Vented Gas Explosions

Bala Mohammed Fakandu, Msc, Bsc (Hons) AIFireE

Submitted in accordance with the requirements for the degree of

Doctor of Philosophy

The University of Leeds

Energy Research Institute

School of Chemical and Process Engineering

June, 2014

The candidate confirms that the work submitted is his own, except where work which has formed part of jointly-authored publications has been included. The contribution of the candidate and the other authors to this work has been explicitly indicated below. The candidate confirms that appropriate credit has been given within the thesis where reference has been made to the work of others.

This copy has been supplied on the understanding that it is copyright material and that no quotation from the thesis may be published without proper acknowledgement.

The right of Bala Mohammed Fakandu to be identified as Author of this work has been asserted by him in accordance with the Copyright, Designs and Patents Act 1988.

List of Publications and Award

Results from the present work as reported in this thesis had led to publications of papers in high ranking journals and well recognised conferences. Some of the publications formed part of chapters of the thesis and are mentioned as such in the list of publications below, and contributions of various authors are also highlighted.

Publications by the Author

1. Fakandu, B.M., Kasmani, R.M., Andrews, G.E., and Phylaktou, H.N. (2011). Gas Explosion Venting and Mixture Reactivity. Proceedings of 23th International Colloquium on the Dynamics of Explosions and Reactive Systems (ICDERS 2011), California.
   (Chapter 7 of the thesis contains part of the publication)
   Contribution of Authors:
   ➢ Fakandu, B.M analysed the result and wrote the paper.
   ➢ Kasmani, RM designed and constructed the vessel used for this work.
   ➢ Andrews, G.E. and Phylaktou, H.N, supervisors of the research and gave advice on the result.

2. Fakandu, B.M., Kasmani, R.M., Andrews, G.E., and Phylaktou, H.N. (2012). The Venting of Hydrogen-Air Explosions in an Enclosure with L/D=2.8. Proceedings of Ninth International Symposium on Hazardous Process Materials and Industrial Explosions (IX ISHPMIE), Cracow, Poland.
   (*Chapter 6 of the thesis contains part of the publication*)
   Contribution of Authors:
   ➢ Fakandu BM analysed the result and wrote the paper.
   ➢ Kasmani RM designed and constructed the vessel used for this work and did similar work which was discussed.
   ➢ Andrews G.E. and Phylaktou, gave advice and supervision.

3. Fakandu B. M. , Yan Z. X. , Phylaktou H. N. and Andrews G. E. (2013). The Effect of Vent Area Distribution in Gas Explosion Venting and Turbulent Length Scale Influence on the External Explosion Overpressure. *Proceedings*

of 7th International Seminar on Fire and Explosion Hazards, Boston, USA (5-10 May 2013).

(Chapter 5 of the thesis contains part of the publication)

Contribution of Authors:

➢ Fakandu BM analysed the result and wrote the paper.

➢ Yan Z.X assisted with the experiment.

➢ Andrews G.E. and Phylaktou, advice and supervision.

4.   Fakandu, B.M., Andrews, G.E., and Phylaktou, H.N. (2014).Gas Explosion Venting: Comparison of Square and Circular Vents. Chemical engineering transactions vol. 36, 2014

(Chapter 5 of the thesis contains part of the publication)

Contribution of Authors:

➢ Fakandu BM analysed the result and wrote the paper.

➢ Andrews G.E. and Phylaktou, gave advice and supervision.

5.   Fakandu, B.M., Andrews, G.E., and Phylaktou, H.N. (2014). Vent static burst pressure influences on explosion venting. Proceedings of Tenth International Symposium on Hazardous Process Materials and Industrial Explosions, Bergen, Norway (10-14 June).

(Chapter 9 of the thesis contains part of the publication)

Contribution of Authors:

➢ Fakandu BM analysed the result and wrote the paper.

➢ Andrews G.E. and Phylaktou, gave advice and supervision.

6.   Kasmani, R. M. Fakandu, B.M. Kumar, P. Andrews, G. E. Phylaktou, H. N. (2010). Vented Gas Explosions in Small Vessels with an L/D of 2. Proceedings of the Sixth International Seminar on Fire and Explosions Hazards, Bradley, D., Makhviladze, G., and Molkov, V., (Eds.), University of Leeds, Leeds, UK (April 11-16, 2010), 2011. pp. 659-670.

7.   Fakandu B.**M**, Sattar H., Andrews G.E. and Phylaktou, H.N. (2011). Vented Gas Explosion in Small Vessels of L/D of 2.8. Proceedings of 23th International Colloquium on the Dynamics of Explosions and Reactive Systems (ICDERS 2011), California.

8. Fakandu, B.M., Andrews, G.E., Stride, D. Witty, L. and Phylaktou, H.N."The Flameless Venting using Polyurethane Foam". To be presented during the 7th International Seminar on Fire and Explosion Hazards in Boston, USA (5-10 May 2013).

9. Yan Z. X. , Fakandu B. M. , Phylaktou H. N. and Andrews G. E. (2013). Vented Hybrid Explosions of Methane and Coal Dust. Proceedings of 7th International Seminar on Fire and Explosion Hazards, Boston, USA (5-10 May 2013).

10. Fakandu, B.M., Andrews, G.E., and Phylaktou, H.N. (2014). Impact of non-central vents on vented explosion overpressures. Proceedings of Tenth International Symposium on Hazardous Process Materials and Industrial Explosions, Bergen, Norway, (10-14 June) .

11. Fakandu, B.M., Andrews, G.E., and Phylaktou, H.N. (2014). Comparison of central and end spark position for gas explosions in vessels with L/D of 2.8 and 2.0. Proceedings of Tenth International Symposium on Hazardous Process Materials and Industrial Explosions, Bergen, Norway (10-14 June).

Award

The paper titled "**The Effect of Vent Area Distribution in Gas Explosion Venting and Turbulent Length Scale Influence on the External Explosion Overpressure**" was selected as one of the best student presenter award at Seventh International Seminar on Fire and Explosion Hazards (ISFEH), 5-10 May 2013. The award was presented to the Author for the quality of its scientific content, and the work also forms part of **chapter 5** of this thesis.

Acknowledgements

x

Abstract

This investigation generated new experimental data on premixed gas/air vented explosions. A small (0.01 m^3) and medium scale (0.2 m^3) cylindrical vessels were used with L/D of 2.8 and 2 respectively, with range of vent area coefficients K_v of 2.7-21.7. The initial set of experiments considered free venting, so that the flame propagation during the venting process was laminar and also the short distance of the vessels would reduce the effects of flame self-accelleration. Covered vents were later used with vent static burst pressure P_{stat} from 35 to 450mb in the 10L vessel. Different gas mixtures were used throughout this work including methane-air (10%), propane-air (4 and 4.5%), ethylene-air (6.5 and 7.5%), and hydrogen-air (30 and 40%) gas mixtures. The ignition position at the far end opposite the vent and central location mid-way the length of the vessels were compared. Current venting guidance is based on experimental vented explosions with central ignition, but this work shows that end ignition opposite the vent is the worst case.

The current design procedures for the protection of explosions using venting is shown to be inadequate for hydrogen-air explosions. New data has been presented which indicates that for hydrogen explosions, the vent flow behaves differently as compared to other gas mixtures investigated. Hence, the need for more research in hydrogen-air mixtures in order to have better understanding of hydrogen venting process.

Experimental data from the current work also shows that multiple vents and vent shapes have significant effects on explosion overpressure and flame speeds. This is contrary to the assumption of the current venting standards.

The effect of static burst pressure on explosion venting was shown to be quite different to that in the design standards, which is supported by other work in larger vessels. Other aspects of vent design that the standards say are not important were shown to be significant: the number of vents, the position of the vent, the shape of the vent, the ignition position. Laminar flame venting theory was shown to be a good predictor of the results and those from the literature where larger vessels were used.

Table of Contents

List of Tables

List of Figures

Nomenclature

A	Area (m²)
a	Bartknecht's (1993) reactivity term
A_f	Area of flame
A_s	Internal surface area of the vessel (m²)
A_v, V_r	Area of the vent (m²)
Br	Bradley number
c, c_0, c_{ui}	Speed of sound (m/s)
C	Deflagration characteristic constant
C_D, C_d	Discharge coefficient
D, d	Diameter (m)
(dP/dt)	Rate of pressure rise (bar/s)
$(dP/dt)_{max}$	Maximum rate of pressure rise (bar/s)
E, E_p, E_v	Expansion factor ($E_p = constant\ pressure, E_v = constant\ volume$)
f	Frequency (Hz)
G_u	Unburnt gas-air sonic flow mass flux = 230.1kg/m²-s
G'	Maximum incompressible (sub-sonic) mass flux through the vent
h	Height (m)
k	Thermal conductivity
K_G	Deflagration index for gases
K_{st}	Deflagration index for dusts
K_v	Vent coefficient ($\frac{V^{\frac{2}{3}}}{A_v}$)
L	Length (m)
l	Integral or characteristic length scale
L	Turbulent length scale
L/D	Ratio of length to diameter

L_e	Lewis number
m	Molecular weight
Ma, M	Mach number
m_b	Mass burning rate
n	Number of moles
P	Pressure (bar)
P_{max}, P_m	Maximum pressure in confined explosion (barg)
P_{red}	Reduced pressure in a vented explosion (barg)
P_{int}	Internal pressure
P_{stat}, P_v	Pressure that activates a vent cover when pressure was increased slowly
P_{burst}	Pressure peak due to vent opening pressure
P_{fv}	Pressure peak due unburned gas flow through the vent
P_{ext}	Pressure peak due the external explosion
P_{mfa}	Peak due to maximum flame area inside the vessel
P_{rev}	Peak due to the reverse flow into the vented vessel after external explosion
P_{ac}	Peak due to high frequency pressure oscillations and acoustic resonance
$P_i, \ P_0$	Initial pressure (which may be ambient)
Pa	Atmospheric or ambient pressure
R	Gas constant ($= 8.314 \text{J mol}^{-1}\text{K}^{-1}$)
r	Vessel radius (m)
R_e	Reynolds number
S_f	Flame speed (m/s)
S_g	Unburnt gas velocity (m/s)
$S_L, \ S_u$	Laminar burning velocity (m/s)
S_T	Turbulent velocity (m/s)
T	Temperature (K)
T_n	Flame detectors (with position number n)

PTn	Pressure transducers (with position number n)
t	Time (s)
U	Mean flow velocity – steady state
U_L	Laminar burning velocity (m/s)
$u^{'}$	Root mean square (rms) value of the fluctuating component of velocity
V	Volume (m^2)
v	Viscosity
w	Molecular weight
x	Distance (m)

Subscript

a	Denotes ambient condition (not necessarily the same as initial)
b	Denotes burnt gas
i	Denotes initial condition (not necessarily the same as ambient)
max	Maximum value recorded
u	Denotes unburnt gas

Greek letters

Φ	Equivalent ratio
λ, β, χ	Turbulent enhancement factor
ρ	Density (kg/m^3)
ΔP	Pressure differential (bar)
γ	Ratio of specific heat at constant P to that at constant V
$\overline{A}$	Dimensionless area
$\overline{S}$	Dimensionless reactivity term ($\overline{S} = \frac{S_u}{C_o}\left(\frac{\rho_u}{\rho_b} - 1\right)$)
δ	Flame thickness
ε	Compressibility factor

CHAPTER 1

Introduction to Gas Explosions

1.1 Background

1.2 Industrial explosion Accidents

1.3 Overview of explosion Problem

1.4 Explosion Prevention and Protection Techniques

1.5 Explosion Venting

1.6 Conclusion

1.1 Background

Over the past decades, there has been major problems dealing with safety issues regarding releases of flammable gases in process industries caused by leakage. A good example of an uncontrolled explosion was the Piper alpha disaster of 1988, where the oil production platform of the North Sea was destroyed due to an accidental explosion resulting from gas leakage from faulty valve, recording 167 deaths and 61 survivors (Shallcross, 2013). The vent design in this case proved to be inadequate. Explosions can occur in dust/air mixtures, but this thesis concentrates on gas/air explosions although explosion protection measures are similar for the two types of explosions. Dust explosions cannot occur without turbulence to disperse the dust, whereas laminar gas/air explosions can occur and does occur for low leak rates and for vessel that operate a process with a flammable atmosphere. This work is only concerned with the venting of laminar gas explosions. It is possible for an explosions to start as a laminar propagating flame and interact with obstacles and generate turbulence, but this interaction is not considered in this work, but is recommended as a future extension of the present work.

The effect of a gas release can be an accidental gas explosion, which may lead to significant damage and also may contribute to an escalation of events to cause more damage such as at Piper Alpha and in the Buncefield incidence of 2005 (Johnson, 2010). At Piper Alpha the initial explosion was relatively mild but the bulging of the compartment walls by the explosion overpressure, which was not adequately vented, caused disruption to the water drench and other safety systems. At Buncefield the initial gasoline leak spread across a car park and across obstacles including a nearby row of trees and bushes and when eventually ignited the initially laminar explosions escalation through the generation of turbulence and is now considered to have reached detonation. This was due to the size of the cloud of flammable gas and the turbulence generated in its interaction with trees and bushes, allowed there to be sufficient distance for the flame to accelerate to detonation.

When explosion accidents occur in enclosed volumes, they involve the generation of a pressure rise due to the temperature rise by the flame in a closed volume. This thesis is concerned with the process of explosion venting that relieves this pressure rise and ensures that the containment vessel is not destroyed. The explosion process

happens in a very short period of time and capable of causing damage and any explosion protection technique must be rapid in its action. Venting requires no sensors and is the simplest and lowest cost of the explosion protection measures. A confined controlled explosion of fuel and oxidants is used in the internal combustion engine for power generation and the related physics of closed vessel explosions are the same for these intentional explosions in engines and the accidental explosions following a gas leak.

In most process plants where petroleum products or flammable gases are produced, the risk of accidental explosion cannot be completely eliminated and this means that plant structures must be protected against any accidental explosion. In this regards, several techniques and methods have been design to protect structures from damage and to ensure the safety of personnel in the process plants. The most cost effective of all the techniques is explosion protection by the explosion venting method, in which part or all part of the process plant wall is designed to fail in the event of an accidental explosion, in order to reduce the impact on the structure. In this instance, the structure is constructed to a certain strength, the vessel failure pressure, in which the expected reduced pressures from the explosion venting most not exceed and a safety margin on this of at least 1/3 is usually applied (NFPA 68, 2013), to give the desired design reduced explosion overpressure, P_{red}. This is the maximum overpressure that can occur in a vented explosions and the vent design aims to calculate the vent area that will produce this P_{red} or lower.

The standard for the explosion protection by deflagration venting (NFPA 68, 2013) and the European venting standard (EN 14994-2007), gives guidelines for the design of the appropriate vents to protect structures against accidental explosions. These will be presented in more detail later in the thesis, but their considerable differences are reviewed here. Also aspects of vent design that are stated not to matter in the design procedure were investigated in this research work. The aim of this work was to produce a better physical understanding of the venting process, to provide a large body of new vented explosions data and to interpret this data in the light of spherical laminar flame venting theory to give some recommendations on the vent design process.

The venting design guidance, as adopted by European vent design standards (EN 14994-2007), was based on the original work of Bartknecht (Bartknecht, 1993) and

the NFPA 68 of the United States relies on the work of Swift (Swift, 1988). Most of the equations in the European standards (EN 14994-2007) are not correlations of all available experimental data in the literature, but is the data for a 10m^3 vented vessel and does not have a safety margin (Andrews and Phylaktou, 2010). It will be shown in the review section of this thesis that this data does not agree with any other data in the literature for larger or smaller vessels and does not agree with Bartknecht's own data for vessels of larger or smaller size. Also, it will be shown that there are many aspects of vent design that is in the two standards for which no experimental data is referenced to support the contention. This thesis explores issues related to the number of vents, the shape of vents and the position of vents as well as the position of the spark, all of which the standards say do not matter and are shown to matter in this work.

The European design equation restricts the length to diameter ratio L/D of the vessel to that of 'compact vessels' which is define in terms of the length to diameter ratio, L/D or minimum dimension to maximum dimension in rectangular rooms. In the European vent design standard a compact vessel is taken as an L/D of <2 (Bartknecht's recommendation) but gives correlations based on very limited data for higher L/D up to 10. The US design equation for a compact vessel is valid up to an L/D of 2.5 and a procedures to design for higher vent areas is given for L/D 2.5 − 5 and these are different from those in the European vent design standards. There is little open literature data to support these effects of L/D, even in the L/D = 1 − 2.5 region. As the effect of elongated vessels is to require a larger vent area for the same volume it is clear that an L/D of 2 or 2.5 is likely to have a larger overpressure than an L/D. As a consequence this work investigated the worst case geometry that could still be considered a compact vessel and an L/D of 2 and 2.8 were investigated.

The reason for the limitation of the basic vent design equations to compact vessels is because, as will be shown in the thesis, spherical flame propagation theory is assumed in vent design. This theory says that the pressure rise is independent of the vessel volume and that the vent coefficient, $K_v = V^{2/3}/A_v$, is a scaling parameter for vented explosions where the flame propagation is spherical. This is the only term in the European vent design procedures that includes the vent volume and the design procedures are valid for all volumes below 1000 m^3, even though no experimental data was undertaken by Bartknecht on volumes above 60 m^3 or below 1 m^3. The applicability of the design procedures to volumes above 60 m^3 and below 1 m^3

entirely relies on spherical laminar flame venting theory, which is reviewed in this thesis. As there is no limit of the vented vessel volume a very small vessel of 0.01 m^3 was used for most of this research with some limited work on a 0.2 m^3 vessel. Comparison with vented explosions in larger vessels would then test the validity of K_v being the only vessel volume term in the vent design. In NFPA 68 (2013) the vessel volume comes into the design procedure through terms relating to the Re of the spherical flame and the Re of the vent flow. Both of these Re increase with vessel volume and so the US design procedures have a mechanism that requires larger vents in large volume vessels and this is not a feature of the European procedures.

NFPA 68 (2013) and BS EN 14994.2006 do not use the same parameter to characterise the mixture reactivity, K_G (see later for definition) for the European standard and the laminar burning velocity for the US standard. The US standard limits the applicability to burning velocities <3 m/s which excludes the maximum burning velocity of hydrogen-air and the European standards have no limit and have a design values for the maximum reactivity of hydrogen.

The European venting standards are limited to a P_{red} of 2 bar and in the US standard this is 0.5 bar, with a different design standard for P_{red} with no limits on this higher P_{red}. The US standard has no influence of the vent static burst pressure, P_{stat}, up to a P_{red} of 0.5 bar (with a limitation that P_{stat} must be <P_{red} by a margin of 24mb for P_{red} <0.1 bar and a margin of 25% for 0.1 < P_{red} < 0.5). In contrast the European vent guidance is not valid for P_{stat} < 0.1 bar, but has design procedures for P_{stat} up to 0.5 bar and are not valid above this. The European design guide is also not valid for P_{red} <50mb above P_{stat} (there is no experimental evidence to justify this) or for P_{stat} < 0.1 bar (which was the limit of Bartknecht's vent design equation). In the draft European guidance a reference to the Swift approach, as in NFPA 68, for P_{stat} < 0.1 bar was mentioned, but this was removed by the final version. These is thus some confusion over the effect of P_{stat} and this work has one Chapter devoted to obtaining more experimental data on this effect including P_{stat} < 0.1 bar.

It is obvious that most of the vent design equations adopted by the standards (BS EN 14994:2006, BS EN 14994:2007, NFPA 68, 2007, 2013) have limitations in their applicability as design guides and limitations in the data base that the design recommendations are based. Also the US and European design standards are quite

different and it is difficult to see how both can be correct. Thus, the issue of gas venting design was the basis of this thesis and many of the design 'rules' were investigated and a large body of new experimental data was produced.

1.2 Industrial Explosion Accidents

Over the last century there has been a series of industrial explosion accidents which made history due to the nature of the devastation in number of casualties and property loss of millions of pounds. Most of these accidents influenced safety legislations, design codes and standards. Furthermore, these accidents has led to extensive research on explosion hazards, in order to get good understanding and proffer better solutions to prevent future occurrence. Some of the well known accidents include the Flixborough, BP Texas, Piper Alpha, Buncefield and the BP oil spill and fire at Deepwater Horizon in the Gulf of Mexico. Table 1.1 gives a summary of explosion incidences (case studies) raging from oil production, chemical and nuclear plants, with particular interest in confined explosions.

These explosions are well known as they were major events that made national news. However, there are thousands of smaller explosions in process plants and in gas leaks in homes that do not reach the national news and this research was directed at understanding the common explosion protection technique of venting. Venting protection is used where the hazard is a gas or dust/air mixture in a closed volume where the mixture is flammable and a spark may accidentally occur. This is the most common industrial and domestic explosion hazard. Although, explosion protection using venting dates back a century or more, there has been no official guidance in Europe on vent design, until that provided as part of compliance with the ATEX (Explosive Atmospheres) Directive, which were implemented by the HSE DSEAR Regulations in the UK. There had been UK industrial recommendations in vent design from British Gas prior to their privatisation in 1990 and some guidance from the Fire Research Station work, as reviewed in Chapter 2. None of this earlier guidance had a legal status and there was a scant body of experimental venting data, as reviewed by Lunn (1984).

In the US the NFPA 68 vent design guidance has existed for many years and this largely recognised the German guidance which was based on the work of Bartknecht

(1993), which effectively became the European guidance. However, in 2013 the US abandoned this approach largely because Bartknecht's results could not be duplicated in vented explosions carried out at FM Global (Bauwens, 2010) and were not supported by any other data in the literature, as shown in the review chapter. The present research was carried out mainly to try to understand why vent design procedures were incompatible in the two design guides and to provide new venting data for gas/air explosions.

Table 1.1 Summary of selected explosion accidents

Serial	Incident	Date	Casualty	Damage	Causes	Reference
1.	Explosion in Gerdau Ameristeel Mill, Tennesee, US	16/05/2014	1 killed and 6 injured	Damaged structures over 1km from site	Equipment failure	(The Daily Times, 2014)
2.	Soma, holding mining tragedy, Turkey	13/05/2014	245 killed and several injuries	Damaged most equipment and high causality rate	Negligence on the part of the factory owners	(The World Post, 2014)
3.	Surat, Recycling Plant explosion, India	12/05/2014	10 died and 30 injured	Damaged to structure and other structures around the site	Gas cylinder explosion caused by fire from short circuit	(SifyNews, 2014)
4.	Chemical plant blast, East Jiangsu, Province	16/04/2014	5 killed 9 injured	Damage to part of the factory	Leaks of palm oil and accidental explosion	(CRIENGLISH, 2014)
5.	Chemical factory reactors explosion, Tarapur, MIDC area, India	14/04/2014	No casualty	Damages to reactors, company building and nearby sttlement	Overheating of the reactor caused the initial explosion and subsequent 5 explosions from other reactors.	(The Times of India, 2014)

Table 1.1 continuation

Serial	Incident	Date	Casualty	Damage	Causes	Reference
6.	Yanhou Tunnel explosion	1/03/2014	31 died, 9 missing and several injuries	The explosion engulfed over 42 car and trucks with cargo	Collision with a truck carrying methanol leading to explosion within the tunnel.	(Wireupdate, 2014)
7.	Explosion at Mitsubishi material chemical plant, Japan	9/01/2014	5 people killed and over 12 Injured	Damaged part of the plant	Heat exchanger exploded while maintenance and cleaning operation was going on.	(BBC NEWS ASIA, 2014)
8.	Clacton gas explosion in dwelling, UK	5/02/2014	10 people were injured	Flattened 2 houses and one partly damaged	Gas maintenance carried a day before the incidence	(BBC NEWS ESSEX, 2014)
9.	Keeper chemical factory Zhaixian explosion	28/2/2012	25 deaths and 46 injured	Breach of safety procedure and management incompetency	Damage to factory surrounding structure extending 2km	(CHINADAILY USA, 2012)
10.	Yeosu chemical plant explosion, South Korea	14/3/2013	7 killed and 13 injured	Breach of safety and operating procedure	Killed the contractor and damage the tanks within the site	(Hazardex, 2013)

1.3 Overview of the Explosion Problem

Safety must be given high priority in areas with potential high fire and explosion risk or areas where the use of flammable substances is unavoidable. Explosions are be defined as a combustion reaction which results to increase in volume, rapid rise in pressure and the release of energy at very high temperature (Bjerketvedt et al., 1997). For an explosion to occur a flammable gas/oxidant mixture must be present with an ignition source. For there to be an overpressure this mixture must in enclosed and the present work is directed at situations where the mixture is totally enclosed inside a process plant or a building. In dust explosions there must be dispersion of dusts or agitation to force mixing with air within a confinement or enclosure resulting in rapid rise in pressure. Gases disperse and mix by diffusion without the necessity for there to be turbulent air dispersion. Leakage of gas and vapours is a common risk in industries and process plants. In most cases, the leakage of associated gases forms a flammable cloud within the explosion limits.

In the process industry flammable atmospheres in process vessel are a common risk. For example every heating plant using a fossil fuel is a potential explosion hazard. The burner has fuel and air fed to it in stoichiometric proportions. If the flame does not ignited and stabilise on the burner then a premixed stoichiometric mixture fills the furnace and this explodes when the ignitor is pressed to ignite the flame. It was this hazard that led British Gas to undertake extensive closed vessel vented explosion research in the 1950 – 1990 periods. There were numerous industrial oven explosions in industry in the 1950's and the venting of process ovens was the solution to the hazard. In the petrochemical industrial large scale furnaces are used in crude oil distillation and all are potential explosion hazards and must be protected. The other area that led British Gas to undertake explosion research was that of buildings supplied by gas for heating having a gas leak and explosions that killed the inhabitants. These still occur today and are ongoing research area in the gas industry.

The Fukushima explosion in a nuclear plant as a result of the Japan earthquake of 2011 was a good example of an accidental explosion caused by natural disaster (Watanabe et al., 2013). This was caused by a cooling water leak onto high temperature nuclear components that dissociated the water into hydrogen and

oxygen which were contained in the nuclear pressure vessel. A closed vessel hydrogen oxygen explosion then occurred for which no vent protection had been provided. The hydrogen explosions blew apart the pressure vessel, which was shown on National news around the world.

1.4 Explosion Prevention and Protection Techniques

There are different methods employed to prevent any accidental explosion and this includes the control technique, ignition source limitation, and use of chemical inerting. The protective measures try to reduce or eliminate the magnitude of damage to the affected structure. Among the most popular explosion protection techniques ventilation, containment, suppression, isolation and venting

1.4.1 Explosion Prevention

Explosion prevention techniques seek to ensure that the causes of accidental explosion are reduced or eliminated. The most common preventive measures are:

1.   **Ventilation:** In many process plants the accidental release of flammable gases or vapour may be inevitable as it is part of the process. In view of this, ventilation techniques are essential in order to reduce or dilute the concentration of the releases gases within the enclosure or confinement. The aim is to ensure that the concentration of the mixture of the gas and air is well outside the explosion limit (lower explosion limit) to support any explosion (EN 1127, 2011). The aim will be achieved by having sufficient flow of air within the confinement, which is done by natural or artificial ventilation.

2.   **Ignition Elimination:** This involves the elimination of all potential spark ignition sources, including those that arise by electrostatic charge generation. However, it can never be assumed that there can be no explosion because there is no ignition source, as past incidents shows that often the ignition source in an explosion event has never been identified. Thus another explosion protection measure is always required.

3. Inerting: The use of inert gas is another method used in limiting concentration of combustible components in process plants. The common inert gases are carbon dioxide, nitrogen and Argon and their mixtures. Inert gases added to a stoichiometric gas air mixture lower the flame temperature as they act as a heat sink. Hydrocarbon

flames have a critical flame temperature for flame propagation of 1400K and the critical amount of inert is that required to reduce the stoichiometric flame temperature below 1400K. The most effect inert gas is carbon dioxide as it has a higher specific heat than nitrogen. Water mist is also effective as water is close to CO_2 in its specific heat. The addition of inert gases displaces oxygen, but this is NOT the mechanism that inerting works. As less CO_2 is required to cool a flame to below 1400K than for nitrogen, the corresponding critical oxygen levels are different (16% for CO_2 and 12% for N_2) which is why it is not the depletion of oxygen that puts the flame out.

4. **Zoning:** The grouping or classification of areas within the process plants based on the risk of hazard associated with these areas is termed zoning. Most of these classifications are done to limit or eliminate the use of any source of ignition within such areas. The classifications are based on frequency or use or duration of occurrence of hazardous explosive atmosphere within the premises (EN 1127, 2011).

Zone 0 is where a flammable atmosphere is normally present and intrinsically safe equipment (Type 1) is required.

Zone 1 is where a flammable atmosphere may be present and Type 1 and 2 equipment are required.

Zone 2 is where a flammable atmosphere is not normally present and Type 1, 2 and 3 equipment (no special explosion protections measures) can be used.

The aim is to keep the most hazardous process in a fenced area and to ensure that equipment that cannot cause ignition of a flammable mixture is used in that zone.

1.4.2 Explosion Protection

All efforts must be taken to prevent explosion from happening, but the plant must still be protected against an explosion. The ultimate purpose of employing the explosion protection techniques is to reduce or protect structures and personnel from explosion hazards in an event of an explosion. Different methods are employed to achieve this as explained in more detail below.

1.   **Isolation:** Isolation is used to prevent an explosion going from one part of a process plant into another enclosure or vessel. Connected vessel or room explosions

can occur via the use of connecting pipes or corridors (Andrews, 2010).The explosion in the connecting vessel or the receiving vessel is more severe due to the generation of turbulence in the connected vessel through the air jet generated down the connecting pipe by the initial explosion venting out of the first vessel into the connecting pipe or corridor (Phylaktou and Andrews, 1993). Connected vessel explosions in process plant can protected using a slam shut isolation valve or by fast injection of explosions suppressant powder together with fast explosions detection.

2. **Containment:** In containment, the equipment to be protected is designed to withstand the maximum overpressure without any damage to the structure. This is normally a very expensive solution to the problem. It would only be used where the materials processed may be dangerous or exposing the combustion product may to be toxic, hence contains the explosion. This method or technique requires some element of isolation in order to prevent the explosion been transmitted or getting into other vessels or connecting pipes from the main vessel. In most cases, containment leads to deformation of the main vessel due to high pressure involved and the vessel may require replacement.

3. **Suppression:** Suppression is the detection of an explosions using a pressure transduced and then injecting a dry powder suppressant very fast at a set static pressure rise of typically 50 mb. The suppressant powder is delivered very fast by stored nitrogen at 60 bar pressure actuated by a fast acting ball valve controlled from the pressure rise transducer. Typical suppressant powders are sodium bicarbonate and mono-ammonium phosphate (MAP), they have flow additives added and are sold under various trade names. Water is also a good suppressant as the nitrogen high pressure injection creates an atomised mist. Design guides for suppression systems are based on extensive experiments and are the property of the suppressant manufacturers. Usually the manufacturer guarantees that the design will work and the manufacturer takes the insurance risk. However, these systems are expensive to install and maintain, compared to venting. They would be used where vent protection was not viable, due to the vessel being near where people worked.

4. **Venting:** Explosion venting is the explosion protection measure designed to ensure the unacceptable pressure build up within the enclosure is released by venting the explosions flame outside the enclosure, so that the flame expansion occurs outside as a free flame and not inside the vessel where the high temperature causes the pressure to rise. A vent is a weak part of the wall of the enclosure that is

designed to fail in the event of an explosion at a set fail pressure, P_{stat}. This is the most cost effective and widely accepted explosion protective measure. The design of a vent for explosion protection in closed vessels requires P_{stat} and P_{red} to be specified as well as the mixture reactivity. The design method then predicts the required vent area to achieve the desired P_{red}. This design process is the research theme of this thesis.

1.5 Explosion Venting

The developing pressures from an explosion are relieved through vents to provide:

a.   An opening of area A_v to allow the explosion flame to escape from the vessel or enclosure, so that pressure rise in the enclosure ceases.

b.   Reduce the internal pressure within the enclosure, to the design P_{red}.

c.   Minimise the damage to the enclosure and the effect of the external explosions on people and buildings close by.
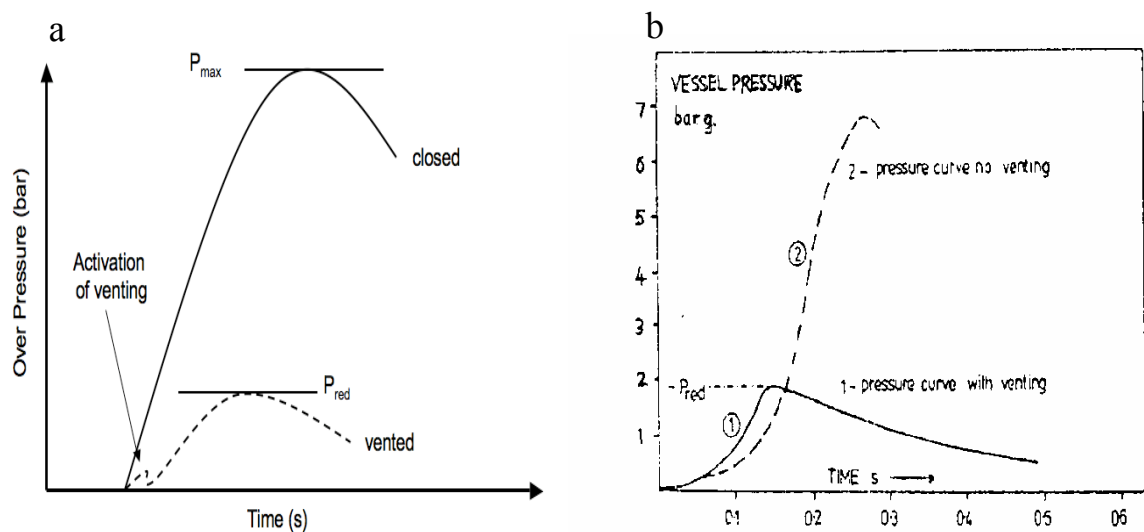
Figure 1.1 Pressure behaviors for normal and vented explosion as a function of time (Bartknecht 1971, Siwek 1996)

The reduction of the peak closed vessel explosions overpressure by a vent is illustrated in Fig. 1.1It is important to note that venting does not prevent an explosion, it reduces the overpressure effect to the minimum as seen in Figure 1.01a. Furthermore, Figure 1.2b also shows the closed vessel explosion peak overpressure at 7 bar (P_{max}=7 bar), while when vented it reduces to $P_{red}<2$ (Siwek, 1996). The P_{red} is an important factor considered when designing a vent for explosion protection

with the activation pressure for the venting mechanism P_{stat} (vent static opening pressure) (Maidstone, 1973, Chappell, 1977).

1.5.1 Design of Explosion Vent

The design of explosion vents relies on empirical correlations of vented explosions guided by laminar flame venting theory (Bradley and Mitcheson, 1978a, Molkov et al., 1999, Molkov et al., Razus and Krause, 2001, Yao, 1974). These vents are designed at P_{stat} to give an open vent area, A_v. The design of the vent for venting explosion protection requires that the design strength of the vessel to be known and that P_{red} be set well below (1/3) the design strength of the vessel being protected. The reduced pressure P_{red}, which is the maximum pressure as a result of venting is expected to be 2/3 of the vessel design strength (Cooper et al., 1986). P_{red} can be predicted using the design equation, which are based on experimental data and laminar flame theory (NFPA 68, 2013, BS EN 14491, 2007, Bradley and Mitcheson, 1978a, Swift, 1988, Molkov, 2000).

The design equations adopted in the standards have some important parameters to assist achieving the vent design as follows:

1.   The maximum reduced pressure (P_{red}) must not exceed two-third of the design strength of the vessel. Provided the deformation of the vessel can be tolerated, P_{red}, must not exceed the ultimate strength.

2.   The vent panel or vent material used must be selected to meet the requirement of venting standards, based on the recommended vent activation pressure or vent static pressure (P_{stat}). This P_{stat} also affects the P_{red} or A_v, depending on the vent design correlation used.

3.   The vent area A_v is the vent opening where the explosion pressure is discharged from the vessel, which must be designed to withstand the intended P_{red}.

4.   A mixture reactivity parameter is a key parameter in explosion venting design. It can be selected depending on the design correlation adopted, and this could be the deflagration index, K_G for gases or K_{st} for dust or the fundamental burning velocity S_u.

5.   Vessel volume V is an important factor in vent design, and this influences the required P_{red}.

6.   The vent coefficient $K_v = V^{2/3}/A_v$ which is a dimensionless parameter to accommodate different vessel sizes in the vent design correlation.

$$K_v = V^{2/3}/A_v$$

7.   Another important factor is the possibility of turbulence at the start of an explosion or turbulence generated as a result of gas flow interaction ahead of the flame in the presence of obstacles within the protected vessel. Turbulence is accounted for by the use of turbulence factor, β. The influence of turbulence can also be predicted using based on the laminar burning velocity provided the turbulent factor or other related parameters are known (Al-Khishali et al., 1983, Andrews et al., Tamanini, 2001, Tamanini and Chaffee, 1991). However, neither the European nor US guidance gives any procedures to take into account turbulence.

$$S_T = 1 + \beta S_L$$

In venting of explosion, the pressure obtained is due to the flow of unburnt gases through the vent and this increases if the burning velocity increases due to turbulence or due to change in mixture reactivity.

The venting design guidance as adopted by European vent design standards relies on the original work of Bartknecht (Bartknecht, 1993) and his equations are based only on his original data and that of his co-workers Donat and Siwek. The US NFPA 68 (2013) standard were based on the original work of Swift. These vent design guides have their limitations which will be discussed in more details when reviewing the literature and in the results section.

This work focuses on gas explosion venting with particular interest on vent area sizing, explosion overpressure, flame speeds and the effect of vessel volume, considering the applicability of the vent design standards (NFPA 68, 2007, 2013, BS EN 14994, 2007) and other vent design correlations in the literature. This was aimed at achieving improved vent design procedures. It is necessary to study the gas-dynamics behaviour, combustion and associated parameters affecting it in order to have a better understanding of the mechanism of venting explosion. Even though this work focuses on gas explosion venting, the venting process is similar for dust explosions although these are always turbulent.

1.6 Conclusion

Explosion venting technique is a simple and the most cost effective explosion protection technique. In the design of explosion vents, various factors are considered and the vent design standards are the primary documents required to guide this design. This work is focused on explosion vent design, and most of the design rules of the venting standards were investigated for better and more improved safety.

CHAPTER 2

Review of Correlations and Published Experimental Data on Explosion Venting

2.1 Introduction

2.2 Closed vessel explosions

2.2.1 Spherical vessel explosion

2.2.2 Spherical flame propagation in non-spherical vessel

2.4 Review of explosion venting experimental instigations

2.3.1 Experimental Investigations in Large and Small Scale

2.3.2 Pressure generation in explosion venting

2.3.3 Effect of Vent Shape on Explosion Venting

2.3.4 Impact of Non-central and Multiple Vents on Vented Explosion Overpressures

2.3.5 Review of the Influence of Ignition Position on Vented Explosion

Overpressure

2.3.6 Review of the Laminar Burning Velocity and Gas Reactivity Parameter K_G

2.3.7 External Explosion in Explosion Venting

2.3.8 Effect of Turbulence and Turbulent Length Scale

2.3.9. Review of Hydrogen Explosion Venting and Mixture Reactivity

2.4 Explosion Venting Standards, Theory and Venting Correlations

2.5 Application of Explosion Vent Design Standards and Correlations

2.6 Conclusions

2.7 Aims and Objectives of the Study

2.7.1 Aims

2.7.2 Objectives of the study

2.1 Introduction

This chapter reviews the explosion venting experimental data base and correlations for explosion vent design in the literature. Also presented is the theoretical laminar flame models of premixed gas/air mixture explosion venting. Another area of concern in venting is the effect of the vent external explosion and turbulent flame propagation in the external jet flame, which in many venting situations is the dominant overpressure. The secondary explosion downstream the vent was shown to affect the overall overpressure in explosion venting (Harrison and Eyre, 1987). This is associated with the turbulent nature of the flame as it exits the vent. Explosion venting data on external explosion, turbulent generation, and turbulent length scale and other associated parameters will also be discussed.

The burning velocity (S_u) and the gas deflagration index (K_G) are two important parameters used to determine the reactivity of the gas mixtures. The review will discuss these two mixture reactivity parameter and their measurement variability in in the literature, for which the vent design correlations depend. The review will concentrate on the physics of the vented explosion process and causes of the various peak pressures that have been found to occur. The cause of the peak pressure in vented explosions will be shown to vary depending on K_v, P_{stat} and K_G and the vessel volume, V.

An important aspect of explosion safety is the knowledge of the amount of gas, mist, aerosol, or dust particles required to support explosion when mixed with oxidant. Furthermore, other vital areas including burning velocity, turbulent flame propagation, detonation and other related areas of explosion are also vital. However, most of these areas are discussed in more detail in the literature, and this work only focuses on deflagration venting of laminar flames.

2.2 Closed vessel explosions

To understand explosion venting, firstly the mechanism of closed vessel explosions without venting needs to be understood.

2.2.1 Spherical vessel explosion

In a closed vessel explosion with central ignition a spherical flame propagates. If the vessel is spherical then the explosion is close to adiabatic as the flame does not touch the walls of the vessel until all the mixture has been burned. The expansion of the burned gases behind the flame front pushes the flame forward and this generates a gas velocity, S_g, or wind ahead of the flame. As the flame propagates the hot burned gas expansion also increases the pressure in the explosion vessel. When the flame reaches the wall and has burned all the mixture the peak pressure and temperature are reached and this can be calculated using adiabatic constant volume flame temperature calculations. In a spherical vessel these calculations agree with the measured peak pressures.

The flame temperature at constant volume and the maximum pressure have a relationship relative to the initial pressure and temperature as shown in equation 2.1.

$$P_m = P_i \frac{T_b}{nT_u} = P_i \frac{\rho_u}{\rho_b} = EP_i \qquad [2.1]$$

A typical spherical vessel explosion is shown in Figure 2.1 from Nagy and Verikas (1983). This shows for spherical acetylene air explosions that the adiabatic pressure rise calculations agree with the measurements.

The pressure rise in Figure 2.1 occurs in two stages, an initial period when the pressure rise is small and a later period when it rises rapidly. Figure 2.1 shows that these two periods are roughly of the same time of 5 ms. The first period of flame propagation is known as the constant pressure period of flame propagation and this occupies about half the flame travel time (Andrews, 2014). For a spherical vessel when the flame is half way across the diameter, it has burned 1/8 of the initial volume of gas/air mixture. However, the density of the burned mixture is about 1/7 that of the unburned mixture and so it has only burned about 1/56 of the initial mass or about 2%. The fractional pressure rise in a closed vessel explosion is proportional to the fraction of the mass burned (Lewis and Von Elbe, 1968) and so when the flame is half way across the spherical vessel diameter it only produces a 2% pressure rise. In Figure 2.1 the pressure rise at half the propagation time is about 0.2bar and the pressure rise is 6.2bar so that the pressure rise at half the propagation time was about 3%. Half the propagation time is only half the propagation distances if the

flame speed is constant. However, the results in Figure 2.1 agree with this simply analysis.
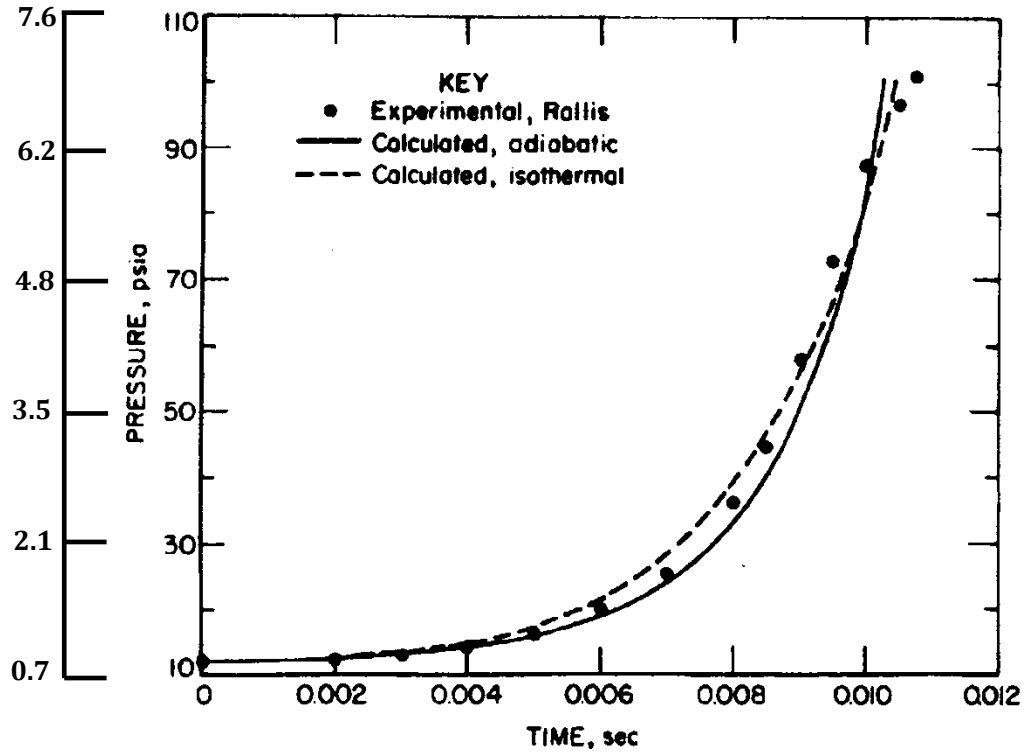
Figure 2.1 Calculated and experimental data for pressure-time for acetylene-air explosion in spherical vessel (Nagy and Verikas, 1983)

In a vented explosion if the peak overpressure is to be low, essentially the explosion has to be vented during this initial near constant pressure combustion.

A spherical flame propagates with an initial spherical flame front pushing the unburnt gases ahead of the flame with flame speed S_f and burning velocity S_u related as given in Equation 2.2 and gas velocity also related by Equation 2.3.

$$S_u = S_f \frac{\rho_b}{\rho_u} = S_f n \frac{T_u}{T_b} \qquad\qquad [2.2]$$

$$S_g = S_f - S_u = S_u(E - 1) \qquad\qquad [2.3]$$

where E is the expansion factor or ratio $= \frac{\rho_u}{\rho_b} = \sim \frac{T_b}{T_u}$.

In closed vessel explosions the rate of pressure rise $(^{dP}/_{dt})_{max}$ is an important factor which is unique to the mixture type and used to determine the reactivity of the fuel mixture. The value of rate of pressure rise is used to determine the constant K_G

which is used to characterise the reactivity of gas mixtures based on the spherical vessel cubic law which is dependent on vessel volume as given in Equation 2.4. The cubic law was based on the spherical flame propagation in spherical volume with flame expanding equally in all directions before reaching the wall of the vessel.

$$K_G = (^{dP}/_{dt})_{max}.V^{1/3}$$ [2.4]

Where, K_G = the reactivity constant for gases and V = the vessel volume

The European standard (EN14994, 2007) for explosion deflagration venting used K_G as the mixture reactivity constant using the values of Bartknecht who used a 5 Litre spherical vessel (Bartknecht, 1993, NFPA68, 2013). While K_G was used as the mixture reactivity constant by the European standard for venting, the US standard (NFPA68, 2013) used the laminar burning velocity S_u as the mixture reactivity. Also, most other correlations for explosion venting design in the literature used S_u as the mixture reactivity constant (Bradley and Mitcheson, 1978b, Molkov et al., 2000, Runes, 1972, Swift, 1989). Bartknecht assumed that his value of K_G was a constant for each gas but it was found that K_G to increased with vessel volume (Cashdollar et al., 2000, Chippett, 1984). This was due to the development of cellular flames due to flame front instabilities, which resulted in flame acceleration. Thus, the use of K_G as the reactivity term in the Bartknecht vent design equation should not be a constant, but should be a function of the vessel volume. In NFPA 68 (2013) this effect has been included in the laminar burning velocity term, as the self-acceleration has been taken into account used the Re of the flame and this is greater for the same pressure rise for flames in vessels of larger volume.

In explosion modelling S_u as the reactivity term is only constant in the contant pressure period of combustion, discussed above. Once the pressure starts to rise the compression of the gas ahead of the flame and the rise in pressure changes the burning velocity. The relationship (Andrews and Bradley, 1972) for methane air is:

$$S_u = S_{uo} \, T^2 P^{0.5}$$ [2.5]

Where S_{uo} is the reference burning velocity at ambient P and T. However, this change of burning velocity (S_u) is small at about 20% (Bradley and Mitcheson, 1977).

Assuming there is constant burning velocity through the pressure rise and since majority of the pressure rise (98%) happens in the last half of the flame propagation. Hence, Equation 2.6 gives the relationship between K_G and S_u considering the adiabatic pressure rise (Andrews and Phylaktou, 2010).

$$K_G = 3.16(^{P_m}/_{P_i} - 1)S_u E \qquad\qquad [2.6]$$

Kumar et al (1992) derived an equation to relating K_G and S_u , with the assumption also that S_u was a constant without any effect of radius, temperature and pressure as shown in Equation 2.7 (Kumar et al., 1992).

$$K_G = 4.84 S_u \left(^{P_m}/_{P_i}\right)^{1/\gamma} (P_m - P_i) \qquad\qquad [2.7]$$

Both of these equations show that the two mixture reactivity parameters used in explosion venting are linearly related and in this work Equation 2.7 will be used to convert venting equations with K_G as the reactivity parameter into its equivalence with S_u as the reactivity parameter.

Nagy (1983) developed a theory of adiabatic spherical closed vessel explosions which he compared with the similar equation for the Isothermal process(Nagy and Verakis, 1983), as shown in Figure 2.1. In his work, the rate of pressure rise was finally obtained as a function of laminar burning velocity, considering that S_u was a constant in Equation 2.8 (Nagy, 1983).

$$\frac{dP}{dt} = \frac{3S_u}{R} \cdot \frac{\gamma P_m^{2/3\gamma}}{P_o^{(2-1/\gamma-\beta)}} \cdot (P_m^{1/\gamma} - P_o^{1/\gamma})^{1/3} \left[1 - \left(\frac{P_o}{P}\right)^{1/\gamma}\right]^{2/3} P^{(3-2/\gamma-\beta)} \qquad [2.8]$$

From Equations 2.6-2.8 above, it was obvious that the rate of pressure rise, $\frac{dP}{dt}$, was dependent on the laminar burning velocity S_u. Hence, this gives a linear relationship between K_G and S_u, as thus $K_G = (Constant)S_u$ with all the other terms constants for a particulate gas/air mixture. This is similar to K_{st} for dust explosion but with exception of the turbulence enhance factor which is unique to dust explosions (Andrews, 2011).

2.2.2 Spherical flame propagation in non-spherical vessels

It is much easier to predict explosion development in spherical vessel with central ignition based on the spherical flame mass burning rate (Andrews, 2011, Nagy, 1983, Lewis and von Elbe, 1968), as there is no contact with the walls before all the mixture is burned. However, non-spherical vessels are more common in explosion venting and then the flame touches the walls before all the mixture has been burned. Heat losses then occurred and the process is non-adiabatic and the peak explosions overpressures and the peak rate of pressure rise are lower than for spherical vessels.
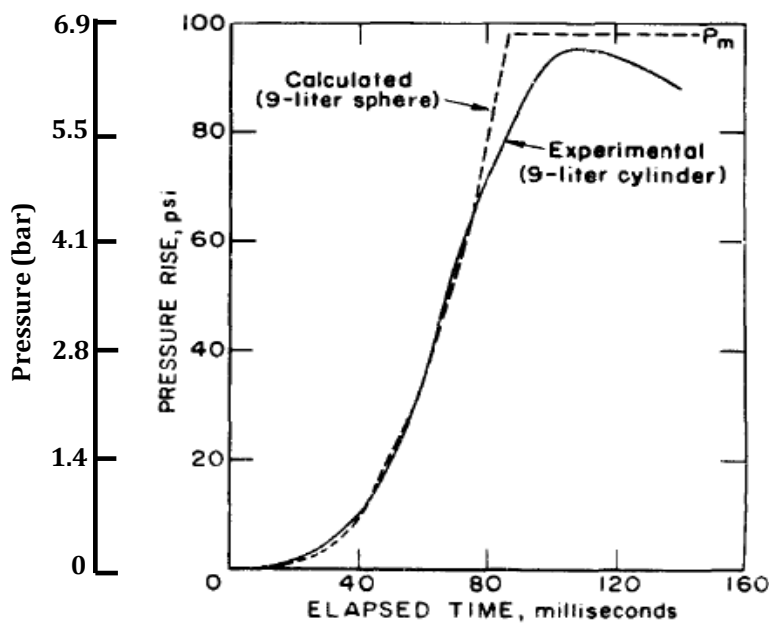
Figure 2.2 Comparing pressure-time records of 9L cylindrical and spherical vessels for 10% methane-air (Zabetakis, 1965)

For a cylindrical vessel, the prediction of flame propagation is difficult after the flame touches the wall of the vessel, and experimental evidence shows that the flames propagate with initial shape of a hemisphere, gets distorted before touching the wall and later assumes a shape closer to that of the vessel (Andrews, 2011). In this regard, the assumed adiabatic nature of explosion development cannot be achieved, since there is heat loss before the burning of the gas mixture is completed. In Figure 2.2, the cylindrical vessel was shown to give lower maximum pressure when compared to the calculated pressure of spherical vessel of equal size due to the flame touching the wall earlier, thereby losing heat before all the gas mixture was

burnt (Zebatakis, 1965). The European vent design correlation restricts the L/D < 2 for compact vessels and assumes that the flame spread spherically in the venting process. If the vessel shape is much different from a cube which is the closest to the sphere or the L/D > 2, then the flame will touch the vessel wall before there is any significant pressure rise (Andrews, 2011).
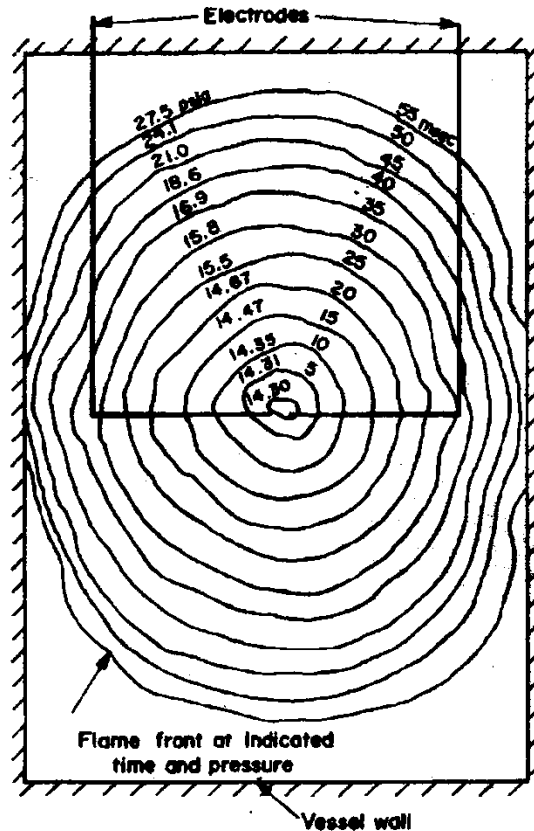
Figure 2.3 Flame development in a cylindrical glass vessel for methane-air
(Nagy and Verikas, 1983)

Nagy and Verikas (1983) have used high speed photography in a rectangular closed vessel with glass walls to show the flame shape as it propagates to the wall. This is shown in Figure 2.3. This shows that when the flame touched the wall the pressure rise was only about 0.9 bar and that all the mass was compressed into the corner regions. However, in this near cubic vessel, provided that the overpressure in a vented explosion is desired to be <0.9 bar, which is normally the case, then spherical flame propagation can be assumed in modelling the vented explosions. What happens after the flame has left the vent and the peak pressure has been achieved does not need to be modelled. For a cubic vessel a spherical flame that touches the walls has a volume burn fraction of $\pi D^3/6D^3$ or 52%, but this is about 1/7 of the density of the unburned gas so that the mass burned is about 7.5% and this would

produce a pressure rise of about 7.5% of 8 bar or about 0.6 bar, which is close to that in Figure 2.3. Thus a cube is a compact vessel and venting will all be for a spherical flame up to an overpressure of 0.6 bar. For a rectangular vessel with an L/D of 2 and a square cross section it is obvious that only 3.7% of the mass will be burned when a flame from a central ignition hits the walls, which is a pressure rise of about 0.3 bar. Normally peak overpressures are desired to be lower than that and so the assumption of spherical flame propagation in venting modelling is valid for an L/D of 2. For larger L/D this assumption becomes less valid as the overpressure during the spherical flame period becomes lower than 0.3 bar.

For a cylinder the mass burned when the flame touches the walls for central ignition is 0.096/(L/D). In the present work an explosion cylinder with an L/D of 2.8 was used and for central ignition the mass burned when the flame touched the walls is 3.4% which will give a pressure rise of about 0.27 bar. This is just on the limit of acceptability for spherical flame propagation provided low vented overpressures are desired. The aim was to study the limit of applicability of the venting correlations for compact vessels.

Thus, spherical flame propagation can be used to model venting in compact vessels and this is the basis of laminar flame venting theory that is reviewed below.

2.3 Review of Explosion Venting Experimental Investigations

Most explosion venting models are correlated either based on theory or experimental data from large scale explosion test. In any case, the validation of the correlations with experimental data from the literature is an important aspect of safety, as these models are developed for application in explosion venting design. This section of the thesis focuses on the review of explosion venting data base by concentrating areas relevant to the present work.

2.3.1 Large and Small Scale Experimental Investigations

In the application of the relevant safety technique or measures in the industries particularly against explosion accidents, understanding the mechanism of the technique is an important factor in achieving the aim of employing such measures as explained above. Most process industries or offshore modules prone to explosion

safety hazard are normally large in size, with the volume of a typical offshore module reaching up to 10,000m^3. This shows the importance of large scale experimental test in analysing explosion safety concerns since it gives exact or similar to realistic scenario.

A large scale experiment was carried in a 550m^3 vessel which was about one half or one third in linear dimension of a typical offshore module(Bimson et al., 1993). This work which was part of the SOLVEX (Shell Offshore Large Vented Explosion) programme designed to give explosion scenario closer to reality and investigated empty and congestion with two different gas mixtures. The effect of self-acceleration flames was demonstrated as this was one of the key findings of this work. Also, the linear increment of flame area over distance, effect of flame interaction with obstacles and the significant of external explosion in explosion venting were emphasised (Bimson et al .1993). A self-acceleration factor 2.9 was observed when the overpressure were compared with vessel 1/6th the linear scale of the main test vessel for methane-air and 3.4 for propane-air, to show the influence of vessel volume. However, only 50% vent area was investigated which is a large area as this will give lower overpressure, small vent area may give higher self-acceleration factor, and hence variation of the vent area was necessary. In the last few decades, the reasonable large explosion venting experimental data available in the data base of different sizes and shapes. These include the venting data on 200m^3 (Bromma, 1957), 81m^3(Howard, 1972), 70m^3(Bromma, 1957), 64m^3(Bauwens et al, 2010), 60m^3(Bartknecht, 1993), 35m^3(Solberg et al., 1981), and the most recent 112m^3 and 182m^3 (Tomlina and Johnson, 2013).Most experimental studies in the literature on vented explosion were large scale, as these were close to the industrial set up and also used to validate models for explosion vent predictions. However, there are very few small scale experimental data in vented explosion. Hence it is necessary to compare most of the large scale test with the similar set up on the small scale for better understanding of experimental scaling and safety margin.

Palmer and Rogowski (1968) in their work on the use of flame arrester to protect enclosed equipment considered the use of small scale cubical vessels of volumes 0.014m^3, 0.028m^3 and 0.085m^3. In this work, open vent experiments were carried and based on this, a simple correlation was found between the maximum explosion overpressure and the vent area. Even though the work varied the ignition location

and concluded that the end ignition location gives higher explosion overpressure, the main focus of the work was on the analysis of the flame arrestors used than other aspect of explosion venting process(Palmer and Rogowski, 1968). A similar work on cubical vessel of $0.0041m^3$ by volume was carried out where the second pressure peak was analysed and ignition location farthest from the vent was shown to produce the worst explosion overpressure(Sato et al., 2010). However, most of the small scale explosions venting experimental data are mostly carried out in either spherical or cubical vessels, with very few cases of cylindrical vessel venting data for both large and small scale.

Nagy and Verikas (1983) carried out experimental work in small 10L glass cylindrical vessel in order to examine the pressure development and flame propagation in vented vessel, and the volume of the vessel is similar to one of the vessels reported in this work. It was shown that the flame propagation was initially spherical and overpressure increases as the vent area decreases with methane-air mixtures for unrestricted vents as shown in Figure 2.4.
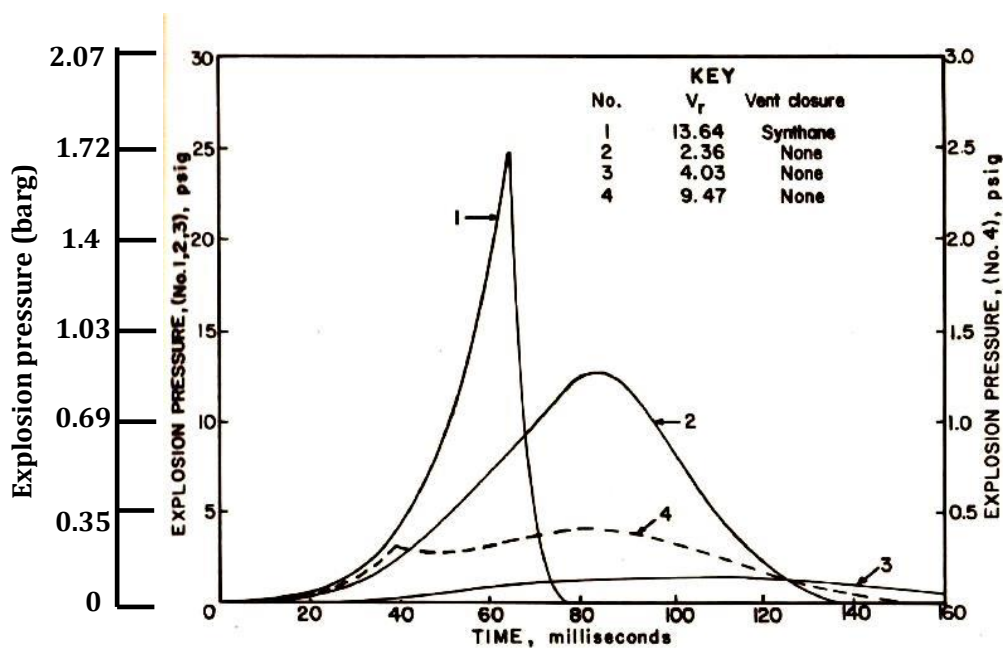
Figure 2.4 Typical pressure-time record for methane-air explosion Centre ignition (Nagy and Verakis, 1983)

For very high K_v of 58.5 and 34.9, the maximum pressure occurred when the flame touched the wall of the vessel (Nagy and Verakis, 1983), and this was in agreement with the literature (Runes, 1972, Cooper et al, 1986 and Bradley and Mitcheson,

1978a, Bauwens et al, 2010). Vessel walls absorb heat from the expanding flame there by reducing the rate of pressure and temperature, and this was usually the case in most closed vessel explosion. Similarly in vented explosions and when the size of the vent is so small, it allows for expanding flame to reach the wall of the vessel before burnt gas venting begins. On the contrary, the flame was shown to touch the wall of the vessel after the maximum reduced pressure was reached for lower K_v or lower vent areas (Nagy and Verikas, 1983). This may be possible with more central ignition location where the distance of flame travel is short and at the time of burnt gas venting, the expanding flame could not have touched the wall. Also, the flame propagation is faster with the large vents and the flame must have exited the vent before it touches the wall irrespective of the ignition location. It was also shown in Figure 2.4 that the first peak pressure (P_v) was the dominant overpressure and the maximum overpressure for this large vent area. This was contrary to the literature where P_{red} was assumed to be additive and always greater than P_v (Bartknecht, 1993). This assumption may be based on theory and not be applicable to large vents as shown in Figure 2.4.

Figure 2.5 is the pressure-time curve for methane-air vented explosions with different ignition locations as reported by Nagy and Verakis (1983). For the 10 L cylindrical vessel, 3 different ignition locations were analysed and it was shown that the ignition location have significant effect on the explosion overpressure and flame speed with the ignition location farthest away from the vent as the worst case. This is in agreement with similar work of Fakandu et al (2011) where 10L small cylindrical vessel was shown to give much higher overpressure for end ignition opposite the vent as compared to more central ignition, for 10%Methane-air mixture(Fakandu et al., 2011). This was contrary to the work in the literature where central ignition location was considered to be the worst case scenarios as compared to the farthest position from the vent and most data used for the venting standards were based on central ignition location (Bradley and Mitcheson, 1978a, EN14994, 2007, NFPA68, 2013, Solberg et al., 1981, Cubbage and Simmons, 1955).It is possible for spherical vessel to produce higher overpressure for central ignition location as compared to end ignition, as the vessel allows the flame to touch the wall of the vessel at some point thereby cooling the flame. However, that may not be the case with other shapes of the vessel.
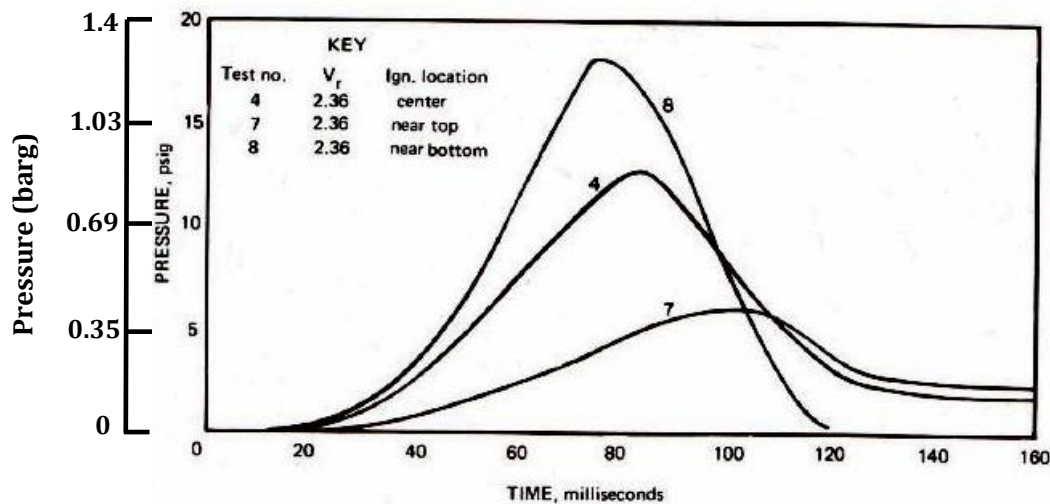
Figure 2.5 Typical pressure-time record for methane-air different ignition locations (Nagy and Verakis, 1983)

Another small scale experimental study on cylindrical vessel was carried by Wu and Swithenbank (1992) to study the gas dynamics of explosion venting. The work considered a small cylindrical vessel of 3.7Litre by volume, hydrocarbon-air mixtures including methane, ethylene and propane, and circular orifice plate as vents. It was shown that highest peak overpressure and the shortest exit time was close to Stoichiometric concentration for all the gases and the influence of external explosion in the overall pressure peak was highlighted(Wu and Swithenbank 1992). This was in agreement with the literature where the external explosion was shown to have significant influence on the peak pressures depending on the vent area (Harrison and Eyre, 1987, Fakandu et al., 2013). Even though the work also looked at the combustion heat release which is not part of the scope of the present work, there are alot of similarities with the work reported in this thesis. Firstly, they are both small scale experiments, and the present work of 10Litre vessel is 2.7 times in volume as the work of Wu and Swithenbank (1992). Secondly, in both cases, the same gas mixtures and circular orifice plates were used as vents.

2.3.2 Pressure generation in explosion venting

Another area of interest in explosion venting analysis is the multiple peaks associated with explosion venting, after the issue of double pressure peaks as discovered by Cubbage and Simmond (1955, 1957). Several authors later discussed the multiple pressure peaks in explosion venting with particular emphasis on the

vent opening pressure and the maximum reduced pressure in explosion venting (Bradley and Mitcheson, 1978a, Harris, 1983, Nagy and Verakis, 1983, Solberg et al., 1981). Furthermore, external explosion was also shown to contribute to the pressure peaks generated during vented explosion (Bauwens et al., 2010, Fakandu et al., 2013, Harrison and Eyre, 1987). This is an indication that the maximum reduced in explosion venting is not influenced by a single factor but many other factors.

An extensive study to identify the physical mechanism responsible for the generation of substantial pressure peaks during venting explosion was conducted by Cooper et aI (Cooper et al., 1986). A near cubic enclosure using low failure pressure explosion panels was employed. In this work, cubic volumes of $0.76m^3$, $2.55m^3$ and $2.41m^3$ were used at the initial stage. Central ignition was employed in generating different pressure peaks in venting explosions, taking into account the physical mechanism of each pressure generated and four different peak pressures were identified. In the study, the first pressure peak (P_1) was associated with the failure pressure (P_v) of the relief panel, and this was the dynamic pressure effect to allow the beginning of the unburnt gas venting when the relief panel fails (Cooper et al, 1986).This pressure was shown to increase as P_v increases and P_1 has a linear relationship with the weight per unit mass of the panel. The second pressure peak pressure (P_2) was influenced by external explosion, P_3 caused by the maximum flame area after touching the wall of the vessel and P_4 was enhanced by acoustic vibration (Cooper et al, 1986). The detail analysis of the various pressure peaks was key contribution to explosion safety and in particular to explosion venting design. It was concluded that the peak pressures due to influence of acoustic combustion will not be of relevance to practical situation after comparing the result with other literature(Cooper et al., 1986). However, the work was restricted to cubic and near cubic vessels and only a more central ignition location was considered. Most of the vent design correlations or models as discussed later, relied on the classic laminar flame venting theory which suggests that maximum pressure could be obtained when the flow of unburnt gas through the vent is at its maximum (Bradley and Mitcheson, 1978a). This was usually obtained at the point of burnt gas venting and prior to pressure due to external explosion, P_3 (Fakandu et al, 2013). Also, the first pressure peak (P_{fv}) was the beginning of the unburnt gas venting and not the maximum as reported by the authors (Cooper et al, 1986). Hence, the important

aspect of explosion venting mechanism was overlooked, and it is considered as a significant aspect of explosion venting process.

Similar work was carried out by Bauwens et al (2010) and Chao et al (2011) where the mechanism for the generation of multiple peaks in vented explosions were analysed in large cubical vessel of $63.7m^3$ by volume(Chao et al., 2011). In the work, various ignition locations were considered including end ignition opposite the vent, centre and front ignition (Bauwens et al, 2010). The work showed P_1 was generated as a result of external explosion and Taylor's instability, P_2 associated with flame surface acoustics and the structure of the chamber, and P_3 caused by the flame interaction with obstacle. The work concluded that no ignition location could be considered to be the worst case, as the end ignition gave P_1 as the highest pressure peak, while front ignition gave P_2 as the highest overpressure (Bauwens et al 2010). Since work of Cooper et al (1986) showed that pressure due to acoustic instability is irrelevant in explosion venting application, hence P_2 should not be considered as important, since it can be eliminated. Hence, the end ignition location should be considered as the worst case. Also, Bauwens and his co-authors recommend a model for prediction of reduced pressure based on the basic theory considered in the work of Bradley and Mitcheson (1987a) as mentioned earlier. Also, a significant contribution of the work was the recognition of the influence of external explosion in the overall peak pressure, which was in agreement with the work of Cates and Samuels (1991). Most correlations for explosion venting design do not accommodate the influence of external explosion. However, the work of Bauwens et al (2010), also omitted the influence of the mass flow of unburnt gases through the vent in the analysis of pressure peaks as included in the model.
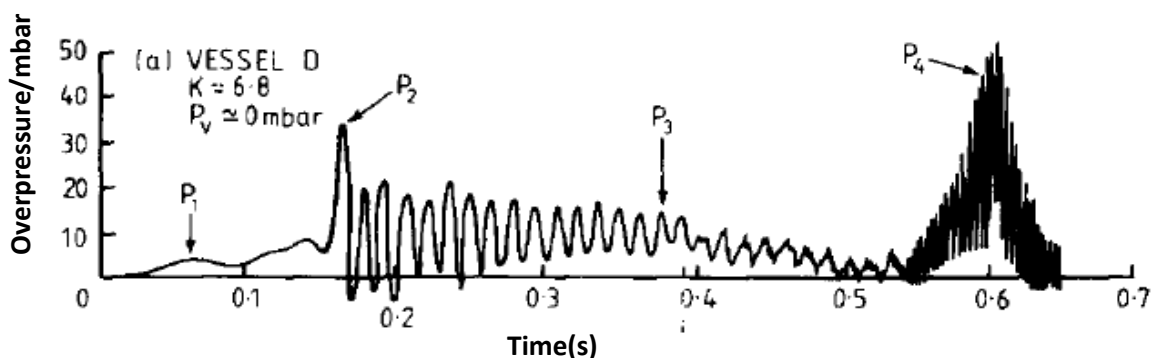
Figure 2.6 Typical pressure-time record in cubical vessel Centre ignition
(Cooper et al, 1986)

In Figure 2.6 and 2.7, P_{fv} is the pressure as result of mass flow of unburnt gases through the vent a reported in the present work. As shown above, neither Cooper et al (1996) nor Bauwens et al (2010) discussed the pressure peak associated with mass flow through the vent, after the bursting of the diaphragm and prior to the pressure peak as a result of external explosion. This was shown to be an important aspect of explosion venting development as most of the vent design correlations were based on the principle of mass flow of unburnt or burnt gases through the vent(Fakandu et al., 2013, Kasmani et al., 2013) .
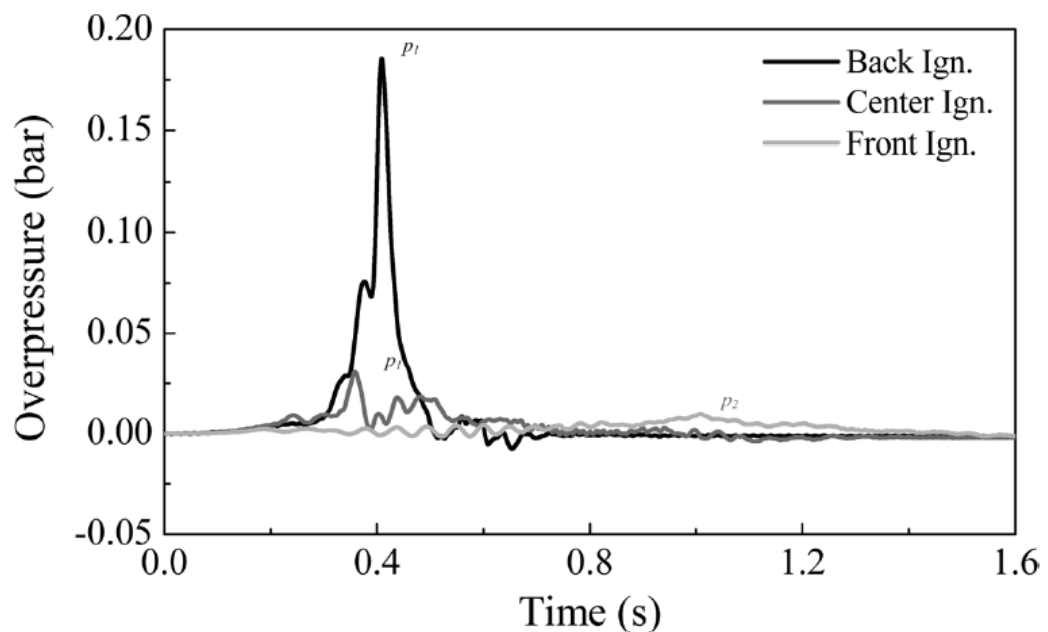
Figure 2.7 Pressure-time record showing effect of ignition position (Bauwens et al 2010)

Since the pressure-time record for vented explosion generated in practice consist of two or more pressure peaks (Marshall, 1977), it may be difficult to predict the individual pressure peaks as most correlations for vent design only predicts the maximum reduced pressure. When explosion venting is carried out with initially uncovered vent, the vent opening pressure (P_1) is eliminated and the initial turbulence associated with bursting of the diaphragm also avoided. But for closed vents, the magnitude of first pressure peak depends on the strength of the material and the size of the vent. In the work of Cooper et al (1986), P_v was the static burst pressure obtained by the slow increase of compressed air to show the strength of the material, referred to as P_{stat} in the standard (NFPA 68, 2013). It was shown that P_1 is always higher than P_{stat} for most vent materials as reported in the literature (Cooper

et al, 1986). The dynamic effect of the explosion phenomena increases the magnitude of P_1, and the fact that the vent cover will only fail when P_1 exceeds P_v. This present work intends to use new nomenclatures for the pressure peaks, different from that of Cooper et al (1986) with P_{stat} (P_v) and P_{burst} (P_1), details are discussed in chapter 5.

The pressure record measured during vented explosions differs depending on the vent area, the mixture reactivity, and the position of the ignition. The first peak pressures (P_1 in most work or P_{burst} in this work), which is the vent opening pressure, depends on the vent area and the vent material used. This first pressure peak is absent when explosion venting is carried out with an unobstructed or free vent. The first pressure peak was shown to be linearly dependent on the inertia of the vent cover in the work of Cubbage and Simmonds (1955) as shown in equation 2.9.

$$P_1 = a\,w + b \qquad\qquad\qquad\qquad\qquad [2.9]$$

Where "a" and "b" are constants and "w" is the weight of the material divided by the area. In this work, it was shown that as the inertia of the vent material increases so also is the first peak pressure. However, the static burst pressure of the vent material, P_{stat} (or P_v as used in the literature) was not considered to be of importance or it was assumed that the first peak pressure was the same as the vent opening pressure ($P_{burst}=P_{stat}$). On the other hand, Rasbash (1969) determined Equation 2.10 for the pressure generated in vented explosion using data from his studies of propane-air in small vessel. His work considered P_{stat} (P_v) as part of the effect of the relief material on the explosion over pressure, with the first term denoting the first pressure peak and the second term is influence of the vent area(Rasbash, 1969).

$$P_{red} = 1.5P_v + 0.5K \qquad\qquad\qquad\qquad [2.10]$$

(K = vent coefficient as cross sectional area in plane divided by the vent area, P_v = the vent static opening pressure)

$$P_{red} = 1.5P_v + S_o[(0.45Kw + 2.6)/V^{1/3} + 7.76K] \qquad [2.11]$$

(S_o= burning velocity, V= volume of the vessel)

Rasbash et al. (1976) gave a correlation in Equation 2.11 that included the gas reactivity and vessel volume (Rasbash et al., 1976). The two correlations have the same dependence of P_{red} on P_{stat} and this implies that the P_{stat} effect is not dependent

on the mixture reactivity. Both of these equations assume that the overpressure due to the vent opening and that due to the effect of the vent area and mixture reactivity are simply additive. The present work will show that this is not the case for low K_v and relatively high P_{stat}.

Cubbage and Marshall (1972) formulated an equation for the prediction of pressure developed in a simple vented explosion with explosion relief for use in industrial plant of different strength as shown in Equation 2.12 (Cubbage and Marshall, 1972). This equation also considers the influence of burning velocity and vessel volume in the determining the maximum reduced pressure in explosion venting which is similar to Equation 2.22. However, Equations 2.12 shows that $P_1= P_v$ from the first term of equation which is different from the Equations 2.10 and 2.11.

$$P_{red} = P_v + [0.5KwS_o{}^2/V^{1/3}][1 - \exp\left\{-\frac{E-E_o}{E+E_o}\right\}] \qquad [2.12]$$

It is obvious that authors either regard P_{burst} as a function of P_{stat} as in equation 2.10 and 2.11 above or considers both P_{burst} and P_{stat} to be the same as in equation 2.12. The main difference between P_v (P_{stat}) and P_1 (P_{burst}) is that the materials used as vent cover are stronger under short dynamic pressure short loading than they are under slow pressure loading. Hence both peak pressures cannot be the same. Furthermore, some explosion venting correlations completely ignores the ratio of the pressure peaks (Bartknect, 1993) and the influence of P_{burst} in most cases is to increase P_{red}, which may not always be the case.

2.3.3 Effect of Vent Shape on Explosion Venting

Venting of explosions involves the expanding flame pushing unburned gas through the vent, which behaves as an orifice in a pipe flow. In venting theory and in some standards, the classic orifice plate flow equation is used and this has an effective area that is a discharge coefficient, C_d, multiplied by the geometrical area, A_v. The discharge coefficient, C_d, for a small vent or large K_v ($V^{2/3}/A_v$) is normally 0.61, which is due to the contraction of the jet flow through a circular vent and can be predicted from ideal fluid flow. C_d increases as K_v decreases, as detailed by Kasmani et al. (2010) and is 0.7 for a K_v of about 2. In NFPA 68 (2013) C_d was taken as a fixed value of 0.7, even though the methodology they used was based on the work of Swift (1980) who used a C_d of 0.61. NFPA 68 (2013) venting design standard uses

the constants from Swift's work adjusted for the C_d difference. NFPA 68 (2013) also says if A_v occupies an entire wall of the enclosure, then a C_d of 0.8 shall be permitted to be used. The European Venting Standard (2007) does not specifically include C_d in the design methodology, as it is based on the work of Bartknecht (1993) who used circular vents and so C_d was incorporated into the empirical coefficients in the design equation. Both vent design standards thus have no procedure to take into account any influence of the vent shape on the vent design.

Fakandu et al. (2013) have shown that the assumption in the venting standards that the number of vents does not influence the vent design is not justified, where the overpressure is controlled by the external explosion. An increase in the number of vents reduces the length scale of turbulence in the external turbulent jet flame which reduces the turbulent burning velocity and the overpressure. The use of several vents is encouraged in the vent design standards for large vented vessels, but not because they reduce the overpressure. The European standard (2007) in Section 6.2 states that 'the location of multiple vents to achieve uniform coverage of the enclosure surface to the greatest extent practicable is necessary', but no reason for this is given. As the pressure inside an enclosure is uniform across the surface, the number of vents should not matter for the same vent area, unless the number influences the vent process, as found by Fakandu et al. (2013).

For free venting the pressure loss of the flow of unburned gas through the vent is one cause of the vent overpressure, P_{fv}, (Fakandu et. al., 2011, 2013; Kasmani et al., 2011) and the other is the external explosion, P_{ext} (Cooper et al 1986 and Bauwen 2010). Both of these causes of the overpressure are potentially influenced by the shape of the vent. The flow through the vent is influenced by any change in C_d with the shape of the vent. The shape of the vent may also influence the shape and area of the flame upstream of the vent, which influences the flame speed and flow through the vent. The pressure loss in pipe flow is related to the flow area base on the hydraulic diameter and this requires a square duct to have 28% greater flow area than a circular duct for the same pressure loss. The implication of this is that for the same flow area the pressure loss would be higher for the square duct for the same mass flow rate. If the same considerations applied to flow through circular and square orifices then the implication would be that C_d would be lower for square orifice. Andrews and Ahmad (1994) have shown that non-circular orifices do have

lower C_d than circular orifices and rectangular orifices had the greatest difference(Andrews and Ahmad, 1994). If a vented explosion overpressure was controlled by the pressure loss of unburned gas through the vent, then it would be expected that a square vent would have a higher overpressure than a circular vent. However, this would only occur if the shape of the vent did not reduce the upstream flame speed and hence reduce the mass flow of unburned gas through the vent.

The external explosion is also influenced by changes in C_d through changes in the pressure loss and the turbulence in the external jet flow and this influences the external flame speed. Thus a lower C_d for square vents would be expected to increase the external jet turbulence through the increase in pressure loss. This would lead to higher flame speeds in the external jet and potentially higher overpressures. However, jets that are not round were shown by Koshigoe et al. (1989) and Gutmark et al. (1985) to influence the rate of spread of the jet and non-circular jets were shown to spread faster than circular jets(Koshigoe et al., 1989, Gutmark et al., 1985). This would mean that a non-circular vent would have a greater entrainment of air and the jet would slow down more quickly and have lower flame speeds and overpressures as a consequence. This was the effect of the vent shape found in this work which shows that square vents had a lower overpressure than circular vents.

The only previous work we have found on the effect of the vent shape in relation to vent design is in the work of Nagy (1983). He describes an extensive series of tests using compressed air and measured the pressure as it flowed through the orifice type vents. Different vessel volumes and sizes of vents were used with three different vent shapes: circular, square and rectangular. He concluded that the shapes of the vent (circular, square and rectangular) did not significantly influence the orifice C_d and a mean value of 0.9 was recommended for all vent areas and all volumes. This is probably the origin of the neglect of vent shape in the vent design standards. Nettleton (1975) also found that the pressure generation in vented vessel with different vent shapes had little or no effect on the explosion over pressure. However, there were three issues with the experiments of Nagy (1983): firstly, no vented explosions were carried out with vents of different shape; secondly, the tests were carried out for very small vents relative to the volume and the lowest K_v was 19; thirdly, the values of C_d were too high and some were >1 which is impossible. When the Nagy (1983) data is examined there is a difference in C_d for circular and square

or rectangular vents, when the lowest values are examined and this was 0.72 for circular vents and 0.82 for square or rectangular vents. The effect of this difference would, for the same vent area, give a lower overpressure for square vents compared with circular vents, which is exactly the finding of the present work. However, in the work of Andrews and Ahmad (1994) the C_d for a thick circular hole was 0.9 and for a rectangular hole of similar thickness it was 0.74 and in their work no C_d greater than 1 was measured. The high C_d for a circular hole was due to using a thick plate, which allowed flow re-attachment within the hole.

2.3.4 Impact of Non-central and Multiple Vents on Vented Explosion Overpressures

Explosion venting is the most common explosion mitigation technique. However, there is limited data that supports current vent design standards and poor agreement with the design standards and experimental data (Fakandu et al., 2011, Fakandu et al., 2013). The European Standard (EN14994:2007, 2007)states "*If the enclosure is small and relatively symmetrical, one large vent is as effective as several small vents of equal combined area. For large enclosures, the location of multiple vents to achieve uniform coverage of the enclosure surface to the greatest extent practicable is necessary.*" This is echoed in almost identical wording by the NFPA 68 (2013). Although there is clearly encouragement to use multiple vents the implication from the first sentence is that the number of vents does not make much difference provided that the total area provided is the same. The source and scientific basis for these statements is unclear. Also, most vent design correlations and theories are developed considering a single vent and the use of single vent was recommended for symmetrical geometry by (Howard and Russell, 1974). The present work was undertaken to investigate these two aspects (positioning and number of vents) of current vent design procedures. Also most models of explosion venting do not specifically take into account the vent location or the number of vents (Andrews and Phylaktou, 2010, Bradley and Mitcheson, 1978a, Molkov, 2001b).The use of unrestricted vents (i.e vents open from the start of the explosion) approximates to conditions with very low vent burst pressure.

Most vented explosion experiments use a central position of the vent with limited data on the position of vent other than the central position. Solberg et al (1981)

carried out vented explosion for initially uncovered and covered vents with the vent position non-central. This work did not discuss the influence of vent position or reasons for considering the vent at the bottom rather than central, instead the ignition position and the effect of instability was the main focus of the work. Bartknecht (1993) varied the vent area by removing the blank flanges used to block the fixed vents at different positions including central and other positions. No justification was given for this approach and the implication of departing from the traditional central position was not given. Hence, there is the need to consider the implications of considering a different position of vents other than the central position, in order to understand how it affects overpressure and flame speed.

The displaced gases from the vented vessel result in external combustion by the emerging flame. The external explosion increases in overpressure with the vent flow velocity (Harrison and Eyre, 1987). This external explosion was shown to influence the internal pressure as well as the peak overpressure generated during explosion venting (Fakandu et al., 2011, Fakandu et al., 2012, Harrison and Eyre, 1987). The turbulence levels and the severity of the external explosion is a function of the vent coefficient, K_v, and the gas velocity through the vent determines the peak turbulence and peak flame speed and this can generate sufficient overpressure to be greater than the pressure loss of the unburned gas flow through the vent. The external explosion is turbulent flame propagation with a length scale determined by the vent blockage or K_v and by the number of vents. Increasing the number of vents decreases the length scale and this reduces the external flame overpressure (Fakandu et al., 2013). This was contrary to the assumption of the venting standards that the number of vents does not influence the vent design. As discussed earlier the European standard (2007) states that "for large enclosures the location of multiple vents to achieve uniform coverage of the enclosure surface to the greatest extent practicable is necessary", and no justification is given for this statement. Furthermore, the increase in turbulent length scale was shown to have significantly increased the flame speed downstream the vent irrespective of the K_v or the mixture reactivity (Fakandu et al, 2013).

The overpressure, flame speeds and other parameters downstream the vent was shown by Harrison and Eyre (1987) to have a close relation with the flame acceleration in the presence of obstacles ahead of the propagating flame. Extensive

studies on the affect the flame interaction with a single obstacle were shown to significantly affect the overpressure and flame speed downstream of the vent as a result of the characteristic length scale (Andrews et al., 1990, Na'inna et al., 2012, Phylaktou and Andrews, 1991a, Phylaktou et al., 1994). In most of these studies, the obstacle scale was varied by simply changing the number of holes in the grid plates for a fixed K_v. Abdul-Gayed et al (1984) used the length scale (l) to analyse the intensity of turbulence and turbulence straining of premixed flames. The work and other similar works use the turbulent Reynolds number based on l as shown in equation 2.13 for the description of the turbulent flow field when premixed flame propagates through obstacle or a vent (Abdel-Gayed et al., 1989, Abdel-Gayed and Bradley, 1981, Abdel-Gayed et al., 1984).

$$R_l = \frac{u'l}{\upsilon} \qquad\qquad [2.13]$$

where R_l = is the turbulent Reynolds number.

There are three reasons why the vent area alone may not be a sufficient design parameter for explosion venting: firstly, the vent discharge coefficient may change; secondly, the flame shape and area upstream of the vent will be different as the flow splits between the different vent areas and this may influence the flame speed upstream of the vent; and thirdly for external explosions the turbulent length scale of the external turbulent flame is reduced as the number of vents increases for the same vent area and this may reduce the external flame speed and overpressure. The experimental influence of turbulent integral length scale on the turbulent burning velocity is a $L^{0.25}$ or $L^{0.32}$ (Phylaktou et al., 1994) dependence, which with L varied by a factor of 4 gives a $1.4 - 1.6$ variation in the turbulent burning velocity. The link between overpressure and turbulent burning velocity, U_T, is roughly U_T^2 and this would give an effect on overpressure of the change to a 16 hole vent in the range $2 - 4$ This is sufficiently large to be able to detect in the venting explosion measurements as a change in P_{ext}.

Additionally, the effect of non-central vent on the explosion overpressure and flame speed needs to be investigated, as the venting standards have no clear guidance with regard to the vent position. Depending on the vent size, the free flow of flame propagation on the axial line could be disrupted forcing the flame to change

direction of propagation path with slower velocity. Changing the direction of propagating flame was shown to significantly affect the overpressure depending on the configuration (Alexiou et al., 1997).

2.3.5 Review of the Influence of Ignition Position on Vented Explosion Overpressure

The ATEX directive requires that for the design of safety systems the worst possible scenario must be considered (European Parliament and the Council, 1994). It should be noted that for compact vented vessels with L/D close to 1, central ignition has been assumed to have the highest overpressure, in spite of the work of Nagy and Verakis (1983) showing that this was not the case. More recently Sato et al. (2010) have shown that ignition closer to the vent and away from the centreline of the vessel have higher P_{red} than for central ignition. Ignition at the vent outlet can in some circumstances be the worst case (Bauwens et al., 2010). This was found in a $64m^3$ vessel and was shown to be higher for front and central ignition as compared to end ignition and was due to the pressure oscillations caused by acoustic interactions, P_{ac}, at the end of the explosion. Cooper et al (1986) showed that P_{ac} was not significant for practical application, as it could be eliminated using an acoustic absorber (Cooper et al, 1986). As Bauwens et al. (2010) used a relatively thin walled vessel this oscillatory pressure peak was also likely to be an artifact of vessel wall resonance. In the present work with thick walled vessel no acoustic pressure peak was found. Bauwens et al. (2010) concluded that which ignition position (end, central or vent outlet) is the worst case depends on the mixture and the vent coefficient.

In experiments carried out by Cubbage and Simmond (1955) for the design of explosion reliefs in industrial drying ovens central ignition was shown to be the worst case, as compared to positions away from the centre (Cubbage and Simmonds, 1955). The actual position of the various ignition positions and vent panels relative to the shelves were not specified, hence cannot be used as a yardstick for considering the central position as the worst case.

Other data in the literature also shows lower overpressure for end ignition as compared to central ignition(Burgoyne and Newitt, 1955, Harris and Briscoe, 1967, Maisey, 1965). Solberg et al (1981) showed for a 35 m^3 cubic vessel that the front

and central ignition gave higher overpressures compared to end ignition opposite the vent and they attributed this to Taylor instabilities. The vent position was off centre (bottom) and so there was no direct acceleration path from the ignitor to the vent and this may have prevented the fast flame development that is seen with wall ignition opposite the vent. Most of the researchers that found higher overpressure for central ignition argued that for the end ignition, the flame contacted the vessel wall before reaching the vent thereby cooling the flame earlier, as compared to central ignition which did not contact the wall before emerging from the vent. This reasoning may be based on spherical flame theory rather than experimental verification. Fakandu et al. (2011) showed for the present 0.01 m^3 cylindrical vessel that the flame touched the wall of the vessel well after the flame had exited the vent.

Willacy et al. (2007) showed, for a L/D of 2, using a 0.2 m^3 cylindrical vented vessel explosions with a high K_v of 16.4 and a vent pipe, that ignition on the wall opposite the vent had a much higher overpressure than for central ignition. Similar work on methane-air explosion venting through a vent pipe showed that a more intense burning rate was expected for rear ignition as compared to central ignition with much higher overpressures (Ferrara et al., 2008). However, Ferrara et al (2008) were of the opinion for venting with a vent pipe that central ignition gives higher overpressure as compared to rear ignition for propane-air mixture, even though the rear ignition has a higher burning rate compared with the central ignition location. This was in agreement with other works in the literature in favour of the central ignition as the worst case overpressure for venting with a vent pipe attached (Ferrara et al., 2006, Ponizy and Leyer, 1999b).

The work of Palmer and Rogowski (1966) found that the worst case explosion overpressure was for end ignition even though the vessel was similar in shape to that of Cubbage and Simmonds (1955). Hence, there is a need to have closer look at the effect of ignition position on explosion venting and in this work in a cylindrical configuration ignition at the end wall opposite the vent was compared with central ignition. This follows the finding of Nagy and Verakis (1983) that P_{red} increased as the spark was moved further away from the vent on the vent centreline. A spark on the end wall is thus the worst case according to their findings, which are in agreement with those of Palmer and Rogowski (1966) but contradict many other investigations, as discussed above.

In NFPA 68 (2013) in the discussion of the determination of the vessel L/D it is assumed that for a vent on the wall of the vessel that the worst case ignition position is that furthest from the vent and that the distance of this to the vent should be used in determining the L/D. This is recognition in a design standard that ignition furthest from the vent is the worst case. Cates and Samuels (1991) also showed that the farthest location away from the vent produced the highest overpressure, even in the presence of obstacles.

2.3.6 Review of the Laminar Burning Velocity and Gas Reactivity Parameter K_G

Severity of any explosion phenomena depends on some factors including the concentration of the mixture, volume and shape of vessel, ignition position and turbulence (Catlin, 1991, Hermanns et al., 2010, Hjertager, 1984, Phylaktou and Andrews, 1993, Razus and Krause, 2001). The concentration of mixture of gases is particularly important due to its influence in the determination of the fundamental burning velocity and gas reactivity represented by the gas reactivity parameter (K_G).Burning velocity of any gas mixture can be defined as "the velocity with which a very large, flat flame front propagates relative to the unburnt gas in the direction of the normal" (Scholte and Vaags, 1958). Also, the laminar burning velocity is the velocity at which unburnt gas of a given composition, pressure, and temperature flows into a flame in a direction normal to the flame surface (Andrews and Bradley, 1972b). Early studies were conducted by Drell and Belles (1957) to determine the combustion properties of hydrogen-air mixture. In this work, the experimental tests were carried out by varying the conditions of temperature and pressure to determine the properties and results compared with other data from the literature. Among other properties, Drell and Belles determined the burning velocity of hydrogen by getting the maximum average of 310 cm/s which is for 43% hydrogen (Φ=1.8) from different sources. Furthermore, the maximum burning velocities obtained rages from 193-232cm/s with an average 215 cm/s was obtained for the Stoichiometric concentration of hydrogen-air mixture (Drell and Belles, 1957). The burning velocity of hydrogen-air and other hydrocarbon-air mixtures were measured by Scholte and Vaags with 5% accuracy (Scholte and Vaags, 1958). Bunsen Flame with cylindrical burners was employed and the nozzle diameter of the burner was

varied in order to obtain accurate readings. The result of this work showed that 42.2% concentration of hydrogen gave the maximum burning velocity of 280cm/s. Additionally, maximum burning velocities for methane, propane and ethylene to air were obtained to be 40cm/s, 41.4 cm/s and 70cm/s respectively (Scholte and Vaags, 1958). Raezer and Olsen used the Double kernel method to measure the laminar burning velocity of Ethylene-air and propane-air mixture (Raezer and Olsen, 1962). This method involves two flame Kernels propagating towards each other and permits the use of direct measurement in obtaining the flame speed as well as the space velocity. Result of this work gave a burning velocity of 79 cm/s and 44cm/s for Ethylene-air and Propane-air respectively at Stoichiometric concentration (Raezer and Olsen, 1962). There are different methods of measuring the burning velocity of gas-air mixture as shown in the literature (Andrews and Bradley, 1972b). In their review work, Andrews and Bradley (1972) surveyed the different experimental techniques for measuring burning velocity with particular reference to the maximum burning velocity of methane. The result of this work suggested that the double Kernel method in closed vessel is simple to understand and has high accuracy. The work recommended that at 1 atm and 25$^\text{O}$C the maximum burning velocity for methane-air to be 45±2 cm/s (Andrews and Bradley, 1972b).

The double kernel method was also used by Andrews and Bradley (Andrews and Bradley, 1973) to determine the burning velocities of gas-air mixtures in order to explore the capabilities of this method. Measurements of burning velocities were carried for methane-air and hydrogen-air over a wide range of equivalent ratio. The conclusion from this work showed that the result from this method were in agreement with the nozzle burner particle track method. It also gave a maximum burning velocity of 350cm/s for hydrogen-air mixture with less experimental error (Andrews and Bradley 1973).The counter flow method was used by researchers in recent times for measuring burning velocity including Egolfopoulos (Egolfopoulos and Law, 1991) Other authors looked at measuring burning velocity by exploring the closed vessel method which could be double kernel or others (Andrews and Bradley, 1973, Gu et al., 2000). Maaren and Goey (1994) used the heat flux method and compared the result with the counter flow method for measuring the burning velocity of methane-air and propane-air. The heat flux method were also used by (Bosschaart et al., 2004)further reviewed other different methods used for measuring

burning velocity and comparing the result with the heat flux method. This work concluded that the different techniques when compared do not vary by a margin of 1cm/s (Bosschaart et al., 2004). However, this result seems to contradictory because the result for methane-air by Bosschaart (2004) was 36cm/s, while the NFPA 68 (NFPA 68 2007) gave 40cm/s for the same concentration. This gives a margin of 4cm/s or more when compared the results of other authors. The values of burning velocity used in this work were based on the given values in the current venting standard of NFPA 68 (2013) as shown in Figure Table 2.1.

Table 2.1 Selected values of Burning velocity (NFPA 68, 2013)

Gas mixture	Burning velocity (cm/s)
Methane-air	40
Propane-air	46
Ethylene-air	80
Hydrogen-air	312

The burner method was also exploited for measuring the burning velocity of gases earlier on as reported in the literature (Clingman et al., 1952, Edmondson and Heap, 1969, Edmondson et al., 1970, Singer, 1952, Wu and Law., 1984). Recently, Pareja (2010) carried out experimental measurement of hydrogen-air by the slot-type nozzle burner using the Particle Tracking Velocimetry (PTV) technique and schlieren photography technique. Other methods including the numerical calculation and angle method were exploited by this authors and results compared with his experimental work. He concluded that there was close agreement of the experimental and the numerical result with the literature (Pareja et al., 2010). Also, when the slot-type nozzle was used with the angle method, there was high reliability of the data of the burning velocity when the flame curvature was reduced (Pareja et al., 2010). It is important to note that all the methods used for measuring Burning velocity have shown similar trend with concentration and equivalent ratio depending on the type gas used. However, it can be concluded that different values were obtained for different gas mixtures and this depends on the measuring technique and method, but with all the values are within an acceptable difference of less than 20% from different authors.

Another important parameter used in the characterisation of explosion reactivity other than the burning velocity is the K_G. The values of the K_G vary depending on the concentrations of gas in the combustion reaction, so also the laminar burning velocity. Since K_G is a constant value which was determined by the vessel volume and the rate of pressure rise, there should be a relationship between K_G and Su. Kumar (1992) derived an equation for K_G as function of S_u, assuming that S_u is constant and is not influenced by Pressure and temperature as mentioned earlier. The literature also showed that the relationship between the burning velocity and rate of pressure rise is almost linear (Lunn, 1984).

The maximum rate of pressure rise was reported to be inversely proportional to the cube root of the volume and the constant of proportionality is termed to be the K_G (Bartknecht, 1981). Thus the K_G for a given mixtures is termed to be constant value as given in equation 2.14.

$$K_G = (\frac{dP}{dt})V^{1/3} \qquad\qquad\qquad [2.14]$$

Bartknecht (1993) recommended the use of constant values of K_G for different gas mixtures and for use as a scaling parameter based on the reactivity of gas mixtures. These values were measured in the 5Litre spherical vessel and recommended for application for all vessel sizes not exceeding $1000m^3$ (Bartknecht, 1993, EN 14994, 2007, NFPA 68, 2007). The work of Chippett (1984) compared the measured and calculated K_G values for different vessel volumes. It was shown that K_G increases with the vessel size, and flame acceleration in large vessel and wall quenching in small vessels also affects the K_G values. Hence, the use of K_G as a simple scaling parameter is not practically possible.

Based on the cubic law above, the value of K_G cannot be a constant, even if the all vessel give the same rate of pressure rise for the same gas mixture. Swift (1989) in his work analysed the cubic law and based on the assumption that K_G must be a constant value as recommended by vent design standard (NFPA 68, 1988, Swift, 1989). It was shown that the value of K_G depends on vessel volume and the ignition energy used, this was based on the experimental data obtained from the US Bureau of mines (Swift, 1989).

The relationship between S_u and K_G even though not completely linear, equation 2.15 shows a linear interpolation for S_u if the K_G is unknown (NFPA68, 2007a).

$$(K_G)_2 = (K_G)_1 \left(\frac{(S_u)_2 \times (P_{max})_2}{(S_u)_1 \times (P_{max})_1} \right) \quad \text{(NFPA 68, 1988)} \quad\quad [2.15]$$

Where Subscript 1 = gas whose K_G is known, Subscript 2 = gas whose K_G is not known, K_G = Deflagration index for gases, bar-m/s, S_u = Fundamental burning velocity, m/s, P_{max} = maximum pressure obtained for gas to air in closed vessel at initial pressure and temperature in bar.

$$(K_G)_2 = (K_G)_1 \cdot \left(\frac{(S_u)_2}{(S_u)_1} \right) \quad \text{(NFPA 68, 2007)} \quad\quad [2.16]$$

Equation 2.16 was recommended in the old version of the NFPA 68 (2007) both K_G and P_{max} given in the standard, were measured in a 5L spherical vessel. Furthermore, Bertknecht (1981, 1993) results on 5L gave K_G to be 55 bar-m/s and 100bar-m/s for methane and propane respectively which was also in the NFPA 68 and as recommended to be used for the design equation containing K_G as constant. However, the effect of test volumes on K_G are obtained for various spherical vessels was included in the NFPA 68(2007). Also, experimental work by Cashdollar (2000) considered 20L spherical and 120L chamber for to determine the flammability limits as well as the K_G values of methane-air, propane-air, and hydrogen-air at different equivalent ratio. A maximum K_G value of 72 bar m/s and 95bar m/s were obtained 20L and 120L respectively, while worse case concentration of propane-air gave a K_G of approximately 170bar m/s for 120L vessel (Cashdollar et al., 2000). These values of K_G are much higher than the values obtained by the Bertknecht's 5L vessel as mentioned above.

The K_G values are not constant for different vessel volumes, as wrinkling effect on flames in larger volumes increases the values of K_G and the effect of wall quenching lowers the rate of pressure rise as well as the K_G in smaller vessel volumes. Hence, the use of constant value of K_G measured in 5L vessel for all vessel volumes up to $1000m^3$ as recommended by the European vent design guide and the old version of NFPA 68 (2007) is not practicable. More analysis on the reactivity influence of K_G and S_u are discussed in chapter 7.

2.3.7 External Explosion in Explosion Venting

The use of mixture reactivity variation is a common way of enhancing the burning velocity in order to accommodate certain phenomenon including flame self-acceleration and influence of turbulence. It was earlier discussed that an aspect of debate in explosion prediction is the value to adopt in order to accommodate vent flow turbulence and other associated issues. In view of this, turbulence generation and experimental scaling has attracted the interest of most researchers in recent years as a result of safety concerns with some current happenings including the flame vegetation interaction of the Buncefield explosion incidence (2005). Thus, this section intends to give an overview of few experimental data and models associated with obstacle generated turbulence and experimental scaling directly related this work.

In gas explosion venting in large vessels, the propagating laminar flame front becomes unstable after certain distance, thereby increasing the flame speed as well as the flame surface area. These instabilities are caused by different factors, and the common acoustic instability is associated with the vibration of the vessel walls during explosion for mostly empty vessel without obstruction or obstacle (Ciccarelli and Dorofeev, 2008). Flame self-acceleration also occurs when flame travel over a long distance and flame instability caused by self-acceleration leads to smooth laminar flames breaking into smaller cells known as cellular flames. These flame instabilities and self-acceleration eventual leads to turbulent regime during flame propagation (McCann et al., 1985). Other factors that cause turbulence in explosion venting include turbulent flame generated flow, turbulence caused by the bursting of vent disc or vent cover, obstructions or obstacle within the test vessel, and turbulence generated downstream as the flame passes through the vent. All the factors mentioned disrupt the normal flame propagation pattern of the flame due to flame front interaction thereby changing it shape, direction, and pattern during propagation.

Harrison and Eyre (1987) in their work conducted series of test in a $30m^3$ chamber to investigate the effect of external explosion in explosion venting. In the work 3 different vent areas were fitted at the end face , and 3 different ignition positions were used including front, centre and end ignition locations. The emerging jet flame

from the test vessel was shown to iginite the cloud of unburnt gas outside the vent which caused the secondary explosion (Harrison and Eyre, 1987). The rear ignition was shown to give higher overpressure as compared to central and front ignition. Peak external overpressure was shown to increase with speed of emerging flame, and external explosion affects the generated internal overpressure (Harrison and Eyre, 1987). However, causes of the different external overpressure and higher speed of flame emergence were not considered in the work. Similar work by Jiang et al (2005) looked at the effect of external explosion on explosion overpressure for different conditions. Higher blockage ratio of the obstacle within the duct was shown to give lower external overpressure, as only smaller section of the unburnt gas forms external cloud as most of the gases were burnt as a result of the high blockage (Jiang et al., 2005). The work also showed that the lean and rich methane-air mixtures gives lower overpressure as compared to the stoichiometric mixtures. It was reasonable for the lean mixture to give lower overpressure as the cloud of the unburnt gas mixture outside the vent may be insufficient to support combustion or give significant overpressure. However, it is surprising that the rich mixture gave lower overpressure as it was expected to have sufficeint mixture cloud to suppport combustion and generate significant overpressure.

External jet explosion was also discussed by Catlin (1991) in the field-scaled experimental study where confined explosion gas jets into cloud of same mixture both internal and external the main test vessel(Catlin, 1991). The work of Wu and Swithenbank (1992) studied the gas dymanics of vented explosions in small vessel for different gasmixtures. It was shown that the external flame which exit through the orifice as a jet causes secondary combustion by igniting the unburnt cloud mixture outside the vent. The key findings were that the external combustions influences the generated internal pressure but not significant, and approximately 50% of the total heat release happens during this external combustion (Wu and Swithenbank, 1992). Furthermore, about 95% of the combustion heat release occured inside the vessel for small vent areas (Wu and Swithenbank, 1992) and this is in agreement with the literature where the inernal pressure (P_{fv}) was shown to be higher than all other peak pressure (Harrison and Eyre, 1987, Fakandu et al ,2013). This shows that most of the combustion process occurs prio to burnt gas venting. Most of the work on external explosion above either focuses only on the secondary

explosion or the jet of the emerging flame that leads to the secondary explosion. The relationship between the external explosion and the internal pressure caused by mass flow of unburnt gas through the vent was negleted. This is an important aspect of explosion venting, as this will help in generating data for safe prediction of explosion venting considering both pressure peaks.

In explosion venting, most correlations for explosion venting prediction only predicts the maximum reduced pressure and do not consider the effect of external explosions (Forcier and Zalosh, 2000, Razus and Krause, 2001). There are limited data in the literature which considrers external explosion in prediction of explosion venting overpressure. The work of Cates and Samuels (1991) recommended a correlation for the prediction of explosion venting design considering the influence external explosion. The work showed that the maximum reduced pressure was obtained by adding the internal pressure with half of the external generated pressure as shown in equation 2.17.

$$P_{max} = P_{int} + \frac{1}{2}P_{ext} \qquad\qquad [2.17]$$

Where P_{max} is the maximum reduced pressure, P_{int} is the internal pressure and P_{ext} pressure as a result of external explosion (Cates and Samuels, 1991). However, the internal pressure and external explosion data were obtained from two different experimental sources and the correlation was considered to be applicable to mostly congested regions with end ignition opposite the vent. The use of only cubical vessel in most of the experiments was a limitation which was not factored in the recommended model (Cates and Samuels, 1991). The model was also not applicable to empty enclosures and smaller vent areas, which are also part of the limitations. The work of Bauwens et al (2010) also recommended a model for the prediction of vented explosion which showed the influence of external explosion. This work was based purely on theory but was validated with the experimental work from a 64m^3 cubical vessel (Bauwens et al, 2010). Forcier and Zalosh (2000) reviewed the existing correlation for the prediction of vented explosion blast pressure and later attempted to apply the blast wave theory to predict external explosion using the volume and vent area as the main input parameters. None of these correlations above was able to predict the external explosion based on the experimental result and relating the internal and external overpressure over a wide range of vent areas.

Another area of much concern is the analysis of the influnces of duct in explosion venting. The mechanism and dynamics of flame interaction in vessel duct was carried out by the work of Ponizy and Leyer (1999a, 1999b), where the vent areas, duct length and shape of the vessel-duct area change were varied. The vent duct was shown to significantly increase the overpressure when compared with the simply vented results. Also, the increase in length of the duct was shown to increase overall peak pressure, increases the flame speed upstream but reduces the flame speed down stream the vent (Ponizy and Leyer, 1999a). This is in agreement with the literature as most data show that the length of the duct have significant effect on the severity of the explosion (Bartknecht, 1981, Molkov and Alexandrov, 1995, Ural, 1993). The work also showed that the impulse generated by the burn out in the duct is a factor which intensifies the combustion phenomenum within the duct (Ponizy and Leyer, 1999b). Furthermore, rear ignition opposite the vent was shown to give the highest burning rate for both initially uncovered and covered vents, and reverse flow was not considered to have significantly affect combustion within the vessel (Ponizy and Leyer, 1999a, Ponizy and Leyer, 1999b). Other similar works where the ignition location were varied include the work of De Good and Chatrathi (1991), Ferrara et al (2008) and Ferrara et al (2006)(DeGood and Chatrathi, 1991, Ferrara et al., 2006, Ferrara et al., 2008). The burnt up responsible for higher overpressure in the vent duct was observed irrespective of the surface roughness, and a strong shear stress was shown to be generated on contact with the surface of the vent duct(Ponizy et al., 2014). The reverse flow which occured due to external combustion within the vent duct was shown to reduce as the vent area reduces, and the effect of the vent duct on a smal vent area was neglegible as most of the combustion process occured within the vessel (Ponizy et al ,2014). A similar work which focuses on the external explosion as it affects explosion venting with duct, and the work showed the effect of duct on ignition position and the maximum overpressure (Ferrara et al, 2008). Most of the work mentioned on explosion venting with duct only considered the duct diameter smaller than the diameter of the actual test vessel, and this was shown to signifacantly increase the maximum pressure up to 10 folds as compared to vented vessels without the duct attached. On the contrary, the present work intends to look at the attached vessel similar to duct venting downstream the vent but with the same daimeter as the test vessel for further analysis.

2.3.8 Effect of Turbulence and Turbulent Length Scale

The increase in flame speed and pressure generated during vented explosion as a result of flame obstacle interaction has been an area of much concern and has attracted intense research in recent times. The rate of pressure rise and explosion overpressure increases when flame travel through obstacles in a tube (Phylaktou and Andrews, 1991a, Phylaktou and Andrews, 1994). It has been shown that the presence of obstacles can significantly affect the free propagating flame in a cylindrical vessel (Moen et al, 1982). The work showed that with appropriate sizing and separation, the flame speed of 10% methane-air was increased 24 times with repeated obstacles when compared with a free propagating flame without obstacle. Large scale flow field distortion and the size of the obstacle were the controlling factors for such increase in flame speed (Moen et al., 1982). Other studies on obstacle generated turbulence including the work of Hjertager et al (1988), Cates and Bimson (1991), Bimson et al (1993) and Bauwen et al (2010), have similar views as overpressure and flame speeds are affected by obstacles on the propagation path. However, obstacle separation distances were not considered for all the work mentioned above.

The work Nainna et al (2012) looked at the obstacle separation distances or pitch as an important factor in the analysis of flame interaction with obstacles and relating to the cold flow turbulence work of Banes and Peterson (1951). It was shown that fewer obstacles can generate much higher overpressure and flame speed if the appropriate obstacles separation distance was achieved (Na'inna et al., 2013, Na'inna, 2013). Prior to the work, increasing the number of obstacle was the yardstick for scaling up the overpressure or flame. This implies that lower overpressure would be obtained if the obstacle separation distance is outside the position of maximum intensity. Hence, the flame may go to extinction if the separation distance was overstretched or less than the required to obtain the optimum intensity.

In large scale explosion venting, the flame speed as well as the overpressure are normally higher due to influence self-acceleration of flame and hydrodynamic instabilities as compared to small scale. In order to replicate large scale experiments, the scaling technique was used to show the relationship between the large and small

scale test. Catlin and Johnson (1992) in their work on experimental scaling attempt to reproduce 1/5 geometrical scale of a large scale experiment. In the work, the laminar burning velocity increased by enriching the air with oxygen and increasing the roughness of obstacles in order to compensate for scale effects in the combustion process. When 24.7% oxygen was used, about 50% increase in burning velocity was achieved, and the scaled model gave overpressure up to twice the large-scale experiments and in some cases a factor of five over prediction for small scale experiment(Catlin and Johnson, 1992). High energy ignition was shown to give the closest agreement with the scaled result, and it was concluded that this scaling technique for estimation of large scale overpressure will be more conservative. The authors also assumed that for Kalovizt number (Ka>0.2), the rms burning velocity (u') are the same for small and full scales based on the turbulent burning velocity correlation recommended by Abdel-Gayed et al (1987). However, the assumption is not realistic, since u' is shown to vary with mixture reactivity due to change in the burning velocity(Phylaktou and Andrews, 1995).

Another way of scale up is the use of more reactive mixture for example using ethylene-air mixture instead of methane-air(Taylor and Hirst, 1989). In this work, a fractal model was developed for the scaling of the behaviour of fast flames with congested obstacle arrays based on the initial work Gouldin (Gouldin et al., 1989). It was concluded that the fractal-scaling model could be applied to vented explosion but not explosion detonation (Taylor and Hirst, 1989).

Most scaling techniques similar to the fractal method above are obtained using existing turbulent models and researchers rely on the turbulent burning velocity models to scale up experiments to large scale. Phylaktou and Andrews (1995) carried out an extensive analysis of turbulent combustion models on explosion scaling. In this work, it was shown that most models have little or no variation of scales as one of the weaknesses of the existing models. A turbulent combustion correlation was later derived based on experimental data and the importance of scale was emphasised, as establishing the exact dependence on rate of turbulence was key to scaling large scale explosions (Phylaktou and Andrews, 1995). Other parameters influencing the turbulent burning velocity includes the laminar burning velocity (S_L), rms burning velocity (u'), Lewis number (Le), Reynolds number (Re) and turbulent length scale (*L*). The length scale (L) is the most important factor in

turbulent combustion determined by the turbulent initiators and the main turbulent initiators are obstacles, width of solid material or grid plate obstacles on the flame propagation path (Baines and Peterson, 1951, Na'inna, 2013, Phylaktou, 1993).

Several experimental studies on gas explosion and flame turbulent interaction have shown the effect of characteristic length scale on turbulent generation. The study on influence of obstacle scale on turbulent generation using perforated grid plates were carried out by Phylaktou et al (1994).The variation of characteristics length scale was achieved by using a fixed blockage ratio or total vent area but variation of number of holes, in different sized cylindrical closed vessels. Result from this work showed that the turbulent length scale and not the overall size of the vessel have significant influence on the turbulent burning velocity (Phylaktou and Andrews, 1994).The overpressure as well as the flame speed were shown to be enhanced with the increase in characteristic length. This was in agreement with earlier work, where obstacle was shown to accelerate flame propagation in a closed tube (Phylaktou and Andrews, 1991a), and other related work on flame obstacle interaction(Andrews et al., 1975, Harrison and Eyre, 1987, Kumar et al., 1989, Phylaktou et al., 1990). Most of these are either carried out considering obstacle array within confined or unconfined vessels. The relationship between overpressure and flame speed upstream and downstream the obstacles were not considered in most of these studies.

The explosion induced gas flow of unburnt gases with interaction with obstacle results to the generation of high turbulence downstream the obstacle which results to fast flame speed as well as higher overpressure. Prediction of this phenomenon is an area of much concern in the industries and also of intense research in recent years. Phylaktou and Andrews (1994) used the steady state flow to obtain the pressure loss coefficient and established a method of predicting the maximum intensity of turbulence generated downstream a grid plate. Other turbulence combustion models based on the characteristic length scale "*l*" were reported by authors to show the influence of the length scale in turbulent prediction (Abdel-Gayed et al., 1985, Bradley et al., 1991, Gouldin et al., 1989, Phylaktou and Andrews, 1995). A recent work of Nainna(2013) derived a turbulent combustion model which was used to derive an equation for the prediction of overpressure based on "*l*" and validated with good agreement with small and large scale data. Hence, in the analysis of turbulent

combustion, the length scale was shown to play a vital role. However, most of these models are applied to obstacle within the vessel without considering the jet of flame emerging from the vent to the open atmosphere. The present work intends to focus on turbulence generated downstream the vent and how the characteristic length scale affect the generated pressure both inside and outside the vent due to limited data in this area, with more detail discussion in chapter 5. A summary of some of the reviewed literature is as shown in Table 2.4.

2.3.9. Review of Hydrogen Explosion Venting and Mixture Reactivity

The reduction in CO_2 emissions from energy generation is leading to consideration of hydrogen's use as a carbon free energy carrier. This has led to increased concern for the safety aspects of the use of hydrogen. For safe hydrogen use in a confined space the space has to be protected against explosions and explosion venting is widely accepted as the lowest cost effective protection measure for gas and dust explosions. The key problem in venting is the appropriate design of the vent area, A_v, necessary to achieve a desired reduced pressure, P_{red}, below the plant strength. Bartknecht's (Bartknecht, 1993) work is the basis of current vent design procedures in the USA and Europe (EN14994:2007, 2007, NFPA 68, 2013). These give a correlation for the vent coefficient K_v ($V^{2/3}/A_v$) as a function of the mixture reactivity, K_G, and the reduced overpressure, P_{red}.

In explosion venting prediction, most of the available correlations only predict single peak pressure normally reduced pressure (P_{red}). Experimental evidence in recent years has shown that multiple peaks generated during vented explosions contribute to the pressure generation in the whole combustion process (Bauwens et al., 2010, Cooper et al., 1986, Fakandu et al., 2013). The generated peak pressures were also shown, including the present work to be governed by different physical phenomenon. Experimental data for hydrogen-air mixtures in FM Global's 64m^3 vessel for different ignition position also presented double peak pressures in there pressure traces (Bauwens et al., 2011). The work involved only 18% hydrogen-air concentration and the aim of the experiment was to compare the result with stoichiometric concentrations of methane-air and propane-air mixture. A comprehensive study of pressure generated vented hydrogen explosion was carried out by Kumar et al (1989) in a 6.85m^3 spherical vessel with 2.3m diameter. In this

work, the influence of ignition position, vent sizes and mixture concentration between 6% -20% by volume were presented. It was also shown that conservative estimate can obtained for the maximum peak pressure using simple empirical correlation(Kumar et al., 1989).Most of these experiments on hydrogen-air that of Pasman et al (1974) in 0.95m^3 vessel and Sato et al (2006) in 37.4m^3 vessel only considers hydrogen concentration of 30% concentration by volume or less (Bauwens et al., 2012, Kumar et al., 1989, Pasman et al., 1974, Sato et al., 2006). In view this, there is the need to generate new data set for 30% and 40% hydrogen-air concentration by volume due to limited data particularly for 40% hydrogen-air mixture.

2.3.9.1 Vent Design and Mixture Reactivity

For compact vessels the vent design equation of Bartknecht (1993) is given by Equation 2.18 for gases.

$$Av = [(0.1265 \log K_G - 0.0567)P_{red}^{-0.5817} + 0.1754P_{red}^{-0.5722}(P_{stat}-0.1)]\ V^{2/3} \qquad [2.18]$$

The first terms is valid for $P_{stat} = 0.1$ bar and the second term gives an additional vent area when higher P_{stat} are used, which has had very limited validation. Equation 2.19 for $P_{stat} = 0.1$ bar is more conventionally expressed in terms of the vent coefficient, $K_v = V^{2/3}/A_v$.

$$1/K_v = (0.1265 \log K_G - 0.0567)\ P_{red}^{-0.5817} \qquad [2.19]$$

The mixture reactivity parameter in Equations 2.18-19 is K_G, which is the maximum rate of pressure rise in a closed spherical vessel times the cube root of the vessel volume, $K_G = dP/dt_{max}.V^{1/3}$ bar/ms, it is often referred to as the 'Deflagration Index'. Bartknecht's values for K_G, measured in a 5 litre spherical volume, have to be used if the measured values of P_{red} are to be predicted. For the most reactive hydrogen/air mixture, Bartknecht's value for K_G was 550 bar m/s. An example of recent measurements of a different values is the work of Tang et al. (Tang et al., 2009) with a value of 440 bar m/s in cylindrical explosion vessel of L/D=1.17 and volume of 5.3L. The difference in K_G is likely to be due to the use of a cylindrical instead of spherical explosion vessel.

Andrews and Phylaktou (Andrews and Phylaktou, 2010) have shown that K_G for initial pressures different from atmospheric should be expressed as the normalized rate of pressure rise with units of m/s, where it is clearly a rate of flame propagation term and could be compared with the more usual laminar burning velocity. This is relevant in the present work, as apart from Bartknecht's data (1993), which was carried out at 1 bar initial pressure, the only other experimental data on maximum reactivity vented hydrogen explosions was carried out at initial pressures higher than atmospheric (7- 9) Recently, Bauwen et al. (2011, 2012] carried out vented experiments in a $64m^3$ rectangular enclosure for 12- 18% hydrogen-air. This was done as part of a study to compare methane, propane and hydrogen explosions at the same spherical flame speed (not the same burning velocity)(Bauwens et al., 2011, Bauwens et al., 2012). Also Lowesmith et al. (Lowesmith et al., 2011) have investigated methane/hydrogen mixtures up to 50/50 in a vented 69.3 m^3 vessel with the vent coefficient K_v ($V^{2/3}/A_v$) close to unity. However, for EU ATEX (1994) compliance it is the worst case scenario that has to be protected against and this requires vented explosion data for 40% hydrogen-air (EuropeanParliament and Council, 1994). The only data for 40% hydrogen-air vented explosions is that of Bartknecht and data for other gas mixtures or equivalence ratios is not relevant to ATEX compliance, when hydrogen/air explosions are the risk being protected against.

The EU vent design standard (EN14994:2007, 2007) and the old version of US NFPA 68 vent design guidance (NFPA68, 2007b) apply Equations 2.18 and 2.19 to compact vessel of L/D<2 and the worst case explosion occurs in vessels with L/D>1 when the spark is in the end wall opposite the vent (EuropeanParliament and Council, 1994). The worst case scenario is for an L/D close to 3 with end ignition and this was the configuration used in the present work. It could be argued that all current vent design procedures do not comply with ATEX as they are based on data from L/D=1 vessel with central ignition, which is not the worst case explosion venting scenario.

Bartknecht (1993) provided experimental vented explosion data for the most reactive propane/air mixture in vessels of different volume from 1 m^3 up to 60 m^3 over a range of K_v for all volumes. The dependence on K_v in Equation 2.19 was that for a 10 m^3 vessel (Kasmani et al., 2006). All other vessel volumes had a lower vent

reduced pressure (Kasmani et al., 2010b, Kasmani et al., 2006). The dependence of P_{red} on K_v was shown to be very similar for methane and hydrogen in the 1 m^3 vessel. Methane was tested in 1 and 30 m^3 vessel and the 30m^3 results were close to the 30 m^3 results for propane as a function of K_v. The only vented results for hydrogen/air were for experiments in the 1m^3 cylindrical vessel at two K_vs and this shows the paucity of data on which current vent design guidance is based for 40% hydrogen/air. The K_G effect in Equation 2.18 was determined from propane in the 10 m^3 vessel, hydrogen in the 1 m^3 vessel and methane in a 1 and 30 m^3 vessel (no results were reported for a 10 m^3 vessel). The vessels were also of different shapes – cylinders for 1 m^3 and cubes above 10m^3. The net result is that the K_G term in Equation 2.19 was not determined at the same vessel volume or shape. This is at the root of the problem, as buried in the constants in the K_G effect in Equations 2.18 and 2.19 is a vessel volume effect that is not accounted for in the K_v term. The propane results of Bartknecht (1993) show a strong influence of vessel volume on the vent overpressure (Kasmani et al., 2010b). Equation 2.19 must include some vessel volume effect in the K_G term and this is the explanation for the overpressures predicted for hydrogen air explosions being too low, as shown in the present work and as shown by classic venting theory. This is the prime reason why the current vent design standards under predict the overpressure for hydrogen relative to those for methane and propane. However, it will be shown in this work that the location of the pressure transducer on the end wall opposite the vent could also have led to an underestimation of the peak overpressure in fast hydrogen explosions with strong dynamics effects.

For the gases methane, propane and hydrogen it is preferable to use the actual constant that was developed in Bartknecht's experiments, as summarized in Table 2.2. Bartknecht (1993) also provided data for Coal Gas (mainly a CO/H$_2$ mixture), but as the composition was not given it is not data that can be readily used and has been omitted. Coal Gas is not currently used as a distributed gas and has ceased production in most countries around 1970 due to the building of the pipeline infrastructure to distribute natural gas.

Table 2.2 Venting and Reactivity KG constants for the three pure gases used by Bartknecht (1993) for a P_{Stat} of 0.1 bar

Gas/air	K_G bar/ms, 5L	a	b	S_um/s (AB)	E_p	P_m/P_i E_v (N)	K_G Eq4 Using Ep	K_G Eq4 using E_v
CH_4 10%	55	0.164	0.5729	0.4	7.5	8.9	75	89
C_3H_8 4.5%	100	0.2	0.5797	0.45	8.1	9.6	99	117
H_2 40%	550	0.29	0.585	3.5	7.1	7.8	544	587

(AB= (Andrews and Bradley, 1972, 1973), N= (NFPA 68, 2013), Eq4=Equation 4)

The experimental vented explosion data was plotted (Bartknecht, 1993) as Equation 2.20.

$$1/K_v = a\ P_{red}^{-b} \qquad\qquad\qquad [2.20]$$

The experimentally derived values of the constants a and b are shown in Table 2.2, together with values of K_G from experiments in a 5 litre spherical vessel (Bartknecht, 1993). The alternative gas reactivity parameter, the laminar burning velocity, S_u, is also listed in Table 2.3, this is the reactivity term adopted in the current vent design equation based on the original work of Swift (NFPA 68, 2013, Swift, 1988) . The exponent b is shown in Table 2.2 to be similar for all the four fuels and an average value of 0.5817 was used in Equation 2.18. However, the reactivity term 'a' is clearly a function of K_G and a plot of 'a' vs. Log K_G gave a linear correlation which is the reactivity term in Equation 2.18. It is important that when using Equation 2.18 in vent design that no other values of K_G are used than those in Table 2.2, otherwise the overpressure will not be that measured by Bartknecht (1993). For venting of the three gases in Table 2.2 it is preferable to use Equation 2.20 with the constants in Table 2.2 rather than Equation 2.18 or 2.19.

Prior to the use by Bartknecht (1993) of K_G as the reactivity parameter for gaseous explosions, the laminar burning velocity, S_u, was used. It may be shown that the two methods are directly related (Andrews and Phylaktou, 2010). For a spherical vessel with central ignition the only assumption needed is that the flame speed is constant

throughout the radial flame propagation. This is not strictly correct as the increase in pressure and temperature, as the gases ahead of the flame are compressed by the flame propagation, changes the laminar burning velocity. However, the pressure effect decreases S_u ($S_u \sim P^{-0.5}$) and the temperature effect increases S_u ($S_u \sim T^2$). The net result is that there is only a 20% change in S_u throughout the flame propagation distance (Bradley and Mitcheson, 1976) and there is more uncertainty in the measurement of S_u than this (Andrews and Bradley, 1972b). There is a further assumption that the vessel diameter is not large enough for the laminar flame transition into a cellular flame and then to accelerate (Bradley, 1997, Bradley et al., 2001). It is to avoid this self-acceleration that the small 5L (106mm radius) spherical explosion vessel was used for the measurement of K_G.

Table 2.3 Relative Reactivity taking Methane as the reference gas

	a	K_G	S_u	K_G Equation 6.04
Propane 4.5%	1.22	1.82	1.12	1.32
Hydrogen 40%	1.77	10	8.75	7.01

For flame propagation in a sphere of diameter D, there is minimal pressure rise in the first half of the flame travel, as shown recently for hydrogen-air explosions by (Dahoe, 2005, Tang et al., 2009). The minimal pressure rise when the flame is half way across the spherical vessel diameter may be shown by considering the fraction of the initial mass burnt. The pressure rise in a closed vessel explosion is directly proportional to the fraction of the initial mass that has been burnt (Lewis and Elbe, 1987). For a sphere the volume of burnt gases when the flame is half way to the wall is 1/8 of the spherical volume. This volume is filled with burned gases of density $\sim 1/E_p$ of the unburned gases. Thus when the flame is half way across the radius there is only 1/60 of the initial mass burned for methane and 1/63 for hydrogen, which is less than 2% of the initial mass. Thus 98% of the mass burned and 98% of the adiabatic pressure rise occurs in the second half of the flame travel. The maximum rate of normalized pressure rise is then 98% of (P_m/P_i - 1) divided by the time for the flame to propagate half way across the radius at the assumed constant propagation rate. An expression for K_G in the form of the normalized pressure rise, P_m/P_i, can now be derived.

$$K_G = V^{1/3}[(0.98\ P_m/P_i) - 1] / \{(D/4) / Su\ E_p\} = 3.16(P_m/P_i - 1)S_uE_p\quad m/s\qquad [2.21]$$

This is used as a consequence of the assumption that the initial flame speed at constant pressure is constant throughout the flame travel. However, the pressure rise occurs in the outer 50% of the vessel radius when the expansion ratio at constant volume might be more appropriate, in which case E_v should be used in place of E_p in Equation 2.21. The effect of this is to increase the predicted value of K_G.

A feature of Equation 2.21 is that K_G should be independent of the spherical vessel volume, but experimental data shows that K_G increases with vessel volume (EN14994:2007, 2007, Kasmani et al., 2010b, Kasmani et al., 2006) due to transition to cellular flames and associated flame acceleration. The use of the 5L vessel by Bartknect (1993) should be small enough to avoid cellular flames for methane and propane, but this may not be small enough for hydrogen. This effect is also the reason that there is an additional influence of vessel volume at constant K_v on the vented explosion overpressure (Kasmani et al., 2010b), yet this effect is currently not taken into account in any approved vent design procedure.

The predicted K_G based on Equation 2.21 is shown in Table 2.2 and these agree well with the results of Bartknecht for propane and hydrogen but predict a significantly higher value for methane. A burning velocity of 0.29 m/s would have to be used in Equation 2.21 to force agreement with the measured K_G of 55 and this is not a reasonable value for S_u for methane/air (Andrews and Bradley, 1972b). Cashdollar et al. (2000) measured K_G for methane-air in two spherical vessels of 20L and 120L and gave values of 50-70 and 90 bar/m/s for the two vessels respectively(Cashdollar et al., 2000). There was a large data scatter for repeat tests in the 20L sphere, but the results would average out at 60, a little above Bartknecht's value of 55. The value of 90 in the 120L vessel is closer to the values predicted from Equation 2.21. Table 2.3 shows the values of K_G and S_u normalized to the values for methane. This shows that the relative impact of mixture reactivity is inconsistent. The relative K_G value for methane is inconsistent relative to propane compared with that based on a wide range of data for the burning velocities of methane and propane (Andrews and Bradley, 1972b).

For gases where a value of K_G may not be known but a value of S_u is, Equation 2.21 shows that the scaling should be $K_{G1}/K_{G2} = (S_{u1}/S_{u2}).(P_{m1}/P_{m2})$ which is the

procedure adopted in previous version of NFPA 68 (2007). In this equation P_m is gauge pressure, whereas in Equation 2.21 P_m is the absolute pressure, so the two equations are in agreement. For hydrocarbons and hydrogen the variation in the values of P_m/P_i for different gases is ignored, as shown by the vent design Equations 2.18-2.20 which do not include the P_m/P_i value. However, for dust explosions P_m/P_i varies between 6 and 15 due to the large differences in calorific values of dusts. This means that the value of P_m/P_i is included in the vent design equation for dust explosions of Bartknecht (1993). The significant difference in P_m/P_i in Table 2.2 for different gases indicates that vent design correlations for gases should include this difference in P_m/P_i. In the Bartknecht method any effect of $P_m P_i$ is included in the constant 'a' in Equation 2.21 and then in the correlation of 'a' that gives the K_G term in Equation 2.18 and Equation 2.19.

For hydrogen-air there are some vented explosion data that is for mixtures other than 40% hydrogen. To use Bartnecht's equation and the laminar flame theory discussed below, the value of K_G as a function of mixture is required. Andrews and Bradley (1973) have used the explosion technique with double ignition to determine the laminar burning velocities across the flammable range of hydrogen/air. This burning velocity data for hydrogen-air over the flammable range enables K_G to be calculated for different hydrogen-air mixtures using Equation 2.21.

There is a significant problem with the values of 'a' in Table 2.2 as they do not scale with either of the measures for reactivity, S_u or K_G as shown in Table 2.3. The value of 'a' for hydrogen is only 1.8 times the value for methane. The ratios of the reactivity constants should be in proportion to those for S_u and K_G at 8.75 or 10, respectively. For methane and propane the differences in the reactivity parameter ratios for K_G, S_u and K_G from Equation 2.21 is probably reasonable if the uncertainties in the experimental values of S_u and K_G are taken into account. However, the hydrogen/methane ratio for 'a' of 1.77 in Table 2.3 has complete disagreement with the ratios for K_G and S_u, that is well outside any uncertainty in the values of S_u and K_G.

It is considered that the problem in the relative values of 'a' in Table 2.3 is due to the use of different sized vessels in the venting experiments of Bartkencht (1993). For Propane, where Bartknecht published results for 1, 2, 10, 30 and 60 m^3 vessels

the value for 'a' was that for the 10 m^3 vented vessel and all the smaller and larger vessel had lower P_{red} for the same K_v. However, the methane results were for the 30 m^3 vessel as the only other volume investigated was 1m^3. For propane the difference in volumes, assuming the same trend as for propane, would increase the value of 'a' by 1.25 giving a volume corrected value of 2.21 for hydrogen. However, if flame speed measurements in free 30% hydrogen/air explosions are taken into account (Andrews and Bradley, 1973) then a flame acceleration factor of 2.5 would be expected for the change in flame radius between a 1 m^3 and 10 m^3 vessel and this would increase the corrected normalised 'a' to 5.5, which would give a value for a of 0.90. This is closer to the methane normalized values of 1.77 in Table 2.3; the difference may be due to greater flame acceleration in a 40% hydrogen/air flame. However, the above considerations do indicate that it was the use of different vent vessel sizes and differences in flame self-acceleration that explains the very low values for 'a' for hydrogen/air in the work of Bartknecht (1993). The derivation of values of 'a' from equation 2.21 from the laminar flame free venting theory and the influenced of various gas mixtures including the current NFPA 68 (2013) are discussed in more detail in chapter 7.

Table 2.4 Review of large and small scale explosion venting experimental studies

Reference	Experimental conditions	Conclusion	Remark
Cubbage and Simmonds (1955,1957)	Geometry: Cubical sized industrial ovens of volumes 0.23-17m^3 and varying the vessel size, vent area and the weight of the explosion relief Gas Mixture: Town gas mixture of various concentration. End, Centre and front ignition used.	The explosion relief was recommended for use in industrial ovens to mitigate against accidental explosions. Relief should be constructed to occupy the whole back of the oven or to be placed in more central that other positions. There is increase in overpressure as the shelving increases.	Double peak pressures were discovered including P$_1$ and P$_2$ and a procedure was recommended for the design of explosion relief. More central ignition was shown to give explosion overpressure as compared to end ignition. The issue of turbulence generation was critical as demonstrated by the shelves.
Palmer and Rogowski (1968)	Geometry: cubical vessels of volumes 0.009m^3, 0.028m^3 and 0.085m^3 to use flame arresters for the protection of the enclosures. Propane-air mixture used. Ignition location remote from the vent, central and near the vent were used	A simple relationship was found between the maximum explosion overpressure and the vent area. The larger volume was successful protected using the crimped-ribbon flame arresters.	Even though the more focus was on the use of flame arresters, it was found that the farthest ignition location away from the vent gives worst ignition location when multiple vents were used. But central ignition gives higher overpressure for single vent.
Nettleton (1975)	Geometry: Tank of volumes 0.7 Litre and 2.5 Litre. The aim was to test the influence of central or end expansion of pressure. Gas Mixture: Ignition location: Centre and end	The peak pressure for centre expansion was equal to the cross sectional area of the vessel, similar to the theory. A key issue was the pressure reversal for the expansion wave opposite the vent.	Change in the vent shape does not have any effect on the shape of the pressure record. Explanation of the multiple peaks as shown in the literature was explained based on the recorded falling expansion waves.
Harris and Briscoe (1967)	Geometry: Cylindrical vessel with dished ends and varying the vent areas. Pentane-air with varied concentration. Ignition location at Central, end and front were used.	The difference between closed vessel explosion and relationship between the maximum reduced pressure and the vent opening pressures were all demonstrated. Also the effect of turbulence.	Even though central ignition was confirmed to produce higher overpressure, no result was shown to demonstrate that. The effect of vent area was not analysed. Also, the relationship between static and dynamic burst pressure was not shown.

Table 2.4 Continuation

Reference	Experimental conditions	Conclusion	Remark
McCann *et al* (1985)	Geometry: cubical vessel of volumes 5.8 litre and 55.9 Litre with circular vents. Gas Mixture: gas mixtures Ignition location: End and Central ignition	Venting on the large and intermediate vents was shown to exhibits flame front wrinkling and instabilities but did only have marginal effect on the internal overpressure. Self-acceleration and cellularity were observed in the later stage of explosion development in the 55.9L vessel.	The flame cellularity in the 55.9L was shown at the later stage of explosion. This was associated with large scale explosion. Also the onset of flame acceleration in the centre ignition was not expected as flame instabilities may be the expected phenomena at this stage considering the vessel size.
Bimson *et al* (1993)	Geometry: A $550m^3$ and $2.5m^3$ chambers, to study on gaseous deflagration of large scale module as part of SOLVEX. A single 50% vent. propane and methane-air mixtures at 1.1 Stoichiometric concentrations, and end ignition used.	Self-acceleration of flames was observed at large flame area. The importance of external explosion was shown to be significant in overall explosion venting overpressure.	The 50% vent area is reasonably large, using small vent area would generate higher self-acceleration factor. Hence, the need to vary the area and the ignition position for better prediction.
Cooper et al (1986)	Geometry: Near cubic vessels of $0.76m^3$, $2,55m^3$, and $2.41m^3$ cuboid. Natural gas mixture was main gas but propane-air and ethylene-air were considered. Central ignition location used.	Four pressure peaks were discovered to be part of the combustion process in explosion venting process in cubic vessel with central ignition. It was concluded that the pressure peak due to acoustic combustion is of no importance in practical application.	The pressure peak associated with the flow through the vent is an important aspect of venting and not identified in this work. Only central ignition location was considered without considering other locations. Peak pressure due to acoustics may not too visible in some circumstances.
Solberg et al (1981)	Geometry: A prismatic steel module of volume $35m^3$ were used for explosion venting. Propane-air mixture, Front, Centre and End ignition, were used.	Central ignition and front ignition location gives higher explosion overpressure as compared to end ignition. The scaling of vented deflagration based on constant volume was shown to be invalid for vessels up to $35m^3$	The location the vent on the side instead of more central position may influence the overpressure. All pressure signatures exhibits Taylors instabilities with central and front having higher instabilities.

Table 2.4 Continuation

Reference	Experimental conditions	Conclusion	Remark
Bartknecht (1993)	Geometry: The vessel volumes include $1m^3$, $2m3$, $10m3$, $30m3$ and $60m^3$ of different shapes and vent sizes. Gas Mixture: Gas mixtures used are methane, propane, town gas and hydrogen-air. Ignition location: Central ignition.	Determined a correlation for predicting maximum reduced pressure using the experimental data. The correlation had limitation as mentioned earlier and the reactivity term used is K_G instead the U_L as applied by other authors.	Only central ignition position was considered in all the experiments. The K_G values was determined only from the 5litre spherical vessel and used to determine the correlation. The correlation only fits the data for $10m^3$ for propane and $30m^3$ for methane as presented.
Cubbage and Marshall (1972)	Geometry: Vessels include $0.95m^3$ and $31m^3$ cubical volumes. Wide range of vent areas where considered. Gas Mixture: manufactured gas natural gas. Ignition location more central was used.	Data was presented for the safe prediction of explosion relief in rigid panels. The result was used to deduce an empirical correlation. Various factors affecting this kind of explosion were observed.	The position of the ignition location was not considered in the analysis and the position used was not completely central. The limitation given for applying the correlation was not also justified.
Wu and Swithenbank (2005)	Geometry: A 3.7m3 cylindrical chamber, with varied circular orifice as vents. Gas Mixture: Methane-air, propane-air and Ethylene-air mixtures. Ignition location: End ignition opposite the vent.	The work showed the dependence of the internal overpressure and flame speed on mixture reactivity and concentrations. External combustion due to exit of external jet flame influenced the rate of combustion and series of external explosions.	For small vent areas, about 95% of the combustion heat releases occurred inside the vessel, this may be responsible for higher overpressure for small vent area. Varying the ignition location may vary the outcome of the internal and external combustion and not considered in this work.
Nagy and Verakis (1983)	Geometry: The vessel use is 0.91Litre, 95Litre, 460Litre. To determine the influence of vent shape on overpressure air flow through chamber. compressed air was used ignition front, end central used.	This experiment shows that varying the vent shape for the same vent area have negligible influence on pressure.	It is may be possible to have this conclusion with the use of compressed air in the vessel, this may be different with explosion with fuel mixture considering the dynamic nature.

Table 2.4 Continuation

Reference	Experimental conditions	Conclusion	Remark
Kumar *et al* (1987)	Geometry: vented explosion in 6.3m3 spherical vessel connected to a 10.3m3 vessel. 6 to 42% Concentration of hydrogen-air used, Ignition location: near end, far end and centre used.	The ignition location relative to the vent has only minor effect on average combustion. Only marginal reduction in peak pressure as observed when vent area was increased by a factor of 2.Turbeulence had no effect on overpressure for high concentration.	The position of the vent midway the connecting vessel between the main test vessel and the cylindrical vessel may have huge influence on the outcome of the result.
Kumar *et al* (1987))	Geometry: A 6.3m3 spherical vessels connectd to 3m long and 0.45m diameter. Gas Mixture: 8.5 to 20% hydrogen-air Ignition location: far end, near end and central ignition.	Central ignition location gives higher overpressure as compared to far end and near end ignition. Reasonable prediction of pressure transient can be obtained using two burning enhancement factor, one pre and post instabilities.	It was shown that the use of constant value of turbulent factor is not realistic and may differ before and after flame instabilities. The view of the ignition position may be different with vessel shape or the influence of the duct.
Hochst and Leuckel Johnson (1998)	Geometry: A 50m^3 silo with H/D=4. Gas Mixture: methane-air Ignition location:	The mass of vent covering panel resulted in higher overpressure in the early stage of the flame propagation and resulted in faster flame front propagation.	Ignition source location with respect to the vent may have some influence on the explosion overpressure and the overall outcome of the explosion.
Proust and Leprette (2010)	Geometry: 1m^3, 10m^{3}and 100m^3 cylindrical vessels. Gas Mixture: Methane, propane and hydrogen.Ignition location:	External explosion was shown to contribute significantly to the maximum overall reduced pressure. It mostly the dominant overpressure and the internal pressure much smaller in magnitude.	In order to reduce the dominance of the external explosion, the author suggested reducing the vent size, which is true. However, this will means increasing the maximum reduce overpressure.
Harrison and Eyre (1987)	Geometry: A 30m^3 vessel. Gas Mixture: Natural gas and propane-air. Ignition location: End and central ignition	In vented explosion chamber, the emerging flame result in external explosion and this external pressure temporary exceeds the internal pressure. It is more violent with far end ignition.	The Size of the external pressure depends on size of vent. Using single peak for the prediction of explosion venting is not realistic; it does not adequately accommodate internal and external pressure.

Table 2.4 Continuation

Reference	Experimental conditions	Conclusion	Remark
Burgoyne and Wilson (1960)	Geometry: Two cylindrical vessel of volume 1.7m³ and 5.7m³. Gas Mixture: Different gas mixtures of pentane-air up to 3.5%. Ignition location: Central, end and front ignition	Spherical envelope of flame in explosion has the minimum surface area and the minimum rate of burning. But obstruction to this envelop leads higher burning rate. The higher the explosion relief also increases the final peak pressure.	The vent near the source of ignition is more effective in reducing the magnitude of the explosion overpressure as compared to the ignition source remote or farther away from the vent which gives higher overpressure.
Catlin (1993)	Geometry: A 0.65m³ vessel to study the external jet explosion. Gas Mixture: methane-air and oxygen enriched mixture. Ignition location: End ignition.	A correlation to determine the external combustion was recommended based on the jet exit velocity since it is not affected by quenching ($\Delta P_{max} \propto U^{4.5}$).	The maximum unburnt gas velocity downstream is used as the jet velocity and recommended for use in the prediction of the maximum external overpressure aa most burnt gas velocities are affected by quenching.
Phylaktou and Andrews (1991)	Geometry: Explosion venting in long tubes, 76mm diameter vessel L/D=21.6, 162mm diameter L/D=6.2-18.4. Gas Mixture: Methane-air mixture. Ignition location: End ignition (flush, x/D=0.33)	Small changes in spark position have significant influence in explosion overpressure, as ignition near the vent is safer. First rate of pressure rise was shown to be inversely proportional to the length of the vessel.	Burnt gas venting is shown to very low explosion overpressure, hence consideration to be given worse unburnt gas venting which gives the worst case explosion for explosion prediction for better safety margin.
Alexious *et al* (1996)	Geometry: Explosion venting in long tubes, 76mm diameter vessel L/D=13.6, with other connecting vessels Gas Mixture: 6% and 10% methane-air. Ignition location: End ignition (Flush).	High flame was observed during this venting process and was found to decrease as the K_v increases. Three pressure peaks associated large L/D vessels were identified, and the mechanism responsible for the dominance of any of the pressure peaks.	The slowing down of flame for high K_v may be as a result of restriction of the expanding flame to accommodate the small the small vent area as it propagates towards the vent.

Table 2.4 Continuation

Reference	Experimental conditions	Conclusion	Remark
Sato et al (2010)	Geometry: A cubical vessel of 4.1 litre by volume. Gas Mixture: Propane-air mixture Ignition location: front, centre and end ignition.	Prior to the rapture of the vent, flame front instability were observed irrespective of the concentration of the gas. Rayleigh-Taylor instability plays important role in intensified combustion.	Turbulence caused by vent opening pressure may be responsible for most of the instability observed in the small vessel. Second pressure peak was low for central ignition as compared to end ignition, may be due to early venting of burnt gases.
Bauwens *et al* (2010)	Geometry: A 63.7m3 chamber with two square vents of 5.4m^2 and 2.7m^2. Also 2.42m^3 cylindrical vessel. Gas Mixture: Stoichiometric propane, methane and 18% hydrogen-air. Ignition location: back, centre and front wall ignition.	The three main physical phenomena responsible for pressure peak generation including external explosion, acoustics, and increased flame area due to obstacles were observed. A model for predicting the reduced pressure was recommended.	The importance of the external explosion in pressure generated in vented explosions was shown, and included in the recommended model. But did not recognise the pressure peak associated with flow through the vent as an important physical phenomenon.
Lowesmith et al (2011)	Geometry: A 69.3m^3 large test vessel. Gas Mixture: methane, methane/hydrogen mixtures Ignition location at Centre and end Ignition	Increase in concentration of hydrogen increases the overpressure and flame speed. Modified shell SCOPE model was used to predict the overpressure with close agreement.	Rear end ignition was shown to give highest overpressure as well as flame speed for the gas mixtures. The work the relationship between overpressure and flame speed in explosion venting.
Jiang et al (2005)	Geometry: A 7.6 cylindrical vessel. Gas Mixture: methane-air. Ignition location: Centre and end Ignition	Several factors including the vent area, the vent failure pressure, external combustible as well as the ignition affects the external explosion caused by the exit flame jet.	Small portion of unburnt gases are venting into the external cloud, there leads to low external explosion. Higher the equivalent ratio gives higher the external explosion due to sufficient fuel in the external cloud.
Tomlin and Johnson (2013)	Geometry: Two different geometries 112m^3 cube and 182m^3 cuboid. Gas Mixture: Methane, propane and ethylene, Ignition at centre and End.	Addition of congestion outside the vent generally increased both the internal and external overpressure by factor of 2. Decreasing the diameter of congestion region of 5% blockage increases P$_{red.}$	Importance of external explosion in maximum explosion in explosion venting shown. External explosion shown to also influence the internal overpressure. Effect of ignition location not analysed.

2.4 Explosion Venting Standards, Theory and Venting Correlations

The design of the explosion vent against explosion deflagration of gas mixtures are based on the gas explosion venting standard, NFPA 68 (2013, 2007) and the European gas venting design guide (2007). For the European design standard and the old version of NFPA 68(2007), the vent design correlations were based on the original work of Bartknecht (1993), and applicable for compact vessel of L/D<2, while the new NFPA 68 (2013) relied on the work of Swift (1989). Bartknecht (1993) in his work provided experimental data for various vessel sizes up to 60m^3 and different gas mixtures including methane-air, propane-air, hydrogen-air, and coal-gas. The experimental data was used to derive explosion vent design correlation as given in equation 2.22, with the vent area A_v as a function of reduced pressure showing the influence of the vessel volume (V).

$$A_v = \left[\frac{0.1265 log_{10} K_G - 0.0567}{P_{red}^{0.5817}} + \frac{0.175(P_{stat} - 0.1)}{P_{red}^{0.5717}} \right] V^{2/3} \qquad [2.22]$$

From equation 2.22, the first part of the equation shows the relationship of the A_v on the pressure loss across the vent, and second term shows how the vent area affects the P_{stat}. Furthermore, the dependence of the equation on K_G shows that the correlation is mainly empirical since the values recommended for K_G where results determined from the 5L spherical vessel (Bartknecht, 1993), different from the large vessels which his correlation was based. It was also mentioned earlier the use of constant value of K_G is not appropriate as the value was shown to have dependence on vessel volume. Bartknecht correlation would be shown later to have no theatrical or fundamental bases as and mainly empirical equation which was adjusted to fit some of his experimental data (Bartknecht, 1993), with the analysis of the data not shown. When Equation 2.22 was applied to P_{stat} of 100mbar, considering that the P_v and w (vent weight inertia) were negligible, then Equation 2.23 was derived (Kasmani et al 2010).

$$\frac{1}{K_v} = (0.1265 log_{10} K_G - 0.0567)P_{red}^{-0.5817} = (Constant)P_{red}^{-0.5817} \quad [2.23]$$

$$\frac{1}{K_v} = a P_{red}^{-b} \qquad [2.24]$$

From different values of P_{stat}, Bartknecht derived a simple equation similar to equation 2.23 with constant "a" for four different gases including methane, propane, town gas and hydrogen (Bartknecht, 1993). This transformed to equation 2.24, with values of constant "a" and exponent "b" depending on the gas mixture, with $K_v(\frac{V^{\frac{2}{3}}}{A_v})$ known is the vent coefficient to accommodate all vessel sizes. The values obtained for constant "a" in his extrapolation, was discovered to be based on K_G values of 55, 100, 140 and 550 for methane, propane, town gas and hydrogen gas mixtures respectively. These K_G values given above were results of the 5 litre spherical vessel and yet still applied on this correlation without considering the huge difference in volume. The exponent value "b" in Equation 2.24 was given for different gases as shown in the literature (Kasmani et al., 2010b), however, an approximate value of 0.5817 was used by Bartknecht (1993) in his design equation 2.22 and 2.23.

The old version of NFPA 68 (2007) had in addition to the Barknechts correlation which was meant for high strength enclosures, also adopted the Swift's (1983) equation, mainly for low strength enclosures. Furthermore, the swift equation has limitation, as it was only applicable to enclosures that can withstand reduced pressure P_{red} not exceeding 100mbar and burning velocity should not to exceed 0.6m/s (NFPA 68, 2007). These limitations restrict the applicability of this equation to only certain vessel volumes and gas mixtures with burning velocities greater the 0.6m/s. However, the swift correlations as given in equation 2.25 is applicable for $P_{red} < 1$, and was shown to have good agreement with certain experimental data in the literature (Harris and Briscoe, 1967, Donat, 1977).

$$A_v = \frac{CA_s}{P_{red}^{0.5}} \qquad\qquad [2.25]$$

Where A_v the vent area, A_s the vessel internal surface area and C the deflagration characteristics constant, which can be obtained experimentally or calculated based on the burning velocity as the reactivity term as shown in equation 2.26 (Swift, 1987). Furthermore, swift (1988) used a typical value of 0.7 as the discharge coefficient (C_D) and turbulence enhancement factor (λ) of 5 which is not included in Bartknecht correlation (Swift, 1988).

$$C = \frac{S_u \rho_u \lambda}{C_D G'} \left[\left(\frac{P_{max}}{P_o}\right)^{1/\gamma b} - 1 \right] P_o^{1/2} \qquad\qquad [2.26]$$

The most recent version of NFPA 68 (2013), abandoned the Bartknecht correlation to adopt the swift equation 2.25 for gas explosion venting design of all type of enclosures with little modification. In this standard, the equation is limited to L/D of 5 or less, and the maximum reduced overpressure (P_{red}) must not exceed 0.5bar. Similarly, additional modification was made to accommodate high strength structure or vessel with$P_{red} < 0.5bar$, also $L/D > 5$ and different equation for the determination of turbulence enhancement factor (λ) (NFPA 68, 2013). All these limitations are different from the old version of NFPA 68 (2007) and the original swift equation (Swift, 1988). Swift's equation has some experimental data which was used to validate the correlation and looks simple to apply. However, there are also key problems with the correlation, firstly, the correlation did not consider the effect of vent opening pressure (P_v) and it means the turbulence associated with the opening of the vent was negligible, which is not practically possible. Secondly, the use of a constant value of 5 for turbulence enhancement factor (λ) is not realistic because this is gross underestimation of large scale condition or explosion associated with different scales and dimensions of obstacles. The use of constant value as turbulence enhancement factor has been an issue of contention with researchers, and recent work on flame obstacle interaction has shown that obstacle generated overpressure are affected by length scale, aspect ratio among other factors (Nain'na et al, 2012, Fakandu et al, 2013). The current NFPA 68 (2013) gave an equation to calculate λ, but still did not consider P_v or P_{stat}. Furthermore, there was no justification for the modifications made from original Swift's equation and no reference was made in that respect. It was necessary to give adequate information on the new vent design correlation for easy application and better safety awareness. More discussion on the application of the vent design correlation is given in the results section.

$$\frac{1}{K_v} = Constant P_{red}^{-0.5} \qquad\qquad [2.27]$$

As shown from equation 2.24, Bartknecht equation included the vessel volume($V^{2/3}$), while the Swift equation considered the use of A_s instead. Swift's use of A_s was followed by the work of Bradley and Mitcheson (1978a, 1978b) and it was considered that for the same reduced pressure (P_{red}), the cubic volume requires larger area than the spherical volume (Swift, 1983). Hence, it shows that the effect

of vessel or geometry is important in the prediction of explosion overpressure, and Bartknecht only considered the effect of volume only without considering how the shape affects the overall outcome of explosion. However, A_s was shown to be related to $V^{2/3}$ by simple relation of $A_s = constant V^{2/3}$ and the value of the constant depending on the vessel volume shape, with 4.84, 6.3, 6 and 5.81 for spherical, rectangular, cubical and cylindrical volumes respectively (Kasmani et al, 2010). Hence, equation 2.25 was used to derive equation 2.7 similar to equation 2.24 in terms of K_v.

Explosion venting correlation was derived by Bradley and Mitcheson (1978a, 1978b) to predict reduced pressure (ΔP_{red}) for initially covered and uncovered vents based on dimensionless parameters, $\overline{A}/\overline{S}$. The correlation which has theoretical backing was presented after comparing with large collection of previous correlations and experimental data. This work which is mostly referenced in explosion venting design analysis or studies is also based on the burning velocity reactivity term and the, A_s, similar to swift's correlation as shown in equation 2.28 and 2.29 (Bradley and Mitcheson, 1978a).

$$P_{red} = 2.43(\overline{A}/\overline{S})^{-0.6993} \text{ for } P_{stat} \geq 1 \, barg \qquad [2.28]$$

$$P_{red} = 12.46(\overline{A}/\overline{S})^{-2} \quad \text{ for } P_{stat} \leq 1 \, barg \qquad [2.29]$$

$$\overline{A} = \frac{C_d A_v}{A_s} \qquad [2.30]$$

$$\overline{S} = \frac{S_u}{C_o}\left(\frac{\rho_u}{\rho_b} - 1\right) \qquad [2.31]$$

The above correlations (equations 2.28 and 2.29) can be expressed in terms of the vent coefficient (K_v), similar to Barknecht's and Swift's equations to give equation 2.32 and 2.33. It was indicated that for smaller vent areas the cross-sectional area of vessels with sharp edges should use $C_d = 0.6$ (Bardley and Mitcheson, (1978a). The use of constant value of C_d, was shown be a more restrictive and conservative approach and the use of constant value C_d large vent areas not realistic as it was shown to vary or increases with the increase of the vent area (Kasmani et al ,2010). Furthermore, $C_d = 1$ was recommended when the entire wall is used for venting, while $C_d = 0.98$ when the vent opening is a well rounded nozzle (Yao, 1974). The

main shortfalls of equations 2.28 and 2.29 is that it reflect a venting scenario where the P_{red} does not exceed the vent opening pressure (P_v) and only valid for one pressure peak (P_{red}). This is a possibility particular for high P_v or P_{stat}, and large vent areas where significant pressure rise is not achieved as a result of effective release of gas mixture or venting induced turbulence not sufficient to enhance the reaction to give significant pressure rise. If the vent area was small, this approach may not be applicable, and also this is contrary to the literature where the maximum reduced pressure (P_{red}) was shown to be additive or a function of P_v or P_{stat} (EN 14491, 2007). In view of the above, Bradley and Mitcheson (1978a) recommended another equation (equation 2.24) which is dependent on P_{stat} and also shows explosion venting scenario with two peak pressures (Bradley and Mitcheson, 1978a).

$$\frac{1}{K_v} = \frac{0.281 S_u(E-1)}{C_d C_o P^{1.43}} = Constant P_{red}^{-1.43} \qquad\qquad [2.32]$$

$$\frac{1}{K_v} = \frac{3.53 S_u(E-1)}{C_d C_o P^{0.5}} = Constant P_{red}^{0.5} \qquad\qquad [2.33]$$

$$P_{red} = 4.82 P_{stat}^{0.375} (\overline{A}/\overline{S})^{-1.25} \qquad\qquad [2.34]$$

In most correlations used to predict explosion venting, it is either assumed that the pressure reduction is effective by the venting of burnt gases or by the venting of unburnt gases. Pressure reduction because of venting of burnt gases is associated with early venting and this may be used considering the ignition location as supported by some studies(Rasbash et al., 1976, Yao, 1974, Maisey, 1965). On the other hand, pressure reduction as a result of venting of unburnt gases which was the main focus of the correlation of Bradley and Mitcheson (1978a), is considered to be the worst case scenario as compared to the venting of burnt gases. This is a safe approach to explosion venting and also in compliance with the ATEX regulation which requires considering the worst case scenario in the design of explosion venting systems (European Parliament and Council, 1994).

This correlation which is the most classic is supported by fundamental theories and a pool of experimental data, to be used as explosion venting prediction tool. However, the correlation was based on central ignition position and in spherical vessel without considering other ignition locations (Bradley and Mitcheson, 1978a and 1978b). It is

difficult to determine the position of ignition source in an accidental explosion and the authors considers the central ignition location in a spherical vessel as the worst case scenario (Bradley and Mitcheson, 1978a). This may be possible in closed vessel explosion (without vent), but this is contrary to the position of other experimental studies that the end ignition opposite the vent gives higher overpressure as compared to central ignition location (Willacy et al. 2007, Sato et al.2010). Another key concern on the correlation of Bradley and Mitcheson is the effect of turbulence on the expanding flame front with the gas flow ahead of the flame which leads higher overpressure. Prior to the venting phase of explosion venting process, the bursting of diaphragm generates turbulence and turbulence generated as a result of flame front interaction with obstacle on the propagation path, which increases the burning velocity as well as the overpressure. In this regard, Bradley and Mitcheson used a turbulent factor (χ) of 4, assuming that increasing the burning velocity four times would assist the theory to agree with the experimental data in all cases (Bradley and Mitcheson, 1978b). In the work of Yao (1974), an empirical turbulence factor (χ) was introduced as a multiplier of the laminar burning velocity (S_u), and $\chi=2$ to $\chi=2.5$ was used for free venting (initially uncovered vent) and $\chi=3$ to $\chi=4$ to accommodate turbulence for the bursting of the diaphragm (Yao,1974). This is similar to the turbulence factor $\chi=5$ used by Swift (1983) as mentioned earlier to force the theory to fit the experimental data and the argument of using a constant turbulence for vent design may not be practicable.

Another correlation was recommended by Molkov et al (1999, 2001), named as the universal correlation, after carrying detail analysis of numerous existing correlations including all the extrapolations and beyond their recommended valid range(Molkov et al., 1999, Molkov et al., 2000). The correlation presented was based on the dimensionless Bradley number (Br) and the turbulence parameter χ/μ, as key parameters. As part of his correlation, the turbulence parameter (χ/μ), known as "deflagration-outflow-interaction number (DOI)" was obtained using the best fit of calculated pressure curves on existing experimental data (Molkov,1999). Also, the Bradley number (Br) is related and similar to the dimensionless parameter,$\overline{A}/\overline{S}$, used in the work of Bradley and Mitcheson (1978a), and the universal correlation for the prediction of vent area and maximum reduced pressure was first introduced by Molkov in 1995 (Molkov and Alexandrov, 1995). The author recommended the use

of these equations (equation 2.35 and 2.36) for unobstructed vessel or some congested enclosures, and a later modified version for initial elevated vessel (Molkov, 2001).

$$\pi_{red} = Br_t^{-2.4} \quad (\pi_{red} \leq 1; \; Br_t \geq 1) \tag{2.35}$$

$$\pi_{red} = 7 - 6.Br_t^{-0.5} \quad (\pi_{red} > 1; \; Br_t < 1) \tag{2.36}$$

$$Br_t = \frac{\sqrt{E_i/\gamma_u}}{\sqrt[3]{36\pi_o}} . Br \frac{\mu}{\chi} \tag{2.37}$$

$$Br = \frac{A_v}{V^{\frac{2}{3}}} \frac{c_{ui}}{S_u(E-1)} \tag{2.38}$$

$$\frac{\chi}{\mu} = \alpha \left[\frac{\left(1+10V_{\#}^{\frac{1}{3}}\right).(1+0.5Br^{\beta})}{1+\pi_v} \right]^{0.4} \tag{2.39}$$

Where the value of the coefficient α and β are the same for hydrocarbon-air mixtures ($\alpha = 1.75$, $\beta = 0.5$) and for hydrogen ($\alpha = 1.00$, $\beta = 0.8$), $\pi_v = \frac{P_v(bar\ absolute)}{P_i}$, $E =$ the expansion ratio $\frac{\rho_u}{\rho_b}$, $\gamma =$ specific heat ratio, $c_{ui} =$ speed of sound. The above correlations (equation 2.35 and 2.36) consider the use of the vessel volume term similar to Bartknecht correlations (equation 2.22) instead of the total surface area ,A_s. Hence, these equations can be transformed based on the K_v term as in equations 2.31 and 2.32.

$$\frac{1}{K_v} = \frac{\sqrt[3]{36\pi}}{\sqrt{E/\gamma}} \frac{\chi}{\mu} \frac{S_u(E-1)}{C_{ui}} \frac{1}{P_{red}^{0.417}} = \frac{Constant}{P_{red}^{0.417}} \tag{2.40}$$

$$\frac{1}{K_v} = \frac{\sqrt[3]{36\pi}}{\sqrt{E/\gamma}} \frac{\chi}{\mu} \frac{S_u(E-1)}{C_{ui}} \left(\frac{7-P_{red}}{6}\right)^2 = Constant \left(\frac{7-P_{red}}{6}\right)^2 \tag{2.41}$$

In the work Molkov (2001), he recommended that the correlations could be used for congested enclosures as well as unobstructed vessels, and this was based on the flexibility of the DOI to accommodate some of these conditions(Molkov, 2001b).

The use of empirical relationship to account for turbulence as a result of venting commenced by increasing the burning velocity term, relevant Reynolds number and including a combination of experimental and best fit approach (Munday, 1963).

Furthermore, over the years the use of turbulence factor has been either a fixed value which were obtained based on narrow, selected experimental data (Swift, 1989, Yao, 1974) or using the turbulent effect on flame front and vent outflow Reynolds number to accommodate the changes of the turbulent parameter on explosion (Chippet, 1984, Molkov, 2000). The main setback of the first approach was that it was difficult to obtain an average value when range of experimental data was used, and also obtaining an equation to correlate the constant value turbulence factor ($\beta = contant$) and the alternative approach ($\beta = f(Re)$) by different authors (Zalosh, 1995). Zalosh also showed some concerns on most of assumptions made in correlations including mixture reactivity or composition, correlations to account for turbulence, the flame area in relation to the geometry and flame acceleration as result of flame instabilities (Zalosh, 1995). Hence, the use of correlation for explosion venting design requires careful examination of all the parameters, to be as realistic as possible based on wide range of experimental data with high flexibility in order to accommodate wide range of scenarios.

In explosion venting modelling, there are numerous models for the prediction of explosion venting scenarios and most of the vent design models have some similarities in their approach. For any approach considered, the fundamental theory or physics concerning fluid flow, mass transfers and thermodynamics must be adequately accommodated in order to get the appropriate mathematical model to accurately predict flame propagation and pressure development in explosion venting. There are two different approaches to explosion vent modelling (Andrew, 2011). Firstly, is to assume that the only pressure difference is created as a result of mass flow of unburnt gas through the vent and this mass flow is the same as the maximum mass burning rate at the flame front. Secondly, is to assume that the maximum pressure occurs when the vent unburnt flow rate is at maximum and equal to the maximum unburnt gas displaced flow by the flame front. On the other hand, the vent can be treated an orifice by using the incompressible flow equation for gas mixtures flowing through the orifice and this can be used for low reduced pressure. The use of the orifice flow equation was shown to agree with the experimental made in the laboratory in the literature (Nagy and Verakis, 1983). These two different approaches will be discussed in relation to other vent design correlations subsequently.

The first approach (**Method 1**) is based on the assumption that the main pressure difference in explosion venting is created by the mass of unburnt gas through the vent, and the mass flow rate is equal to the mass burning rate of the unburnt gas by the flame (m_b). This approach assumes that when the mass burning rate is at its maximum, is the mass flow through the vent. This has been the bases for some correlations in the literature including Munday (1963), Molkov (2001) and has also been simplified by Swift (1983), as given in equation 2.42.

$$\text{Vent maximum mass flow rate} = m_b = S_u A_s \rho_u \qquad [2.42]$$

From the above equation, it implies that the vent discharges the unburnt gases through the vent at the same rate as the flame is generating burnt gases, and this is if the combustion is not a near constant volume (Andrews, 2011). If this is the case, then the only increase in pressure in the vessel will be due to flow pressure loss through the vent. Normally as the flame propagates towards the vent, the thermal expansion of the burning gases pushes the unburnt gases a head of the flame. Hence, the maximum pressure loss and vent mass flow occurs prior to the flame vent exit, once the flame exit the vent, the flame reduces drastically to S_u, while expansion continues outside the vent. In view of the above, this approach is more valid at the later stage of venting process when the venting of burnt gases commences, which still gives maximum flow as proportional to the burning velocity. On the other hand, burning of burnt gases are associated with early venting where the ignition source is near the vent, which seek to give lower overpressure as compared to the unburnt gas venting (Bjerketvedt et al, 1997). In reality, not all unburnt gases are ejected through the vent by the time the burnt gases start to vent, and once the burnt gases exit the vent, there is no further expansion within the vessel, with any other combustion would be at velocity (possibly the burning velocity). Hence, this method is most likely applicable to cubic and rectangular vessels where the trapped unburnt gases are left within the vessel to burn at S_u. It was also shown that the burning of trapped unburnt gases occurred in small cylindrical vessel after the flame had exited the vent, but was not sufficient to generate significant pressure rise (Kasmani, 2008). Thus by implication, this method assumes that there is no expansion of burnt gases inside the vessel pushing the flame into the urburnt gases and the flame propagates at S_u into these gases, and this method may predict very low overpressure.

The second approach (**Method 2**), the modellers believe that the maximum vent overpressure occurs when the vent unburnt gas flow rate is at a maximum and that is equal to the maximum unburnt gas displaced by the flame front. This approach that has been adopted by Runes (1972), Bradley, and Mitcheson (1978a), was based on the gas velocity ahead of the flame (unburnt gas velocity) as shown in equation 2.43.

Vent maximum mass flow rate $= m_b = S_g A_f \rho_u = S_u (E - 1) A_s \rho_u$ [2.43]

The use of S_g shows that the expansion of the burnt gases by pushing the unburnt gases ahead of the flame is recognised and this gives up to 6.5 times higher than equation 2.42 which uses only S_u by additional the expansion factor parameter $(E - 1)$. Runes (1972) in his work on safe design of explosion vent considered maximum burning rate as the upper limit and assumed that this can be achieved when the surface area is at the maximum (A_f). The work also assume that the burning rate and A_f can only be at its peak when A_f is equal to the internal surface area of the vessel (A_s) and starts to decreases after that (Runes, 1972). By implication as shown from equation 2.34, A_f, which is the maximum flame area of the propagating flame, is assumed to be equal to A_s in order to achieve the maximum burning rate (m_b). This assumption is based on spherical flame propagation with central ignition and is valid when the flame approaches the wall with higher reduced pressure(P_{red}). The use of maximum flame area (A_f) as mentioned earlier is more conservative and this could lead to overestimation of the maximum flow. The work of Cates and Samuels (1991) recommended a correlation for explosion venting based on this approach, and assumed that the flame reached the wall of the vessel with it surface area equal to twice the internal surface area of the vessel $(A_f = 2A_s)$. This work and that of Runes are similar as they both relate the internal surface area of the vessel to the flame area, but the main difference the correlation was based on rectangular vessel end ignition location as compared to more central ignition location considered by Runes (1972)(Runes, 1972).

Considering both approaches, while method 1 is likely to me more applicable to cubic and rectangular vessels at high P_{stat} when the flame exits the vent and trapped unburnt gases are left to burn (Andrews, 2011), method 2 is more applicable to spherical explosion. Both methods agree with experimental data but method 2 agrees with more experimental data. However, both methods require enhancement of the

burning velocity to force the equations agree with experimental data either due to flame self-acceleration or vent flow induced turbulence. Assuming that equations 2.37 and 2.38 are based on spherical flame propagation with central ignition and treating the vent as an orifice. Equation 2.44 and 2.45 can be obtained by correlating the orifice meter equation for incompressible flow to equations 2.42 and 2.43.

$$m_b = S_u A_s \rho_u = C_d \varepsilon A_v (2\rho_u P_{red})^{0.5} \qquad [2.44]$$

$$m_b = S_g A_f \rho_u = S_u (E-1) A_s \rho_u = C_d \varepsilon A_v (2\rho_u P_{red})^{0.5} \qquad [2.45]$$

$$\varepsilon = 1 - [0.41 + 0.35 \left(\frac{1}{K_v}\right)] \frac{P_{red}}{\gamma(P_i + P_{red})} \qquad [2.46]$$

From the equations above, the discharge coefficient (C_d) is a constant which varies depending on the vent area or K_v, with sharp edge the $C_d = 0.61$, which is also considered in equation 2.45 and 2.46. Also, the compressibility factor (ε) decreases as P_{red} increases and for incompressible flow a values of 1.0 is used, 0.8 for flow approaching the sonic regime at the nozzle and the standard equation to obtain compressibility as in equation 2.43 (BS 1042, 1992). Thus equation 2.47 and 2.48 can be transformed to a standard equation in terms of A_s similar to that of Swift (1987).

$$\frac{A_v}{A_s} = \frac{S_u \rho_u^{0.5}}{C_d \varepsilon (2P_{red})^{0.5}} \qquad [2.47]$$

$$\frac{A_v}{A_s} = \frac{S_u (E-1) \rho_u^{0.5}}{C_d \varepsilon (2P_{red})^{0.5}} \qquad [2.48]$$

$$\frac{1}{K_v} = C_1 C_2 \varepsilon^{-1} \rho_u^{-0.5} P_{red}^{-0.5} \qquad [2.49]$$

Since method 1 and 2 are assumed to base on spherical vessel explosion, and the relationship between A_s and volume ($A_s = C_2 V^{2/3}$), equation 2.47 and 2.48 can be obtained in terms of K_v with C_2 on the vessel shape (Kasmani, 2010). Furthermore, equation 2.40 can be used for either method 1 or method 2 with the value C_1 depending (method 1 $C_1 = \frac{S_u \rho_u^{0.5}}{C_d \varepsilon (2)^{0.5}}$ and method 2 $C_1 = \frac{S_u (E-1) \rho_u^{0.5}}{C_d \varepsilon (2)^{0.5}}$). Also, equation 2.49 do not accommodate the effect of any turbulence generated either due to P_v or self acceleration of flames. Hence, the use of a burning velocity enhancement factor could be used to predict the reduced pressure based on turbulent burning velocity

($S_T = \beta S_u$), where β is the turbulence factor. The validity of the equation 2.49 is for $P_{red} \leq 900mbar$, but above this value, the ${P_{red}}^1$ to be used instead of ${P_{red}}^{-0.5}$.

Most of these correlations mentioned above have similarities in the underlying theories but the main differences are the enhancement factor required to accommodate certain scenarios. Other areas of major differences are the limits of applicability of the correlations which differs from one author to another. A good example is while the Swift (1988) correlation is only applicable to propane-air and methane-air, the new NFPA 68(2013) which was based on the Swifts' equation only accommodates gases with $S_u < 3m/s$. Also, the mixture reactivity term in the two vent design standards considered in this work either used S_u or K_G , while most of the correlations in the literature used S_u. Another issue of concern is that most correlations only considered the prediction of only the P_{red} or at most two peaks ($P_{red} and P_{stat}$). The issue of the explosion venting peaks pressure are not fully addressed in most correlations, as most recent publications have shown the existence of more than one pressure peaks (Cooper et al 1986, Buawen et al. 2010). It was also shown that the P_{red} may be influenced either by flow through the vent or as result of external explosion depending on the size of the vent (Fakandu et al 2013), which is yet to be accommodated into the vent design correlations. Hence, there is the need to compare most of these correlations with the existing vent designs standards of NFPA 68 (2013) and the European gas venting design Guide (EN 14994, 2007) for better understanding of the design fundamentals.

2.5 Application of Explosion Vent Design Standards and Correlations

In order to adequately implement the venting technique, several experimental and theoretical studies were instrumental to the development of the design guidance of NFPA 68 (NFPA 68 2007, 2013) and the European standard (BS EN 14994, 2007) for the application of the venting technique for gas mixtures. The recommendations provided by this design guide are used for the predictions of the appropriate vent for different structures and flammable gases. For over a decade, the venting standard had undergone series of reviews in order to accommodate recent discoveries and areas of explosion hazards not initially covered by the standards. However, there are

still areas of safety concerns in explosion venting literature both experimental and theoretical approach in the data base which are not covered by these standards.

The venting design guidance as adopted by European vent design standards(BS EN 14994, 2007) and the old NFPA 68 (2007) of the United State relies on the original work of Bartknecht (Bartknecht, 1993) and his equations are based on his original data. Most of the equations of this data are not the representation of experimental data and the experimental result does not have the safety margin (Andrews and Phylaktou, 2010)
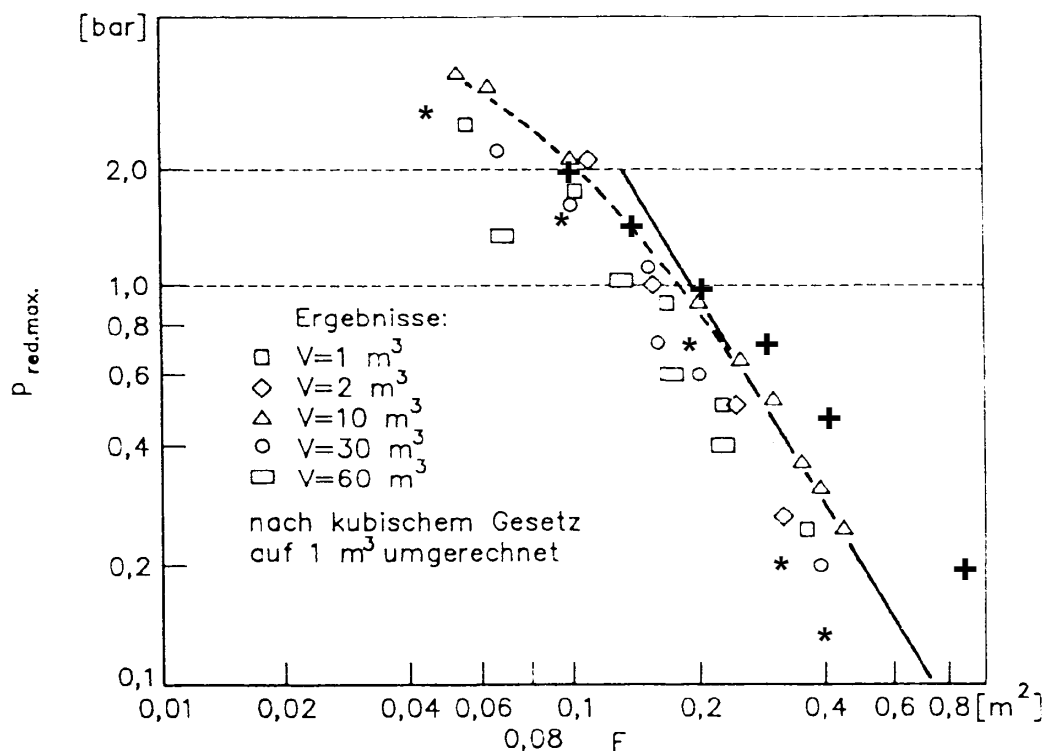
Figure 2.8 P_{red} as a function of F(vent area) for different vessel volumes (Bartknecht, 1993)

Bartknects original data for experimental work using propane-air for different vessel volume (1m^3-60m^3), where the correlation was derived is show in Figure 2.8 (Bartknecht, 1993). The figure shows the maximum reduced pressure P_{red}(bar) against vent area F (m^2). It was shown from the figure that the correlation was based on experimental data in 10m^3 vessel rather than all the test results. Furthermore, the correlation was used to re-plot some of the vessel volumes, with the 2m^3 and 30m^3 showing poor agreement with the main line of fit of the correlation. Siwek (1996) in his work noted that the Bartknechts correlations were mainly empirical derived from

his experimental work, with no other published work used (Siwek, 1996). Figure 2.8 shows the overpressure for larger vessels than $10m^3$ vessel were decreasing as the volume increases, while the others increases as the volume increases. This is not realistic in practice, as the overpressures were meant to increase as the vessel increases in size due to effect of self-acceleration of flame (Bradley and Mitcheson, 1978).

Figure 2.8 was showing the overpressure as function of the vent area, F (m^2) with the vent increasing from 0.01-0.8. However, the figure was re-analysed and it was discovered that the x-axis was supposed to be the reciprocal of the vent coefficient $(1/K_v)$. It is evident that Bartknect correlation is mainly empirical as there was no theoretical or physical evidence to support it. Also it was not based on all his experimental results and not validated with published data. Other concerns with the correlation including the volume effect and reactivity will be discussed later.

$$A_v = \frac{CA_s}{P_{red}^{0.5}}$$ [2.50]

$$C = \frac{\lambda S_u \rho_u}{C_D G'} \left[\left(\frac{P_{max}}{P_o}\right)^{1/\gamma b} - 1 \right] P_o^{1/2}$$ [2.51]

$$C = \frac{\lambda S_u \rho_u}{2 C_D G_u} \left[\left(\frac{P_{max}+1}{P_o+1}\right)^{1/\gamma b} - 1 \right] (P_o + 1)^{1/2}$$ [2.52]

The vent design correlation (equation 2.50) in the current standard for explosion protection by deflagration venting (NFPA 68, 2013) is based on the original work of Swift (1988) and abandoned the Bartknechts (1993) correlation of the previous standard (NFPA 68, 2007). Swift had followed the same approach as Bradley and Mitcheson (1978a) by using the burning velocity (S_u) as the reactivity term instead of K_G. The constant (C) in equation 2.51 was derived theatrically, with $C_D = 0.7$, $\gamma b = 1.1$ and G' is the maximum incompressible mass flux through the vent (Swift, 1989). Since, G' is mass flux through the vent, then it will depends on S_u and then C should not depend on S_u if we are to follow the basic approach to obtain theoretical value of the constant (C). A turbulence enhancement factor of 5 was obtained when the constant C was forced to agree with the experimental data from the original work. This was to account for vent induced turbulence, self acceleration of flames or other flame instabilities (Swift, 1988). Figure 2.9 shows large scale experimental

data to determine the empirical value used in NFPA 68 (2013), with Swift showing a safe prediction of the equation for methane and propane, but the main concern is the theoretical approach used to obtain the constant. Furthermore, the correlation does not accommodate the vent opening pressure, P_v, for subsonic venting but only for sonic venting (Swift, 1988).

There are some differences between the original vent design correlation of Swift and the NFPA 68 (2007, 2013). The old version of the standard (NFPA 68, 2007) recommended the swift equation for low strength enclosures with 0.1bar as the limit, while the new version (NFPA 68, 2013) limits the application of the equation to 0.5bar for subsonic venting.
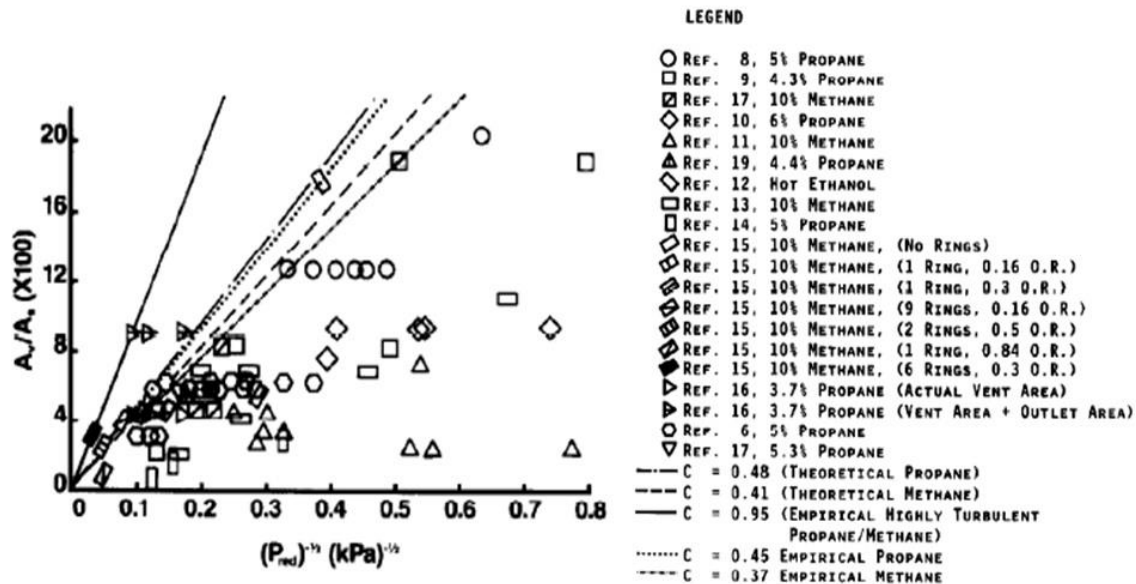
Figure 2.9 Large scale explosion venting data used to determine the deflagration characteristic value-C (Swift, 1988)

However, Swift (1988) equation is applicable up to one bar overpressure ($P_{red} < 1bar$), and there are no justifications given for the change in the limits of applicability of the design equations in the design standards. Equation 2.43 is used to determine the constant value in the New NFPA 68 (2013), and the use of $P_{red}^{0.5}$ in equation 2.44 shows that the equation is mainly for subsonic venting. However, the use of the term $(P_o + 1)^{1/2}$ in the new standard in equation 2.52 shows that the initial pressure must be higher than atmospheric, this may result in sonic venting and also different from the original equation 2.51.

$$C = 0.0223\lambda S_u bar^{1/2} \text{ for } S_u \text{ in m/s} \tag{2.53}$$

Equation 2.52 above was used to determine the value of the constant C as shown in equation 2.53 in the new NFPA 68 (2013). When the constant $0.0223\lambda S_u$ was reanalysed, with the constant value $C = 0.045 bar^{0.5}$ given by swift (1988) for propane, using a burning velocity of 0.46, It was discovered that the new standard used a $C_d = 0.61$ instead of 0.7 as used by Swift. However, the $C_d = 0.61$, is more acceptable and regularly used by authors in venting models for sharp edged vents (Bradley and Mitchenson, 1978a). The standard also specified that the P_{red} is always more than $1.33 P_{stat}$, this unusual limitation is not always the case in reality for large vents areas with low external explosion (Lunn, 1984). More review on the venting standards to be discussed more in other chapters of this thesis.
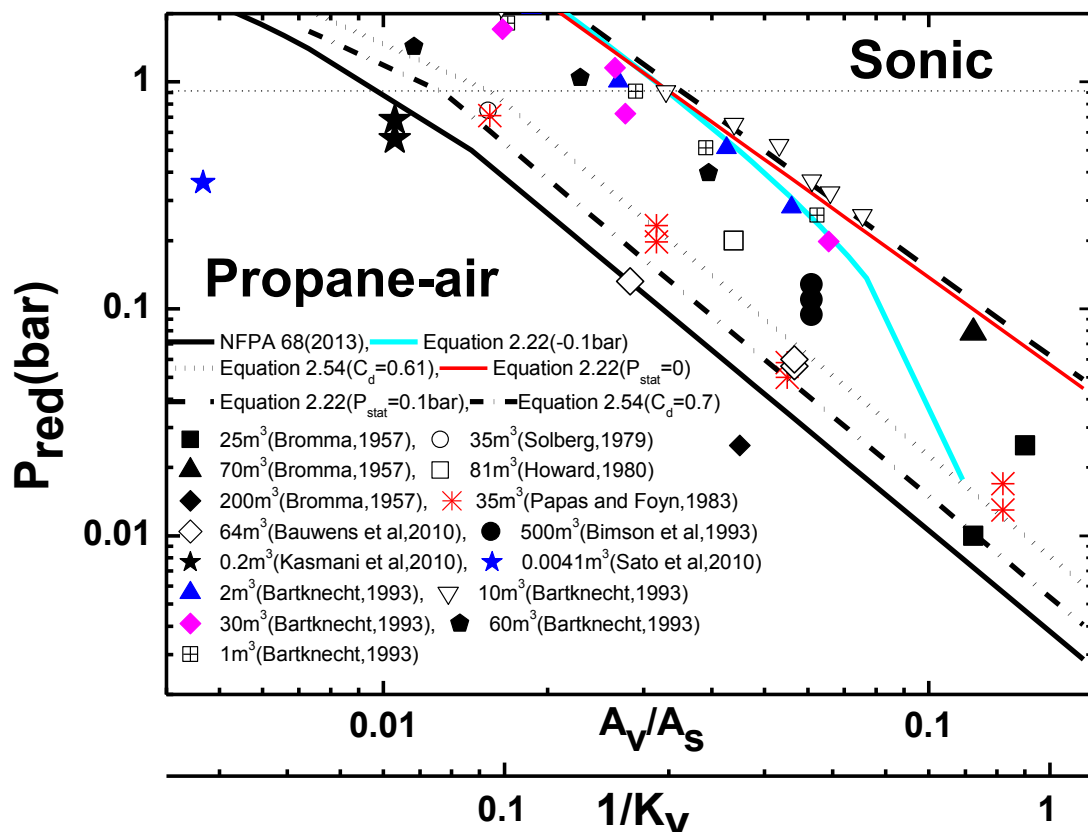
Figure 2.10 Comparison of vent design equations with experimental data for propane-air as Pred v. 1/Kv = Av/V2/3

There are two different approaches to explosion vent modelling suggested in the literature as discussed previously. In both cases the maximum flame area A_f is required to be known at the point of the maximum overpressure. Runes (1972)

introduced the assumption that the maximum possible flame area is the surface area of the vessel, A_s. However, this should give an over prediction of the mass of unburned gas flow rate, as the assumption that flame area is equal to the surface area of the vessel at the point of maximum pressure depends on the vessel type and other factors. Most correlations developed for prediction of overpressure generated during explosion venting based on the theory of mass flow through the vent is termed the laminar flame venting theory. The classic laminar venting theory was reviewed by Bradley and Mitcheson (1978a) in his correlation to show that the unburnt gas venting gives higher overpressure than the burnt gas venting. One of the features of the laminar flame theory was the use of the orifice flow equation and Andrews and Phylaktou (2010) derived equation 2.54 after reviewing the laminar flame venting theory. The laminar venting theory will be discussed in more detail later in chapter 7.

$$A_v/A_s = C_1\varepsilon^{-1}\lambda S_u(E_p - 1)P_{red}{}^{-0.5} \qquad \text{with } P_{red} \text{ in Pascals} \qquad [2.54]$$

where $C_1 = \rho_u{}^{0.5}/(C_d\,2^{0.5}) = 1.27$ for $\rho_u = 1.2$ kg/m^3 and the vent discharge coefficient $C_d = 0.61$.

Figure 2.10 shows the comparison of the vent design correlations with experimental data from the literature with free venting (uncovered vent) for propane-air mixture. The Bartknecht (1993) correlation was shown to be based on only his experimental data on 10m^3 vessels and not his experimental. Also, the correlation was shown to have overestimated the overpressure for most of his experimental data and other data including the vessels larger and smaller than the 10m^3 as seen in Figures 2.10 and 2.11 (Bartknecht,1993). It was expected that the overpressure should increase with vessel size but this was not the case, and the reason for the choice of only propane data for 10m^3 is still not known. All venting data in Figure 2.10 from the literature for vessel volumes up 550m^3(Bimson et al, 1993) were shown be lower than the Bartknecht (1993) correlation and all his experimental data. Also, the maximum volume used by Bartknecht in his experiments was 60m^{3}and minimum vessel was 1m^3. Hence, there is no justification for the limits of applicability of his correlation of 1000m^3.

It was expected that the overpressure should increase with vessel size but this was not the case, and the reason for the choice of only propane data for 10m^3 is still not

known. The laminar venting model based of equation 2.54 was compared with the experimental data for propane, considering that this work was for free venting, as no turbulence factor was included. Figure 2.10 shows that laminar flame grossly under predicts the Bartknecht correlation but overpressure predict the venting standard. Furthermore, the changing of the discharge coefficient was shown to make significant difference and the model also in agreement with some experimental data. When that data for Methane-air was analysed as shown in Figure 2.11, Bartknecht correlation was shown to only fit his data on the $30m^3$ and $1m^3$ vessels (Bartknecht, 1993). Furthermore, the other correlations also show similar trend to Figure 2.10 as discussed earlier. There are more discussions on correlations and the new NFPA 68 when compared with the experimental results from this work in chapter 7.
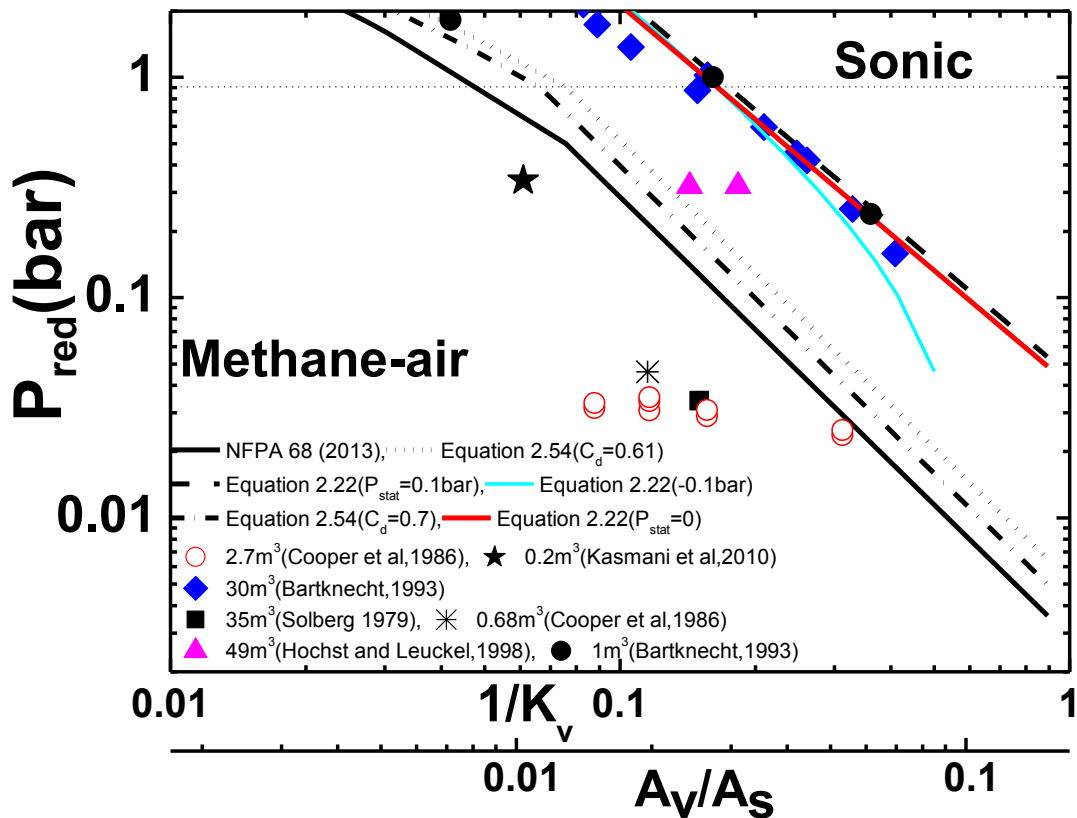
Figure 2.11 Comparison of vent design equations with experimental data for Methane-air as Pred v. 1/Kv = Av/V2/3

This was similar to the work of the Cates and Samuels (1991), were both internal generated pressure and external explosion were used to the determined the P_{red}. The application of venting technique by predicting the overpressure regenerated in industrial oven by Cubbage and Simmonds (1955), gained recognition in the history of explosion venting prediction. Series of other correlations were later developed to

accommodate various scenarios with improvements over time, with latest "a novel correlation for vented hydrogen-air deflagration" by Molkov(2013) and the current most recent vent design guide (NFPA68, 2013, Molkov and Bragin, 2013). Thus, Table 2.5 gives the summary of reviewed correlations for gas venting of explosion deflagration as considered in this work.

Some of the correlations including Bartknecht (1993), Swift (1988), Bradley and Mitcheson(1978a), and the Laminar flame model (Andrews and Phylaktou,2010) were compared with experimental data in Figure 2.12a. It was shown that the Swift correlations (Equation 2.25) and the equation of Bradley (equation 2.34) had the highest over predictions due to the influence of the turbulence factor, while the laminar model with the lowest prediction had no turbulence factor. The influence of the turbulence was also demonstrated in Figure 2.12b when different value of turbulence factor was included. The figure also shows how the models are having agreements with experimental data from the literature for different size volumes.
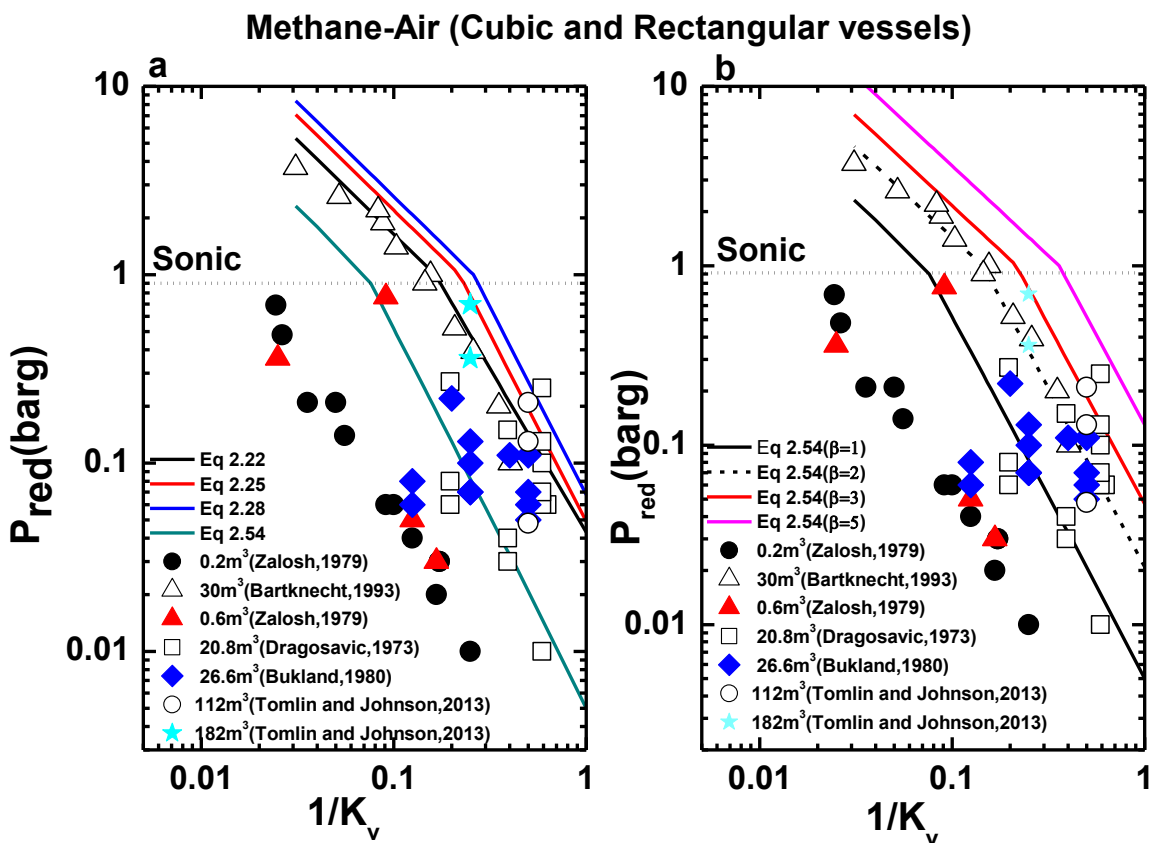
Figure 2.12 vent design equations and experimental data for cubic and rectangular vessels

A model for the prediction of vented explosions was also given in the work Buawens et al (2010), and it recognised the importance of external explosions as a key factor in the outcome of the maximum reduced pressure (Bauwens et al, 2010).

Most correlations are derived either based on theoretical analysis or experimental data for the prediction of explosion venting. The issues with some of the correlations are conditions considered in the theory or experiments to derive some of the equations and other considerations including vessel shapes or size of the vessel influences the outcome of the correlations. John Nagy (1983) in his work recommended some equations for the prediction of vented explosions for both uncovered and covered vents. In the work, separate vent equation was recommended for closed cylindrical vessel, vented cylindrical vessel with central, end and near vent ignition locations, and the spherical vessel with central ignition (Nagy and Verakis, 1983).

Table 2.5 A review of explosion venting deign correlations

Reference	Equation	Methodology	Restrictions	Remark
Cubbage and Simmonds (1955)	$P_1 V^{1/3} = S_o(0.45Kw + 2.6)$ $P_2 = 5.8S_oK$ $P_2 = 5.8S_oKV^{1/3}$	Based on experimental investigation of industrial explosion relief in industrial oven and similar low strength facility. Geometry: Vessel volumes from 0.3m³ to 17m³. Gas mixture: Varieties of flammable mixtures were investigated. Varied the ignition locations.	$L/D < 3$, $K < 5$ $V < 1000m^3$ The larger of the two peaks $P_2 or P_1$ should be taken as the maximum	Concluded that central ignition was worse case but there are no restrictions on the force to be applied or effect of P_v or P_{stat} is not given.
Rasbash (1969)	$P_m = 1.5P_v + 0.5K$ (Original equation in imperial unit). $P_m = P_v + 7.76S_oK$ (modified equation)	Carried out studies on small enclosures using propane-air, and also correlated the results from other authors to derive at the empirical equation.	$L/D < 3$, $1 \le K \le 5$, the weight of vent cladding not more than $24kg/m^2$, $P_v \le 0.07bar$	The original equation did not account for reactivity, was only restricted to propane but modified accounted different fuel mixtures. However, the volume effect was not considered.
Cubbage and Marshall (1972)	$P_{max} = P_v + 2.44S_o{}^2Kw/ V^{1/3}$ $P_{max} = P_v + 0.7S_o{}^2Kw/V^{1/3}$	Analysis of extensive series of experimental data on both small scale test chambers and large including buildings.	$S_o < 0.5m/s$ $S_o < 1m/s$	An improvement of the work of Cubbage and Simmonds (1955). The P_v pressure up to 0.5bar and fuels with burning velocities up to 1m/s

Table 2.5 Continuation

Reference	Equation	Methodology	Restrictions	Remark
Runes (1972)	$A_v = \frac{\pi}{200} * \frac{L_1 * L_2 * V_f}{\sqrt{\Delta P}}$ $* \left[\frac{M_f}{M_i} * \frac{T_f}{T_i} - 1\right]$ Or $P_{red} = 1.804 * 10^{-4}[D^2 S_f(E_o - 1]A_v^{-2}$	It is a theatrically based model which was validated by comparing with the NFPA 68 (1954) and experimental data of propane-air from 154m³.	Normal ignition spark to be used, flame velocity below the speed of sound and burning velocity not exceeding 3.4m/s at atmospheric pressure. Not for detonation explosion.	It based on spherical flame propagation. The correlation is based on flame speed and considers that peak pressure is obtained when, $A_f = A_s$. Considers flow through the vent and volumetric flow.
Yao (1974)	$P_{red} = \left[\frac{0.375\chi^{0.675}E_o^{7/6}}{E_o - 1}\right]^2 (\bar{A}/\bar{S})^{-2}$	Empirical correlation for low bursting pressure. Considered the spherical vessel with free venting and later closed vent. Correlated result for propane in 8.3m³ vessel and other experimental data	Turbulence enhancement factor $\chi = 3\ to\ 4$ for busrting diapharm and $\chi = 2\ to\ 2.5$ for free venting	Used enhancement factor for covered and free venting. Equation based on the mass flow through the vent based laminar burning velocity term. Considers explosion with central ignition.
Swift (1988)	$A_v = \frac{CA_s}{P_{red}^{0.5}}$ $C = \frac{\lambda S_u \rho_u}{C_D G'}\left[\left(\frac{P_{max}}{P_o}^{1/\gamma b}\right) - 1\right]P_o^{1/2}$	Empirical correlation based on initial theoretical model, correlated with actual experimental data, with a lumped parameter to account for turbulence.	$C_D = 0.7, \gamma b = 1.1, \lambda = 5,$ $P_{red} \leq 0.9$	Based on central ignition. Uses $\lambda = 5$ for turbulence, determined constant for propane and methane only. Not for sonic venting, and does not account for P_v.

Table 2.5 Continuation

Reference	Equation	Methodology	Restrictions	Remark
Bradley and Mitcheson, 1978a)	$P_{red} = 4.82 P_{stat}^{0.375} (\overline{A}/\overline{S})^{-2}$	A modification with some scaling dimensions of $\overline{A}/\overline{S}$ to accommodate P_{stat}.	Turbulence factor (β=4) $C_d = 0.6$	Two pressure peaks exhibited with dependence of P_{red} on P_{stat}.
Simpson (1986)	$P_{red} = \left[\dfrac{1}{dVf \exp(gP_{stat})}\right]^{1/h} A_v^{1/h}$	Based on the Bartknecht nomogram for prediction of overpressure and cited by Razus *et al* (2001)	$1 \leq P_{stat} \leq 1\, barg$ $P_{stat} + 0.1 \leq P_{red} \leq 2\, barg$ $1 \leq V \leq 5000 m^3$	The constants in the equation including d,f,g.h depends on the nature of flammable mixture.
Cates and Samuels (1991)	$P_1 = \frac{1}{2}[(1/C_d)^2 + a\gamma C_g(n)]\rho[\frac{2AU_t(E-1)}{A_v}]^2$	A theoretical model based on the rectangular vessel and end ignition location. It was validated with large data from the 35m³ DNV vessel reported by Pappas and Foyn (1983).	Applicable to congested region and maybe used for empty vessels.. Only incompressible flow and considered for box with aspect ratio close to 1.	The term $a\gamma C_g(n)$ accounts for the turbulence within the vessel. It assumed that the peak pressure is achieved when $A_f = 2A_s$, based on end ignition and not central ignition location
Bartknecht (1993)	$A_v = \left[\dfrac{0.1265 log_{10}K_G - 0.0567}{P_{red}^{0.5817}} + \dfrac{0.175(P_{stat}-0.1)}{P_{red}^{0.5717}}\right]V^{2}/3$	Based on experimental data for large vessels from 1m³-60m³. With K_G used instead of Su to accommodate reactivities of the various fuel mixtures.	$K_G \leq 550 bar.m/s$, $0.1 bar \leq P_{stat} \leq 0.5 bar$, $P_{red} \leq 2bar$, $V = 1000m^3$, $L/D \leq 2$	The K_G are considered to be constants and measured in 5 Litre spherical vessel. Correlation only fits 10m³ for propane and 30m³ vessel for methane. All test based on central ignition location.

Table 2.5 Continuation

Reference	Equation	Methodology	Restrictions	Remark
Molkov (2001)	$\pi_{red} = Br_t^{-2.4}$ $(\pi_{red} \leq 1;\ Br_t \geq 1)$ $\pi_{red} = 7 - 6.Br_t^{-0.5}$ $(\pi_{red} > 1;\ Br_t < 1)$	Based on the dimensionless Br and $\frac{\mu}{\chi}$. The DOI, $\frac{\mu}{\chi}$, derived from best fits of experimental data from different authors.	For hydrocarbon-air mixture, $\alpha = 1.75, \beta = 0.5$ For hydrogen-air, $\alpha = 1.00, \beta = 0.8$	Br is closely related to $\overline{A}/\overline{S}$ of Bradley (1978a). Can also be applied in congested regions.
NFPA 68(2007)	$A_v = \left[\frac{0.1265log_{10}K_G - 0.0567}{P_{red}^{0.5817}} + \frac{0.175(P_{stat} - 0.1)}{P_{red}^{0.5717}}\right]V^{2}/3$	Adopted the Bartknecht (1993) correlation above, for high strength structures.	Same as Bartknecht (1993) correlation.	Same as Bartknecht (1993) correlation.
NFPA 68 (2007)	$A_v = \frac{CA_s}{P_{red}^{0.5}}$ $C = \frac{\lambda S_u \rho_u}{C_D G'}\left[\left(\frac{P_{max}}{P_o}^{1}/\gamma b\right) - 1\right]P_o^{1/2}$	Adopted the Swift (1988) correlation, required for low strength structures.	$C_D = 0.7, \gamma b = 1.1,$ $\lambda = 5, P_{red} \leq 0.1 bar$	Different equations to determine the constant C. Some deviation from original Swifts equation.
EN BS 144994(2007)	$\frac{1}{K_v} = \left[\frac{0.1265log_{10}K_G - 0.0567}{P_{red}^{0.5817}} + \frac{0.175(P_{stat} - 0.1)}{P_{red}^{0.5717}}\right]$	Adopted the Bartknecht (1993) correlation above.	$K_G \leq 550 bar.m/s,$ $0.1 bar \leq P_{stat} \leq 0.5 bar,$ $P_{red} \leq 2 bar, V = 1000 m^3,$ $L/D \leq 2$	Same as Bartknecht (1993) correlation.
Bauwens et al (2010)	$\frac{P}{P_o} = \frac{P_e}{P_o}\left(1 - \frac{G}{A_v^{*2}}\right)^{-1}$ $\frac{P_e}{P_o} - 1 = \frac{20\gamma(\sigma - 1)\sigma S_u R_e \sqrt{K_T a}}{a_o^2}$	Model for the estimation of maximum pressure for each of the pressure transient. Validated with experimental data of 64m³ vessel.	$K_T a$ estimated from the experimental data and the flame depends on the location of ignition.	Considers different pressure peaks and shows the influence of external explosion in the model.

Table 2.5 Continuation

Reference	Equation	Methodology	Restrictions	Remark
Rasbash (1976)	$P_m = 1.5P_v + S_o[(\dfrac{0.45Kw + 2.6}{V^{\frac{1}{3}}}) + 7.76]$	An improvement to the old version of the equation.	$L/D < 3$, $1 \le K \le 5$	A modification of the Rasbash 1969 to account for back pressure other conditions including back pressure by restricting of gases through the vent.
Bradley and Mitcheson, 1978a)	$P_{red} = 2.43(\overline{A}/\overline{S})^{-0.6993}$ $P_{red} = 12.46(\overline{A}/\overline{S})^{-2}$	Correlation from theory and validated with experimental data for both uncovered and covered vent. The equation was based on the dimensional parameter $\overline{A}/\overline{S}$.	for $P_{stat} \ge 1\ barg$ and $P_{stat} \le 1\ barg$	Past models in the literature considered. Problem of effect on turbulence and did not account for P_v or P_{stat} . Based on central ignition and spherical vessel.
Siwek (1996)	$A_v = \left[\dfrac{0.1265log_{10}K_{max}-0.0567}{P_{red}^{0.5817}} + \dfrac{0.175(P_{stat}-0.1)}{P_{red}^{0.5717}}\right]V^{2/3}$	Initially recommended equation for the design of vents for dust and hybrid mixture. And later gaseous mixtures based on the correlation of Bartknecht(1993)	$K_G \le 550bar.m/s$, $0.1bar \le P_{stat} \le 0.5bar$, $P_{red} \le 2bar$, $V = 1000m^3$, $L/D \le 2$	The K_{max} (max explosion constant) is K_G in Barknecht's empirical equation. Valid for cubic and non-turbulent mixtures.
NFPA 68 (2013)	$A_v = \dfrac{CA_S}{P_{red}^{0.5}}$ $C = \dfrac{\lambda S_u \rho_u}{C_D G'}\left[\left(\dfrac{P_{max}}{P_o}^{1/\gamma b}\right) - 1\right]P_o^{1/2}$	Adopted the Swift (1988) correlation with some modifications.	$C_D = 0.61$, $\gamma b = 1.1$, $\lambda = 5$, $P_{red} \le 0.5\ bar$	Different equations to determine the constant C and λ. Some deviation from original Swifts equation
Molkov (2013)	$\pi_{red} = 0.33Br_t^{-1.3}$ $\pi_{red} = 0.33Br_t^{-1.3}$ (more Conservative estimate)	Correlation was validated with wide range of experimental data from vessel up to 120m³. H₂-air mixture from 6%-30% (v/v).	$(\pi_{red} < 1;\ Br_t > 1)$	Mainly for H₂ mixture not exceeding 30 %(v/v). End, central and front ignition. Valid for initially quiescent and turbulent mixtures.

2.6 Conclusions

Explosion protection using the venting method was known to be the most economical and simple to apply. Furthermore, the application of venting technique requires careful understanding of the mechanism of explosion venting and required the parameters to use as provided by the vent design standards or the vent design guides. However, the design of vents in complex petrochemical plants is still based on empirical correlations, although recognised by EU and US standards, do not include practical effects (Andrews and Phylaktou, 2010). After an extensive literature review on gas explosion venting design, the following conclusions were made:

1.   The venting design guidance as adopted by European vent design standards and the old NFPA 68 (2007) of the United State relies on the original work of Bartknecht (Bartknecht, 1993) and his equations are based on his original data. Most of the equations of this data are not the representation of experimental data and the experimental result does not have the safety margin (Andrews and Phylaktou, 2010). Furthermore, the new NFPA 68 (2013) is based on the original work of swift (Swift 1983 and 1988) and has a maximum burning velocity of 3m/s.

2.   The current vent design equations are as a result of Bartknecht experimental data for $10m^3$ vessel for propane and methane, and also for $1m^3$ vessels for hydrogen. It was observed that Bartknecht data for propane predicts lower values of P_{red} for volumes lower or higher than $10m^3$ (Andrews and Phylaktou, 2010).

3.   Bartknecht correlations as well as the European design equations (EN14994, 2007) which is based on the gas reactivity (K_G), over predict the vent area A_v when compared with other experimental results from the literature.

4.   The European design equation restrict the length to diameter ratio L/D of <2 and valid for compact vessel assuming that the venting process spreads as a spherical flame. It is however difficult to make accurate prediction of the pressure rise when the L/D is >2.

5.   The new standard for explosion protection by deflagration venting of US (NFPA 68, 2013) which is based on burning velocity term (U_L), is applicable only to U_L< 3m/s and mixture concentration not above 10%. This means that Hydrogen-air venting at the maximum reactivity composition is excluded (3.5 m/s U_L and 40% H_2 in air).

6.   The new guidance (NFPA 68, 2013) is not applicatable to hydrogen-air venting, but the European guidance (EN14994,2007) which is the same guidance in the old US guidance (NFPA 68, 2007) are applicable to hydrogen-air, but shown be inaccurate in predicting hydrogen-air mixtures.

7.   Both venting standards assume that the $P_{red}>P_{stat}$ always and have restriction on the applicability of Pstat. Also the new US guide (NFPA 68, 2013) has no provisions for P_{stat} for $P_{red} < 0.5bar$.

8.   Most explosion vent design correlations including the desising equations in the explosion venting standards predicts only one peak pressure and that is the maximum reduced pressure. However, there surficient evidence that in explosion venting, more than one pressure peaks are involved depending on the initial and physical conditions (Cooper et al, 1986, Bauwen et al, 2010, Fakandu et al, 2013).

9.   In planning and design of systems for explosion protection, the ATEX regulations requires that the maximum possible pressure and the extreme or worst case senario to be considered (European Parliament and Council, 1994). In this regard, all possible factors affecting the combustion process or explosion venting including ignition position, vent area, must be given attention and the extreme condition considered. It is obvious that worst-case ignition position is still inconclusive, and other areas of research interest including the effect of external explosion as mentioned in earlier.

10.   The venting standards assumed the use of single or multiple vent of total equal size would give the same results. Also, the shape of the vent has no influence on the outcome of explosion venting. All these design rules need to be investigated and assumptions verified. Other design rule including the position of the venting relative to the natural flame propagation path needs to be investigated.

11.   Influence of reactivity is an important aspect of gas explosion vent design. It is important to estbalish the relative influence of reactvities for different gas mixtures, as this was not adequately accommodated in the current european standard.

12.   Most gas explosion venting data considers only few vent areas for investigation and this may not be applicable to different vent sizes. Investigating wide range of vent areas would give better understanding of the physics of explosion venting process.

13.   The Laminar flame venting theory was shown to be a good predictor of explosion venting data, but varies depending on the turbulent enhancement factor. It is important to apply the laminar flame model to small scale and free venting in order to verify the applicablility of the model for explosion venting design.

In view of the above, there is the need to address these limitations and some other areas of research interest as discussed in this chapter. Hence, the present work as reported in this thesis intends to give closer look at these challenges in the subsequent chapters in line with the objectives of the work for better safety.

2.7 Aims and Objectives of the Study

2.7.1 Aims

The aim of this work was to produce a better physical understanding of the venting process and the parameters for explosion venting modelling. To also investigate the problems with current design procedures and provide a large body of new vented explosions data.

2.7.2 Objectives of the study

The main objective of this work is to investigate and generate new experimrntel data on the hazard associated with premixed explosions by application of venting technique in small and medium scale geometries. In this regard, the research will focus on:

➢ Carrying out explosion venting using small and medium scale geometries with free venting (initially uncovered vent), where self-acceleration of flame and vent flow turbulence is unlikely to occur. This will separate turbulence generation as a result of venting from self-acceleration associated with large scale venting. The main result from this work would be compared with large scale experimental results and the vent design correlations of venting standards, the literature and the spherical laminar flame model.

➢ To investigate the vent area by comparing variation of vent areas, different vent shapes and single with multiple vents, and different ignition locations. This is to determine how these factors affect the explosion overpressure and flame speeds in explosion venting.

➢ Investigate the influence of static burst pressure for different material with P_{stat} <0.5bar in comparison with initially uncovered or free venting. In addition, to study the phenomena of external explosion and the relationship with internally generated pressure.

➢ Determine the influence of mixture reactivity in explosion venting by carrying experiment with different hydrocarbon and hydrogen to air mixtures.

➢ The relationship between the internal generated pressure and the external combustion is also of concern and needs to be addressed. Analysis of the parameters upstream and downstream the vent would help in this aspect.

➢ Generate new experimental data on explosion venting of hydrogen-air mixtures for 30% and 40% concentrations, and compare the result with the current venting standards.

CHAPTER 3

Experimental Methodology

3.1 Introduction

3.2 Equipment and Facilities

3.3 Equipment Design and Geometry Construction

3.4 Design of Vent and selection of Vent cover material

3.5 Equipment and Instrumentation

3.6 Experimental Procedure and Technique

3.7 Hazard Identification and Safety Procedure

3.1 Introduction

The nature of hazard associated with explosions requires a robust facility that can accommodate it dynamics and other safety concerns, hence the choice of location and facility for this area of research was a key factor for it success. The indoor explosion facility, which commenced operation on 4th March 1997, has two compartments separated by concrete wall as shown in Figure 3.1. The first compartment, which was the control room, comprises of the computer system with the software for capturing data, the filing system with record of all the test carried out, documentation for all equipment in the Lab and reference materials. Also in this section are the ignition button connected to the ignition system, the sequence generator connected to the test vessels and other computer systems for general use. The hardware data logging system, which has the instrumentation connected to it, was connected electrically to the computer system in the control room. Test vessels, and all other equipment used for various explosion tests are all located in the second compartment. The concrete wall between the compartments was installed for safety purpose. Apart from separating the test area from the control room, it was part of a safety interlock system. This interlock system was connected to the ignition systems linked to the access doors to the main test room, and these doors must be properly locked for any test procedure to be completed. This helps to achieve the overall safety of the test procedure, which will be explained in more detail later.

The equipment used for this research was adopted from previous work carried out in this facility, and this to a very large extent influenced the direction of work reported in this thesis. This was because equipment used was designed with high flexibility to accommodate range of explosion scenarios without compromising safety. Furthermore, the availability of large dump vessel in this indoor explosion facility makes it possible to demonstrate the practical application of explosion venting into the atmosphere as obtained in the industries. In view of the above, present study involves the vented explosions of gaseous mixtures with different vent sizes and length to diameter (L/D). Hence, the use of dump vessel was necessary to accommodate wide range of explosion venting scenarios presented in this thesis and duct venting which is not included in this work.
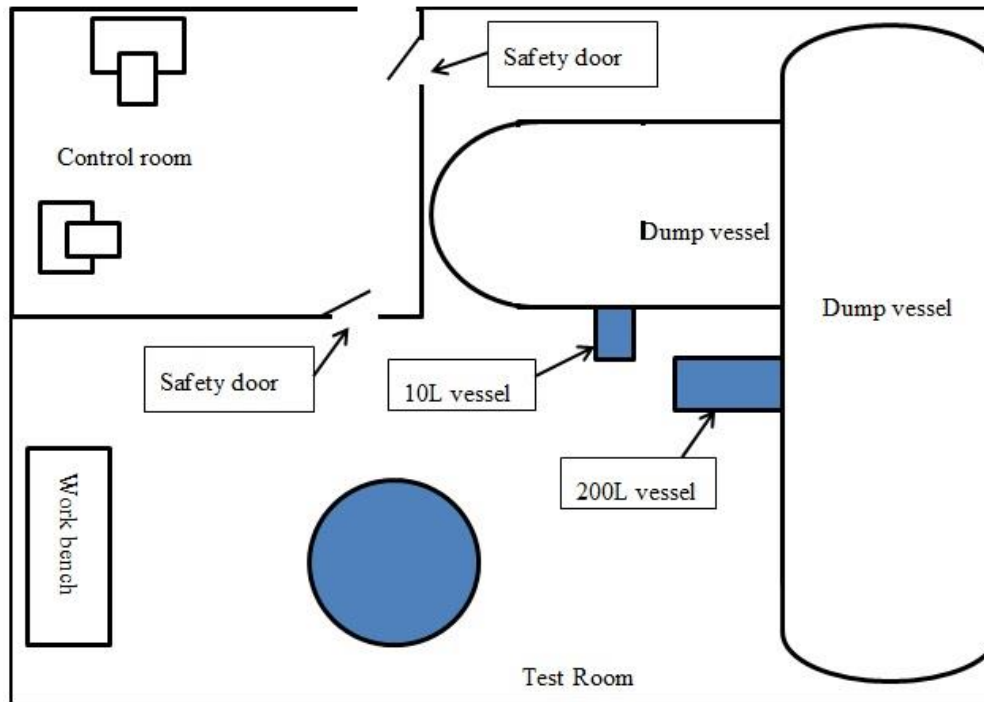
Figure 3.1 Schematic Diagram of Test Facility

3.2 Equipment and Facilities

3.2.1 Factors Affecting The selection of Geometry

3.2.1.1 Test Geometry

The vessel characteristic including the dimensions and shape are important factors affecting the maximum overpressure in closed vessel explosion and reduced pressure in explosion venting(Andrews and Phylaktou, 2010). Most vent design correlations in the literature including the venting standards of NFPA 68 (NFPA68, 2007) and the European Design guide (BS EN 14994, 2007)for gas explosion venting do not accurately accommodate the influence of vessel volumes. Most large scale experiments used to correlate the vent design equations including the venting standards, considered centre ignition location and use spherical, cubical or rectangular vessels, with limited data on cylindrical vessels.   Hence, the use of cylindrical vessel has become imperative. Furthermore, the objective of this work and other factors as motioned above influenced the choice of vessel type. In this regard, two different cylindrical vessels were considered for vented explosions including Test Vessels 1 and 2 as the geometries in this work. The first geometry (Test vessels 1) had diameter of 0.162m with length of 0.46m, while test vessel 2

had a diameter of 0.5m and 1m long. For all the vessels, bosses were drilled and tapped around each vessel section to allow for instrumentation, where additional instruments when necessary. All vessels were connected a 0.5 diameter vessel of 0.5m length to allow for instrumentation downstream the vent in line with the objective of this research.

All the geometries used for this work were existing vessels with little modifications to meet current challenges and objective of this project, without comprising the functional requirement of the vessels and safety in general. In view of this, the following were considered:

1. This work aimed to investigate the dynamic of flame propagation and mechanism of pressure generated during vented explosion. The instrumentation within the vessel will allow for analysis of the pressure and flame speed upstream the vent. Furthermore, the attached 0.5m diameter vessel after the vent gives the flexibility of analysing the flame speed and external explosion downstream.

2. All vessels used are pressure rated between 25 to 35bar; this was within the range of deflagration explosions pressure of the gas mixtures considered in this work. However, the vessels were also capable of withstanding some potential detonation which may occur with some of the gas mixtures used.

3. The flexibility of the existing vessels to accommodate different explosion scenarios in order to meet more realistic industrial set up was a key factor.

4. All vessels used complied with the limit of compact vessel of L/D=2 as prescribed by the NFPA 68 2007and the European standard at the commencement of the project. However, the vessels were also in compliance with the new NFPA 68 2013 which accommodates L/D=5.

5. Most of the existing vessels were made of Austenitic Chromium-Nickel (low-carbon) stainless steel construction (304L). The choice of the material was influenced by it high anti-corrosion properties and a better stress characteristics when compared to mild steel pipes.

6. A cylindrical vessel shape gives more uniform distribution of shear wall stress due to internal pressure rise. In addition, there was ease in the manufacture and construction of this shape of vessel as compared to other vessels.

3.2.1.2 Dump vessel

In the design of the explosion vents for industrial use, the position of the vent matters, and the burnt gases and other product of combustion must be directed to safe direction in order prevent harm to people and structures as specified by the standard (NFPA68, 2013). Hence, the availability of the dump vessel in this facility for safe capture of vented gases was a key factor in achieving explosion venting at laboratory scale. The vent end of the test vessel connects to the dump vessel through flange openings on the dump vessel to accommodate safely the vented products of combustion, until these products were later purged out. This geometry was design with flange openings with varying diameter of vessels to be connected and this was able to match all the existing test vessels. Furthermore, the vessel was designed such that pre-test conditions both inside and outside the test vessels could be controlled. In this regard, other factors also influenced the design and use of the dump vessel as follows:

1. The flange openings where made to accommodate the diameters of the test vessels and consideration was also given to the length of vessel to be used in relation to the space within the test room/other independent test vessels.

2. Blank flanges were made available to cover the openings not been used at any time in order to have all openings sealed not to allow the escape of vented gases into the test room.

3. The flange openings were made with high flexibility to accommodate different explosion scenarios and vent vessel sizes to meet desired objectives.

The size and other dimensions of the dump vessel was made to safely and sufficiently contain the vented gases with negligible or no effect on the explosion overpressure or other parameters in the main test vessel. Furthermore, all the

existing test vessels for explosion venting were relatively small as compared to the size of the dump vessel such that the dump vessel sufficiently simulates venting into the open atmosphere as obtained in the industries. The ideal gas law was used as bases for the design of the dump vessel based on the relationship of dump vessel with test the vessel(Gardner, 1998). The influence of combustion of hydrocarbon in the test vessel (V_t) and vented gases into the dump vessel (V_d) could increase the total pressure in the combine total volume (V_T) as given in equation 3.1,

$$V_T = V_t + V_d \qquad\qquad\qquad [3.1]$$

Assuming that adiabatic combustion at 1 atm constant pressure and adiabatic expansion factor of 7.5, then the burnt gas volume (V_b) in equation 3.2 is,

$$V_b = 7.5V_t \qquad\qquad\qquad [3.2]$$

And the ideal gas laws applied as shown in equation 3.3-3.5 gives,

$$P_2 = P_1 \frac{V_1}{V_2} \qquad\qquad\qquad [3.3]$$

Where, P_1 = absolute pressure prior to combustion (1 atm), P_2 = absolute pressure after combustion (atm), V_1 = system volume after combustion ($V_T = V_t + V_d$)(m^3), V_2 = system volume before combustion ($V_T = V_t + V_d$)(m^3). When this is applied to this work, we obtain:

$$P_2 = 1 \times \frac{7.5V_t + V_d}{V_t + V_d} \qquad\qquad\qquad [3.4]$$

Hence, after combustion of the fuel mixture the total system pressure becomes,

$$P_2 = \frac{6.5V_t}{V_t + V_d} \qquad\qquad\qquad [3.5]$$

It is necessary to calculate the total system pressure after the combustion for each test vessel connected to the dump vessel.

3.3 Equipment Design and Geometry Construction

The flexibility use of the dump vessel and other factors as outlined in the previous section were vital in determining use of both the test and dump vessels for explosion venting. However, some adjustments and configurations were made in order to achieve the main objective of the current work. Two different test geometries were used for this work, Test vessels 1 and Test vessel 2. All the vessels were connected

to the dump vessel to the appropriate flange openings for the diameter size of the vessels, and cranes were used to support the test vessels at the centre line. The details of construction of the test vessels and dump vessel to be later discussed in more detail.

(a)
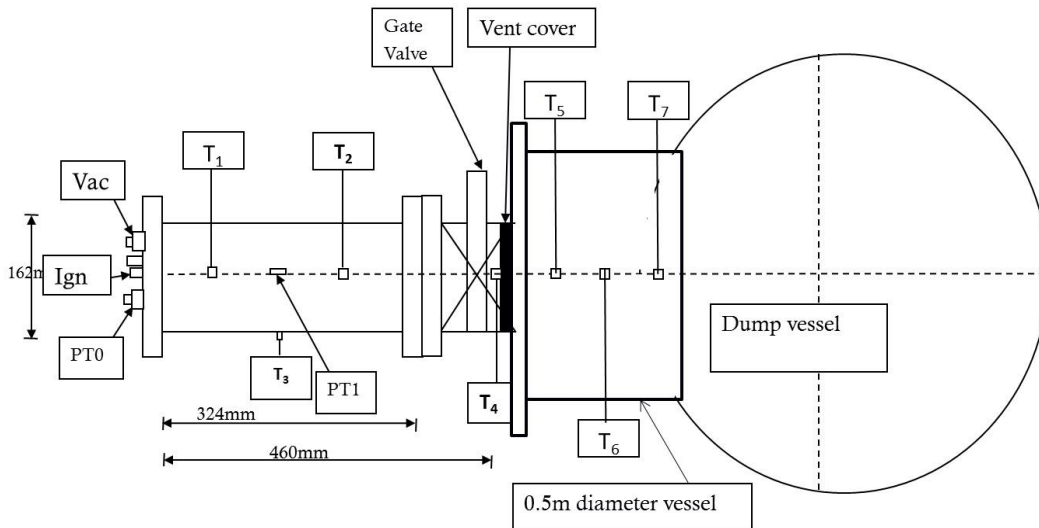
Legend

Connection point for purging =	**Vac**	
Ignition Spark Position	=	**Ign**
Pressure Transducers	=	**PT0, PT1 and PT2**
Thermocouples	=	$T_1, T_2, T_3, T_4, T_5, T_6, T_7$

Figure 3.2 Schematic diagram and setup for Test Vessel 1

3.3.1 Test Vessel 1

All test vessels used for this work were existing vessels of cylindrical shape with simple design to aid the analysis of flame propagation. Test vessels 1 was made from cylindrical pipe section with the diameter of 0.162m and lengths of 0.46m. It was designed to BS EN 1759 requirement, with 35.5 bar pressure rating as this could accommodate high overpressure from deflagration of the fuel mixture used or possibly detonation pressure (BS EN 1759-1, 2004). It was manufactured from

rolled welded stainless steel along its length and slip-on flanges welded on at each of the pipe diameter to support connection to dump vessel or blank flange. Along the vessel length are also drilled tapped bosses, which allow pressure transducers and thermocouples to be connected. A removable blank flange, which is used to close one end of the vessel, was also drilled at the centre to allow for the spark plug to be tapped and provisions for other auxiliary fitting connections or pipe work.

In order to achieve part of the objectives of this project, different size orifice plates were used as vent areas. The orifice plates were positioned before or after the gate valve depending on the scenario. Test vessels 1, can be adjusted to form another vessel by changing the position of the vent opening, which makes a lot of difference. When Test vessel 1 has the vent before the gate valve the length to 0.32 with L/D=2, while with the vent after the gate valve, it increases the length to 0.46m with L/D of 2.8 as shown in Figure 3.2. Table 3.1 gives more details on the dimensions of the vessel.

3.3.2 Test Vessel 2

Test vessel 2 was a bigger vessel as compared to the other test vessels motioned above. This geometry was a cylindrical vessel of 1m length and 0.5m in diameter (L/D=2). The vessel was constructed by rolling and welding of 12.7mm thick steel layer along the 1 m length, and was manufactured by Veirod and Woods Ltd, Leeds (Gardner, 1998). It had slip-on flanges welded on at both ends of the pipe. Furthermore, a number of bosses welded and tapped along the length of vessel to accommodate the use of thermocouples, with an additional boss specifically for spark plug when the central ignition location was required. A removable blank flange was attached at one end of the vessel, drilled and tapped to accommodate instrumentation and other fittings, while the other end with the vent, was connected to a vacuum gate valve. At the open end, the vacuum gate valve also connected to a 0.5m x 0.5m vessel before the dump vessel. This vacuum get valve was required to separate the main test vessel from the dump vessel and allow for preparation of the gas mixtures prior to ignition. Test vessel 2 as shown in Figure 3.3a and 3.3b was meant to scale up size of the Test vessel 1 up to 20 times and Table 3.1 gives more details on the design of the vessel.

(a)

(b)
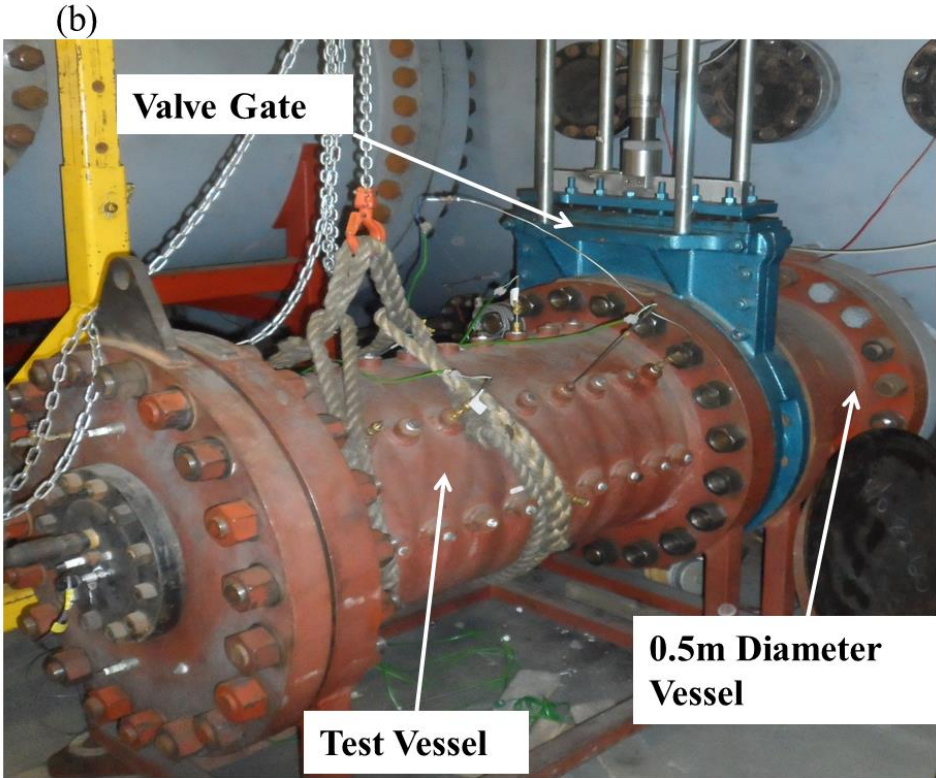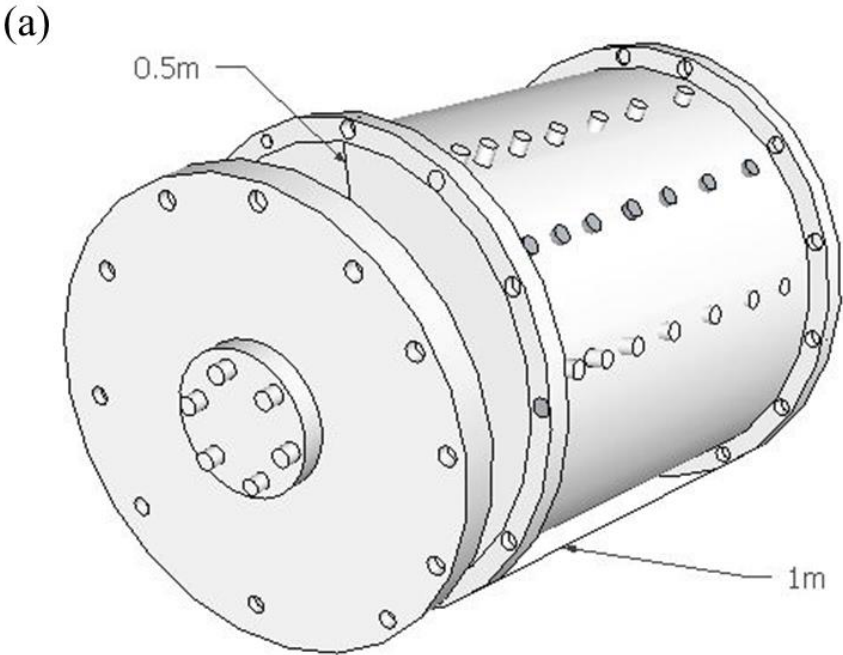
Figure 3.3 Schematic Diagram and Setup of Test Vessel 2(a) Schematic (b)
Photograph

Table 3.1 Design Details for Test Vessels

Description	Test-vessel 1	Test-vessel 2
Pipe sections		
Internal diameter (nominal) (mm)	162	482
Section length (nominal) (m)	0.46	1
Wall thickness (mm)	3.4	12.7
Design pressure (bar)	35.5	28
Flanges		
Class (BS1560, 1970)	300	300
Flange Thickness (mm)	36.5	68
Number of bolts	12	20
Bolt-hole diameter (mm)	22	42
Bolt-hole PCD (mm)	269.9	670
Diameter of bolts (mm)	19	38
Assembled test-vessels Hydraulic pressure rating (baro)	30	40
Length to diameter ratio (L/D) Volume, V_t (m^3)	2.8	2
Ratio of total system volume to test-vessel volume, V_T/V_t	0.010	0.2
System overpressure due to adiabatic combustion, P_{sys} (mbar)	486	19

3.3.3 Dump Vessel

The dump vessel was design in order to carry out vented explosion within the indoor facility thereby simulating explosion venting in to the atmosphere as applicable in the industry. It allows for safe explosion venting to contain the burned and unburned gases ejected from the vented end of the main test vessel, until later purged to the open atmosphere at the end of the test for the day. The design of the vessel was such that flange openings were made to accommodate variety of test vessels to be used for explosion venting. The flange openings were made to fit the diameters of existing test vessels and other test vessels yet to be made.

The vessel was constructed from a rolled steel plate with 15mm thickness, was design, and manufactured by Hustlers of Yeadon Ltd. It was designed to

specification and the design was restricted or limited by the space available within the test facility. The cylindrical shell vessel was constructed within the test facility and due to the limitation of the room size, a total length of 8m; diameter of 2.5m and total volume of $40m^3$ was finally obtained. More details on the dimensions of the vessel as given in Table 3.2 and the specifications were based on the governing standards (BS EN 1759-1, 2004, BS EN 1092-2, 1997).

In order to monitor the conditions within the dump vessel, instrumentation ports were fitted to accommodate pressure transducers and thermocouples at different locations of the vessel to suit different scenarios. For this work, the pressure transducer in the dump vessel was used to monitor and ensure that there was no pressure build-up. Some of the fittings were tapped with bosses at the side of the dump vessel back wall opposite the position of the test vessel and some other on the front wall same side as the test vessel.

The flange openings were numbered from N1 to N5 with different vessel flange openings as shown in Figure 3.4 and other details in Table 3.2 One of the two large openings with diameter 1.5m on the right side was fitted with a blank torispherical dished end , while the left side had two 3m long and 1.5m diameter vessels connected, thereby increasing the total size of the dump vessel to $52m^3$. This extra $12m^3$ side of the dump vessel also has two flange openings of 0.5m diameter each and one of the openings was used for this work, where Test Vessels 1, was connected through 0.5m diameter vessel. All other flange openings in the dump vessel and it extension were covered (sealed) with blank flanges when not in use so as to prevent any interconnection vessel effect or allow the safe containment of the vented gases. Also, pipe work were connected to the dump vessel to allow the purging or evacuation of vented gases and ball valves were used to isolate connected ancillary equipment from the dump vessel prior to ignition of the main test vessel. Before the dump vessel was commissioned, a certified hydraulic pressure testing was carried out by pressurising the water-filled dump vessel to pressure up to 11.25bar.
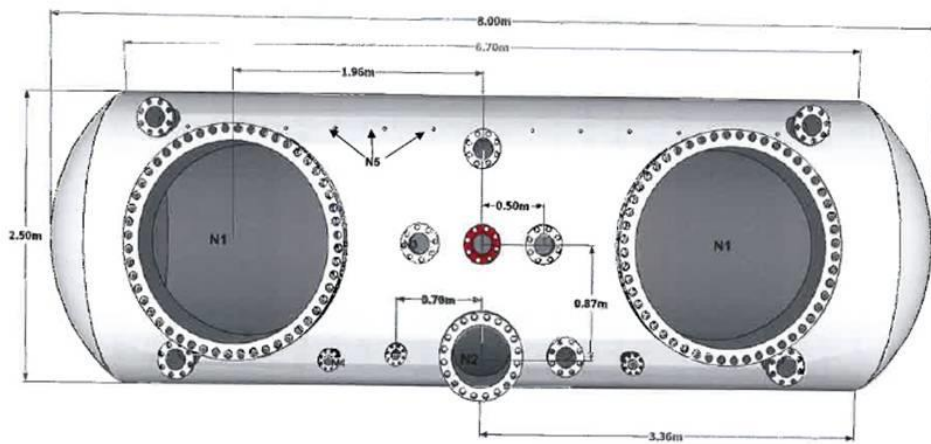
Figure 3.4 Schematic Diagram of the Dump Vessel(Willacy, 2008)

Table 3.2 Dump vessel design details

Section					Dimension	
Shell						
Internal diameter: (mm)					2470	
Length: (mm)					6720	
Shell thickness: (mm)					15	
Torispherical (2:1) Dished Ends						
Outer diameter: (mm)					2500	
Nominal plate thickness: (mm)					10	
Assembled structure						
Total Length: (mm)					8000	
Design Pressure: (bar)					9.0	
Certified pressure (hydraulic test) (baro)					11.25	
Flanged Openings						
Type	**Nominal bore**	**Neck thickness**	**Flange**	**Number of bolts**	**Bolt-hole PCD (mm)**	**Rating**
N1	1524 mm O/DIA	20 plate	Special	52	1759	Special
N2	508 mm O/DIA	10 plate	RFSO	20	635	BS 4504 40/3
N3	162 mm	SCH 40	RFSO	12	269.9	BS 1560 class 300
N4	76.2 mm	SCH 40	RFSO	8	168.3	BS 1560 class 300
N5	¼″ BSP	COUPLING			-	Special

3.4 Design of Vent and Selection of Vent Cover Material

3.4.1 Vent Design

In explosion venting, the area of the vent is an important parameter in determining the severity of explosion. For this research work, circular orifice grid plates were used as vent areas, placed at the open end of the test vessels connected to the dump vessel. The position of the vent was made adjustable such that the disc plate could be replaced to vary the vent area or to accommodate other scenarios. The grid plates were made of single and multi-hole orifice with different vent areas. Majority of the grid plates were circular in natures with few square vents orifice plates used to investigate the effect of shape of the vent or discharge coefficient.

For Test Vessel 1, the grid orifice plates used was a solid steel metal sheet circular in nature and metal thickness (t) of 3.2mm. The vent opening was defined in terms of orifice plate blockage ratio (BR) which relates to ratio of the block area to the total area of flow. For single-hole grid plate, the BR can be obtained from equation 3.6.

$$BR = 1 - \frac{A_h}{A} \qquad\qquad [3.6]$$

Where $A_v = $ cross-sectional area of the orifice.

For a vent of multi-hole grid-plate with holes of equal diameter,

$$BR = 1 - N_h \left(\frac{d_h}{D}\right)^2 \qquad\qquad [3.7]$$

where $N_h = $ the number of holes, $d_h = $ hole diameter and D= diameter of the approach to open flow (diameter of test vessel).

For this work, single-hole circular grid plates of BR 0.2 to 0.9, multi-hole and square-hole vents of BR of 0.4, 0.6 and 0.8 were used. In addition, BR 0.3-0.9, were considered for Test Vessel 2 including the single and multi-hole grid plates. For the multi-hole grids, the measured width of solid material between holes varies for individual plates and the average value was obtained and used as the obstacle scale 'b'. This value can also be obtained in the single-hole grid plate when viewed as part of an imaginary larger arrangement with the b given as (D-d_h). Other important parameters associated with the grid plates were the aspect ratio (t/d) and the pressure loss coefficient K, Table 3.03 gives more details on the grid plates used for Test

vessel 1 and 2. But for analysing the data, the vent coefficient ($K_v = \frac{V^{2/3}}{A_v}$) was preferred to using BR for the purpose of standardization of the vessels and Figure 3.5 shows samples of the orifice plate.

Figure 3.5 Sample of different configuration of the vent orifice Grid-Plates

3.4.1 Vent cover material

Different vent cover materials were used for explosion venting on Test vessel 1. The selection of the vent cover was based on the limitation of P_{stat} between 50-200mbar. In this regard, four vent cover materials were used and given nomenclature of A1, A2, A3 and A4 based on the value of P_{stat}. These values were determined experimentally by introducing compressed air gradually into the vessel as specified by the vent design standard (NFPA 68, 2013). The vent material was clamped between two steel plates before it was placed at the open side of the test vessel during the experiment.

Table 3.3 Details of the orifice grid plates

TEST-VESSEL 1				
Shape	**BR**	**N_h / N_b**	**t/d**	**b (mm)**
Multi-holes	0.4	4	0.051	15.5
	0.4	16	0.1	7.2
	0.6	4	0.062	25.3
	0.6	16	0.13	11.7
	0.8	4	0.088	38.8
	0.8	16	0.18	20.1
Single-hole	0.9	1	0.062	110.8
	0.8	1	0.044	89.6
	0.7	1	0.036	73.3
	0.6	1	0.031	59.6
	0.5	1	0.028	47.5
	0.4	1	0.026	36.5
	0.3	1	0.024	26.5
	0.2	1	0.022	17.1
	0.1	1	0.021	8.3
TEST-VESSEL 2				
Shape	**BR**	**N_h / N_b**	**t/d**	**b (mm)**
Single-hole	0.9	1	0.021	153.7
	0.8	1	0.015	217.3
	0.7	1	0.012	266.2
	0.6	1	0.010	307.4
	0.5	1	0.009	343.7
	0.4	1	0.009	376.5
	0.3	1	0.008	406.6

3.5 Equipment and Instrumentation

The analysis of explosion phenomena requires robust set of equipment and high speed measurement techniques to be able to withstand it dynamics. Hence, the choice of the right and appropriate equipment are key factors in this work, and some set of equipment were chosen bearing in mind the dynamic nature of the explosion phenomena and explained in more details later. Some of the key parameters analysed in this work were the speed of the propagating flame and the pressure generated in this process. The pressure was measured by set of pressure transducers and the thermocouples measured the time of flame arrival at different location during propagation. All pressure transducers, thermocouples and other ancillary

equipment were connected to the main test vessel through tapped bosses as mentioned earlier. Another important aspect explosion analysis which is flame visualisation technique to monitor flame propagation, but safety consideration ruled out optical access of the vessels for photographic study. However, the available instrumentation was maximised to assist satisfactory analysis without compromising safety as discussed in more details subsequently.

3.5.1 Thermocouples

The exposed junction mineral insulated type-K thermocouples were used to measure the time of flame arrival as it propagates towards the vent. These thermocouples supplied by TC Ltd UK have shaft of 3mm in diameter and the exposed conduction wire was 0.5mm in diameter and the thermocouples were positioned axially along the centreline of the test-vessels. All the test vessels were fitted with thermocouples and were connected through the tapped bosses on the walls of the vessels sealed with threaded Swagelok compression fittings. Furthermore, each thermocouple was connected to the data acquisition system through a standard thermocouple cable extension and the cables conforming to BS EN 60584 (BS EN 60584-3, 2008).

Table 3.4 Type K thermocouple margin of error and response time

Temperature (^{o}C)	Tolerance		Average Response Time
	^{o}C	%	
-200 to -110	± 2	0.75	0.03 sec
-110 to 0	± 2.2	0.75	0.03 sec
0 to 275	± 2.2	0.75	0.03 sec
275 to 293	± 2.2	0.75	0.03 sec
293 to 1260	± 2.4	0.75	0.03 sec

When taking measurement, the sudden temperature rise on the output of the thermocouple indicates the time the flame arrives at the thermocouple. These thermocouples have large thermal lag due to the 0.5mm thermocouple bead used and that makes it unsuitable for use for temperature measurement. However, there was no obvious dead time in the thermocouple response and can withstand explosions, hence, was considered suitable for this purpose. Furthermore, the use of

thermocouple was a more logical option when gases like hydrogen was used as compared to the ionisation probes or UV detectors. Table 3.4 gives the average response time and the margin error for the standard mineral insulated exposed junction Type K thermocouple as obtained from the manufacturers (TC Limited).

The impact from high gas velocity flow was likely to cause high dynamic loads and considering that the thermocouples were located through the wall to the centre line, there was the need to ensure the position integrity of the thermocouples through the test. In this regard, the shaft of the thermocouple was reinforced with a 5mm steel sheath with some modification to hold the support in place by Swagelok fittings from outside the vessel. Also, at least 20mm gap was given between the reinforced sheath and the exposed tip of the thermocouple. This approach was adopted on all the test vessels used for this work with Figure 3.6 showing a model of type-K thermocouple and the support.

Figure 3.6 Model Type K Thermocouples and the Support

3.5.2 Pressure Measurement

As part the instrumentation for all test vessels to achieve the objective of this work, it was necessary to get robust equipment to measure the fast explosion pressures, while keeping the integrity and sensitivity of the equipment. For this work, Keller type pressure transducers were employed to measure internal pressure of all the test vessels during the experiment. The Keller type PAA-11/10bar/800592 piezoresistive pressure transducers with measurable range 0-10bar and a maximum pressure of

15bar were used for Test vessels 1. One of the transducers (PT0) was located at the end flange of the vessel opposite the vent and the second (PT1) was midway the total length of the vessel. Furthermore, a transducer (PT2) was located on the wall of the 0.5m diameter vessel attached to the vessels immediately after the vent in order to accurately measure external explosion and it time of occurrence. A transducer PT3 was located at the end wall of the dump vessel extension were the test vessel was connected in order to measure the pressure pile up in the dump vessel.

For test vessel 2, also five Keller type-PAA/11 piezoresistive pressure transducers were used at similar positions as Test vessel 1 in order to achieve same purpose. All the pressure transducers used for the work were highly sensitive with high stability, high water resistance and thermal shock. The transducers were all connected to tap bosses on the wall of the vessels as mentioned above and details of the pressure measurement would be discussed subsequently.

A standard dead-weight calibration method was used to calibrate all the pressure transducers with the transducers connected to the data logging Equipment. This was ensuring that accurate reading was achieved and to eliminate possible error due to connection to an electronic system.

3.5.3 Pressure Monitoring System

The preparation of fuel mixture was carried out accurately in the test vessel using the partial pressure method; hence, there was the need to employ reliable piece of equipment in order to achieve accuracy in this process. A pressure monitoring system the Edwards Barocel Pressure sensor type 600AB Trans 100MB was used to enable the accurate measurement of the vacuum pressure within vessel. The unit with 0.15% accuracy was connected to the test-vessel through the fuel line to monitor the fuel pressure at all times during mixture preparation. Its operating principle was to transduce absolute vacuum pressure into dc output voltage precisely proportional to input pressure. An Edwards's diametric type 1500 digital display with reading accuracy of ±0.05 was connected to the Barocel. For example assuming the final pre-ignition pressure of 1013mbar, an accuracy of 0.05% could be obtained if a 10% methane-air mixture was to be prepared.

An alternative means of measuring pressure within the vessel in case the pressure exceeds the normal atmospheric pressure by the use of an analogue display gauge pressure with a measurement range of 0 to 2.5 bara. Furthermore, additional two way valve could be connected from the control panel to the test vessel either side of the gate valve, this was a feature that enable the Barocel to measure pressure within the test-vessel and the dump vessel.

3.5.4 Spark Ignition System

The standard combustion engine spark plug of 16J ignition energy was used to ignite the gas mixture in the test vessel. For end ignition (flush), the normal spark plug was used but in order to accommodate other positions within the vessel, the spark plug was extended by welding stainless steel strip of same diameter to the existing electrodes to the length required. And for the extended spark plug, the central electrodes had ceramic beads around the walls and secured firm using electrical tape and this was to prevent multiple parks from other locations other than the designated park gap. Figure 3.7 shows a normal and extended spark used in this work.
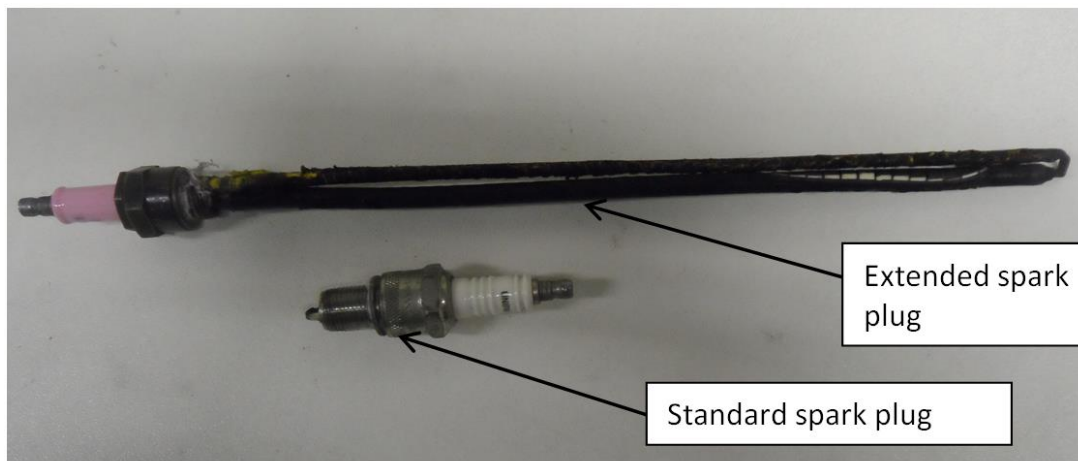
Figure 3.7 The standard and Extended 16 J Spark Plug

Ignition location was determined based on the experimental scenario of choice and this work considered flush end ignition, protrude side ignition and central ignition location for Test vessel 1. For Test vessel 2, only end and central ignition location were used; however, there are other ignition positions previously used which are not considered for this work. The spark energy required was supplied from the

electricity mains and this energy was passed through the spark box which contains capacitors and consistent amount of energy was released upon ignition. To ensure maximum safety which was part of the safety procedure, the ignition system was incorporated into a number of safety features connected to the interlock system. This integrated ignition and interlock safety system as shown schematically in Figure 3.8 was also meant to maintain the integrity of the equipment. Furthermore, the supply of energy to actuate the ignition was only possible if certain criteria were met, and these were:

> ➢ The fuel supply line must be disconnected from the main test vessel.
> ➢ All the interlocking doors must be closed and properly locked.
> ➢ The vacuum gate valve must be open at the point of ignition.

All the above conditions must be met in order to have a successful ignition, as this completes the integrated ignition and interlock safety system circuit. And the ignition was initiated by depressing the fire button in the control room after satisfying all the conditions.
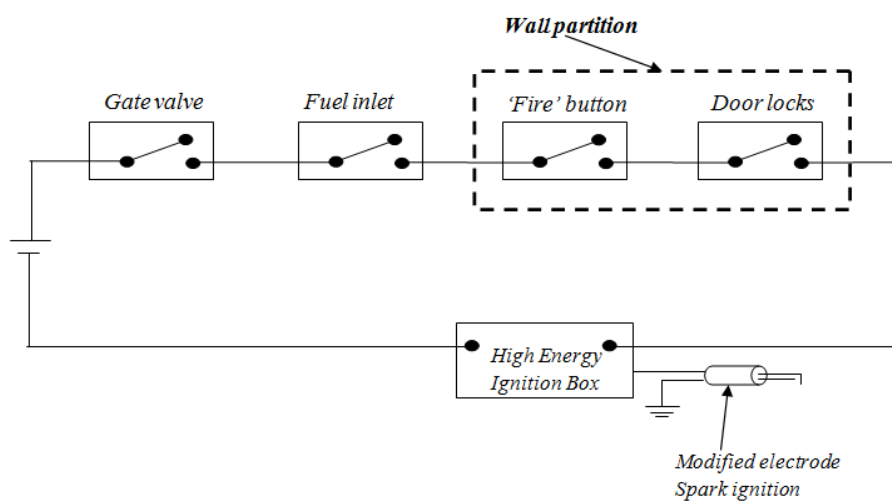
Figure 3.8 Schematic diagram of ignition and interlock safety system

3.5.5 Evacuation System

Evacuation and purging of the vessel was a routine and also an important aspect of experimental procedure for all vessels investigated in this work. For test vessels with smaller volume, vacuum pump A was used to assist fuel mixture preparation and purging out the burnt gases. On the other hand vacuum B was used for similar

purpose i.e the evacuation and purging of Test vessel 2 and the dump vessel. Subsequent paragraphs discussed the vacuum pumps in more details.

3.5.5.1 Vacuum Pump A

The smaller of the two vacuum pumps was vacuum pump A which was an 'Edwards E1M18' single direct drive, rotatory vacuum pump. The pump which had a pumping mechanism of the slotted rotor/sliding vane type, had a nominal displacement rating of 340l/min. It direct-drive was supplied through a flexible coupling from an enclosed motor normally cooled with fan integrated within the system. This pump was operated through an on/off switch on the mixture preparation equipment, and Figure 3.9 shows photograph of vacuum pump A.

Figure 3.9 Edwards E1M18' Vacuum pump A for Test vessel 1

3.5.5.2 Vacuum Pump B

Vacuum pump B was a large pump which has the capability of both working at laboratory level and industrial use for a longer period of time. This was an 'Edwards E2M175' rotary vacuum pump with two-stage, having a nominal displacement rating of 2967 1/min. It has high and low rotor and stator assemblies with sliding vane type pumping mechanism. It also has a direct drive, but this drive was provided via a flexible couple made up of a four-pole, three-pole motor to IP54 enclosure ring. An electric isolation valve was used to control the water cooling of the pump from the mains supply as shown Figure 3.10 In order to allow recycling of the oil and to prevent spilling of oil within the room, oil filter was fitted to the side of the

pump which was changed periodically during maintenance. Soft starter button and isolation valve from the mains was used to operate the pump.

The pump was used for the purging and evacuation of most test vessels through hose connections to the network of pipe works within the facility. Individual vessels were attached with flexible vacuum rated one inch diameter pipes, which were also connected to Vacuum pump B through one inch diameter pipes. Furthermore, the evacuation and purging of dump vessel were achieved by connecting the vacuum pump to the dump vessel through two inch pipes with ball rated valves to regulate flow.
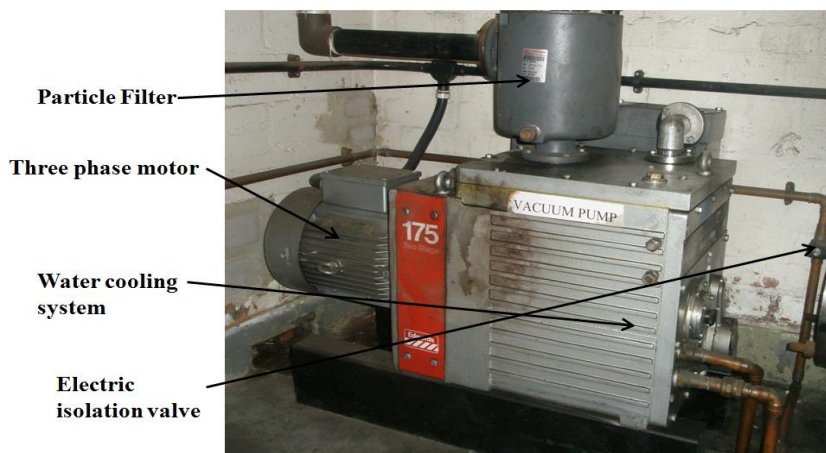
Figure 3.10 Edwards two stage high vacuum pump

3.5.6 Fittings, Pipe network and Valves

A network of piping was carried out to assist the activities within the facility without compromising safety. All pipe fittings and valves were put in place to suite different purposes with little adjustment to accommodate changes when required. The evacuation and purging of the smaller vessel (Test vessel 1) were carried out using vacuum pump A, through a 12.7mm copper pipe which was sufficient for the purpose. While, purging and evacuation of other larger vessels and the dump vessel, was through 25.4mm and 50.8mm pipes respectively using the vacuum pump B. Furthermore, a network of one inch pipe work allows the Vacuum pump B to be connected to test vessels within the facility via flexible hoses. The one inch rubber hose has 25.4mm ball valve used for isolation during evacuation of the test vessels. Similarly the 50.8mm pipe connecting vacuum pump B and the dump vessel also provides a 50.8mm ball valve for the purpose of isolation.

The control panel of the fuel mixing and pressure monitoring apparatus has a whitey four way valves used for selection either fuel, ambient air or compressed air required to be injected into the vessel. Also available were different whitey ball and needle valves to aid regulation of flow and for isolation purposes. On the fuel line, a flexible stainless still pipe of 6.4mm diameter was used to inject fuel into the vessel. Furthermore, a similar construction was made for the pressure monitoring line, which also monitors the fuel pressure with a flexible 12.7mm pipe. Both lines were connected to the vessel through a Swagelok click-lock fitting on the access point provided on blank flange of the vessel, which were disconnected prior to ignition. When introducing compressed air to the test vessel, 6.4mm diameter nylon pipe was used from a 4bar line through the control panel. All access ports on the vessel were provided with either a 12.7mm or 6.4mm pressure fittings including adaptors and connectors, with the relevant Swagelok ball valves and other fitting for control and isolation during injection.

3.5.6 Vacuum Gate Valve

For this work, two different vacuum gate valves were used in order to isolate the vessels from dump vessel, and to allow for mixture preparation and opened immediately prior to ignition from the control room. For the smaller test vessel (Test vessel 1), a 12 model DN160 (152mm) series vacuum gate valve was used. One-sided 0.162m diameter and length of 0.14, was supplied by VAT Vacuum Products, London. It was constructed from a lightweight aluminium body with Viton seals and has a pneumatic actuator of double acting cylinder provided with solenoid valve with a 4 bar supple feed control. The gate valves as shown in Figure 3.11 were part of the integrated ignition and interlock safety system and managed from the control room.

3.5.7 Data Acquisition System

The nature and dynamics of explosion phenomena requires speed and accuracy in data capture, especially with the highly transient explosion capturing a lot of data within a short period. All the generated data were recorded and processed using set of data logging system comprising the data logger equipment and specialised software known as the wavecap. The wavecap software allows sampling frequency,

before and after sampling times to be varied by synchronising the captured data and the ignition time.
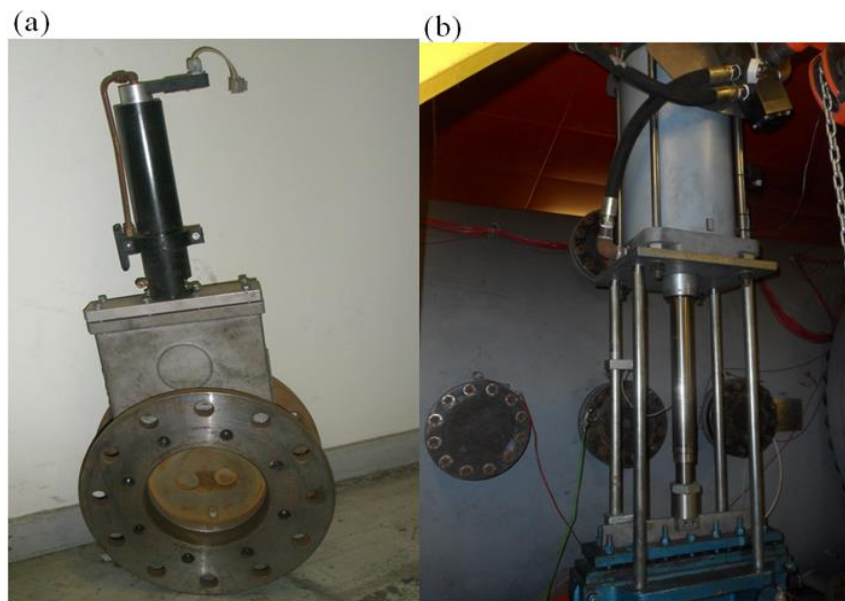
Figure 3.11 Photographs of the vacuum gate valve connected to (a) Test vessel 1-10L vessel (b) Test vessel 2-200L vessel
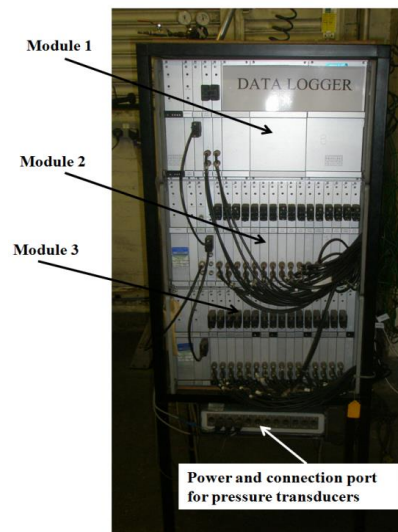
Figure 3.12 Microlink 4000 modular 34-channel data logging system

The outputs of the thermocouples and pressure transducers were recorded by the data logging system through the computer system installed with the Wavecap software and FAMOS software. The data logging system was a 32-channel Microlink 4000 system which was designed to capture high speed waveform with a sampling frequency of 200 KHz per channel with photograph in Figure 3.12. The

wave signals were captured by the data logger and transmitted to Wavecap software in the form of digital signal with a sampling rate of 5000 samples/sec. The Wavecap data was saved in the form of FAMOS outputs and the analyses of the results were also done using the FAMOS software.

3.6 Experimental Procedure and Technique

The experiments conducted were part of a tick box operating procedure which was mandatory to follow for all test vessels. The purpose of using a tick procedure was to ensure that all the steps were followed and also to attain maximum safety of the equipment as well as personnel. At the start of every test, the date, fuel type, test number, concentration of the gas to be used, blockage ratio and the ignition location were indicated. Furthermore, it was important that area around the rig was cleared so as to avoid slip and trip hazard. There were initial procedures which was to turn on all the systems and testing the functionality of the apparatus prior to the experiments. The description of the experimental procedure and the technique used to analyse the flame speed and pressure records are discussed subsequently.

3.6.1 Preparation of mixture

The main gas mixtures analysed in this work were methane-air, propane-air, ethylene-air and hydrogen-air mixtures. Furthermore, the gases were used considering the explosive limits or flammability limits with various concentrations by volume, and only premixed mixtures were used in order to have homogeneous mixture without stratification. The gas was introduced directly into the vessel using the partial pressure method. This was followed by thoroughly induced mixing by fast intake of air from one of the valves. This process of fast injection of air assists in achieving faster homogeneity of the mixture to achieve the required gas mixture concentration for a particular test. This was evident from the repeatability of the test.

Before the gas mixture was prepared, the gate valve was meant to be closed separating the vessel from the dump vessel to allow for the mixture preparation. The ambient pressure in the vessel was noted, the vessel pressure was then evacuated to a very low level before the required fuel was introduced followed by the fast injection of air to the initial ambient pressure. For example if the pre-ignition ambient pressure was 1016 mbar, the required fuel pressure would be 101.6mbar for

10% methane-air mixture (10% of the ambient). The use of ambient pressure not standard pressure was to maintain the same pre-ignition pressure or with minimal difference between the dump vessel and the test vessel. Hence, the final pre-ignition pressure set for all vessel was the ambient pressure for that day and must be recorded in the vessel and dump vessel pressure to mixture preparation for each test.

3.6.2 Ignition and Vessel Purging Procedure

All procedures after gas mixture was prepared were taking with extra safety because of the availability of volatile gas mixture in the test vessel. And high level of safety was enhanced during the ignition procedure with the availability of the ignition and interlock safety system. After preparing the mixture, all isolating valves were closed, and fuel mixture and pressure monitoring lines were disconnected from the test vessel following the tick box test procedure. The ignition box was connected to the spark plug attached to the vessel and turned on from the electricity mains, before all personnel leave the test room to the control room and all doors leading to the control room locked. Furthermore, the data acquisition software was armed with all the lights on the ignition control panel turning on showing the integrity of the safety circuit with the exception of the gate valve opening light. The gate valve was opened immediately prior to ignition with the gate valve opening light as signal to press the FIRE button on the panel. More so, the sampled data was saved once sampling time was over so that the data captured could be viewed using the FAMOS software. The pressure rise and ignition signal on the FAMOS raw data was an indication of successful ignition of the mixture.

After the ignition procedure, the door was opened and the spark system disconnected to begin preparing the test vessel for the next test by first purging the vessel. Depending on the test vessel in use, the vacuum pump A or B was turned on in order to evacuate the remaining gases or burnt gases within the test vessel which begins the purging process. The evacuation was stopped after low vacuum pressure was sufficiently attained, then air was allowed into the test vessel until the ambient pressure was reached. This process was repeated for at least three times to ensure that system matched the ambient air outside the vessel, and the test vessel was then ready for another test. Details of all the experimental tests carried out are shown in Table 3.5 with different test conditions.

Table 3. 5 Details of Experimental tests

Gas Mixture	Concentration (%)	Vessel type	Ignition Location	K_v	BR (%)	Vent Orientation	Vent Condition
Methane-air	10	1	End	2.4 to 21.7	10 to 90	Single centre vent	Free venting
Methane-air	10	1	End	5.4 and 10.9	60 and 80	Single side vent	Free venting
Methane-air	10	1	End	21.7, 7.2, 3.6 and 1	90, 70, 40 and 0	Single centre vent	Vent cover used
Methane-air	10	1	Centre	21.7, 7.2, 3.6 and 1	90, 70, 40 and 0	Single centre vent	Vent cover used
Methane-air	10	1	End	3.6, 5.4 and 10.9	40, 60 and 80	16 vents	Free venting
Methane-air	10	1	End	Closed vessel	Closed vessel	No vent	No vent
Methane-air	10	1	Side	2.4,4.3,10.9 and 21.7	20,50,80 and 90	Single centre vent	Free venting
Methane-air	10	1	Centre	3.1, 5.4 and 10.9	30, 60 and 80	Single centre vent	Free venting
Methane-air	10	1	Centre	closed	Closed vessel	No vent	No vent
Methane-air	10	1	End	3.6, 5.4 and 10.9	40, 60 and 80	4 vents	Free venting
Methane-air	10	1	End	3.6, 5.4 and 10.9	40, 60 and 80	Square vents	Free venting
Propane-air	4	1	End	2.4 to 21.7	10 to 90	Single centre vent	Free venting
Propane-air	4.5	1	End	2.7 to 21.7	20 to 90	Single centre vent	Free venting
Propane-air	4.5	1	End	Closed vessel	Closed vessel	closed	closed
Propane-air	4.5	1	Side	2.7,4.3 and 10.9	20,50 and 80	Single centre vent	Free venting
Propane-air	4.5	1	Centre	Closed vessel	Closed vessel	No vent	No vent
Propane-air	4.5	1	End	5.4 and 10.9	60 and 80	4 vents	Free venting
Propane-air	4.5	1	End	Closed vessel	Closed vessel	No vent	No vent

Table 3.4 Continuation

Gas Mixture	Concentration (%)	Vessel type	Ignition Location	K_v	BR (%)	Vent Orientation	Vent Condition
Ethylene-air	6.5	1	End	2.4 to 21.7	10 to 90	Single centre vent	Free venting
Ethylene-air	7.5	1	End	2.7 to 21.7	20 to 90	Single centre vent	Free venting
Ethylene-air	7.5	1	End	5.4 and 10.9	60 and 80	Single side vent	Free venting
Ethylene-air	7.5	1	End	21.7, 7.2, 3.6 and 1	90, 70, 40 and 0	Single centre vent	Vent cover used
Ethylene-air	7.5	1	Centre	21.7, 7.2, 3.6 and 1	90, 70, 40 and 0	Single centre vent	Vent cover used
Ethylene-air	7.5	1	End	3.6, 5.4 and 10.9	40, 60 and 80	16 vents	Free venting
Ethylene-air	7.5	1	End	Closed vessel	Closed vessel	closed	closed
Ethylene-air	7.5	1	Side	2.4,4.3,10.9 and 21.7	20,50,80 and 90	Single centre vent	Free venting
Ethylene-air	7.5	1	Centre	3.1, 5.4 and 10.9	30, 60 and 80	Single centre vent	Free venting
Ethylene-air	7.5	1	Centre	Closed vessel	Closed vessel	No vent	No vent
Ethylene-air	7.5	1	End	3.6, 5.4 and 10.9	40, 60 and 80	4 vents	Free venting
Ethylene-air	7.5	1	End	3.6, 5.4 and 10.9	40, 60 and 80	Square vents	Free venting
Hydrogen-air	30	1	End	2.4 to 21.7	10 to 90	Single centre vent	Free venting
Hydrogen-air	40	1	End	2.7, 3.6, 4.3, 5.4 and 10.9	20, 40, 50, 60 and 80	Single centre vent	Free venting
Hydrogen-air	40	1	End	2.4 and 3.6	10 and 40	Single centre vent	Vent cover used
Hydrogen-air	40	1	Side	2.7,4.3 and 10.9	20,50 and 80	Single centre vent	Free venting
Hydrogen-air	18	1		3.1 and 5.4	30 and 60	Single centre vent	Free venting

Table 3.4 Continuation

Gas Mixture	Concentration (%)	Vessel type	Ignition Location	K_v	BR (%)	Vent Orientation	Vent Condition
Methane-air	10	2	End	2.5 to 17.3	30 to 90	Single centre vent	Free venting
Methane-air	10	2	End	2.9, 4.3 and 8.7	40, 60 and 80	4 vents	Free venting
Methane-air	10	2	End	4.3 and 8.7	60 and 80	16 vents	Free venting
Methane-air	10	2	End	Closed vessel	Closed vessel	No vent	No vent
Methane-air	10	2	Centre	2.5, 4.3 and 8.7	30, 60 and 80	Single Centre	Free venting
Methane-air	10	2	Centre	Closed vessel	Closed vessel	No vent	No vent
Ethylene-air	7.5	2	End	2.5 to 17.3	30 to 90	Single centre vent	Free venting
Ethylene-air	7.5	2	End	2.9, 4.3 and 8.7	40, 60 and 80	4 vents	Free venting
Ethylene-air	7.5	2	End	4.3 and 8.7	60 and 80	16 vents	Free venting
Ethylene-air	7.5	2	End	Closed vessel	Closed vessel	No vent	No vent
Ethylene-air	7.5	2	Centre	2.5, 4.3 and 8.7	30, 60 and 80	Single Centre	Free venting
Ethylene-air	7.5	2	Centre	Closed vessel	Closed vessel	No vent	No vent
Propane-air	4.5	2	End	2.5 to 17.3	30 to 90	Single centre vent	Free venting
Propane-air	4.5	2	End	Closed vessel	Closed vessel	No vent	No vent
Propane-air	4.5	2	Centre	2.5, 4.3 and 8.7	30, 60 and 80	Single Centre	Free venting
Propane-air	4.5	2	Centre	Closed vessel	Closed vessel	No vent	No vent
Hydrogen-air	30	2	End	2.5, 3.5 and 8.7	30, 50 and 80	Single centre vent	Free venting
Hydrogen-air	40	2	End	2.5 to 17.3	30 to 90	Single centre vent	Free venting
Hydrogen-air	40	2	End	Closed vessel	Closed vessel	No vent	No vent
Hydrogen-air	40	2	Centre	2.5, 4.3 and 8.7	30, 60 and 80	Single Centre	Free venting
Hydrogen-air	40	2	Centre	Closed vessel	Closed vessel	No vent	No vent

3.6.3 Flame Speed Analysis

The use of thermocouples for measuring was a technique used and validated by comparing with the photographic technique in a closed spherical vessel at the University of Leeds (Gardner, 1998, Phylaktou, 1993). In this work, thermocouples were arranged axially on the centre line to detect the position of the flame as it propagates away from the spark position. The distinct change in the output of the thermocouples within the test vessel where it shows rise in temperature (Figure 3.13a and Figure 3.13b), indicates the time of flame arrival. This distinct change for each thermocouple was recorded and difference in time between adjacent thermocouple was used to obtain the flame speed between two distinct points. Similarly, there were thermocouples downstream the vent also at the centre line to allow for the calculation of the flame speed downstream the vent before the dump vessel. The flame speeds calculated from these thermocouples were used for analysis of external explosion or secondary explosion. In some cases where the flame was so fast and flame arrival time at all the thermocouples could not obtained particularly the downstream thermocouple. Hence, the time of flame arrival of only the first and last thermocouples could be used to provide an average flame speed through that vessel. The thermocouples upstream and downstream the vents were numbered from T1 to T7 in sequential order along the length of the vessel from the closed end. With the exception of thermocouple T3 which was midway the test vessel to measure the time of flame arrival at the wall of the vessel. Thermocouples T_1, T_2 and T_4 were located on the centreline of the main test vessel, while thermocouples T_5, T_6, and T_7 were on the centreline of the 0.5m dia. connecting vessel. The time of flame arrival was detected from the thermocouples and the flame speed between two thermocouples was calculated and plotted as the flame speed for the midpoint between the two thermocouples. There was also another thermocouple, T_3, located on the wall of the main test vessel to measure the time of flame arrival at the wall of the vessel. These event times are marked on the pressure time results with the thermocouple location, so that the position of the flame when a peak in the pressure time record occurs can be determined. This enabled precise determination of whether the highest overpressure was generated by an external explosion or by the internal flame displacing unburned gas through the vent.

(a)

(b)

Figure 3.13 Thermocouple output traces (a) a typical trace (b) Time measurement

The measured time of flame arrival at the thermocouples were used to calculate the flame speeds between two adjacent thermocouples considering the distance between the thermocouples. Furthermore, the use of this technique using equation 3.9 was adequate for laminar flame within the test vessel before the vent. However, the jet of

flame after vent may enter contraction region particular for the 0.5m extension of Test vessel 4, the flame was seen recording randomly on the thermocouples without order. This was as a result of the high flame speed of the jet and also reactivity within that region. In this regard, two clear time of flame arrival could be used as the average flame speed within that region.

$$S_f = \frac{x_{T_n} + x_{T_{n-1}}}{t_{T_n} + t_{T_{n-1}}}$$
[3.8]

Where S_f = flame speed, x = the distance from ignition location, t = time of flame arrival at thermocouple T and n = the corresponding number of the thermocouple.

3.6.4 Explosion Pressure Analysis

All the test vessels had threaded bosses tapped to allow the use of pressure transducers to record the pressure history of a particular test. For this work, the explosion pressure was measured using the Keller type-PAA/11 piezoresistive pressure transducers as mentioned earlier in this section. Two of the transducers were connected to the test vessel to measure the internal pressure, while the 0.5m diameter vessel attached to the vessel a transducer to assist recording the pressure records outside the vent. Additionally, a transducer was attached to the wall side of the dump vessel to assist in monitoring the pressure build up within the vessel. All pressure transducers were connected to a different section of the data logging system as the thermocouples. Furthermore, the raw data as captured after every test was viewed and analysed using the FAMOS software.

Most of the pressure traces have reasonable amount of pressure oscillations caused by acoustic noise present within the vessel or the dump vessel, and also has the ignition time at certain point of the trace. The oscillations were eliminated from individual traces by a smoothing function to clearly present this pressure trace. Furthermore, pressure traces were normalised to t=0 and in some cases ambient pressure (P_i) =0 in order to assist in accurate comparisons. There was no difference between the raw pressure trace and the smoothened one, but the smoothened was obtained at the centre of the acoustic frequency. The smoothening principle involved averaging of the trace over a certain time frame. Some of the pressure traces have more oscillations than the others, and experiments with large vent areas and pressure recorded in the dump vessels have higher oscillations. More details of

the various pressure traces are discussed in the result sections. A typical pressure trace for vented vessel with small vent area is shown in Figure 3.14a, while Figure 3.14b shows a typical pressure-time trace from a closed vessel explosion.

(a)

(b)
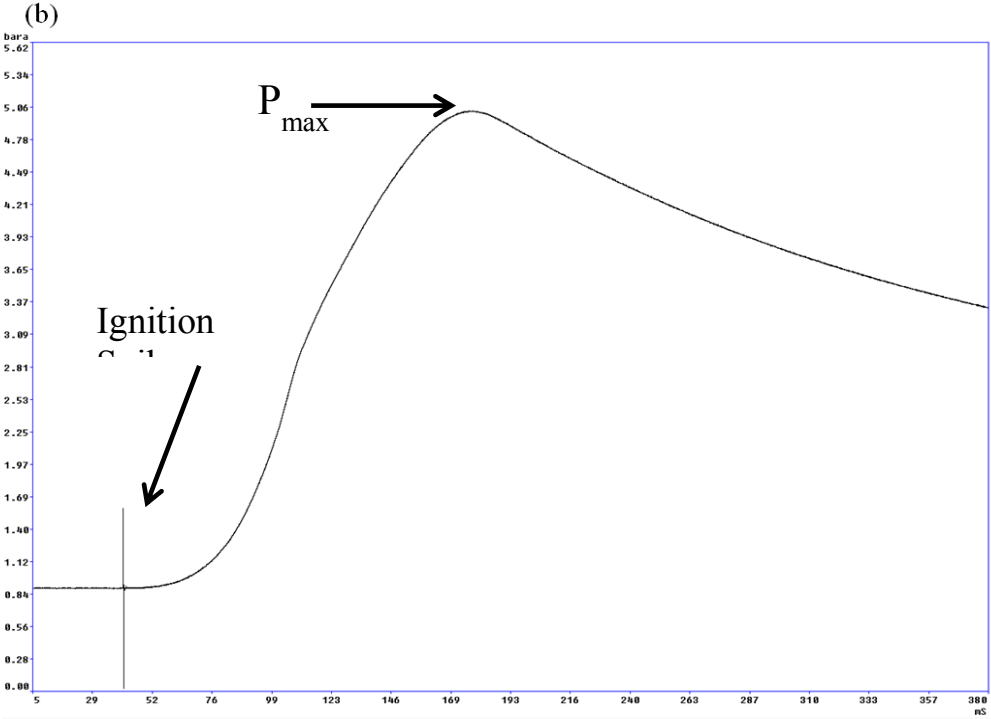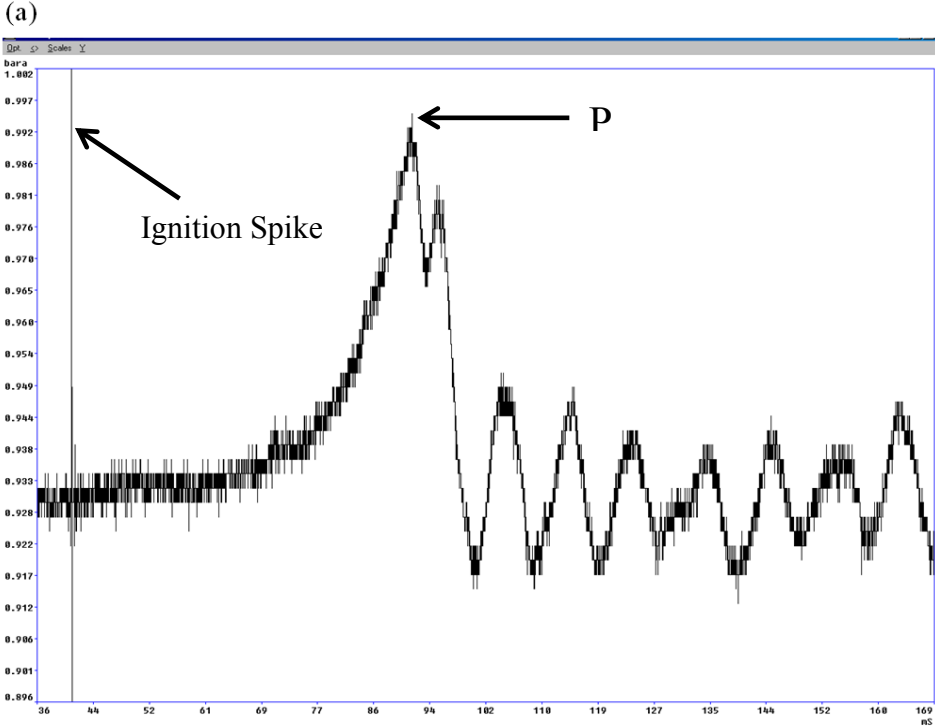
Figure 3.14 Typical of pressure transducer response traces (a) vented explosion (b) confined explosion

3.7 Hazard Identification and Safety Procedure

The safety of the facility, personnel and equipment are integral part of the safety procedures and practice for experimental test carried out in this facility. Each individual test require separate safety procedure, this comprises a safety procedure and hazard identification form for each vessel. Also an approved test schedule was required which must be approved by the managers of the facility. The approved test schedule for individual test scenario includes the gases to be used, the vessel to be used, and the required concentration, vent areas and maximum pressure which must not be exceeded. A tick box safety record sheet was to be strictly followed for each test conducted and every vessel has such record sheet to accommodate the steps through the test. Even though the operating procedure follow similar methods, the procedure was constantly modified and improved to accommodate other circumstances, with total revision between vessels without compromising safety. This section discusses the main safety consideration and other hazard identification, and attached in Appendix 1 and 2 are the hazards identification and step by step tick box record/safety sheet.

3.7.1 Vessel Leak Test

Leaks from the test vessel could be as a result of fittings of vessels not having proper seal, leaks from the tapped bosses or any other part of the vessel. This could lead to the potentially explosive mixture allowed to leak into the test facility which has safety implications and could also reduce the required concentration of the gas mixture within the vessel. In view of the above, leak test were carried any time the vessels were assembled or commissioned and prior to any test. This was done by monitoring the increase in pressure within the vessel while under-vacuumed using the digital barocel. In case of any leak, that is when the rate of pressure rise was above acceptable level for most vessels (standard 2mbar/min), the vessel was pressurised using compressed air and all joints/ fittings were checked for leak using liquid surfactant-water mixture. This process clearly highlights the leak for it to be corrected and re-tested until no leak condition was achieved.

3.7.2 Vessel Failure

All vessels used for this experiment were normally pressure tested and certified to ensure that they could withstand pressure above 8 bars. The 8 bar pressure used was the maximum overpressure that could be obtained for most gas mixtures with the initial pressure of 1 bar. In order to accommodate any possibility of transition to detonation, Test vessels 1,2 and 3 were designed to 35bar pressure rating, while Test vessel 4 was design to 28bar pressure, with all exceeding the detonation pressure. Furthermore, the dump vessel was hydraulically tested and certified prior to commission at 11.25bara on the bases of the standard regulation. All pressure relief valves and fittings were design to meet the design pressure of the vessels.

3.7.3 Transmission of explosion to Auxiliary equipment

The auxiliary equipment are shown to be very vital in most work carried out in this facility and these equipment are either connected permanently or temporary during the experimental procedure, hence stand the risk of explosion transmission to the equipment. In view of the above, series of valve on the test vessel and the mixture preparation panel were used to isolate vessel from the apparatus. Furthermore, pipes connecting the vacuum pump to the vessel were also isolated from the vessel immediately after use by pressure ball valves. To ensure maximum safety in this respect, the procedure was controlled in sequence by the checking and recording made on the mandatory tick box test sheet procedure for each test conducted.

The fuel line and pressure monitoring line were also disconnected from the fittings on the test vessel immediately after use in order to prevent transmission of explosion into the fuel cylinder bottle. Furthermore, flame arrestor was fitted to the bottle prevent any accidental transmission of flame through the fuel line to the fuel cylinder. To further enhance the safety measure, the fuel filling line when disconnected from the vessel, must be connected to a click and lock on the panel which was part of the ignition and interlock safety system. This ensures that the fuel mixture panel and fuel cylinder were isolated from the vessel, also prevent any ignition process while the fuel line was still connected to the vessel.

3.7.5 Combustible gas release to the test room

The use of highly volatile and flammable gases within this facility makes it prone to accidental release of gas and other related accidents, hence the need the have a reliable safety measure in place in the event of it occurrence. In this regard, efforts were made to prevent leaks within the facility by ensuring all pressure valves for the apparatus and vessels were isolated. Additionally, pressure testing was carried out before the commencement of any test, isolation of fuel cylinders and strict adherence to the tick sheet test procedure. Furthermore, the large cross-section of the wall windows of the facility was made of a weak structure design to give away in the event of any accidental explosion as a result of leaks. The window which was made of glass was covered with tin plastic sheet to reduce fragmentation of the glass on breaking. It was intended that the weak structure would fail thereby releasing the pressure before any significant structure damage was done to the facility.

3.7.4 Failure of Spark Ignition or Non-ignitable Mixture

As part of the pre-test procedure on the mandatory tick box test sheet, the ignition system must be tested prior to start of the test for the day to ascertain the integrity of the ignition system. In the event that the ignition system fails during the test, the special procedure was carried which was also specified in the protocol folder for each set of experiment. The first step was to repeat ignition procedure from the same spark or different spark already connected to the vessel. If no ignition still, abandon the test and carry out special procedure for 'No ignition' as specified in the protocol folder. There were also special procedures for excess fuel, excess initial pressure or when the fuel did not ignite for gas mixture outside the flammable range of the spark. All these are part of the robust safety measure to assist in sustaining the integrity of the equipment, structure, and safety of the personnel within the explosion facility.

CHAPTER 4

Discussion of Pressure Peaks in Confined and Vented Explosions

4.1 Introduction

4.2 Explosion in confined enclosure

4.2.1 Maximum overpressure and rate of pressure rise in closed vessel

4.2.2 The influence of vessel volume and Ignition position in closed vessel

4.2.3 Explosion pressure and rates of pressure rise

4.3 Explosion venting Mechanism

4.4 Characteristics of Pressure Peaks in Vented Explosions

4.5 The Determination of P_{red} as P_{fv} or P_{ext} or P_{rev} or P_{mfa}, Illustrations where each of these Pressure Peaks is P_{red}

4.8 Conclusion

4.1 Introduction

Explosion overpressure is a key parameter in confined explosions for closed and vented vessels. This chapter is initially concerned with explosions in closed empty enclosures for premixed gas-air prelude to the application of the venting technique. Then the features of vented explosions are discussed with the pressure traces analysed in detail to identify the physical features of the vented explosions that give rise to a range of pressure peaks, any one of which can be the peak overpressure, depending on the venting circumstances. Large scale experiments were conducted by Bartknecht (1993) in both closed and vented enclosures and part of his original work were accommodated in the vent design correlations in the current European venting guide (EN14994:2007, 2007). Most of the vent design correlations in the literature rely on the data from initially closed vessel explosion to successfully predict explosion venting (Bartknecht, 1993, Bradley and Mitcheson, 1978a, EN14994:2007, 2007, Swift, 1988). To justify the application of the venting technique, there is also the need to first understand the extent of hazard associated with closed vessel explosion.

4.2 Explosion in Confined Enclosure

When an explosion occurs in a confined space, the expansion of burnt gases causes a rise in temperature and pressure, and the severity of the explosion is measured by the maximum pressure attained (P_{max}) and the maximum rate of pressure $(^{dP}/_{dt})_{max}$ during the process. The magnitude of this pressure rise can be affected by numerous factors including the gas composition, concentration of the mixture, the initial conditions of P and T prior to the explosion and the location of ignition source. Studies have shown that a lot of effort has been channelled into understanding the evolution of pressure generated when explosion of gas mixtures is carried out in confined enclosure (Bradley and Mitcheson, 1976, Fairweather and Vasey, 1982). The literature has shown that mixture reactivity of different gas mixtures at initial temperature and pressure affects the maximum overpressure for explosion deflagration in closed vessel (Bartknecht, 1993, Cashdollar et al., 2000, Harris and Briscoe, 1967, Nagy and Verakis, 1983, Razus et al., 2009). In most cases single fuel-air mixtures were analysed by variation of the mixture

concentration with one gas-air mixture but limited data comparing different gas mixtures and it effects.

In mixture reactivity, the burning velocity (S_u) and the gas reactivity parameter (K_G) are two parameters used to indicate the reactivity of gas mixtures in gas explosion prediction. K_G can only be determined from closed vessel experiments, but S_u can be determined by both closed vessel flame propagation studies and on stabilised flames on laboratory burners. Andrews and Bradley (1972) have shown in their review of methods of measuring S_u that there is considerable variations in the measured values of S_u in the literature and the value obtained is equipment dependant. The main cause of systematic error in the measurements is the assumption of an infinitely thin laminar flame reaction zone, which means that flame curvature or stretch effects are neglected. Stoichiometric methane-air flames are a little over 1mm thick and this thickness increases as the mixture is made leaner or richer. Most flames that are stretched with a burnt gas area greater than the unburnt gas area (as in a Bunsen burner type flame) have a measurement error or the order of 20% of that for a flame with negligible curvature effects. In closed vessel explosions with central ignition the burned gas surface of the flame has an area less than the unburned gas surface and so the stretch is the opposite of that for a Bunsen burner. Sattar et al. (2014) have shown that a 1 m³ explosion vessel is the minimum size necessary for the assumption of an infinitely thin flame front to be valid in a closed vessel explosion. For this size they showed that the flame speed measured in the constant pressure period of the explosions when multiplied by the adiabatic expansion ratio gave a maximum burning velocity for methane-air of 0.42 m/s. If measurements are made in much smaller vessels, as is common, then values around 0.36 m/s are commonly reported, which is 17% below the unstretched value of Satter et al. (2013).

The gas reactivity index K_G is also determined from closed vessel explosion and the current European standards for gas explosion venting (BS EN 14994, 2007), which was based on the original work of Bartknecht (1993) and recommended values of K_G for different gases. The values were based on measurement carried out in a 5 Litres (0.005m³) spherical vessel and recommended for application for vessel up to 1000m³. However, if 1 m³ is the minimum size to measure the laminar burning velocity from the flame speed, then it must also be the minimum size to measure K_G reliably. Thus all of Bartknecht's K_G values are likely to be specific to his small

volume. It was shown in Chapter 2 that K_G is volume dependant, it changes with increase or decrease of the volume of the vessel. The reason for the change in K_G at small volume is the flame stretch effect. However, it is know that for volumes greater than 1 m^3 K_G continues to increase and in large volumes has quite high values. Cashdollar and co-workers (2000) had previously shown that K_G is not a constant as assumed by the European venting standard (BS EN 14994, 2007), but the values were dependent on vessel volume. This is due to the phenomena of flame self acceleration through the formation of cellular flames, which increase the mean flame speed and burning velocity.

The maximum pressure (P_{max}) and the rate of pressure rise $(^{dP}/_{dt})_{max}$ are key factors in determining the severity of explosions. For spherical vessels of at least 1 m^3 volume with central ignition the measurements of P_{max} and dp/dt$_{max}$ are close to adiabatic and compare well with adiabatic flame computations. If the flame touches the wall before peak pressure is reached then there are burned gas heat losses and the peak pressure is measured lower than the adiabatic value. This occurs in non-spherical vessels. In addition to the factors mentioned above the type and energy of ignition, and temperature and pressure prior to explosion affect the rate of pressure rise as well as the maximum overpressure for any gas mixture (Bartknecht, 1981, Lunn, 1984, EN13673-1, 2003).

The European standard (EN 13673-1, 2003) recommends that only central ignition in spherical and cylindrical vessels of L/D=1 and vessel volume (V≤ 5Litres) must be used to determine the maximum overpressure in a closed vessel explosion. There is no reason to limit the vessel volume, other than that self acceleration will increase the rate of pressure rise. In closed spherical vessel explosions, the expansion of gases is equal in all direction and the maximum overpressure is obtained when the flame reaches the wall of the vessel, the pressure then declines declines afterwards due to heat losses. In a spherical closed vessel explosion, a central spark will produce the worst case explosion, as compared to other ignition locations, as any other ignition position will result in the flame touching the wall before it has burned all the mixture. The heat losses then reduce the peak pressure. This is in agreement with most studies on closed vessel explosion where central ignition positions were used (Bradley and Hundy, 1971, Razus et al., 2010, Runes, 1972). However when L/D > 1, the result may not be the same and there are no reasons given for not using

other shapes of vessels in the recommendation of the standard or how this may be applied (EN 13673-1, 2003).

This section of the thesis presents the results of closed vessel explosions in the vessels that are used with venting later in the Chapter. These are base line experiments prior to the venting experiments and were undertaken to give a better understanding of the mechanism of flame propagation in the closed vessel explosion. Also when a vent cover is used the flame propagation up to the time the vent bursts should be the same as for a closed vessel explosion and hence will be compared with the results presented here for closed vessel explosions.

4.2.1 Maximum Overpressure and Rate of Pressure Rise in Closed Vessel

In closed vessel explosions, there are various stages or phases of flame propagation. The first phase is the constant pressure phase which commences from the time of ignition of the gas mixtures reaching up to ¾ of the total travel time of the flame. Fig. 4.1 shows that only 3% of the total pressure rise fell within this constant pressure flame propagation time in a 1 m^3 closed vessel explosion (Sattar et al., 2014). The second phase is that pressure rise which occurs in the later stage of combustions, while the last phase is the decay period after touching the wall of the vessel. For a spherical vessel, the maximum pressure generated was obtained when the flame reached the wall of the vessel as shown in Figure 4.1.

In the present work two cylindrical vessels of L/D 2.8 and 2 were used in vented explosions with vessel volumes of 10 and 200 litres respectively. They were used in the closed vessel configuration in this section with 10% methane-air, 4.5% propane-air, and 7.5% ethylene-air. The vessel complies with the European standard for the measurement of maximum overpressure and rate of pressure rise in closed vessel, with the exception of the L/D, as the standard required the L/D =1 while vessel used in this case have L/D of 2.8 and 2 (EN 13673-1, 2003).
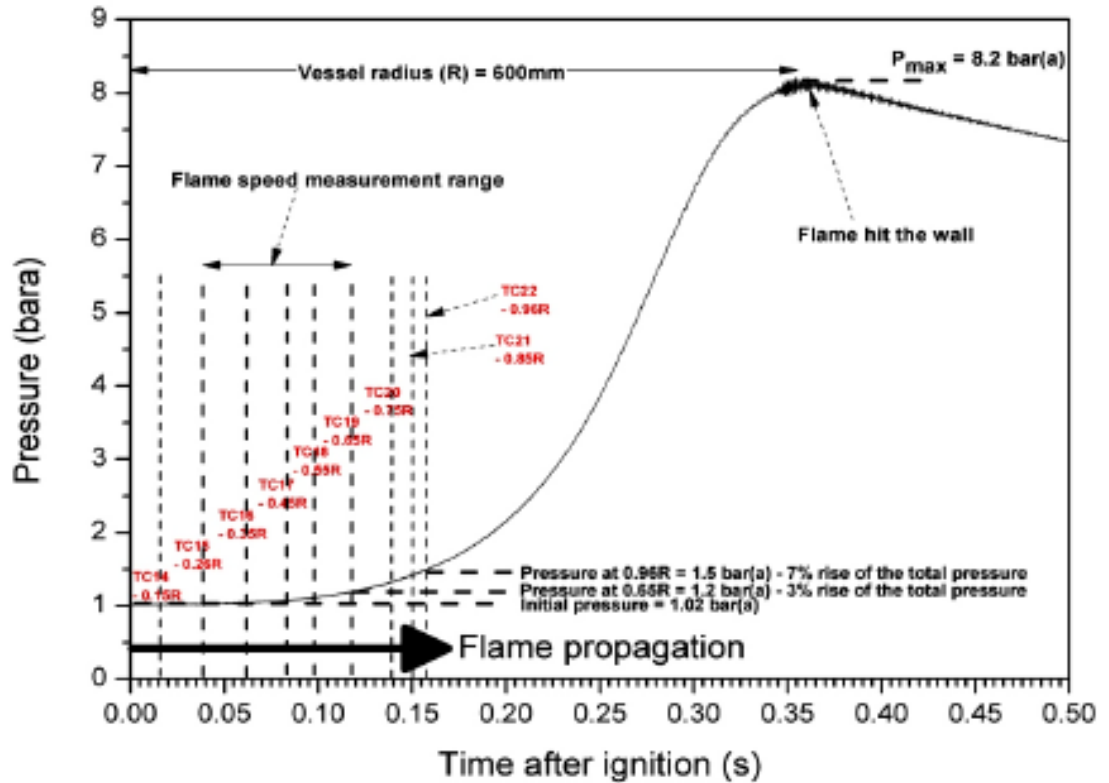
*Figure 4.1 Laminar 10% methane explosion pressure-time trace
along with the time of flame arrival (Sattar, 2013)*

Figure 4.1 shows pressure-time profile for 10% methane-air with central ignition position for the 10 litre vessel (L/D=2.8). The time of flame arrival at the thermocouples along the centre line are indicated as T_1, T_2, and T_4, while T_3 located at the wall of the vessel was to indicate when the flame touches the wall on the vertical to the normal plane. Thermocouple T_1 was located at 152mm away from the spark location on one side, while T_2 and T_4 were located at 81mm and 230mm on the opposite side along the vessel length. Fig. 4.2 shows that after the flame arrived at the wall at T_3 the pressure rise was 3 bar. After this the rate of pressure rise was lower than before the flame touched the walls and this was due to heat losses with the burned gases in contact with the walls. However, in vented explosions the overpressure is normally desired to be < 0.5 bar and Fig. 4.2 shows that venting of this explosion with central ignition would take place while the flame was still spherical and not in contact with the walls. Spherical laminar flame propagation would then apply.
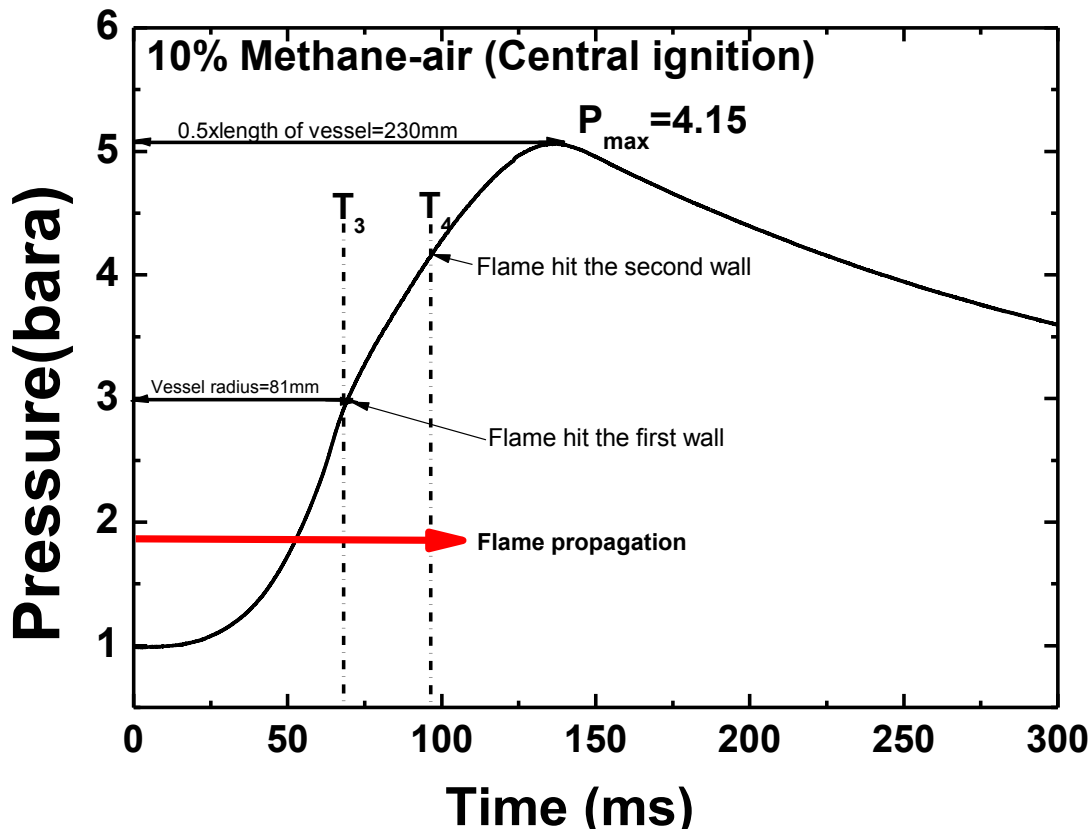
Figure 4.2 Pressure-time record for 10% methane-air with the time of flame arrival in 10 Litres cylindrical vessel

The rate of pressure rise was shown in Figure 4.2 to change again when the flame reached the wall of the vessel at T_4 after 95 milliseconds from time of ignition. This is when the flame reached the end wall of the vessel (a greater distance than the wall from the spark). Comparing Figure 4.1 and Figure 4.2 it as seen that the peak pressure is much lower in the cylindrical vessel due to the heat losses after the flame touched the walls. In larger L/D, Phylaktou and Andrews (1991) have shown lower peak pressure than in Fig. 4.2 due to the greater flame contact. Hence, the adiabatic situation can only be achieved in a cylindrical vessel when the L/D=1, otherwise the peak pressure is reduced by heat losses before the combustion process is completed.

4.2.2 The Influence of Vessel Volume and Ignition Position in Closed Vessel Explosions

When explosions occur in confined enclosures, the adiabatic compression of the unburnt gas ahead of the flame is caused by the expansion of the burned gases, which also increases the temperature as well as the pressure. It was shown in Figure 4.1. that the first half of the total flame propagation time, there was only a slight

increase of pressure from the initial pressure (Zabetaskis, 1965, Sattar, 2013). This is the constant pressure period of combustion and the constant pressure flame speed and burning velocity can be measured in this phase of the explosions. The work of Zabetaski (1965) had suggested that the two stages of closed vessel explosion (i.e the initial constant pressure and rapid rise periods) have a similar time period, and the pressure generated only becomes significant when the flame diameter was half the diameter of the flame (Zabetaskis, 1965).
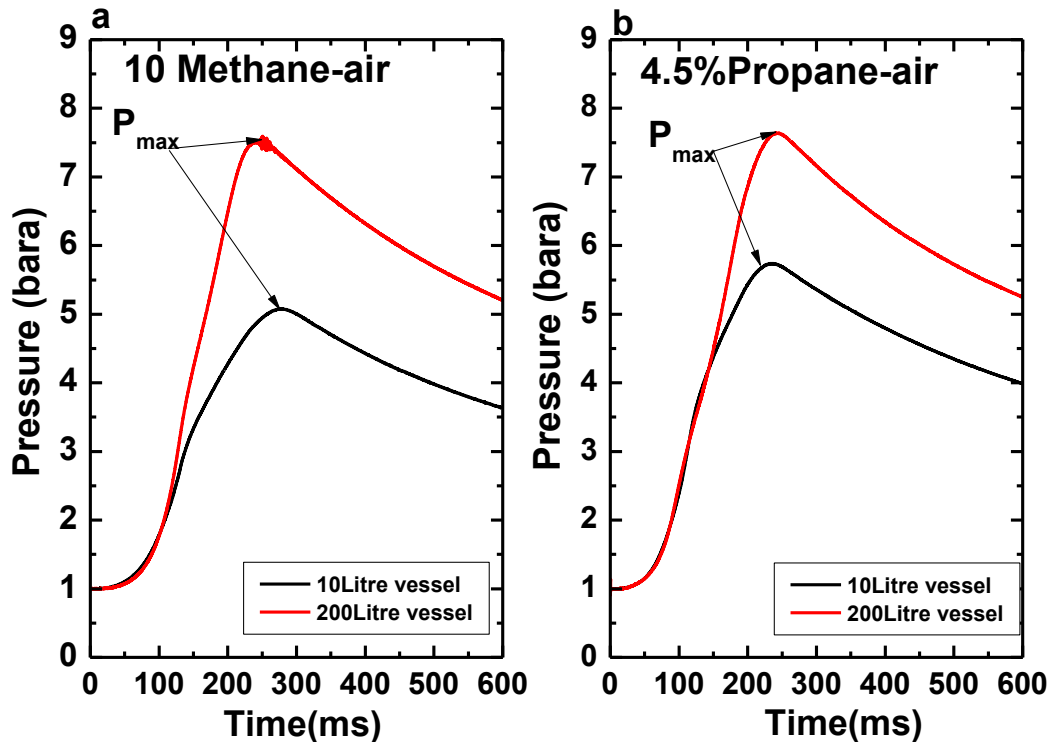
Figure 4.3 Comparison between 10L and 200L cylindrical vessels (a) 10% methane-air (b) 4.5% propane-air

Figure 4.3 compares the pressure-time profile for the two vessels used in this work. The flame propagation time for the 10L vessel was scaled up by $V^{1/3}$ to align with the result from the 200L vessel for better comparison. The maximum pressure generated for the 200L vessel was almost twice the value obtained for 10L vessel with 10% methane-air and central ignition as shown in Figure 4.3a. The reason for the higher pressure in the larger vessel is that the heat losses decrease with the size of the vessel. The peak pressures never exceed the adiabatic pressure rise. Heat losses from the hot gases that touch the walls scale with the ratio of surface to volume, S/V. For a cylinder this is proportional to 4/D and the diameter ratios for the two vessels is 162/500 = 0.324 or the smaller vessel has 3.1 times the heat losses of the larger vessel. The reason for the heat losses to scale with S/V is that the

convective heat transfer is proportional to the surface area and the temperature difference (which should be the same in the two vessels). However, the total heat is proportional to the mass which is proportional to the volume. Hence, the heat losses scale with the ratio of the heat losses to the mass of hot gas. Also the differences in L/D between the two vessel will result in more wall contact with the burned gases in the smaller volume larger L/D vessel.
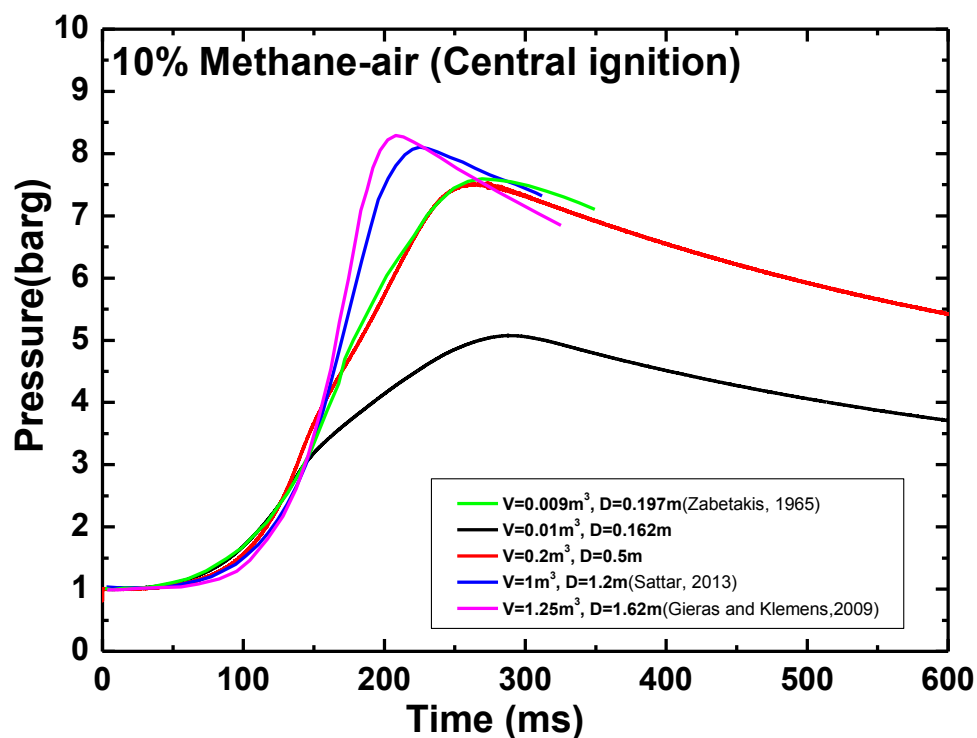
Figure 4.4 Comparison of pressure-time record for different vessel volumes and diameter

Figure 4.4 compares different closed vessel explosions with the present work, considering central ignition for spherical and cylindrical chambers. This shows that the maximum pressure increases as the vessel volume increases. In addition, a 9L (D=0.197m, L/D = 1.5) vessel from the work of Zabetakis (1965) was shown to give a much higher maximum pressure when compared to the 10L (0.162) vessel from the present work as seen in Figure 4.4. The difference was due to the difference in L/D of 1.5 and 2.8 in the present work. This gives much more wall flame contact in the present work.

The current European venting standard recognises K_G as a constant and as a design parameter to represent the combustion behaviour of gas mixtures. The "cubic law" $((\frac{dP}{dt})_{max} V^{1/3})$ which has been used for explosion scaling in the industries were

shown not be applicable to vessel with large L/D (Phylaktou and Andrews, 1991b).,
which is why the standard vent design procedures do not apply for large L/D
vessels. In large L/D vessel very fast flames are generated along the axis of the
vessel at the onset of flame propagation. The flame does not touch the wall until
later in the explosion, by which time the pressure rise is greater than would be
desired for P_{red} in a vented explosions. Thus the flame in a large L/D vessel has to be
vented during the fast flame period.

Apart from the mixture reactivity, initial temperature and pressure, and the vessel
volume, the location of ignition was known to affect the maximum explosion over
pressure in closed vessel particularly for spherical vessels (Bartknecht, 1993,
Cashdollar et al, 2000, Razus et al, 2003, 2006, 2010). For spherical vessels, central
ignition gave higher P_{max} as compared to any other position away from the central
location. Lower P_{max} were obtained when non-central ignition locations were used,
as the flame reached the wall before the combustion was completed thereby losing
heat, decreasing the rate of pressure rise. The current work, presents the result for
central and end ignition farthest away from the central location for cylindrical vessel
of L/D > 1.
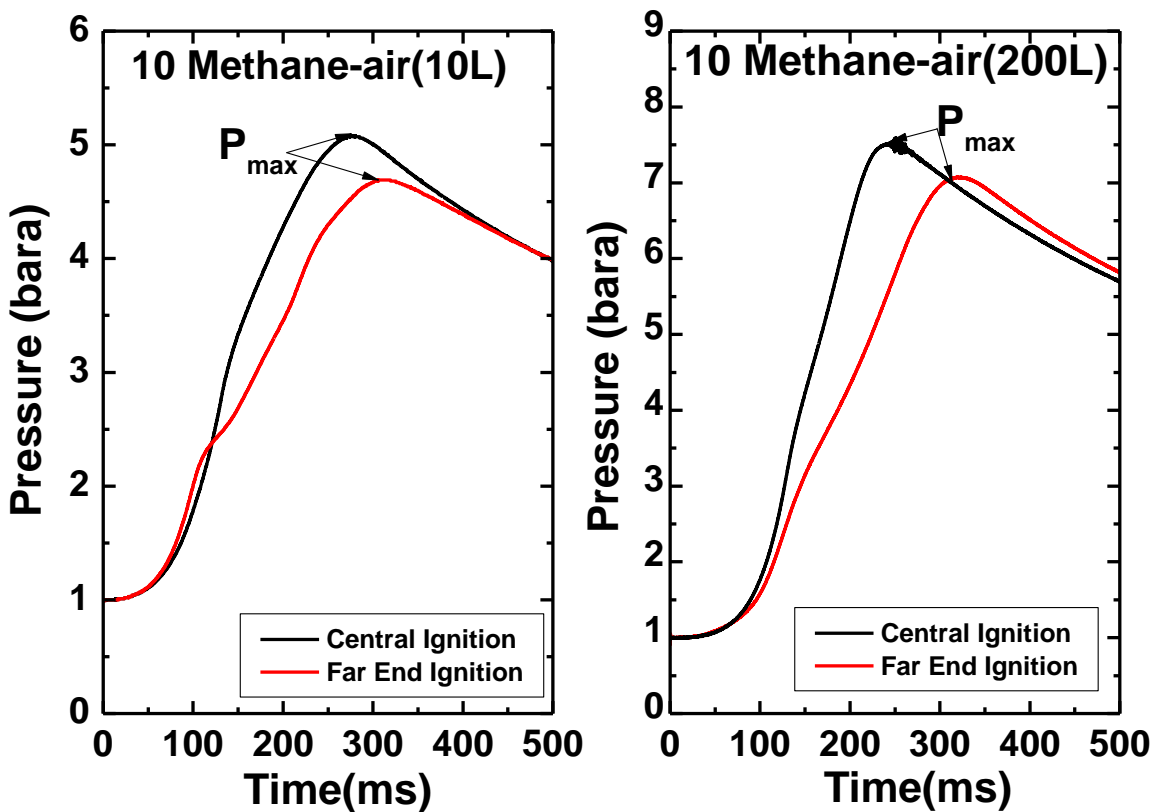
Figure 4.5 Comparison pressure-times profile for Central and far end ignition

Figure 4.5 shows that the central ignition location produced higher overpressure when compared to end ignition away from the centre. This was as result of the heat losses caused by the flame contact with the wall of the vessel with end ignition, leading to a reduction in rate of pressure rise and the maximum pressure. This was in agreement with the literature where central ignition location was shown to produce higher overpressure as compared to other remote locations (Andrews and Bradley, 1972b, Bartknecht, 1993, Bradley and Mitcheson, 1978a, Razus et al., 2006, Razus et al., 2003). In the design of explosion systems, the ATEX directive based on the European parliament required that the most extreme condition to be considered (EuropeanParliament and Council, 1994). It was only appropriate to consider the central ignition locations as the worst case in compliance with the ATEX regulation for closed vessel explosion.

However, the use of the central ignition for vented explosions will be shown in this work not to be the worst case, with end ignition being shown to be the worst case for vented explosions (Fakandu et al., 2013, Kasmani et al., 2010b, Willacy, 2008). It will be shown that the reason for this is the fast flames in the initial part of the explosion, as reported by Phylaktou and Andrews (1991). The fast flame occur before the flame has touched the walls and venting has to occur in this fast flame period as the pressure rise is already too high by the time the flame contacts the wall and starts to lose heat. The presence of the vent outflow of unburned gases also keeps the fast flame period in existence longer and the flame will be shown not to touch the walls until well after the peak vented overpressure had occurred. Thus the higher heat losses responsible for the lower peak overpressures in the closed vessel explosion in Fig. 4.6, do not matter as the flame is not in contact with the wall during the venting process, where peak pressures are often <100mb for free venting.

4.2.3 Explosion Pressure and Rates of Pressure Rise

Confined explosions in cylindrical vessels give lower peak pressure as compared to spherical vessel with the heat losses to the wall as the main cause particularly when the L/D >1. Heat losses as result of flame contact with the walls are the cause of lower pressure for end ignition in spherical and cylindrical vessel. Figure 4.6 shows the effect of rate of pressure rise as well the maximum pressure in cylindrical vessel. The continue contact to the vessel wall and the heat loss is also responsible for lower

overpressure as shown in Figure 4.6. Only spherical enclosure with central ignition can achieve the adiabatic combustion peak pressure rise, as all other vessel shapes or ignition location may not complete the combustion process without losing heat to the wall. Table 4.1 gives a summary of the maximum overpressure for the two vessels and the rate of pressure rise, for different gas mixtures. Two different rates of pressure rises, $(dP/dt)_1$ and $(dP/dt)_2$, were observed in all the experiments conducted in vessel 1 (10L) and vessel 2 (200L). For central ignition location, $(dP/dt)_1$ was shown to always give a higher value as compared to $(dP/dt)_2$ for both vessel 1 and 2. This was because of the short period of total explosion time for the central ignition location and more than half of the pressure total time was consumed before the flame contacted the first wall. This in agreement with the fact that an initial spherical flame in a compact cylindrical vessel occupies 50% of the diameter and only 1% mass was burnt within this period and the remaining mass burnt at the later stage (Phylaktou and Andrews, 1991). This shows that the rate of pressure rise at the initial phase reaches its peak when the flame first touches the wall, which will be higher for central ignition with shorter total explosion time. This was a different scenario for end ignition where $(dP/dt)_2$ was much higher as the flame touches the wall much earlier with more than half of the total propagation time left. Once in contact with the cylindrical wall, the rate of pressure rise falls and starts to increase until it touches the end wall of the cylindrical vessel.
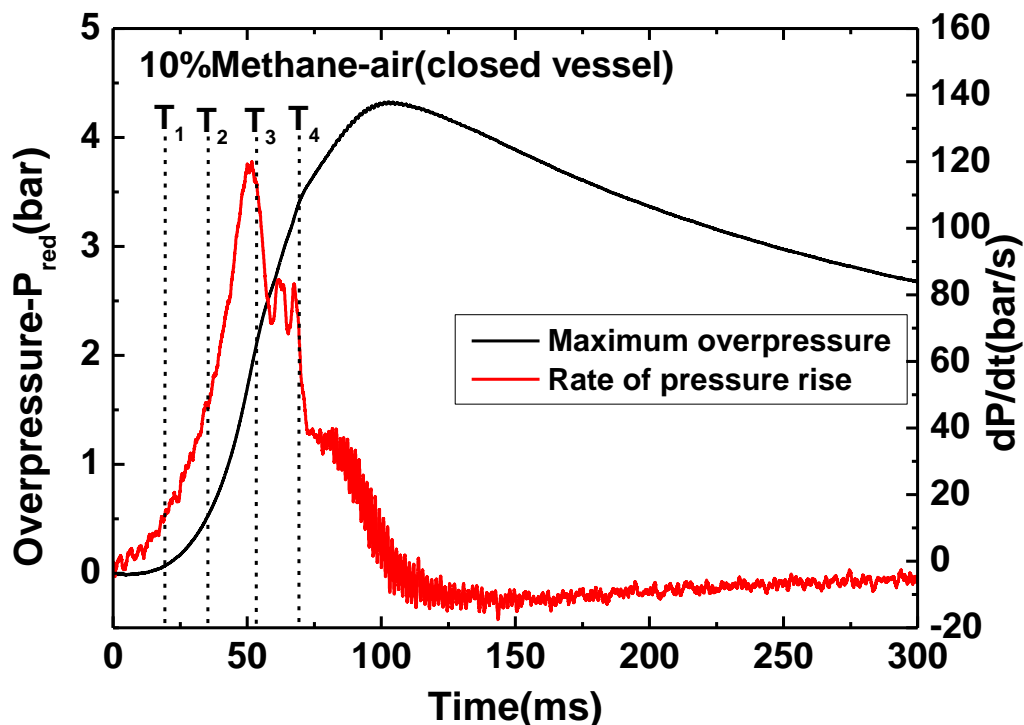
Figure 4.6 Pressure-time profile for 10% methane-air with rates of pressure rise for 10L vessel

Table 4.1 Pmax and dP/dt for different gas mixtures in 10L vessel Pmax and dP/dt for different gas mixtures in 10L vessel

Gas	Concentration (%)	Ignition Location	Volume (L)	P_{max}(bar)	dP/dtmax	K_G
CH_4	10	Centre	10	3.78	68	14.7
CH_4	10	Centre	10	4.17	85	18.3
CH_4	10	Centre	10	4.14	85.6	18.4
CH_4	10	End	10	3.69	59	12.7
CH_4	10	End	10	3.6	56	12.1
CH_4	10	End	10	3.4	52.9	11.4
C_2H_4	7.5	Centre	10	5.83	345	74.3
C_2H_4	7.5	Centre	10	5.93	301.9	65.0
C_2H_4	7.5	End	10	5.1	192	41.4
C_2H_4	7.5	End	10	5	170	36.6
C_2H_4	7.5	End	10	5.2	228	49.1
C_2H_4	7.5	End	10	5.1	197	42.4
C_3H_8	4.5	Centre	10	4.8	130.9	28.2
C_3H_8	4.5	Centre	10	4.73	135.2	29.1
CH_4	10	End	200	6.07	39.6	23.2
CH_4	10	End	200	6.14	41.9	24.5
CH_4	10	Centre	200	6.54	66.7	39.0
CH_4	10	Centre	200	6.47	69.75	40.8
C_2H_4	7.5	End	200	7.1	151.7	88.7
C_2H_4	7.5	End	200	7.134	147.2	86.1
C_2H_4	7.5	Centre	200	7.14	201.3	117.7
C_2H_4	7.5	Centre	200	7.14	211.6	123.7
C_2H_4	7.5	End	200	7.39	143.9	84.2
C_3H_8	4.5	End	200	7.13	140	81.9
C_3H_8	4.5	End	200	6.64	62.8	36.7
C_3H_8	4.5	End	200	7.13	116.7	68.2
C_3H_8	4.5	Centre	200	7.15	95.05	55.6
C_3H_8	4.5	Centre	200	7.15	55.27	32.3

Table 4.1 shows that the K_G values were significantly lower than those for the 5 Litre vessel used by Bartknecht, where methane was 55 and Propane 100. A value for ethylene was not determined. The present lower values were due to the heat losses in explosions in cylindrical vessels as the peak pressure occurred after the flame touched the walls.

Table 4.1 is the central ignition result for 10% methane-air in vessel 1, showing the pressure time profile and the rate of pressure through the combustion process. The initial period of flame propagation was followed by rapid period of pressure rise prior to the contact with the first wall at T_3, and this period of rapid pressure rise was shown to occur the first 5-10% of the total explosion time (Phylaktou and Andrews, 1991). The distance from the spark position to the wall was half the diameter and this took 50% of the total combustion time to achieve. There was a sudden drop in the rate of pressure after touching the wall at T_3 and later starts rising (second rate of pressure rise-$(dP/dt)_2$) before final pressure drop in pressure on getting to the end walls at T_4. There was still an increase in pressure after T_4, this was the burning of remaining unburnt gas mixtures in the corner regions of the vessel.

4.3 Explosion Venting Mechanism

The process of venting in explosions is the intended to reduce the explosion contained in an originally closed vessel such that the design pressure of the vessel or containment is not exceeded. The explosion vents are placed permanently and are activated in the event of any accidental explosion in order to relieve the build-up of pressure at certain activation pressure, P_{stat}. In closed vessels, the maximum explosion attained is the, P_{max} , while P_{red}, is the maximum reduced pressure obtained as a result of the application of the venting technique (Siwek, 1996). Similarly, the maximum rate of pressure rise in a confined explosion also has a different designation from that of the vented explosion, with $(^{dP}/_{dt})_{red}$ and $(^{dP}/_{dt})_{max}$ for vented and confined explosions respectively (Swift, 1996). The maximum reduced pressure P_{red} in vented explosions is required not to exceed $^2/_3$ of the total pressure strength of the vessel or structure to be protected (NFPA 68, 2013). The vent area must be correctly sized for the P_{red} to meet this requirement.

Figure 4.7 shows the pressure-time history of a typical vented and unvented explosion with particular concern to the vent area design, such that the burst static pressure P_{stat} is set to be less than the design strength of the vessel and also the P_{red} (Lunn, 1984). The literature has also shown that the vent is related to the reduced pressure such the lager the vent area, the lower the P_{red} (Lunn, 1984). A study of flame development in vented explosion was reported by Harris (Harris, 1983). It

showed that pressure due to the flow of unburnt gases moving ahead of the flame and out of the vent is always the highest pressure in venting. It is higher than the burst static pressure (P_{stat}) unless the P_{stat} is very high and the vent area (A_v) is quite large (Harris, 1983). The reduced pressure P_{red} is usually predicted to be the maximum pressure and the primary cause of this overpressure in a vented explosion is the flow of unburnt gases through the vent or as a result of the external explosion of the vented gases (Fakandu et al. 2011). Apart from the vent area, many other factors are contributory to the magnitude of the maximum reduced pressure, P_{red} , including the mixture reactivity, ignition location, vessel size, vent materials and available obstacle or obstructions.
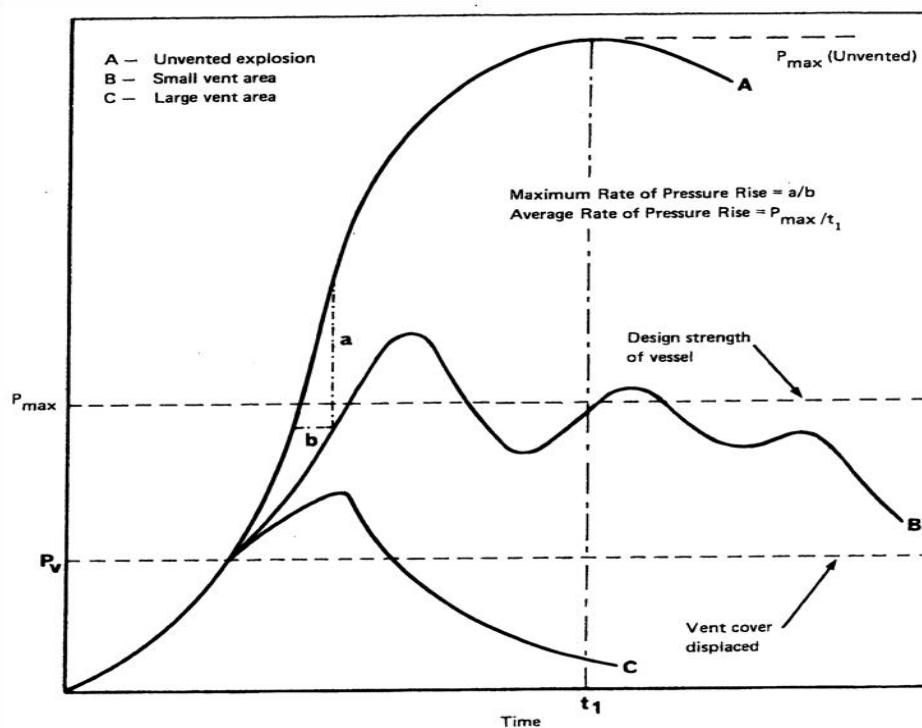
Figure 4.7 Typical Pressure-Time history of vented and unvented explosion (Lunn 1984)

From the pressure-times profile in Figure 4.7, it can be seen that the venting process passes through 3 different stages, from the time ignition. Firstly, on ignition the flame propagates normally with a spherical flame assuming the confined explosion scenario. At this stage, there continues the burning of the gas mixtures and the expansion of the flame increases the flame area, the rate of pressure rise $((dP/dt)_{max})$ as well as the mass burning rate of the gas mixture. This also leads to the rise in pressure as for the confined vessel explosion pressure development

process, until the vent opening pressure, P_v, is reached in Figure 4.7. However, in a vented explosion with uncovered vent (free venting), the situation is different, as the flame propagates with an initial spherical shape and later distortes in the direction of the vent. Furthermore, the flame propagates with an increase in flame speed with the increasing mass burning mass burning rate until it exits the vent. Figure 4.7 and Figure 4.8 shows the pressure-time record comparing the closed vessel with that of free venting and initially covert vents respectively. Figure 4.9 shows a typical confined explosion in the 10L cylindrical vessel with central ignition location compared with the vented explosion for 7.5% Ethylene-air. For the confined explosion, the initial stage was smooth with high rate of pressure rise as a result of fast flame propagation, while the later stage was characterised by oscillatory combustion. This oscillatory combustion was caused by pressure wave interactions as the flame burned into the trapped volumes in the corner regions of the vessel (Cooper et al., 1986). This was similar to the oscillatory explosion obtained in large closed vessel due to high initial flame speeds associated with large L/D (Phylaktou and Andrews, 1991b). The faster flame associated with more reactive ethylene flame was a key factor when compared with the methane-air pressure trace of Figure 4.2. This type of oscillation was also shown to exist with vented explosions with central ignition (Cooper et al, 1986).

The second stage of the venting process involves the opening or removal of the vent panel. In the design of explosion vent, the vent panels or vent material covering the vent is designed to fail at a certain pressure known as the vent opening pressure, P_v, (or P_{stat} as used in this work and by Bartknecht, 1993) which should be as low as possible (Cooper et al. 1986). At the opening of the vent, the pressure drops from the confined vessel pressure propagation pattern to generate the first peak pressure, P_1 (Cooper et al. 1986, Cubbage and Simmonds 1955). The spherical flame propagation pattern is distorted at this point and the flame propagates towards the direction of the vent with the flame still expanding, increasing the mass burning rate as well as rate of pressure rise ($(\frac{dP}{dt})_{red}$) leading to the second peak pressure.

Figure 4.8 and 4.9 shows the deviation from the confined explosion, while Figure 4.9 clearly shows the first peak pressure P_1 (P_{burst}) and subsequent pressure rise. The magnitude of P_1 depends on the strength of the vent panel or vent cover and this

can also influence the initial turbulence as a result of the vent opening pressure or the P_{red} (McCann et al, 1985). Hence, there is the need to use P_v as low as possible in order to avoid turbulence generated as a result of the vent opening pressure or else this may lead to very high P_{red} and jeopardise the objective of venting. For free venting, this stage of the venting process is completely eliminated and since there is no vent cover involved P_1 is not generated. Figure 4.10 shows the pressure-time profile for 7.5% ethylene-air from the 10 Litre vessel for a small vent area, with a vent cover of $P_{stat} = 0.057\ bar$, showing the different stages of explosion venting process.
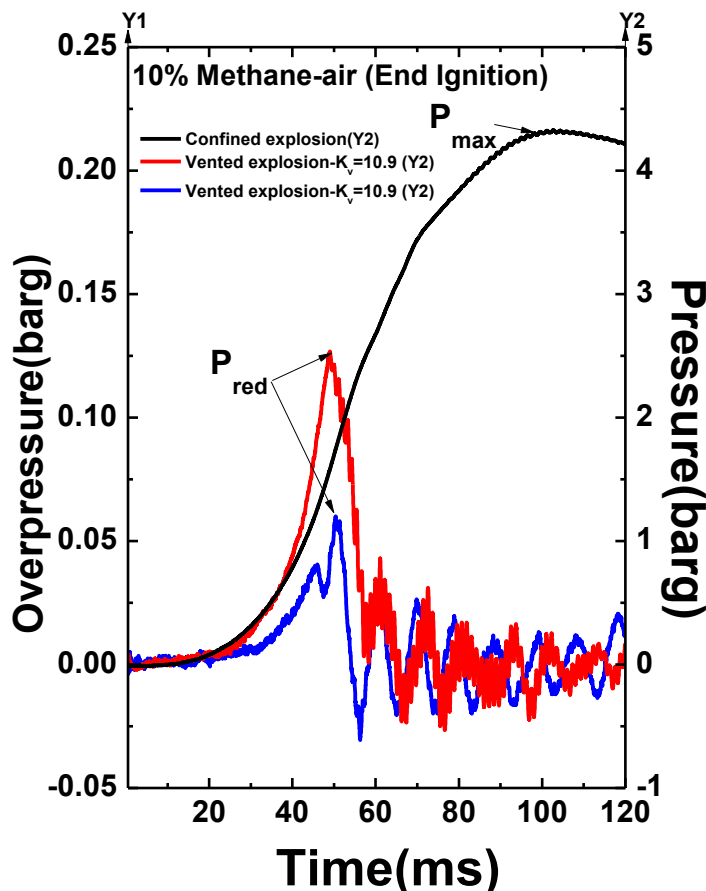
Figure 4.8 Closed vessel pressure-time for 10% methane-air and free venting explosion pressure for two vent areas in 10L vessel

The last phase of the explosion venting process is the mass gas flow through the vent. At this point the pressure drops due to unburned gases flowing out of the vessel vent. When the flame arrives this external volume of gas is ignited and this generates an external explosion which generates the second peak pressure P_2 (Cooper et al., 1986). After the bursting of the diaphragm, the longer period of venting of unburnt gases and increasing mass burning rate increases the overall pressure within the vessel until the point flame exit through the vent, when the pressure drops to form the second peak pressure P_2 (Cubbage and Simmons, 1955).

At this point, the pressure-time profile as a result of the venting process generates another pressure peak. This was shown by Cubbage and Simmond (1957), where double peak pressure was discovered in the investigation of explosion overpressure in industrial drying oven. Other authors have shown that multiple peak pressures exist in explosion venting but have different nomenclature for different peak pressures (Cooper et al. 1986, Bauwen et al. 2010).
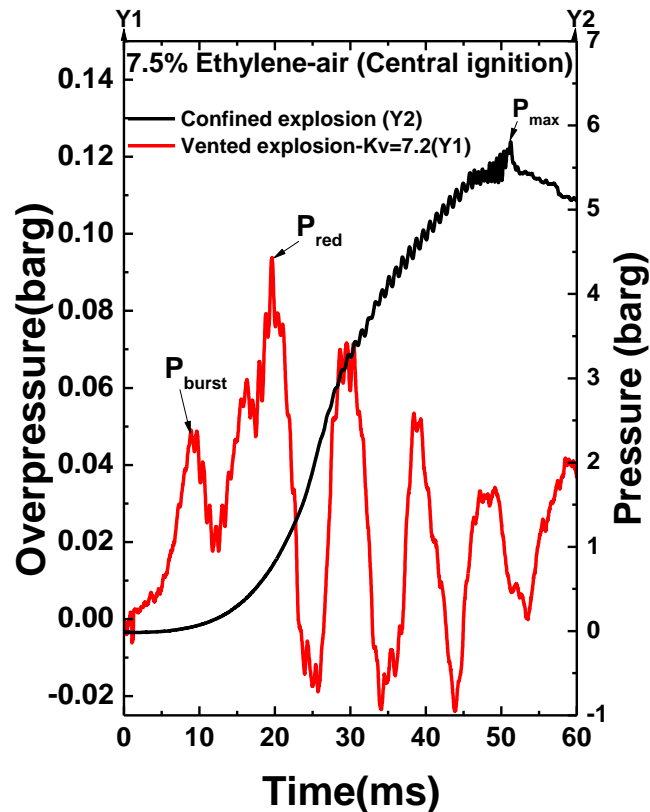
Figure 4.9 Closed vessel pressure-time for 7.5% ethylene-air and vented explosion pressure for initially closed vent in 10L vessel

Harris (1983) showed that the vent panels or covers with high vent opening pressure usually gives one peak pressure, the once with the lowest vent opening pressure gives a double peak as shown in Figure 4.11. In this case if different materials were used as vent covers and the area of the vent was the same, the vent opening pressure may be the dominant peak pressure in the former as compared to the later where the second peak is dominant. The sudden opening of the vent cover in the second phase enhances the effective surface area of the flame front and this also increases the combustion rate inside the vessel. Furthermore, this increases the pressure as shown in Figure 4.10. The thermocouple T_4 gives the precise time of the flame exiting the vent, while pressure transducer PT_2 located in the connecting vessel shows the pressure rise due to external flame propagation, which coincided with the time of

flame arrival at that position. It was shown that any of the pressure peaks generated during the vented explosion can be the maximum reduced pressure, and this depends on various factors including vent area, mixture reactivity, and vent opening pressure (Fakandu et al., 2013).
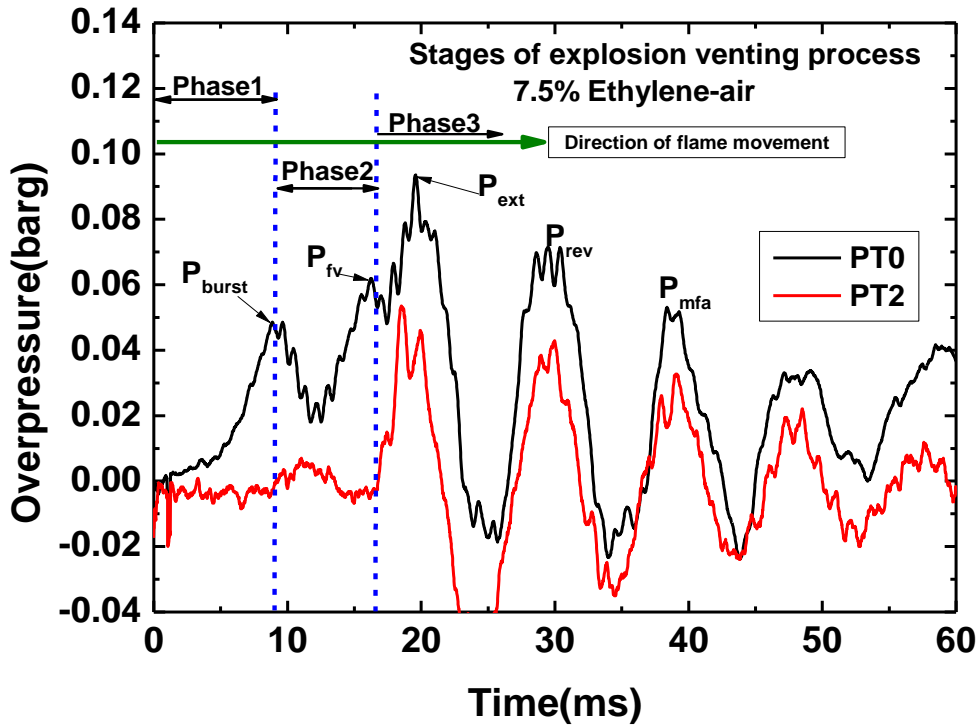
Figure 4.10 Phases of explosion venting process for 7.5% ethylene-air and 10L vessel

($K\_v=7.2, P_{stat}=0.057bar$)
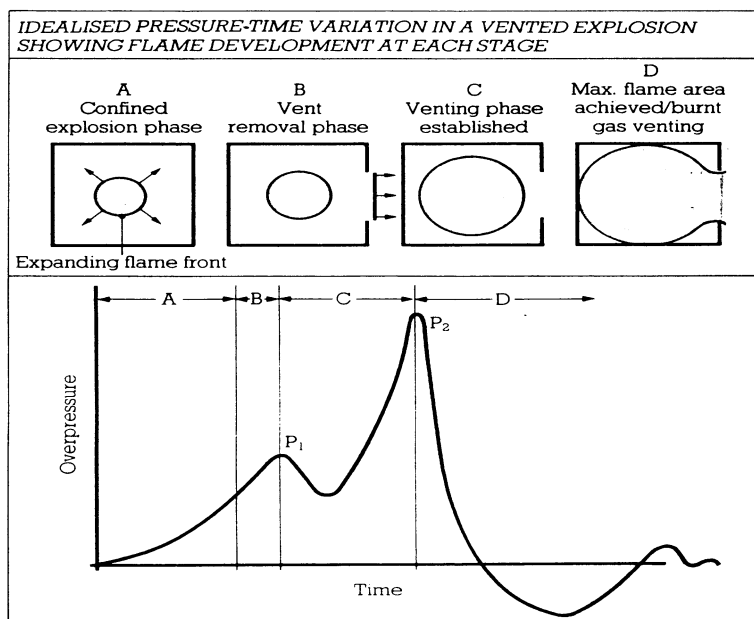
Figure 4. 11 Pressure-time trace with stages of explosion venting process
(Harris, 1983)

4.4 Characteristics of Pressure Peaks in Vented Explosions

There are range of events in vented explosions that can cause a peak in the pressure time record of a vented explosion. Each event will be illustrated in the results section with an explosion pressure record where that pressure is the maximum overpressure. There are six possible causes of the peak overpressure pressure, as summarised in Table 4.2. In many vented explosions all six pressure peaks may be present and which one is the peak overpressure, P_{max} or P_{red} (Bartknecht, 1993) depends on K_v, K_G, P_{stat} and the ignition position. The six pressure peaks were numbered from 1-6 in the order that they normally occur in vented explosions in previous work by the authors (Fakandu et al., 2011, Kasmani et al., 2010b, Fakandu et al., 2012), but have been given a more descriptive nomenclature in the present work as summarised in Table 4.2 and compared with the terminology used by other investigators.

P_{burst} is used for the pressure peak associated with the vent static pressure (P_{stat}), which was zero in the explosion venting with initially uncovered vent (free venting). The bursting of the diaphragm or the vent covers leads to sudden drop in pressure as a result of pressure difference within the vessel and outside the vessel thereby creating this pressure peak. A typical pressure-time profile for 7.5% Ethylene-air shown in Figure 4.10 with P_{burst} in the first phase of explosion venting process as explained earlier.

The overpressure due to the pressure loss caused by the flow of unburned gas through the vent (fv) is referred to as P_{fv} in the present work and this is the overpressure predicted by laminar flame theory. This pressure peak is caused by the onset of gas venting, due to pressure difference, and P_{fv} and P_{burst} occurs before the flame leaves the vent. Following the P_{fv} pressure peak there is usually a pressure peak, P_{ext}, due to an external explosion and this may be larger or smaller than P_{fv}, depending on the mixture reactivity and K_v. The pressure peak P_{ext} is caused by the turbulent flame propagation of the vented flame in the cloud of turbulent unburned mixture expelled from the vent. It will be shown in the results section that in most vented explosions in the present work either P_{fv} or P_{ext} is the peak overpressure, depending on K_v, K_G and ignition position.

In some explosions there is an overpressure peak that occurs at the point of maximum flame area (mfa) inside the vented vessel and this will be referred to as P_{mfa} in the present work. This peak is significant as the laminar flame theory assumes that P_{fv} and P_{mfa} occur at the same time, as discussed below, but the present experiments show that they often occur at different times and that in most cases P_{fv} occurs before the time of maximum flame area and has a higher overpressure than P_{mfa}.

In some vented explosions there is a pressure peak, $P_{rev,}$ that occurs after the external explosion, which is caused by the cooling of the gas mixture in the vessel which causes a reduction in the vessel pressure and a subsequent reverse flow of the external gases into the vented vessel, creating turbulence and causing a second explosion in the vessel in the unburned mixture that remained in the vessel. In some vented explosions P_{mfa} and P_{rev} occur at the same time. This occurs because the reverse flow turbulence coupled with a reactive gas mixture can lead to all the mixture inside the vessel suddenly burning.

This reverse flow explosion is followed by an oscillating mass flow out of the vent and then back into the vessel, which gives a low frequency pressure oscillation. This is quite different from the high frequency acoustic pressure oscillations referred to by Cooper et al (1986), which are referred to as P_{ac} in the present work. P_{ac} is caused by oscillatory combustion inside the vessel and unburned gas trapped in corner regions of the vessel and burning after the flame has left the vent. Which of these six pressure peaks is the maximum will be shown in this work for free venting to depend on K_v, K_G and the ignition location.

Table 4.2 summarises the present terminology and that of other investigators for the various peaks in vented explosions. Most investigations of vented explosions do not give the pressure time diagrams and simply report P_{red} with no comment on whether this is P_{fv}, P_{ext}, P_{mfa}, P_{rev} or P_{ac}, using the present terminology. Cooper et al (1986) did not refer to a pressure peak associated with the maximum flow of unburned gas through the vent, nor do Bauwens et al. (2010). This is not surprising as it may be difficult to observe P_{fv} particularly for large vent areas in large enclosures which were the case with Cooper et al (1986) and Bauwens et al (2010). This is an important pressure peak in explosion venting as the classic laminar flame venting theories are all based on predicting P_{fv} for free venting(Bradley and Mitcheson,

1978a, Cates and Samuels, 1991, Molkov et al., 2000), and should be mentioned. None of the previous investigators refer to the present P_{rev} reverse flow pressure peak. The present results will show that this is a significant pressure peak in central ignition vented explosions, but is rarely the dominant overpressure. The present vented vessel was instrumented with flame position detectors and external pressure transducers to ensure the unequivocal identification of the various pressure peaks.

Table 4.2 Comparison of terminology for the various pressure peaks in vented gas explosions

Peak pressure events	This work	Fakandu et al. [2011,2012] Kasmani et al. [2010b]	Cooper et al [1986] Central ignition	Harrison and Eyre [1987] End ignition	Cates and Samuels [1991]	Bauwens et al. [2010] Central ignition
Peak due to vent opening pressure	P_{burst}	P_1	P_1			
Peak due unburned gas flow through the vent	P_{fv}	P_2		P_{emerg}	ΔP	
Peak due the external explosion	P_{ext}	P_3	P_2	P_{ext}	Dominant	P_1
Peak due to maximum flame area inside the vessel	P_{mfa}	P_4	P_3	P_{max}	Max.burning rate	P_3
Peak due to the reverse flow into the vented vessel after the external explosion and a subsequent internal vessel turbulent explosion. Sometimes co-incident with P_4	P_{rev}	P_5				
Peak due to high frequency pressure oscillations and acoustic resonance.	P_{ac}	P_6	P_4			P_2

4.5 The Determination of P_{red} as P_{fv} or P_{ext} or P_{rev} or P_{mfa}, Illustrations where each of these Pressure Peaks is P_{red}

All the freely vented explosions in the present work showed pressure peaks associated with the flow of unburned gas through the vent, P_{fv}, and an external explosion, P_{ext}. Some also showed P_{mfa} or P_{rev} as the peak overpressure and these will be illustrated in this section. Fakandu et al. (2012) investigated the influence of K_v on P_{fv} and P_{ext} for 40% hydrogen-air in the present test facility. This showed that P_{fv} and P_{ext} were close together as a double peak and which one was highest depended on K_v. At low K_v (<4) P_{ext} was always the largest overpressure and at high K_v (>4) P_{fv} was the greatest overpressure. It is assumed that for the same flame front mass burning rate, the square root of the pressure loss across the vent orifice increases linearly with the decrease in vent area, as shown by the laminar flame venting model (Andrews and Phylaktou, 2010). For K_v around 4 P_{fv} and P_{ext} were similar. When the vent area is large and the flow pressure loss that creates P_{fv} is low then the external explosion dominates. This critical K_v of 4 was for 40% hydrogen-air and may be different for 10% methane-air. Different K_vs were used in the present work (K_v= 3.1-21.7), and 4 gases of different reactivity were chosen to give the external explosion, P_{ext}, as the largest overpressure at the low K_v and P_{fv} as the largest overpressure at the higher K_vs and the results show that this did occur.

A typical end ignition vented explosion smoothed PT1 pressure record is shown in Figure 4.12 for 10% methane-air for K_v=5.4. Also shown in Figure 4.12 is the PT2 pressure record for the pressure transducer mounted downstream of the 162mm diameter vessel. This shows that the peak identified as P_{ext} was due to an external explosion, as there was no pressure rise externally until the flame had exited the vent, at the time recorded by thermocouple T_4 in the plane of the vent and shown in Figure 4.12. The overpressure peak P_{fv} due to the flow of unburned gas through the vent is shown in Figure 4.12 as occurring just before the flame passed through the vent and was, for this K_v of 5.4, lower than the external explosion P_{ext}. The pressure peak, P_{mfa}, associated with the maximum flame area occurred just after the flame reached the wall at time T_3 and this was associated with the start of pressure oscillations and pressure peak P_{rev}. The pressure peak P_{mfa}/P_{rev} in Figure 4.12 could be due to the common action of a reverse flow into the vessel which generated

turbulence that completed the combustion of the mixture in the vessel. Figure 4.12 shows a significant negative pressure in the vessel due to cooling of burnt gases in the vessel after the explosion was vented. This vacuum sucks gas from outside the vent back into the vessel creating turbulence and a further explosion in the unburned gas still inside the vented vessel and this causes the low frequency pressure oscillation shown in Figure 4.12.
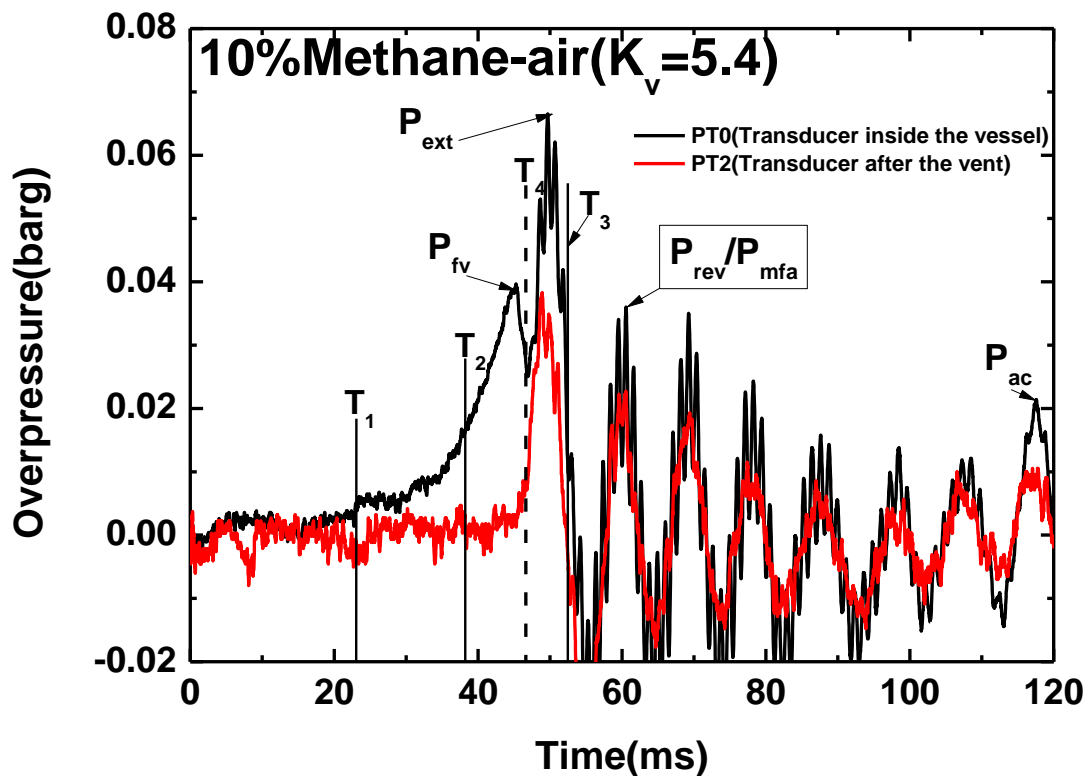
Figure 4.12 Pressure profiles for 10% methane-air for Kv=5.4 with end ignition, for pressure transducers PT1 and PT2

Figure 4.13 shows the results for 7.5% Ethylene-air vented explosions with the same K_v=5.4 as for the methane-air explosions in Figure 4.12. Both central ignition and end ignition were investigated and Figure 4.13 shows much higher peak overpressure for end ignition than central ignition, 0.35 bar compared with 0.09 bar respectively. For central ignition the peak overpressure was clearly caused by the external explosion as it occurred after T_4 and the external pressure transducer had a peak pressure at the same time as the internal pressure transducer. The pressure peak P_{fv} due to the flow of unburned gas through the vent was a distinctive peak, lower than P_{ext}, and occurred after T_2 and before T_4. For central ignition there was a clear P_{mfa} and P_{rev}, both lower than P_{ext} but higher than P_{fv}. P_{rev} occurred before P_{mfa} and this was distinguished by the time of flame arrival at T_3, which occurred just after the negative pressure after P_{ext} and was caused by the reverse flow into the vented

vessel and the turbulence this created. However, the maximum flame area with central ignition is when the flame reaches the end flange and passes T_1 and this occurred on the second pressure oscillation, as shown in Figure 4.13a.
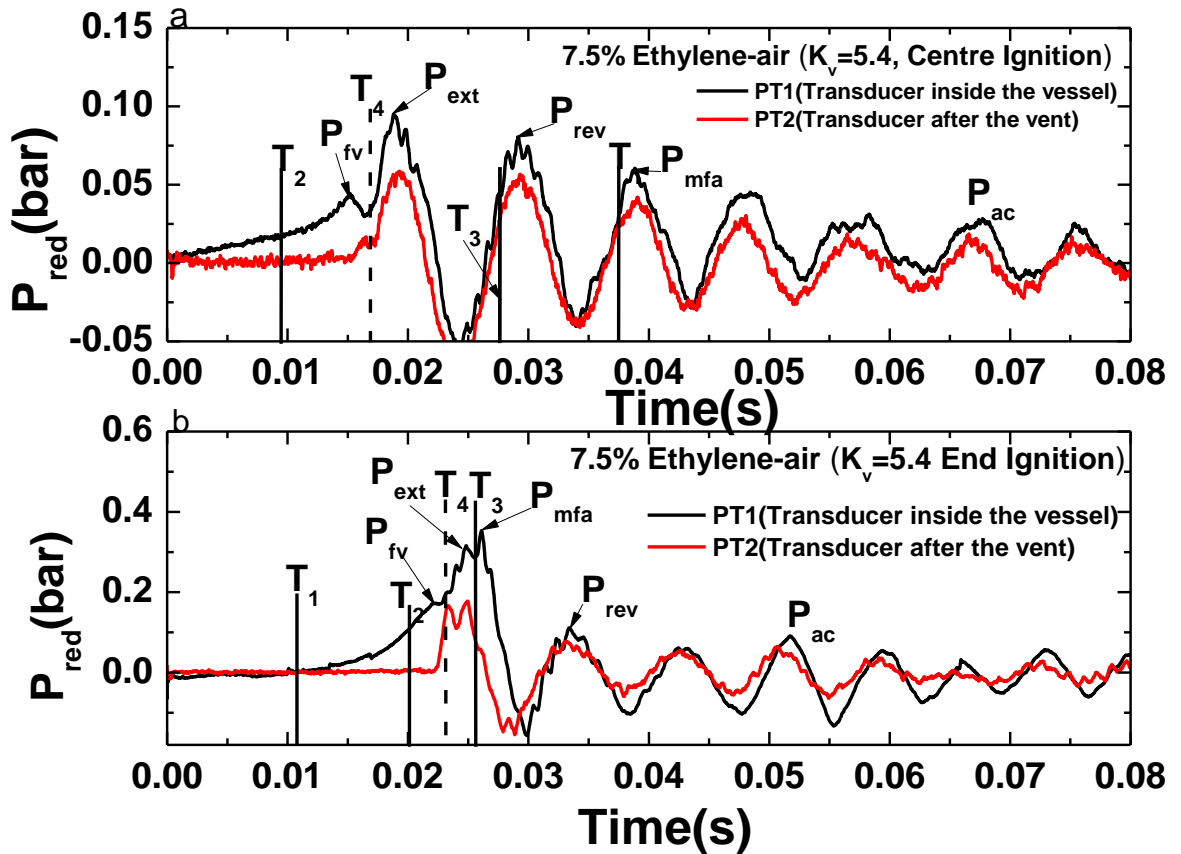
Figure 4.13 Pressure profiles for 7.5% ethylene-air for Kv=5.4 with (a) central and (b) end ignition, for pressure transducers PT1 and PT2

For end ignition Figure 4.13b shows that the P_{fv} and P_{ext} pressure peaks occurred either side of the time of the flame arrival at the vent, T_4. P_{ext} was the larger of the two peaks. The alignment in time of the external pressure record with the internal record is shown for peak P_{ext} in Figure 4.13b. However, in this case Figure 4.13b shows that the peak overpressure occurred at the time of peak flame area, P_{mfa}, with the flame arriving at the wall at T_3. This was followed by a small reverse flow pressure peak, P_{rev}. This was one of the very few vented explosion cases where the peak flame area, co-incident with the flame arrival at the wall thermocouple, T_3, gave the highest overpressure. Figure 4.13b shows that P_{mfa} was the highest overpressure, but it was only slightly higher than the external explosion, P_{ext}. In most cases, the P_{mfa} occurs well after the flame had left the vessel particularly for less reactive mixtures of methane-air and propane-air mixtures. This was due to fast axial flame acceleration as the flame propagates towards the vent as a result of high

combustion rate. However, the flame could not touch the wall before exiting the vent, due to the small vessel vent and as such the first pressure for the free venting was P_{fv}. This was contrary to result obtained for large L/D where the first pressure peak was caused by cooling effect after contacting the wall of the vessel (Alexiou et al., 1996a). This was contrary to the assumption that the P_{mfa} was always the peak pressure (Bradley and Mitcheson, 1978b, Runes, 1972), this is the case as shown in the two cylindrical vessels considered in this work.
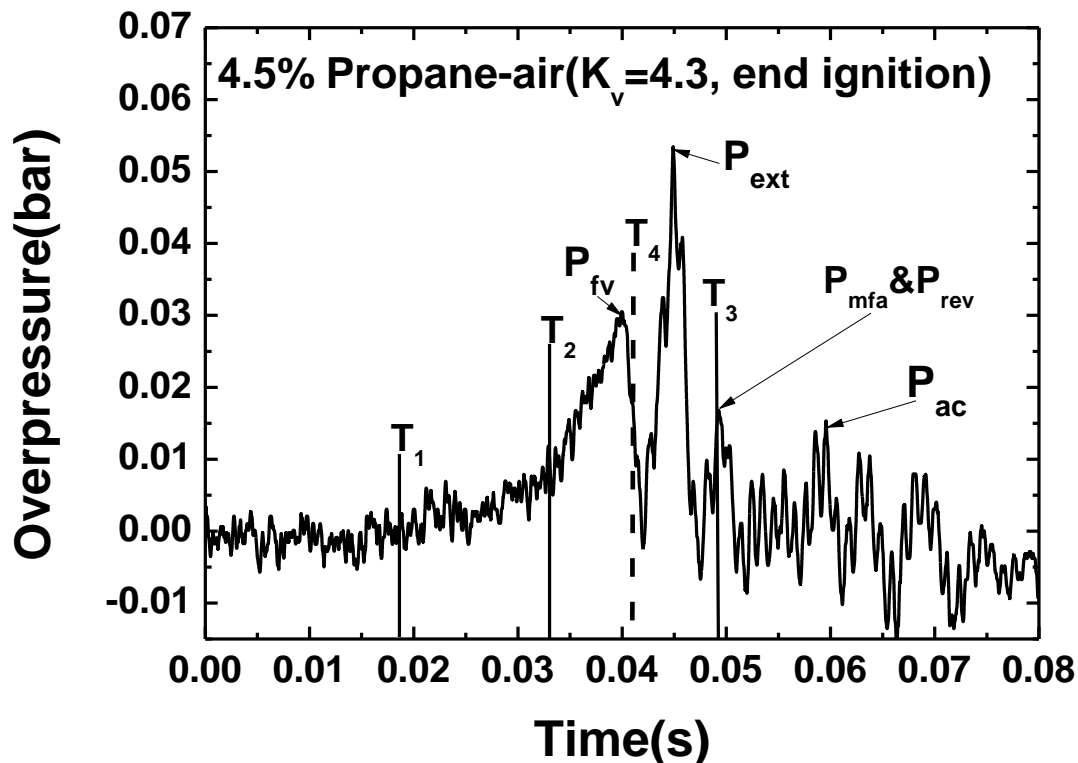
Figure 4.14 Pressure profiles for 4.5% propane-air for Kv= 4.3 with end ignition, for

pressure transducer PT1

Figure 4.14 shows the pressure record for a 4.5% propane-air explosion with end ignition and $K_v = 4.3$. This shows a very clear pressure peak for P_{fv} and P_{ext} either side of the flame arrival at the vent, T_4, and a clear maximum flame area peak, P_{mfa}, after the negative pressure and subsequent reverse jet flow and ignition of residual unburned gas in the vented vessel. In this case peaks P_{mfa} and P_{rev} are caused by the same event, as the reverse jet flow causes turbulent burning of the residual mixture that burns all the mixture and arrives at the wall at T_3 in Figure 4.14. However, of these three pressure peaks it is the external explosion peak, P_{ext}, which is significantly higher than P_{fv} or P_{mfa}. Similar results are shown in Figure 4.15 for 7.5% ethylene-air at the same K_v of 4.3, with the external explosion, P_{ext}, as the dominant overpressure. In this case P_{mfa} is not a separate peak, but occurs rapidly

after P_{ext} on the pressure decay from the P_{ext} peak and is identified by the time of arrival at T_3. The peak overpressure with ethylene is much greater than for propane at 0.18 bar compared with 0.052 bar for propane. The ratio of these two pressure peaks, 3.46, is very close to that predicted by as shown by the laminar flame venting model (Andrews and Phylaktou, 2010) as U_L^2 which is $(0.8/0.45)^2 = 3.16$.

The above vented explosions were for K_v=5.4 or lower and all but one showed that the external explosion, P_{ext}, was the highest overpressure. This is in agreement with the hydrogen results (Fakandu et al., 2012), but with the critical K_v for P_{ext} to be the dominant overpressure moved from 4 for hydrogen to at least 5.4.
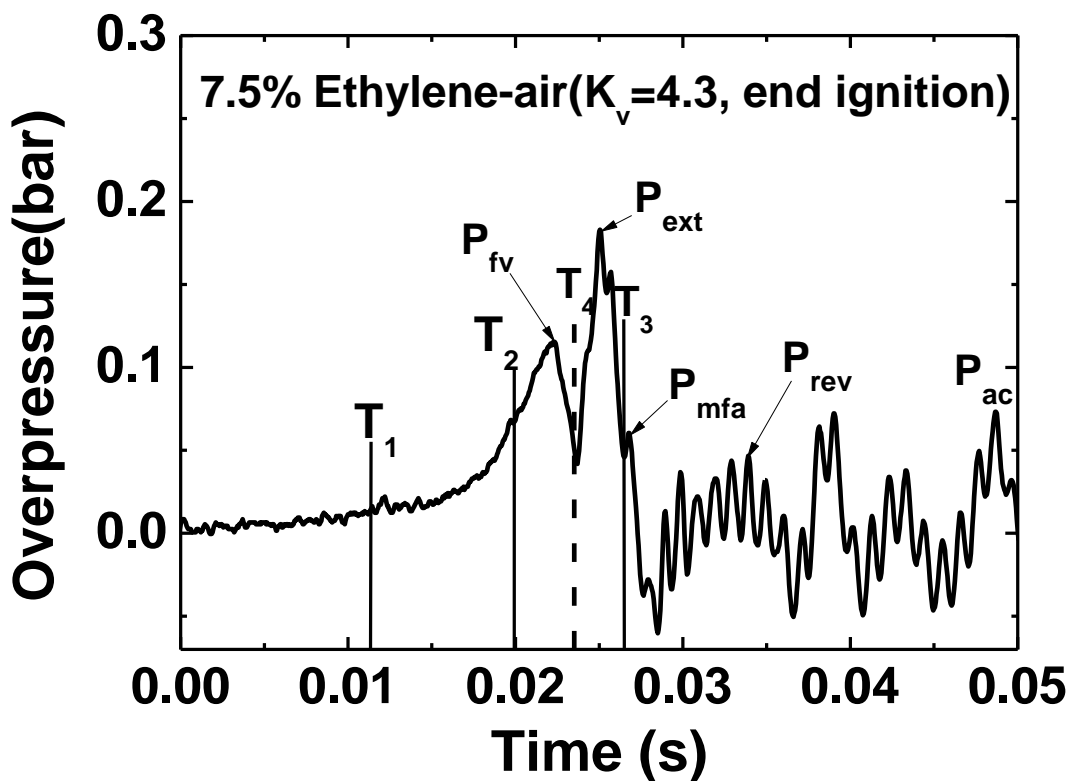
Figure 4.15 Pressure profiles for 7.5% ethylene-air for Kv=4.3 with end ignition, for pressure transducer PT1

Vented explosions for 10% methane air for the higher K_v of 10.9 (80% blockage) are shown in Figure 4.16 for end ignition This shows that for end ignition P_{fv} was the dominant overpressure at 0.125bar and occurred just before the flame arrived at the vent at time T_4. The external explosion and the maximum flame area pressure peaks occurred on the decay from the P_{fv} pressure peak and were identified from the T_4 time for the external explosion and T_3 for the P_{mfa} pressure peak. However, there was only one overpressure peak and the above three pressure peak events were not separated much in time. It was typical of higher K_v for P_{fv} to be the dominant

overpressure particularly for 10% methane-air and 4.5% propane-air. More detail discussions on the effect of vent area and reactivity will be given in subsequent chapters, as this section aims to introduce the various pressure peaks as observed from the present work.
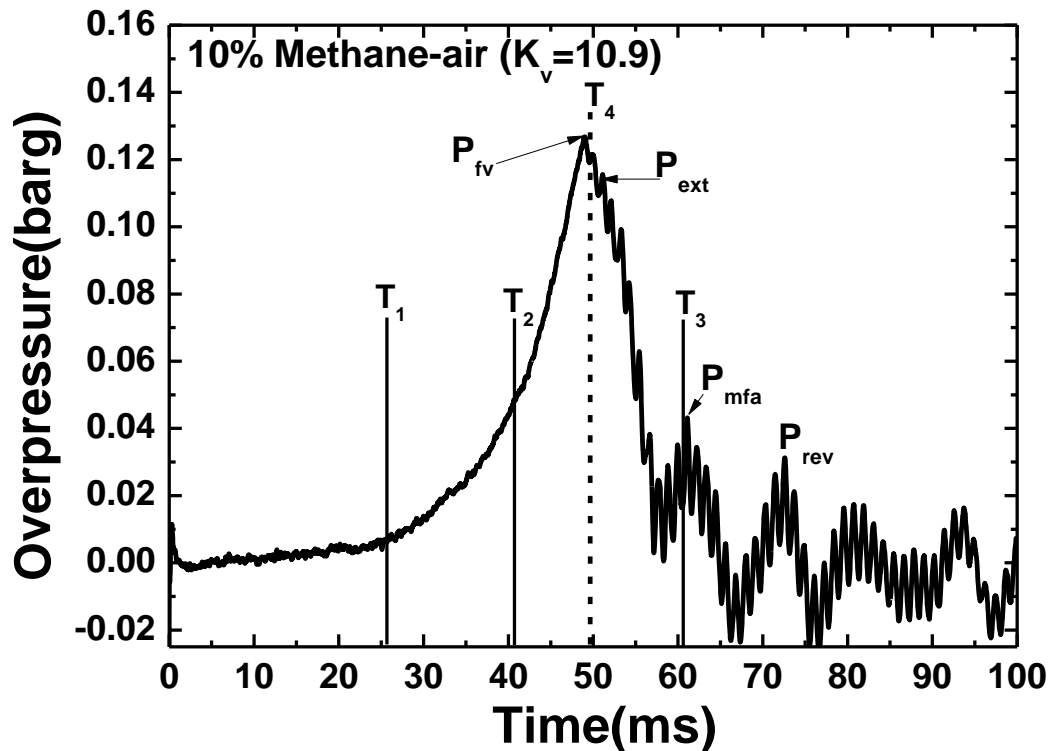
Figure 4.16 Pressure profiles for 10% methane-air for Kv= 10.9 with end ignition, for pressure transducer PT1

4.8 Conclusion

1.   It was shown that the maximum pressure in cylindrical vessel behaves differently from that of spherical particularly when the vessel length is greater than the diameter. Heat losses as a result of flame contact with the wall was a major cause of lower P_{max} in cylindrical vessel, and this was also the cause of lower P_{max} in ignition positions other than central in confined enclosure. P_{max} was shown to increase as the vessel volume increased and this was due to the influence of the vessel surface area to volume ratio, S/V, which produces higher wall convection losses as the volume decreases for the same vessel shape.

2.   Central ignition location in closed spherical vessels was shown to produce the highest P_{max}. However, this does not mean that this is the worst case ignition location for vented explosions, as these do not reach the peak pressure of a closed vessel explosions and P_{red} is controlled by the fast initial flames that propagate to the vent without touching the walls in L/D of 2.8 vented explosions.

3.   Pressure peaks generated as a result of explosion vented are influenced by different physical phenomenon. This chapter gave a breakdown of different pressure peaks with new nomenclature to replace the once used previously as part of this work. The maximum reduced pressure (P_{red}) may either be P_{fv} or P_{ext} depending on certain factor including the vent area and mixture reactivity. Some of the other pressure peaks could dominate in certain circumstances.

CHAPTER 5:

Factors Affecting the Overpressure and Average Flame Speed in Explosion Venting

5.1 Introduction

5.2 Influence of vent area on explosion overpressure and flame speed

5.2.1 Influence of vent area on explosion overpressure

5.2.2 Influence of vent area on flame speed

5.3 Impact of non-central and multiple vents on vented explosion overpressures

5.3.1 Influence of non-central vents on explosion overpressure and flame speed

5.3.2 Effects of single vent and four vents on the explosion overpressure and flame speed

5.3.3 Change from one to 16 vents and effect of characteristic length scale on the turbulence downstream the vent at constant Kv

5.3.4 Comparison of the present single vent results with Cooper et al. (1986) in a larger volume vessel

5.4 Ignition position effect in explosion venting

5.5 Influence of vent shape on gas explosion venting

5.8 Conclusion

5.1 Introduction

Most current vented explosion data in relatively large explosion vessels cannot be predicted using laminar flame propagation models, without including an empirical turbulence factor to make theory and experiments match. However, part of the flame acceleration may be the self-acceleration of laminar flames over the large distances involved in large explosion vessels. The generation of flame acceleration due to turbulence created in the venting process should not change significantly with vessel size. This section present the result of a small 10L explosion vessel with an L/D of 2.8 with small flame propagation distance to the vent so that self-acceleration of the flame should be small or may not exist (Kasmani et al., 2010b).

Different scenarios of experiments were carried out with this vessel with free venting (without a vent cover – i.e. open from the start of the test). Pressure peaks of vented explosions as introduced earlier in chapter 4 will be discussed in more detail in this section, and the flame speed associated with premixed gas-air mixture.

The result of influence of vent area, position of the vent, multiple distributed vents, position and shape are presented. Furthermore, the influence of ignition position which is ignored in the current venting standard was also discussed. The present results and other data from the literature show that the vent design guides may not be based on sufficiently conservative data and need to be reviewed.

5.2 Influence of Vent Area on Explosion Overpressure and Flame Speed

In general, there are series of experimental data on vented explosions in order to generate substantial data for the for accurate prediction of appropriate vent size in applying the venting technique ((Lunn, 1984). The current vent design guidance gave the appropriate sizing of the vented vessels based on the experimental data of swift (1988) and the European guide based on the work of Bartkecht (1993), and the work considered different vessel volumes, vent areas as well as lower L/D. A most of the experimental data were large scale, as these are close to reality as applied in the industries. Large scale vented experimental data was carried out by Bauwen et al (2010) with two different vent sizes, and the work showed that the vent size had significant influence on the various pressure peaks depending on the ignition

location(Bauwens et al., 2010). The relationship between the vent area and maximum pressure in a vented $35m^3$ was shown to also depend on the ignition location (Solberg et al., 1981). In large L/D vented vessels, the various peak pressures were shown to differ with the size of the vent (Alexiou et al., 1996b). The magnitude of the P_1 increases while that of P_3 decreases with vent area, for the two vent sizes of $K_v=1$ and 5 considered in the work. Most of the work discussed above and in the literature did consider only selected vent sizes, with limited data on wide range of K_vs especially for small scale explosion venting (Chow et al., 2000, Cooper et al., 1986, Sato et al., 2010, Solberg et al., 1981, Wu Y and Swithenbank, 1992, Alexiou et al., 1996b). A typical experiments where wide of range K_v were used (K_v= 1-64) was carried out by Rasbash and Rogowski(1960) for large duct L/Ds using propane-air and pentane-air mixtures (Rasbash and Rogowski, 1960). It was shown that the explosion overpressure was directly proportional to the vent area or inversely proportional to the K_v. This was in agreement with the work of Tite et al (1991) in long enclosure where proportional relationship between vent area and the maximum pressure was also established (Tite et al., 1991).

It was extremely important that some of studies mentioned above established a linear relationship between vent area and vented overpressure, which could be useful in explosion venting prediction particularly for large L/D based on experimental result. However, there is little or insufficient data for wide range of K_vs related to small vessels and lower L/D within the applicability of the NFPA 68 (2013) and the European gas venting guide (EN14994:2007, 2007). Hence, this section seeks to present the result for vented explosion in 10L vessel with L/D =2.8 for range of $K_v=3.1$ to $K_v=21.7$. This is to establish the effect of vent area on explosion overpressure and to generate explosion venting data for such geometry as cylindrical vessel with practical relevance due to insufficient data.

5.2.1 Influence of Vent area on Explosion Overpressure

The range of experiments in this section, a16 J ignition energy was used and the spark plug was located at the centreline of end flange opposite the vent. This was shown to produce the most severe overpressure as compared to other locations for geometry of this configuration, in compliance with the ATEX regulation(EuropeanParliament and Council, 1994, Kasmani et al., 2010b, Willacy

et al., 2007).Each test was carried out at least three times and where possible all repeat measurements are shown. Figure 5.1 shows the pressure-time profile for 10% methane-air with different K_vs. After the initial spherical flame propagation period, there was sudden rise in pressure with increasing rate of pressure until P_{fv} was achieved for the higher K_v of 21.7. This shows similar behaviour with the closed vessel explosion pressure rise as shown in the previous chapter but with the sudden drop in pressure after the flame had exited the vent. For this particular set of experiments, only free venting (initially uncovered vent) was considered and the first peak pressure (P_{burst}) was not observed. A peak pressure of 370mbar was observed for K_v of 21.7 and this was caused by onset of burnt gas venting (P_{fv}), while P_{ext} as a result of the external combustion of the unburnt gas cloud occurred almost at the same time. The reduction of venting rate as a result of restricted vent area for the small vent and faster mass burning rate is responsible for much higher overpressure for higher K_vs as compared to the larger vent area. Small vent areas or higher K_v =8 was shown to give much more overpressure of 243mbar as compared to K_v=2 with 16mbar due to more reduced venting rate associated with smaller vents (Chow et al., 2000).
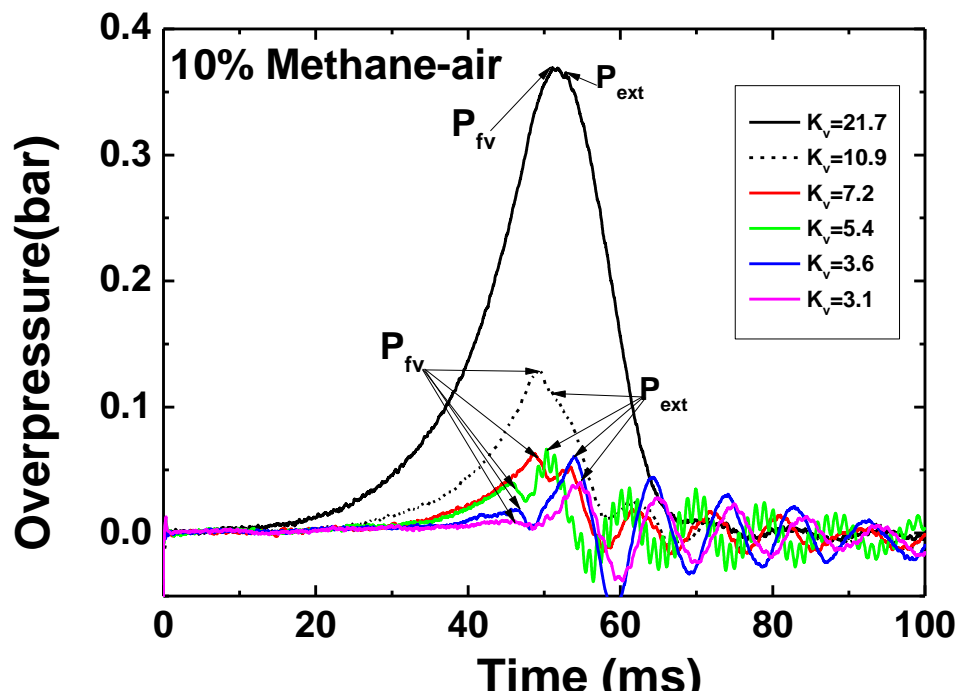
Figure 5. 1 Influence of Kv on pressure-time profiles 10% methane-air

 Figure 5.1 also shows that the rate of pressure rise was faster with higher K_vs and decreases as the K_v decreases. Similarly onset of burnt gas venting is faster with

smaller K_vs and decreases with increase in K_v. The mass flow rate of unburnt gas is faster for large vent areas as compared to the rate of burning of he gas mixture resulting to early burnt gas venting as well as lower P_{fv}. Additionally, the large vent areas were shown to generate higher P_{ext} as compared to smaller vents areas with P_{fv} as the dominant pressure peak. The large unburnt gas cloud expelled from the large vent areas due to higher venting or mass flow rate was responsible for the higher external combustions. The magnitude of P_{fv} increases with increase in K_v and this is in agreement with the literature where P_1 was shown to increase with increase in K_v due to difference in volumetric flow rate and time of burnt gas venting (Alexiou et al., 1996b). Figure 5.2 also gives similar trend for 4.5% propane-air with the result in Figure 5.1 where the P_{fv} was the dominant peak pressure for K_v=21.7 to 7.2, while P_{ext} was the dominant peak pressure for K_v=5.4 to 3.1. Additionally, the higher the Kv the longer it takes for the maximum reduced pressure to be attained similar to trend obtained for 10% methane-air in Figure 5.1. The main difference between Figure 5.1 and 5.2 are the magnitude of the peak pressure at constant K_v. While P_{red} of 370mbar and 131mbar where obtained for Kv of 21.7 and 10.9 for 10% methane-air, 450mbar and 156mbar were obtained for the same Kv for 4.5% propane showing the influence of reactivity. This is in agreement the work of Chow et al (2000) where the fuel type was shown to influence the peak overpressure due to different combustion rate and other fundamental properties.
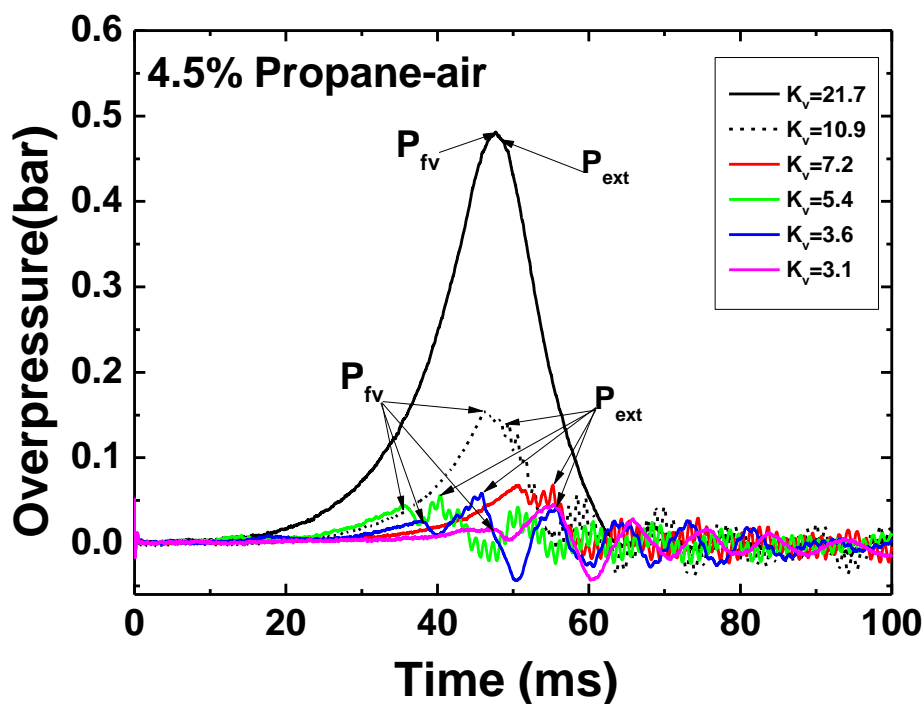
Figure 5.2 Pressure-time record for 4.5% Propane-air for different Kv

For more reactive mixture of 7.5% ethylene, the high rate of combustion and fast nature of flame propagation was shown to affect the trend pressure-time as shown in Figure 5.3 when compared to that of propane-air and methane-air. The peak overpressure increases as the vent coefficient increases, while P_{fv} show increase in magnitude as the K_v increases similar to other gas-air mixtures mentioned above. However, P_{ext} was shown to be the dominant pressure peak for all vent areas, which is the main difference with the other gas mixtures due to it reactive nature of the gas mixture and reactivity of the gas mixtures is explained in more detail in chapter 7. A negative pressure as seen in most pressure profiles after the external combustion was due to back flow of the flame into the test vessel caused by the higher pressure generated as a result of the external explosion. This is a characteristic trend of the pressure-time traces of vented explosion as demonstrated in this work. The negative pressure decreases as the vent area increases with deep becoming more obvious with larger vents, as shown in Figures 5.1-5.3. The pressure peak generated after the pressure deep is termed P_{rev} as discussed in the previous chapter.
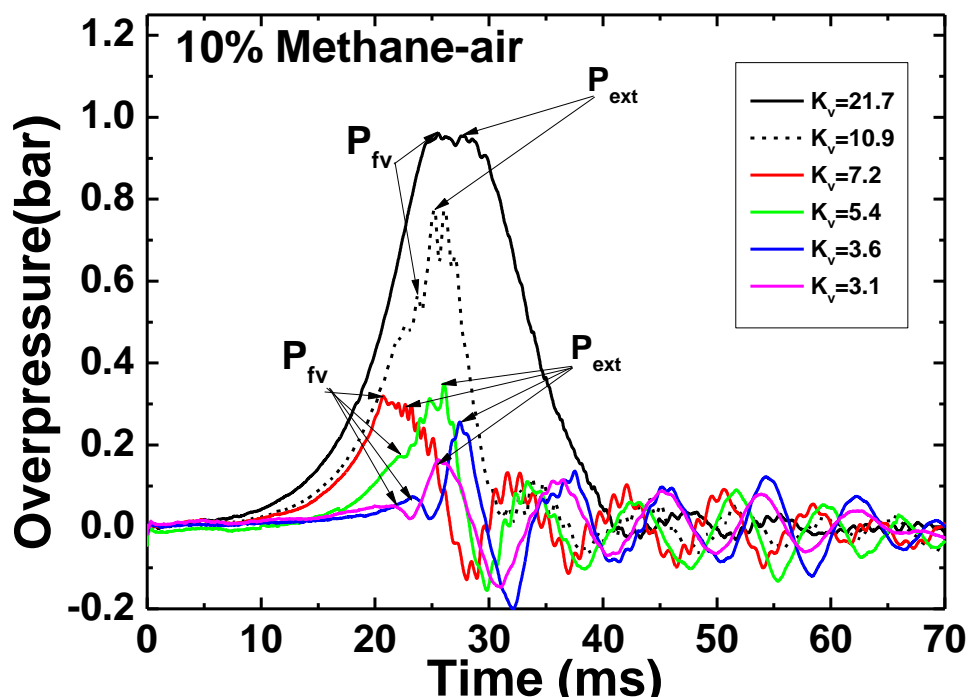
Figure 5.3 Pressure-time record for 7.5% Ethylene-air for different Kv

The pressure associated with acoustic oscillation (P_{ac}) was not seen to be visible in most of pressure-time records in Figures 5.1-5.3. It is typical of end ignition opposite the vent to produce low Pac and high Pac are associated with more with

central and front end ignition caused by external explosion (Cooper et al., 1986, Harrison and Eyre, 1987).
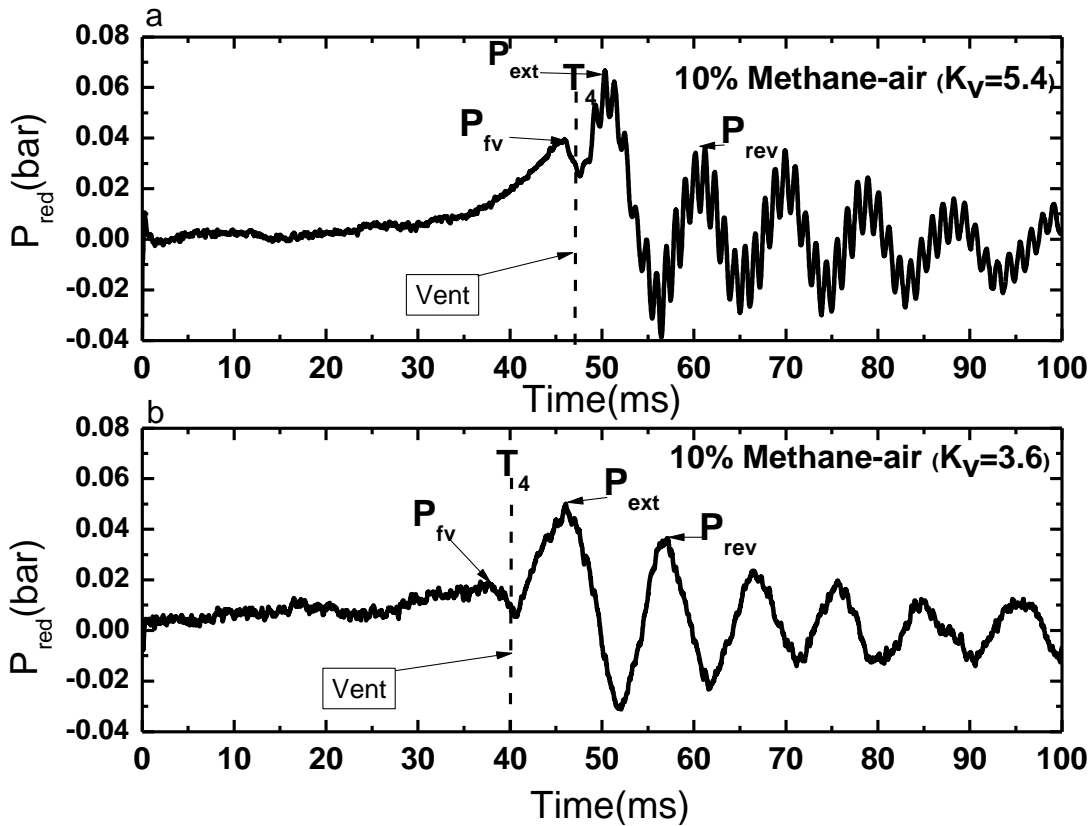
Figure 5.4 Pressure-time record for 10% methane-air with end ignition,(a) Kv=5.4 (b) 3.6.

A typical end ignition vented explosion smoothed PT0 pressure record is shown in Figure 5.4a for 10% methane-air for K_v=5.4. Also shown in Figure 5.4b is the PT0 pressure record for the pressure transducer mounted upstream of the 162mm diameter vessel at the end flange opposite the vent for 10% methane-air for K_v=3.6. This shows that the peak identified as P_{ext} was due to an external explosion, as there was no pressure rise externally until the flame had exited the vent, at the time recorded by thermocouple T_4 in the plane of the vent and shown in Figure 5.4. The overpressure peak P_{fv} due to the flow of unburned gas through the vent is shown in Figure 5.4 as occurring just before the flame passed through the vent and was, for this K_v of 5.4 and 3.6, lower than the external explosion P_{ext}. The pressure peak P_{rev} in Figure 5.4 could be due to the common action of a reverse flow into the vessel which generated turbulence that completed the combustion of the mixture in the vessel. Figures 5.1-5.3 shows significant negative pressure in the vessel due to cooling of burnt gases in the vessel after the explosion was vented. This vacuum

sucks gas from outside the vent back into the vessel creating turbulence and a further explosion in the unburned gas still inside the vented vessel and this causes the low frequency pressure oscillation shown in Figure 5.4.
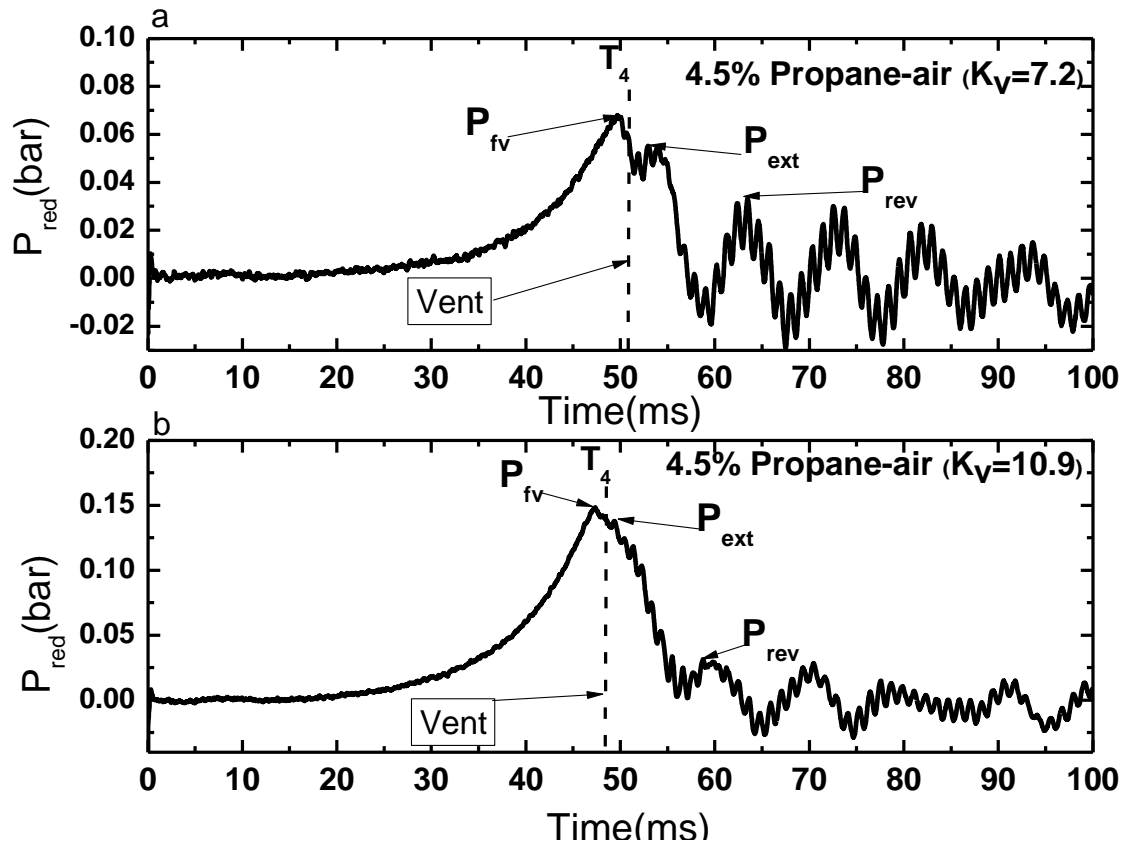
Figure 5.5 Pressure-time record for 4.5% Propane-air with end ignition, (a) Kv=7.2 (b) 10.9

Figure 5.5 shows the pressure record for a 4.5% propane-air explosion with end ignition for $K_v = 7.2$ and 10.9. This shows a very clear pressure peak for P_{fv} and P_{ext} either side of the flame arrival at the vent, T_4. These two pressure peaks shows that P_{fv} was the controlling peak pressures which was contrary to Figure 5.4 where P_{ext} was the dominant pressure peak. In this case peaks P_{rev} caused by the reverse jet flow causes turbulent burning of the residual mixture that burns all the mixture as shown in Figure 5.5. However, the negative pressure seen in Figure 5.4 was not too obvious in Figure 5.5 this was because since of the dominant pressure peak in Figure 5.4 was P_{ext} , the pressure moves into the vessel more due to difference in pressure. This was also similar with the small vent areas for 10% methane-air.
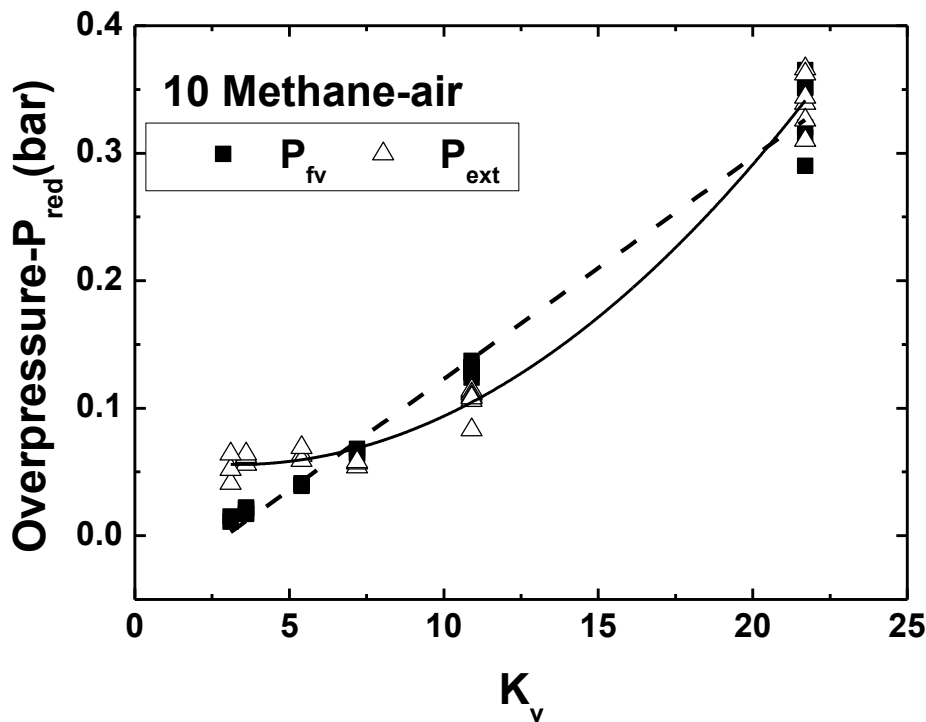
Figure 5.6 Overpressure against Kv for 10% methane-air with end ignition

For free venting the pressure loss of the flow of unburned gas through the vent is one cause of the vent overpressure, P_{fv}, (Fakandu et. al., 2011, 2012, 2013; Kasmani et al., 2011) and the other is the external explosion, P_{ext} (Cubbage and Simonds, 1955, Cooper et al, 1986 and Bauwen et al, 2010). Both of these causes of the overpressure are potentially influenced by the shape of the vent. It was reported that the flow of unburnt gas through the vent, P_{fv} was dominant peak pressures for small vent areas while the P_{ext} was the controlling peak pressure for most large vent areas (Fakandu et al 2011). This present work, exploits further by defining the range of K_v for which either P_{fv} or P_{ext} was dominant peak overpressure. Figure 5.6 shows two peak pressure (P_{fv} and P_{ext}) as against K_v for range of vent coefficients (K_v=3.6-21.7) for 10% methane-air mixture. There was increase in overpressure for P_{fv} as the Kv increases showing the dependent of overpressure on the vent area. Also, Figure 5.6, shows that the P_{fv} was the dominant pressure for lower K_v up to 5.4, while the P_{ext} was the controlling pressure peak for all K_vs above 5.4 when result of 10% methane-air. This was in agreement with the work of Harrison and Eyre (1987) and Fakandu el al (2011) where pressure as result of external explosion was the controlling pressure peak for large vent areas. The result was also shown to be similar when 4.5% propane-air was analysed as shown in Figure 5.7, but more reactive mixtures

may have different trend as seen in these mixtures shown in Figure 5.6 and Figure 5.7.
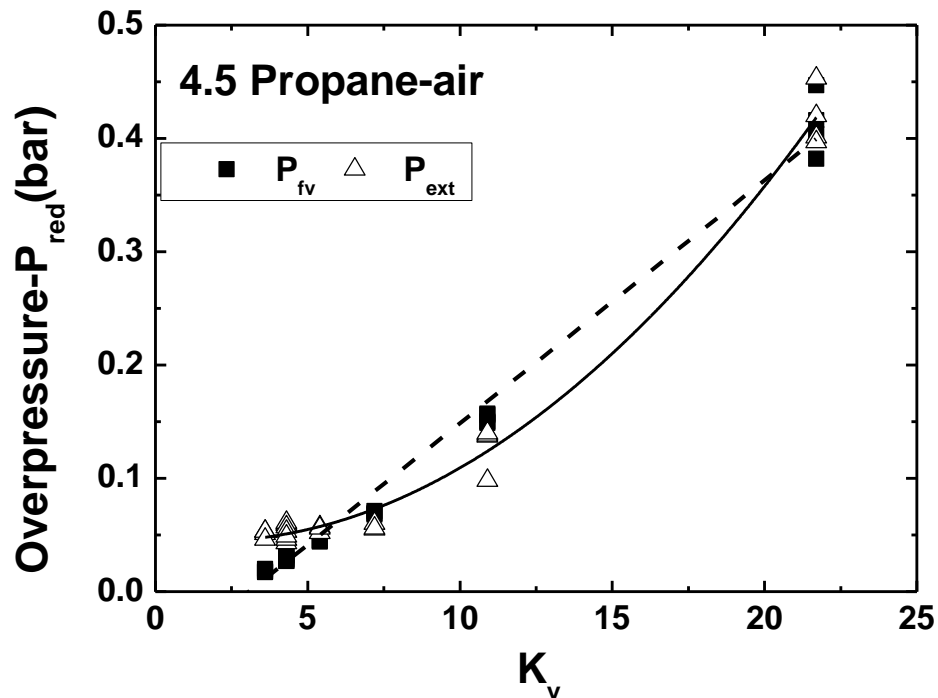
Figure 5.7 Overpressure against Kv for 4.5% Propane-air with end ignition

All the above vented explosions were for K_v=5.4 or lower and all showed that the external explosion, P_{ext}, was the highest overpressure. This is in agreement with the literature (Harrison and Eyre, 1987, Fakandu et al., 2011, Fakandu et al., 2012) but with the critical K_v for P_{ext} to be the dominant overpressure with limiting value 5.4. For all K_v above 5.4, it was shown that the P_{fv} was the controlling peak pressure for 10% Methane-air and 4.5% and Propane-air.

For methane the large vent areas were shown to allow more backflow of pressure due to higher external explosion, showing negative dip of pressure in the pressure profile. For small vent areas or higher K_v the P_{fv} was the higher overpressure, hence reducing the reverse flow of pressure. For all the gas mixture as shown in Figure 5.6 and 5.7, the proportional relationship between the vent and maximum overpressure in vented explosion is demonstrated. This is in agreement with the work Tite et al (1991) and Cubbage and Simmond (1955), where the maximum pressure was shown to increase as the vent area increases (Cubbage and Simmons, 1955, Tite et al., 1991). Additionally, the P_{fv} has a linear relation with the K_v irrespective of the gas mixture as shown in Figure 5.6 and 5.7. The maximum explosion pressures obtained

in vented explosions is directly proportional to the vent coefficient irrespective of the position of vent (Palmer and Rogowski, 1968).

5.2.2 Influence of Vent Area on Flame Speed

The flame travel time was recorded by mineral insulated, exposed junction type-K thermocouples, arranged axially at the centreline of both the main test and the 0.5m dia. vessel. Thermocouples T_1, T_2 and T_4 were located on the centreline of the main test vessel, while thermocouples T_5, T_6 and T_7 were on the centreline of the 0.5m dia. connecting vessel. The time of flame arrival was detected from the thermocouples and the flame speed between two thermocouples was calculated and plotted as the flame speed for the midpoint between the two thermocouples. There was also another thermocouple, T_3, located on the wall of the main test vessel to measure the time of flame arrival at the wall of the vessel. These event times are marked on the pressure time results with the thermocouple location, so that the position of the flame when a peak in the pressure time record occurs can be determined. This enabled precise determination of whether the highest overpressure was generated by an external explosion or by the internal flame displacing unburned gas through the vent.

Figure 5.8 is the flame speed result for 10% methane-air and 7.5% ethylene-air for Kv= 21.7 to 3.1 against distance from the ignition position. The flame upstream the vent was seen to propagate at the initial spherical flame speed of 3.2m/s for 10% methane-air in Figure 5.8a, and this is the initial flame speed from the time of the flame to travel from the spark to the first thermocouple. A range of initial flame speed of 3.01-3.5m/s was obtained for the small vessel with the average flame speed of 3.2m/s from the time of ignition to the first thermocouple at a distance of 0.078m from the ignition position. There was no significant influence of K_v on this initial flame speed which was close to the expected 3m/s spherical flame speed that has been measured in laminar flames in spherical vessels (Andrews and Bradley, 1973, Bradley et al., 2000). The flame speed increased in the later stage of the explosion reaching up to twice the initial flame speed at the second thermocouple and approximately 10 times the flame speed before reaching the vent as shown in Figure 5.8a. An average maximum flame speed of 25.8m/s was obtained for 10% methane-air irrespective of the K_v. The maximum flame speed upstream and closer to the vent

was significantly affected by the vent coefficient, the flame speed increases as the K_v was increased. This was expected as the unburned gas velocity at the vent throat increases as K_v increases and this was expected to result in an increase in the flame speed approached the vent as the vent area was reduced (higher K_v). However, there also this issue as K_v increases the vessel end wall becomes increasingly closed and the mean velocity in the vessel decreases due to the flame essentially propagating towards a flat wall with a small hole in it.

For ethylene there was an initial flame speed of about 6 m/s and a maximum upstream flame speed of 71m/s at the vent and the flame speed was shown to be independent of Kv which is not expected as shown in Figure 5.8b. Propane also showed a steady initial flame speed of 3.3m/s for most of the vent sizes as shown in Figure 5.9a. This is close to the spherical flame speed for propane and a maximum upstream flame speed of 23m/s with little dependence on K_v different from the trend to the trend observed in Figure 5.8a. Faster flames speed associated with more reactive mixtures accelerating axially towards to the vent may be responsible for the flame not recognising the vent size. This is contrary to the result presented for large L/D vessel where flame speed was shown to decreases as the K_v increases (Alexiou et al., 1996b). The large L/D vessel and the flame propagation pattern are different from what is obtained in compact vessel.
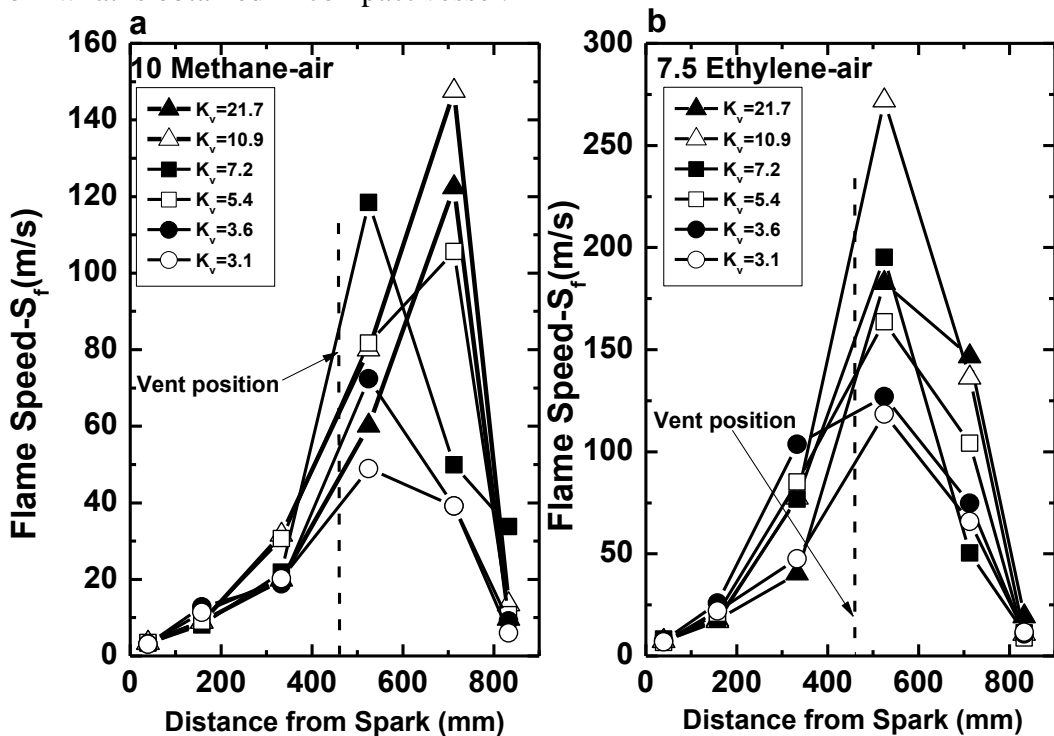
Figure 5.8 Flame speed as a function of Kv for (a) 10% methane-air (b) 7.5% ethylene-air

The downstream flames speeds for all K_v were also calculated for different gas mixtures as seen in Figure 5.8 and 5.9. For all gas mixtures, the maximum flame speeds observed downstream were shown to increase as the K_v increases, with the exception of $K_v=21.7$ which shows lower overpressure as compared to $K_v=10.9$. The increase in blocked area of the vents represented by the length scale (*l*) is responsible for increase in flame speed after the flame exit the vent. The effect of characteristics length was shown to affect flame speed (Andrews et al, 1990, Phylaktou and Andrews, 1991, Phylaktou et al, 1994). Figure 5.9b demonstrate the effect on length scale by presenting the maximum flame speed obtained downstream as a function of K_v. The maximum flame speed downstream was shown to increase as the K_v increases with the $K_v=10.9$ as the thresh hold and starts going down after that. For all the gas mixtures used, the maximum flame downstream for $K_v=21.7$ was shown to be lower than that of $K_v=10.9$ even with it higher length scale. In the study of flame interaction with obstacle, the flame speed increases as the turbulent scale increases up to certain length scale after which it starts to decline ((Na'inna, 2013). In this case, the Kv=10.9 is the threshold turbulent length scale where the maximum flame speed could be achieved as demonstrated from this work.
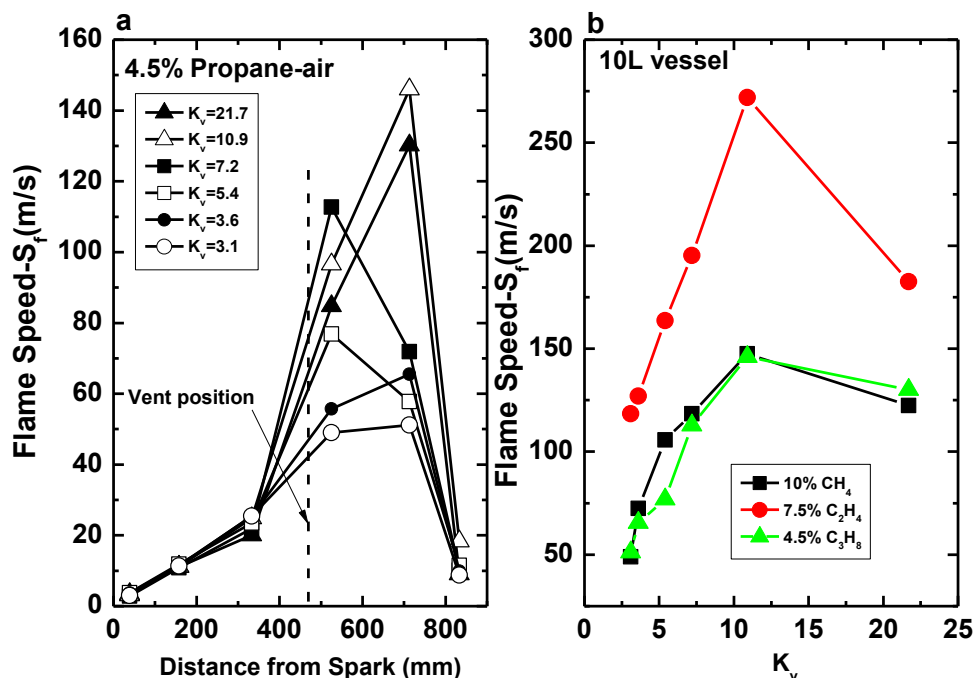
Figure 5.9 (a) flame speed for 10% methane-air (b) maximum downstream speed as function of Kv

5.3 Impact of Non-central and Multiple Vents on Vented Explosion Overpressures

In this section values of K_v were chosen to cover values that produce the external explosion, P_{ext}, as the dominant overpressure at low K_v and where the flow of unburnt gas through the vent is the dominant cause of the peak overpressure, P_{fv}, which occurs at high K_v (Fakandu et al., 2011). The vent numbers investigated were 1, 4, and 16 for the same K_v as this is 1:4 ratios in vent size and in turbulent length scale.

The 10L cylindrical vessel (L/D=2.8) was used for vented explosions with free venting (without a vent cover). Three different vent areas (without a vent cover – i.e. open from the start of the test) with vent coefficients (K_v) of 3.6, 5.4 and 10.9 for central, non-central single hole vents and for distributed 4 and 16 hole vents. Figure 5.10 shows sample of hole orifice grid plates used in the experiments of this section. Methane-air (10% v/v) and ethylene-air (7.5%) mixtures were investigated to determine the influence of the mixture reactivity.
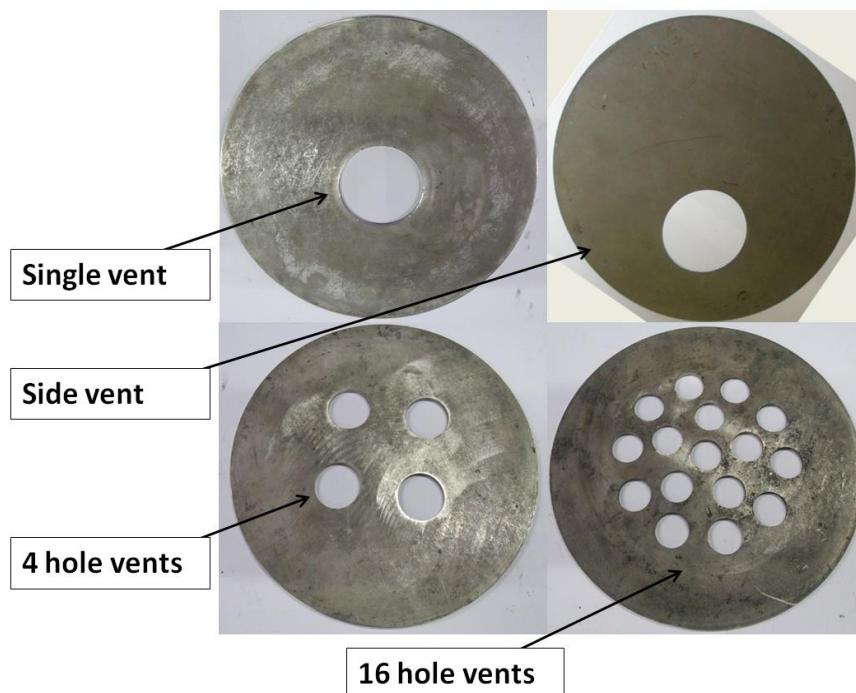
Figure 5.10 Samples of hole orifice grid plates

5.3.1 Influence of Non-central Vents on Explosion Overpressure and Flame Speed

Figure 5.11, shows the pressure-time records of the 7.5% ethylene-air and 10% methane-air for a single hole vent of K_v of 10.9 as either a central vent or an offset "bottom" vent. The time of flame arrival at the vent is identified as "vent". For both cases P_{fv} was slightly higher for the bottom vent case compared to the central vent. The stretching of the flame surface towards the vent was shown by Solberg et al. (1979) to bring an early end to spherical propagation and increase burning rate because of the increased flame area. Naturally the tubular flow is faster in the centreline of the tube and the alignment of the central vent with this preferred direction of flame propagation allows the flame to move axially much faster than radially. In the case of the offset vent the misalignment between the preferred flame flow path and vent exit path slows the axial flame speed – this would have the effect of reducing the overpressure as the flow through the vent would be lower. However, this counterbalanced by an increase in the flame area and (hence the combustion rate) as the offset vent arrangement forces a non-symmetrical flow towards the vent. Furthermore as bulk of flow has to flow closer to the wall this results in higher friction losses and therefore higher pressures, P_{fv}. P_{fv} was the dominant overpressure for low reactive mixtures of methane-air and propane-air (Fakandu et al, 2011).
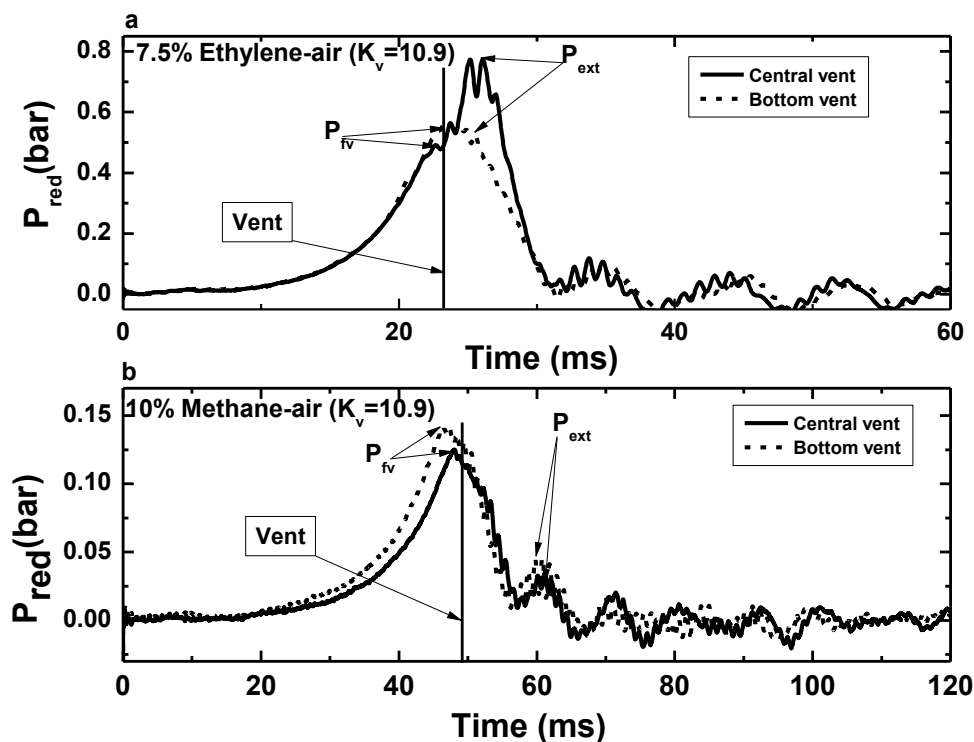
Figure 5. 11 Pressure-time records of central and bottom vent positions for Kv=10.9. (a) Ethylene-air (b) Methane-air
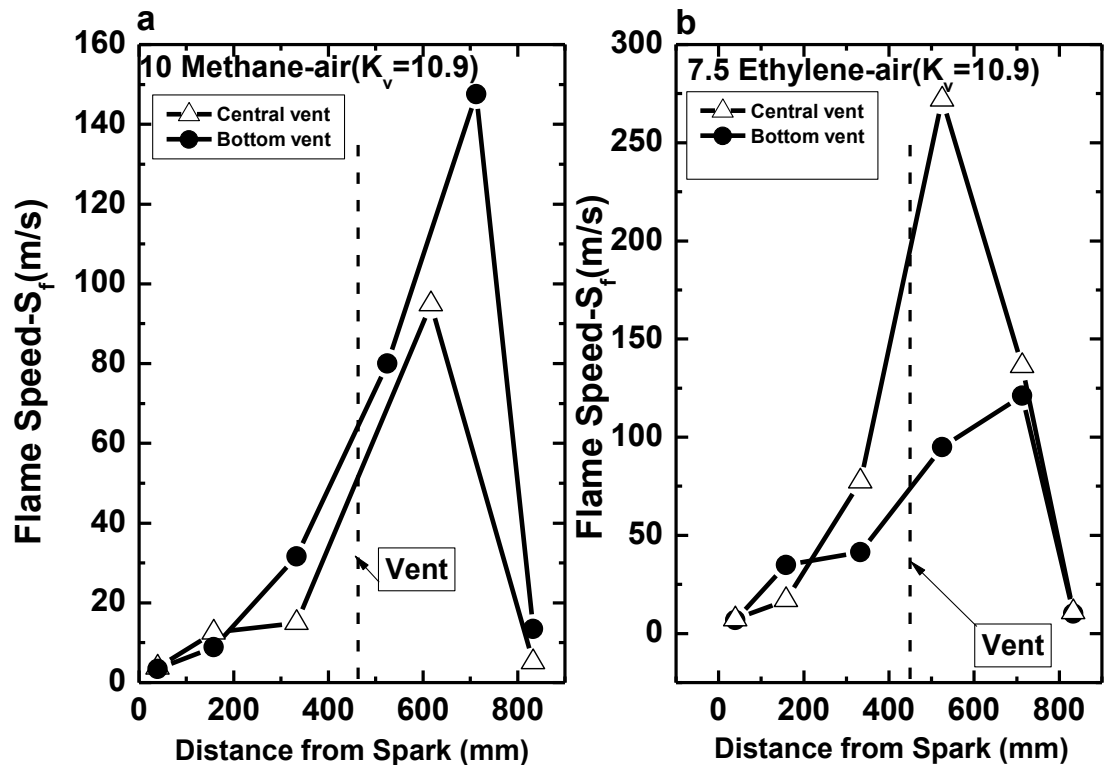
Figure 5.12 Flame speed vs distance from spark of central and bottom
vent positions for Kv=10.9

When the more reactive mixture of 7.5% Ethylene-air was used P_{ext} was much higher for the central vent as compared to offset vent for this K_v, This was due to the much lower flame speed generated by the downward movement of the flame when the vent was located offset from the centreline. This lower flame speed reduced the vent exit velocity and hence reduced the external jet turbulence.

This mechanism is supported by the corresponding flame speed measurements in Figure 5.12. The offset vent position slowed the flame upstream of the vent as compared to the central vent and this decreased the burning rate and gave a lower overpressure for methane explosions, as shown in Figure 5.11. For the ethylene tests the relative slowdown was far greater with the effective result of offset vent resulting in a significant reduction of the external explosion severity and a reduction in the maximum internal pressure as shown.

5.3.2 Effects of Single Vent and Four Vents on the Explosion Overpressure and Flame Speed

Comparison of the pressure time records for single and four-hole vented explosions for 10% methane-air for K_v=10.9 are shown in Figure 5.13a and in Figure 5.13b for a K_v of 5.4. The time of arrival at the vent thermocouple T_4 is marked as 'vent' and it is clear that P_{ext} was well after the flame passed through the vent and P_{fv} was well before this. For the small vent area (K_v=10.9), the peak pressure was P_{fv} as a result of the internal explosion pushing unburnt gas through a small orifice which gave a high flow pressure loss. Figure 5.13a shows that the single vent increased the peak overpressure for this vent area by more than 20%, as compared to peak pressure when the 4 holes vent was used. This was caused by the flame spreading out to pass through the four vents thereby increasing the flame surface area and rate of combustion just before reaching the vents.
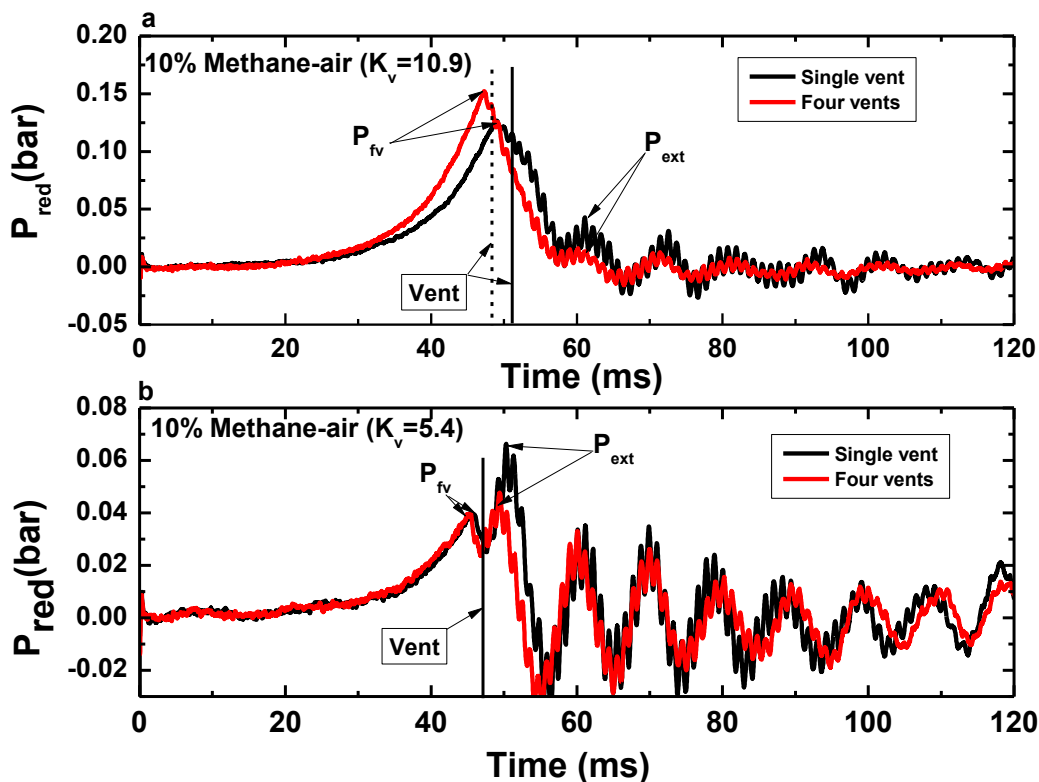
Figure 5.13 Pressure-time records of single and four vents for 10% Methane-air Kv=10.9 and 5.4

Figure 5.13b shows the opposite results were obtained for K_v = 5.4, due to the lower vent flow velocities at the large vent area. In this larger-vent-area explosion the vent flow pressure loss was low and the external explosion dominated the overpressure. This overpressure was reduced with the four-hole vent compared with the single-

hole one due to the reduced turbulent burning rate as a result of with the smaller length scale turbulence associated with the multiple hole vent. The benefits of using multiple distributed vent was also shown by Bjerketvedt et al, (Bjerketvedt et al., 1997).

When the more reactive mixture of 7.5% Ethylene-air was used, the single-hole vent was shown to significantly increase the peak pressure as compared to the four-hole vent. This was due to increase in characteristic length scale for the single vent as compared with the smaller scale for the multiple vents. The relevant characteristic length scale in these tests is the width of the solid material between the vents.

This is in agreement earlier were the effect of length scale on explosion overpressure and flame speed when single vent was compared to 16 holes vent (Fakandu et al, 2013). Furthermore, the P_{ext} was shown to be the dominant peak overpressure irrespective of the vent area as a result of influence of reactivity.
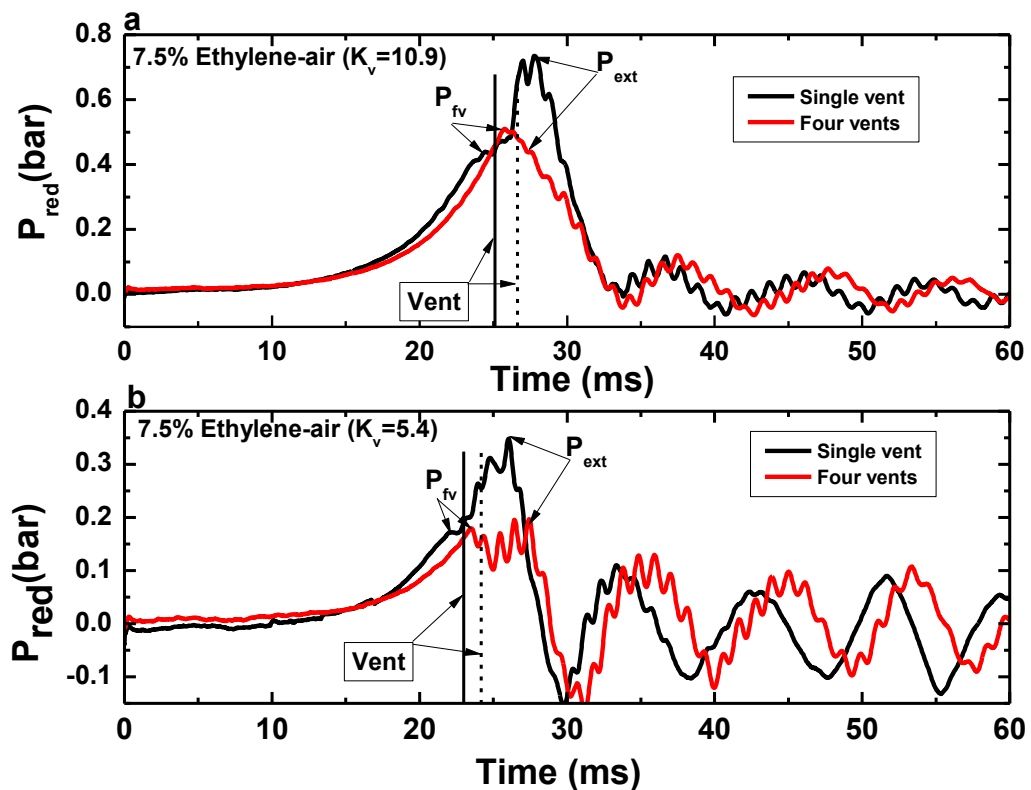
Figure 5.14 Pressure-time records for single and four vents for 7.5% Ethylene-air Kv=10.9 and 5.4

Figure 5.14 shows more than 30% increment in P_{red} when the single vent was compared with the 4 vents and this is significant for both K_v of 10.9 and 5.4. Since

the single vent was considered as the worst case as mentioned above, it was necessary to consider the worst case in explosion vent design as recommended by the ATEX regulation (The European Parliament and the Council, 1994).

For less reactive mixtures of methane-air and propane-air, P_{fv} was shown to be the dominant overpressure for small vent areas or large K_v, while P_{ext} dominates for large vent areas (Harrison and Eyre, 1987, Fakandu et al, 2011). P_{fv} is controlled by the mass flow through the vent which also controls the level of turbulence downstream of the vent and the turbulent burning velocity is reduced if the number of vents increases, as the length scale is reduced and this reduces the external flame speed as shown in Figure 5.15.

The results from the present work are in agreement with the work of Fakandu et al (2013), where the single hole vent was compared to 16 hole vents with the same total equal length. The work also recommended the use of scaling effect as used by this approach of reducing the overpressure by reducing the scale of the vents to smaller vents of total equal size, when considering the influence of vessel volume for external vented explosions (Fakandu et al, 2013).
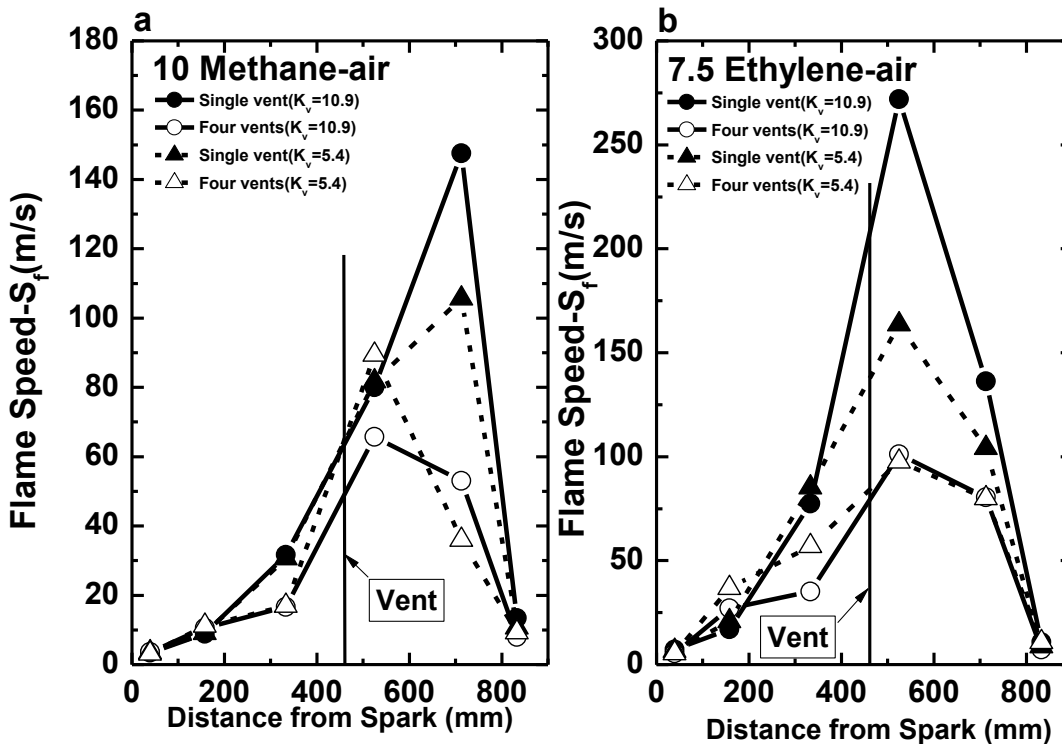
Figure 5.15 Flame speed vs distance from spark of single and four vents for Kv=10.9 and 5.4

The degree or intensity of turbulence generally depends on various factors but mainly on the flow velocity and geometry of the confinement (Phylaktou and Andrews, 1994). The pressure loss across a grid plate is characteristic of geometry and flow velocity of the unburnt gas ahead of the flame and relates to the conversion of flow energy to kinetic energy of turbulence. The pressure loos can be obtained from the pressure loss coefficient K from Equation 5.1.

$$K = \frac{\Delta P_T}{\frac{1}{2}\rho U^2}$$

[5.1]

Where, ΔP_T is the total pressure loss, ρ density of the gas, U is the gas flow velocity. The pressure loss coefficient K can be used to predict the intensity of turbulence downstream which was shown to be dependent on K and the aspect ratio ($^t/_d$ = orifice thickness/orifice diameter) as given by Equation 5.3 (Phylaktou and Andrews, 1994).

$$^{u'}/_U = 0.225\sqrt{K} \quad \text{for} \quad (^t/_d < 0.6)$$

[5.2]
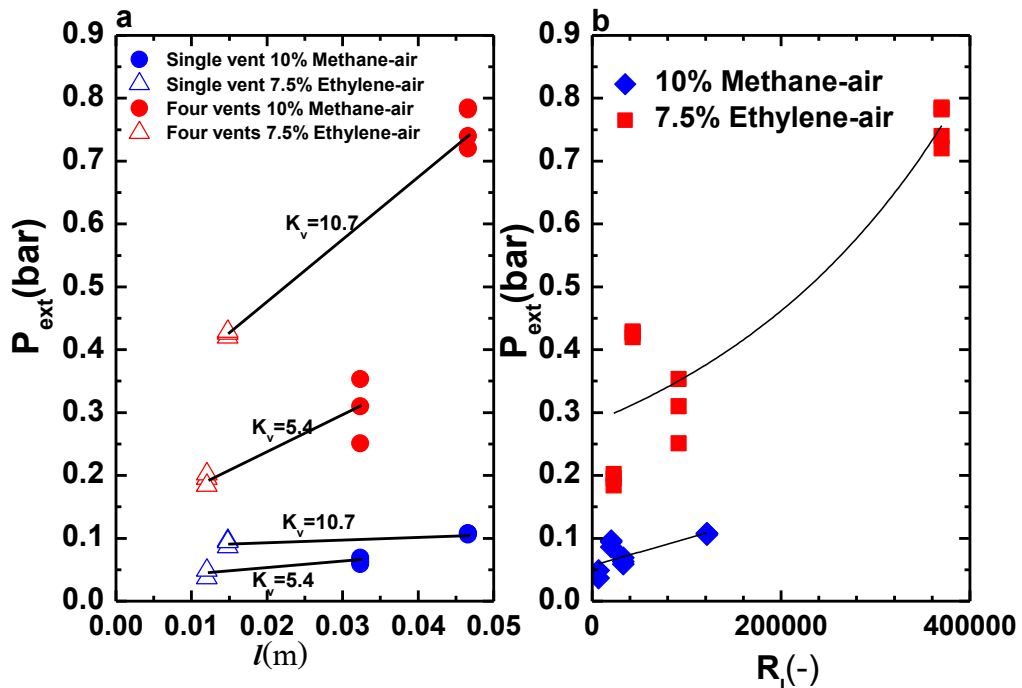
Figure 5.16 External pressure peak as a function of (a) vent length scale and (b) turbulent Reynolds number

Since mean velocity of flow is a key factor in estimating the intensity of turbulence and the mean velocity was shown to be approximated to about 80% of the maximum flame speed upstream the obstacle (Phylaktou and Andrews, 1994), then the turbulence downstream of the vent can be estimated using the flame speeds obtained

from the present work. The intensity of turbulence can then be expressed in terms of the turbulent Reynolds number based on the length scale (l) using Equation 5.1.

Figure 5.16 shows the pressure peak associated with the external explosion as a function of the vent length scale and of the turbulent Reynolds number for the different gas mixtures. It should be noted that in all the test conditions P_{ext} was the maximum pressure recorded **except** for the 4 hole, K_v of 10.7, methane/air test, where P_{fv} was the highest pressure peak.

Figure 5.16a shows for a given fuel mixture P_{ext} increased with both increasing K_v (decreasing vent area) and increasing in vent scale (decreasing number of vents). Decreasing vent area results in higher pressure loss across the vent and hence (according to Equation 5.2) increasing turbulence levels (u'). Increasing the mixture reactivity causes higher flow velocities towards the vent and again according to Equation 5.2, this increases u'. Higher u' results in a faster external explosion and hence a higher pressure peak. This figure also clearly shows that increasing the characteristic scale of the vent causes an increase the size of turbulence eddies and this also results in higher overpressures.

The effects of u' and length scale are embodied in the turbulent Reynolds number and Figure 5.16b tries to capture the effect of this parameter on P_{ext}. The spread of the data in Figure 5.16b would suggest that there is as separate effect of the mixture chemistry, however other effects such partial flame quenching at high straining rates may also come to into play. There were insufficient data to try and resolve these effects.

5.3.3 Change from One to 16 Vents and Effect of Characteristic Length Scale on the Turbulence Downstream the Vent at Constant Kv

Comparison of the pressure time records for single and 16 hole vented explosions for 10% Methane-air for K_v=10.9 is made in Figure 5.17a for a K_v of 10.9 and in Figure 5.17b for a K_v of 5.4. The time of arrival at the vent thermocouple T_4 is marked as 'vent' in Figure 5.17 and it is clear that the external explosion marked as P_3 was well after the flame passed through the vent and P_{fv} was well before this. Thus, although P_{fv} and P_{ext} are close together they can be separated with the aid of a thermocouple at the vent. For K_v of 10.9 P_2 was the dominant overpressure for both

1 and 16 holes. However, the 16 hole P_{fv} was greater than that for the 1 hole vent and this was considered to be due to the greater radial spread of the flame upstream of the vent. This was caused by the physical location of the vents covering the vessel vent wall with equal gaps between the vents. The external explosion was lower for the 16 hole vent compared with the 1 hole vent, as expected for the smaller turbulent length scale in the external explosion.
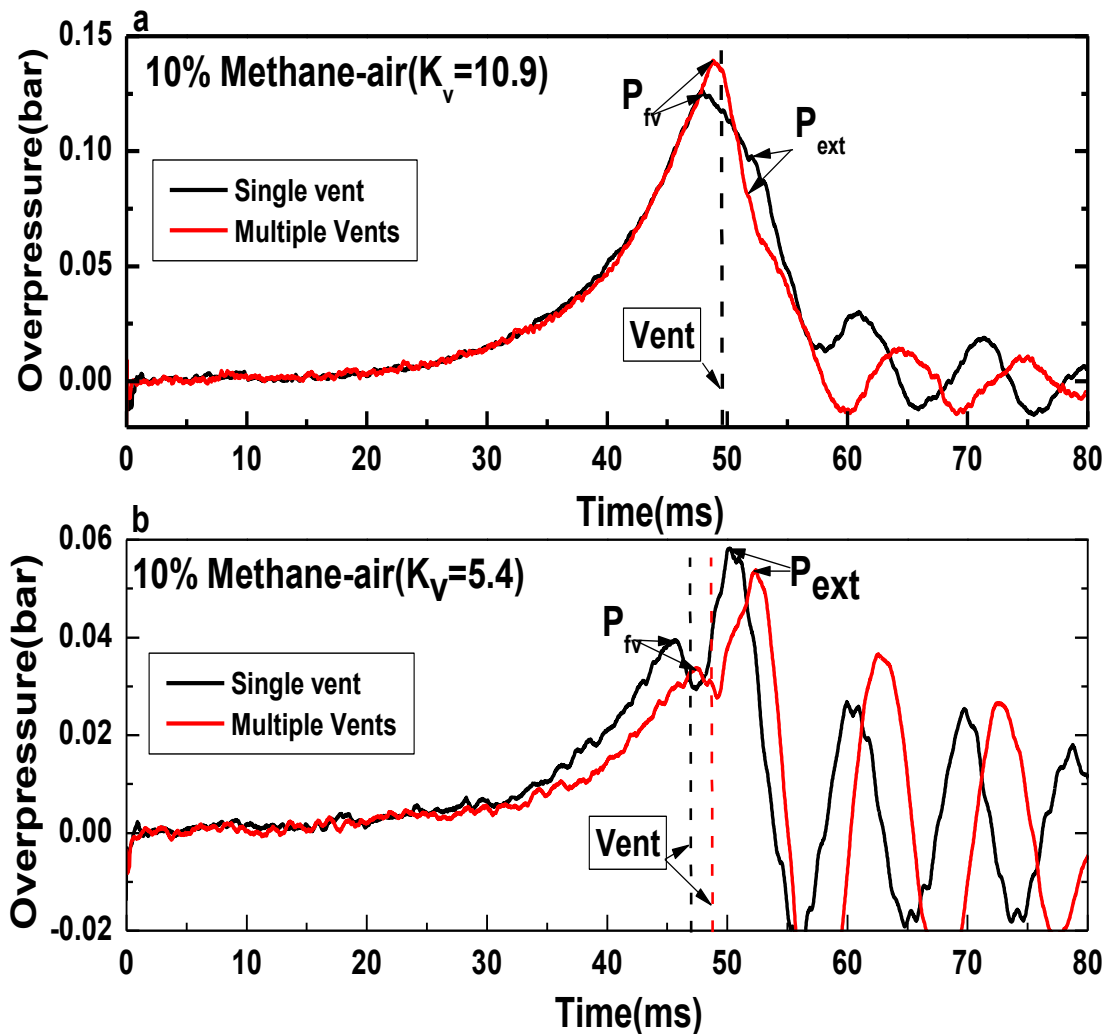
Figure 5.17 Comparing Single and multiple vents for 10% Methane-air (a)
Kv=10.9 (b) Kv=5.4

For the larger vent area, $K_v = 5.4$, the results in Figur 5.18b show the opposite trend to those found for $K_v = 10.9$. At this low K_v the external explosion overpressure, P_{ext}, was larger than P_{fv} for both the 1 and 16 hole vents. However, the influence of the number of vents on P_{ext} was the same as at the higher K_v in Figure 5.17a. P_{ext} was significantly lower for 16 holes than for 1 hole and this was considered to be due to the smaller turbulent length scale in the external turbulent flame explosion.

However, the reduction in P_{ext} with the 16 hole vent was relatively small at about 12 %. Figure 5.18b also shows that the peak overpressure due to the flow of unburned gas through the vent, P_2, was also lower for the 16 hole vent compared with the 1 hole vent, which was not the trend found at the higher K_v in Figure 5.17a. Also the peak overpressure occurred later for the 16 hole vent, implying a slower flame speed upstream of the vent. This indicates that the radial spreading of the flame upstream of the vent was significant for 16 vent holes of high blockage or high K_v but not at low K_v. The key parameter that is changing with K_v is the unburned gas velocity through the vent as the upstream flame speeds starts off the same and does not know there is a different number of vents until it receive feedback from the influence of the high velocity at the vent.
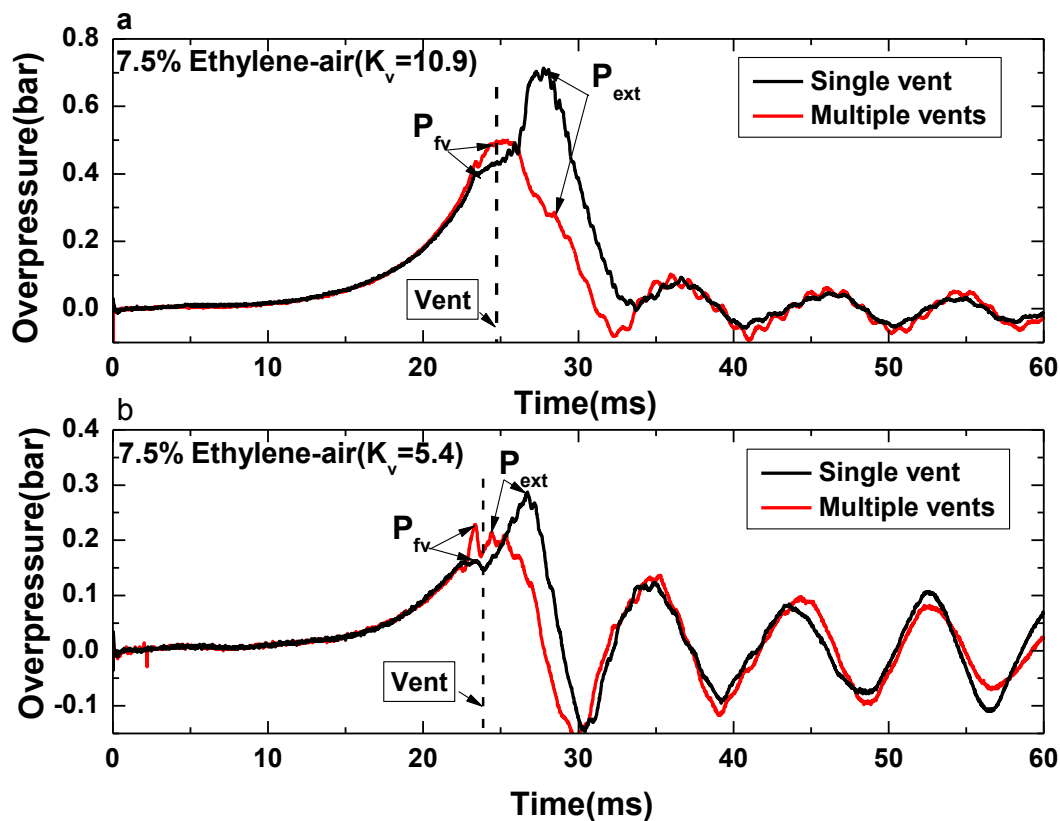
Figure 5.18 Comparing Single and multiple vents for 7.5% ethylene-air

(a) Kv=10.9 (b) Kv=5.4

Figure 5.18a shows that for the more reactive mixture of 7.5% Ethylene-air, the single hole vent was the worst case for both K_v. Both explosions had the peak overpressure for the external explosion with the higher external overpressure, P_{ext}, being 40% higher for the 1 hole vent compared to the 16 hole vent. The influence of the smaller turbulent length scale was to decrease the turbulent burning velocity at

the lower length scale and hence decrease the overpressure. The reason for the change in location of the peak pressure at the higher K_v in Figure 5.18a compared with Figure 5.17a, was due to the higher burning velocity of the external flame at the higher mixture reactivity. For both K_v, P_{fv} was higher for the 16 hole vent compared with the 1 hole vent, although lower than the external overpressure, P_{ext}, in both explosions. This was due to the increase in the bulk flame area as the main flame split to pass through the 16 vents. This resulted in the flame speed induced flow through the vent being higher for 16 holes than for one hole and thus P_{ext} was higher for the 16 hole vents than for the 1 hole vent.
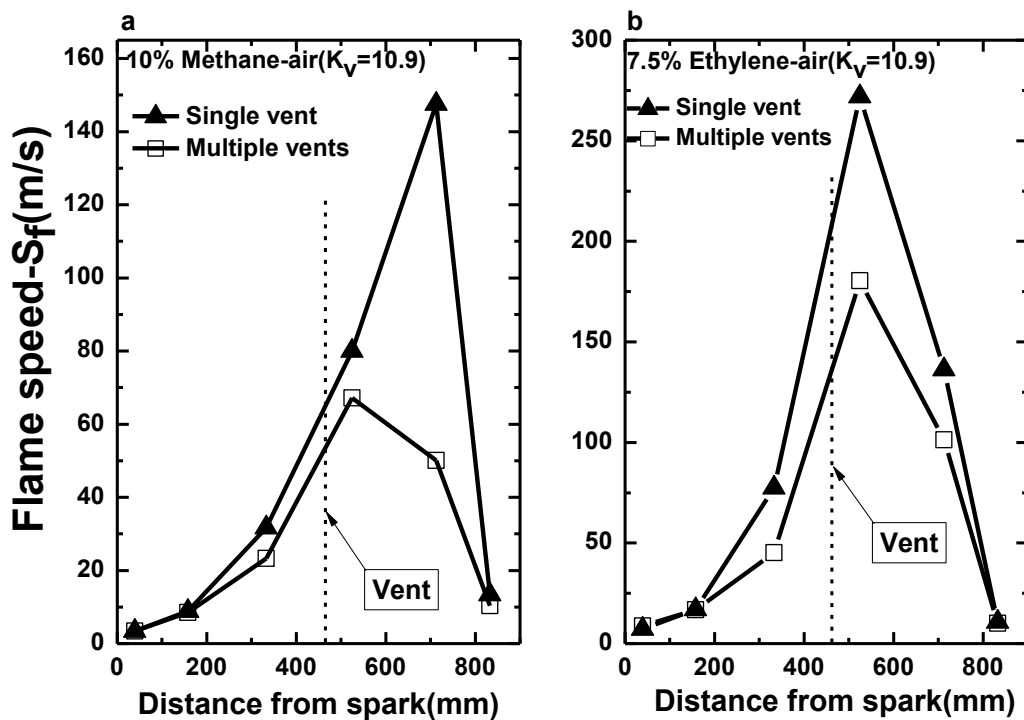
Figure 5.19 Flame speeds as a function of distance from the end wall for 10% methane-air (a) and 7.5% ethylene-air (b) for single and multiple vents at Kv=10.9

The measured axial centre line flame speeds for K_v = 10.9 are shown in Figure 5.19 as a function of the distance from the end flange where the spark is mounted. The vent was located 454mm from this face and the flame speed increases substantially downstream of the vent. The peak flame speed upstream of the vent was about 30 m/s for 10% methane-air and 60 m/s for 7.5% ethylene-air. This flame speed was reduced for the 16 hole vent to about 23 and 40 m/s respectively. Phylaktou and Andrews (Phylaktou et al., 1990) showed a large L/D (18.4) closed tube had a fast initial maximum flame speed of 25m/s followed by a much slower flame speed after

the flame had attached to the wall (Phylaktou et al., 1990). A similar trend was observed for the present small vessel with L/D of 2.8. There was an initial hemispherical flame speed of 3.4m/s and a maximum upstream flame speed of 30m/s for 10% Methane-air. The initial flame speed was in agreement with the laminar spherical flame speed, which indicates that the flame was propagating hemi-spherically at the initial stage, when there was no significant change in pressure. However, the flame speed of 30m/s was higher than 25m/s of Phylaktou and Andrews (1990) because it was for an open vent rather than a closed ended tube. This allows the gas velocity ahead of the flame to flow out of the vent instead of stagnating on the end wall.

Figure 5.19 shows that there was a sudden increase in the flame speed downstream of the vent due to the turbulent flame propagation in the external unburned gas cloud. There was a significant difference in the axial flame speed downstream of the vent between the 1 and 16 hole vents. For the single vent, a flame speed of 147m/s was obtained downstream the vent as compared to 67m/s for the multiple vents for 10% methane air with $K_v = 10.9$. This is an increase in the flame speed by a factor of 2.19. For 7.5% ethylene air Figure 5.19 shows a peak flame speed downstream of the vent of 272 m/s for the single vent and 180 m/s for the 16 hole vent. This is a flame speed ratio of 1.5 which is a little lower than the relative flame speeds for methane-air.

This increase in flame speed was as a result of fast flames jetting out of vent, induced by turbulence generation as it passed through the vent. It was argued in the introduction that for a reduction in the number of holes by a factor of 16 would result in the reduction in length scale by a factor of 4 at constant hole area. For a constant turbulence velocity, u', the turbulent burning velocity would scale by a maximum factor of 1.6, using a turbulent burning velocity length, L, scaling of $L^{0.32}$ (Phylaktou et al., 1994). However, for the turbulence velocity, u', to remain constant the upstream flame speeds would have to be the same, so as to generate the same gas flow through the vents. Figure 5.19 shows that this was not the case and the 16 hole vent had much lower flame speeds approaching the vent by a factor of 1.35 for 10% methane-air and for 7.5% ethylene-air. This was due to the action of the 16 hole vent forcing the flame to spread radially outward due to the wide distribution of the vents. For the single vent the flame could travel directly to the vent and this

minimized the radial spread and increased the flame speed. The turbulence created by a grid plate in a flow normal to the grid plate scales linearly with the upstream mean velocity (Phylaktou and Andrews, 1994)and hence in the present work the turbulence for the single hole vent should increase by a factor of 1.35 relative to that for the 16 hole vent. This would give a combined turbulent burning velocity effect of 1.35 x 1.6 = 2.16. This agrees very well with the maximum turbulent flame speed ratios downstream of the vent of 2.34 for 10% methane-air and 2.1 for 7.5% ethylene air.

5.3.4 Comparison of the Present Single Vent Results with Cooper et al. (1986) in a Larger Volume Vessel

The present 0.01 m^3 vented vessel was designed to have laminar flame propagation upstream of the vent and hence have results that could be compared with laminar flame venting theory (Andrews and Phylaktou, 2010). The present results for single hole vents are well below the vent design equation of Bartknecht (Bartknecht, 1993), but so are most of the experimental venting overpressures in the literature for large vent volumes(Fakandu et al., 2011, Kasmani et al., 2010a, Kasmani et al., 2010b) . Cooper et al. (1986) have presented overpressure data for vented explosions in a vessel with and L/D of 3 and volume of 0.68 m^3. They found for a K_v of 8.7 that the external flame overpressure, P_3, was 0.045 bar compared with 0.10 bar in the present work in Figure 5.17a for K_v =10.9 and 0.059 bar for K_v = 5.4 in Figure 5.17b. The result of Cooper et al. (1986) was below both of these results and this was probably because they used central ignition instead of the worst case end ignition. This comparison indicates that the present results in a very small volume compare with similar geometry results in larger volumes.

In both the present work and that of Cooper et al. (1986) the peak overpressure was for the external explosion for a K_v of 8.7 and for a K_v of 5.4 in Figure 5.17b. In the work of Cooper et al. (1986) the external overpressure was 0.045 bar compared with 0.059 bar in Figure 5.17b. In comparison the P_{fv} results were 0.04 bar in Figure 5.17b and 0.036 bar in the work of Cooper et al. (1990). For the higher K_v of 10.9 the present results were much higher than Cooper et al. (1986) reported for K_v=8.7. This shows that for a similar geometry the present results gave a higher overpressure than reported by Cooper et al. (1986) for a volume 68 times larger. Comparison with

the wider range of the vented explosion results of Cooper et al. (1986) shows a consistently higher overpressure in the present work (Fakandu et al., 2011). This was unexpected as lower overpressures were expected due to the smaller volume. However, comparison with larger volume vented experiments shows the present test facility gives overpressures about a factor of 2 below those in vessels in the 30-60 m^3 range (Phylaktou and Andrews, 1991a, Pappas and Foyn, 1983) for the same K_v. However, the present results are in agreement with the large volume vented explosion results of Bromma (Bromma, 1957) .

Where the overpressure is controlled by the external explosion outside the vent there is a volume effect related to the turbulent flame propagation. For bigger volumes, V, and the same K_v the vent area becomes physically bigger and this increases the turbulent length scale. Now the length scale in a cubic volume scales as $V^{1/3}$ and the dependence of the turbulent burning velocity on length scale, L, is $L^{0.32}$ (Phylaktou et al., 1994). This gives a scaling of the turbulent burning velocity with the test geometry of $V^{0.106}$. The external explosion turbulent flame gives proportionality on turbulent burning velocity of the overpressure of U_T^2. This then gives a dependence of turbulent burning velocity on volume of $V^{0,212}$. Scaling up the present results by a volume 1000 times greater than the test equipment will give about a factor of 4.3 increase in the turbulent burning velocity. This will produce about a factor of 18.5 increase in the overpressure. This would take the overpressure in Figure 5.17b from 0.059 bar to 1.09 bar at 10 m^3, which is close to the result of Bartknecht (1993) for a 10 m^3 vessel. Thus, the scaling effect shown in the present work to predict the reduction in overpressure by decreasing the scale by using 16 times the number of vent holes, can be used to determine the influence of vessel volume for externally vented explosions.

5.4 Ignition Position Effect in Explosion Venting

The principle of explosion venting is to reduce the peak explosion overpressure, P_{red}, so as to minimise the resulting damage, by providing sufficient vent area, A_v, that opens early enough to release the explosion pressure successfully. Experimental evidence has shown that the resulting explosion overpressures are controlled by different physical mechanisms depending on the vent design and the vessel volume, V(Bauwens et al., 2010, Cooper et al., 1986, Fakandu et al., 2013, Nagy and Verakis, 1983). The spark position for the worst case overpressure is not addressed

in current design procedures or explosion venting models, as all assume that central ignition is the worst case and are based on experiments in vented explosions with central ignition (Bradley and Mitcheson, 1978a, Cooper et al., 1986, Molkov et al., 2000, NFPA 68, 2013). Nagy and Verakis (1983) showed, for a rectangular enclosure with an L/D = 1.4 and a square cross section, that the peak explosion overpressure increased as the spark was moved away from the vent towards the wall opposite the vent. However, this was carried out for a very small vent area, A_v, with a $K_v = V^{2/3}/A_v$ and the present work were carried out to investigate these phenomena at more realistic values of K_v. Also the literature on the influence of spark position on P_{red}, reviewed below is confusing with contradictory findings.

5.4.1 Central Ignition Experimental Results are the Basis of Vent Design Methodology

Most of the experimental explosion venting data is for central ignition, including the vent European venting standard and the NFPA (NFPA, 2013, BS EN 1449, 2007). This was also the assumption used by Bradley and Mitcheson (1978), Molkov (2000) as well as in the work of Bartknecht, on which the European venting standard (BS EN 14491, 2007) is based. Similarly, the data used by Swift (1989) to generate his vent design equation was for central igntion and is the basis for the correlation used in the new NFPA (2013) vent design guide for gas explosion deflagration venting.

For a totally closed vessel (no vents) explosion, the central ignition location is the worst case, since the flame propagates at relatively constant speed and the flame will develop to its maximum possible surface area just before touching the walls. For any other ignition position in a spherical vessel the flame will touch the walls before all the mixture has been burned and there will then be heat losses from the burned gas to the wall which will reduce the peak pressure. However, this is not be the case with end ignition in a vented explosion, as the flame accelerates towards the vent and ignition at the furthest point from the vent gives the greatest flame acceleration distance and the rate of propagation of the flame is much higher than that for a laminar spherical flame (Fakandu et al., 2011).

The flame in most vented explosions with end ignition has emerged from the vent before the flame spreads to the walls of the vessel, as will be shown in the present

work. The worst case scenario should be used in order to meet the requirement of the ATEX directive and ignition with the maximum overpressure must always be considered in this regard. The aim of this work was to investigate whether end ignition was the worst case for vented explosions with ignition on the centre line midway the length of the vessel.

5.4.2 Influence of Ignition Location on Explosion Overpressure for Low K_v of 5.4 and 3.1 for 10% Methane-air

Figure 5.20 compares the pressure-time profile for central and end ignition with K_v = 5.4 for 10% methane-air for (a) the $0.2m^3$ vessel and (b) for the $0.01m^3$ vessel. Figure 5.20 shows that the end ignition opposite the vent gave much higher overpressures compared with central ignition for both test vessels. For both cases with end and central ignition the external explosion controlled the peak overpressure as shown by the peak overpressure occurring after the flame had emerged from the vent and past thermocouple T_4. For both vessel volumes the ratio of the end ignition P_{ext} to that for central ignition was 3.1 for the $0.2 m^3$ vessel and 2.7 for the $0.01m^3$ vessel and it would be reasonable to take a ratio of the two peak pressures as 3.
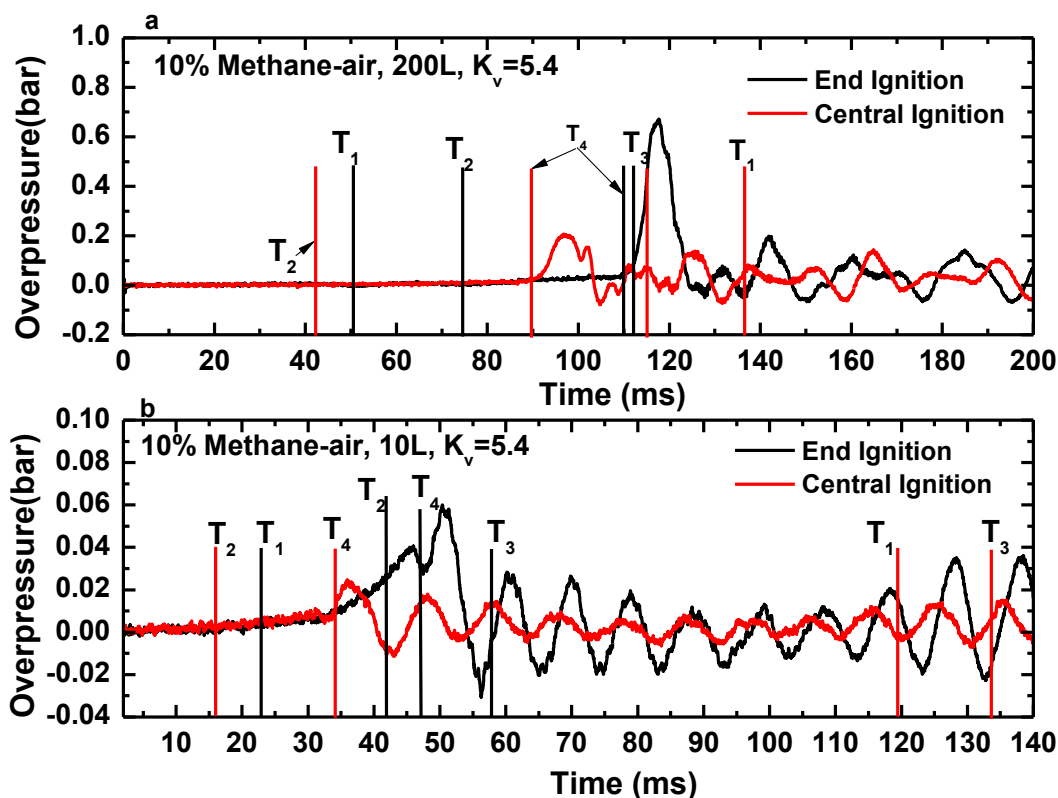
Figure 5.20 Comparison of central and end ignition for Kv = 5.4 for 10% methane-air for(a)the 0.2 m3 vessel and (b) the 0.01 m3 vessel

Figure 5.20 shows that for central ignition the flame propagation was entirely towards the vent and this left a large volume of unburned gas behind the flame front inside the vessel. This is shown by the very long time, well after the peak pressure had been reached, for the flame to reach thermocouples T_2 upstream of the spark and T_3 at the wall in the plane of the spark. This time was proportionately longer in the smaller vessel than the larger vessel, indicating faster flame propagation in the larger vessel. In the larger vessel there was no discernable pressure peak due to the unburned gas flow through the vent, P_{fv}, but this was a clear peak in the smaller pressure peak. This may be because for the larger vessel the external explosion overpressure was much larger than for the smaller vessel that P_{fv} cannot be seen in the scale of Figure 5.20. This paper is concerned with the influence of the ignition position and will not be discussing the reason for the higher overpressures in the larger vented vessel.
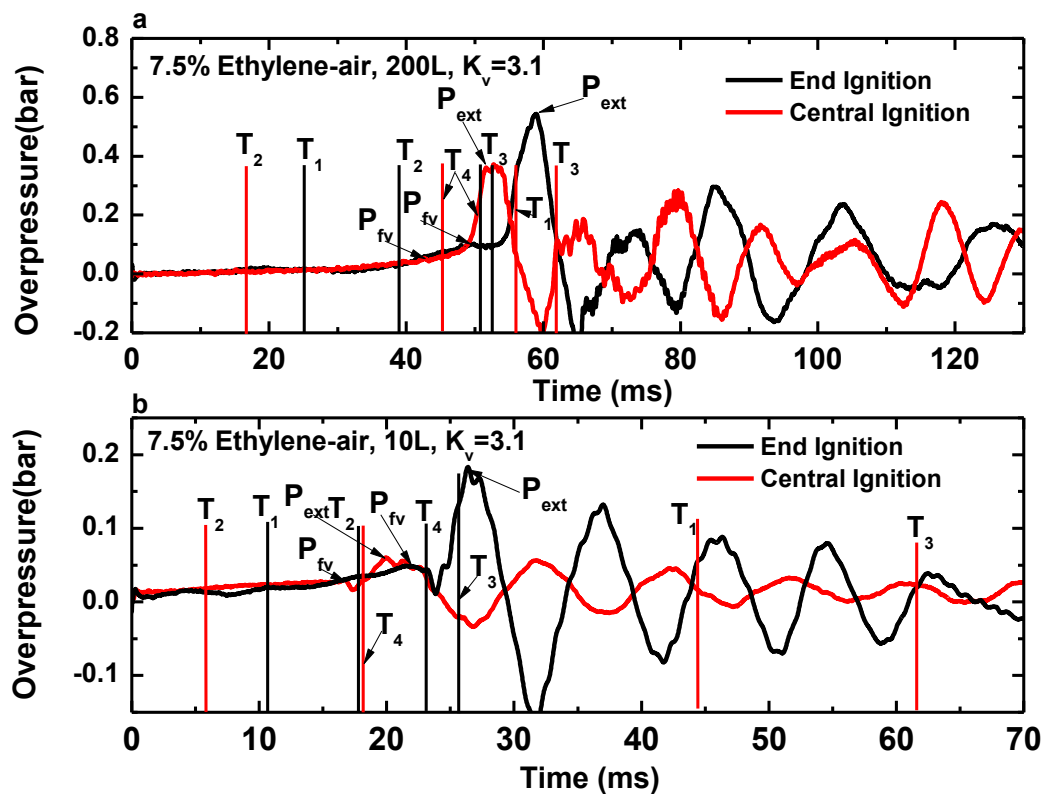
Figure 5.21 Comparison of central and end ignition for Kv = 3.1 for 10% methane-air for(a)the 0.2 m3 vessel and (b) the 0.01 m3 vessel

This large difference in overpressure between end and central ignition was due to the expansion of the flame in the direction of the vent with convection of the flame by the vent outflow. This effect was greater for the larger distance of the spark from

the vent and results in a fast flame approaching the vent, as will be shown later. This fast flame drives unburned gases ahead of it so that the unburned gas mass flow through the vent is higher for the end vented case. This creates a greater volume of unburned gas outside the vent and a higher external explosion overpressure as a result for the end ignition case. Also as the flame velocity upstream of the vent is higher than for central ignition, there is more turbulence in the external unburned gas cloud and hence a faster external explosions and higher external overpressure.

With central ignition the flame leaves the vent earlier than for end ignition with a smaller external cloud of unburned mixture. Also the flow of unburned gas through the vent is lower due to the slower upstream flame speed. This results in lower turbulence in the external unburned gas cloud and hence a lower external flame overpressure. The earlier flame arrival at the vent also marks the start of burned gas venting, which is more efficient in reducing the overpressure than unburned gas venting.

For the lower K_v of 3.1 Figure 5.21 shows that the pressure due to the flow of the unburnt gas through the vent, P_{fv}, was very low and the external explosion, P_{ext}, dominated the overpressure for both vessel volumes and for both ignition positions. The ratio of P_{ext} for end to central ignition was 2 for the larger vessel with L/D = 2 and 3.7 for the smaller vessel with L/D = 2.8. For the larger vessel the flame reached the wall at T_3 well after the peak external pressure and reached T_1 after this, as shown in Figure 5.21a. There was no evidence of rapid combustion of the unburned gases left in the vessel after venting with central injection. The same occurred in the smaller vented vessel, but was even slower to reach T_1. For end ignition in the larger vessel the flame reached T_3 soon after it passes through the vent at T_4 and before the peak external pressure. The burning of the unburned gas inside the vessel thus contributed to the peak external overpressure. However, in the smaller vessel the flame did not reach T_3 until after the peak explosion pressure.

5.4.3 Influence of End and Central Spark Location for $K_v = 5.4$ and 3.1 for 7.5% Ethylene-air

For higher mixture reactivity the flame speeds in the direction of the vent will be greater and this will increase the mass flow through the vent and the turbulence in the external unburned mixture expelled out of the vent. Ferrara et al. (2008) found

that for vented explosions with a vent pipe propane gave central ignition as the worst case, whereas methane explosions had a worst case with end ignition. In the present work propane had very similar end ignition results to methane with the external explosion dominating the peak overpressure and with a much larger peak external pressure than for central ignition. However, a greater test of the influence of mixture reactivity is that of 7.5% ethylene-air mixtures, and these were investigated in the 0.01 m^3 explosion vessel for the low K_v of 5.4 and 3.
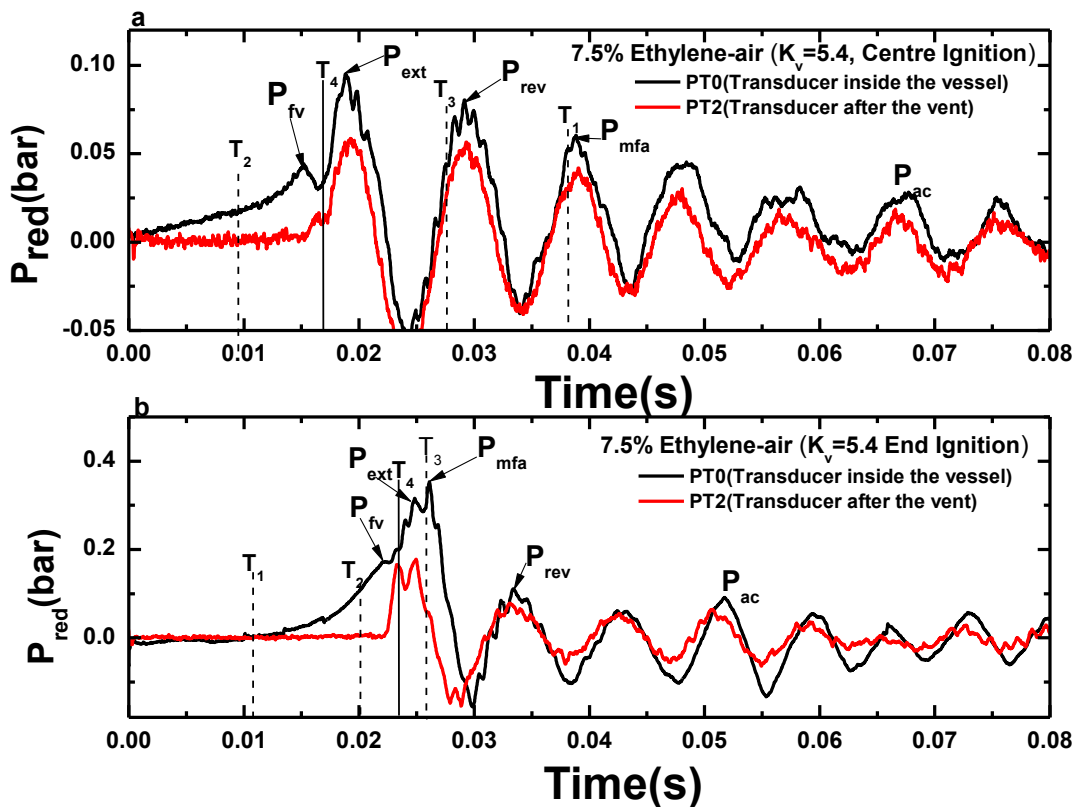
Figure 5.22 Comparison of (a) central and (b) end ignition for 7.5% ethylene/air vented explosions for Kv = 5.4 in the 0.01 m3vessel

Ethylene air vented explosions were carried out with central and end ignition in the 0.01 m^3 explosion vessel, using the most reactive mixture of 7.5% ethylene in air. Figure 5.22 compares central and end ignition for pressure transducers inside and outside of the vessel. Figure 5.22b shows that for end ignition the peak overpressure was much higher than for central ignition by a factor of 3.9, which is greater than the factor of 3 found for methane-air explosions in Figure 5.20. However in this case, neither the pressure peak due to the flow though the vent, P_{fv}, nor the external explosion overpressure, P_{ext}, was the highest overpressure. The peak overpressure occurred when the flame reached the vessel wall and was thus due to the maximum

flame area, P_{mfa}, which occurred after the flame had left the vent. This maximum flame area pressure peak was only slightly higher than the external explosion overpressure but occurred after the external explosion overpressure had started to decay. This explosion also had a reverse flow pressure peak at a similar magnitude to the central ignition case, but it was nowhere near the peak overpressure.
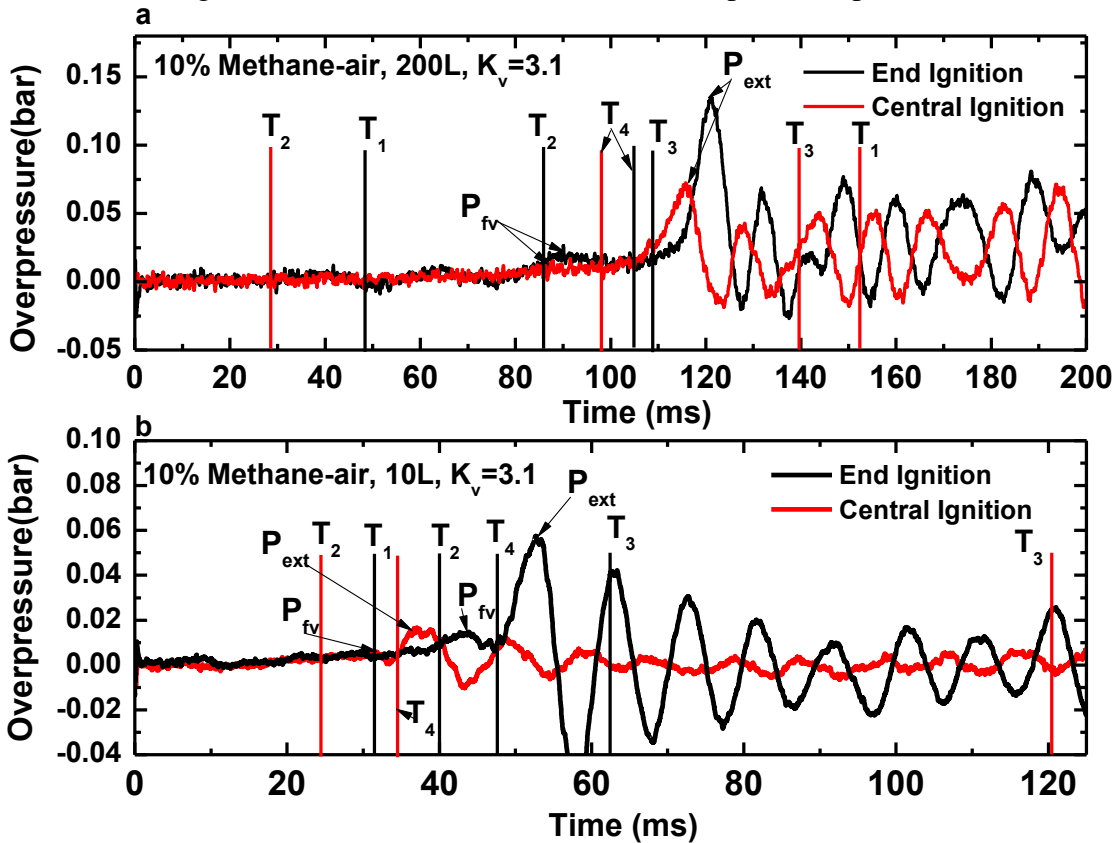
Figure 5.23 Pressure-time record for 7.5% Ethylene-air for Kv= 3.1 with end and central ignition (a) 200L vessel (b) 10L vessel.

Central and end ignition for 7.5% ethylene/air mixtures were also compared on the 0.2 and 0.01 m^3 explosion vessels for $K_v = 3.1$ and the results are shown in Figure 5.23. For both vessels the end ignition results gave a higher peak overpressure than for central ignition, but the difference was greater in the smaller vessel. The external explosion was also the cause of the peak overpressure for both vessel sizes. The overpressure for end ignition as a ratio of that for central ignition for 7.5%% Ethylene-air for the 200L vessel was a factor of 1.5 increase. This is the smallest increase in the overpressure for end ignition in the present work. The overpressure for end ignition as a ratio of that for central ignition for 7.5% Ethylene-air for the 10L vessel was a factor of 4.3 increase. This is larger than the effect in Figures 5.20

and 5 for K_v = 5.4, where the difference was close to a factor of 3. This may indicate that the effect of spark location is greater for lower K_v.

5.4.4 Influence of Central and End Ignition for K_v = 10.9 for 10% Methane-air

Reducing the size of the vent increases the velocity through the vent for the same upstream mass burning rate and this increases the vent flow pressure peak, P_{fv}, which scales inversely with the square of the vent area (Andrews and Phylaktou, 2010). The external explosion will also be increased due to the higher vent flow velocity, which will create more turbulence in the downstream jet. However, this is a linear increase in velocity with increase in K_v, or reduction in A_v. This will produce a linear increase in the external jet turbulence and roughly a linear increase in the jet turbulent burning velocity. The external overpressure scales with the square of the external flame speed and so both the internal and external overpressure could increase in proportion and it would be difficult to predict which would dominate.
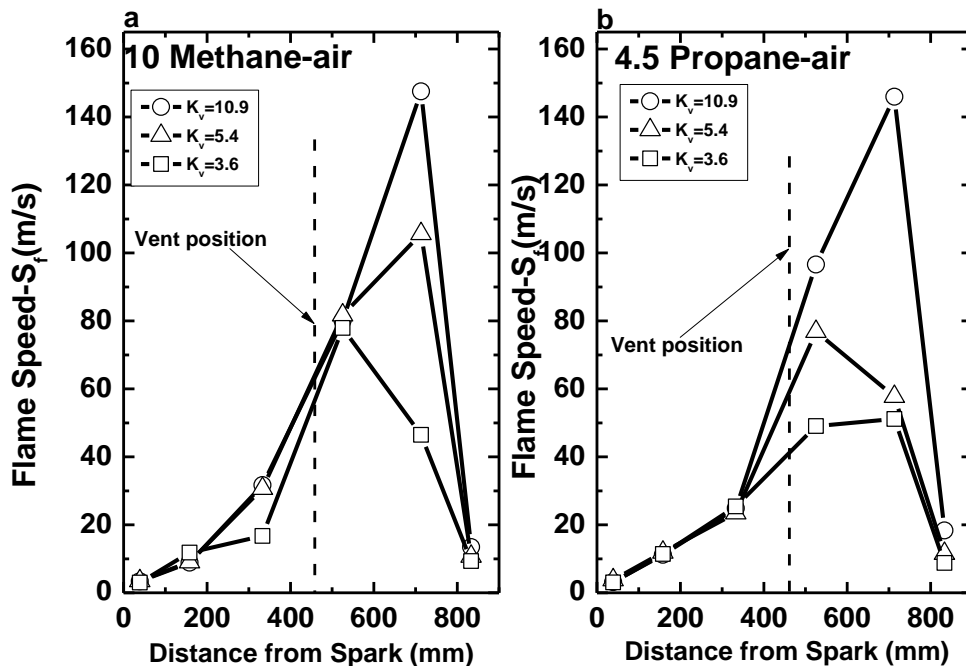
Figure 5.24 Flame speeds as a function of the distance from the end wall ignition through to the external flame for the L/D = 2.8 vessel for Kv 3.6 – 10.9

All of the above considerations rely on the assumption that the upstream flame speed and mass burning rate of the flame will be unaffected by the reduced vent outflow. Figure 5.24 for end ignited vented explosions for 10% methane-air and 4.5% propane air shows that increasing K_v from 3.6 to 10.9 does not change the

upstream flame speed significantly, but does increase the external flame speed. However, Figure 5.24 shows that the external flame speed does not increase in proportion to K_v as argued above should occur. This means that the internal vent flow overpressure, P_{fv}, is likely to rise faster than the external overpressure, P_{ext}, as K_v is increased and this is what the experimental results show. The reason for the external flame velocity not scaling with K_v is that the external flame speed is a function of the turbulent burning velocity which depends on the turbulent length scale as well as the turbulent fluctuating velocity, which should scale with K_v. As K_v is reduced the diameter of the vent is reduced and this controls the length scale and the position in the external jet at which the peak turbulence occurs.

The present L/D = 2.8 and 0.01 m^3 cylindrical vessel end vented results with central and end ignition for a K_v of 10.9 are compared for 10% methane-air vented explosions in Figure 5.25 with those of Cooper et al. (1986) for their L/D=3 vessel with central ignition and a K_v of 8.7 in a 0.68 m^3 rectangular volume. This difference in K_v would reduce the overpressure a little for the Cooper et al. (1986) results. To compare with comparable time scales the present results were scaled in time using $V^{1/3}$ time scaling of the present results to the time scale for the larger volume Cooper et al. (1986) results.

For central ignition Figure 5.25 shows that the present pressure records were very close to those of Cooper et al. (1986) for a similar vessel L/D, but much larger volume. The present results with central ignition had a slightly lower peak pressure than found by Cooper et al. (1986). The P_{ext} external explosion was the highest overpressure and Figure 5.25b shows that this occurred after the flame had passed through the vent plane at time T_4, when the peak pressure due to the flow through the vent occurred, P_{fv}. This was followed by a short period of pressure reduction while the flame propagated outside the vent to reach the peak external turbulence which produced a fast flame that gave the peak overpressure, P_{ext}. These two peaks were present in the results of Cooper et al. (1986), but the flame position information was not available to determine which event caused the peak pressure, which was slightly higher than in the present work. Also, the oscillatory pressure peak, P_{ac}, was slightly higher than P_{ext} in the work of Cooper et al. (1986) as shown in Figure 5.25b, but they discounted these oscillatory peaks as an artifact of using a thin metal box in the experiments. They showed that they disappeared when an

acoustic absorber was used as a wall liner in the chamber. Overall the present central ignition results are in good agreement with those of Cooper et al. (1986) for a vessel with similar L/D but larger volume. This indicates that the much larger 0.68 m^3 vessel volume (x70 of the present volume) of Cooper et al. (1986) has little effect on the overpressure. In this work the distance from the spark to the vent was 0.9m compared with 0.3m in the present work for central ignition. This would indicate that self-acceleration was not significant for a spark to vent distance of at least up to 0.9m.
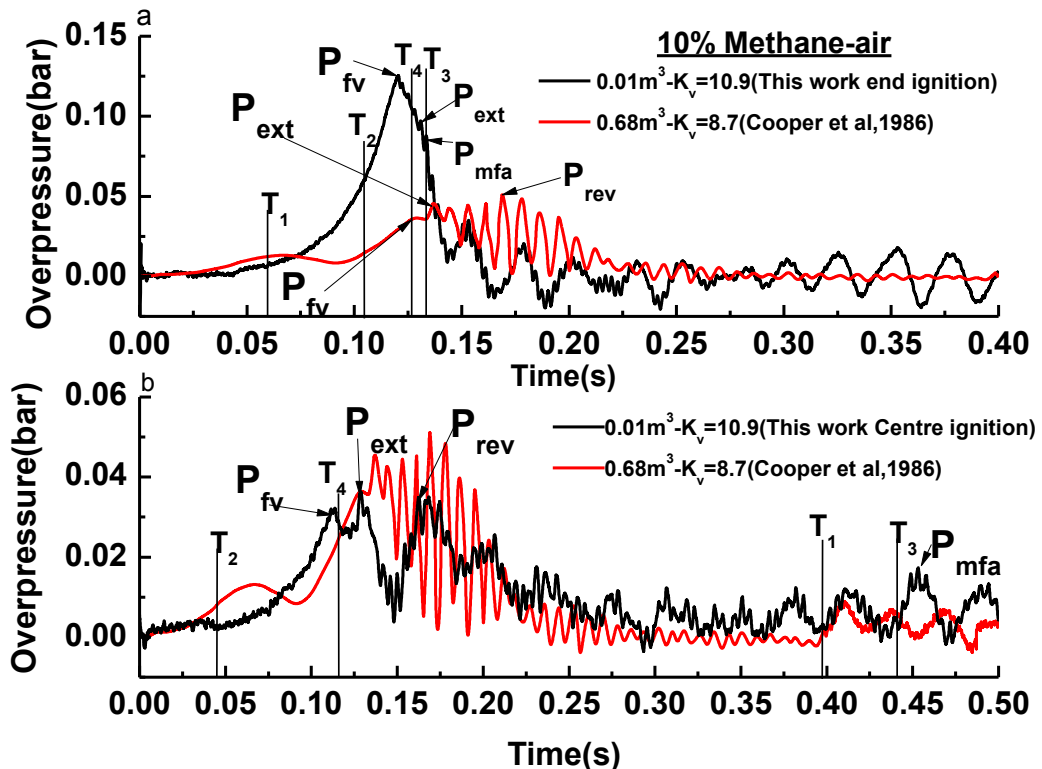
Figure 5. 25 Pressure-time record for 10% methane-air for Kv= 10.9 with end (a) and central (b) ignition, for pressure transducer PT0

Figure 5.25a shows the end ignition results for $K_v = 10.9$, which have much higher overpressures than for central ignition in Figure 5.25b. The peak pressure was due to the flow of unburned gas through the vent, as P_{fv} occurred before the flame reached T_4. The external explosion occurred on the decaying pressure and is a slight peak on the pressure decay. The flame arrives at T_3, indicating that the maximum flame area inside the vessel occurred after the peak pressure and was not the cause of the peak pressure. The ratio of the peak pressure for end ignition to central ignition was 3.6 and this supports the results above, all of which have end to central ignition peak pressure ratios between 1.5 and 4.3. Thus end ignition had a major increase in the

peak overpressure and vent design based on experiments with central ignition may not be safe designs. Current procedures based on the vented explosion results of Bartknecht (1993) are safe, in that his results are much higher than any others in the literature, even for experiments in much larger vessel than he used (Fakandu et al., 2011, Kasmani et al., 2006).

5.4.5 Influence of Central and End Ignition for $K_v = 10.9$ for 7.5% Ethylene-air

Figure 5.26a, shows the vented explosion pressure record for the more reactive mixture with 7.5% ethylene-air and a K_v of 10.9. The external pressure transducer PT2 records are also shown. For central ignition the external overpressure P_{ext} (0.17 bar) was just higher than P_{fv} (0.16 bar). The external pressure record confirms the location of P_{ext}.
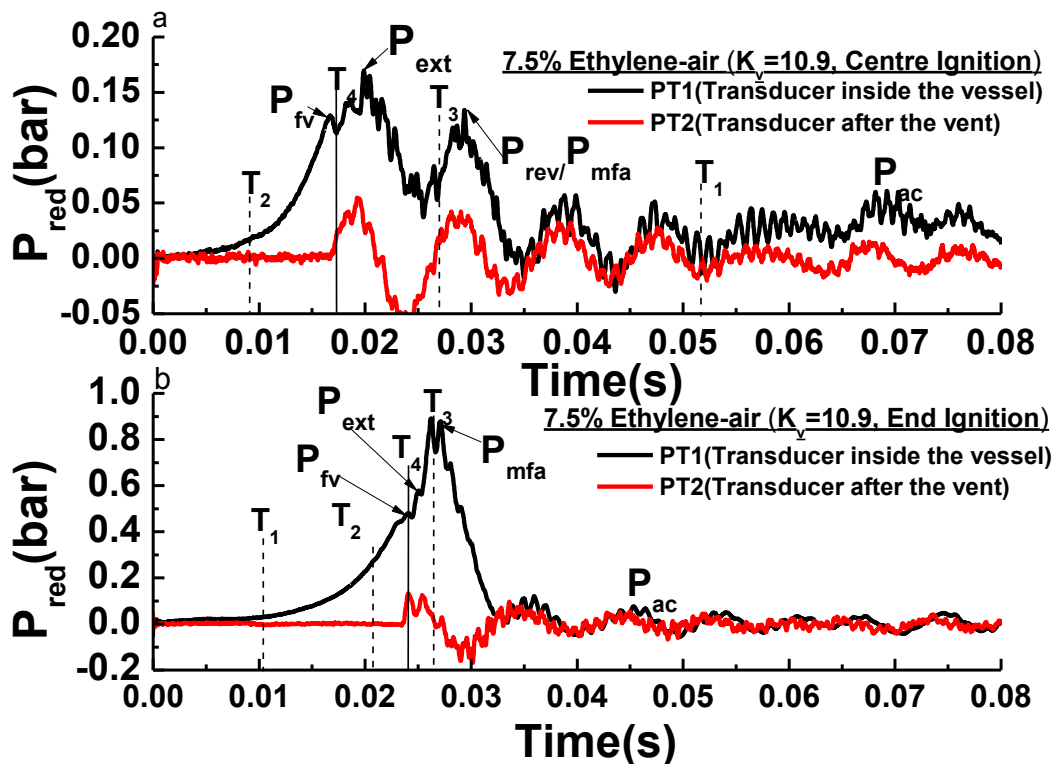
Figure 5.26 Pressure-time record for 7.5 % ethylene-air for Kv= 10.9 with central (a) and end (b) ignition, for pressure transducer PT0 and PT2

The pressure peak for the maximum flame area that occurs just after T_3 was quite high at 0.13 bar. Comparison to the methane results shows that for both mixtures the external explosion was the largest overpressure for central ignition. For end ignition Figure 5.26 shows that the external explosion P_{ext} (0.59 bar) was larger than P_{fv} (0.47 bar) but the highest overpressure was P_{mfa} (0.88 bar). This was confirmed by

the external overpressure measurement aligning in time with P_{ext} and P_{mfa} aligning in time with T_4 and T_3 respectively. The ratio of the peak overpressure for end ignition to that of central ignition was 5.2, much higher than for methane at 3.6 at this K_v.

Figures 5.20-5.26 shows that the peak overpressure can be due to any of the events (P_{fv}, P_{ext} or P_{mfa}), depending on K_v, gas reactivity and the ignition location. Without the present thermocouple sensors to detect the location of the flame just before a pressure peak and the use of the external pressure transducer PT2, it would be difficult to separate the cause of the various pressure peaks. However, the first two pressure peaks P_{fv} and P_{ext} are more commonly responsible for the peak overpressure. The present results for end ignition indicate that for $K_v <\sim 5.4$ P_{ext} would be the dominant overpressure and for $K_v >\sim 5.4$ P_{fv} would be dominant.

5.4.6 Influence of Ignition Location on Flame Speeds

Figure 5.27 shows the flame speeds for 10% Methane-air and 7.5% Ethylene-air for Kv=10.9, as a function of the ignition position. With end ignition, the flame propagated axially towards the vent and accelerated as it approached the vent, with maximum flame speed of 31m/s for 10% methane-air and 84m/s for 7.5% ethylene-air (just upstream of the vent).
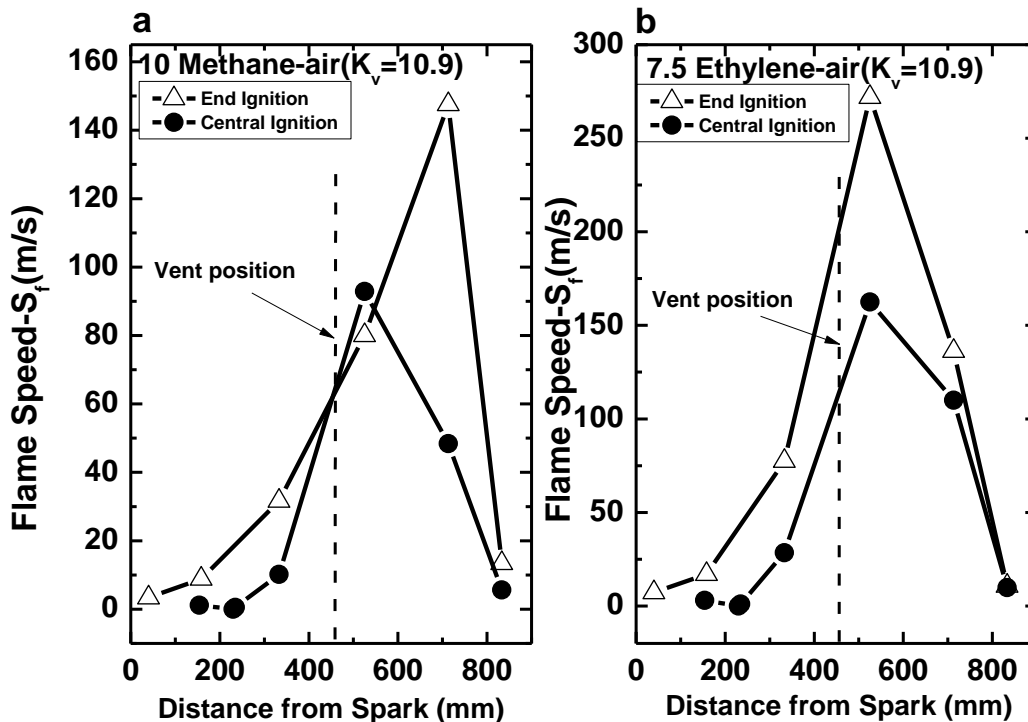
Figure 5.27 Comparing flame speeds of Centre and End Ignition for Kv= 10.9
(a)10% methane-air (b) 7.5% Ethylene-air

For 10% methane-air, the maximum flame speed of 31m/s upstream the vent was 5 times the value obtained for the centrally ignited mixtures of approximately of 6m/s and this is similar for 7.5% Ethylene-air as a factor of 4 difference in flame speeds occurred when the two ignition locations were compared, as seen in Figure 5.27b. The trend of development in the upstream flame speeds, which is responsible for the maximum flame speeds obtained downstream the vents, also influences the rate of pressure rise and the final peak overpressures.

5.5 Influence of Vent Shape on Gas Explosion Venting

The European Standard (2007) in section 6.2 states that 'rectangular vents are as effective as square or circular vents'. This work presented in this section was undertaken to determine if this statement and the assumption of a constant C_d for all vent shapes in NFPA 68 (2013) are justified.

Figure 5.28 Sample of square and circular for Kv=10.9 (BR=80%)

Three different vent coefficients, K_v, of 3.6, 5.4 and 10.9 were investigated with both the circular and square vents located at the centre of the vented cylindrical vessel end wall. Two gaseous reacting mixtures were investigated: 10% methane-air and 7.5% ethylene-air mixtures, these mixtures were the most reactive concentration for the fuel gases (Kasmani, 2008b). Figure 5.28 show sample of the square and circular used for in the work presented in this section.

5.5.1 Effect of the Change from Square to Circular Vents on Explosion Overpressure, P_{red}

Figure 5.29 shows the ethylene pressure v. time results for $K_v = 3$ with a circular vent for pressure transducer end wall and external discharge vessel pressures. The latter pressure, PT2, does not change until the flame exits the vent and thus determines the time that the external explosion occurred. Figure 5.29 shows that this aligns with the peak overpressure, P_{ext}, thus showing that it was the external overpressure that controlled the peak overpressure in this case. The time of arrival of the flame at the vent is marked as Vent in Figure 5.29, which also shows that the flame was external to the vent at the peak overpressure. The pressure peak for the flow through the vent, P_{fv}, was much lower than P_{ext} and occurred before the flame reached the vent, as it was due to unburned gas flow through the vent.
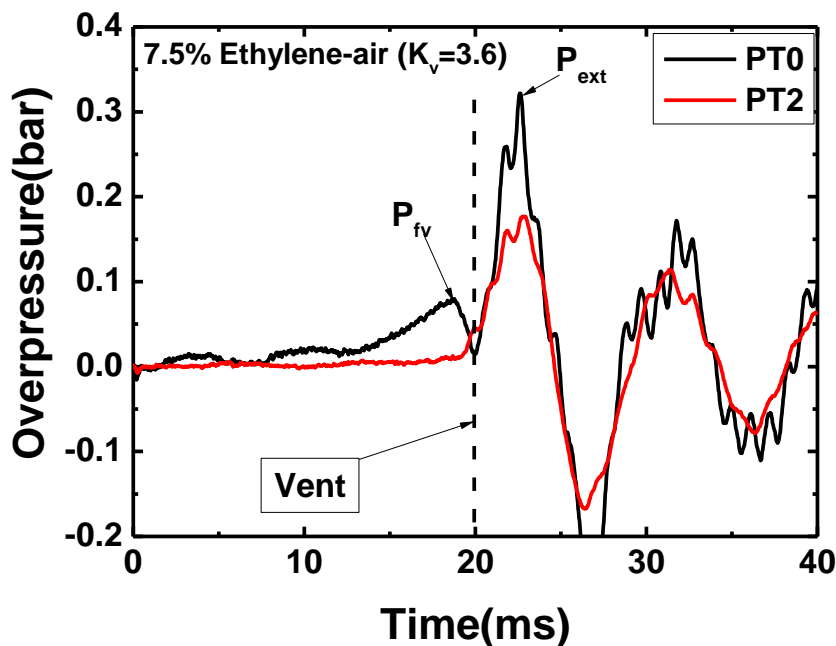
Figure 5.29 Pressure time records for PT0 and PT2 for 7.5% ethylene-air with circular vent

Figure 5.30 compares the pressure time records for circular and square vents for 10% methane-air for K_v of 10.9 and 3.6. The overpressure due to the flow through the vent, P_{fv}, was the dominant overpressure for both circular and square vents for $K_v=10.9$ and the overpressures were very close in magnitude for the two vent shapes. Kasmani et al. (2010) has previously shown that for high K_v the dominant overpressure was P_{fv}.

For the larger vent area, $K_v = 3.6$, the results in Figure 5.30b shows that P_{ext} was the dominant overpressure for both circular and square vents. The influence of vent shape was small for P_{fv} similar to Figure 5.30a, but a significant influence of vent shape was found in the dominant external overpressure, P_{ext}. The circular vent had more than 30% higher external explosion overpressure than that of the circular vent. This significant change was a result of the greater rate of jet spreading for non-circular jets, as reviewed above, which resulted in faster entrainment of air into the jets and hence reduced the external flame speeds which reduced the external overpressure for the square vent. For $K_v=10.9$ Figure 5.30b shows a major reduction in P_{ext} for the square vent, but in this case P_{ext} was not the dominant overpressure.
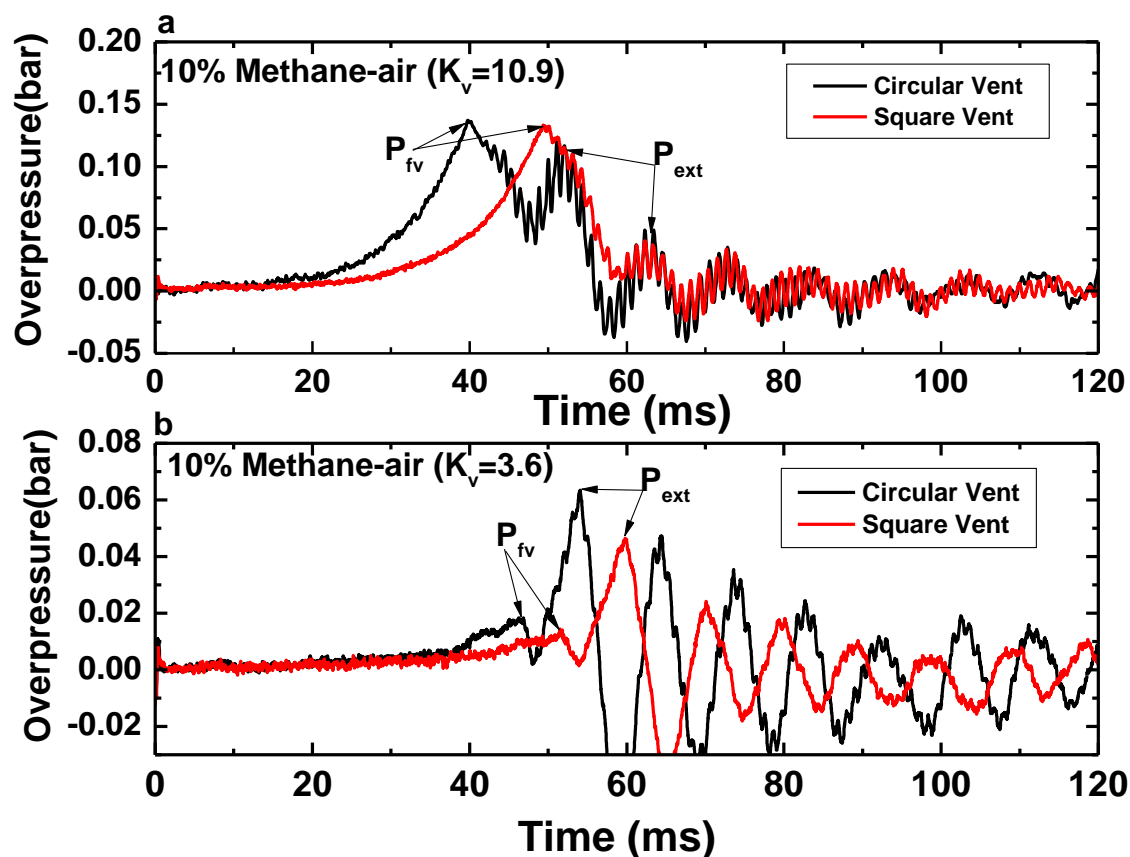
Figure 5.30 Square and circular vents compared for 10% methane-air (a) Kv=10.9 (b) Kv=3.6

Table 5.1 shows the summary of all the experiments conducted for both circular and square vents by varying the vents for three K_v, with three repeat tests for each K_v. Table 5.1 also shows whether the peak overpressure was due P_{fv} or P_{ext}. Also shown is the average percentage decrease from the overpressure obtained with the circular vent, when compared to the square vent for the two gas mixtures. Table 5.1 shows

that for methane and ethylene at all K_v the square vents always had a lower overpressure than the circular vents. The difference varied but was typically 30% lower. For methane with $K_v = 10.9$ the two vent shapes had practically the same overpressure, as also shown in Figure 5.30a. For ethylene the results were very consistent with >30% lower overpressures with square vents at all K_v. These results clearly show that for most venting conditions a square vent will give a significantly lower overpressure than a round jet and hence give better protection.

Table 5.1 Summary of maximum reduced pressure for different gas mixtures and vent shapes

Kv	10% Methane-air (P_{red}-bar)			7.5% Ethylene-air (P_{red}-bar)		
	Circular	Square	Increase (%)	Circular	Square	Increase (%)
3.6	0.062 P_{ext}	0.046 P_{ext}		0.30 P_{ext}	0.23 P_{ext}	
3.6	0.076 P_{ext}	0.051 P_{ext}	35	0.29 P_{ext}	0.24 P_{ext}	30
3.6	0.064 P_{ext}	0.049 P_{ext}		0.32 P_{ext}	0.23 P_{ext}	
5.4	0.069 P_{ext}	0.056 P_{ext}		0.35 P_{ext}	0.23 P_{ext}	
5.4	0.063 P_{ext}	0.055 P_{ext}	17	0.31 P_{ext}	0.23 P_{ext}	46
5.4	0.059 P_{ext}	0.052 P_{ext}		0.31 P_{ext}	0.21 P_{ext}	
10.9	0.133 P_{fv}	0.129 P_{fv}		0.74 P_{ext}	0.57 P_{fv}	
10.9	0.137 P_{fv}	0.133 P_{fv}	3	0.72 P_{ext}	0.56 P_{fv}	31
10.9	0.137 P_{fv}	0.132 P_{fv}		0.78 P_{ext}	0.59 $_{fv}$	

The flame speeds for Kv = 5.4 are shown in Figure 5.31 as a function of the distance from the end flange, where the spark was located. The maximum or peak flame speed with the circular vent for 10% methane-air downstream of the vent was 30m/s and 85m/s for 7.5% ethylene-air. However, when the square vent was used the peak flame speed was reduced to 21m/s and 75m/s for the 10% methane-air and 7.5% ethylene-air respectively. This was caused by the faster entrainment of air for the square vent thereby reducing the speed of the propagating flame as shown in Figure 5.31.
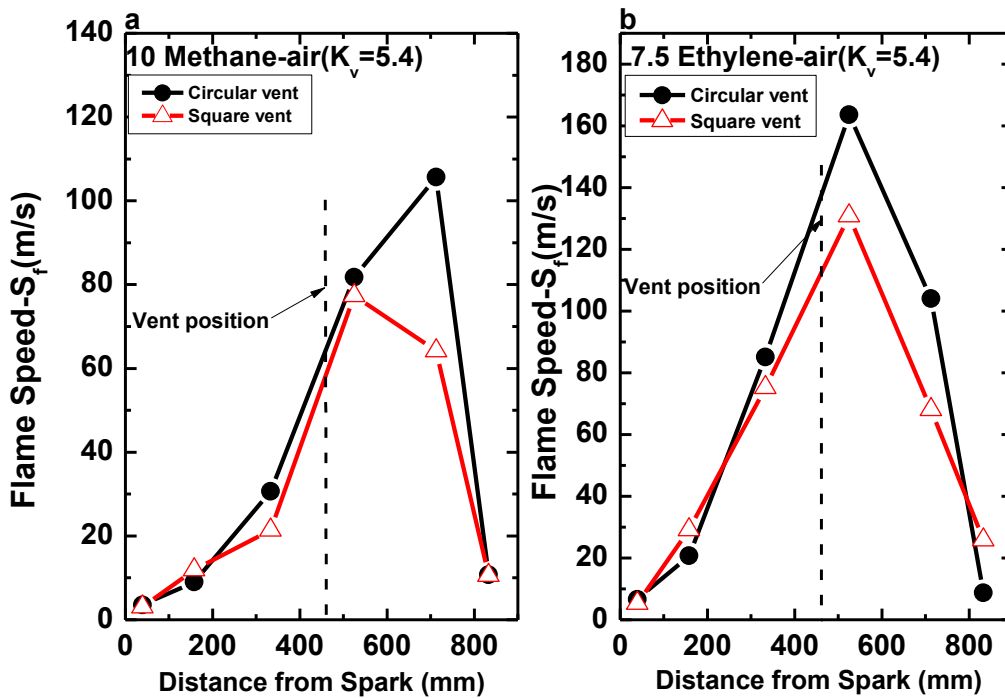
Figure 5.31 Comparison of the flame speeds for square and circular vents for Kv=5.4

The flame speed upstream of the vent is also shown in Figure 5.31 to be lower for square vents than circular vents. This effect was greater as K_v increased. This lower flame speed would produce a lower mass flow of unburned gas through the vent and hence reduce the overpressure for square vents. However, as discussed in the Introduction, square vents have a lower C_d than circular vents and this would increase the overpressure for square vents. The combined effects nearly cancel out. For methane with K_v of 10.9 the change in overpressure between circular and square vents was very small and this is the only condition where the overpressure was caused by the flow through the vent and not the external overpressure. For ethylene with $K_v = 10.9$ Table 5.1 shows that square vents had the overpressure due to flow through the vent as the greatest, but the two overpressures P_{fv} and P_{ext} were nearly the same at this condition.

5.6 Conclusion

This chapter has presented new experimental data which shows the effect of vent area in different venting scenario for 10L small vessel. In view this, the following conclusions were made:

1.   Overpressures were shown to be affected by the vent area and it was shown that the maximum reduced pressure is linearly depending on K_v for all the gas mixtures used this work. The large vent areas slowed down flame as it approaches the vent, while the fasters burning rate as well as rates of pressure rise were also shown to increases as the vent area reduces. The flame speeds downstream the vent increases as the K_v increases. This was as result of increase in the characteristics turbulent length by the obstruction caused by the vent, as the vent reduces. Vent area was also shown to affect the jet of the flame exiting the vent and the cloud of the unburnt gas mixtures outside vent, thereby affecting the pressure-time records of the gas mixture as a result of the external explosion (P_{ext}).

2.   It was demonstrated in this geometry that non-central vents increased pressure transient peak due to the maximum unburnt gas flow through the vent. The non-central vent was shown to slow down the flame as it propagates towards the vent but at the same time distorts the flame front and hence increases the flame area. This was caused by the flame diversion from the normal centreline propagation path as it moves toward the offset vent position. The influence of characteristic obstacle scale was also demonstrated to have significant effect on the external overpressure and flame speed downstream of the vent. Having more vent openings (for the same overall vent area) results in a smaller characteristic scale and this reduces the pressure peak due to the external explosion. None of these factors are mentioned in the venting standards.

3.   The result from this work for central ignition in a 0.01 m^3 vessel with an L/D of 2.8 was compared with that of Cooper et al. (1986) for a 0.68 m^3 rectangular vessel with an L/D of 3. The peak overpressures were due to an external flame in both cases and were very similar for the two test facilities. The ratio of the peak explosion overpressure for end and central ignition was found to vary from 1.5 to 5.2, depending on K_v, mixture reactivity, and vessel size. P_{ext} was the dominant cause of the peak overpressures for K_v of 5.4 or lower and P_{fv} was the dominant cause of the overpressure for K_v of 10.9. The results clearly demonstrate that the ignition position relative to the vent is important and that that the highest overpressures are not generated by central ignition, which is the basis of the current vent design correlations. There is therefore a clear need to consider the effects of ignition locations in vent design correlations in order to meet the ATEX directive

(European Parliament and Council, 1994) requirement for the worst case conditions to be considered.

4.   The use of square vents is preferable to circular vents, which give at least 30% higher overpressure than square vents. Vent design guidance should encourage the use of square or rectangular vents. The circular vents were shown to give higher external overpressure (P_{ext}) when compared with the square vents, while small differences were found for the internal pressure (P_{fv}). This effect was concluded from literature work on non-circular jets, to be due to the faster entrainment of air by the square vent jet flow as compared to the circular vent jet flow. This resulted in slower external flames. For methane with a K_v of 10.9, P_{fv} was the higher overpressure and in this case there was very little difference in the overpressures for circular and square vents. Where the peak overpressure was due to the external explosion the square vent always had a lower overpressure than for circular vents. The more reactive ethylene/air mixtures showed more than 30% increase in overpressure at all K_v for round vents compared with square vents.

CHAPTER 6

The Venting of Hydrogen-air Explosions

6.1 Introduction

6.1.1 Vent Design and Mixture Reactivity

6.2 Experimental Setup and Procedure

6.3 Pressure Time Records for Vented Hydrogen Explosions

6.4 Flame Speeds

6.6 Conclusions

6.1 Introduction

The increase in the awareness of greenhouse effect and the quest for the reduction in the use of fossil fuel necessitates the search for alternative energy in order to reduce the emission of greenhouse gases. In recent years, hydrogen gas has been identified as a good replacement for fossil fuel and the demand for hydrogen has also increased. In view of the above, there is the need to consider the hazards associated with the combustion of hydrogen gas mixtures. The literature survey in chapter 2 showed that the current gas explosion design standards do not adequately accommodates hydrogen mixtures.

In view of the above, this section presents vented hydrogen-air explosions results for range of K_vs for 30% (stoichiometric) and 40% (most reactive) hydrogen-air concentrations, at the limit of applicability of the compact vessel definition of L/D<2 in the EU venting standards or L/D< 5 current NFPA 68 (2013). New data for explosion venting of hydrogen-air mixtures were generated and the limitations of the explosion venting standards as regards the design of explosion vents for protection against hydrogen explosion hazards was demonstrated .

6.3 Pressure Time Records for Vented Hydrogen Explosions

The pressure time records for two repeated vented explosions for 40% hydrogen-air (maximum reactivity mixture) are shown in Figure 6.1 for a K_v of 10.9. The pair of pressure records in Figure 6.1 are for pressure transducer PT0 on the end ignition flange (left) and pressure transducer PT1 on the vessel wall in the centre (right). The terminology for the pressure peaks is that P_{burst} is the pressure peak due to the vent burst pressure, which was zero in all the present work for free venting. P_{fv} is the pressure peak due to the flow of unburned gas through the vent. P_{ext} is the pressure caused by the external explosion, which is caused by the flame emerging from the vent and then igniting the external turbulent cloud of vented unburned gases as explain earlier.

The thermocouple T_1 was 81mm downstream of the rear face of the vessel and T_2 was 217 mm upstream of the vent and thermocouple T_4 was at the vent. Thermocouple T_3 was at the wall in the centre of the vessel and was placed there to determine the time at which the flame propagated to the wall, which was assumed to

be the time the peak overpressure occurred in the laminar flame theory. The time of arrival of the flame at these thermocouples enables the location of the flame at the time of the maximum overpressure to be determined as well as the axial development of the flame speed. These flame arrival times are marked in Figures 6.1-6.4 and if the peak pressure occurs after the flame has reached T_4 then the peak pressure is due to an external explosion, but if the peak pressure occurs before the flame reaches T_4 or at the same time as T_4 then it is due to the flow of unburned gas through the vent.

Figure 6.1 Pressure records for two repeat vented explosions for 40% hydrogen-air with Kv = 10.9 (blockage ratio 80%), comparison of the PT0 (left) and PT1 (right) pressure transducers

There was a significant time difference for events at the two pressure transducers and the thermocouples to respond, due to the finite speed of sound at which pressure waves travelled. The vessel was 0.46m long from the rear wall where PT0 was mounted to the vent and the velocity of sound in 40% hydrogen/air at ambient temperature is 427 m/s. A pressure change event at the vent would then take 1.08ms to reach the pressure transducer PT0. This means that PT0 will lag events at the vent by about 1ms. This makes P_{fv}, which in Figure 6.1 for PT0 appears to align with the

time the flame is at T_2, to be when the flame is at T_4. However, this still leaves P_{ext} as the peak pressure.

For pressure transducer PT1 as mentioned in chapter 3 has a distance of 0.3m from the vent and a pressure event at the vent would take 0.70ms to reach PT1. This is sufficient to move the pressure spike in Figure 6.2 from occurring between the times T_2 and T_3 aligning with the time the flame emerged from the vent at T_4. This then leaves the P_2 pressures in Figure 6.1 for PT0 and PT1 time aligned and occurring when the flame passed through the vent. Figure 6.1 shows that the time of P_{fv} and P_{ext} is the same at both pressure transducers and it is only their magnitude that was different, with PT1 pressure transducer recording P_{fv} as the maximum pressure and PT0 recording P_{ext} as the maximum pressure. This indicates that the pressure wave decays in magnitude in the distance between PT1 and PT0. The fact that PT1 had a larger overpressure than PT0 was unexpected as PT0 should record the total pressure in a dynamic flow and PT1 should record the static pressure. However, PT0 was <PT1 for all times after the flame reached T_2.
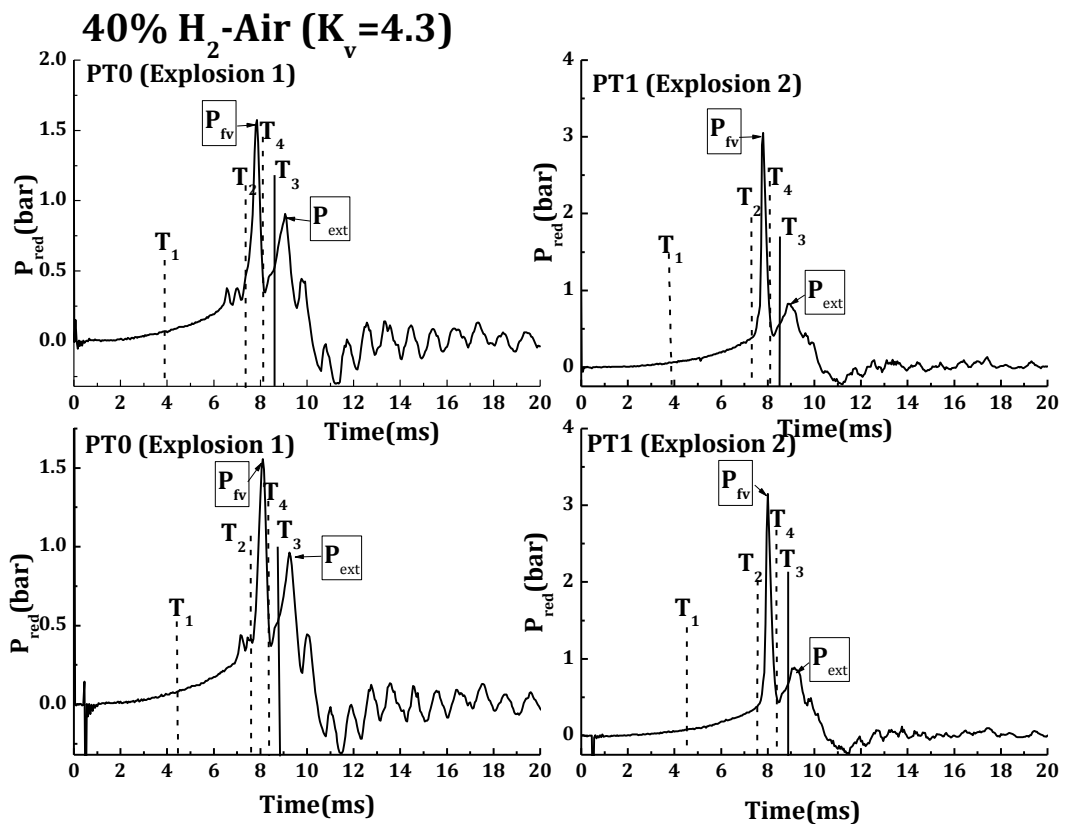
Figure 6.2 Pressure records for two repeat vented explosions for 40% hydrogen-air with Kv = 4.3 (blockage ratio 50%), comparison of the PT0 (left) and PT1 (right) pressure transducers

The difference between PT1 and PT0 in the magnitude of P_{fv} is a crucial problem, as at PT0 the external explosion was dominant at 1.6 bar, but at PT1 the flow through the vent overpressure P_{fv} was dominant at 4.4 bar. In the graphs of P_{red} as a function of $1/K_v$ which are presented later, both P_{fv} and P_{ext} are plotted for all explosions and P_{red} is shown for both pressure transducer locations. It is considered that this problem has not been reported previously as Bartknecht (1993) only had a pressure transducer at the present PT0 position and hence his peak overpressures may be low and this may explain why his results do not fit laminar flame venting theory.

The pressure time records for 40% hydrogen with K_v of 4.3 are shown in Figure 6.2. As in Figure 6.1 both the PT0 and PT1 pressure records are shown and there is similarity in the measurements of where the peak overpressure occurred, although not in the magnitude. The time for the pressure wave to move between the event at the vent and the two pressure transducers was taken into account, as discussed above. And also, both PT0 and PT1 show in the first explosion that a peak overpressure, P_{fv}, occurs when the flame reaches the vent and arrives at T_4. The external explosion occurs much later after the flame has left the vent and has a much lower magnitude due to the larger vent area and lower external turbulence.

The magnitude of the overpressure was 4.4 bar for PT1 and 1.4 bar for PT0. As for Figure 6.1, it may be concluded that most of the mixture in the vessel was burned just before the flame exited the vent. This is in contrast to methane and propane vented explosions on this test facility, where most of the mixture remained unburned in the vessel when the flame left the vent and burns slowly, with T_3 occurring well after the peak external pressure.

The repeat explosion in the bottom pair of graphs in Figure 6.2, showed different results, with PT0 showing that P_{fv} was the maximum P_{red} at 0.7 bar with an external explosion P_{ext} at 0.65 bar. However, PT1 records the maximum P_{red} as the external explosion P_{ext} at 1.5 bar with P_{fv} at 0.5 bar. However, when the 0.7ms time delay is taken into account between T_4 and PT1 the first of the two pressure peaks for P_{ext} occurs as the flame passes through the vent. Thus it is very difficult to separate events upstream and downstream of the vent, as the peak pressure occurs as the flame passes through the vent.
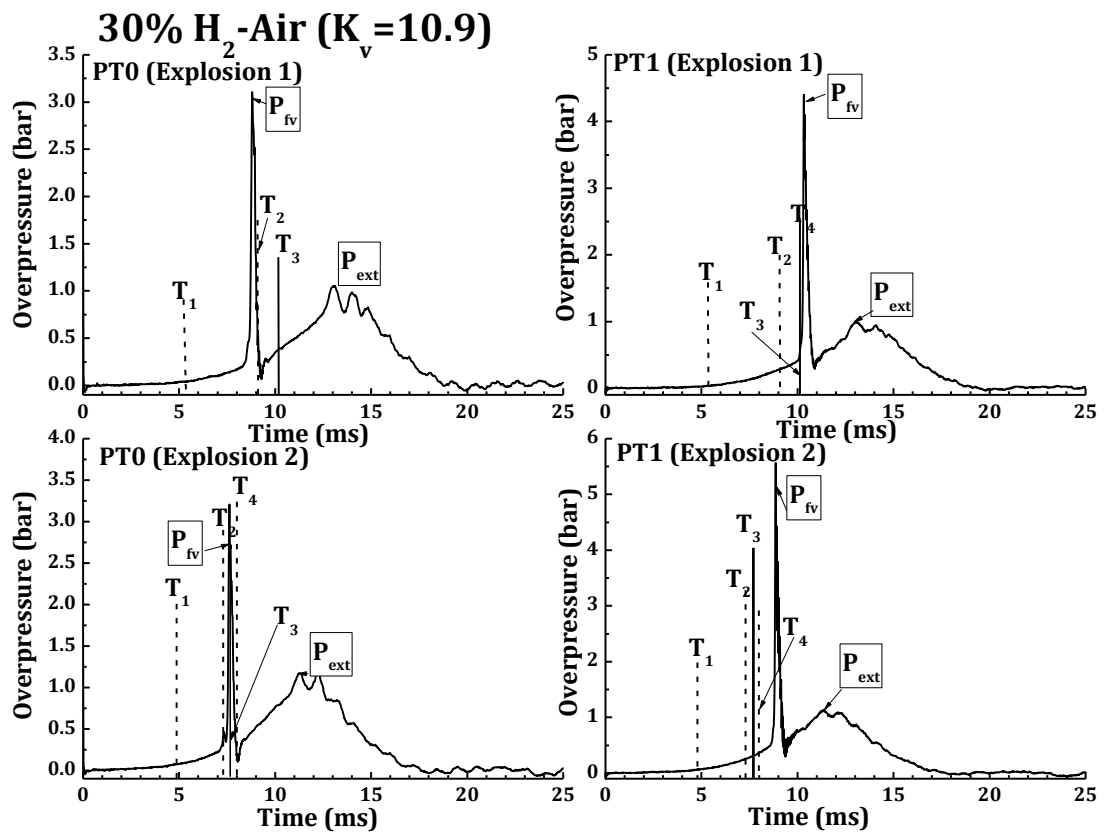
Figure 6.3 Pressure records for two repeat vented explosions for 30% hydrogen-air with Kv = 10.7 (blockage ratio 80%), comparison of the PT0 (left) and PT1 (right) pressure transducers

Figures 6.3 and 6.4 show the pressure-time records for 30% hydrogen-air vented explosions with K_v of 10.7 and 4.3 respectively, with two repeats for each and for both pressure transducers. The thermocouple T_4 at the vent exit was not available in these explosions. However, in Figures 6.1 and 6.2 T_4 and T_3 occurred at a very similar time and so it will be assumed that the time for the flame to reach T_3 is roughly the time it exited the vent. Figure 6.3 shows a different behaviour to the 40% case in Figure 6.1, with all four pressure records in both explosions and both pressure transducers showing a large spike in pressure occurring at a similar time to that in Figure 6.1 for PT1, with it occurring earlier at PT0 than PT1. The pressure spikes in Figure 6.3 all occurred before the flame exited the vent and were thus due to the high velocity flow through the vent. In Figure 6.1, the PT1 pressure transducer had a higher overpressure of 5 bar compared with 3 bar at PT0. The 5 bar pressure at PT1 was greater than the peak PT1 value of P_{fv} of 4 bar in Figure 6.1. These results show that the worst case explosion for peak pressure was the 30% hydrogen

explosions not the 40% and the vent flow dominated the overpressure. The external explosion P_{ext} was much lower than P_{fv} in all cases in Figure 6.3. The external explosion overpressure was around 1 bar in both explosions and at both pressure transducers, this was lower than the 1.5 bar in Figure 6.1.
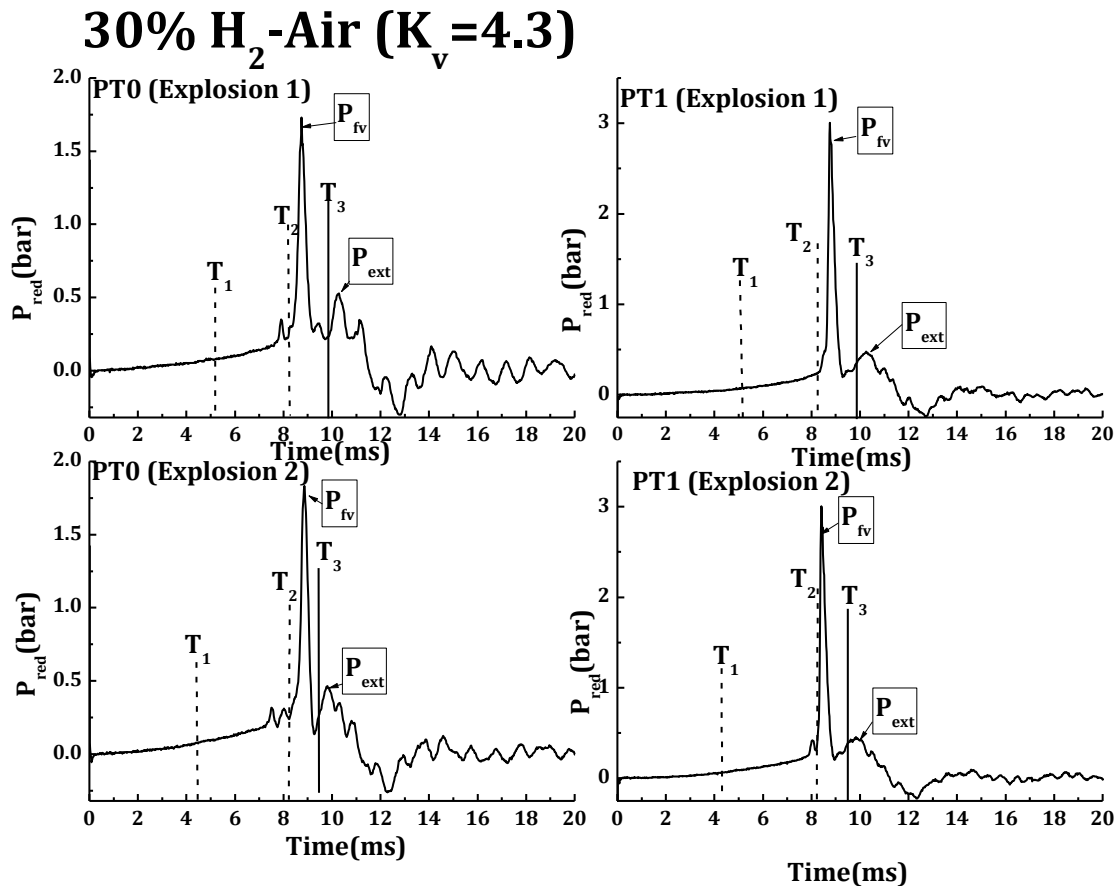
Figure 6. 4 Pressure records for two repeat vented explosions for 30% hydrogen-air with Kv = 4.3 (blockage ratio 50%), comparison of the PT0 (left) and PT1 (right) pressure transducers

For K_v=4.3 the pressure time records are shown in Figure 6.4 for 30% hydrogen and for two repeat explosions. For the both explosion the peak overpressure at PT1 and PT0 was a 3 bar pressure spike that occurred before the flame reached the vent and hence was due to the vent outflow. The repeat explosion was very similar with a slightly lower P_{ext}.

For lower K_v than 4.3 the P_{red} measurements were not as consistent in the repeat explosions and between PT0 and PT1. An example of this is given in Figure 6.5 for K_v = 3.6 (40% vent blockage). This shows that the repeat explosions had different results for the location of the peak pressure. For the first explosion the peak pressure

spike occurred when the flame was outside the vent and in the repeat explosion it occurred when the flame passed through the vent. This occurred for the PT0 and PT1 pressure transducers, which showed the same event timing, but at different magnitudes. The reason for this difference may be associated with the larger upstream flame speeds at low K_v as discussed in the next section.
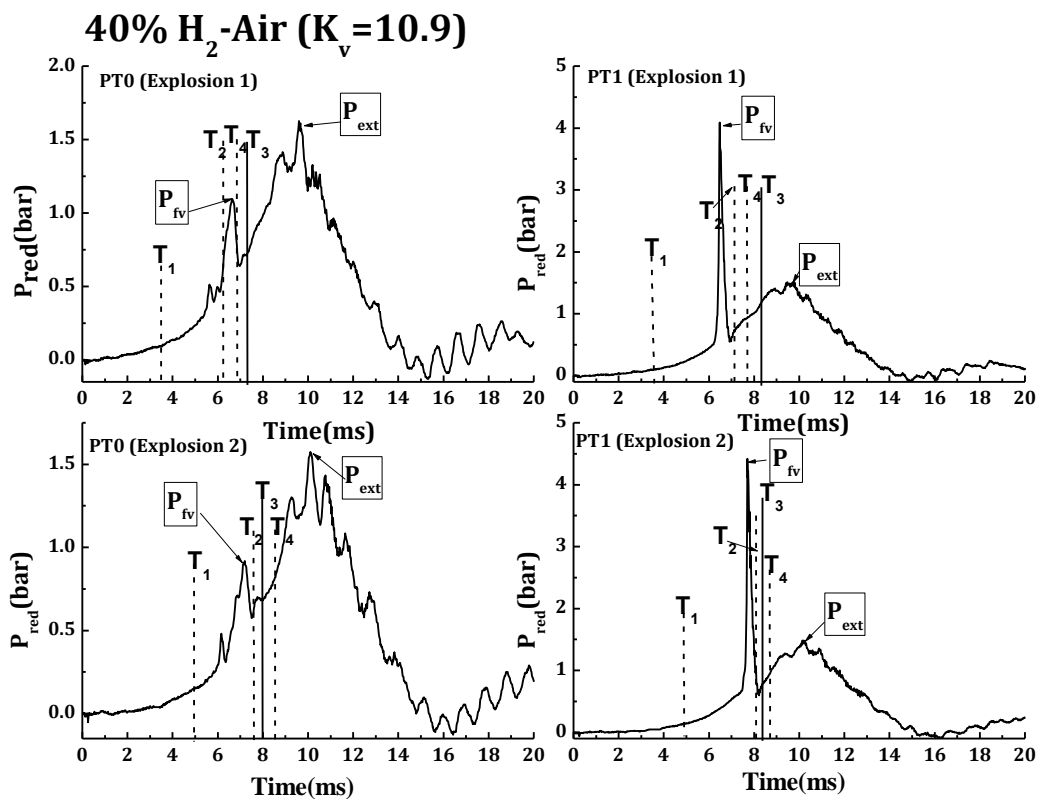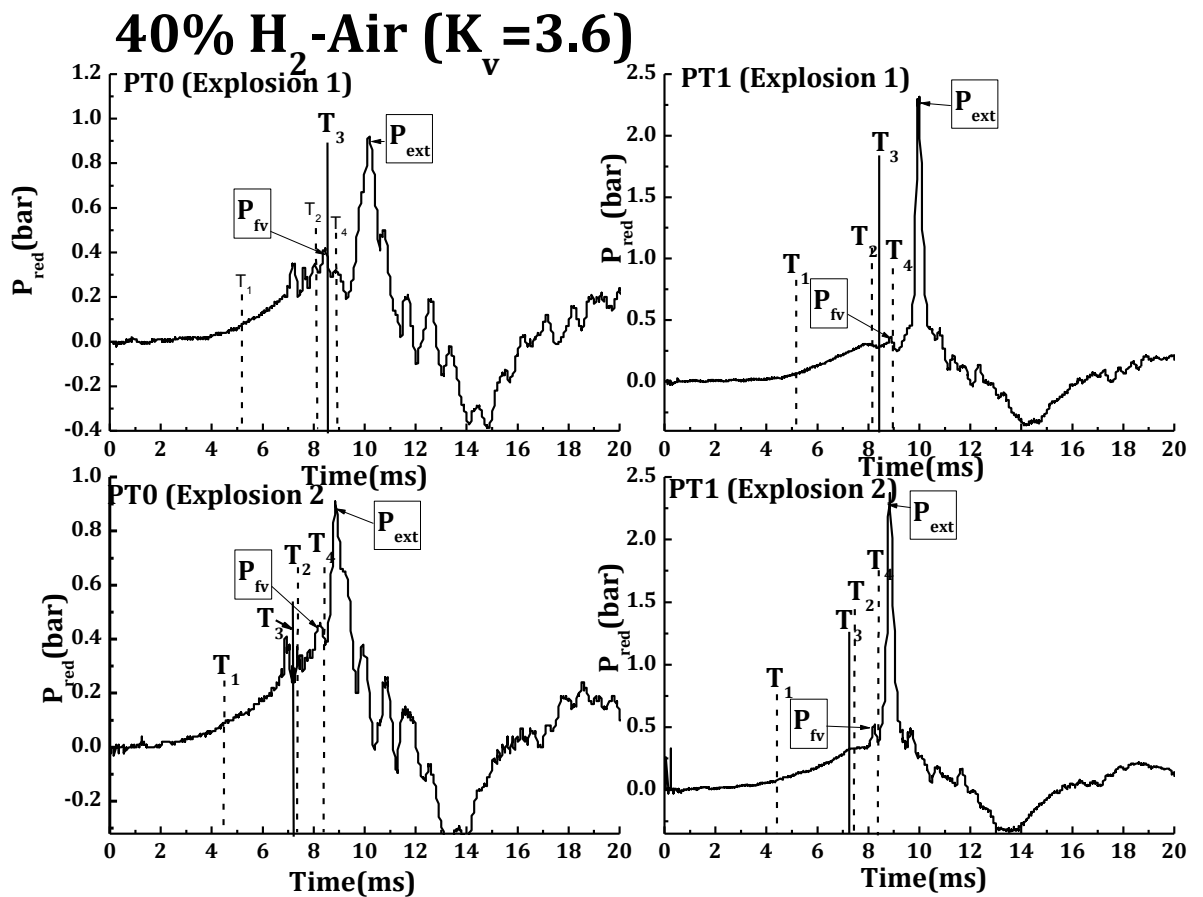

Figure 6.5 Pressure records for two repeat vented explosions for 40% hydrogen-air with Kv = 3.6 (blockage ratio 40%), comparison of the PT0 (left) and PT1 (right) pressure transducers

Figure 6.6 shows the pressure-time for 40% and 30% hydrogen-air, compared with the time of flame arrival from the thermocouple records. It was clear from the thermocouple records that there are no unusual events as the flame passes through the vent to suggest the causes of the pressure spike. The only explanation is the pressure spike generated was caused by the fast flow of unburnt gases through the vent. However, there is the need for further investigation in order to give better understanding of the possible causes of the pressure spikes and sonic venting as discovered the present work for hydrogen-air mixtures.
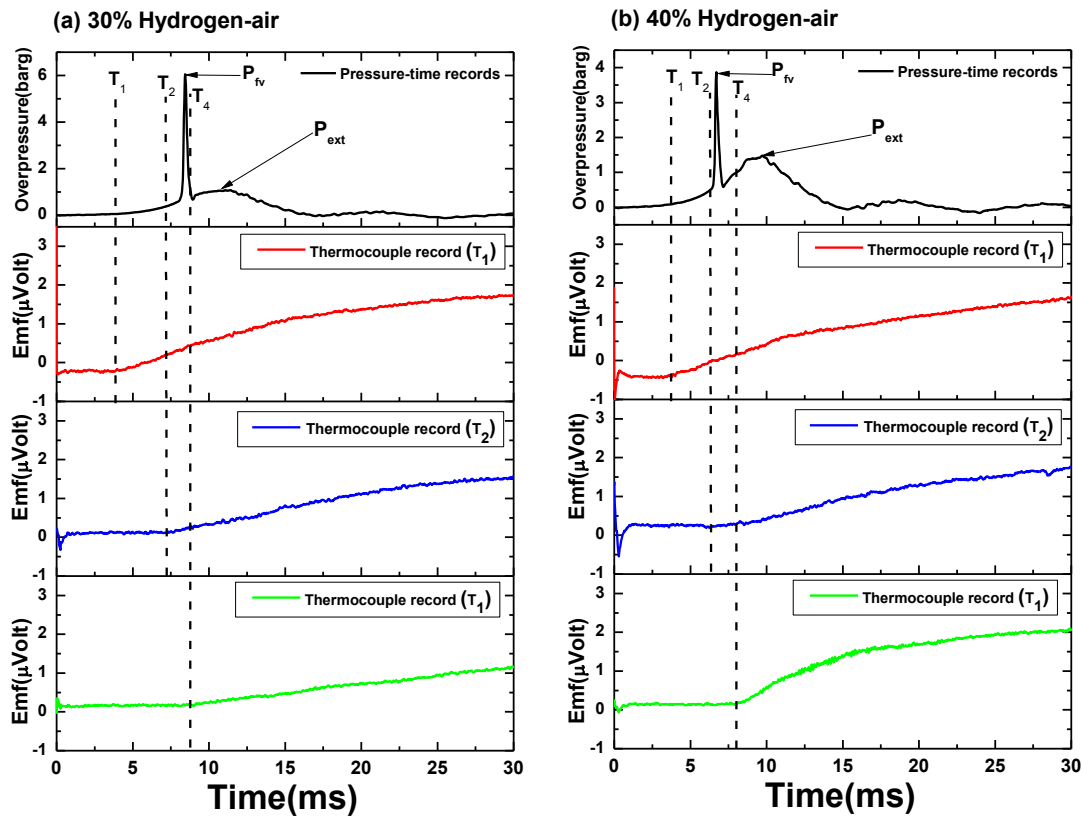
Figure 6. 6 Comparing pressure-time record and thermocouple records

6.4 Flame Speeds

The flame speeds between the line of thermocouples on the vessel and vent centerline are shown for 40% hydrogen in Figure 6.7 for K_v=3.6 and 10.9. This shows that there was a very fast acceleration of the flame from the spark to the vent and further acceleration outside the vent for K_v=10.9, due to turbulence generation in the vent outflow for this high blockage vent. The high flame speed between T_2 and T_4 is crucial for the vent overpressure as this pushes unburned gas ahead of it at $(E_p-1)/E_p$ times the flame speed, which for 40% hydrogen is 86% of the flame speed. For the two flame speeds approaching the vent in Figure 6.7 of 350 and 300 m/s respectively for K_v=10.9 and 3.6 this is gas velocities of 301 and 258 m/s. This is the velocity in the 162mm diameter vessel pipe area (assuming the flame is near planar, which is unlikely). This would give a mean gas velocity at the plane of the vent of 505 m/s and 387 m/s respectively. The sonic velocity for 40% hydrogen air is 427 m/s in the unburned gas and ~1000m/s in the burnt gas. This means that the unburned gas flow ahead of the flame at the vent is likely to be sonic and choked

vent flow will occur at most of the K_v investigated. This is the principle cause of the high pressure spike as the flame passes through the vent in Figures 6.1-6.5 and T_2. Also the initial Flame speeds upstream of the vent were determined from the travel time between T_1 and T_2. These two flame speeds are shown as a function of K_v in Figure 6.8 for 30% hydrogen-air and in Figure 6.9 for 40% hydrogen-air. The initial flame speed at low K_v was about 12 m/s at 30% hydrogen-air and 20 m/s at 40% hydrogen air, which were relatively independent of K_v.
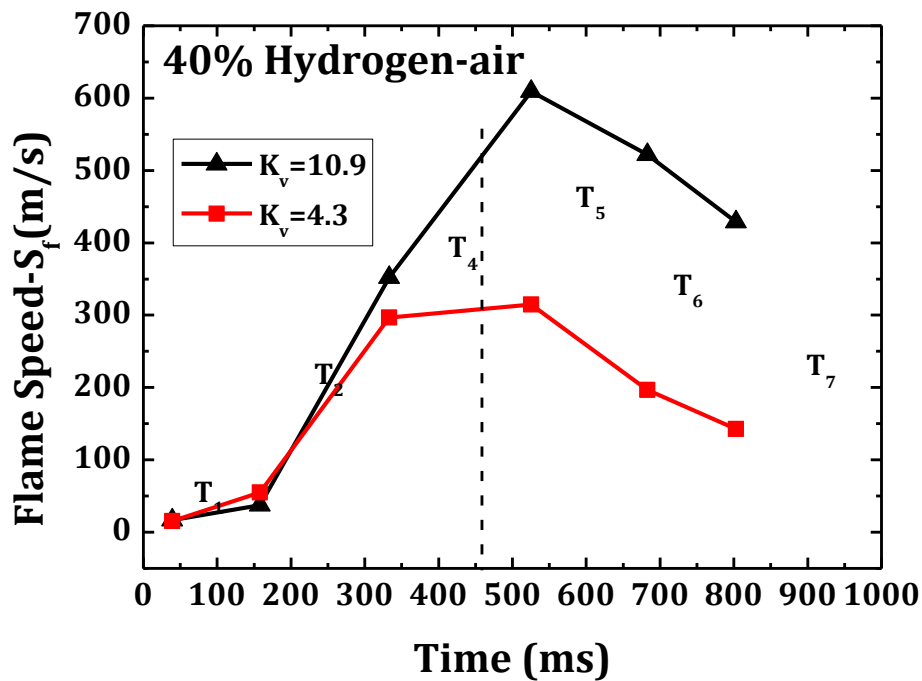
Figure 6.7 Flame speeds as a function of the distance from the rear face. T4 is the time the flame passed through the vent

This was expected as the initial flame is too far away from the vent to have any feedback from the vent open area. The spherical laminar flame speed for hydrogen air for diameters 50-100mm (Fakandu et al., 2011) was 14 m/s for 30% hydrogen-air and 17.5 m/s for 40% hydrogen-air and these are in reasonable agreement with the present initial flame speeds in Figures 6.7 and 6.8. Thus it may be concluded that the initial flame speed is a hemispherical laminar flame that propagates from the spark in the axial and radial direction at the spherical laminar flame speed.

The flame speed approaching the vent, between T_1 and T_2, is shown in Figure 6.8 and 6.9 to be much higher than the initial flame speed and to be about 50m/s at low K_v for 30% hydrogen-air and 60m/s for 40% hydrogen-air. These flame speeds are about a factor of 3.5 higher than the laminar value of the initial flame and they show that for end ignition opposite the vent that the flame accelerates towards the vent on

the axis of the vessel. It is considered that it is the outflow of gases that induces the vent flow and accelerates the flame towards the vent. Phylaktou and Andrews (1990) have shown, for large L/D vessels with no venting, that there is a initial fast flame of 'U' shape propagating along the vessel axis with a slow flame accelerating radially towards the wall. This is a feature of explosions in large L/D vessels irrespective of the presence of a vent (Phylaktou et al., 1990).
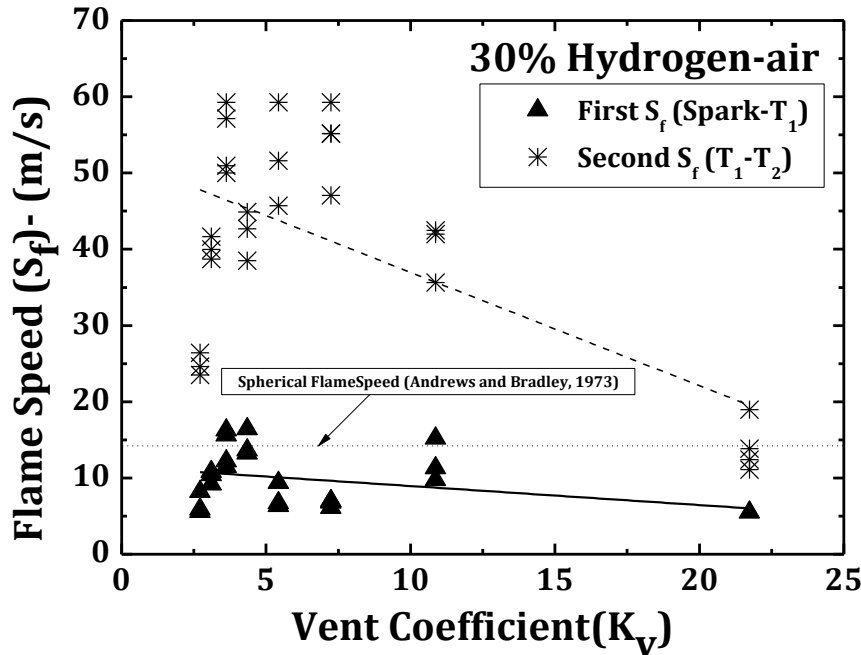
Figure 6.8 Initial and vent approach flame speeds as a function of Kv
for 30% hydrogen-air (stoichiometric)
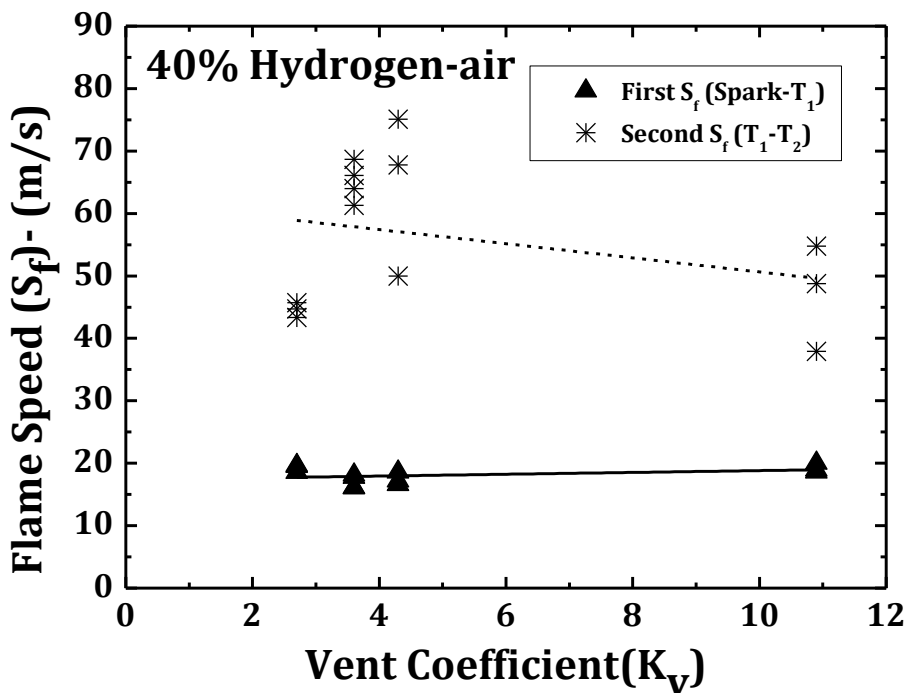
Figure 6.9 Initial and vent approach flame speeds as a function of Kv for
40% hydrogen-air (maximum burning velocity condition)

If it is assumed that the flame propagation is adiabatic then there is an unburned gas velocity ahead of the flame that is 86% of the flame speed. This would give mean velocities in the vessel cross sectional area of 43 m/s for 30% hydrogen-air and 52 m/s for 40% hydrogen air. The thermocouple T_4 at the vent was not in place for all of this work and so the $T_2 - T_4$ flame speed was not available for all K_v. However, the results shown in Figure 6.7 show that there was substantial acceleration of the flame after thermocouple T_2 to 300- 350 m/s, relatively independent of K_v. These fast flames will give sonic flow at the vent plane at all K_v investigated. Part of the cause of these high vent plane velocities could simply be due to flow acceleration into the vent. Assuming that the velocity at the vent is simply the velocity averaged across the vessel area multiplied by the vessel area to vent area ratio then this is a multiplication factor of 2 for $K_v = 4.3$ and 5 for K_v-10.9, which gives vent unburned gas velocities of 83 and 215 m/s for 30% hydrogen-air. For 40% hydrogen-air the equivalent velocities are 104 and 260 m/s. These velocities should be increased due to the sharp edged orifice vents used which would form a vena contracta downstream with a contraction coefficient of 0.61. This would then give vena contracta velocities of 136 and 352 for K_v=4.6 and 10.9 respectively for 30% hydrogen air and 171 and 425 m/s for 40%. However, as shown in Figure 6.7 there is some further acceleration of the flame after T_2 and the high velocities for T_2 to T_4 are not all due to flow acceleration due to the area change. Nevertheless, the above rough calculations show that sonic velocities will be created at the vent plane and hence shock waves and possible detonations. These events are then responsible for the sharp pressure rises shown in Figure 6.1-6.6.

6.5 P_2 and P_3 Overpressures as a Function of K_v for PT0 and PT1 Pressure Measurements

The maximum reduced pressure is shown as a function of K_v in Figure 6.8 for 40% hydrogen air. This shows the data for the rear face pressure transducer PT0 on the left and for the wall mounted pressure transducer in the middle of the vessel, PT1, on the right. In each sub-figure the value of the maximum value of P_{red} of the internal, P_{fv}, and external, P_{ext}, overpressures are shown as separate symbols. Comparison is also made with the Bartnecht (1993) vent design Equation 6.1 and with his two vented hydrogen explosion data points. This shows that for K_v<5 Bartknechts design line and his data points are in agreement with the present

measurements at PT0 and it is thus likely that his pressure transducer was mounted on the rear wall opposite the vent.
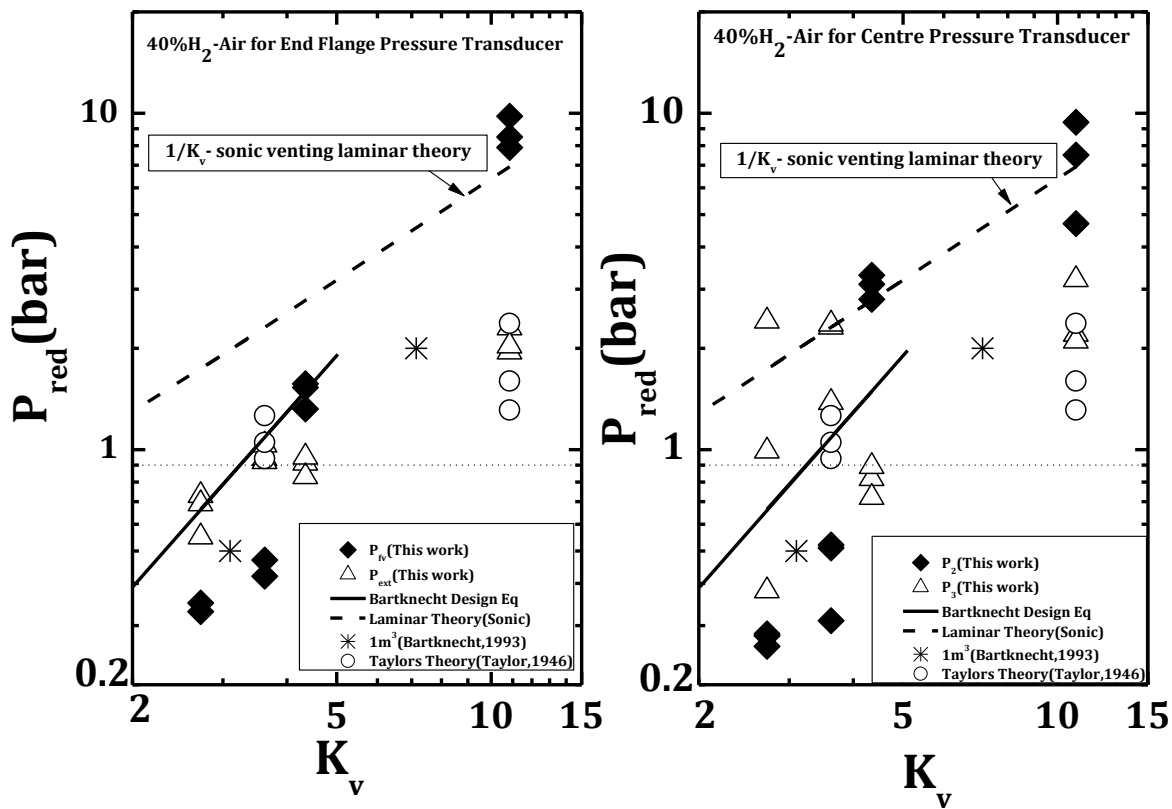
Figure 6.10 P2 and P3 free venting overpressures for 40% hydrogen-air as a function of Kv for PTO (left) and PT1 (right) pressure transducers, with comparison with Bartknecht's equation and data for 0.1 bar static burst pressure

Figure 6.10 shows that for $K_v > 4$ PT1 measured the highest P_{red} and this was the overpressure due to flow through the vent, P_{fv}. For $K_v < 4$ PT1 was still the highest overpressure, but the external explosion, P_{ext}, was the highest overpressure. For PT0 the highest overpressure was also P_{fv} for $K_v > 4$ and P_{ext} for $K_v < 4$. This change in the dominant cause of the overpressure at $K_v > 4$ is considered to be due to the relative independence of the upstream flame speed on K_v, shown in Figures 6.6 and 6.7 for 40% hydrogen-air. At low K_v the vent blockage to the explosion is low and the flow pressure loss is low.

The external unburned gases ejected at high velocity through the vent will create a fast external explosion with a dynamic pressure greater than that due to flow through the large vent. Use of the Taylor (Taylor, 1946) Equation 7.1 shows that the high external flame speeds in Figure 6.6 predict a P_{ext} of 0.8 bar, close to that measured

for K_v= 3.6, whereas for K_v=10.6 the Taylor external fast flame overpressure was less than P_2 due to sonic vent flow.

$$P = \frac{2\gamma M^2}{1+M}$$

[7.1]

It is also shown in Figure 6.10 that the Bartnecht vent design equation underestimates the peak P_{red} measured at PT1, but is in good agreement with that measured at PT0 on the end flange. The laminar flame theory for sonic venting agrees well with the experimental data for peak P_{red} measure at PT1. The peak overpressures were much less than the detonation pressure which is 12.4 for 40% hydrogen(James, 2001) and were due to fast deflagrations close to detonation transition.
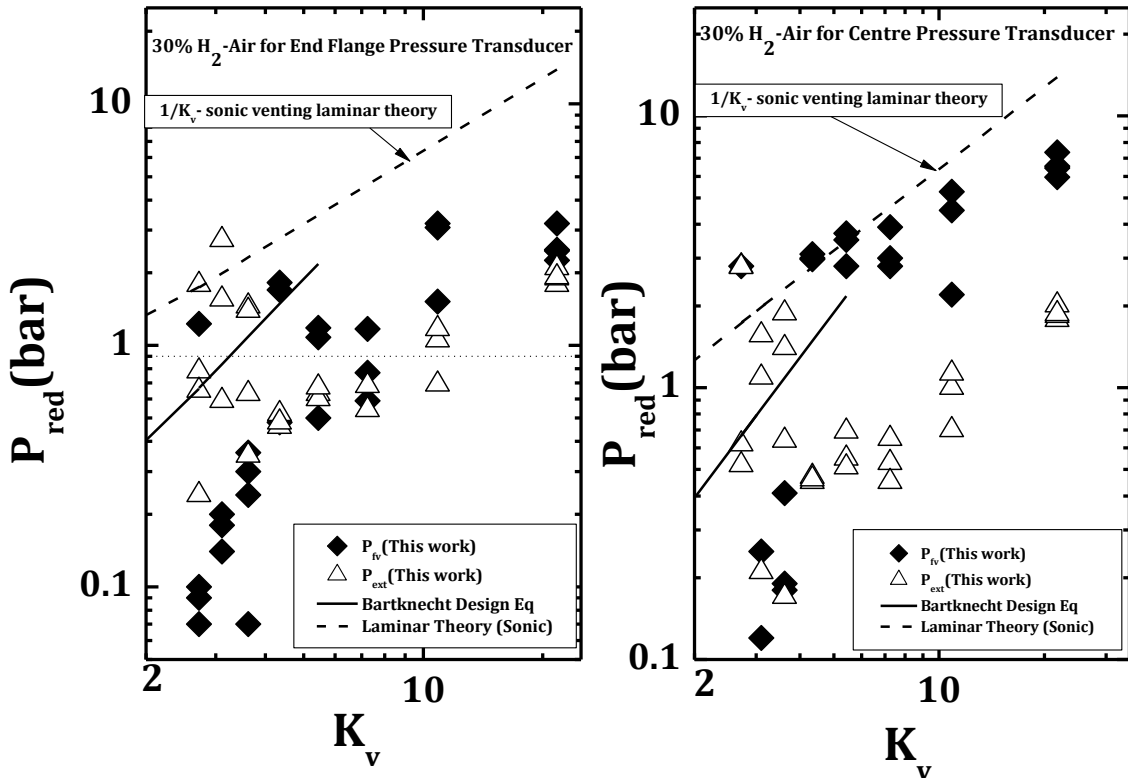
Figure 6.11 P2 and P3 overpressures for 30% hydrogen-air as a function of Kv for PTO (left) and PT1 (right) pressure transducers, with comparison with Bartknecht's equation and data

Figure 6.11 shows the equivalent data as Figure 6.9 for 30% hydrogen-air. At low K_v P_{red} is higher than for 40% hydrogen in Figure 6.10. There was considerable data scatter in the repeat tests. At PT1, P_{fv} had the highest P_{red} for K_v>4 and P_{ext} was highest for K_v<4, as was found for 40% hydrogen and for the same reasons. At PT0 P_{fv} had the highest P_{red} for all K_v, but with a few explosions at low K_v with P_{ext} as

the highest P_{red}. The Bartknect vent design equation was in poor agreement with the experimental results and is therefore unsafe for hydrogen. This is in contrast to methane and propane vented explosions in this test facility, where the Bartknecht design equation grossly over predicts the measured overpressures (Fakandu et al., 2011, Kasmani et al., 2006). The laminar flame sonic venting predictions are in good agreement with the measurements.
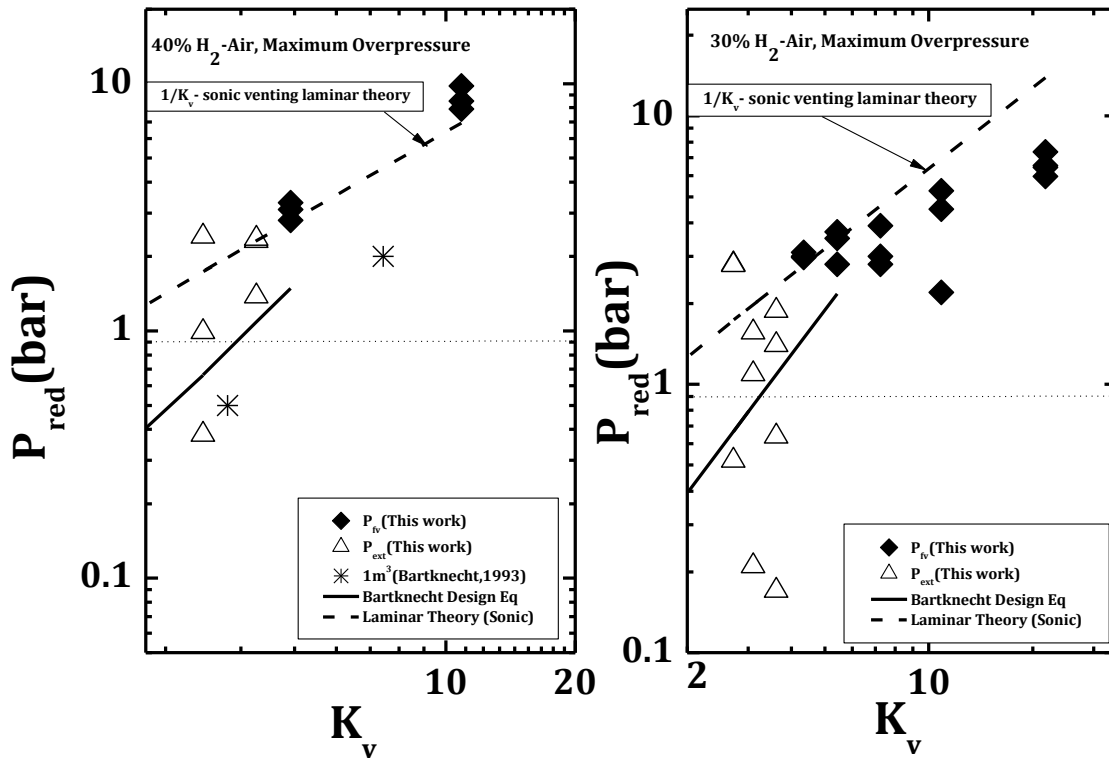
Figure 6.12 Maximum Pred for PT0 or PT1 as a function of Kv for 40% and 30% hydrogen

The maximum P_{red} at either pressure transducers for P_{fv} or P_{ext} is shown in Figure 6.12. This demonstrates again for both mixtures that the Bartknecht vent design equation is much lower than the measured P_{red} for both 40% and 30% hydrogen. The two experimental vented 40% hydrogen results were also well below the present measurement, but were in agreement with the PT0 measurements. The data in Figure 6.12 provides a much better design line for hydrogen free venting than is in the current design standards. However, there is likely to be an increase in the overpressure with higher vented vessel volumes, as occurs with methane and propane vented explosions.

The laminar venting theory with incompressible flow at the vent predicted higher overpressures than the measured values, which has also been found for methane and propane vented explosions (Fakandu et al., 2011, Kasmani et al., 2006). This was due to the assumption of A_s as the flame surface area and indicates that the actual surface area at the time the flame reached the vent was much lower than A_s at the peak P_{red}.

6.6 Conclusions

1. The current gas explosion venting design guides, based on the work of Bartknecht (1993) have a design constant for hydrogen explosions that is incompatible with the known relative reactivities of methane, propane and hydrogen.

2. These gas explosion venting design guides underestimate the measured peak overpressures in the current vented hydrogen explosions, even though for methane and propane there is a gross overestimation.

3. Hydrogen vented explosions for a vessel with L/D=2.8 and end ignition, which is within the range of applicability of the design guides, show very fast flame effects with flame velocities approaching the vent of 60m/s, acceleration to 300 m/s at the vent and 600m/s in the turbulent flow downstream of the vent. In all cases these flame speeds at all K_v create sonic flow of unburned gas through the vent with very large P_2 overpressures as a consequence.

4. The dynamic flame pressure events result in difference in the pressure recorded at the end flange and at the wall in the centre of the vessel and it is the latter position that showed the highest overpressures. It is likely that the lower overpressure reported in the work of Bartknecht (only two vented hydrogen explosions in a 1 m³ cylindrical vessel) was due to the location of the pressure transducer on the end wall opposite the vent.

5. For K_v<4 the peak explosion overpressure was due to an external explosion created by the very high flames speeds approaching the vent and the low resistance to this flow at low K_v, which left the external flame speeds very high with an overpressure that was well predicted by the Taylor equation for the static pressure behind a fast flame.

CHAPTER 7

Vent Design and Influence of Mixture Reactivity

7.1 Introduction

7.2 Mixture reactivity parameters in gas explosion venting

7.3 Self Acceleration of Flames in Explosions in Large Vented Vessels and its Link to Mixture Reactivity

7.4 Comparison of the Bartknecht Vent Design Equation with other Experimental Data for Vented Explosions

7.5 Laminar Flame Venting Theory

7.6   Experimental Methods

7.7 The Influence of Gas Reactivity

7.7.1 Influence of gas reactivity at K_v=4.3 (50% vent blockage) for Stoichiometric gas/air mixtures where the external explosion, P_{ext}, was the dominant overpressure

7.7.2 Influence of Gas Reactivity at K_v=21.7 (90% vent orifice blockage)

7.8 P_{red} as a Function of Mixture Reactivity

7.9 Conclusions

7.1   Introduction

The knowledge of the pressure development in closed vessel and vented explosions are important consideration in the application of explosion venting correlations including the vent design standards. Experimental scaling of explosion scenarios correlated by the use of vessel volume from small scale to larger volumes, and the self-acceleration of flames and other associated turbulence could be responsible for much higher overpressures in larger vessels. Another parameter used to scale up explosion is the use of more reactive mixtures in order to generate higher combustions rates as well as higher mass burning rate(Bimson et al., 1993, Na'inna, 2013). The previous chapter has seen the explosion venting analysis of individual gas mixtures for hydrocarbons and hydrogen gases. On the other hand the results presented in this chapter are based on the analysis of different gas mixtures used in the current study, and comparing the reactivity influences.

Explosion venting is influenced by the reactivity of the gas mixture and venting design correlations based on the NFPA 68 (2013) and European standard (BS EN 14994, 2007) considered the use of reactivity parameter. This is normally correlated using either the laminar burning velocity, U_L, or the deflagration index, $K_G = (dp/dt)_{max}V^{1/3}$. This work used a small 10 litre vessel that was considered to give a laminar flame explosion and enabled laminar flame venting theory to predict the influence of reactivity through the U_L term. It was shown that U_L is directly related to K_G and hence that laminar flame venting theory can be expressed in terms of K_G, which is used in the experimental presentation of venting data and in venting design standards. It is shown that the treatment of hydrogen in the standards, significantly underestimates the overpressure for vented hydrogen explosions.

7.2 Mixture reactivity parameters in gas explosion venting

The reduced overpressure, P_{red}, of any vented explosion depends on the reactivity of the mixture, the volume and shape of the vessel, the ignition position and the initial turbulence levels (Catlin, 1991, Hermanns et al., 2010, Hjertager, 1984, Phylaktou and Andrews, 1993, Razus and Krause, 2001). This complexity of influences on the venting of gaseous explosions led Hattwig and Steen (2004) to conclude that current knowledge does not permit satisfactory predictions of P_{red} for vented gas

explosions(Pappas and Foyn, 1983). The reactivity of the mixture of gases is taken into account using either the laminar burning velocity, U_L, or the deflagration parameter, $K_G=(dp/dt)_{max}V^{1/3}$. Current gas explosion vent design standards are based on experimental results in empty compact vessels (L/D~1) with central ignition. NFPA 68 (2007) and EN14994 (2007) use K_G as the reactivity parameter, but NFPA 68 (2013) has abandoned this approach and now uses the burning velocity, U_L, approach for mixture reactivity influences, up to a maximum of 3 m/s and for mixture concentrations <10%, which excludes hydrogen/air venting at the maximum reactivity composition (3.5 m/s U_L and 40% H_2 in air). No guidance is thus given in NFPA 68 (2013) for hydrogen-air venting, but such guidance is given in EN14994 (2007) which is that same guidance that used to be in NFPA 68 2007.

The burning velocity was used in the laminar flame venting theory developed by Swift (1983, 1988) which was recognised in NFPA 68 (2007) and EN14994(2007) for low (<0.1 bar) P_{red} and in NFPA 68 (2013) for P_{red} up to 0.5 bar. The Swift [1988] methodology for higher overpressure with compressible flow at the vent was also used in NFPA68 2013, with no stated limitation on the maximum P_{red}. As sonic flow occurs at $P_{red} = 0.9$ [$(P_{red} + 1)/P_i = 1.9$] this must be the upper limit of applicability of the design approach in the new NFPA 68 (NFPA 68, 2013). For $P_{red}>0.9$ bar sonic flow venting occurs and this is not addressed in NFPA 68 2013, although for high initial pressures venting is sonic and vent design procedures are given for this, based on the sonic venting flow methodology of Epstein (Epstein et al., 1986). All theories of vented explosions (Bradley and Mitcheson, 1978a, Cates and Samuels, 1991, Molkov et al., 2000, Molkov, 1999b, Swift, 1988) use the laminar burning velocity, U_L, as the reactivity parameter.

The methane, propane and hydrogen vent design procedures in current standards using K_G as the reactivity parameter, show a very low influence of the high reactivity of hydrogen and a high reactivity difference between methane and propane. This is difficult to understand in relation to the well established large differences in reactivity between hydrogen and propane based on U_L as the reactivity parameter. Also, the small difference in U_L between methane and propane makes a large difference in the vented vessel overpressures difficult to understand. This indicates that the measurement of mixture reactivity and its influence on vented explosions is an area of uncertainty and this work was aimed at providing further

experimental evidence and further understanding on the influence of mixture reactivity in vented explosions.

The K_G and U_L approaches to the inclusion of mixture reactivity in explosion venting design are directly related and can be interchanged. Andrews and Phylaktou (2010) derived Equation 7.1 from spherical flame propagation theory(Andrews and Phylaktou, 2010). In a spherical vessel 98% of the pressure rise occurs in the second half of the flame travel distance. If a constant flame speed is assumed across ¼ of the vessel diameter, then the time to achieve the last 98% of the pressure rise can be calculated and the adiabatic pressure rise used to determine the mean rate of pressure rise, as in Equation 7.1. The chief approximation in the derivation of Equation 7.1 is that U_L is assumed to be constant throughout the flame travel. This is not valid as for hydrocarbons U_L decreases as pressure increases and increases as the unburned gas temperature increases due to compression. However, the computations of Bradley and Mitcheson (1976) show that this effect is a maximum change in U_L of 20% from the initial value. A mean value of U_L 10% higher than that at ambient conditions would be reasonable in Equation 7.1. However, there is no agreement on a standard method to determine U_L and published values vary widely, by much more than 10% (Andrews and Bradley, 1972b).

$$K_G/P_i = [d(P/P_i)/dt]_{max}/V^{1/3} \ = 3.16 \ [P_m/P_i - 1]U_LE_p \quad m/s \qquad\qquad [7.1]$$

The flame speed, which governs the actual time taken to burn the unburnt gas mixture, is the burning velocity times the expansion ratio. In Equation 7.1 the constant pressure combustion expansion ratio, E_p, has been used. It could be argued that in the final stages of combustion it is the temperature at high pressure that is more important in the expansion and hence the constant volume expansion ratio, E_v, should be used to determine the flame speed from the burning velocity. In this case Equation 7.2 relates K_G and U_L. The expansion ratio at constant volume, E_V, is the ratio of peak pressure to initial pressure, as shown in Equation 7.2.

$$K_G/P_i = 3.16 \ [P_m/P_i \ \text{-}1] \ U_L E_v \ = \ 3.16 \ U_L \ [P_m/P_i - 1] \ [P_m/P_i] \ m/s \qquad\qquad [7.2]$$

Where P_m is the maximum adiabatic pressure (bara) in a closed spherical vessel.

   P_i is the initial pressure (bara)

E_v is the unburned gas to burned gas density ratio or expansion ration at constant pressure

A very similar expression to that in Equation 7.2 was also derived by Kumar et al. (1992) and Hattwig and Steen (2004) and this is shown in Equation 7.3. This was derived from the theory of spherical flame propagation in a closed spherical vessel which gives the pressure rise as a function of the radius of the flame, differentiation of this to determine the maximum dP/dt then enables K_G to be predicted. Kumar et al. (1992) and Hattwig and Steen (2004) also assumed a constant burning velocity in the derivation of Equation 7.3. The value for the ratio of specific heats, γ, in Equation 7.3 is that for the unburnt gases and is close to that of air, which with some preheat is about 1.38. Equation 7.2 is derived as the average rate of pressure rise from the first 2% pressure rise to peak pressure and Equation 7.3 as the peak rate of pressure rise. In practice in real explosions there is little difference between the maximum and average, measured from the start of pressure rise.

$$K_G/P_i = 4.84 \ U_L \ [P_m/P_i - 1] \ [P_m/P_i]^{1/\gamma} \qquad\qquad [7.3]$$

Hattwig and Steen (p. 571, 2004) have suggested the approximation in Equation 7.4 for the link between U_L and K_G, which is essentially a scaling function based on a U_L of 0.48 m/s for propane/air with $K_G/P_i = 100$ m/s, if the NFPA 68 accepted value of 0.46 m/s for propane is used instead then Equation 7.4 becomes the relationship between K_G and U_L.

$$K_G/P_i = \sim 217 \ U_L \ \text{m/s} \qquad\qquad [7.4]$$

Equations 7.1-7.4 show that if the rate of pressure rise is normalised to the initial pressure then the deflagration parameter has units of m/s and is proportional to the burning velocity, U_L. This form of K_G/P_i is preferred as it can be applied to any initial pressure.

The predictions of K_G/P_i from Equation 7.1-7.4 are compared with the measured values of K_G in a 5L sphere by Bartknecht (1993) and for a 1 m^3 vessel in Table 7.1. The values for U_L are taken from NFPA 68 2013, which uses a reference value of 0.46m/s for propane-air taken from France and Pritchard (1977), so the U_L for propane and hydrogen have also been taken from the same literature(France and Pritchard, 1977). The problem with the procedure in NFPA 68 2013 for determining

K_G from U_L is that the procedure does not agree with the measurements of France and Pritchard (1977), which are used as a reference method for propane at 0.46 m/s. The table of values for U_L for 117 gases in NFPA 68 2013 also gives 0.46 m/s as the maximum burning velocity for propane/air, in agreement with the data of Frances and Pritchard (1977). However, the value in the burning velocity table in NFPA 68 is 0.4 and 3.12 m/s for methane and hydrogen respectively, compared with 0.43 and 3.5 m/s in the work of Frances and Pritchard (1977). In this work the Frances and Pritchard maximum burning velocity results have been used for propane, methane and hydrogen and the value of 0.8 m/s for ethylene in NFPA 68 2013.

Table 7.1 Comparison of KG/Pi Measurement and Predictions from UL

Gas Maximum Reactivity Conc.	K_G/P_i m/s Bartknecht (1993), 5L Sphere	K_G/P_i m/s 1 m³ Andrews & Bradley (1972)	U_L m/s France & Pritchard (1977)	E_v GasEq	E_p Adiab. GasEq	E_v/E_p	Eq. 7.1 K_G/P_i m/s	Eq. 7.2 K_G/P_i m/s	Eq.7.3 K_G/P_i m/s γ=1.38	Eq.7.4 K_G/P_i m/s
Methane	55	72	0.43	8.85	7.54	1.17	80	94	79	93
Propane	100	102	0.46	9.53	8.05	1.18	100	118	97	100
Hydrogen	550	693	3.5	7.7	6.47	1.19	479	571	499	760

Table 7.1 shows that Equation 7.4 is too simplistic and takes no account of the influence of P_m/P_i on K_G, its values for methane and hydrogen from Equation 7.4 are too high for both gases. Table 7.1 also shows that the Bartknecht [1993] K_G value of 55 for methane is far too small relative to the 100 bar m/s for propane, to be compatible with measured values of U_L for these gases. Cashdollar et al. [2000] have measured K_G for methane at 65 bar m/s in a 20L vessel (0.168m radius) and 90 bar m/s in a 120L vessel (0.306m radius), which gives an average value of 72 bar m/s. In NFPA 68 1988 other measurement of K_G than those of Bartknecht [1993] are reported with 64 bar m/s for methane, 96 for propane and 659 for hydrogen. All of these results and those measured by the authors in a 1m³ vessel, also included in Table 7.01, indicated that the 55 bar m/s K_G for methane is too low and that a more reasonable value is in the range 70 - 90 bar m/s. This difficulty over a reliable K_G for methane makes comparison with Equation 7.1-7.3 difficult. However, if the K_G of 100 bar m/s is reliable for propane and the same value was found by the authors in a 1m³ explosion vessels, then Equation 7.1or Equation 7.3 could be judged as the most

reliable relationship between U_L and K_G. However, Equation 7.1and Equation 7.3 give quite low values for hydrogen K_G and Equation 7.2 gives the best agreement with measurements for hydrogen.

Table 7.2 Comparison of KG and UL from NFPA 68 2013 data

Gas	K_G	K_G/K_G Propane	U_L	U_L/U_L propane
Propane	100	1	0.46	1
Methane	55	0.55	0.4	0.87
Methanol	75	0.75	0.56	1.22
Butane	92	0.92	0.45	0.98
Ethane	106	1.06	0.47	1.02
Pentane	104	1.04	0.46	1
Carbon disulphide	105	1.05	0.58	1.26
Diethyl Ether	115	1.15	0.47	1.02
Isopropanol	83	0.83	0.41	0.89
Toluene	94	0.94	41	0.89
Acetylene	1415	14.1	1.66	3.61
Hydrogen	550	5.5	3.12	6.78

For compliance with the venting design guides using K_G to measure the mixture reactivity, the values of K_G experimentally measured in a 5L spherical vessel by Bartknecht (1993) have to be used, as the vent design equation is based on the work of Bartknecht (1993) and his values of K_G must be used if the original experimental vent overpressures are to be obtained. Unfortunately, these values of K_G do not correlate with U_L for all gases as is shown in Table 7.2, taken from data in NFPA 68, 2007 and 2013. If the values of K_G and U_L relative to propane are compared then it can be seen that, of the 12 gases where NFPA 68 has both K_G and U_L data, there is agreement to within 10% of Table 7.2 Comparison of K_G and U_L from NFPA 68 2013 data their relative K_G and U_L. However, there are 5 gases that have widely different relative K_G and U_L and these include the common gases methane, methanol, acetylene and hydrogen as well as carbon disulphide. If either of these parameters were to be used in design procedures for gas explosions for different mixture reactivities, then standardisation of the measurement method for K_G and U_L is required. Andrews and Bradley (1972) reviewed measurements of U_L and showed

a strong dependence on the method of measurement, with many methods having systematic errors(Andrews and Bradley, 1972a). Since then, there has continued to be published U_L measurements, particularly for methane-air, with much the same variability as that reviewed in 1972(Andrews and Bradley, 1972b).

There have been relatively few investigations of the influence of mixture reactivity on vent design and the current European design methodology is based on one set of vented explosion data(Bartknecht, 1993). In the USA venting design procedures in NFPA 68 2013, the U_L approach to mixture reactivity is stated to be valid for U_L up to 3.0 m/s and yet there is minimal experimental venting data for mixtures significantly more reactive than propane, such as ethylene and acetylene. There is concern that the current European design methodology is particularly in error in relation to the venting of hydrogen explosions (Kasmani et al., 2010a, Kasmani et al., 2010b) and the new USA guidance has no procedures that apply to hydrogen venting, as they do not apply for mixtures with more than 10% of the reactive gas in air or for $U_L > 3$ m/s and both these criteria exclude hydrogen from the guidance, but include ethylene and acetylene.

The present work presents new experimental data for the influence of mixture reactivity using methane, propane, ethylene and hydrogen-air vented explosions at two values of the vent coefficient K_v ($K_v = V^{2/3}/A_v$) for free venting. The use of K_v in gas explosion vent design equations, with no other term including the vessel volume, implies that the size of the vessel used in the venting experiments is not important. Nevertheless, many investigations of gas explosion venting have involved expensive experiments in very large vented vessels, closer to the vessel size required to have vent protection. This implies a lack of confidence that the K_v term does include all the influences of vessel volume. In the present work a very small 0.01 m^3 vessel was used for two purposes: firstly, to compare the results with experiments in large vessels at the same K_v to see if there was an additional volume effect and secondly, to produce experimental results where the assumption of laminar flames was valid, with negligible self acceleration of the flame due to the development of a cellular structure. It is this feature of large spherical flames, to develop a cellular structure which propagates at a higher flame speed that could give an additional volume effect.

7.3 Self Acceleration of Flames in Explosions in Large Vented Vessels and its Link to Mixture Reactivity

Spherical explosion flames form a cellular structure above a critical diameter, which depends on the properties of the gas. Cellular flames propagate faster than laminar flames and this effectively results in K_G being a function of the vessel volume and not a reactivity constant. Larger volume vessels have greater distances from the spark to the vent and hence the reaction rate, K_G, could be a function of the vessel volume. This was shown by Swift (1989) and discussed in NFPA 68 (2007), but not included in the vent design methodology(NFPA 68, 2007, Swift, 1989).

Laminar flame explosion venting theories using U_L as the reactivity parameter, have to date had poor agreement with experimental vented explosion data and invoke an empirical factor, λ, to account for the predicted overpressure being too low relative to experimental measurements. This factor, λ, accounts for any effect of the vent burst pressure on creating turbulence and for any self acceleration of the flame and is usually about 3-5 in value for agreement with experimental data. The additional influence of vessel size on vented explosions, that is not taken into account by the vent coefficient, $K_v = V^{2/3}/A_v$, is that of self acceleration of the flame over the larger distance to the vent in large vessel explosions. The formation of a cellular flame structure is correlated using one or more of the Karlovitz, Lewis, Markstein and Peclet numbers (Bradley, 1997), all of which are a function of the composition of the mixture in the explosion. This results in a more complex influence of mixture reactivity on vented explosions than that simply due to U_L or K_G. Typical self acceleration factors can be as high as 3.5 (Bradley, 1997) but vary with the gas mixture. Some authors assume little difference between self acceleration and acceleration due to turbulence and use the turbulence factor λ for a combined influence of both effects. However, it is preferable to understand the two effects separately and the use of free venting in the present work minimised any turbulence generated by the bursting of the vent cover.

Chippett (1984) was the first to show that K_G increased as the spherical vessel radius increased, with the value in a small vessel (0.034 m^3) for stoichiometric propane/air of 100 bar m/s increasing to 250 bar m/s at five times the 200mm radius of the small vessel (a volume of 4.2 m^3)(Chippett, 1984). This is a flame acceleration factor of

2.5 over a flame travel distance from 0.2 to 1m. This is similar to the self acceleration effect in spherical flames for large balloon explosions (Harris and Wickens, 1989). The K_G of 100 bar m/s for the $0.035m^3$ vessel is the same as that reported by Bartknecht (1993) for his $0.005 \ m^3$ sphere and hence laminar flame propagation can be assumed to apply up to a vessel radius of at least 0.2m and explosions in vessels larger than this should take into account the self-acceleration of the flame in any explosion venting model. In the present work a $0.01 \ m^3$ cylindrical vented vessel (diameter 0.162m and length of 0.46m) was used and this was designed to minimise the generation of cellular flames in the vented explosion. However, the distance from the spark on the end wall to the vent was 0.46m and hence some self-acceleration may have occurred.

Swift [1989] correlated measurements of K_G with the vessel volume and showed that this effect was greater for propane than methane and highest for pentane(Swift, 1989). These two gases had K_G increasing by a factor of about 3.5 over a vessel radius increase from 0.2 to 4m. This is similar to the maximum increase expected from self acceleration (Bradley, 1997). These results show that the reactivity effect in vented explosions should be related to the vessel volume as well as to U_L or K_G. NFPA 68 has included a similar graph to that in the work of Swift (1989) for many years, but had no firm proposals as to how the effect of volume on K_G can be taken into account in vent design.

In NFPA 68 2013 a procedure to take account of self acceleration of flames has been introduced and included in a new turbulence parameter, λ, in the vent design procedures, as given in Equation 7.5.

$$\lambda_{\text{self acceleration}} = [\text{Re}_f/4000]^{0.39} \qquad\qquad [7.5]$$

where $\text{Re}_f = (\rho_u \ U_L \ D_h/2) / \mu_u$ and Equation 7.05is limited by $\lambda = 1$ if $\text{Re}_f <$ critical value of 4000, with $D_h =$ hydraulic diameter of the vented vessel.

This procedure is based on that of Chippett (1984) with the maximum possible flame size used instead of the flame radius, which gives the largest possible value for $\lambda_{\text{self acc.}}$. The exponent of 0.39 was 0.4 for propane in the work of Chippett and 0.25 for methane. Equation 7.5 does not include any influence of the known dependence of flame self acceleration on mixture reactivity and is probably only

valid for propane explosions. In the present work Re_f was 2400 and hence no self acceleration should have occurred. The critical value of 4000 for propane corresponds to a critical flame diameter for the onset of cellular flames of 0.272m and spherical volume of 10.5L. If the vessel diameter is 10 times this size then λ = 2.45 and the volume would be 38.7 m^3 for a sphere. Equation 7.05 has no limit on the self acceleration term, whereas experimental evidence is that there is a limit on cellular flame $\lambda_{self\ acceleration}$ of about 3.5, as reviewed above. Subsequently, there may be a transition to self-turbulising flame propagation which has the turbulent burning velocity increasing with flame radius. This cellular flame limit would be a vessel size of 6.75m diameter and volume of 161 m^3, which is larger than nearly all experimental data for vented vessels.

 Current vent design is based on the experiments of Bartknecht (1993) in a 10m^3 vented vessels (2.67m dia.), where flames will have accelerated by the self acceleration mechanism. In using a value for K_G that was measured in a small (0.005m^3) vessel, the effect of flame self acceleration must be included as an effective λ factor in the constants in the design vent equation. It would be preferable if this effect of vessel volume was included explicitly in the vent design procedures as is now done in NFPA 68 2013. As self acceleration is different for different gas reactivities, this complicates any investigation of the influence of gas reactivity on vent overpressures. The use of a small explosion vessel in the present work was aimed at measuring overpressures that were likely to be free of significant flame self acceleration complications.

7.4 Comparison of the Bartknecht Vent Design Equation with other Experimental Data for Vented Explosions

Current EU (BS EN 14994, 2007)and previous USA (NFPA 68, 2007)design guidance for gas explosion protection using venting are based on the experimental data of Bartknecht (1993) with no safety factor added. The vent design Equation 7.6 (Bartknecht, 1993) is for a vent static burst pressure, P_{stat}, of 0.1 bar. Equation 7.6 uses the deflagration index, K_G, as the gas reactivity parameter. There is an additional term in the full vent design equation for higher P_{stat}, which will not be discussed in this section as it is directed at free or very low vent static burst pressure explosions.

$$1/K_v = (0.1265 \log K_G - 0.0567) \, P_{red}^{-0.5817} \quad\quad [7.6]$$

where K_v is the vent coefficient $= V^{2/3}/A_v$, which should include all of the vessel volume effects. Equation 7.06 can be converted from the use of the vent coefficient, K_v, to one using the internal surface area of the vessel, as arises in the laminar flame venting theory discussed later and used in NFPA 68 (2013). This is because K_v and A_s are directly related, as $A_s = C_2 \, V^{2/3}$, where C_2 is 4.84 for a sphere, 6 for a cube and 5.54 for a cylinder with L/D=1 and 5.86 for the present cylinder with an L/D of 2.8.
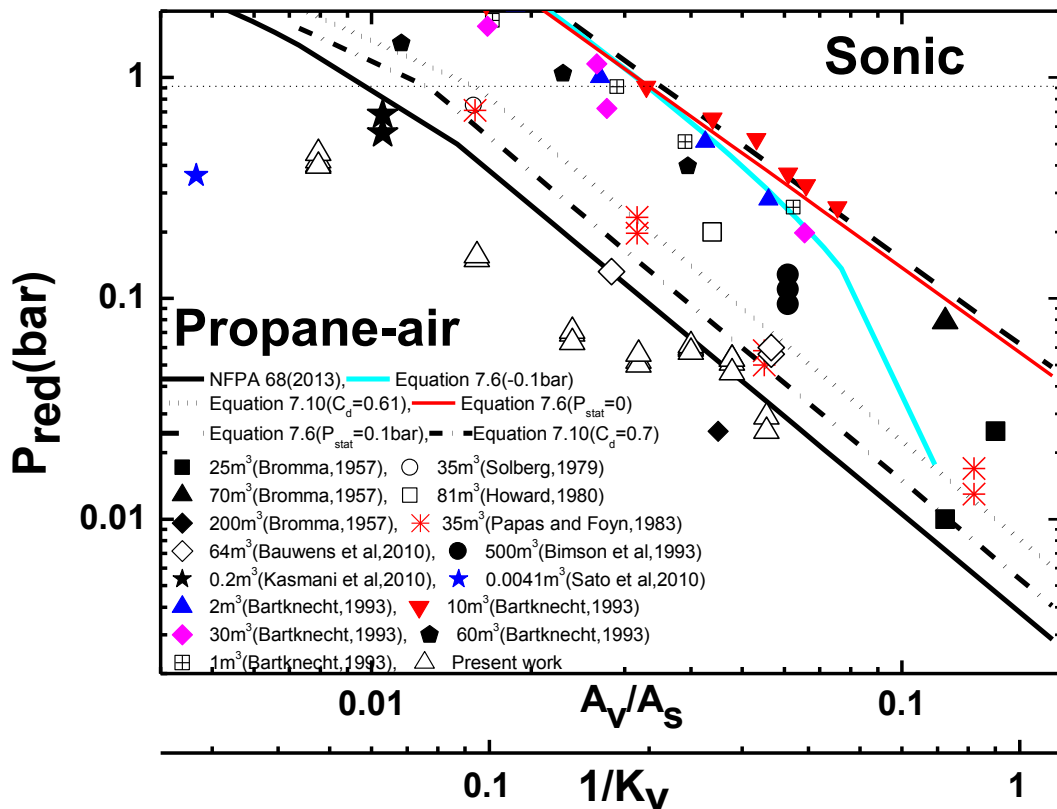
Figure 7.1 Comparison of vent design equations with experiments for propane-air as Pred v. 1/Kv = Av/V2/3

For comparison of experimental data with Equation 7.6 $1/K_v$ or A_s/A_v should be plotted against P_{red}. This is done using A_s/A_v in Figure 7.1 for propane-air maximum reactivity vented explosions and in Figure 7.2 for methane using the $1/K_v$ presentation. Figure 7.2 also includes the experimental data of Bartknecht (1993) for $1m^3$ and $30 \ m^3$ vessels, which is in agreement with Equation 7.6 for methane. Equation 7.6 from Bartknecht has been converted from K_v to A_s/A_v assuming a cubic vessel relationship in Figure 7.1. Figures 7.1 and 7.2 show that Equation 7.6 grossly overestimates the vent design size necessary for smaller vented vessels

(Kasmani et al., 2010a, Kasmani et al., 2010b, Kasmani et al., 2006) and over predicts the overpressures measured by others for large vessels (V > 10 m^3). The data in Figures 7.1 and 7.2 are for free venting with no vent static burst pressure or the lowest static pressure used in the experiments quoted.

The vent design equation in Figure 7.1 is Equation 7.6 with the Bartknecht values for K_G from Table 7.1. These results of Bartknecht (1993) have been corrected to a free vent condition on the basis of extrapolating the vent burst pressure influence to zero using the P_{stat} influence of Bartknecht (1993) and alternatively by simply deducting 0.1 bar from the measured overpressure, following the finding of other investigators that the P_{stat} influence on the overpressure was simply additive to the overpressure for free venting (Harris, 1983). Figures 7.1 and 7.2 show that neither method of correcting Equation 7.6 to a P_{stat} of zero gives good agreement with experimental results of other investigators for $1/K_v < 0.5$ ($K_v > 2$).
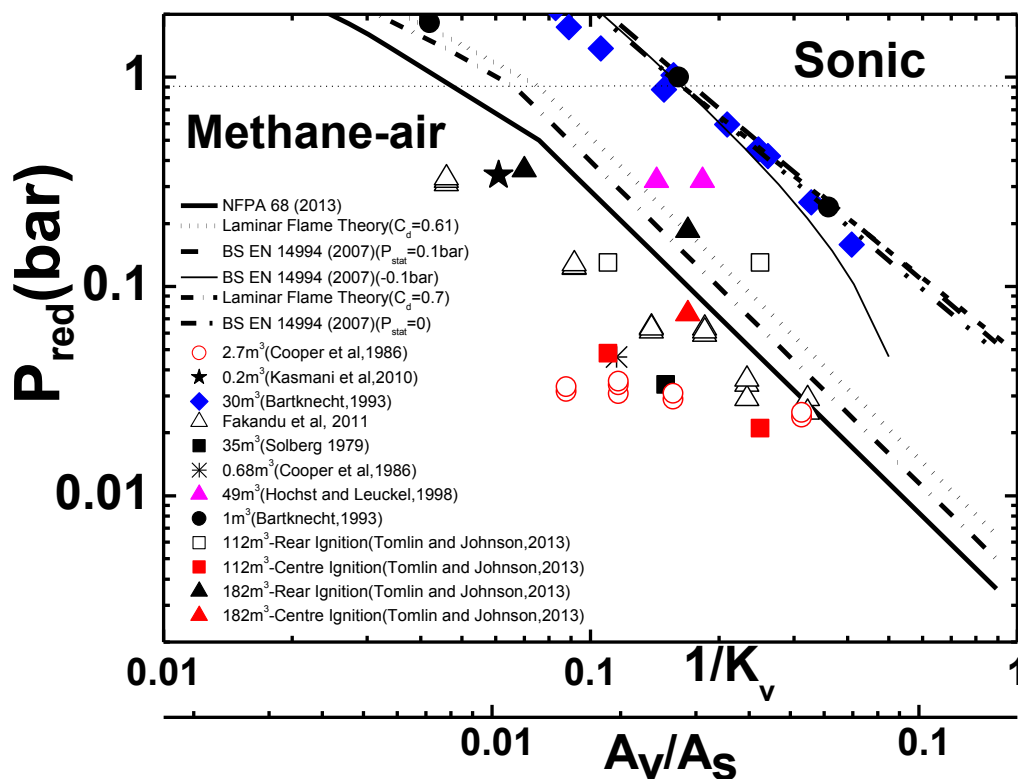
Figure 7.2 Comparison of vent design equations with experiments for methane-air as Pred v. Av/As,

Figure 7.1 shows that the highest over pressures for propane-air vented explosions reported by other workers, including volumes up to 550m^3 (Bimson et al., 1993), were about 1/3 of Equation 7.6, which was for a 10 m^3 vessel. Much of the other literature on venting in large (25 – 81 m^3) explosion vessels with low or no vent

burst pressure is around 1/10 of the Bartknecht equation as shown in Figure 7.1. The highest overpressure in the present results for 4.5% propane and 10% methane with end ignition has been included in Figures 7.1 and 7.2 for comparison. These results are below most of the data in the larger vessels, but in agreement with the data of Bromma (1957) for a 200m^3 vented vessels and above those of Cooper et al (1986) in vessels of about 1m^3 for methane air in Figures 7.2. Figures 7.1 and 7.2 show that there is no consistent influence of the vessel volume on P_{red} for the same K_v and thus incorporating a fixed λ factor would not collapse the data to one line.

The results of Cooper et al. (1986) for natural gas (10% in air) in various vessels of about 1 m^3 volume, including one result for a vessel L/D of 3, are shown in Figure 7.2. In the work of Cooper et al. (1986) there was a final pressure peak, P_{ac}, due to acoustic pressure oscillations(Cooper et al., 1986). They showed that this could be eliminated if an acoustic absorber liner was attached to the vessel walls. They showed that these acoustic pressure oscillations were a feature of their thin walled test vessel. They comment that this pressure peak, which was often the largest P_{red}, could be ignored in most practical situations and hence has been ignored in this comparison of their P_{red} data in Figure 7.1. These are some of the lowest vented explosion overpressures reported in the literature. The present methane-air results are higher than those of Cooper et al. (1986) and show that the present small vessel vented explosion results are reasonable.

The main reason for the higher P_{red} in the present work was the use of end ignition in an L/D 2.8 cylindrical explosion vessel, rather than the central ignition using in the near L/D = 1 explosion vessels used by Cooper et al. (1986). Kasmani et al. (2010b) showed that for 10% methane-air P_{red} increased from 0.18 bar for central ignition to 0.35 bar for end ignition for K_v = 16.4 in a 0.2 m^3 explosion vessel with an L/D of 2. Cooper et al. (1986) also reported the pressure time results for a square cross sectional vessel with L/D of 3, the P_{red} of which is shown in Figure 7.1 to be just below the present results, but there was a difference in ignition position.

Sato et al. (2010) have also investigated vented explosions in a small cubic vessel of 0.004 m^3 volume, which was smaller than in the present work. For a Kv of 36 and P_{stat} of 1.5 bar they investigated the influence of spark ignition location and equivalence ratio for propane-air mixtures. They did not investigate end wall

ignition opposite the vent, but did show that central ignition was not the worst case vented explosion. Their highest reported P_{red} is shown in Figure 7.1 without any correction for P_{stat} and was lower than the extrapolated results for the present $0.01m^3$ vessel, due to the worst case ignition location not being investigated in their work.

Bartknecht (1993) presented experimental venting results for propane in vessel volumes of 1, 2 and 10 m^3 for cylinders with L/D=1 and for cubic vessels with vessel volumes of 30 and 60m^3 and these experimental results are shown in Figure 7.3. For methane the only data was for the 1 and 30m^3 vessels and this is shown in Figure 7.2 and for hydrogen the only data was for the 1m^3 vessel (Bartknecht, 1993). Figure 7.3 shows that Equation 7.6 is not a correlation of the experimental results at different volumes, but the correlation line for the data of vented propane-air explosions in a 10 m^3 vessel with P_{red}<0.7 bar. Comparison of the results of Bartknecht (1993) for a 30 m^3 vessel for methane and propane vented explosions in Figures 7.2 and 7.3 show that there was hardly any influence of the mixture reactivity with practically identical results for the same K_v. This was unexpected as Equation 7.6 correlates the K_G effect with a significant difference between propane and methane.
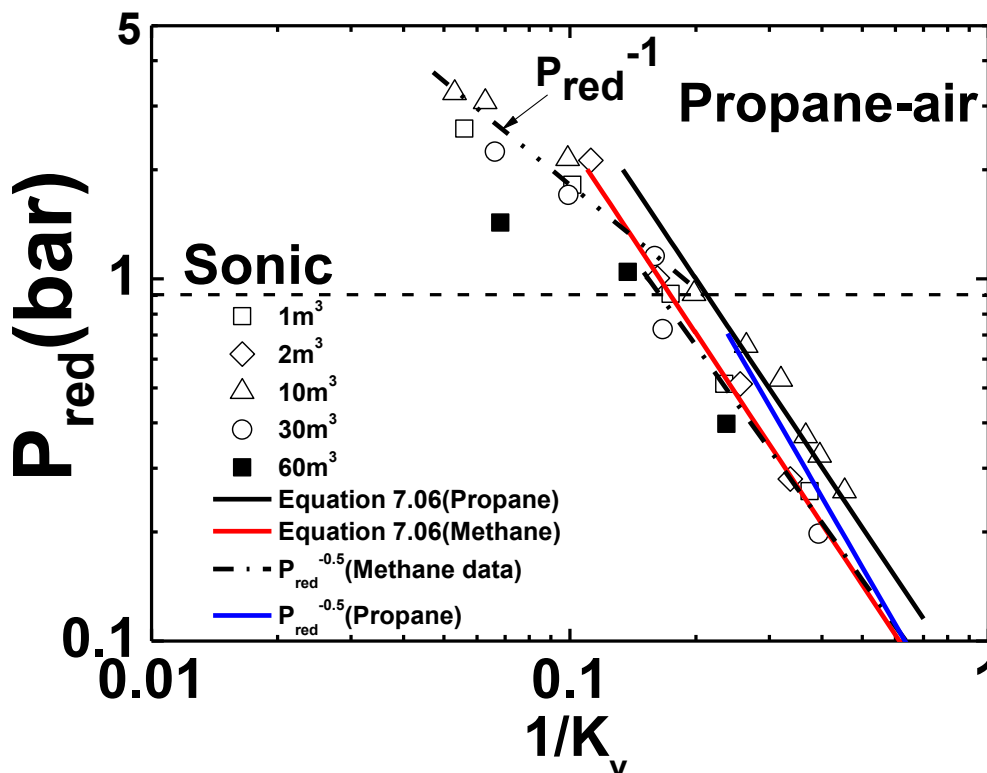
Figure 7.3 Bartknecht's results for Pred as a function of 1/Kv for different volumes (Bartknecht, 1993)

All of Bartknecht's experimental data for propane at volumes smaller or greater than 10 m^3 and the data of others in Figure 7.1 for smaller and larger volume vessels fall below the Bartknecht data for his 10 m^3 vessel. No explanation of this unexpected volume effect has been given or commented on in the present EU standard or in NFPA 68 prior to 2013 that used Equation 7.6. There is a much higher overpressure in the work of Bartknecht for the same K_v and volume than for the results of all other experimental investigators as shown in Figures 7.1 and 7.2. For example the results of Papas and Foyn (1983) for a 35 m^3 vessel and the more recent work of Bauwens et al. (2010) for a 65 m^3 vessel are in agreement with conventional laminar flame venting theory present later, but are well below the P_{red} measured by Bartknecht (1993) in 30m^3 and 60 m^3 vessels for the same K_v, as well as below the line for Equation 7.6.

None of the data in Figures 7.1 and 7.2 was used in the development of the vent design Equation 7.6, which should never be referred to as a correlation of explosion venting data, as it is not even a correlation of Bartknecht's data. Bartknecht's results in Figure 7.3 show that K_v is not a sufficient correlator of the volume effect for vented explosions. Kasmani et al. (2006) have discussed this in more detail and shown that the larger overpressure as the volume increased is likely to be due to self-acceleration of the flame as the vessel radius or width gets larger with increase in volume. However, the reason for the over pressure to be lower for 30 and 60 m^3 vessels is unknown, although the change from cylindrical vessels for volumes up to 10 m^3 to cubic vessel for larger volumes may be significant. Figure 7.3 indicates that all the volumes tested apart from 10m^3 could be correlated by a single line with agreement with the 30 m^3 methane results in Figure 7.2, but this line is about a factor of 2 below the line for the 10m^3 vessel. Figure 7.1 shows that even the data for the 30 and 60 m^3 vessels are still well above data of other workers for similar sized and larger vessels.

The P_{red} dependence in Figure 7.3 clearly shows a change in dependence at $P_{red}=0.9$ bar, which is the condition for the onset of sonic flow at the vent. It is clear in Figure 7.3 that much of Bartknecht's data was for sonic venting and the vent mass flow rate is linear with the upstream pressure in the sonic flow regime, which is shown in Figure 7.3 to fit Bartknecht's data for the 10 m^3 vessel. The application in the pre 2013 US and current EU vent design standards of Equation 7.6 to values of P_{red} up

to 2 bar, as recommended by Bartknecht (1993), is incorrect but safe. If the P_{red} data above 0.9bar is ignored Figure 7.3 does show that the P_{red} exponent of -0.58 in Equation 7.2 is supported by the data for propane in the 1, 10, 30 and 60 m^3 vessels. However, in the 2m^3 vessel for propane and in the 30 m^3 vessel for methane a -0.5 P_{red} exponent is supported, which is that expected from incompressible flow at the vent, as discussed in the laminar flame venting theory later. The action of the 0.1bar vent burst pressure is greatest at low K_v and the effect is to raise the pressure exponent from the -0.5 expected value to -0.58.

Equation 7.6 correlates the gas reactivity effect using K_G, but can be converted into an equation using U_L as the reactivity parameter using Equation 7.2. Bartknecht's (1993) results for the influence of gas reactivity were based on varying K_v with central ignition, but the vessel size used was not given. The results for each gas were correlated by Equation 7.7.

$$1/K_v = a \, P_{red}^{-n} \hspace{4cm} [7.7]$$

This converts to

$$P_{red} = (a \, K_v)^{1/n} \hspace{4cm} [7.8]$$

which shows the strong influence of the reactivity term 'a' on P_{red}. The values of 'a' were plotted by Bartknecht (1993) as a function of the log of K_G and the logarithmic relationship in Equation 7.6 was found. The logarithmic relationship for the reactivity term was unexpected, as this is not the influence of gas reactivity expected from laminar flame venting theory that is discussed below.

Values for the constants a and n in Equation 7.7 were determined by Bartknecht (1993) and are shown in Table 7.3. The average of the P_{red} exponents n in Table 7.3 was -0.5817 which is the value used in Equation 7.06. If the values for K_G in Table 7.3 are substituted in Equation 7.6 then the values for $'a'$ in Equation 7.7 result as shown in Table 7.3 for the 10 m^3 explosion vessel of Bartknecht. When Equation 7.7 is compared with the vented data of Bartknecht for propane it only agrees with the 10 m^3 vented data for propane in Figure 7.3, which is the Bartknecht design line in Figure 7.1. The values in Table 7.3 for 'a' in Equation 7.7 do not agree with the data for any other volume, as shown in Figure 7.3. Bartknecht (1993) gives venting data for P_{red} of 2 barg and 0.5 barg for the 1 m^3 vessel for all the gases in Table 7.3 and these values for 'a' are given for comparison in Table 7.3. They are lower by about

20% than the values for 'a' from the 10 m^3 vessel for propane, as shown in Figure 7.3. The data for the 10 m^3 vessel were not given by Bartknecht (1993) for methane, town's gas and hydrogen, but it must be that the values for 'a' on which Equation 7.6 is based was determined in the 10 m^3 vessel for all four gases, as the 1 m^3 results are all below the values that result from Equation 7.6.

Table 7.3 Bartknecht's (1993) values for the constants a and n in Equation 7.7

Gas	K_G bar m/s	$-n$	a_{10} 10m^3	a_1 1 m^3	a LFT n = -0.5	$a_{10}/a_{laminar}$ TF λ	$a_1/a_{laminar}$ TF λ
Methane	55	0.572	0.164	0.133	0.063	2.60	2.11
Propane	100	0.580	0.200	0.157	0.078	2.56	2.01
Propane Excluding 10m^3	100	0.616		0.154	0.078		
Coal Gas	140	0.590	0.212	0.171			
Hydrogen	550	0.585	0.290	0.231	0.46	0.63	0.50

(LFT=Laminar Flame theory, TF=Turbulence Factor)

Bartknecht (1993) gave vented explosion results for 10% methane-air in the 30 m^3 and 1 m^3 vented vessels and these results are shown in Figure 7.2. The value of 'a' for methane in Table 7.3 gives reasonable agreement with the results in Figure 7.2 for the 30 m^3 vessel, although the P_{red} exponent is closer to 0.5. However, the P_{red} for methane for the 1 m^3 vessel are very similar to those for the 30 m^3 vessel, as shown in Figure 7.2, which is also the case for propane in Figure 7.3. A puzzling feature of Bartknecht's results is that he gives a graph with the values of 'a' with the figures derived from the 10 m^3 vessel in Table 7.1 ascribed to the 1 m^3 vessel, but the actual 1 m^3 results that are given by Bartknecht (1993) for propane and methane at P_{stat} = 0.1 bar do not agree with these values for 'a', as shown in Table 7.3. The methane results from Equation 7.7 using the Bartknecht value for 'a' from Table 7.3 are shown in Figure 7.3 to agree with Bartknecht's propane results for the 1, 2, 30 and 60 m^3 vessels. Thus, if the 10 m^3 vessel results are ignored there is no significant reactivity influence on the vented vessel overpressures, as shown in Figure 7.3. The correlating line for Bartknecht's propane data, excluding that for 10

m^3, is shown in Table 7.3 to have a value for 'a' close to that determined from the 1 m^3 data, but with a slightly higher exponent for 'n' in Equation 7.7.

The results of Bartknecht (1993) in Table 7.3 have some unexpected influences. The reactivity K_G of propane, measured in a 5 litre spherical explosion vessel, is given as 1.82 times that of methane, whereas the ratio of the reactivity constant 'a' for propane and methane is 1.22. The deflagration index, K_G, is proportional to U_L as shown in Equations 7.1-7.4 and the relative values of K_G and U_L for different mixture reactivities should be the similar. The ratio of propane and methane laminar burning velocities, $U_{L,}$ is about 1.15 (0.46/0.4) depending on the data source for U_L and the ratio of K_G in Table 7.3 is 1.82, which is much greater than any other measure of their relative reactivities. Comparison is made in Figure 7.2 of the predictions of Equation 7.06 for methane/air explosions with the experimental data for methane explosions in the $1m^3$ and $30m^3$ vented vessels and with other data in the literature. This shows that the overpressures based on the 1 m^3 results were slightly higher than were found at 30 m^3. Also Figure 7.2 shows that other experimental data in vessels of about 1 m^3 (Cooper et al., 1986) were much lower than the values of Bartknecht.

The reactivity term 'a' for hydrogen in Table 7.3 is only a factor of 1.45 higher than for propane and yet the reactivity K_G is 5.5 times that of propane and the laminar burning velocity ratio is 7.6 (3.5/0.46) times that of propane. Equation 7.8 shows that the impact of reactivity on P_{red} is much greater than its influence on 'a' as the proportionality is $a^{1/n}$. The hydrogen results of Bartknecht (1993) show a much lower dependence on mixture reactivity than that between propane and methane. This indicates that the 'a' term for hydrogen could be unreliable and vented hydrogen explosions were carried out in the present work to check this. The methane, propane and hydrogen results in Table 7.1 indicate that the measurement of mixture reactivity and its influence on vented explosions is an area of uncertainty and this work was aimed at providing further experimental evidence on the influence of mixture reactivity in vented explosions.

Figure 7.1 shows that the only data from other investigators that agrees within 20% of Equation 7.6, is that of Bromma (1957) in a 70 m^3 vessel. All other data, including the $550m^3$ results of Bimson et al. (1993), are well below Equation 7.6.

For agreement with the Bimson et al. (1993) 550 m^3 data, Figure 7.1 shows that a factor of around 3 decrease from Equation 7.6 is required. Also, Equation 7.6 requires a factor of 10 decrease for agreement with the extensive data of Papas and Foyn (1993) and Bauwen et al. (2010). This difference between Equation 7.6 and other large volume experimental data in Figure 7.1 is disturbing as it leads to a large overdesign of vent areas. It is also probably the reason that the USA NFPA 68 2013 vent design standard has abandoned this approach and adopted that based on laminar flame propagation, as developed by Swift (1993, 1988) and discussed below.

A turbulence factor λ to increase the mixture reactivity U_L or K_G is common in vent design theories to achieve agreement with experimental data and is used in NFPA 68 (NFPA 68, 2013). For free venting turbulence is not involved in flame acceleration well upstream of the vent, but cellular flame self acceleration does occur in large volumes with an effective maximum λ of about 3.5. Turbulence will play a role in the external explosion downstream of the vent, which is generated by the flow of unburned gases through the vent, which acts as an obstruction or obstacle to the flow with a blockage that increases as the vent coefficient, K_v, increases. This turbulence downstream of the vent gives rise to an external explosion pressure, P_{ext}, which may dominate the overpressure in some circumstances (Bauwens et al., 2010, Cooper et al., 1986). In much of the present work the flow of unburned gas through the vent dominates the generation of overpressure (P_{fv}) and this is the basis of the laminar flame model of the venting process. However, the pressure time traces for vented explosions do show many cases where an external explosion (P_{ext}) was significant. The classic laminar flame vented explosion theory may still apply as it predicts the vent jet flow velocity, which determines the turbulence in the external flammable gas cloud as discussed in chapter 4 of this thesis.

7.5 Laminar Flame Venting Theory

Most theories of venting to date assume that flow through the vent dominates the overpressure and that P_{fv} is the dominant overpressure (Bradley and Mitcheson, 1978a, Bradley and Mitcheson, 1978b, Cates and Samuels, 1991, Molkov, 1999a, Molkov et al., 2000, Swift, 1988). Bradley and Mitcheson (1978a) reviewed the development of laminar flame venting theories and showed that unburned gas venting had much higher overpressures than burnt gas venting. They also showed

the common features of laminar flame venting theories were: unburned gas venting; the use of orifice plate flow equations; and the maximum induced unburned gas flow rate as the mass flow through the vent. Andrews and Phylaktou (Andrews and Phylaktou, 2010) and Kasmani et al. (2010b) have reviewed laminar flame venting theory based on the pressure loss of the flow of unburned gas through the vent as the dominant overpressure for free venting. The classic laminar flame venting model (Bradley and Mitcheson, 1978a) assumes that a spherical flame in a spherical vessel with central ignition propagates uniformly until all the unburned mixture ahead of the flame is expelled through the vent. The maximum overpressure is then the vent orifice flow pressure loss at the maximum unburned gas vent mass flow rate (Andrews and Phylaktou, 2010). The unburned gas mass flow rate is the flame surface area, A_f, times the unburned gas velocity ahead of the flame, $U_L(E_p-1)$, times the unburned gas density, ρ_u. A further assumption is made that simplifies the theory and this is that the maximum possible flame area is the surface area of the vessel walls, A_s. This was an assumption first proposed by Runes (Runes, 1972).

The laminar flame venting model with the above assumptions leaves the prediction of P_{red} a function of A_v/A_s, as shown in Equation 7.9. (Andrews and Phylaktou, 2010). Bradley and Mitcheson (1978 a, b), Swift (1983, 1988) and Molkov (1999, 2000) all left the theoretical venting equation in terms of A_v/A_s and the Swift [1988] formulation of the laminar flame venting theory has been adopted in NFPA 68 2013. In the original Swift (1983) formulation of Equation 7.10 a turbulence factor of 5 was assumed, but this has been replaced with λ and a procedure given in NFPA 68 2013 to calculate this.

$$A_v/A_s = C_1 \, \varepsilon^{-1} \, \lambda \, U_L \, (E_p-1) \, P_{red}^{-0.5} \quad \text{with } P_{red} \text{ in Pascals} \qquad [7.9]$$

Where $C_1 = \rho_u^{0.5}/(C_d \, 2^{0.5}) = 1.27$ for $\rho_u = 1.2$ kg/m^3 and the vent discharge coefficient $C_d = 0.61$.

With P_{red} in Equation 7.9 converted to bar and the above value for C_1 inserted and an E_p of 8.05 used, which is the adiabatic value for propane, Equation 7.9 becomes Equation 7.10 for P_{red} in bar.

$$A_v/A_s = 0.0283 \, \varepsilon^{-1} \, \lambda \, U_L \, P_{red}^{-0.5} \qquad [7.10]$$

The constant in Equation 7.10 becomes 0.0247 if a C_d of 0.7 is used, as in the work of Swift (1983) which is the C_d value adopted in NFPA 68 2013 as Equation 7.11.

This predicted value of the constant in Equation 7.11 is only 11% higher and so the laminar flame venting theories have very similar results.

$$A_v/A_s = C\ P_{red}^{-0.5} = 0.0223\ \lambda\ U_L\ P_{red}^{-0.5}\ \text{ for } P_{red}<0.5\ \text{bar} \qquad [7.11]$$

There is no reason for limiting this equation to a P_{red} of 0.5 bar as all compressibility effects are contained in the expansibility factor, ε, in Equations 7.9 and 7.10. This shows that the present approach to the laminar flame venting theory produces a very similar vent design equation to that of Swift (1983) adopted in NFPA 68 2013.

It may also be shown that the laminar flame theory of Bradley and Mitcheson (1978a) for free venting can be expressed in the above format as in Equation 5.12.

$$A_v/A_s = 0.831[\lambda\ U_L(E_p - 1)]\ /\ [C_d\ a_v\ P_{red}^{0.5}] = 0.0284\ \lambda\ U_L\ P_{red}^{-0.5} \qquad [7.12]$$

where a_v is the velocity of sound at the vent, taken as 343 m/s for air. E_p has been taken as the adiabatic value for propane of 8.05. Equation 7.12 is identical to Equation 7.10 which shows that the present simple approach gives the same vent overpressure prediction as that based on a full computer solution to the spherical flame propagation. There was a difference in C_d of 0.6 instead of 0.61 used in Equation 7.10, but this only changes the constant in Equation 7.12 to 0.0280. Bradley and Mitcheson (1978b) went on to use a value for the turbulence factor λ of 4.19 to produce a prediction that would encompass data from vented explosions with a static burst pressure at the vent. Equation 7.12 also shows that the artificial dimensional numbers used by Bradley and Mitcheson are unnecessary as the 0.0284 U_L term in Equation 7.12 has units of bar$^{-0.5}$ so that Equation 7.12 is dimensionless. Equations 7.9-7.12 show a common formulation of the laminar flame venting equation for free vents with the present simple approach giving the same result as in the Bradley and Mitcheson (1978a) computer solution and the Swift (1983, 1988) approach, which also involves the use of the sonic velocity of sound at the vent as a parameter to dimensionalise the flame induced unburned gas velocity, which is an unnecessary procedure.

The A_v/A_s formulation of the laminar flame venting equation can be converted into a form using the vent coefficient K_v as $A_s = C_2\ K_v$, where C_2 is 4.84 for a sphere, 6 for a cube and 5.54 for a cylinder with L/D=1 and 5.86 for the present cylinder with an L/D of 2.8. This then converts Equation 7.9 into Equation 7.13 and this has the same

form as in the European vent design guidance (Andrews and Phylaktou, 2010 and Kasmani et al., 2010b).

$$1/K_v = A_v/V^{2/3} = C_1 C_2 \ \varepsilon^{-1} \ \lambda \ U_L \ (E_p-1) \ P_{red}^{-0.5} \qquad\qquad [7.13]$$

If Equation 7.13 is used for a cube and P_{red} is converted from Pa to bar then with E_p = 8.05 Equation 7.12 becomes Equation 7.14.

$$1/K_v = 0.170 \ \varepsilon^{-1} \lambda \ U_L \ P_{red}^{-0.5} \qquad\qquad [7.14]$$

For propane with U_L=0.46 m/s and taking $\varepsilon = 1$ and $\lambda = 1$ Eq. 14 becomes Eq. 15.

$$1/K_v = 0.078 \ P_{red}^{-0.5} \qquad\qquad [7.15]$$

The constant in Equation 7.15 is for propane. For 10% methane –air with U_L is taken as 0.43 m/s and E_p as 7.54 the constant in Equation 7.15 becomes 0.063. For 40% hydrogen –air with U_L taken as 3.5 m/s and Ep as 6.47 the constant in Equation 7.15 becomes 0.46. The laminar flame theory predicted values of the constant for 'a' in Equation 7.7are compared with the Bartknecht experimental values in Table 7.3.

Equation 7.15 is in the same format as used by Bartknecht and his constant for propane in Table 7.3 was 0.200. This implies a λ value of 2.56 for agreement, as shown in Table 7.3, which gives a 6.57 factor difference in P_{red} for the same K_v. If the Bartknecht 10 m^3 vented data is ignored as not agreeing with his data at four other volumes, the a λ of only 2.1 is required for agreement, as shown in Table 3. For methane Bartknecht had a constant in Equation 7.15 of 0.164 and the above prediction needs a turbulence factor λ of 2.60 for agreement (or 2.0 if the 10 m^3 data is ignored), which gives a 6.78 factor difference in P_{red} for the same K_v. These turbulence factors for propane and methane are very similar and are of the magnitude expected for self acceleration of the flame in the larger vented vessel used by Bartknecht. However, for hydrogen Bartknecht's constant in Equation 7.15 was 0.29 which is less than the laminar flame prediction of 0.46. As hydrogen has a greater self acceleration tendency than propane or methane a value of λ greater than the 2.6 value for methane and propane would be expected. Hence, a constant in Equation 7.15 of at least 1.2 would be expected. This leads to the conclusion that the Bartknecht venting constant has to be unreliable and needs re-evaluating in the European gas venting standard. As NFPA 68 2013 has no recommendation for hydrogen venting, there is a clear need for more work on hydrogen explosion venting, which was the impetus for the present work.

Equations 7.9 – 7.15 are based on incompressible flow through the vent with a compressible orifice plate flow correction in the expansibility coefficient, ε. This is the approach used in orifice plate flow metering for the influence of compressible flow and the correlation given (BS 1042-1.4, 1992) is Equation 7.16.

$$\varepsilon = 1 - [0.41 + 0.35(1/K_v)^2] \, P_{red}/[\gamma \, (P_i + P_{red})] \qquad [7.16]$$

For $K_v > 5$ the K_v term in Equation 7.16 is negligible. For a P_{red} of 0.5 bar, $K_v > 5$ and the ratio of specific heats $\gamma = 1.4$ Equation 7.11 gives $\varepsilon = 0.90$. Most other vent theories (Bradley and Mitcheson, 1978 a, b; Molkov, 1999, 2000; Bauwens, 2010) all treat the vent as a theoretical nozzle and not a sharp edged orifice. Compressible nozzle flow cannot be applied to sharp edged orifices due to the minimum flow area being at the Vena contraction, which is in free space with expansion due to compression both axially and radially. For nozzle flow only expansion due to compression in the axial direction is possible due to the nozzle throat area being the minimum flow area.

There are several problems with the above laminar flame theory. The theory assumes that all the unburned mixture is expelled from the vessel before the flame emerges from the vent and this does not occur in reality (Cooper et al., 1986)]. If this was a valid assumption then P_{fv} and P_{mfa} in Table 7.4 would occur at the same time and be the same overpressure, it will be shown in this work that this does not occur. Cates and Samuels (1991) have also shown from experimental results that the flame surface area at the peak overpressure was twice the cross-sectional area of the vessel for low K_v. For a cubic vessel this is equivalent to 1/6 of A_s and for a cylinder, with an L/D of 1, 1/3 of A_s and for an L/D of 3, 1/7 of A_3. Thus the classic laminar flame theory should overpredict measured venting overpressures by a factor of 3-7 depending on the vessel L/D.

A further problem with this theory is that it assumes a uniformly distributed vent area. In reality there is a single vent hole (or a small number of vent holes) and the flame moves with the unburned gas flow towards the vent [(Cooper et al., 1986)] and the flame area assumptions are not valid and will give an over prediction of the overpressure. The assumption that all the unburned mixture is expelled before the flame arrives outside the vent is also not valid, as there is amply evidence, and more provided in this work, that much of the original mixture in the vented vessel remains

in the vessel after the flame has left the vent and ignited the unburned mixture that was expelled. The proportion of unburned gases left in the vented vessel is greater with central ignition and give rise to peaks P_{mfa} and P_{rev} in Table 4, which may merge into one peak, as will be demonstrated in this work.

The laminar flame theory in Equations 7.9 and 7.10 is compared with the present experimental results and those of others in larger vented vessels in Figures 7.1 and 7.2. This shows excellent agreement of the laminar flame theory, Equations 7.9 and 7.10, with the experimental results for near free venting of a 35 m^3 vessel of Papas and Foyn (1983) and of the 64m^3 vented vessel results of Bauwen et al. (2010) and of the 25m^3 vented vessel results of (Bromma, 1957). A further difference between Equation 7.10 and the vent design Equation 7.6 is that the P_{red} exponent is -0.58 in Equation 7.6 and -0.5 in Equation 7.10. The difference is related to the use of $P_{stat} =$ 0.1bar in Bartknecht's work. This is particularly significant at low P_{red}, where the predictions would be <0.1bar for a free vent. Consequently, the difference between the Bartknecht vent design P_{red} exponent and the theory is not considered to be important. It would have been preferable for the design correlation to have the first term for an open vent and then an additional term valid for any value of P_{stat}. In the present work P_{stat} is zero, as open vents were used. The agreement between the form of Equations 7.6, 7.7 and 7.10 shows that the current vent design procedures in Europe, which are based on Equation 7.6, support the assumption, at the heart of the laminar flame venting theory, that it is the flow of unburned gases displaced by the expanding flame that controls the peak overpressure. This flow controls P_{fv} which in turn controls the magnitude of the vented jet velocity and the jet induced turbulent flow that creates the external explosion outside of the vent, P_{ext}.

The key difference between the later Equations (Equations 7.9 to 7.13) when compared with the vent design Equations 7.6 and 7.7 is that the reactivity term is a linear dependence on K_G in Equation 7.12 and log-linear in Equation 7.6 and these is incompatible influences of mixture reactivity. This work was undertaken to provide new data on the influence of mixture reactivity, so as to improve current design procedures as they apply to mixtures of different reactivity to propane. Propane was the gas for which the bulk of the experimental validation of Equation 7.6 was carried out.

If the peak overpressure is controlled by the external explosion, P_{ext}, then the generation of external jet turbulence by the unburned gas flow through the vent is the controlling physics. However, the turbulent energy is directly related to the pressure loss across the vent, which is P_{fv}, which also has a dependence on U_L^2. Turbulent burning velocities have a prime dependence on the mean fluctuating velocity, u', and a lesser dependence on U_L. The external explosion will also be more severe if there is self acceleration upstream of the vent, if a more reactive mixtures is used or if there are obstacles in the vessel that interact with the flame to produce turbulence and generate a faster flame. The additional dependence of external turbulent flame speeds on mixture reactivity potentially leads to a greater influence of mixture reactivity on the overpressure in a vented explosion, if the external explosion dominates the overpressure. The present work explores experimentally the influence of mixture reactivity on P_{fv} and P_{ext} for two K_v. Four gas reactivities were investigated at the two vent areas using the maximum reactivity mixture for methane (10%), propane (4.5%), ethylene (7.5%), and hydrogen air (40%). Additionally, Stoichiometric concentrations of all gas mixtures including hydrogen-air explosions were also investigated in the 10L vessel.

7.6 The Influence of Gas Reactivity

7.6.1 Influence of gas reactivity at K_v=4.3 (50% vent blockage) for Stoichiometric gas/air mixtures where the external explosion, P_{ext}, was the dominant overpressure

The pressure time records for vented explosions for K_v=4.3 for stoichiometric (not the most reactive mixture) propane, ethylene and hydrogen explosions are shown in Figure 7.4 together with the maximum reactive mixture, 10% (Ø=1.05), for methane-air. The pressure records for the most reactive mixture for propane and ethylene with K_v=4.3 are shown and have been discussed in chapter 4 to demonstrate that the identification of P_{fv} and P_{ext} in Figure 7.4 was correct. The time of arrival of the flame at the vent throat was not determined in the explosions in Figure 7.4. Also marked in Figure 7.4 are the time of flame arrival at T_2 and T_3. The results for all gas reactivities show that the flame arrival at T_2 occurred before the peak overpressure, but the flame arrival at the wall T_3 occurred well after the peak pressure and in the case of hydrogen and ethylene the flame arrival at the wall was a

long time after the peak pressure occurred. The late arrival of the flame at the wall shows that the maximum flame area inside the vessel did not create the peak overpressure.

The assumption in the simple laminar flame venting theory that the flame had an area of A_s at the time of the peak overpressure is shown in these results to not be valid. If it was valid the time of arrival at T_3 would be the same as the time of occurrence of peak overpressure. This means that the measured overpressure should be less than that predicted, as was found and shown in Figures 7.1 and 7.2. It will be shown later that the flame speed towards the vent was much greater than the spherical laminar flame speed, so that the assumption in the laminar flame venting theory of spherical laminar flame propagation prior to the vent was also not valid.
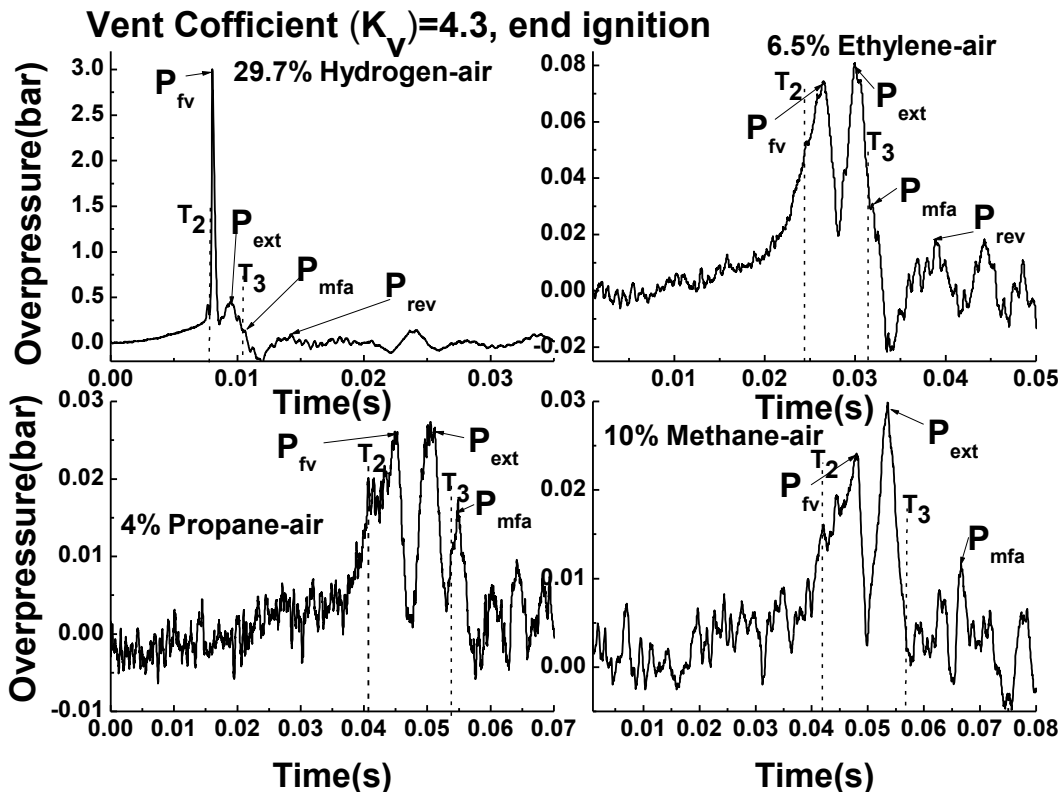
Figure 7.4 Pressure-time and flame time of arrival for different fuels with Kv=4.3.

Figure 7.4 shows that for K_v=4.3 there was a double overpressure peak of similar magnitude in each explosion of P_{fv} and P_{ext} for methane, propane and ethylene. The second of the peak overpressures in Figure 7.4 was due to an external explosion that was in most cases slightly higher than P_{fv}. The problem with developing a prediction procedure for the external explosion, P_{ext}, is that this needs to know the flow rate of

unburned gases out of the vent, in order to compute the vent induced turbulence. This computation is the same as that involved in the simple laminar flame theory here. Also, this computation requires the area of the flame to be known in order to calculate the mass combustion rate and hence the mass flow of unburned gas through the vent. Thus the two approaches to modelling the overpressures, P_{fv} and P_{ext}, are interlinked. In the laminar flame venting theory the flame area at the maximum overpressure was taken as the surface area of the vessel, A_s. Cates and Samuels (1991) stated that their video records of vented explosions supported a flame area at the maximum overpressure that was twice the cross sectional area of the vessel, which for a cubic vessel is 1/3 of A_s. Bauwens (2010) presented empirical expressions for the maximum flame area for venting with rear wall ignition and central ignitionThe stoichiometric hydrogen-air vented explosion results in Figure 7.4 for $K_v=4.3$ were significantly different for those of the other less reactive gases. The overpressure rose to 0.25 bar just as the flame passed T_2, but then there was a very large pressure increase to 3.0 bar just as the flame passed through the vent, which indicates sonic flow at the vent (sonic flow for air occurs at a pressure ratio of 1.9 or an overpressure of 0.9 bar). The second peak pressure P_{ext} at 0.5 bar was due to a very fast external explosion (Harris and Wickens, 1989). Once the vent flow was sonic the mass flow of unburned gas through the vent was a linear function of the upstream pressure. Thus, as the upstream mass burning rate continues to increase the pressure due to sonic flow through the vent increases linearly with the mass burning rate.

It may be considered that hydrogen is a special case as none of the other gases are sufficiently reactive to generate sonic flow at the vent at a K_v of 4.3. In Bartknecht's work in Figure 7.3, sonic flow for propane in the 10 m^3 vessel occurred at a K_v of 5 and at a K_v of about 6 for the other vessel volumes. Figure 7.1 shows that for propane no other workers in large vented vessels record sonic flow overpressures occurring for propane at these K_v. Figure 7.1 also shows that the majority (56%) of the Bartknecht's (1993) vented explosion overpressure data was in the vent sonic flow regime. The sharp fall in pressure for hydrogen in Figure 7.4 was due to the passage of the flame through the vent and the cessation of unburned gas flow through the vent.

The external explosion for stoichiometric hydrogen in Figure 7.4 was significant at about 0.4 bar overpressure, but this was well below the large peak pressure caused by sonic flow at the vent. There was a long period until the thermocouple at T_3 recorded flame arrival at the wall. This was surprising as the radial spread of hydrogen into the wall region would have been expected to be fast, but the results in Figure 7.4 show a very similar time from the flame arrival at T_2 to its arrival at T_3 at about $0.02 - 0.025$s irrespective of the reactivity of the mixture. For a maximum radial flame movement of 81mm, this implies an average radial flame speed of about 4 m/s irrespective of the reactivity. This is close to the burning velocity for stoichiometric hydrogen air, but much higher than the burning velocity for the other gases. This indicates that the flame burned into the trapped unburned hydrogen-air mixture at the laminar burning velocity with the production of burned gas vented out of the vent and not trapped, so that it increased the flame speed.

Fakandu et al. (2012) showed in the present experimental facility that for 40% hydrogen-air explosions, P_{ext} was the dominant overpressure up to $K_v=4.3$, but for higher K_v P_{fv} was dominant(Fakandu et al., 2012). It has been shown above that for methane-air the critical K_v for P_{ext} to be the dominant overpressure was ~<5.4 and the unburned gas vent flow pressure loss, P_{fv}, was dominant at higher K_v. For this reason the influence of mixture reactivity was also investigated at a high K_v of 21.7 ($1/K_v=0.046$).

7.6.2 Influence of Gas Reactivity at $K_v=21.7$ (90% vent orifice blockage)

Figure 7.3 shows that the smallest vent size investigated in the work of Bartknecht (1993) was a $1/K_v$ of 0.03, but most of the data was limited to $1/K_v$ of 0.05 or K_v of about 20. Consequently, in the present work this very low vent area or very high K_v effect was investigated for a K_v of 21.7, which corresponds to a vent with a 90% blockage of the cross sectional area of the cylindrical explosion vessel. The pressure time records for stoichiometric methane, propane, ethylene, and hydrogen are shown in Figure 7.5. As expected, all the overpressures were much higher than for $K_v=4.3$ in Figure 7.4. This work was the first to be completed in this research and thermocouples T_3 and T_4 were not fitted. However, all the results show that the peak overpressures occurred soon after the flame passed thermocouple T_2. Figure 7.5 shows that there was no double overpressure peaks of the type shown in Figure 7.4,

where the pressure dips to a low value before the external explosion occurs. However, Figure 7.5 shows that all the gases apart from propane exhibited a double peak, but without the large pressure drop between the two peaks found for K_v=4.3.

The pressure peak P_{fv} was always the dominant peak for K_v=21.7, in contrast to K_v=4.3 where P_{ext} was the dominant peak for methane, propane and ethylene. For propane Figure 7.6 shows evidence of a second pressure rise event that creates a 'shoulder' in the pressure fall from the main P_{fv} peak at a time of 0.055s. This indicates that for propane the P_{fv} and P_{ext} events were merged into one overall pressure peak. The reason for the dominance of P_{fv} at high K_v is that displacement of unburned gas by the advancing expanding flame upstream of the vent is similar at the two K_vs, as shown below, but the pressure loss of this flow through a smaller vent is much higher and is the dominant source of the overpressure, as assumed in the simple laminar flame theory.
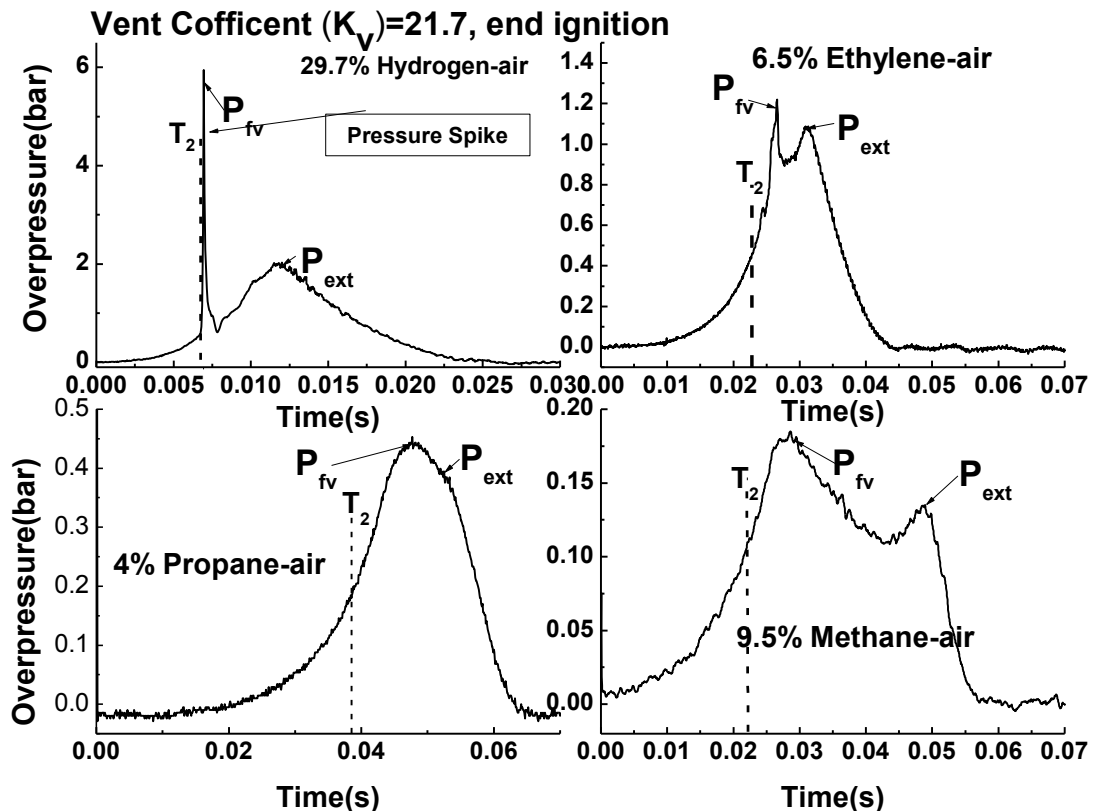
Figure 7.5 Pressure-time and flame time of arrival for different fuels with Kv=21.7

For methane and propane Figure 7.5 shows that the peak overpressure was in the subsonic vent flow regime. However, for ethylene and hydrogen the peak

overpressure was >0.9 bar and hence sonic flow occurred at the vent. This occurred soon after the flame passed T_2. The laminar flame venting theory in Equation 7.09, which assumes incompressible flow at the vent, can be converted into a sonic vent flow version by replacing the orifice plate flow equation with the orifice sonic flow equation and then Equations 7.17 and 7.18 result.

$$U_L(E_p - 1)\rho_u A_s = 0.0404\, P_o/T_o^{0.5} A_v = 0.00233\, P_o A_v \text{ for } T_o = 300K \qquad [7.17]$$

$$A_v/A_s = U_L(E_p - 1)\rho_u\ / 0.00233\, P_o \qquad [7.18]$$

where $P_o = P_a + P_{red}$

In this case the overpressure due to the mass flow of unburned gas scales linearly with the mass flow rate and this dependence has been plotted in Figures 7.1 and 7.2 for $P_0/P_a > 1.9$ where critical flow occurs for air. This is a P_{red} of 0.9 bar. The linear dependence of P_{red} on flow rate has been plotted in Figures 7.1-7.3 to pass through the point at which Equation 7.3 for propane passes through $P_{red} = 0.9$ bar. This shows a good correlation of the data for Bartknecht for the $10m^3$ vessel for $P_{red} > 0.9$ bar. Comparison of Figure 7.4 and 7.5 for hydrogen shows that for K_v between 4.3 and 21.7 the vent flow will be sonic for hydrogen, but for ethylene will only be sonic for the highest K_v.

For ethylene and hydrogen there was a significant overpressure P_{ext} due to the external explosion, which was lower than the P_{fv} overpressure due to sonic flow of unburned gas through the vent. This was because at a K_v of 21.7 the jet velocity through the vent was very high and this created high turbulence in the downstream unburned gas flow as well as a high orifice vent flow pressure loss. For ethylene and hydrogen this second overpressure was above 1 bar and indicates a very high flame speed in the external explosion. The 2 bar P_{ext} overpressure for hydrogen air in Figure 7.5 would need an external flame speed of 450 m/s to account for this and the 1.1 bar P_{ext} for ethylene-air would require 320m/s flame speed (Harris and Wickens, 1989). Downstream flame speeds were not determined in the present work, but the upstream flame speed was and these are presented below. The acceleration by the turbulence created by the vent, as an obstacle to the explosion with 90% blockage, is capable of accelerating the fast flame upstream of the vent into speeds 10 times faster downstream (Phylaktou and Andrews, 1991a).

7.6.3 Influence of Gas Reactivity on Flame Speeds Upstream of the Vent

The time of arrival at the two bare bead thermocouples on the vessel centreline was used to determine two flame speeds: the initial flame speed for the time of the flame travel from the spark to the first thermocouple, T_1, and the later flame speed determined as the time of travel from T_1 to T_2. The two flames speeds are shown as a function of the mixture reactivity K_G and U_L as well as the laminar spherical flame speed U_L E_p in Figures 7.6a-f for K_v=4.3 and 21.7. These results show that the three methods of characterising the mixture reactivity resulted in flame speeds that were reasonably linearly related.
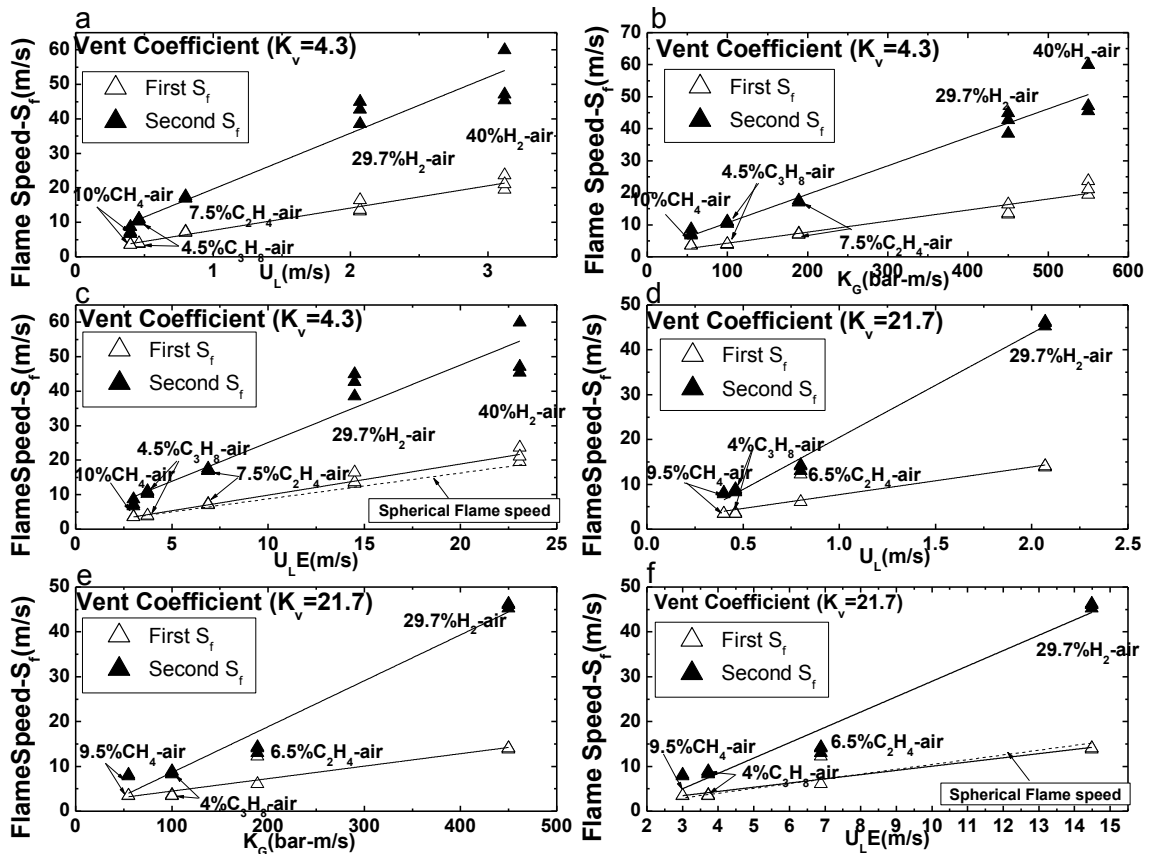
Figure 7.6 Initial and later flame speeds as a function of mixture reactivity for Kv=4.3 (a) – (c) and Kv=21.7 (d)-(f)

Figures 7.6a and 7.6b show for K_V=4.3 the flame speeds as a function of mixture reactivity in terms of K_G and U_L respectively and this shows a more linear relationship with U_L, mainly due to the large differences in K_G for methane and propane, which is not proportional to the U_L differences for these gases. The initial flame speed was close to the spherical flame speed as shown in Figure 7.6c. The

final flame speed was much higher than the spherical flame speed, which is the main reason why end ignition gives higher overpressures than for central ignition (Kasmani et al., 2010b). The linear relationship between the two flame speeds and mixture reactivity U_L shows a constant ratio between the later and initial flame speeds of about 2.5 for all mixture reactivities, as shown in Figures 7.6b and c.

For the high K_V of 21.7 the results in Figures 7.6d-f were quite similar to those for K_v=4.3, with a near linear relationship between the two flame speeds and the mixture reactivity in terms of U_L and the spherical laminar flame speed $U_L E_p$. The initial flame speed was similar to that for a spherical flame, as shown in Figure 7.6f, which was also found in Figures 7.6c for K_v=4.3. This was expected as the flame on the far wall was too far from the vent to be influenced by the vent open area. However, the later flame speed was also similar to that for methane/air at K_v=4.3, but was lower for propane and ethylene and similar for hydrogen to the later flame speeds for K_v=4.3.

These flame speed results show a flame acceleration ratio of the later to the initial flame speeds of about 3 for methane and hydrogen but about 2.3 for propane and ethylene. This ratio for a K_v of 4.3 was about 2.5 for all reactivities. However, the present data would indicate that there is no major influence of K_v on the ratio of later to initial flame speeds and a mean acceleration factor of about 2.5 would be reasonable to assume from these measurements for all mixture reactivities.
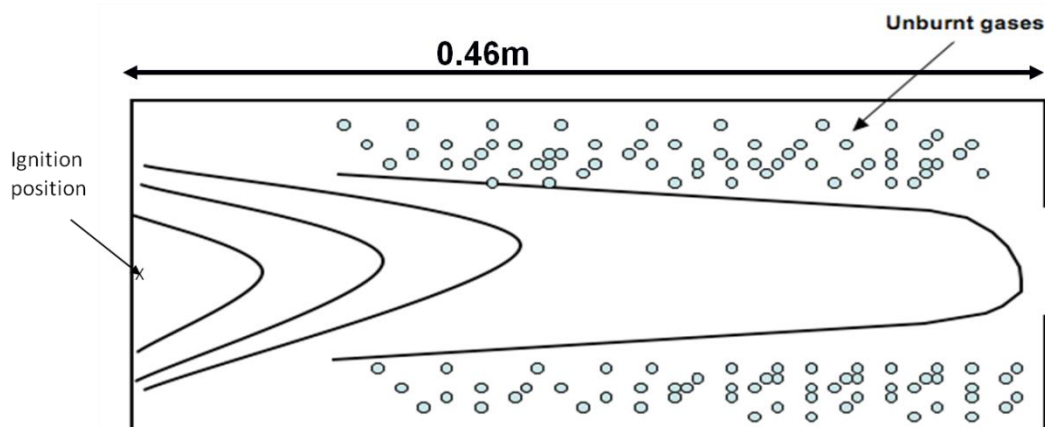
Figure 7.7 Flame Movement Pattern in 0.46m long cylindrical vessel

There are three mechanisms that can cause the flame to accelerate towards the vent:

a. Expansion of the flame by the burned gases is in the direction of the vent flow and not spherically, which is in agreement with earlier work by Phylaktou et al. (1990) as shown in the sketch in Figure 7.7.

b. The 0.46m flame travel distance is sufficient for cellular flames to develop, as for many flames this starts at ~0.1m (Harris and Wickens, 1989). Using the correlation of Cates and Samuels (1991) for this effect would lead to an acceleration distance beyond the critical size of 0.1m for cellular flame development of 0.36m and a cellular flame self acceleration factor of 1.2 for propane.

c. The vent outflow velocity, which increases as K_v increases, drags the flame towards the vent as shown schematically in Figure 7.7.

A constant factor of about 2.5 for all the gas reactivities would not be expected if cellular flames were the cause of the acceleration, the acceleration for hydrogen and propane should be greater than methane (Bradley, 1997). Also the acceleration factor for propane was 1.2 using the Cates and Samuels (1991) correlation and this is too small to account for the observed flame acceleration. As the vent flow velocity increases with K_v and the flame speed upstream of the vent does not, then the suction effect of the vent is unlikely to be the cause of the increased flame speeds. Thus, it is concluded that the increased downstream flame speeds were due to the preferential expansion of the flame in the axial direction of the vent. Andrews and Phylaktou (Phylaktou and Andrews, 1990) demonstrated this for large L/D vessels with no venting. They showed that at an L/D of 3 the axial flame speed was about 3 times the laminar spherical value, close to that found in this work.

7.7 P_{red} as a Function of Mixture Reactivity

The influence of the mixture reactivity K_G on P_{red} is shown as a function of K_G in Figures 7.8 for $K_v = 4.3$. The results for P_{fv} and P_{ext} in Figures 7.4 and 7.5 have been included as well as all the repeat tests (3 at each condition). The values of K_G were those in Table 7.3 from Bartknecht (1993). No value for ethylene was determined by Bartknecht and this was estimated as a linear relationship with the laminar burning velocity using propane $K_G=100$ bar m/s and laminar burning velocities of 0.46 for propane and 0.80 for ethylene, this gave a K_G for ethylene of 174 bar m/s. The

stoichiometric and maximum reactivity mixtures for hydrogen have also been included in Figures 7.8 and the same method as above for ethylene was used to determine the K_G for stoichiometric hydrogen-air, using the burning velocity measurements of Andrews and Bradley (1973) for hydrogen-air as a function of equivalence ratio. The experimental results show a very strong influence of mixture reactivity at $K_v = 4.3$ with sonic venting for both the hydrogen explosions.

The overpressures P_{fv} and P_{ext} are shown separately in Figures 7.8 and these have slightly higher P_{ext} for methane, propane and ethylene and much higher P_{fv} for hydrogen. This was due to the higher velocities through the vent as the reactivity increased and higher vent velocities which created higher vent orifice flow pressure loss and hence higher P_{fv}. The Bartknecht vent design equation prediction of the influence of reactivity in Equation 7.6 is shown in Figures 7.8 for comparison with the experimental data. The laminar flame theory of Equation 7.14 is shown for comparison with the P_{fv} results in Figures 7.8. The theory was corrected for sonic flow at the vent using a linear dependence of vent mass flow on the overpressure, as shown in Equation 7.18, instead of the square root dependence for incompressible flow in Equation 7.14. Figures 7.8 also compares the prediction of the reactivity effect from Equation 7.11 from NFPA 68 (2013) for $\lambda = 1$, with A_s converted to a function of $V^{2/3}$ using a cubic vessel relationship. This is in much better agreement with the present results than that for Equation 7.9.

Figure 7.8 shows that the laminar flame venting theories of Equations 7.11 and 7.14 give much better agreement with the experimental data than that of the Bartknecht vent design Equation 7.6, which grossly over predicts P_{red} at low K_G and under predicts at high K_G. Figures 7.8 shows the square root relationship in Equation 7.14 for the dependence of P_{fv} on K_G is not demonstrated in the experimental results for methane and propane. This is most likely due to the measurement of K_G for methane being too low and their relative values being inconsistent with the more common reactivity parameter U_L. Figure 7.8 shows that the theories in Equations 7.11 and 7.14 over predict the present experimental P_{fv} results for methane, propane and ethylene, but only by a small margin for methane. This was due to the assumption that the flame area was A_s at the time the flame exited the vent. The time of flame arrival at the wall thermocouple T_3, which was shown above to be well after the flame had left the vent, shows that this assumption is not valid. However, the trend

for the influence of K_G is reasonably well predicted, apart from the methane results relative to propane.
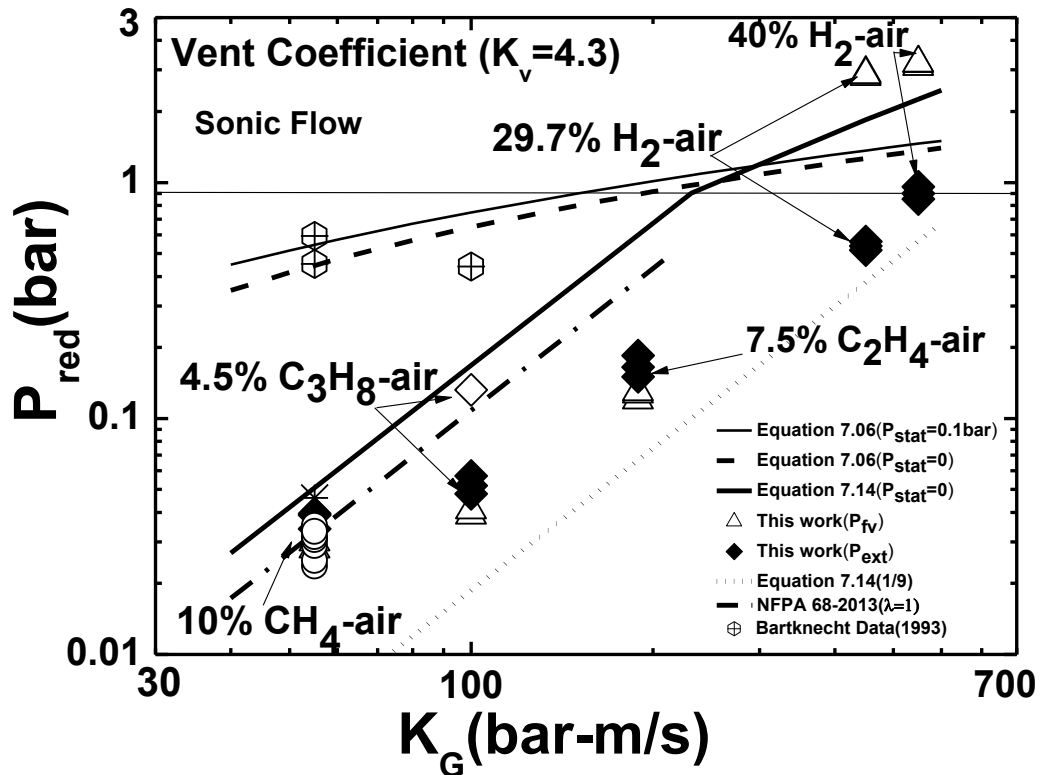
Figure 7.8 Pred as a Function of KG with Comparison with Equations 7.6, 7.11 and 7.14

For hydrogen the theory under predicts the measured P_{fv} results as shown Figure 7.8. This suggests that there was an additional acceleration mechanism for hydrogen, possible self acceleration due to the development of cellular flames. Comparison with Equation 7.6 for Bartknecht's results is also shown in Figures 7.8 which indicates that this does not predict the influence of mixture reactivity adequately. There was a gross over prediction of the low K_G results and a significant under prediction of the hydrogen results. Correcting Equation 7.6 for the 0.1 bar static burst pressure used does not account for the over prediction that occurs. The under prediction of the hydrogen results using Equation 7.6, which is adopted in the EU vent design guidance, is of concern and more work on hydrogen explosion venting is required and the vent design guidance for hydrogen needs to be revised. It is possible that in the Bartknecht results the P_{fv} pressure rise was ignored as too short a pressure pulse for the vessel to respond to and that the peak overpressure was taken as the external flame pressure P_{ext}, which Equation 7.6 does predict reasonably well

for hydrogen. However, the pressure records for Bartknecht's vented explosions have not been published so this cannot be verified.

The P_{fv} and P_{ext} peak pressures for $K_v = 21.7$ are shown as a function of K_G in Figures 7.10, together with the results of repeat tests. At this high K_v the experimental results show that P_{fv} was the dominant overpressure for all gas reactivities. The P_{fv} peak pressures correlate with $P_{fv}^{-0.5}$ in the subsonic vent flow regime as expected by the theory. The ethylene P_{fv} results also lie on the expected line in the sonic flow regime, but as for the $K_v=4.3$ results the hydrogen P_{fv} results are above the expected result based on extrapolation from the lower K_G experiments. It is considered that the explanation may lie in self acceleration of hydrogen flames in this small vented explosion vessel, but no significant self acceleration for the other gases.
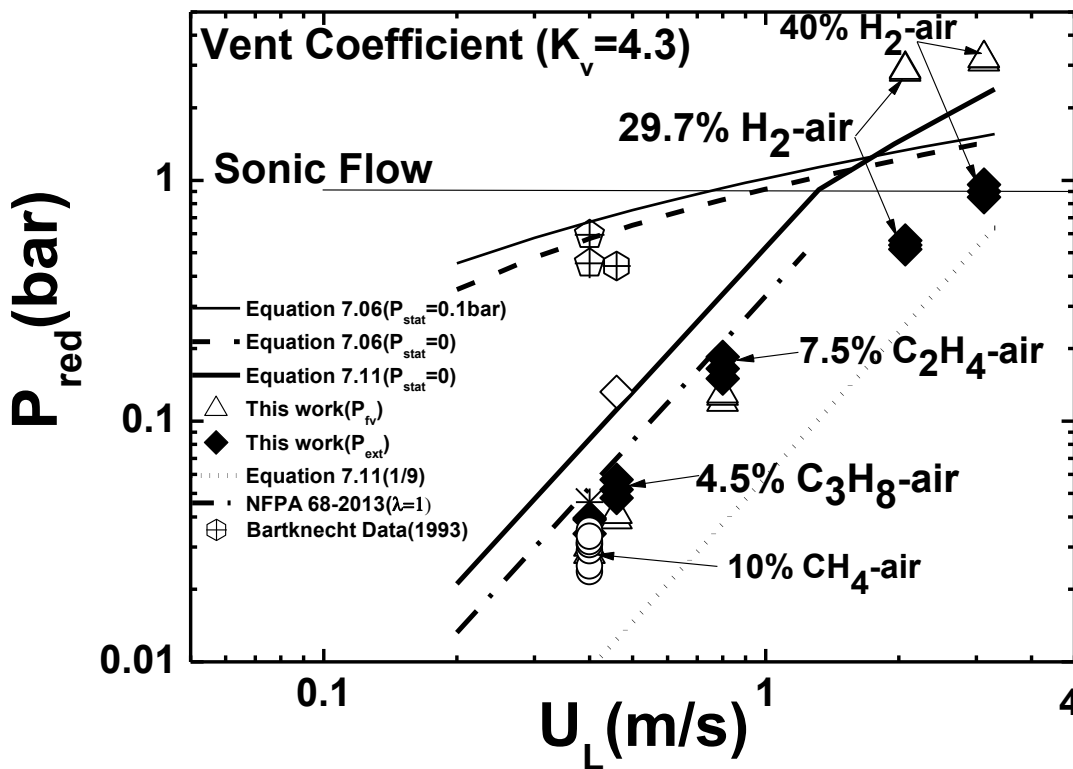
Figure 7.9 Pred as a Function of UL for Kv=4.3 with Comparison with Equations 7.6 and 7.11

Figures 7.9 shows the same data as in Figures 7.8 for $K_v=4.3$ plotted as a function of the laminar burning velocity U_L, which is the more usual combustion theory reactivity parameter. This shows much better agreement of the laminar burning velocity data with the laminar flame theory of Equation 7.9 than is shown in Figure

7.8 using K_G as the reactivity parameter. However, the magnitude of the present results are over predicted by the present laminar flame theory with $C_d = 0.61$, but are only just below the predictions of NFPA 68 (2013) where a C_d of 0.7 is used. The over prediction of the measured overpressures was because the actual flame area at the peak overpressure was not the assumed area of A_s in the theory. The flame area assumption of Cates and Samuels (1991) that the flame area was twice the cross sectional area of the vessel, would for a cubic vessel give a flame area one third of the surface area of the vessel and hence an overpressure 1/9 of that assuming the flame area was A_s would result. However, Figures 7.9 shows that this gives a significant under prediction of the present results. The square root relationship between P_{fv} and U_L from the theory in Equation 7.9 is supported by the experimental data for methane, propane and ethylene. This is because K_G values in Table 7.3 for propane and methane and hydrogen do not scale with the U_L values, which have a better experimental data base than does the K_G values of Bartknecht. More work needs to be done on the measurement of K_G as a reactivity parameter with better relative agreement with the data for U_L. The Bartknecht vent design Equation 7.6 may be converted into a U_L equivalent using Equation 7.2 and this has been plotted in Figures 7.9. This still over predicts P_{red} for low reactivity mixtures and under predicts for hydrogen.
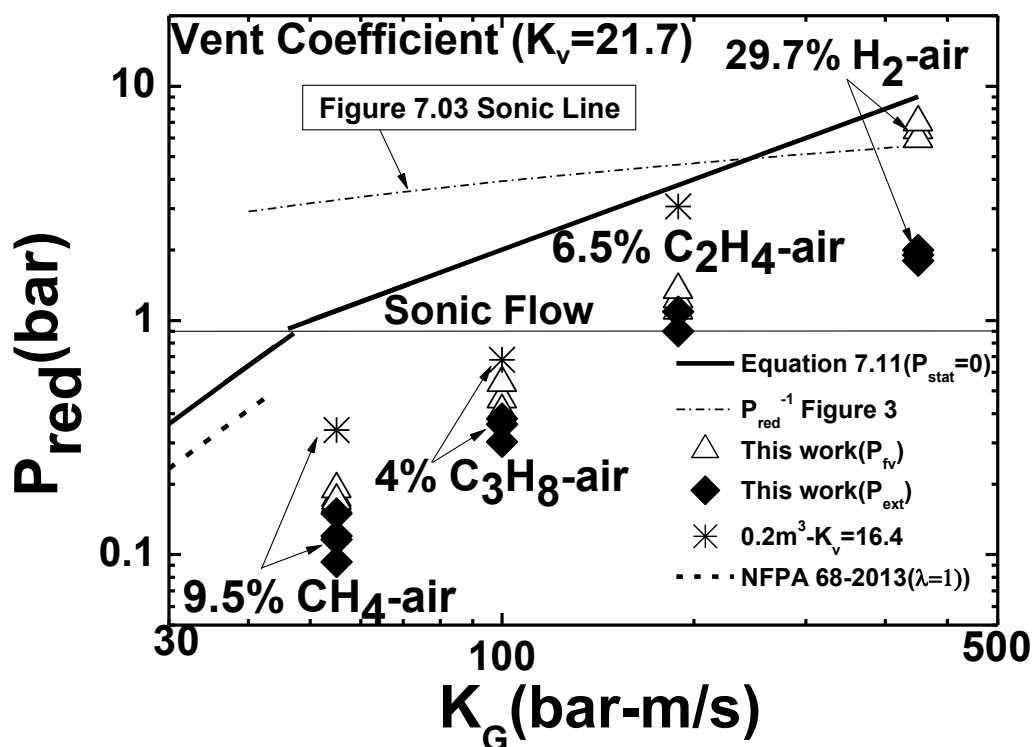
Figure 7.10 Pred as a Function of KG for Kv=21.7 (90% blockage) with Comparison with Eqs. 7.6 and 7.11

Figure 7.10 also compares the present results with Bartknecht's experimental results for the sonic flow regime and the laminar flame venting theory in Equation 7.9. Equation 7.6 predicts that the vent overpressure will be in the sonic flow regime for all values of K_G and this is why Equation 7.6 cannot be used directly as it is not valid for $P_{red} > 2$ bar and is not really valid for $P_{red} > 0.9$ bar, as Equation 7.6 is essentially an incompressible vent flow equation, as discussed above. However, Figure 7.3 shows that all Bartknecht's experimental results for $1/K_v = 0.05$ were for $P_{red} > 0.9$ bar and hence all venting is predicted to be sonic based on these experimental results for propane and methane. The sonic venting line, Equation 7.18, in Figure 7.10 has been taken from Figure 7.3 and anchored on the propane-air data for the $10m^3$ vessel. The K_G trend has then been assumed to be the same as in Equation 7.6. This methodology does enable the hydrogen overpressures to be more closely predicted than direct use of Equation 7.6 would give.

Figures 7.10 shows that the laminar flame theory in its sonic orifice flow version, Equation 7.18, over predicts the measured results substantially and predicts sonic flow at conditions that the experiments showed were well away from sonic vent flow. Again this shows that the assumption in the theory that the flame area at the point of maximum overpressure was A_s cannot be correct. At $K_v = 21.7$ the error is much greater than at $K_v = 4.3$, as shown by comparing Figures 7.8 and 7.10. These results show that although Equation 7.6 or 7.9 give safe overpressure predictions, there are still venting flame shape effects that are not taken into account in the theory. However, the theory does have excellent agreement with vented explosion data in some large scale explosions as shown in Figures 7.1 and 7.2.

Table 7.4 Experimental and Theoretical Influence of Mixture Reactivity for $K_v=21$ and $P_{stat}=0$

Gas	U_L m/s	P_{fv} P_{red} Bar	P_{ext} bar	N P_{fv}	SF $(U_L/0.43)^2$	SF $U_L/0.43$	N K_G	NBR 'a'
Methane	0.43	0.18	0.13	1	1	1	1	1
Propane	0.46	0.45	0.38	2.5	1.14	1.07	1.82	1.22
Ethylene	0.80	1.2	1.1	5.5	3.46	1.86		
Hydrogen	3.5	6.0	2.0	9	66.3	8.14	10	1.77

(N=Normalised, SF=Sonic Flow, NBR=Normalised Bartknecht Reactivity)

The overpressure results in Figures 7.8 and 7.10 are summarised in Table 7.4 and compared with the expected gas mixture reactivity effect normalised to that of methane/air. If the relationship between overpressure and U_L was that in Equation 7.9 then Table 7.4 shows that the reactivity effect is grossly under predicted for propane and grossly over predicted for hydrogen. However, the hydrogen overpressure is in the sonic regime and the vent flow rate is linear with overpressure, which would result in a linear dependence of the overpressure on U_L and the results in Table 7.4 for sonic flow are in approximate agreement with this for hydrogen. However, these results at high K_v indicate a more complex influence of mixture reactivity than in the simple laminar flame venting theory. Table 7.4 shows good agreement between the measured normalised overpressures and the normalised values of the deflagration index K_G. If the flow was incompressible then the relationship should be with K_G^2 and linear with K_G only for sonic flow. Also, the unusual high increase in reactivity between methane and propane in the K_G factor requires further validation as there is no kinetic reason for this. Table 7.4 also shows that the present results show no agreement with the reactivity trends in the Bartknecht vent design Equation 7.6 with the constants for 'a' from Table 7.3.
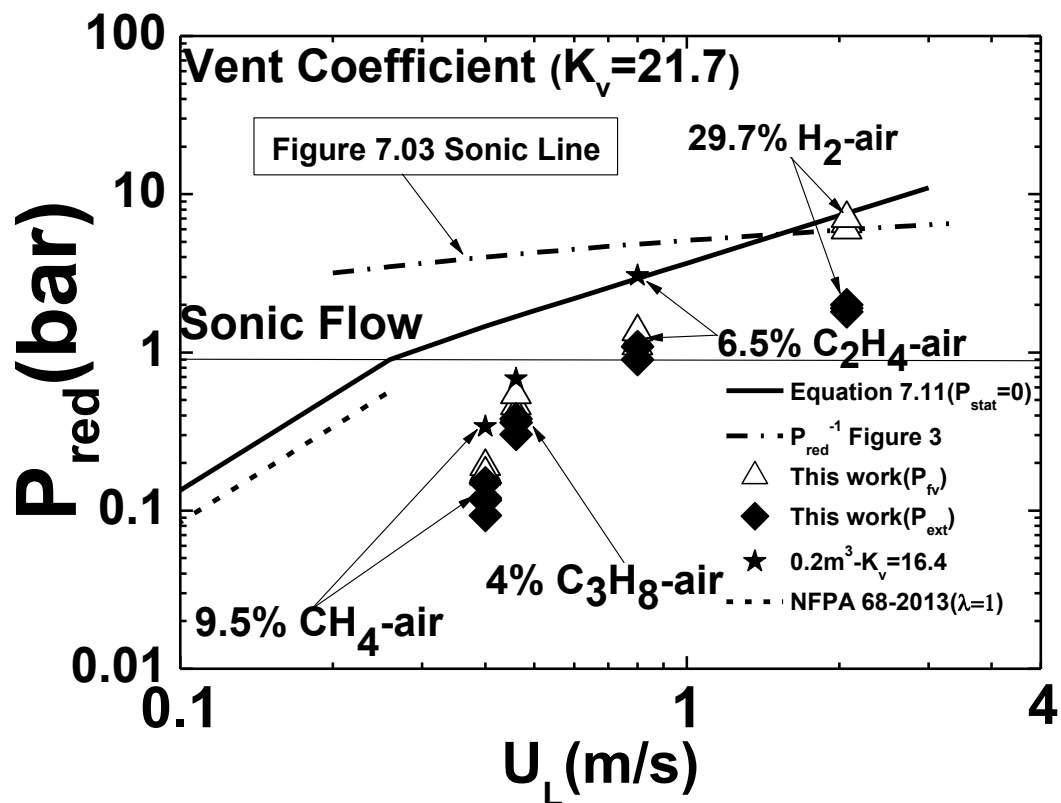
Figure 7. 11 Pred as a Function of UL for Kv = 21.7 with Comparison with Equations 7.9 and 7.11

The vented explosion results as a function of U_L are shown in Figures 7.11 for $K_v =$ 21.7. Comparison with the laminar flame venting theories in Equations 7.9 and 7.11 (NFPA 68) still overpredict the experimental results, but are relatively close. The difference between Equations 7.9 and 7.11 is mainly in the vent discharge coefficient. For methane and propane the experimental results show subsonic venting occurred, whereas laminar flame theory predicted that sonic venting should occur. Again the difference was due to the assumption of A_s as the maximum flame area was not valid. All the overpressures were predicted to be far too high and all in the sonic venting regime for the Barktnecht Equation 7.6.

The over prediction of the measured P_{red} by Equations 7.9 in Figures 7.8-7.11 could be explained by the actual flame area at the time of the peak overpressure being less than A_s. This is equivalent to reducing the assumed flame area A_s by a factor of about 3 or introducing a correction constant on the area in Equation 7.7 of 0.33. For a cubic explosion vessel this reduces the C_2 constant in Equation 7.7 from 6 to 2 and this is in precise agreement with the flame area constant used by Cates and Samuels (1991) based on videos of vented explosions in a Perspex vented box. Cates and Samuels (1991) found that the surface area of the flame at the position of maximum overpressure was twice the cross sectional area of the vessel and for a cubic vessel this is the same as $C_2=2$ in Equation 7.7. However, the time of flame arrival data in chapter 4 indicates that the overpressure due to turbulent flame propagation in the external vent flow is significant.

7.8 Conclusions

1.   The results from this section showed that after an initial period of flame propagation from the spark at the laminar spherical flame speed there was a fast central flame accelerating towards the vent, which left a trapped unburned gas volume in the vessel. This fast flame speed was not significantly influence by K_v and was measured well upstream of the vent and not influenced by the acceleration of the flow into the vent. It was concluded that the increased downstream flame speeds were due to the preferential expansion of the flame in the axial direction of the vent, rather than self acceleration.

2.   The form $1/K_v = a\, P_{red}^{-n}$ of the venting design equations of Bartknecht, for P_{stat}=0.1bar, was shown to be the same as in the Swift approach that is recognised by NFPA 68. For agreement with Bartknecht's results for methane and propane venting the laminar flame venting theory only needs a burning velocity enhancement factor of 2.60 and 2.56 respectively. The theory allows the effect of gas reactivity to be predicted. For the present 10L vented vessel, the theory over predicts the measurements for methane, propane, ethylene and hydrogen. The higher predicted values were due to the assumption of the maximum flame area being A_s and the actual flame area at the time of maximum overpressure being less than this.

3.   The laminar flame venting theory is very similar to that of Bradley and Mitcheson (1978) and Swift (1983) if the same vent orifice discharge coefficient C_d is used. The adoption of the Swift (1983, 1988) approach to laminar flame venting design for P_{red} up to 0.5 bar in NFPA 68 2013 is justified as it is in good agreement with the present results and with many other vented explosion results in the literature. The extension of this approach to hydrogen air venting is justified by the present results.

4.   The laminar flame venting theory expanded to include self acceleration of flames, which give an additional volume effect, is applicable to large scale explosion venting, as it accommodates the influence of vessel volume. The laminar flame theory has perfect agreement with experimental data for a 35m^3 vented vessel without any correction term and also shows agreement with other large vented vessel results. However, there is disagreement with some large vessel results because the flame propagates through a longer distance and the effect of self-acceleration may need to be taking into account.

5.   The explosions at low K_v=4.3 showed two peaks in the overpressure, P_{fv} and P_{ext}. The overpressure due to the external explosion was higher than that due to the vent flow at low K_v, but the reverse occurred for high K_v. Also at low K_v the very reactive hydrogen explosions had sonic vent flow and the pressure loss due to unburned gas flow through the vent dominated the overpressure.

6.   The Bartknecht design Equation 7.6 under predicts the P_{red} for hydrogen in spite of the over prediction for the other gases. In view of this, the approved design

procedures for hydrogen explosion venting need revision and more experimental work is required on vented hydrogen explosions.

CHAPTER 8

External Flame Jets and the Influence of External Vessel Wall

8.1 Introduction

In chapter 5, the external explosion of the unburnt gas cloud outside the vent was shown to affect the maximum pressure in vented explosion. This depends on the vent area as well as the obstacle length as the vent obstructs the free flow movement of the flame as it exits the vent into the open atmosphere. Most of these vented products particular when violent, toxic or blast waves are involved, must be directed to a safe place in order not to constitute hazard to people and the surrounding, as part of the requirement of the vent design standards (EN14994:2007, 2007, NFPA 68, 2013). In this case, the use of duct becomes necessary and duct venting has been shown to generate and likely to increase the severity of explosion venting when compared to simple venting without the use of duct (Bartknecht, 1981, Ponizy and Leyer, 1999b). In chapter 7, the result of Barknecht(1993) in which the European venting guidance is based was shown to over predict most experimental data from the literature. No results over time have been shown to agree to Bartknecht and no much information was provided on the result.

In this chapter, the result of simple venting into the atmosphere in 200L ($0.2m^3$) vessel is presented. The vessel was initially intended to scale up the 10L vessel as presented earlier for further studies on the effect of vessel volume. However, result was later shown to agree with the experimental result of Bartkecht (1993), which was previously shown to over predict most experimental data in the literature. The vessel extension attached to the main test vessel was responsible for this increase in the overpressure downstream the vent, similar to the behaviour of a duct. The result and other similar work are presented as new data to the explosion venting data base for better application of the venting technique. Additional, the external jets flame speed was used to predict the overpressure based on the Taylors acoustic theory. A flame area correction factor was included in the laminar flame model to force the prediction of the experimental data from this work.

8.2 Comparison of Result with Bartknecht Experimental data

The experimental data from the original work of Bartknecht has been adopted as the main vent design correlation for explosion venting design in the current European

standard (Bartknecht, 1993), and was also used in the previous NFPA 68 (2007). This data for propane was shown carried in various vessel sizes up to 60m^3, and shown to be much higher than most venting data in the literature including vessel volumes of 550m^3 (Bimson et al., 1993). The correlation of Bartknecht (1993) in equation 7.6, which is in the venting standard was shown to based on empirical correlation rather than a representation of his experimental data as discussed in chapter 7. It limitation of accurately predicting experimental data was also highlighted in most in various aspect of venting studies (Andrews and Phylaktou, 2010, Molkov, 1999a, Molkov and Bragin, 2013, Swift, 1989). A closer look at the experimental set up of Bartknecht(1993) showed that most of vessels were placed on the flat ground and the vent positions are not place too close to ground. A typical set up of Bartknecht's 60m^3 vessel is shown in Figure 8.1a indicating the vent position in relation to the ground (Bartknecht, 1993). Additionally, Figure 8.01b shows schematic representation of how vent areas were varied by removing and replacing flanges on the surface of the vessel (Bartknecht, 1993).
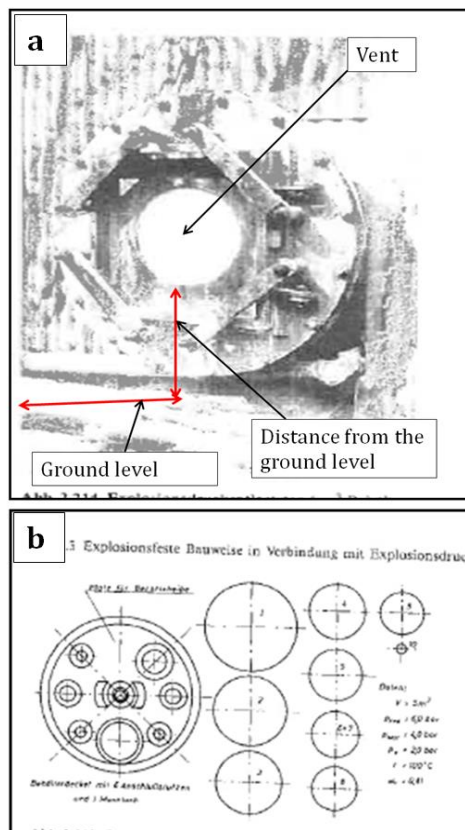
Figure 8.1 (a) vent position in relation to the ground level (b) different vent opening with flanges (Bartknecht,1993)
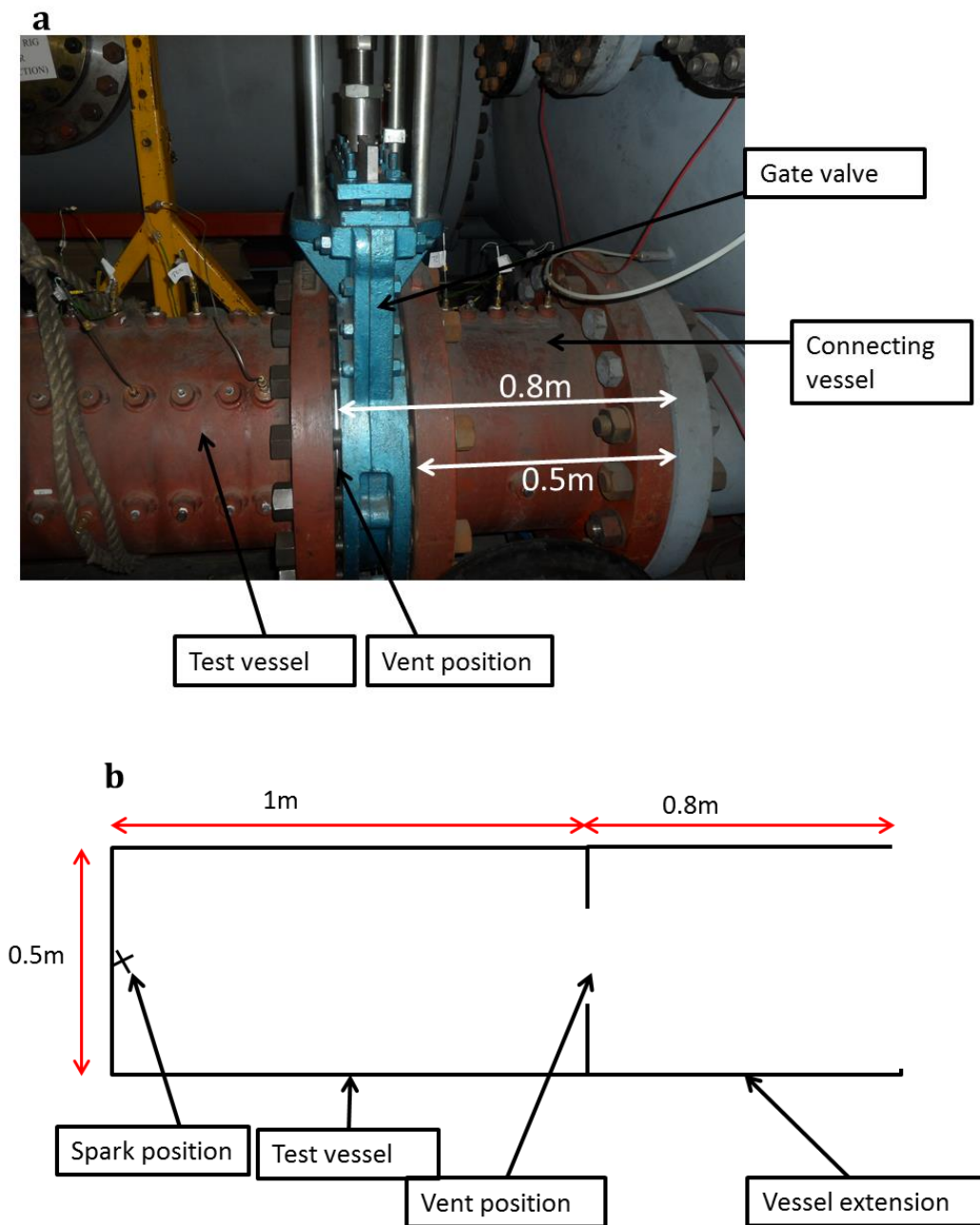
Figure 8.2 Experimental set up 200L (a) photograph (b) schematic representation

A 200 litres (0.2m³, L=1m, D=0.5m) shown in Figure 8.2, was used for vented gas explosion with free venting (open vents). Different vent areas were introduced using a removable vent at the end wall attached to a 0.5m cylindrical vessel which was also connected to a large dump vessel. The connection to 0.5m diameter vessel (same diameter as test vessel) before the dump vessel was necessary to accommodate the weight and height of the gate valve which would not allow direct

connection of the test vessel to the dump vessel. Additional, movement of the valve was restricted for safety reasons and vents were placed between the test vessel and the connecting, making the total length downstream to be 0.8m.

The schematic representation in Figure 8.2b shows how the experimental set up including the vessel extension comprising the total length of the gate valve and the connecting vessel. Spark plug was positioned at the end flange opposite the vent, which was considered to give the worst case explosion overpressure in compliance with the ATEX regulation (EuropeanParliament and Council, 1994, Ferrara et al., 2006, Willacy et al., 2007). The lower level of the vessel extension is similar to the ground level shown in Figure 8.1a.

Figure 8.3 shows the result of 200L vessel with the vessel extension for 10% methane-air compared with that of 10L vessel and experimental data of Bartknecht (1993) for different vessel volumes. The results of the 200L vessel shows much higher overpressure when compared to 10L vessel for low K_v, but agrees with the Bartknecht's data for 1m^3 and 30m^3 vessel. Even though the test is 20 times the size of the small vessel (10L), such a massive difference in overpressure was not expected for K_v of 2.7 to 7.2. This unusual high maximum pressure was a a of the vessel extension downstream the vent, which restricts sufficient air entrainment, thereby allowing for further combustion along the vessel extension. The lower level of the vessel extension is similar to the ground level of the experimental set of Bartknecht (1993) as shown in Figures 8.1a and 8.2b. Similarly, Figure 8.4 also gives similar trend of result for both 10L and 200L vessels. The agreements with Bartknecht's data are $K_v< 7.2$ in which P_{ext} were the controlling peak pressure. In this case, the jet of flame exiting the vent ignites the external cloud close to the vent, within the vessel extension, thereby making contact with the lower and upper walls of the vessel extension. The vortex of the external jets was not allowed to be fully established as the case of venting into the atmosphere. This makes the pressure behave similar pressure generated in duct venting.

For higher $K_v >7.2$, the P_{fv} as discussed in previous chapters and most of the combustion process was almost completed. Additionally, the small vent allows the jet of the flame to ignite the external cloud farther away from the vent, close to the exit of the vessel extension. This was shown to be just slightly higher than result from 10L vessel and overestimated by Bartknechts data as expected.
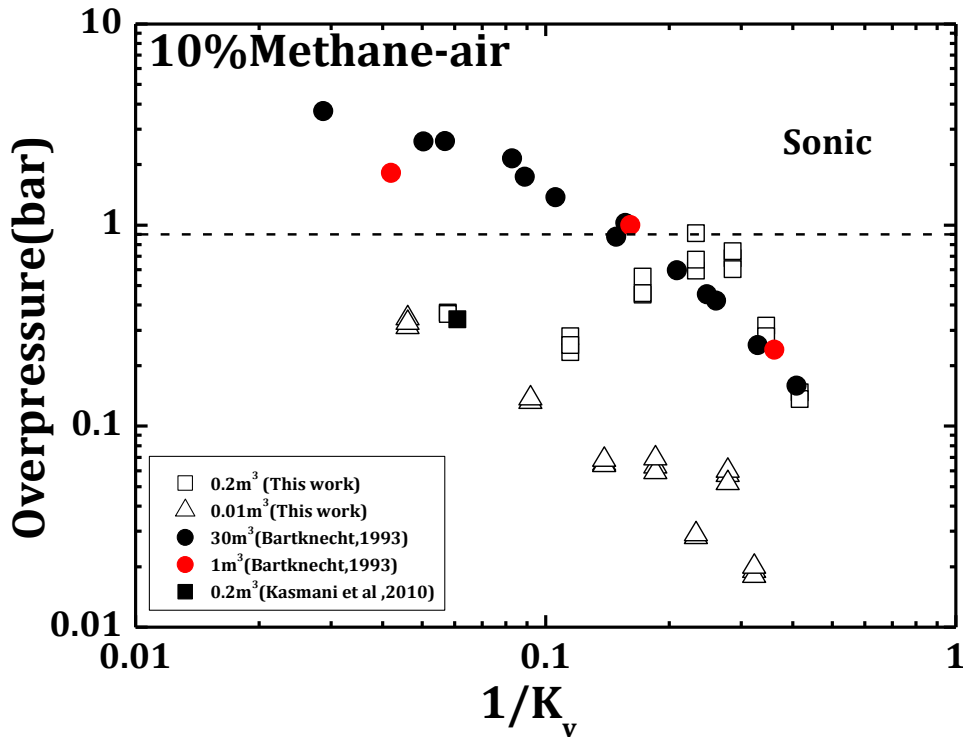
Figure 8.3 Comparison of 10L and 200L result with Bartknecht data for 10% Methane-air
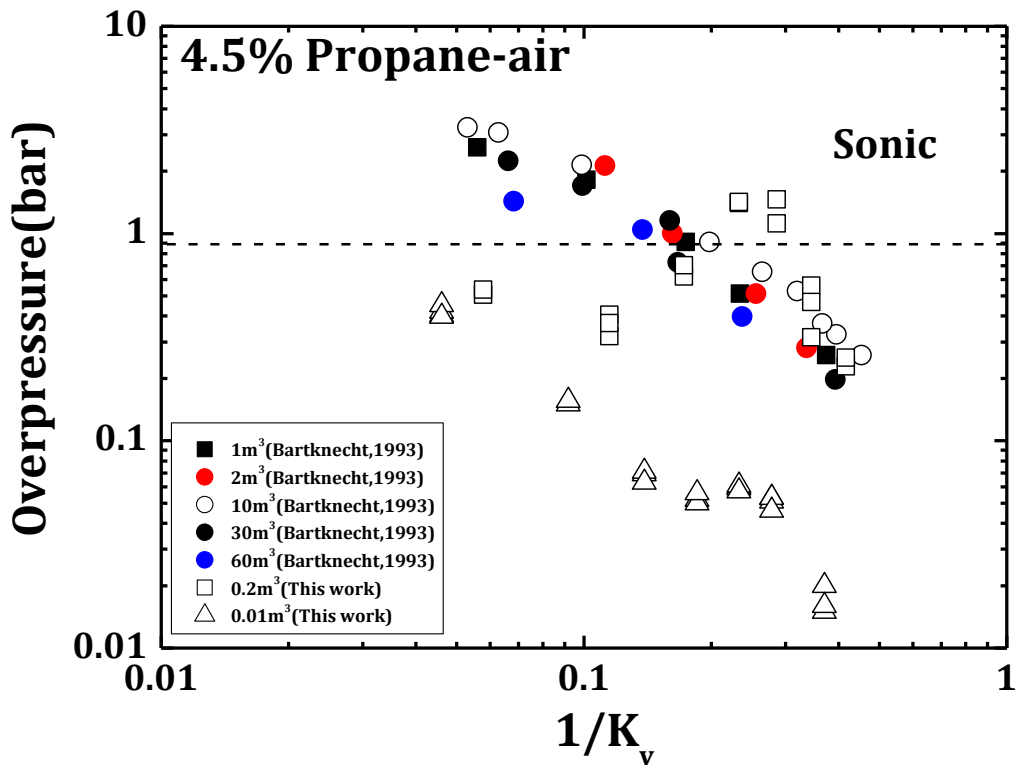
Figure 8.4 Comparison of 10L and 200L result with Bartknecht data for 10% Methane-air

8.3 Effect of External Wall on 10L Vessel

The total length of the vessel extension was 0.8m with diameter of 0.5m, making L/D=1.6. In order to verify the effect of vessel extension, cylindrical vessel of length 0.260m and diameter of 0.162m (L/D=1.6) was attached to the 10L vessel, having same L/D with the vessel extension of 200L vessel. The set up of the 10L vessel and the vessel extension is shown in Figure 8.5, with 10L (+ext) or $0.01m^3$(+ext) used to describe the new 10L vessel with the vessel extension.

Pressure-time pressure for two vent areas for 200L vessel was compared with the 10L (+ext) a shown in Figure 8.6. Since the two vent areas have different K_v due to different L/D and volume, the area blockage ratio (BR) will be used on this Figure 8.6 only, and BR is the ratio of the total blocked area, in relation to the vent area in percentage. For BR=40%, there was significant increase in the maximum pressure (P_{red}) when the two vessels were compared. Even though similar L/D was used for both vessels, the length, is shown to be a more contributing factor rather than L/D. The increases was minimal for BR=80% as expected due to increase in vessel volume as shown in Figure 8.6b.
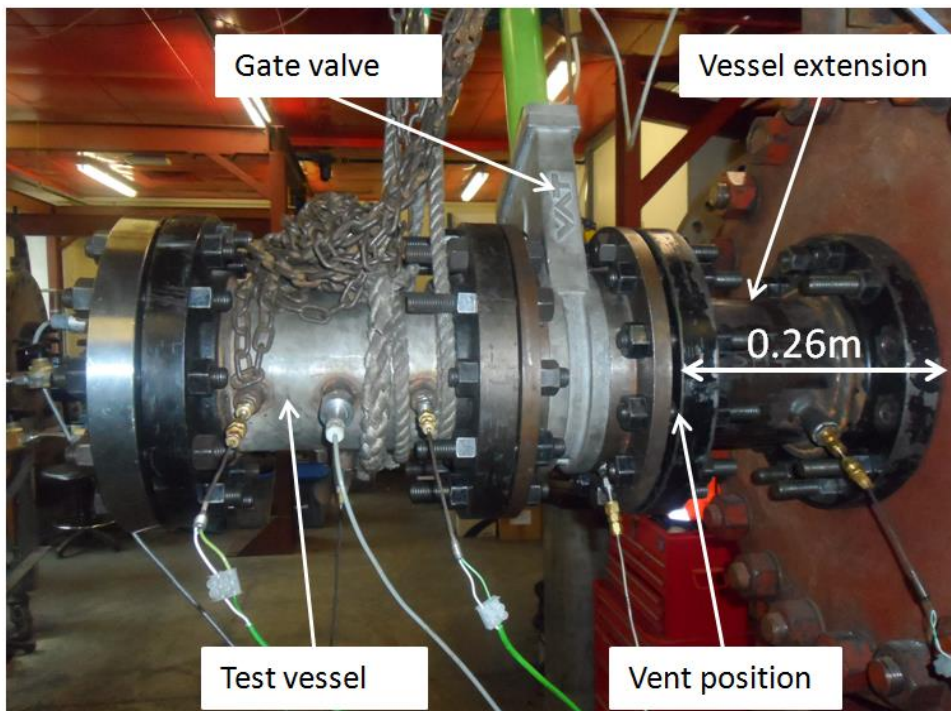
Figure 8.5 Experimental set up of 10L vessel with extension
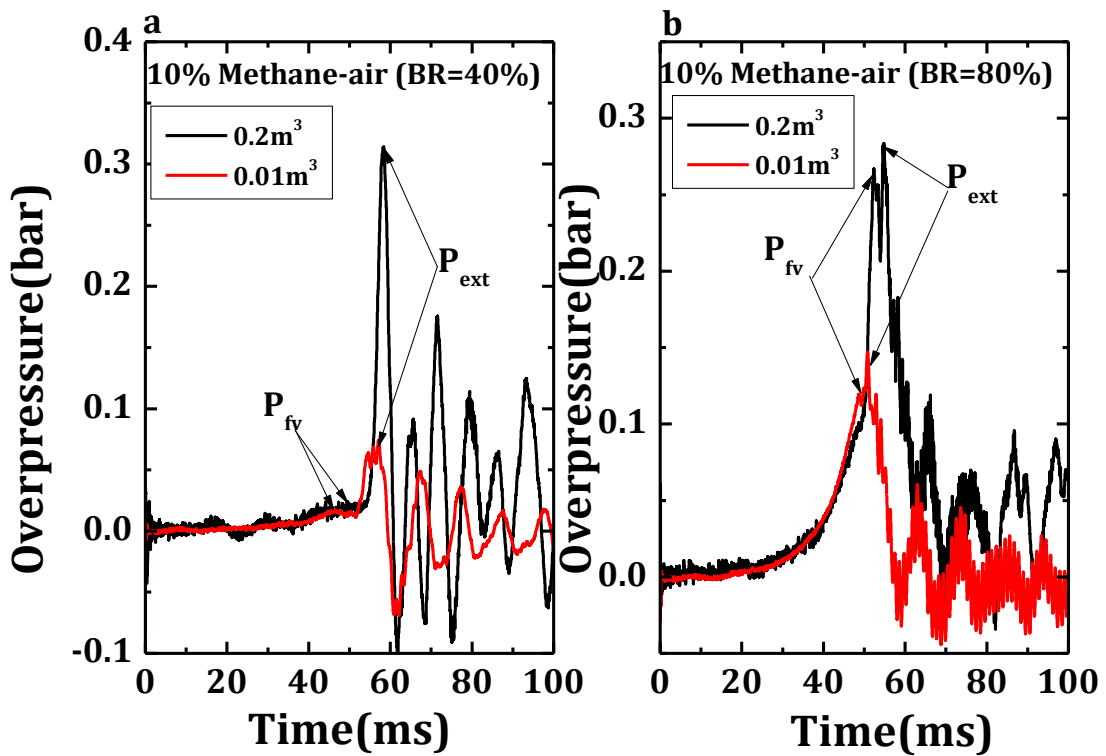
Figure 8.6 Pressure-Time for different vessel volumes for 10% methane-air

Figure 8.7a, the P_{fv} for 200L vessel compared with the 10L vessel for 10% methane-air. The increase was the influence of vessel volume which was expected for larger volume. This also shows s that the vessel extension has no influence on the internal overpressure. Hence, this is also in agreement with the Figures 8.3 and 8.4 where the higher K_v gave realistice result when 10L and 200L vessel where compared and over predicted by the result of Bartknecht (1993). In Figure 8.7b, second peak pressure influenced by the external explosion (P_{ext}) was shown to be much higher for 200L vessel. The vessel extension for 200L had more influence than the vessel extension of 10L, even though the same L/D downstream was used. This implies that the length of the vessel downstream had more influence than the L/D. If sufficient distance was given downstream by increasing the length of the vessel extension of 10L vessel, the position of maximum intensity would have be reached where the maximum overpressure would be obtained (Na'inna, 2013).

When 10L vessel and 10L (+ext) were compared in Figure 8.8, the P_{fv} was shown to be same for both experimental set up. This agrees with the earlier statement that vessel extension has no influence on the internally generated pressure inside the vessel. Figure 8.8b showed higher overpressure for low K_vs for external explosion (P_{ext}), these are K_vs where the P_{ext} were shown to be the controlling overpressure.
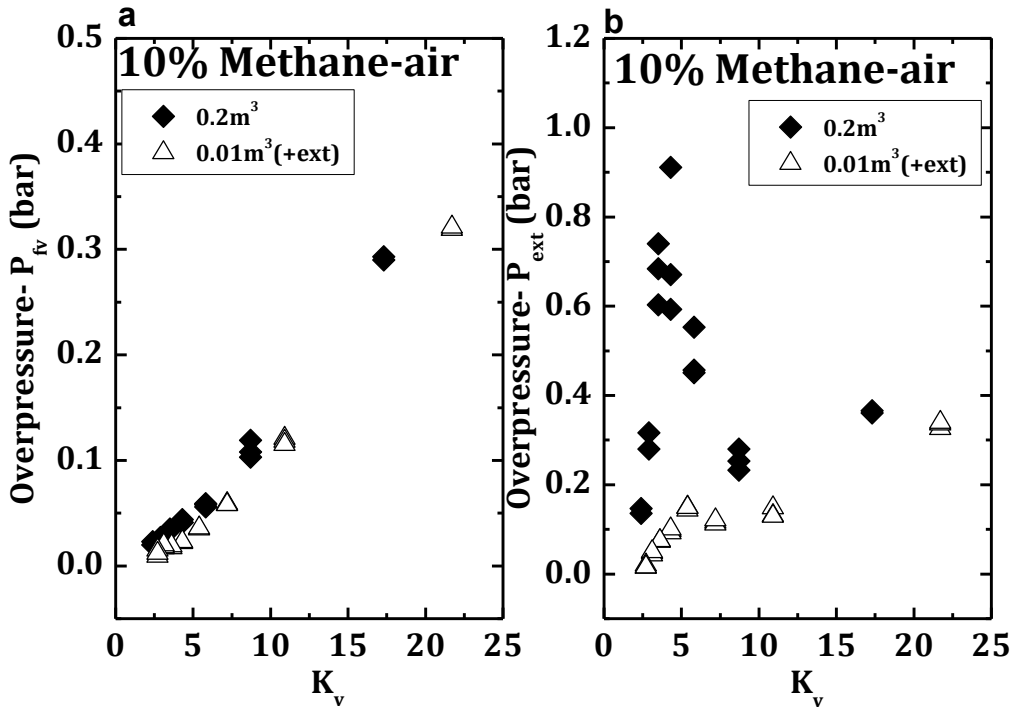
Figure 8.7 Comparison of 0.2m³ with 0.01m³(+ext) (a) P_{fv} (b) P_{ext}
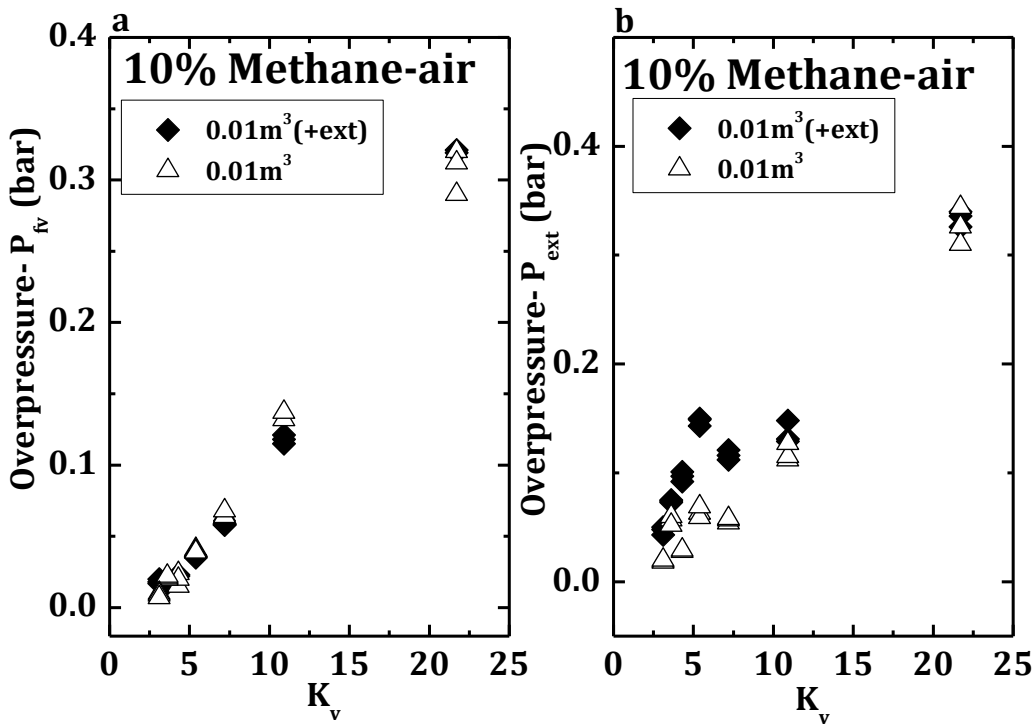
Figure 8.8 Comparison of 0.01m³ with 0.01m³(+ext) (a) P_{fv} (b) P_{ext}

Contact with the wall surface of the external vortex within vessel extension and restriction of air entrainment are the main causes of this unexpected pressure rise for the low K_v. This also agrees with the fact that share layer gives the maximum explosion overpressure (Na'inna, 2013, Na'inna et al., 2012). There is strong

evidence from this work to show the vessel extension has no influence on the P_{fv} but significant influence on the P_{ext}. The increases in length downstream was shown also increase P_{ext} , which is different situation with large L/D where increase in L/D reduces the overpressure(Phylaktou and Andrews, 1991b).

8.4 Flame Speeds in the Internal and External Explosions

Figure 8.9 shows the flame speeds measured for K_v = 10.9 on the axis of the vent from the spark to the external flame. The vent position is also shown. It is clear that for methane, propane, ethylene and hydrogen that the peak flame speed was outside the vent and was 110 m/s for propane and methane, 247 m/s for ethylene and 1000 m/s for hydrogen. These fast external flames give rise to high static pressures behind the flame front. Taylor (1946) showed for spherical waves the static pressure behind the expanding wave could be related to the Mach number by Equation 8.1.

$$\frac{P_+}{P_o} = \frac{2\gamma M^2}{1+M}$$

[8.1]

where P_+ = peak overpressure, Pa = ambient pressure (absolute), $\gamma =$ the specific-heat ratio, and M = Flame Mach number. Harrison and Eyre (1987) showed that this could be used to predict the static pressure behind flame front in vapour cloud explosions in the presence of obstacles.

Equation 8.1 has been applied to the present peak external flame speed measurements and compared with the peak pressure due to the external explosion in Figure 8.9 for hydrogen explosions. A very good prediction of the pressure trace from the flame speed measurements using Equation 8.1is shown. Figure 8.9 shows that the measured peak overpressure correlated well with the measured external flame speed for a range of K_v. Figure 8.10 compares the measured and predicted (from Equation 8.1) peak external overpressures as a function of K_v for ethylene explosions. Good agreement is shown and this indicates that Equation 8.1can be used to predict the external explosion overpressure. To use Equation 8.1in vent design a procedure to predict the external flame speed based on the internal mass burn rate and the laminar flame theory is a good basis to do this. However, this needs a prediction method for the maximum flame area at the time the flame passes through the vent and techniques to do this are being developed by the authors.
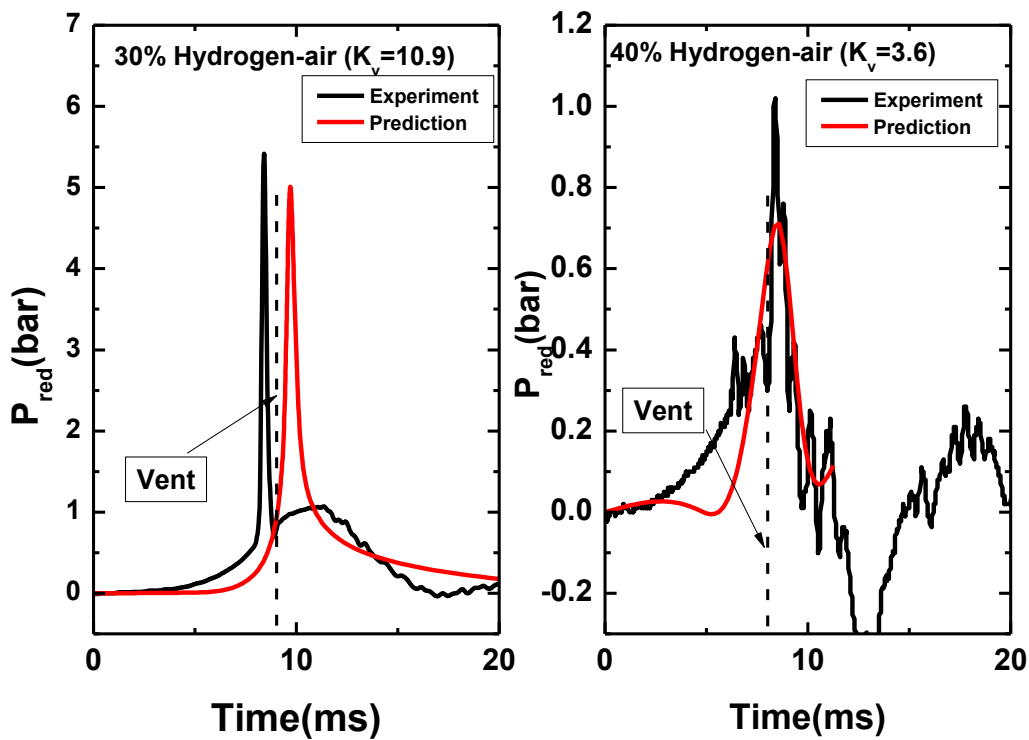
Figure 8.9 Experiment and predicted pressure-time profile for hydrogen-air mixture
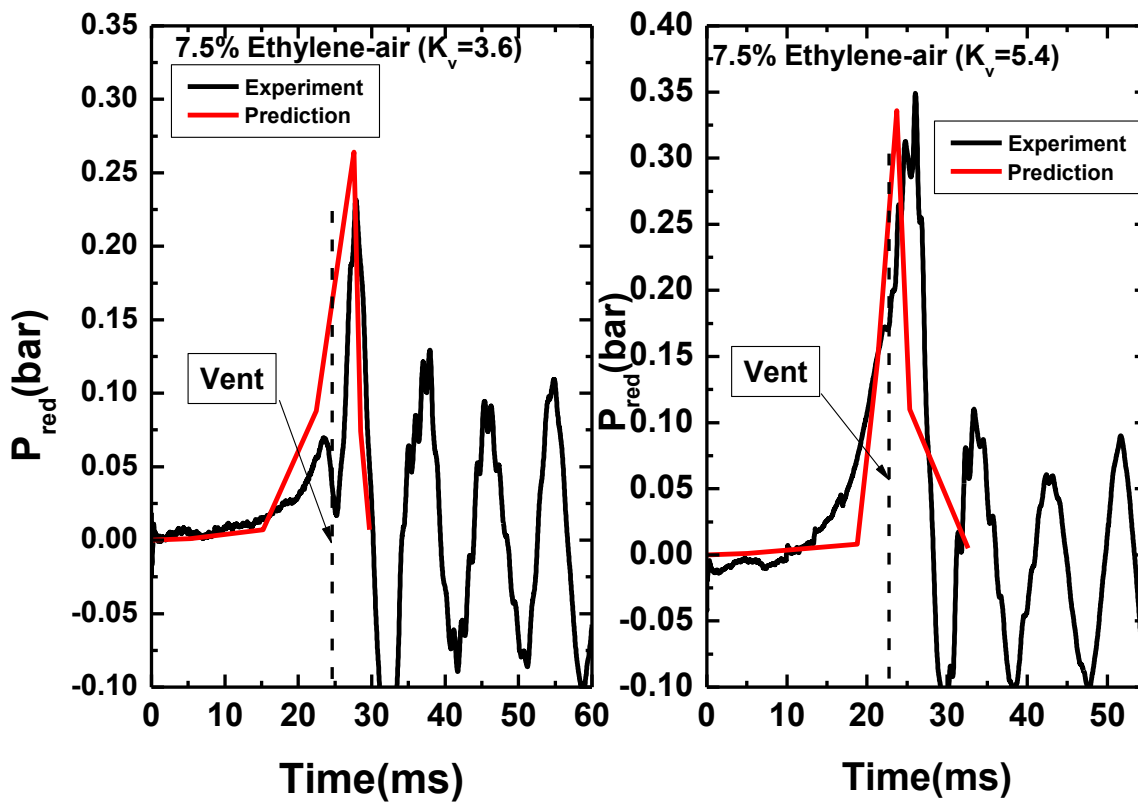
Figure 8.10 Experiment and predicted pressure-time profile for Ethylene-air mixture

8.5 Maximum explosion reduced pressure and effect on maximum flame area

Most current vented explosion data in relatively large explosion vessels cannot be predicted using laminar flame propagation models, without including an empirical turbulence factor to make theory and experiments match. However, part of the flame acceleration may be the self-acceleration of laminar flames over the large distances involved in large explosion vessels. The generation of flame acceleration due to turbulence created in the venting process should not change significantly with vessel size. The present work uses a small 10L explosion vessel with an L/D of 2.8 with small flame propagation distance to the vent so that self-acceleration of the flame should be small or eliminated (Kasmani et al., 2010b). Comparison with laminar flame theory of venting is made to show that turbulence factors are not necessary, as the measured results for open vent explosions are less than those predicted by laminar flame theory. The laminar flame theory assumes a worst case flame area equal to the vessel wall area. US design standards for gas venting are based on compact vessel venting where L/D<5 and in European standard it is L/D<2 and the present L/D is between these values.

8.5.1 Free Venting Theory

There are two different approaches to explosion vent modelling suggested in the literature (Kasmani et al., 2010b). In both cases the maximum flame area A_f is required to be known at the point of the maximum overpressure. Runes (1972) introduced the assumption that the maximum possible flame area is the surface area of the vessel, A_s (Runes, 1972). However, this should give an over prediction of the mass of unburned gas flow rate, as the flame area is almost never equal to the surface area of the vessel at the point of maximum pressure. In the present work the term Δ_a has been introduced, which is the flame area as the fraction of the surface area of the vessel that gives agreement between theory and measurement, with no other turbulence or self-acceleration factors.

The first approach to the prediction of the unburned gas mass flow rate assumes that the maximum vent overpressures occurs when the consumption of unburned gas is at its maximum and this is equal to the mass burnt rate at the flame front (Molkov, 2001a) as given in equation 8.2.

Vent maximum unburned gas mass flow rate, $m_b = U_L \Delta_a A_s$ [8.2]

The second approach as shown in equation 8.3 (Bradley and Mitcheson, 1978a, Runes, 1972) assumes that the maximum vent overpressure occurs when the vent unburnt gas flow rate through the vent is at a maximum and that this is equal to the maximum unburnt gas displaced flow by the flame front (Molkov, 2001a).This is given by:

Vent maximum unburnt gas mass flow rate,

$$m_b = S_g \Delta_a A_s = m_b = U_L \Delta_a (E-1) A_s$$ [8.3]

where U_L = laminar burning velocity, Δ_a = actual laminar flame area at the maximum overpressure / A_s, A_s = surface area of the vessel, Sg=velocity of the unburnt gas ahead of the flame, ρ_u= unburnt gas density (1.2 kg/m^3), E_P = the constant pressure expansion coefficient, where the Stoichiometric value of E_P is 7.5 for methane, 8.1 for propane and 7.9 for hydrogen.

This second assumption assumes that the flame propagates as a sphere in a spherical vessel and all the unburned gas is expelled before the flame exits the vent. The first assumption essentially assumes that there is no flame expansion driving the unburned gas forward, this occurs once the flame is outside the vent and all the expansion is outside and the laminar flame propagates into unburned mixture inside the vessel with continuous expansion of unburned gas outside the vent.. Reality is somewhere between these two extremes and in the present work the second mass flow is used with the flame area correction term Δ_a, to give agreement between the predicted and measured overpressures and is the flame surface area at the maximum overpressure as a fraction of the vessel surface area. This second approach gives a higher predicted unburned gas mass flow rate through the vent and a higher overpressure is predicted, which is in closer agreement with experimental measurements than the predictions using the first method (Kasmani et al., 2010b).

The overpressure due to the maximum flow rate of unburnt gas through the vent, assuming free venting, can be obtained from the orifice plate flow equation for the vent (Kasmani et al., 2010b).This is summarised in equation 8.4 as:

$$m_{bmax} = A_{f\,max} U_L \rho_u = \beta U_L \Delta_a (E-1) A_s = C_d \beta A_v (2 \rho_u P_{red})^{0.5}$$ [8.4]

Where ε = expansibility factor, which is the deviation of compressible flow from incompressible flow for an orifice plate, which is about 0.8 for near sonic flow and 1 for incompressible flow. This factor cannot be predicted and has been experimentally measured for orifice plate flow metering, which will apply here. The vent flow cannot be treated as a nozzle as has been done in most work on venting. The term, C_d = the orifice plate discharge coefficient, which is 0.61 for large K_v or small vents and about 0.75 for small K_v or large vent areas. Other parameters A_v = vent area, m^2, P_{red} = reduced pressure or overpressure in Pa (N/m^2), β = Turbulence enhancement factor such that the turbulent burning velocity $U_T = \beta U_L$. This resulted to equation 8.5.

$$A_v/A_s = \beta U_L \Delta_a \rho_u{}^{0.5}(E-1)/(C_d \beta \varepsilon 2^{0.5} P_{red}{}^{0.5}) \qquad [8.5]$$

Taking the vent gas compressibility factor ε=1, Cd=0.61 and $\rho_u = 1.2$ kg/m^3 for the incompressible flow, then Equation 8.5 becomes A_v/A_s=1.27 Δ_a U_L (E-1) $P_{red}{}^{-0.5}$. Furthermore, considering the vessel volume V in relation to the surface area A_s given as A_s=$C_2 V^{2/3}$, this gives:

$$\frac{A_v}{V^{\frac{2}{3}}} = \Delta_a C_1 C_2 P_{red}{}^{-0.5} = 1/K_v \qquad [8.6]$$

Where $1/K_v = A_v/V^{2/3}$ and the K_v is the vent coefficient of the vessel based on the vent area, C_1= 1.27βU_L (E-1) , C_2 is a constant that is $A_s/V^{2/3}$ and is 4.84 for sphere, 6 for a cube and 5.54 for a cylinder with an L/D of 1, 5.81 for an L/D of 2 and 6.21 for an L/D of 3.

8.5.2 Experimental Results Compared With Laminar Flame Venting Theory

The laminar flame venting theory or free venting theory discussed in detail in chapter 7 was shown to over predict the overpressure for all vent coefficient (K_v) from this 0.01m^3 (Fakandu et al., 2011, Kasmani et al., 2010b). The experimental vented overpressure results are shown as a function of K_v in Figure 8.11a. The data is compared with the predictions of Equation 8.6 with β=1 and $\Delta_a = 1$. The results are less than those predicted by Equation 8.6 for laminar flames for small vent areas but agree with the current result for large vent areas (low K_vs). Also the experimental results are below the predictions of Swift and Bartknecht There was good agreement with Bradley and Mitcheson predictions with a β=1 and the present

prediction, but both were above the experimental results. This was not the conclusion found when Equation 8.6 is compared with other vented experimental results for large volume vessels and a β of between 3 and 5 is normally required to get agreement (Andrews and Phylaktou, 2010, Bradley and Mitcheson, 1978a, Swift, 1989).The difference in the experimental results in Figure 8.11a with the laminar flame predictions from Equation 8.6 can be used to compute a value for the flame area factor Δ_a.
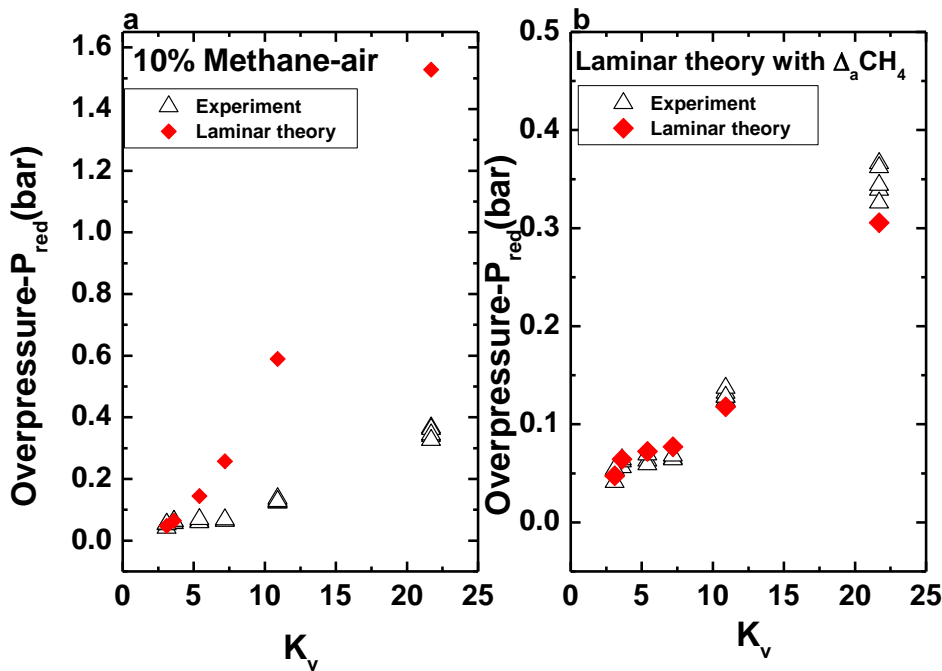
Figure 8.11 Laminar theory flame with Δa for 10% Methane-air

This is shown in Figure 8.11b as a function of K_v for methane-air explosions, the computed factor is given in Table 8.1 for all gases. The agreement of the theory in Equation 8.6 with the experimental data from the present 10 litre vented vessel explosions is shown in Figures 8.11-8.13 for methane, propane and ethylene. These results show that when the vessel is small enough for laminar flame to exist throughout the vented explosions then the laminar flame area is less than A_s but the predictions of laminar flame venting are well supported. It is clear that the higher overpressures recorded in larger vented explosions is due to an increase in the flame reactivity, most likely due to self acceleration rather than turbulence.This shows that at low K_v the maximum flame area is closer to the surface area of the vessel at the peak overpressure, but at higher K_v the flame area is a smaller fraction of A_s. This is evident from Figure 8.11a, 8.12a and 8.13a where large vent areas (low K_v) the predictions agree closer to the experimental result, while the flame area gets small as

the vent area reduces or K_V increases irrespective of the gas mixture. Additionally this indicates that at small K_v with high vent velocities the flame is accelerated towards the vent and does not propagate to the vessel wall at the same rate it propagates towards the vent.
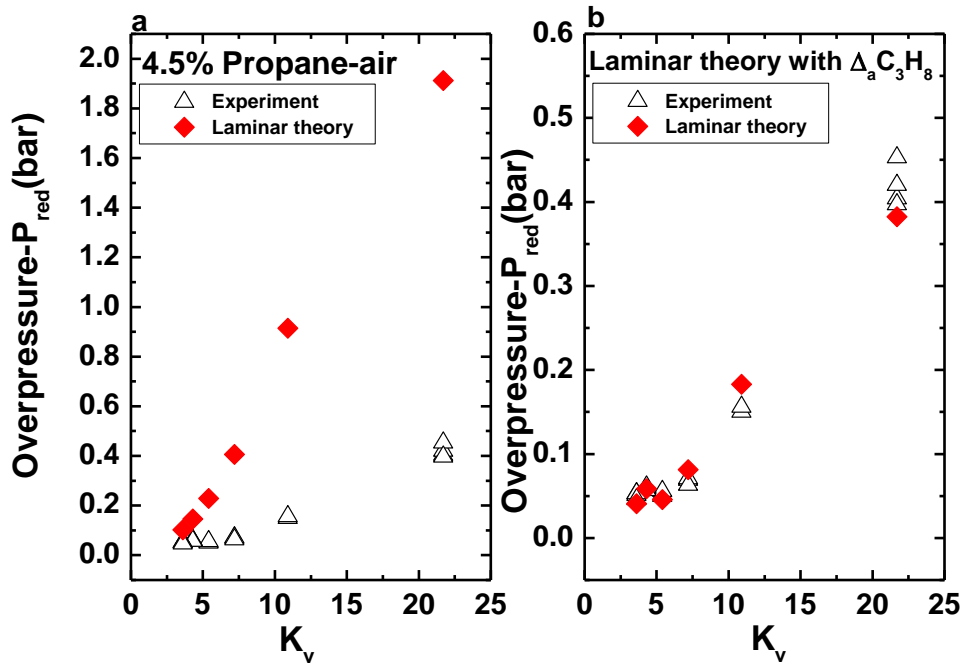
Figure 8.12 Laminar theory flame with Δa for 4.5% Propane-air

Table 8.1 Summary of Δa for different gas mixtures

Kv/Gas-air	CH4	C3H8	C2H4
Kv=21.7	0.2	0.2	0.3
Kv=10.9	0.2	0.2	0.5
Kv=7.2	0.3	0.2	0.3
Kv=5.4	0.5	0.2	0.5
Kv=3.1-3.6	1	0.4	1

The values of Δ_a in Table 8.1 were used to force the experimental data to agree with the Equations 8.6 as shown in Figures 8.11b and 8.12b together with equivalent values and new predictions made. Based on the current result for 10% methane-air and 4.5% propane-air as presented above, Equation 8.7 and 8.8 were derived for Δ_a which can used in Equation 8.6 for the prediction of the result for the current vessel for. Equation 8.7 is the factor for 10% methane-air (Δ_m) while Equation 8.8 for 4.5

propane-air (Δ_p). These equations are yet to be validated with other experimental results, and other factors including turbulence associated with vent opening pressure or obstacles and self acceleration of flames should be considered carefully when applying this factor.

$$\Delta_m = 1.654 K_v{}^{-0.51} \qquad\qquad\qquad\qquad [8.7]$$

$$\Delta_p = 1.083 K_v{}^{-0.403} \qquad\qquad\qquad\qquad [8.8]$$

The agreement of the theory in Equation 8.06 with the experimental data from the present 10litre vented vessel explosion is shown in Figures 8.11-8.13 for methane, propane and ethylene. These results show that when the vessel is small enough for laminar flame to exist throughout the vented explosions then the laminar flame area is less than A_s but the predictions of laminar flame venting are well supported. It is clear that the higher overpressures recorded in larger vented explosions is due to an increase in the flame reactivity, most likely due to self-acceleration rather than turbulence. In future work self-acceleration experimental and theoretical data will be examined as a means of enabling the β factor in Equation 8.6 to be interpreted as a self-acceleration factor. The role of turbulence induced upstream of the vent by the action of the vent flow is likely to be low. Additionally, validation of Equation 8.7 and 8.8 is necessary for application for all vented vessels with all factors incorporated in future work.
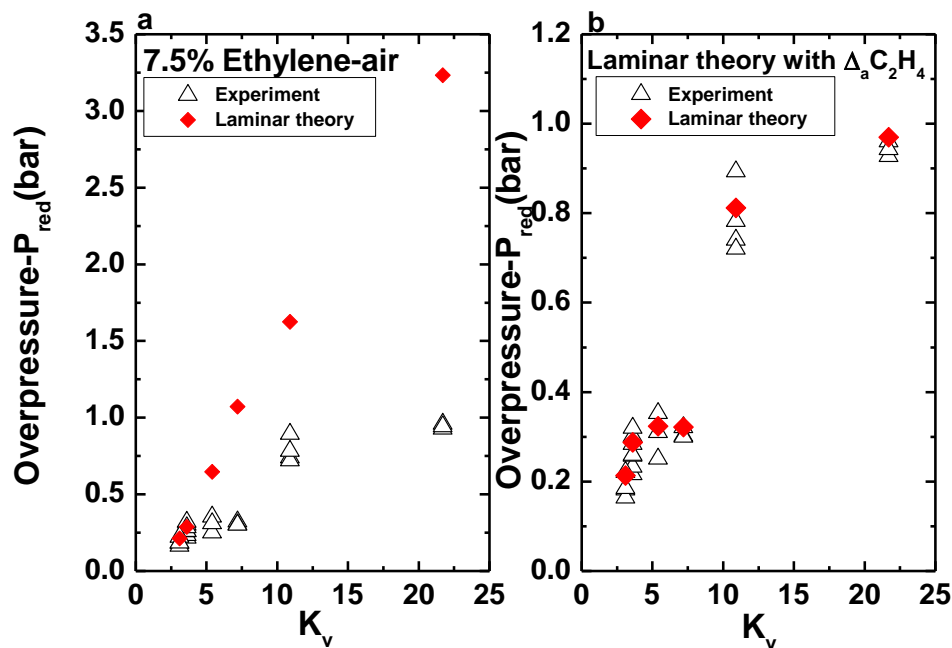
Figure 8.13 Laminar theory flame with Δa for 7.5% Ethylene

8.6 Conclusion

1.   A 0.2m^3(200L) test geometry of L/D of 2 was used for vented explosion for different gas mixtures. The vessel was initially intended to increase the 10L vessel 20 times its size for further analysis on volume effect. The results showed unexpected high maximum overpressure for low K_v caused by the attached vessel connecting the test vessel with the dump vessel. This high overpressure showed have very good agreement with the result of Bartknecht (1993) and the only result shown to agree with his result so far. There is strong indication that floor level of connecting vessel and ground level in Bartknecht experimental were responsible for this high overpressures at low K_v. For high K_v>7.2, a realistic and similar result were obtained which has no agreement with Bartknecht(1993) data. The reason for such high overpressure for high K_v in Bratknecht's result can still not be explained. Hence, there is the need for more studies on attached vessels to vented vessels to give better understanding in this new finding.

2.   The conventional laminar flame venting theory has been extended to include the flame area as a proportion of the vessel surface area, Δ_a. The use of a small 10 litre vented explosion vessel with an L/D of 2.8 was shown to enable laminar flame venting to be achieved so that β=1. Δ_a was determined for methane, propane and ethylene at their maximum reactivity. This is the first time that a turbulence factor β was not required to give agreement between experimental data and laminar flame venting theory. The results show that the flame is accelerated towards the vent from the spark and only part of the mixture has been burned inside the vessel when the flame emerges from the vent and this decreases as K_v increases. Peak overpressure occurs when the trapped unburned gases in the vented vessel burn after the flame has left the vent. This is not taken into account in the laminar flame model, which assumes that all the unburned gas is expelled through the vent before the flame exits the vent. It would therefore be more correct to take Δ_a as a corrected for deviations of the all the assumptions in the theory from reality.

3.   Vented explosions are shown to have a peak pressure that is controlled by the external flame. Very high external jet flame speeds were measured and these were shown to predict the external overpressure using Taylors equation. This should be the basis of vent design procedures for the prediction of the external explosion overpressure.

CHAPTER 9

Vent Static Burst Pressure Influences on Explosion Venting

9.1 Introduction

9.2 Vent Static Burst Pressure and the maximum overpressure

9.3 Vent Design Procedures for the Influence of P_{stat}

9.3.1 Review of Investigations into the Impact of P_{stat} on P_{red}

9.3.2 Relationship between P_{stat} and P_{burst}

9.3.3 Influence of P_{stat} on P_{red} at low, medium, and high K_v

9.4 P_{red} as a function of P_{stat}

9.5 Influence of mixture reactivity on P_{red} and P_{stat}

9.6 Flame speed

9.7 Conclusion

9.1 Introduction

Vented explosion was carried without vent cover for K_v = 3.6-21.7, in order to determine the influence of vent area on peak overpressures for for different gas mixtures as reported in the previous chapters. The aim was to allow for free flow propagation of flame without any obstruction as result of flame self acceleration or turbulence as a result of bursting of the vent cover. When covers are used the peak pressures generated depends on the strength of the vent cover, vent area, combustible mixture, and initial conditions (Bauwens et al., 2010, Bradley and Mitcheson, 1978a, Cooper et al., 1986, Kasmani, 2008b). These factors including the static burst pressure of the vent material (P_{stat}) affects the overall pressure obtained in a vented explosion (P_{red}). In other vent design correlations the ratio of P_{burst}/P_{stat} is assumed to be constant, such as 1.5 by Rasbach et al. (1976) and Cubbage and Simmonds (1957). In NFPA 68 (2013) P_{stat} has to be $<P_{red}$, which is impossible for practical vent covers at low K_v, and also shown not to be true for large vent areas (Nagy and Verakis, 1983).

In this chapter, the overpressure generated in a 10L cylindrical vented vessel with an L/D of 2.8 was investigated, with end ignition opposite the vent, as a function of the vent static burst pressure, P_{stat}, from 35 to 450mb. Three different K_v ($V^{2/3}/A_v$) of 3.6, 7.2 and 21.7 were investigated for 10% methane-air and 7.5% ethylene-air and 40% hydrogen-air. It was shown that the dynamic burst pressure, P_{burst}, was higher than P_{stat} with a proportionality constant of 1.37. For 10% methane-air P_{burst} was the controlling peak pressure for $K < \sim 8$. This was contrary to the assumption that $P_{red} > P_{burst}$ in the literature and in EU and US standards. Literature measurements of the influence of P_{stat} at low K_v was shown to support the present finding and the work reported in this section is aimed at providing additional data on the influence of P_{stat} in gas explosion venting.

9.2 Vent Static Burst Pressure and the maximum overpressure

The prediction of the maximum overpressure, P_{red}, required for the design of explosion vents (Bradley and Mitcheson, 1978a, Bradley and Mitcheson, 1978b, Razus and Krause, 2001) does not have a specific methodology for predicting the effect of the vent static burst pressure, P_{stat}. The explosion venting theories also have

empirical constants, often referred to as turbulence factors, to make the predictions higher than experimental data with a vent static burst pressure. It is usually assumed that the effect of P_{stat} is included in these empirical turbulence factors. The US NFPA 68 (2013) gas vent design standards for P_{red} <0.5 bar has no procedure to account for the influence of P_{stat}, but does require for P_{red} <0.1 bar that $P_{stat} > P_{red} -$ 0.024 bar and for P_{red} >0.1 bar that P_{stat} <0.75 P_{red}. The literature and the present work show that these limitation cannot be complied with as the vent burst pressure, P_{burst}, is always greater than P_{stat} by a $30 - 50\%$ due to materials being stronger under dynamic load that static load, as discussed in detail in A.6.3.2 of NFPA 68 (2013). In the European standards for gas venting (2007) Bartknecht's approach (1993) to the influence of P_{stat} is followed as discussed in more detail later. This is valid for $P_{stat} > 0.1$ bar and has P_{red} linearly increasing as P_{stat} increases with this applying at all K_v and all mixture reactivities. For P_{stat} <0.1bar the European standard (2007) has no design recommendations, in spite of this being an important area of vent projection. Clearly these two vent design standards are incompatible.

Vent design correlations and design standards normally predict the maximum explosion overpressure (P_{red}) without giving considerations to the individual pressures peaks associated with physical phenomena in explosion venting. The literature shows that there are different pressure peaks associated with different events in explosion venting (Cates and Samuels, 1991, Cooper et al., 1986, Harris, 1983, Marshall, 1977, Molkov, 2001b, Runes, 1972, Swift, 1989, Yao, 1974). This was discussed in more detail n chapter 4 of this thesis.

When a vent cover is used, the magnitude of the vent opening pressure depends on the type of vent material used and the vent area. The pressure associated with the bursting of the vent material is referred to as the dynamic pressure (P_{burst}) in this work, while P_{stat} is the static burst pressure from tests where compressed air pressure is slowly increased until the vent cover bursts (NFPA 68, 2013). The difference is because materials are stronger under dynamic short pressure pulse loading than they are under slow static pressure loading, as detailed in NFPA 68 A.6.3.2 (2013). In some vent design procedures (Bartknecht, 1993), the ratio of P_{burst}/P_{stat} is ignored and the influence of P_{stat} is always to increase $P_{red.}$ In spite of its importance, therefore this work aimed to provide more data with better instrumentation of the venting process, so that the physics of the action of P_{stat} could be determined.

9.3 Vent Design Procedures for the Influence of P_{stat}

Only the European vent design procedures (2007) have a procedure for accounting for the influence of P_{stat} on P_{red} and this used the correlation of Bartknecht (1993) given in Equation 9.1, who investigated P_{stat} in a 1 m^3 vessel. Bartknecht's (1993) results are shown in Figure 9.1. The lowest P_{stat} investigated was 0.1 bar and often there are requirement to use lower values than this and these are explored in the present work. Figure 9.1a for 10% methane-air shows that the influence of P_{stat} was strongly dependent on K_v and there was only a linear relationship between P_{red} and P_{stat} at the low K_v of 3.3. In Figure 9.1b the P_{stat} effect is given for a K_v of 3.3 for different mixture reactivities. However, there were no experiments at different mixture reactivity apart from at P_{stat} of 0.1 bar and the data in Figure 9.1b was an assumption that the P_{stat} trend for methane would be the same for the other mixture reactivities. This assumption has been carried through into the EU gas venting standards, without informing the user of the standard that the assumption has not been verified. Also, the linear relationship between P_{red} and P_{stat} that Figure 9.1a shows, only occurs at the low K_v of 3.3 but is applied in the EU standard
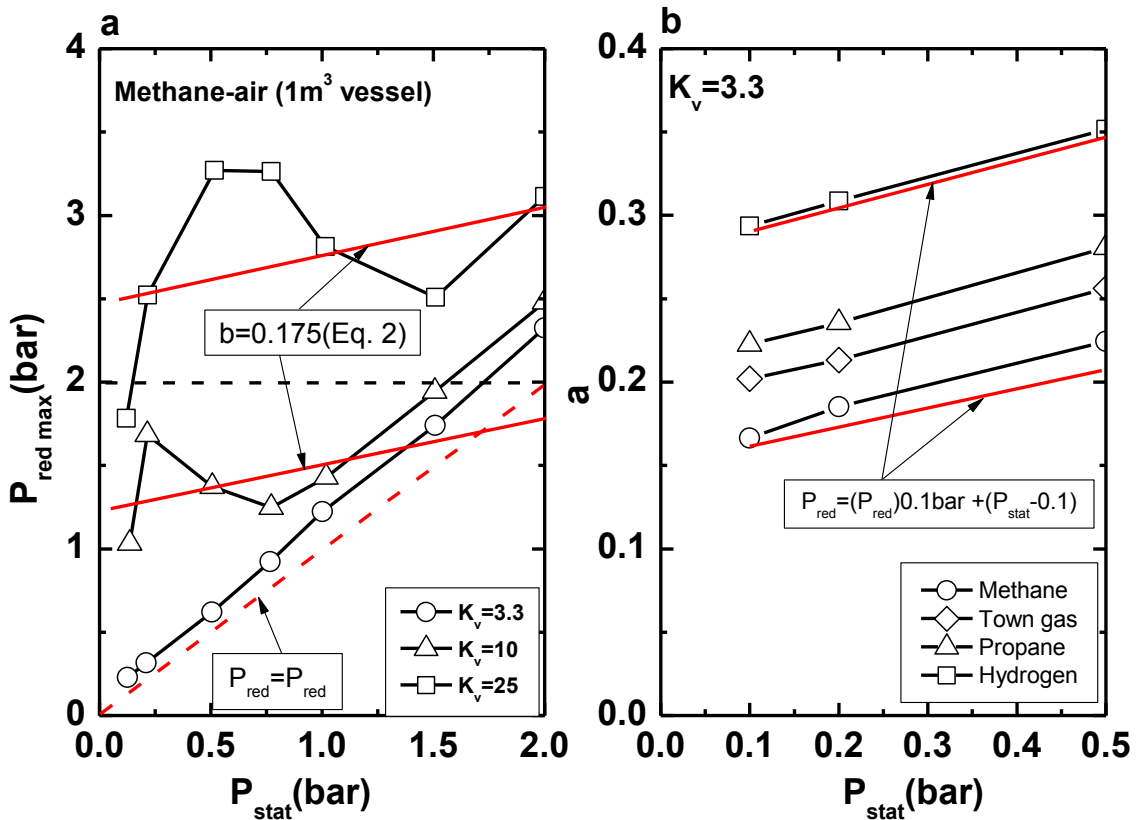
Figure 9.1 Pred as a function of P_{stat} for a 1 m^3 vessel for 10% methane-air

$$\frac{1}{K_v} = \left[\frac{0.1265 log_{10} K_G^{-0.0567}}{P_{red}^{0.5817}} + \frac{0.175(P_{stat}-0.1)}{P_{red}^{0.5717}}\right] \qquad [9.1]$$

for all K_v, which is invalid but there is no mention of this in the EU standard. Equation 9.1 is stated by Bartknecht to be valid up to a P_{red} of 2 barg and P_{stat} of 0.5 bar, with no limit on K_v. Comparison of Equation 9.1 for a K_v of 10 in Figure 9.1 shows that it is valid only up to a P_{stat} of 0.2 bar and not applicable for higher values of K_v, due to the P_{red} limit of 2, Equation 9.1 may be simplified to Equation 9.2 using two significant figures on the constant, as they are not known to the precision implied in Equation 9.1.

$$\frac{P_{red}^{0.57}}{K_v} = a + b(P_{stat} - 0.1) \qquad [9.2]$$

The constant 'a' was evaluated by Bartknecht in a 10 m^3 cubic vented vessel with a P_{stat} of 0.1bar, for methane and propane as 0.164 and 0.200 respectively for a range of K_v from 2.2 to 10. For hydrogen a 1 m^3 vessel was used with 'a' evaluated as 0.290, although this value cannot be correct as it implies hydrogen is only 45% more reactive than propane, whereas the ratio of burning velocities is at least 7 (Fakandu et al., 2012). The use of a different volume for the vented vessel for hydrogen was the problem. The reactivity term in Equation 9.1 is based on a correlation of these values for 'a' with Bartknecht's values for the mixture reactivity K_G measured in a 5L sphere, 55 bar m/s for methane, 100 for propane and 550 for hydrogen.

These problems with Bartknecht's correlation of the P_{stat} and his limited data set, has led to the US venting standards abandoning this approach (NFPA 68, 2013), although it is continued within the European gas venting standard. In NFPA 68 (2013) there is no procedure to account for the influence of P_{stat} for P_{red} <0.5 bar. For 0.1 bar< P_{stat} < 0,5 bar NFPA 68 (2013) requires that P_{stat}<0.75 P_{red} or P_{red}/P_{stat} > 1.33, unfortunately this ratio is exceed by the dynamic burst pressure effect discussed in NFPA 68 (2013) in section A.6.3.2. For 0<P_{stat}<0.1 bar NFPA 68 (2013) requires that P_{stat}< (P_{red} − 0.024bar). It will be shown in the present work that these design rules are difficult if not impossible to comply with for low K_v with relatively high P_{stat}, as P_{stat} dominates P_{red} and P_{burst} is the dynamic burst pressure which is > P_{red} and this is not allowed in NFPA 68. This shows that this new NFPA 68 approach to the P_{stat} effect on vent design present design is also not compatible with experimental data. There is clearly a need for further research and more experimental data on the influence of P_{stat} in vent design and this work was

undertaken to try to provide more data with accompanying interpretation of the physics involved.

9.3.1 Review of Investigations into the Impact of P_{stat} on P_{red}

Cubbage and Simmonds (1955) showed in Equation 9.3 that the P_{burst} overpressure peak was linearly dependent on the inertia of the vent cover(Cubbage and Simmons, 1955).

$$P_{busrt} = cw + d$$ [9.3]

where "c" and "d" are constants and "w" is the weight of the material divided by the area. If w is in kg/m^2 then this can be converted to a static pressure as wAg Pa, where A is the area of the vent cover. Equation 9.3 shows that the P_{stat} pressure was additive to the term 'd' which was related to K_v and U_L. Rasbash (1969) determined Equation 9.4 for the pressure generated in cubic vented explosions using data from his studies of propane-air in small vessel(Rasbash, 1969). Equation 9.4 implies that the influence of K_v is additive to that of P_{stat}. Another way of looking at this type of correlation is that for a free venting with $P_{stat} = 0$ the K_v term is that measured for free venting and P_{stat} is simply an additive pressure to that for free venting. The present results will be shown not to support such a P_{stat} effect.

$$P_{red} = 1.5 P_{stat} + 0.5 K_v$$ [9.4]

Cubbage and Marshall (1972) also correlated the pressure developed in a vented explosion and took the P_{stat} term as additive to the term taking into account the influence of K_v and U_L(Cubbage and Marshall, 1972). They had no multiplier of P_{stat}, similar to that in Equation 9.4, and essentially assume that the dynamic burst pressure was the same as the static burst pressure.

The influence of P_{stat} by various investigators is shown in Figure 9.2 for K_v of 1.72 and 3 and in Figure 9.3 for K_v of 4 and 6. On each graph the line for $P_{red} = P_{stat}$ is shown in bold. For most of the data for $K_v < 4$ P_{red} is close to P_{stat}, with some results below P_{stat}, probably due to an error in the measurement of P_{stat}. For $K_v > 4$ there is evidence of P_{red} being higher than P_{stat}. The present results will show agreement with these results, that P_{stat} determines the overpressure up to a critical value of K_v when there is an additive term that is a function of K_v and U_L.
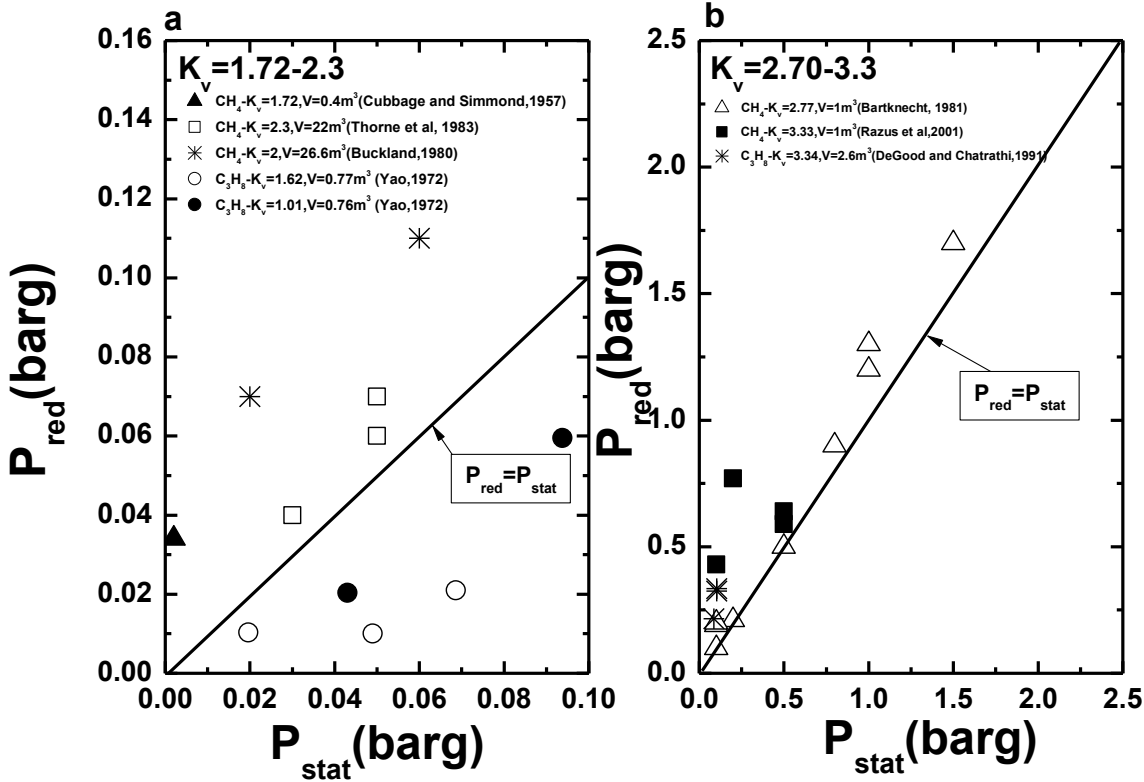
Figure 9.2 P_{stat} verses P_{red} for methane-air and Propane-air (a) K_v=1.72-2.3 (b) K_v=2.7-3.3
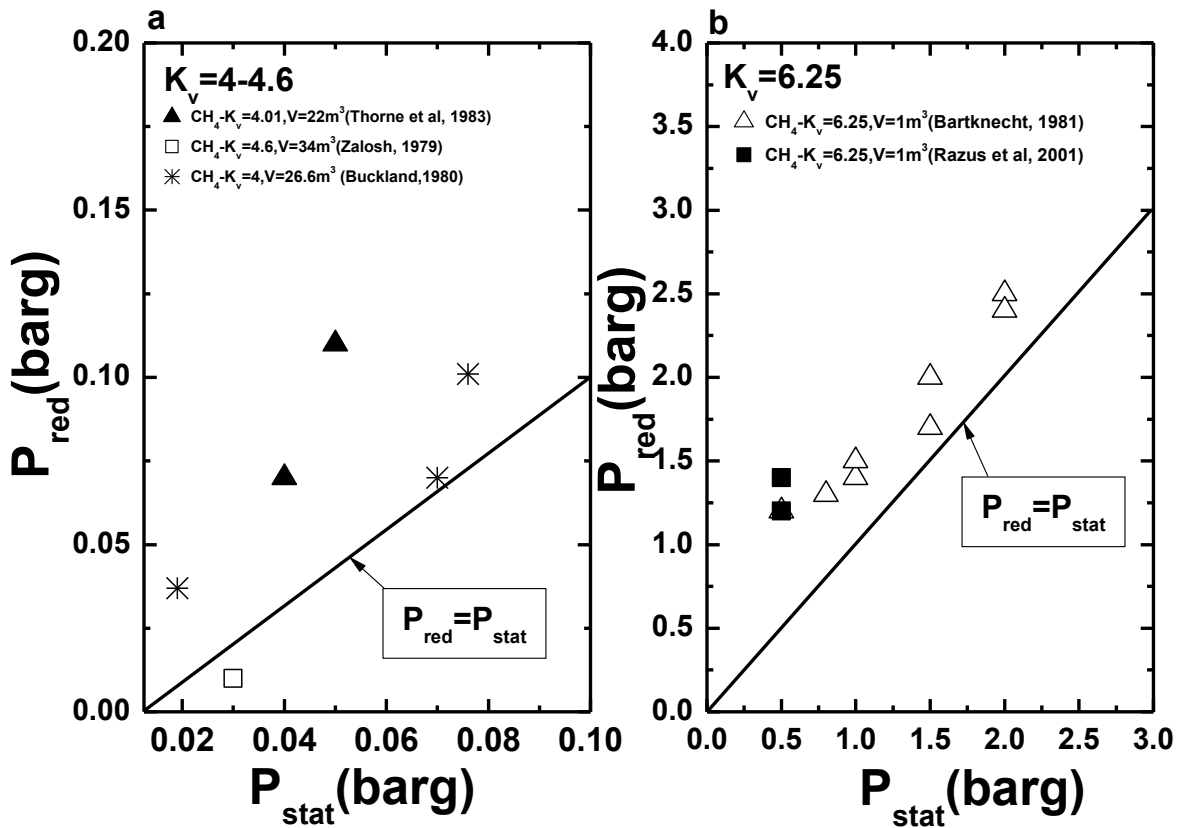
Figure 9.3 P_{stat} verses P_{red} for 10% methane-air (a) K_v=4-4.6 (b)K_v=6.25

9.3.2 Relationship between P~stat~ and P~burst~

Figure 9.4a compares the measured P_{burst} as a function of P_{stat}. The results show close agreement with the P_{burst}/P_{stat} constant of 1.5 in Equation 9.4, as shown in Figure 9.4b. The line of best fit to the present results is given in Equation 9.5.

$$P_{burst} = 1.37 P_{stat} \hspace{4cm} [9.5]$$

Most empirical correlations, as in Equations 9.01-9.04, above assume that the first pressure peak in the pressure time record must be less than the maximum reduced pressure obtained during explosion venting (Cubbage and Marshall, 1972, Rasbash et al., 1976, Rasbash, 1969). In NFPA 68 P_{red} (either P_{fv} or P_{ext}) has to be always greater than P_{burst}, which is impossible for practical vent covers at low K_v.
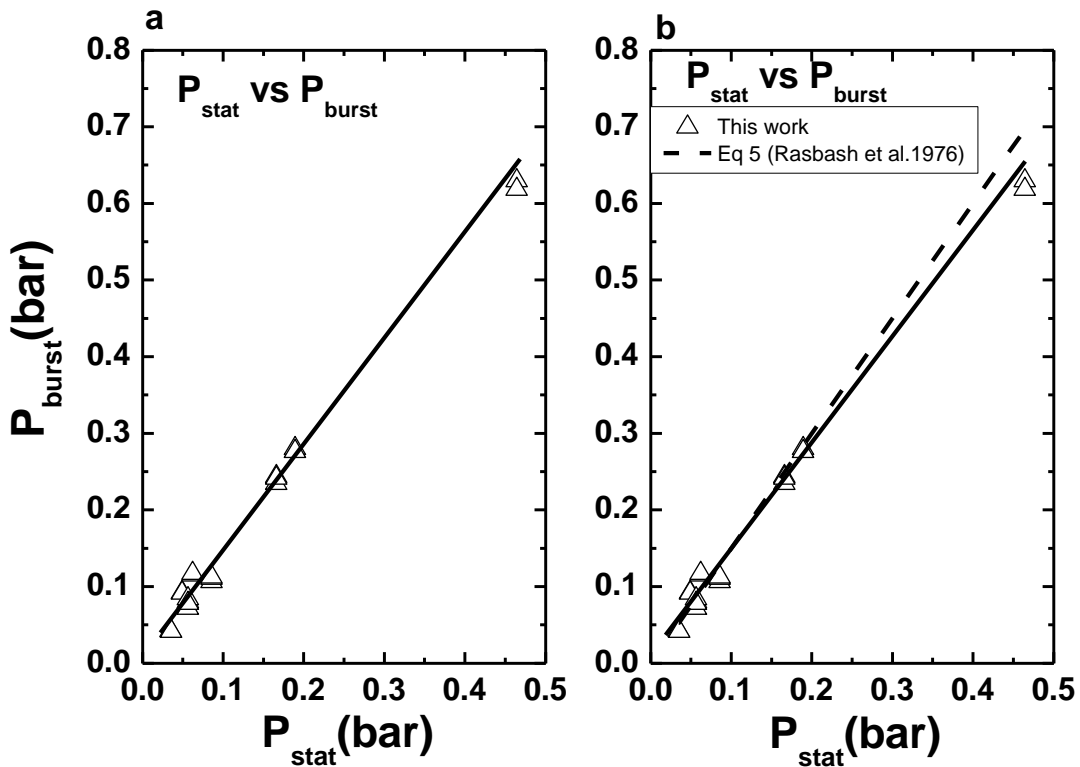
Figure 9.4 Relationship between P_{burst} and P_{stat} for K_v=1-21.7

9.3.3 Influence of P~stat~ on P~red~ at Low, Medium, and High K~v~

The results in Figure 9.5a for P_{stat} = 0.035 bar and K_v of 3.6 show that for low K_v, P_{red} is determined by P_{stat} for 10% methane-air. For the free vent Figure 9.5b shows that P_{red} was controlled by the external explosion at 0.05 bar and it was identified as an external explosions because the peak pressure occurred after the flame had passed thermocouple T_4 at the vent plane. With a P_{stat} of 0.035 bar Figure 9.5a shows that

the P_{burst} was 0.043 bar and the external overpressure was reduced to 0.04 bar, so that P_{burst} was the controlling factor in $P_{red.}$ Figure 9.5b shows that for free venting the pressure due to the flow of unburned gas through the vent was 20mb. With the 35mb P_{stat} the flame took longer to reach the vent compared with free venting. This was because there was no flow towards the vent when it was closed and hence the initial flame spread was slower than for free venting. When the vent burst due to the closed vessel pressure rise, there was then an outflow of unburned gas through the vent and the pressure initially falls. After the vent burst the fall in pressure was so fast that it created a vacuum and this induced a reverse flow of unburned gas back into the vessel. The flame propagation inside the vessel was continuing and the flame expansion pushed unburned gas out of the vent.
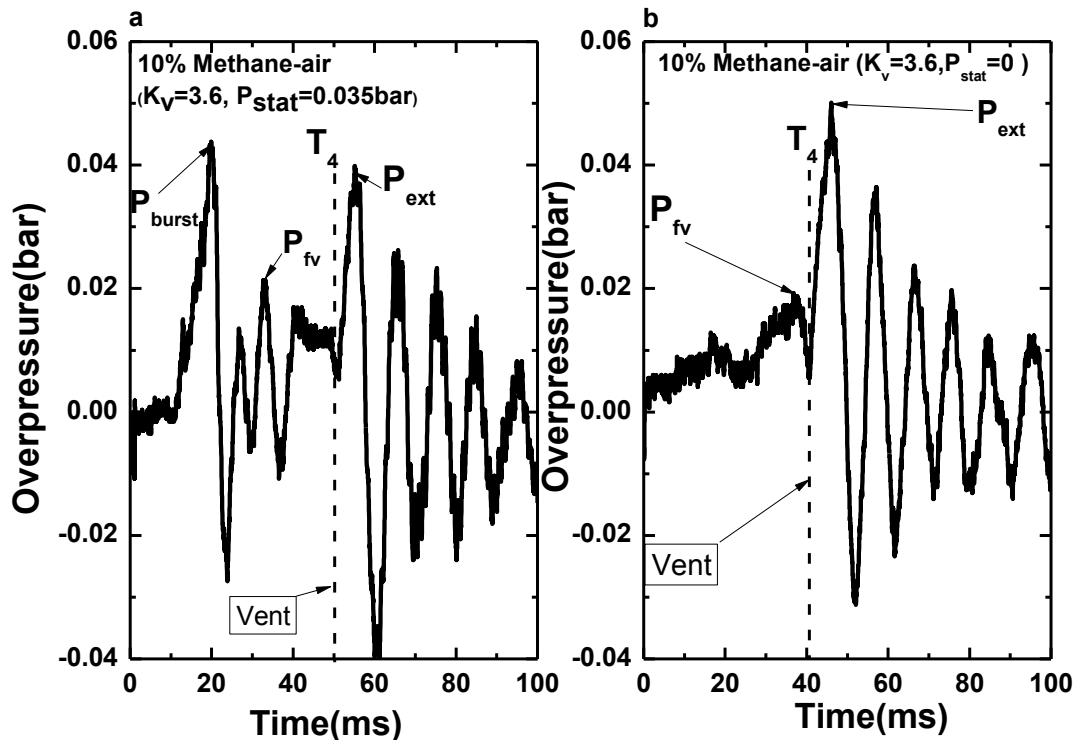
Figure 9. 5 Peak pressures for 10% methane-air with large vent area and a P_{stat} of 0.035bar

The pressure loss on the vent bursting sets off a pressure and flow oscillation and this considerably slowed the progress of the flame to the vent. The P_{fv} peak occurred on an oscillation before the flame reached the vent and was lower than for free venting. This resulted in lower external jet turbulence and a lower external overpressure. The net result was that P_{red} was lower for the vent with the bursting cover than for a free vent, as shown in Figure 9.5.
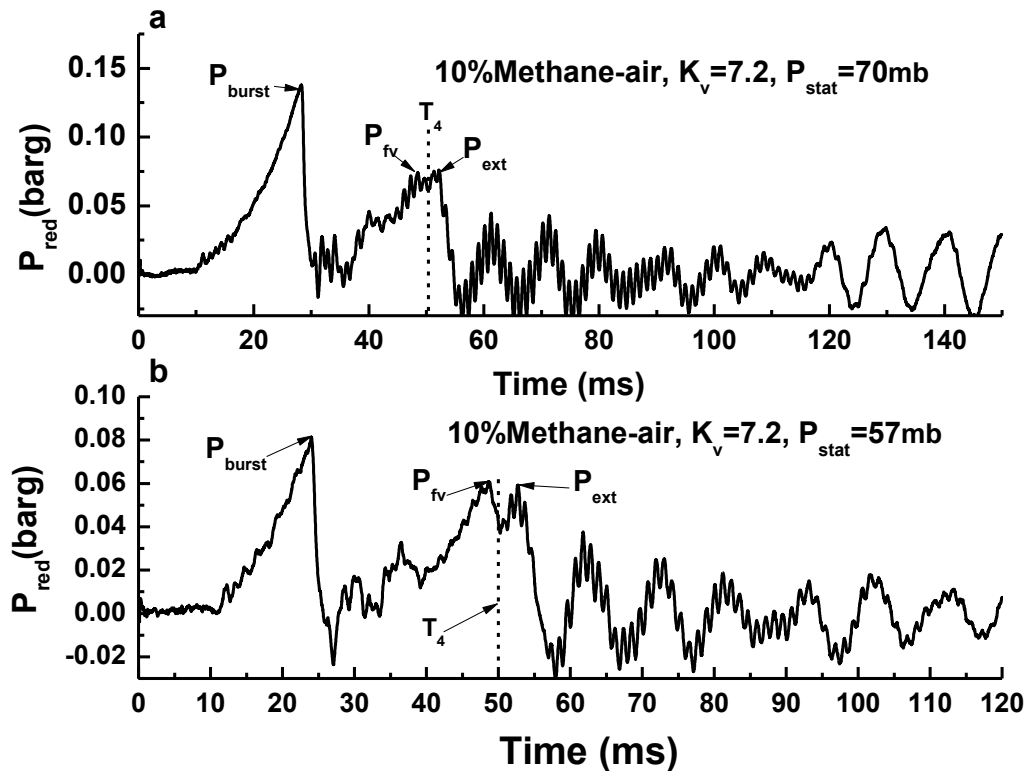
Figure 9.6 Peak pressures for 10% methane-air with (a) P_{stat} =70mb (a) P_{stat} =57mb

The PT0 pressure-time record for 10% methane-air for K_v=7.2 and P_{stat}=70mbar is shown in Figure 9.6a and for a P_{stat} of 57 mb in Figure 9.6b. The results in Figure 9.6b are directly compared with those for free venting in Figure 9.7. These results all shows that for P_{stat} of 57 and 70 mb at K_v of 7.2 P_{red} is still controlled by P_{burst}, as it was at K_v = 3.6 with P_{stat} = 35 mb in Figure 9.5. Figure 9.6a shows that P_{burst} is 135mb and occurs 28ms after ignition, well before the flame emerges from the vent at 50ms. The P_{fv} and P_{ext} pressure peaks are very similar at 75mb, but occur just before and just after the flame emerges from the vent. Similar events occur in Figure 7b with 57mb P_{stat} where the vent bursts at 24ms with P_{burst} of 80mb. The flame arrives at the vent at 50 ms with the P_{fv} and P_{ext} pressure peaks either side of this time with P_{fv} slightly higher than P_{ext} at 61mb compared with 59mb. For free venting the flame arrives at the vent at 52ms, only 2ms later than with the vent covers. The peak overpressure is P_{fv} at 61mb the same as for the P_{stat} = 57mb P_{fv}. With a vent cover the initial flame propagation inside the closed vessel is slower than with free venting. Once the vent bursts this accelerates the flame and creates more turbulence in the external jet. The net result is that the time to reach the vent is very similar for free venting and with a vent cover. Also Figure 9.8 shows that once the vent bursts the subsequent events are very similar to those for free venting. Free venting

overpressures increase with K_v (Bartknecht, 1993, Fakandu et al., 2011, Fakandu et al., 2012, Fakandu et al., 2013) and so there will be a value of K_v at which the P_{burst} is not the dominant overpressure.
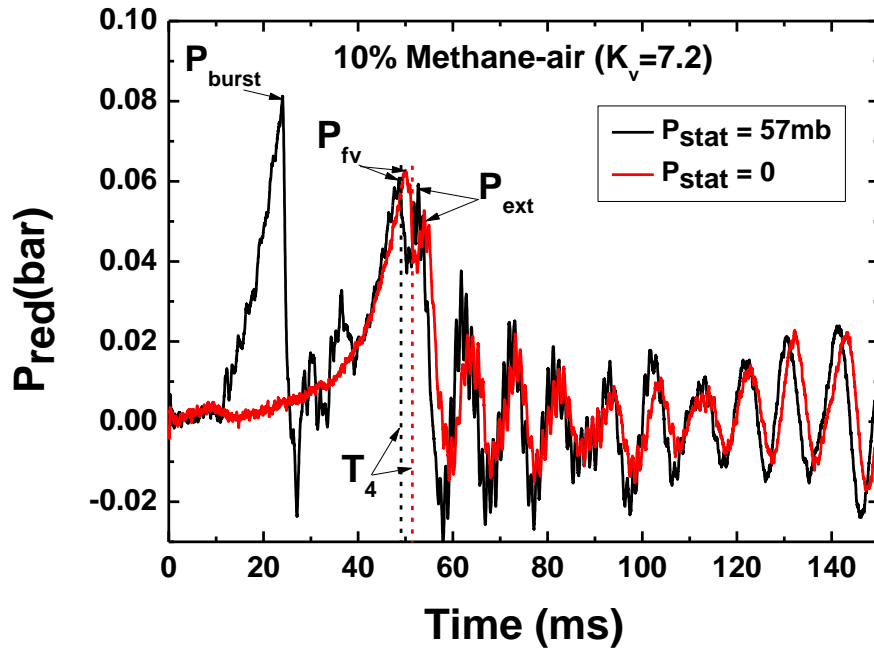
Figure 9.7 Comparison of the pressure time records for 10% methane-air for K_v = 7.2 for free venting and for P_{stat} = 57mb
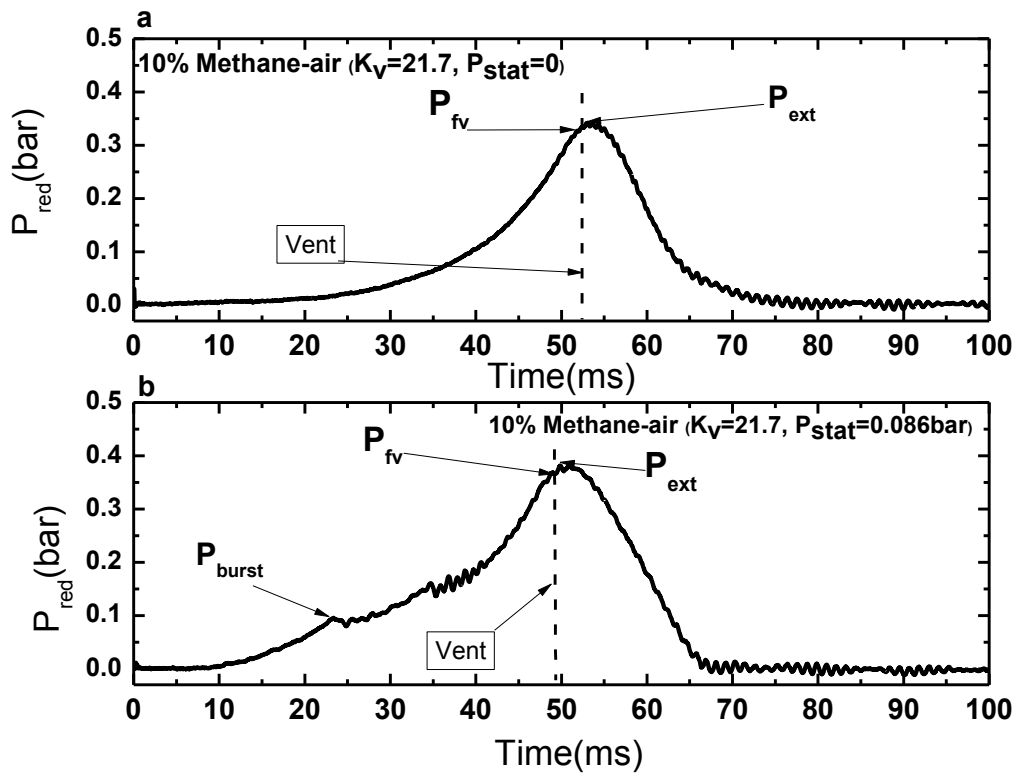
Figure 9.8 Pressure v. time record for 10% methane-air with a K_v = 21.7 (a) free venting and (b) P_{stat}= 86mb

This is illustrated in this work at a K_v of 21.7 in Figure 9.8. For a free venting Figure 9.8 shows that P_{red} was 0.35 bar and was due to the flow through the vent P_{fv}, although the pressure peak occurred at the same time as the flame reached the vent. With a P_{stat} of 0.086 bar the P_{burst} was 0.1 bar and occurred after 24 ms, but P_{red} was much higher at 0.39 bar which is only 0.04 bar above that for free venting. Both pressure peaks occurred at a similar time of 50ms coincident with the flame passing through the vent.

9.4 P_{red} as a Function of P_{stat}

Figures 9.9 and 9.10 show P_{red} as a function of P_{stat} for K_v of 3.6, 7.2 and 21.7, with Figure 9.9a concentrating on the present data for $P_{stat} < 300mb$ and Figure 9.10 comparing the work with the results of other workers for similar K_v. The main result from Figure 9.9 is that P_{red} was controlled by P_{stat} for a K_v of 7.2 or lower, but that at a K_v of 21.7 the flow through the vent controlled P_{red} and the P_{stat} effect was lower, but still significant. Figure 9.10 concentrates on the data for $P_{stat} < 300mb$. This shows, as discussed above, that for K_v of 3.6 the initial influence of P_{stat} up to 50 mb was to reduce P_{red} below that of free venting and at P_{stat} of about 100mb P_{red} was close to that of free venting. This effect was due to the reduced flame speed upstream of the vent. At a K_v of 7.2 this effect was still present, but the reduction was small and the net effect was to have very little influence of P_{stat} on P_{red} up to P_{stat} of 150mb, the limit of the values tested at this K_v.
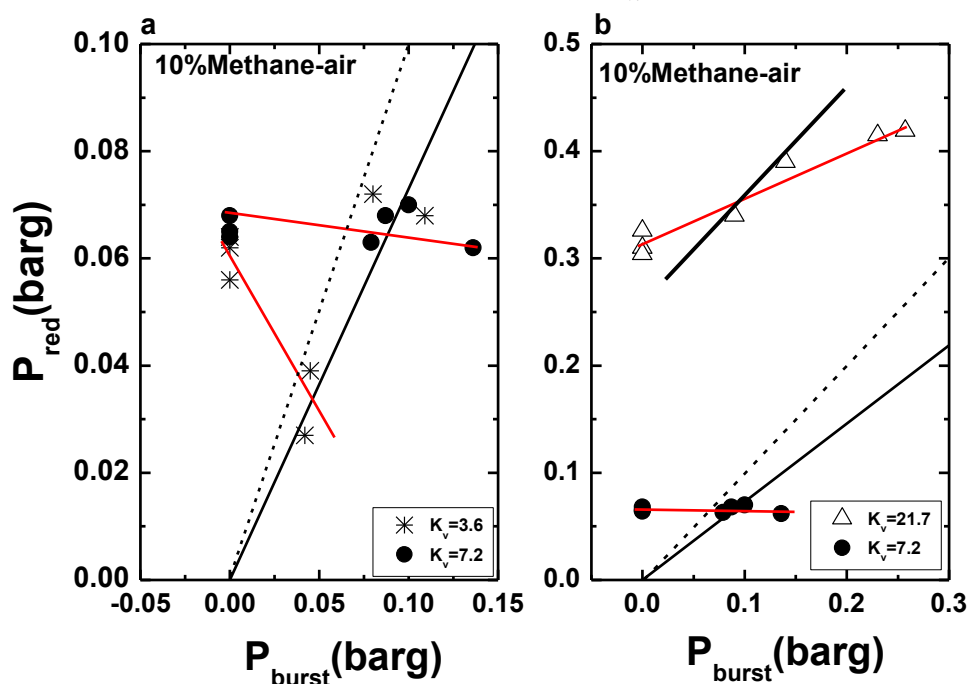
Figure 9.9 Peak pressures as a function of P_{burst} for K_v = 3.6, 7.2, and 21.7 for low P_{burst}

The present results are compared in Figure 9.10 with others in the literature as P_{red} as a function of P_{stat} for a range of K_v. Figure 9.10 shows a linear relationship between P_{stat} and P_{red} for high $K_v=21.7$, which is below that for simple additive effect of P_{stat} similar to the result of Bartknecht (1981). The evidence of the present work and of the literature on the influence of P_{stat} is that for $Kv < {\sim}8$ P_{burst} dominates P_{red} and there is no effect of K_v. For $K_v > {\sim}8$ P_{red} is dominated by P_{fv}. Further work is needed to define the critical K_v more precisely and to investigate the influence of the mixture reactivity. Figure 9.10 shows that the data of Copper et al. (1986) for a K_v of 8.8 agrees with the present results that P_{red} is determined by P_{stat}. The results of Bromma (1967) also agree with the present work that P_{stat} determines P_{red} at low K_v.
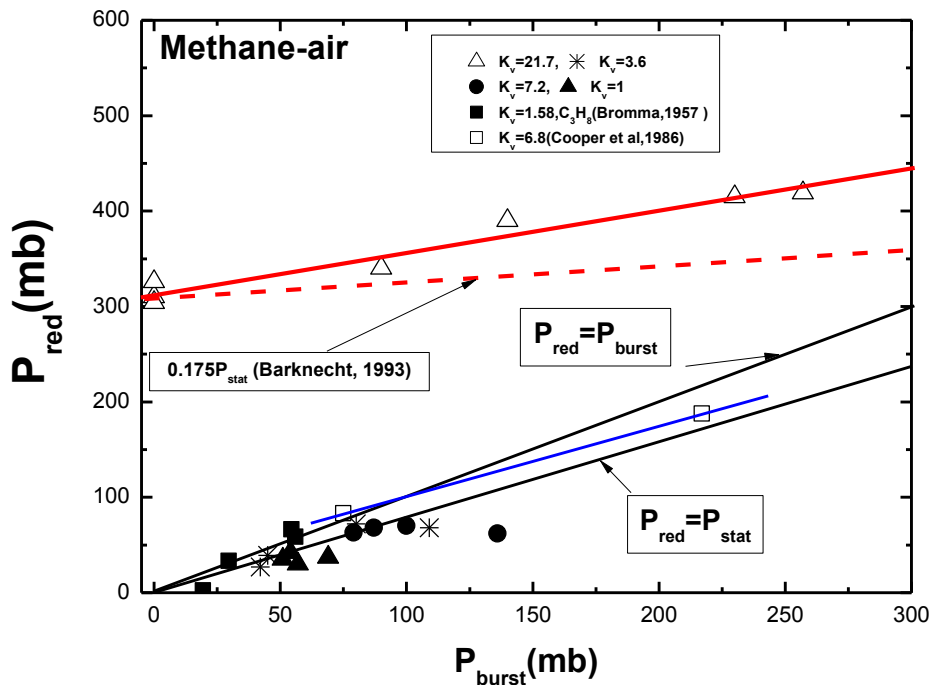
Figure 9.10 eak pressures with Pburst for different Kvs. The dashed line is the 0.175 Pstat constant in Equation 8.01

9.5 Influence of Mixture Reactivity on P_{red} and P_{stat}

When more reactive mixture of 7.5% methane-air was used, the higher combustion rate as well as high propagation rate shows clearly the difference between the covered and initially uncovered vents. Figure 9.11 shows the pressure-time for 7.5% ethylene-air for a small K_v(large vent area) with a P_{stat} of 35mb. For this vent area, the P_{ext} is the controlling peak pressure for both free venting and covered vent which is similar to result of 10% methane-air for the same vent size in Figure 9.5. It is clear from Figure 9.11 that the free venting pressure reached the vent faster when

compared with the covered vent. In the presence of the closed vent in the early part of the flame travel slows the flame and this results in a lower flame speed approaching the vent once it bursts than would apply for an open vent. This also reduces the impact of the external explosion, resulting to lower P_{red} for the covered vent. When Figure 9.11 is compared to the Figure 9.5 with large vent area, Figure 9.11 and Figure 9.12 supports the assumption in the current European standards where $P_{red} > P_{stat}$ even for large vent areas. The high reactive nature of ethylene and hydrogen-air flame jets, are responsible for higher pressure downstream the vent higher than the P_{stat} when compared to methane or propane-air mixtures. However, the use of higher P_{stat} with large vent area for 7.5% ethylene-air may still give similar result to methane-air as motioned earlier. Figure 9.12 shows that flame was slowed down as it approaches the vent with the vent cover as compared to that of free venting from result of PT1 and PT0 in Figure 9.12a and 9.12b respectively. The result for PT0 shows that the free venting pressure profile with higher maximum pressure as compared to that with initial vent cover. This is similar to the result obtained with 7.5% Ethylene-air, but with much higher enhancement on burning rates and overpressure. However, it can be concluded that P_{stat} has no or negligible effect on all vent areas for 40% hydrogen-air as a result of the high reactive nature, as most of the maximum pressure are in the sonic irrespective of the vent area as discussed in the previous chapter.
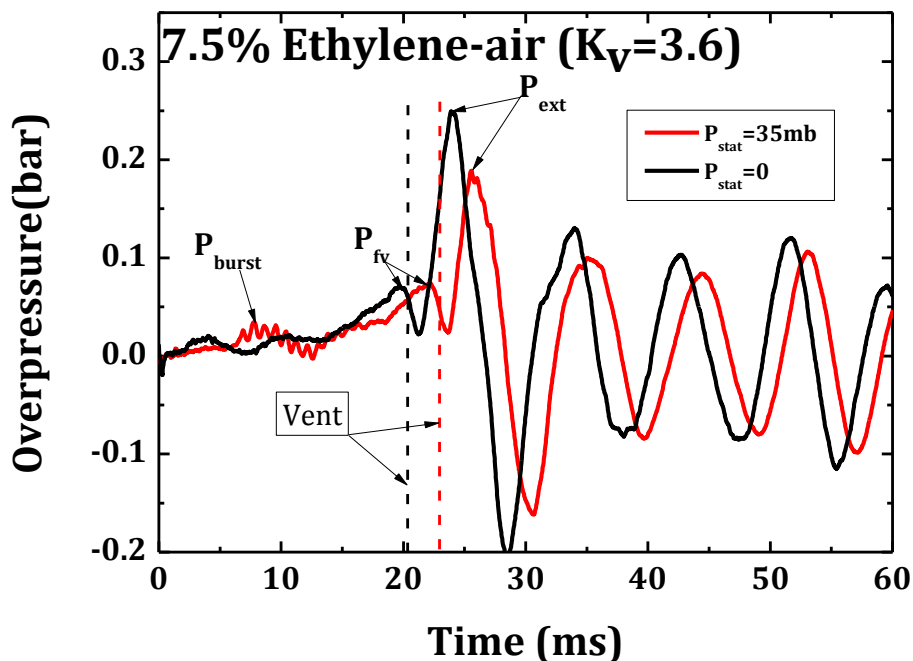
Figure 9.11 Peak pressures for 7.5% Ethylene-air with large vent area and a P_{stat} of 0.035bar
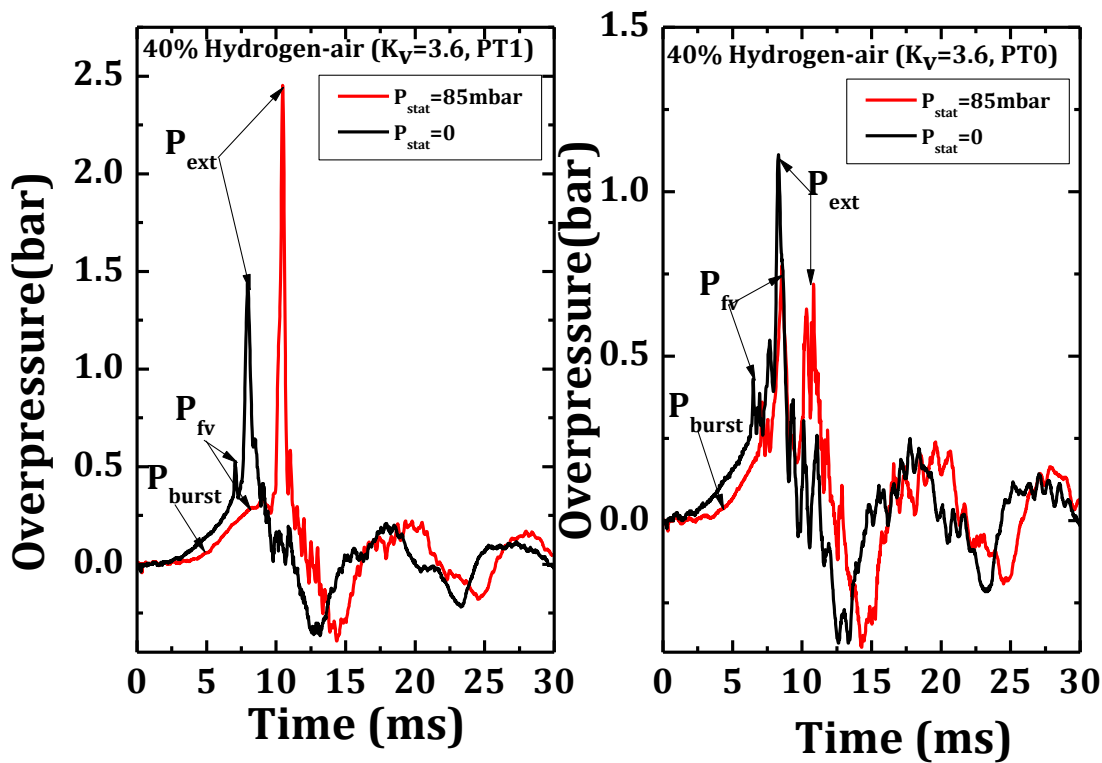
Figure 9.12 Peak pressures for 40% hydrogen-air with large vent area and a P_stat of 0.86bar

9.6 Flame Speed

The centre line flame speed was measured along the flame propagation path within the test vessel and immediately after the vent. With free venting, a maximum flame speed of 28.8m/s was achieved upstream as compared to that with vent covered with 22.7m/s as the flame approaches the vent as shown in Figure 9.13a for 10% methane-air. With the covered vent, the flame propagates at constant rate similarly to the confined explosion before the vent opening pressure was reached, thereby slowing down the flame as compared to the initially open vent. This is similarly to the flame speed of more reactive mixture of 7.5% ethylene-air with maximum upstream flame speeds of 77m/s and 71.9m/s for free venting and covered vents respectively. These high flame speeds upstream for free venting are responsible for higher downstream flame speeds when compared with the covered vents. Figure 9.13b shows maximum downstream flame speed of 195.2m/s compared to 124.2m/s for free venting and covered vents respectively. This higher flame speeds translates and in agreement with the higher P_{ext} observed with the pressure-time profile in Figure 9.11 for ethylene-air and Figure 9.5 for methane-air mixtures.
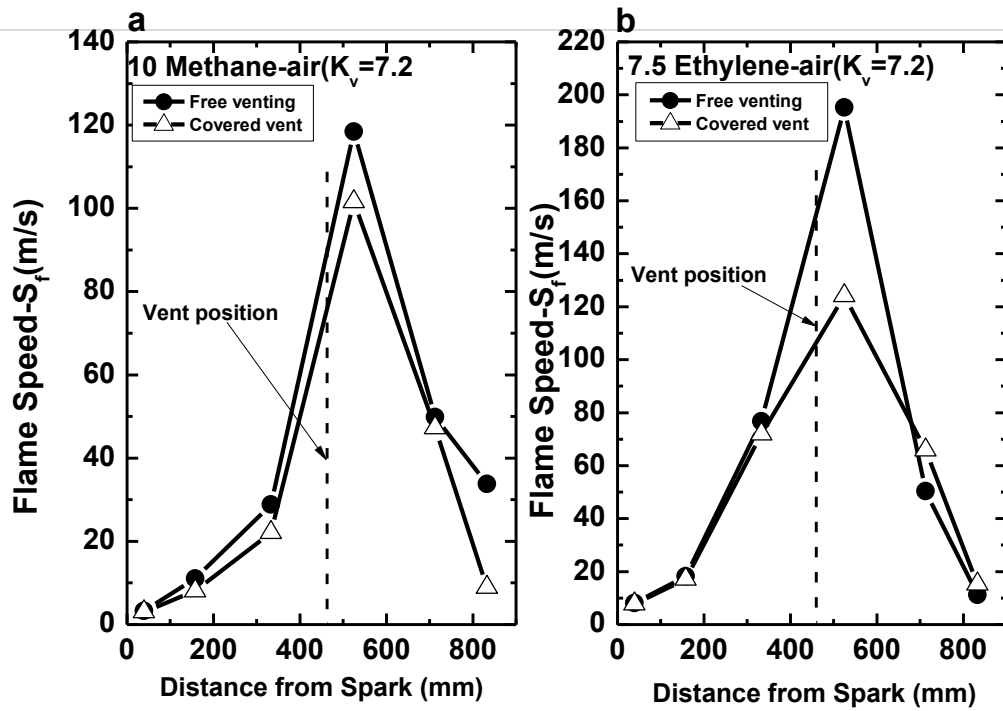
Figure 9.13 Flame speed as a function of distance from spark for
(a) 10% methane-air (b) 7.5% ethylene-air

9.7 Conclusion

1. Current vent design guidance in Europe is incompatible with the experimental data of Bartknecht and of the present work for low K_v. Bartknect's data and the present work show that for $K_v < \sim 8$ P_{stat} determines P_{red}. The US NFPA 68 (2013) guidance is impossible to comply with as P_{red} is determined by P_{stat} and their requirement that P_{red} is always greater than P_{stat} cannot occur at low K_v. The data of Cooper et al. (1987) and Bromma (1967) in larger volume vented vessels support this conclusion.

2. The critical K_v is > 9 and <21.7 and it is recommend that at present $K_v = 9$ should be used as the critical K_v, but more work is required to determine this more precisely and to investigate the influence of mixture reactivity and vessel size. Bartknecht's data for $K_v = 10$ shows that this is beyond the critical condition as P_{red} is significantly higher than P_{stat}, but with a non-linear dependence on P_{stat}.

3. For K_v greater than the critical value P_{fv} controls P_{red} and the influenced of P_{stat} is reduced and can be predicted from free venting correlations with an additive term for the P_{stat} effect that has a constant greater than that in Equation 9.1 at 0.5. The flame speed for explosion with initially covered vent was shown to lower when covered to free venting. This is responsible for higher downstream flame speeds as well as P_{ext} for free venting as compare to the initially covered vent.

CHAPTER 10

Conclusions and Recommendation for Future Work

10.1 Conclusions

10.2 Recommendations for Future work

10.3 Final remarks

10.1 Conclusions

1.   The venting design standards of the USA and Europe have been shown to be incompatible. Both state that a range of vent designs factors do not influence the overpressure that are shown in the present work to be significant. These design factors include: the spark position, the vent location, the number of vents, and the shape of the vent.

2.   It was shown that agreement between the two design standards and experimental results, other than those on which the European standards are based, is poor. Bartknecht's (1993) data on which the European gas venting standard is based had a 0.1bar static burst pressure, but this does not account for the high overpressures that were measured, relative to other data using similar or larger volumes. The review of data in this thesis showed that no one has ever been able to reproduce this data, using larger and smaller vessels. The present work on the 0.2 m^3 of 0.5m diameter with a 0.5m diameter short outlet duct was shown to give overpressure close to those of Bartknecht, but still lower. It was concluded that the presence of a solid surface relatively close to the vent outlet, but at least a few vent diameters away, was increasing the venting overpressure. In Bartknecht's case the explosion vessel were mounted on the ground and were not elevated and this could give a coanda effect that caused the vent external explosion to attach to the ground, resulting in a higher external overpressure. The distance of the ground to the edge of the vent would be an installation effect with significant influence on the overpressure and this should be in the design standards. More work is required in this area.

3.   The new NFPA 68 (2013) standard uses the laminar burning velocity approach rather than the deflagration parameter, $K_G = dP/dt_{max}V^{1/3}$, used in the European standard (2007) and in older editions of NFPA 68 (NFPA 68, 2007). The literature review of venting data in Figure 7.01 shows that the new NFPA method gives better agreement with experimental results. However, there is a wide variation in overpressures measured in experimental results and many results that are higher than the new NFPA 68 predictions. There is clearly a need for a better understanding of the combustion aerodynamics of the venting process.

4.   The laminar flame theory was shown to include a key assumption that the maximum pressure occurred at the maximum flame area inside the vessel, which was assumed to be when the flame touched the wall , where the flame area was assumed to be the internal surface area of the vessel, A_s. It was shown that most current vented explosion data in relatively large explosion vessels can be predicted using laminar flame propagation with the flame area is A_s assumption. This is the reason for the inclusion of A_s in the US NFPA 68 (2013) standard. However, it was shown in this work that A_s was directly related to $V^{2/3}$ with the constant of proportionality varying from 4.84 for a sphere, 6 for a cube, 5.54 for a cylinder with L/D=1 and 5.81 for L/D = 2.

5.   An important feature of the present work was to determine if the maximum explosions overpressure occurred when the flame touched the walls as was due to the maximum flame surface area and thus maximum mass burning rate. A thermocouple, T_3, was fitted on the centreline of the vessel at about 1mm from the wall in line with the centre part of the vessel. The results showed that in most cases the peak overpressure occurred well before the flame arrived at the wall. The fractional area of the flame relative to the vessel surface area was determined and it was shown that putting a factor of 0.6 at low K_v to 0.15 at high K_v. Cates and Samuels (1991) in their laminar flame venting model had assumed a constant shape of the flame at all K_v at the maximum overpressure. An empirical ratio of the flame surface area to A_s as a function of A_v, would enable the peak pressure to be predicted from the laminar venting theory. However, it was considered that the experimental results showed that the assumption that the flame area equalled A_s at the point of maximum pressure was unrealistic physics and an understanding of what caused the peak explosion overpressure was required without arbitrary assumptions.

6.   The difference between laminar flame theory predictions and experimental results often use an empirical turbulence factor to make theory and experiments match and this is particularly the case when predictions are made to match the Bartknecht measurements. In this case turbulence factors in the range of 3 to 5 are often used. This approach falls down in the present work where the predictions are higher than the measurements for free venting. However, part of the turbulence factor may actually be a volume factor with the flame undergoing transition to cellular flame and self-acceleration. The present work used a small vented vessel to

ensure that self-acceleration was unlikely. The laminar flame theory still over predicted the measurements.

7.   There are a range of events in vented explosions that can cause a peak in the pressure time record. Each event was illustrated in chapter 4 with an explosion pressure record where each pressure is the maximum overpressure. There are six possible causes of the peak overpressure were summarised. In this thesis examples of where each of the peaks caused the peak overpressure has been given. In many vented explosions all six pressure peaks may be present and which one is the maximum overpressure, P_{max} or P_{red} depends on K_v, K_G, P_{stat} and the ignition position. The six pressure peaks were numbered from 1-6 in the order that they normally occur in vented explosions in previous work but have been given a more descriptive nomenclature in the present work as summarised in this work and compared with the terminology used by other investigators.

8.   An important aspect of the explosion venting technique is the prediction of the vent area required to reduce the explosion severity to as low as possible. The current research has demonstrated that for $K_v < 7.2$, the P_{ext} dominates while $K_v \geq 7.2$ P_{fv} is the controlling peak pressure for most hydrocarbon mixtures. The initial flame upstream the vent and within the vessel was shown to propagate at the spherical flame speed for the first 80mm for methane, propane and the ethylene-air mixtures. The maximum flame speed upstream of the vent was shown to increase as K_v increased due to the higher velocity of unburned gas through the vent, which acted as a suction flow on the flame. However, the sidewards spread of the flame was decreased and the time to reach the wall thermocouple T_3 increased. An increase in K_v also increased the flame speeds downstream of the vent due to the higher jet velocities caused by the faster flame upstream of the vent.

9.   It was shown that at low K_v the peak overpressure occurred after the flame had left the vent and before the flame reached the wall (arrived at T_3). In this case it was shown that the peak explosions occurred due to the external explosion outside the vent. This was the explosion in the dispelled unburned gases by the upstream explosion. Turbulence is created in these external gases due to the flow through the vent and a gas external turbulence flame speed arises of >100 m/s. The overpressure from Taylor's theory for these fast external flame speeds were shown to predicts the

explosion overpressure for low K_v. There was thus a K_v above which the internal explosion was the controlling overpressure and below which the external was the controlling overpressure. This critical K_v was a function of the mixture reactivity and tended to move to higher K_v as the reactivity increased. This was due to the action of the faster internal flame that caused a higher flow of unburned gas through the vent, which resulted in higher overpressures.

10.   The present research was able to demonstrate that single vents generate higher overpressure and flame speed downstream the vent when compared to multiple vents of total equal area, contrary to the statement above. Four or 16 vent openings compared to one (same overall vent area) resulted in a smaller characteristic scale and this reduced the pressure peak due to the external explosion. A small reduction of over 10% was observed for methane-air, and over 30% reductions for ethylene-air is considered significant and attributed to the reduction of the turbulent length in the external explosion.

11.   The effect of non-central vent on the explosion overpressure and flame speed was investigated, as the venting standards have no clear guidance with regard to the vent position. Depending on the vent size, the free flow of flame propagation on the axial line could be disrupted forcing the flame to change direction of propagation path with slower velocity. Changing the direction of propagating flame was shown to significantly affect the overpressure depending on the configuration. In this work central and bottom round vents of the same K_v were shown to have a significant influence on the peak overpressure. The non-central vent was shown to slow down the flame as it propagated towards the vent but at the same time distorts the flame front and hence increases the flame area. For explosions where the upstream flame dominated the overpressure through the pressure loss of the flow through the vent, the effect of the non-central vent was to increase the overpressure as there was more mass burning upstream of the vent and higher flow through the vent. For venting situations where the external explosion was the dominant overpressure with central vents, the overpressure was reduced with non-central vents. This was due to the size of the external cloud being reduced as a consequence of more of the mixture burning upstream of the vent, due to the deflection of the flame travel direction.

12. The vent design standards state that the shape of the vent has little influence on the overpressure and this was shown not to be true in the present work. Square and round vents on the centreline of the vessel were compared under free venting conditions. The impact of the vent shape was mainly on the external explosion and was significant at low $K_v = V^{2/3}/A_v$, with a reduced overpressure for square vents of about 30%. The work was carried out for the most reactive gas mixtures of methane/air and ethylene/air. The effect of the vent shape was greater for ethylene/air and occurred at all K_v tested from 3.6 to 10.9. There were two contributory factors to the effect, the change in the discharge coefficient of the vent and the greater entrainment of external air into square jets, which caused the jet to spread faster and have lower flame speeds and lower external overpressures.

13. Current explosion vent design correlations and guidance are based on an experimental data base of centrally ignited vented tests. This is in agreement with the current research when confined explosion was carried in 10L and 200L cylindrical vessels, as higher overpressure was generated for central ignition as compared to other ignition locations. On the contrary, vented explosions in the same vessel show that far end ignition is more severe when compared to central ignition location. The ratio of the peak explosion overpressure for end and central ignition was found to vary from 1.5 to 5.2, depending on K_v, mixture reactivity, and vessel size. P_{ext} was the dominant cause of the peak overpressures for K_v of 5.4 or lower and P_{fv} was the dominant cause of the overpressure for K_v of 10.9. The results clearly demonstrate that the ignition position relative to the vent is important and that that the highest overpressures are not generated by central ignition, which is the basis of the current vent design correlations. There is therefore a clear need to consider the effects of ignition locations in vent design correlations in order to meet the ATEX directive (European Parliament and Council, 1994) requirement for the worst case conditions to be considered.

14. The available data on vented 40% hydrogen/air explosions was reviewed and shown to be very limited, so the provision of new data in this work considerably expands the available vented hydrogen explosion data. The current design procedures for the protection of explosions using venting is shown to be inadequate for hydrogen-air explosions. New data is presented that indicates that for hydrogen explosions the vent flow are mostly sonic and not incompressible, as is the basis of

current designs. Very fast flames upstream and downstream of the vent are shown to be a feature of hydrogen venting at all K_v. There were significant differences in overpressure measured on the ignition face of the vessel opposite the vent and that on the wall at the midpoint, due to very fast dynamic flame events. The wall position had the highest overpressures for hydrogen, significantly higher than on the end flange and previous experimental investigations may have missed these dynamic flame effects through only measuring the pressure at the end flange.

15.   The form $1/K_v = a\, P_{red}^{-n}$ of the venting design equations of Bartknecht(1993), for P_{stat}=0.1bar, was shown to convert into the same form as in the Swift approach, that is recognised by NFPA 68(2013). This uses the relation between S_u and K_G and between A_s and $V^{2/3}$ For agreement with Bartknecht's results for methane and propane venting the laminar flame venting theory only needs a burning velocity enhancement factor of 2.60 and 2.56 respectively. The theory allows the effect of gas reactivity to be predicted. For the present 10L vented vessel, the theory over predicts the measurements for methane, propane, ethylene, and hydrogen. The higher predicted values were due to the assumption of the maximum flame area being A_s and the actual flame area at the time of maximum overpressure being less than this. The Bartknecht design Equation which is the adopted in the current European standard under predicts the P_{red} for hydrogen in spite of the over prediction for the other gases. In view of this, the approved design procedures for hydrogen explosion venting need revision and more experimental work is required on vented hydrogen explosions.

16.   The current work also carried out explosion venting experiments in a 0.2m^3(200L) cylindrical geometry with L/D=2, in order to study the volume effect with the existing 10L vessel. The overpressure from this vessel was observed to be unexpectedly high for low K_v with for end ignition opposite the vent. This higher overpressure was caused by the vessel extension of the same diameter as the test vessel connecting it to the dump vessel, and this only affects the range of K_v for which P_{fv} was the dominant peak pressure as observed with the 10L vessel. The overpressures were also shown to agree with the Bartknecht's(1993) data for propane and methane for K_v<7.2. However, the data for K_v >7.2 where P_{ext} was the controlling pressure were shown to be unaffected by the vessel extension and far below the data of Bartknecht (1993). In Bartknecht's experiments the vented

vessels were mounted on the ground and the proximity of the vent outlet to the ground was the same as using an enclosure wall in the present work at the same relative position to the vent edge as in Bartknecht's work. These results explain why Bartknecht's results are higher than those of other workers using large volume venting.

17.   When a vent cover was used, it was shown that the dynamic burst pressure, P_{burst}, was higher than P_{stat} with a proportionality constant of 1.37. For 10% methane-air P_{burst} was the controlling peak pressure for $K <\sim 8$. This was contrary to the assumption that $P_{red} > P_{burst}$ in the literature and in EU and US standards. For higher K_v the overpressure due to flow through the vent, P_{fv}, was the dominant overpressure and the static burst pressure was not additive to the external overpressure. Literature measurements of the influence of P_{stat} at low K_v was shown to support the present finding and it is recommended that the influence of P_{stat} in gas venting standards is revised.

18.   Bartknecht's data at low K_v and the present work show that for $K_v < \sim 8$ P_{stat} determines P_{red} and there is little effect of K_v. However, this finding is not used in the European standard, which is based on results at high K_v with a complex variation of P_{red} with P_{stat} with a constant line used of slope 0.175 for the dependence of P_{red} on P_{stat}. The US NFPA 68 (2013) guidance shows that P_{red} is determined by P_{stat} and their requirement that P_{red} is always greater than P_{stat} cannot occur at low K_v. The data of Cooper et al. (1987) and Bromma (1967) in larger volume vented vessels support this conclusion.

19.   The critical K_v is >8 and <21.7 for the K_v above which there is an influence of P_{stat} needs more work to determine this more precisely and to investigate the influence of mixture reactivity and vessel size. Bartknecht's data for $K_v = 10$ shows that this is beyond the critical condition as P_{red} is significantly higher than P_{stat}, but with a non-linear dependence on P_{stat}. For K_v greater than the critical the influenced of P_{stat} can be predicted from free venting correlations with an additive term for the P_{stat} effect that has a constant greater than that in Equation 9.1. The relationship between P_{burst} and P_{stat} was established to predict the P_{burst} when P_{stat} is known.

10.2 Recommendations for Future work

Throughout the course of this research, a number of related research areas were identified that justify further work in the future.

1. The 0.2 m^3 vessel results indicated that a wall or the ground placed of the order of 1-2 vent diameters from the vent caused a large increase in the overpressure. This is a possible cause of the high overpressures in Bartknecht's (1993) work as his vessels were sat on the ground with a short distance from the vent to the ground. More work is required in this area to establish the reason for this increase in overpressure and the design standards need to be modified to draw attention to the problem.

2. Most of the result with the external explosion as P$_{red}$ the worst case overpressure were usually the slightly reach mixtures. This may be as a result of the dilution of the rich mixtures downstream the vent. Also, the Lewis and Markstien effect downstream influences the rich mixture, hence, more reactivity. This area of work is rarely investigated.

3. Most of the experiments considered in this work where laminar in nature. There is the need to consider the turbulence in future experiments by using obstacles within the test vessel.

4.. The volume effect on the confined and vented explosions has been an area much concern in vent design equations. This area has not been adequately addressed in the vent design and there are limited data on the effect of volume or issue of self-acceleration of flames. NFPA 68 has two indirect volume effects in it: firstly the self-acceleration of a flame is modelled using the Re of the flame based on its diameter. For the same overpressure the flame is bigger and has a higher Re in larger vessels. This is a procedure to account for the self-acceleration of flames, but this needs more validation. Secondly, NFPA 68 (2013) has another Re term that is based on the Re of the vented turbulent jet flame with the dimension as the vent diameter. This is an attempt to include the external explosion in the prediction, which will get bigger as the vessel volume increases because for the same K$_v$ the vent area and diameter is greater for higher volumes. Again more validation of this needs to be undertaken.

5. This work has shown that the link between A_s and $V^{2/3}$ is a constant that depends on the vessel shape. The implication is that for the same K_v and vessel volume the overpressure will depend on the vessel shape. This needs to be validated with explosions in vessels other than cylindrical. This could be done on the small scale using the present test facilities with different shaped vessel of similar volume.

6. The use of L/D=1 should be considered for both closed vessel and vented explosion since most experimental work was carried out with an L/D = 1, generally using cubic vessels.

7. The present work was carried out for an L/D of 2 and 2.8 as these are at the limits of US and European design standard applicability. However, there are few studies of the L/D effect in the range 0.5 − 3 and more work is need in this area as it is not clear why an L/D of 2 should have the same overpressure as for an L/D of 1. Also the effects of ignition position may be different.

8. The use of the 200L vessel was shown to give unusual higher overpressure as result of the vessel extension. Although these results are of interest, this vessel should be relocated in the test facility on the centreline connections of the 2.5m diameter vessel. The 0.5 diameter 0.5m long connecting vessel is not then required.

9. The venting standards are based on vents on the end of cylindrical vessels. Further work is required on vessels with an L/D >1 to compare end and side venting and to explore the statement that the location of the vent is not important in more detail. For end ignition in cylindrical vessel of L/D = 2 or greater, a vent close to the spark is likely to have a very different overpressure to one on the end of the vessel opposite the spark on the end wall. Some work on this for L/D >6 was carried out by Alexiou et al. (1995) and they found that side venting lowered the peak overpressure.

8. The study of higher burning velocity gas mixtures such as pentene and butane may be of interest since both gas mixtures have higher burning velocity than propane-air mixture. This has been an area of little research interest, as the mechanism and behaviour of both gases mixtures has not been fully understood, and possibility of flame cellularity at certain concentration of the gas mixtures. In addition venting experiments are needed for methane/hydrogen mixtures as adding

hydrogen to the gas mains for greenhouse gas control is being seriously considered and the current guidance for explosion venting for hydrogen has been shown in this work to be inadequate, so new data on hydrogen/methane mixtures is required.

9. Interpretation of venting experiments would be aided by high speed videos of the flame propagation and venting process and this should be done in future work. A perspex transparent vessel should be constructed inside the explosion facility with the same size of one of the vessels used in this work.

10. Further work needs to be undertaken on the influence of the spark position, as others workers have found that ignition closer to the vent of off centre can be worse than central ignition. The present finding of end ignition being the worst case my only be valid for the present L/D = 2.8 cylindrical geometry. Ignition away from the rear wall leaves a large proportion of the initial mixture trapped in the test vessel, as the flame exits the vent. CFD modelling should be used to investigate this problem together with specific experiments. The present work shows that the trapped gas behind the initial flame from the spark burns very slowly. Thus the fact that in large volume vessels this trapped gas has burned rapidly indicates that this could be an important effect of vessel volume that is not taken into account in current vent design procedures.

11. Current modelling of vented explosions needs to be extended to venting of higher pressure explosions, where the vent flow is always sonic and the external explosion is always likely to be dominant in the generation of overpressure. Current design guidance in this area is highly empirical, but there is a reasonable experimental data set of high pressure venting in the open literature.

12. This work has been confined to gas explosions but should in future be extended to dust explosions, especially as Leeds University has the experimental facilities to do this. Gas explosion venting is in an equally empirical era for vent design.

10.3 Final remarks

The present research has provided new experimental data for improving explosion protection using venting. The data provided in this thesis is by no means sufficient

but a positives step towards improving the venting standard. More studies are required in hydrocarbon and hydrogen explosion venting in order generate additional as mentioned above.

The results of this research question the validity of the vent design equations in the current European design guide applicable to hydrogen-air mixtures. Several other parameters have been identified that affect the venting overpressure, but are not currently part of European vent design procedures. It is hoped that the data as presented by this research would have a positive contribution to combustion, explosion protection, and explosion mitigation in general.

REFERENCE

Abdel-Gayed, R. G., Al-Khishali, K. J. a. & Bradley, D. (1984). Turbulent Burning Velocities and Flame Straining in Explosions. Proc. R. Soc. Lond. A 1984 391.

Abdel-Gayed, R. G., Bradley, D., Hamid, M. N. & Lawes, M. (1985). Lewis number effects on turbulent burning velocity. *Symposium (International) on Combustion,* 20**:** 505-512.

Abdel-Gayed, R. G., Bradley, D. & Lung, F. K. K. (1989). Combustion regimes and the straining of turbulent premixed flames. *Combustion and Flame,* 76**:** 213-218.

Abdel-Gayed, R. G. a. & Bradley, D. (1981). A Two-Eddy Theory of Premixed Turbulent Flame Propagation. *Phil. Trans. R. Soc. Lond. A 1981*

Al-Khishali, K. J., Bradley, D. & Hall, S. F. (1983). Turbulent combustion of near-limit hydrogen-air mixtures. *Combustion and Flame,* 54**:** 61-70.

Alexiou, A., Andrews, G. E. & Phylaktou, H. (1996a). Side-vented gas explosions in a long vessel: the effect of vent position. *Journal of Loss Prevention in the Process Industries,* 9**:** 351-356.

Alexiou, A., Andrews, G. E. & Phylaktou, H. (1997). A Comparison between End-Vented and Side-Vented Gas Explosions in Large L/D Vessels. *Process Safety and Environmental Protection,* 75**:** 9-13.

Alexiou, A., HN;, P. & GE;, A. (1996b). The effect of vent size on pressure generation in explosions in large L/D vessels. *Combustion Science and Technology,* vol. 114**:** 645-652.

Andrews, G. E. (2010). Explosion Protection and Mitigation Course. University of Leeds. Leeds.

Andrews, G. E. (2011). Explosion Protection and Mitigation Course. University of Leeds. Leeds.

Andrews, G. E. (2014). Explosion Protection and Mitigation Course. University of Leeds. Leeds.

Andrews, G. E. & Bradley, D. (1972a). The burning velocity of methane-air mixtures. *Combustion and Flame,* 19**:** 275-288.

Andrews, G. E. & Bradley, D. (1972b). Determination of burning velocities: A critical review. *Combustion and Flame,* 18**:** 133-153.

Andrews, G. E. & Bradley, D. (1973). Determination of burning velocity by double ignition in a closed vessel. *Combustion and Flame,* 20**:** 77-89.

Andrews, G. E., Bradley, D. & Lwakabamba, S. B. Turbulence and turbulent flame propagation--A critical appraisal. *Combustion and Flame,* 24**:** 285-304.

Andrews, G. E., Bradley, D. & Lwakabamba, S. B. (1975). Measurement of turbulent burning velocity for large turbulent Reynolds numbers. *Symposium (International) on Combustion,* 15**:** 655-664.

Andrews, G. E., Herath, P. & Phylaktou, H. N. (1990). The influence of flow blockage on the rate of pressure rise in Large L/D cylindrical closed vessel explosions. *Journal of Loss Prevention in the Process Industries,* 3**:** 291-302.

Andrews, G. E. & Phylaktou, H. N. (2010). Handbook on Combustion- Explosion Safety. Wiley-VCH Books. Leeds.

Andrews, G. E. a. & Ahmad, S. A. R. (1994). Noncircular Jet Shear Layer Turbulent Diffusion Flames for Ultra Low NOx Gas Turbine Primary Zones,. ASME Cogen-Turbo, Portland. ASME: 411-417.

Baines, W. D. & Peterson, E. G. (1951). An investigation of flow through screens. *Trans. American Society of Mechanical Engineering,* 73.

Bartknecht, W. (1981). Explosion: Course, Prevention, Protection. *Springer Verlag.* New York.

Bartknecht, W. (1993). Explosionsschultz, Grundlagen und Anwendung, Springer Verlag.

Bauwens, C. R., Chaffee, J. & Dorofeev, S. (2010). Effect of Ignition Location, Vent Size, and Obstacles on Vented Explosion Overpressures in Propane-Air Mixtures. *Combustion Science and Technology,* 182**:** 1915-1932.

Bauwens, C. R., Chaffee, J. & Dorofeev, S. B. (2011). Vented explosion overpressures from combustion of hydrogen and hydrocarbon mixtures. *International Journal of Hydrogen Energy,* 36**:** 2329-2336.

Bauwens, C. R., Chao, J. & Dorofeev, S. B. (2012). Effect of hydrogen concentration on vented explosion overpressures from lean hydrogen–air deflagrations. *International Journal of Hydrogen Energy,* 37**:** 17599-17605.

BBC NEWS ASIA. (2014). *Japan: Fatal blast at Mitsubishi Materials factory* [Online].   Available: http://www.bbc.co.uk/news/world-asia-25664195 [Accessed 29 May 2014].

BBC NEWS ESSEX (2014). Clacton gas explosion: Ten injured and houses flattened.

Bimson, S. J., Bull, D. C., Cresswell, T. M., Marks, P. R., Masters, A. P., Prothero, A., Puttock, J. S., Rowson, J. J. a. & Samuels, B. (1993). An Experimental Study of the Physics of Gaseous Deflagrations in a Very Large Vented Enclosure. *14th International Colloquium on the Dynamics of Explosions and Reactive System.* Coimbra, Portugal.

Bjerketvedt, D., Bakke, J. R. & van Wingerden, K. (1997). Gas explosion handbook. *Journal of Hazardous Materials,* 52**:** 1-150.

Bosschaart, K. J., de Goey, L. P. H. & in collaboration with, J. M. B. C. f. F. M. (2004). The laminar burning velocity of flames propagating in mixtures of hydrocarbons and air measured with the heat flux method. *Combustion and Flame,* 136**:** 261-269.

Bradley, D. (1997). Evolution of flame Propagation in Large Diameter Explosions. *Proc. 2nd International Seminar on Fire and Explosion Hazards.* Moscow.

Bradley, D., Cresswell, T. M. & Puttock, J. S. (2001). Flame acceleration due to flame-induced instabilities in large-scale explosions. *Combustion and Flame,* 124**:** 551-559.

Bradley, D., Dixon-Lewis, G., El-Din Habik, S., Kwa, L. K. & El-Sherif, S. (1991). Laminar flame structure and burning velocities of premixed methanol-air. *Combustion and Flame,* 85**:** 105-120.

Bradley, D. & Hundy, G. F. (1971). Burning velocities of methane-air mixtures using hot-wire anemometers in closed-vessel explosions. *Symposium (International) on Combustion,* 13**:** 575-583.

Bradley, D. & Mitcheson, A. (1976). Mathematical solutions for explosions in spherical vessels. *Combustion and Flame,* 26**:** 201-217.

Bradley, D. & Mitcheson, A. (1978a). The venting of gaseous explosions in spherical vessels. I--Theory. *Combustion and Flame,* 32**:** 221-236.

Bradley, D. & Mitcheson, A. (1978b). The venting of gaseous explosions in spherical vessels. II--Theory and experiment. *Combustion and Flame,* 32**:** 237-255.

Bradley, D., Sheppart, C. G. W., Woolley, R., Greenhalgh, D. A. & Lockett, R. D. (2000). The development and structure of flame instabilities and cellularity at low Markstein numbers in explosions. *Combustion and Flame,* 122**:** 195-209.

Bromma (1957). Kommitten for explosionforsok. Slutrapport, Stockholm.

BS 1042-1.4 (1992). Measurement of fluid flow in closed conduits-. *Part 1: Pressure differential devices.* BSI. London.

BS 1042 (1992). Measurement of fluid flow in closed conduits European Committee for standardization, Brussels.

BS EN 1092-2 (1997). Flanges and their joints. Circular flanges for pipes, valves, fittings and accessories, PN designated. Cast iron flanges. European Committee for standardization. Brussels.

BS EN 1759-1 (2004). Flanges and their joints. Circular flanges for pipes, valves, fittings and accessories, class-designated. Steel flanges, NPS 1/2 to 24 European Committee for standardization,Brussels.

BS EN 14994 (2007). Gas Explosion Venting protection system. European Committee for standardization, Brussels.

BS EN 60584-3 (2008). Thermocouples, Extension and compensating cables, Tolerances and identification system European Committee for standardization,Brussels.

Burgoyne, J. H. & Newitt, D. M. (1955). Crankcase explosions in marine engines. *Institute of Marine Engineers -- Transactions,* 67**:** 255-263.

Cashdollar, K. L., A. Zlochower, I., Green, G. M., Thomas, R. A. & Hertzberg, M. (2000). Flammability of methane, propane, and hydrogen gases. *Journal of Loss Prevention in the Process Industries,* 13**:** 327-340.

Cates, A. & Samuels, B. (1991). A simple assessment methodology for vented explosions. *Journal of Loss Prevention in the Process Industries,* 4**:** 287-296.

Cates, A. T. a. & Bimson, S. J. (1991). Fuel and obstacle dependence in premixed transient deflagrations.   13th International Colloquium on Dynamics of Explosions and Reactive Systems (ICDERS), Nagoya University, Japan.

Catlin, C. A. (1991). Scale effects on the external combustion caused by venting of a confined explosion. *Combustion and Flame,* 83**:** 399-411.

Catlin, C. A. & Johnson, D. M. (1992). Experimental scaling of the flame acceleration phase of an explosion by changing fuel gas reactivity. *Combustion and Flame,* 88**:** 15-27.

Chan, C., Moen, I. O. & Lee, J. H. S. (1983). Influence of confinement on flame acceleration due to repeated obstacles. *Combustion and Flame,* 49**:** 27-39.

Chao, J., Bauwens, C. R. & Dorofeev, S. B. (2011). An analysis of peak overpressures in vented gaseous explosions. *Proceedings of the Combustion Institute,* 33**:** 2367-2374.

Chappell, W. G. (1977). Chemical Engineering Progress. *Plant Loss Prevention*.

CHINADAILY USA. (2012). *Oil spill led to factory blast that killed 25* [Online]. Available: http://usa.chinadaily.com.cn/epaper/2012-03/14/content_14834524.htm [Accessed 15 October 2013].

Chippett, S. (1984). Modeling of vented deflagrations. *Combustion and Flame,* 55**:** 127-140.

Chow, S. K., Cleaver, R. P., Fairweather, M. & Walker, D. G. (2000). An Experimental Study of Vented Explosions in a 3:1 Aspect Ratio Cylindrical Vessel. *Process Safety and Environmental Protection,* 78**:** 425-433.

Ciccarelli, G. & Dorofeev, S. (2008). Flame acceleration and transition to detonation in ducts. *Progress in Energy and Combustion Science,* 34**:** 499-550.

Clingman, W. H., Brokaw, R. S. & Pease, a. R. N. (1952). *Proc. Combust. Inst.,* 4**:** 310.

Cooper, M. G., Fairweather, M. & Tite, J. P. (1986). On the mechanisms of pressure generation in vented explosions. *Combustion and Flame,* 65**:** 1-14.

CRIENGLISH. (2014). *5 Dead, 3 Missing in E China Chemical Plant Blast* [Online]. Available: http://english.cri.cn/11354/2014/04/16/2361s822288.htm [Accessed 29 May 2014].

Cubbage, P. A. & Marshall, M. R. (1972). Pressures generated in combustion chambers by the ignition of air-gas mixtures. Hazard IV, IChemE Symposium Series No. 33.

Cubbage, P. A. a. & Simmons, W. A. (1955). An investigation of explosion reliefs for industrial drying ovens. I-Top reliefs in box ovens. The Gas Council: Research Communication GC23. . London.

Dahoe, A. E. (2005). Laminar burning velocities of hydrogen-air mixtures from closed vessel gas explosions. *Journal of Loss Prevention in the Process Industries,* 18**:** 152-166.

DeGood, R. & Chatrathi, K. (1991). Comparative analysis of test work studying factors influencing pressures developed in vented deflagrations. *Journal of Loss Prevention in the Process Industries,* 4**:** 297-304.

Donat, C. (1977). Pressure relief as used in explosion protection. *Loss Prevention,***:** 87-92.

Drell, I. L. & Belles, F. E. (1957). Survey of Hydrogen Combustion property. 1161-1194.

Edmondson, H. & Heap, M. P. (1969). The burning velocity of methane-air flames inhibited by methyl bromide. *Combustion and Flame,* 13**:** 472-478.

Edmondson, H., Heap, M. P. & Pritchard, R. (1970). Ambient atmosphere effects in flat-flame measurements of burning velocity. *Combustion and Flame,* 14**:** 195-201.

Egolfopoulos, F. N. & Law, C. K. (1991). An experimental and computational study of the burning rates of ultra-lean to moderately-rich H2/O2/N2 laminar flames with pressure variations. *Symposium (International) on Combustion,* 23**:** 333-340.

EN13673-1 (2003). Determination of the maximum explosion pressure and the maximum rate of pressure rise of gases and vapours. European Committee for standardization, Brussels.

EN14994, E. (2007). Gas Explosion Venting protection system. European Committee for standardization, . Brussels.

EN14994:2007, E. (2007). Gas Explosion Venting protection system. BSI.

EN 1127 (2011). Explosive atmospheres-Explosion prevention and protection Part 1: Basic concepts and methodology. European Committee for standardization,Brussels.

Epstein, M., Swift, I. & Fauske, H. K. (1986). Estimation of peak pressure for sonic-vented hydrocarbon explosions in spherical vessels. *Combustion and Flame,* 66**:** 1-8.

European Parliament and the Council (1994). "The Explosive Atmosphere Directive (ATEX)" 94/9/EC. Equipment and Protective Systems Intended for Use in Potentially Explosive Atmospheres. *In:* EC (ed.) *94/9/EC.* The Explosive Atmosphere Directive

EuropeanParliament & Council, a. t. (1994). "The Explosive Atmosphere Directive (ATEX)" 94/9/EC. Equipment and Protective Systems Intended for Use in Potentially Explosive Atmospheres. *In:* EC (ed.) *94/9/EC.* The Explosive Atmosphere Directive

Fairweather, M. & Vasey, M. W. (1982). A mathematical model for the prediction of overpressures generated in totally confined and vented explosions. *Symposium (International) on Combustion,* 19**:** 645-653.

Fakandu, B. M., Kasmani, R. M., Andrews, G. E. a. & Phylaktou, H. N. (2011). Explosion Venting and Mixture Reactivity Influences In A Small Vessel. *23rd The International Colloquium on the Dynamics of Explosions and Reactive Systems.* Irvine,California, -- July 24-29.

Fakandu, B. M., Kasmani, R. M., Andrews, G. E. a. & Phylaktou, H. N. (2012). The Venting of Hydrogen-Air Explosions in an Enclosure with L/D=2.8. Proc. Ninth International Symposium on Hazardous Process Materials and Industrial Explosions (IX ISHPMIE), Crakow, Poland.

Fakandu, B. M., Yan, Z. X., Phylaktou, H. N. a. & Andrews, G. E. (2013). The Effect of Vent Area Distribution in Gas Explosion Venting and Turbulent Length Scales on the External Explosion Overpressure. *In:* D. BRADLEY, G. M., V. MOLKOV, P. SUNDERLAND, F. TAMANINI ed. 7th Proceedings of the Seventh International Seminar on Fire and Explosions Hazards (ISFEH7), Providence, RI, USA, 5 – 10 May .717-726.

Ferrara, G., Di Benedetto, A., Salzano, E. & Russo, G. (2006). CFD analysis of gas explosions vented through relief pipes. *Journal of Hazardous Materials,* 137**:** 654-665.

Ferrara, G., Willacy, S. K., Phylaktou, H. N., Andrews, G. E., Di Benedetto, A., Salzano, E. & Russo, G. (2008). Venting of gas explosion through relief ducts: Interaction between internal and external explosions. *Journal of Hazardous Materials,* 155**:** 358-368.

Forcier, T. & Zalosh, R. (2000). External pressures generated by vented gas and dust explosions. *Journal of Loss Prevention in the Process Industries,* 13**:** 411-417.

France, D. H. a. & Pritchard, R. (1977). Burning Velocity Measurements of Multicomponent Fuel Gas Mixtures. Gas Warme International,.

Gardner, C. L. 1998. *Turbulent combustion in obstacle-accelerated gas explosion - the influnce of scale.* PhD, University of Leeds.

Gouldin, F. C., Bray, K. N. C. & Chen, J. Y. (1989). Chemical closure model for fractal flamelets. *Combustion and Flame,* 77**:** 241-259.

Gu, X. J., Haq, M. Z., Lawes, M. & Woolley, R. (2000). Laminar burning velocity and Markstein lengths of methane-air mixtures. *Combustion and Flame,* 121**:** 41-58.

Gutmark, E., Schadow, K. C., Parr, D. M., Harris, C. K. a. & Wilson, K. J. (1985). The Mean and Turbulent Structure of Noncircular Jets. Proceedings of AIAA Shear Flow Control Conference,.

Harris, G. F. P. & Briscoe, P. G. (1967). The venting of pentane vapour-air explosions on a large vessel. *Combustion and Flame,* 11**:** 329-338.

Harris, R. J. (1983). Investigation and control of Gas explosion in Buildings and Heating Plant. *British Gas and F.N. Spon*.

Harris, R. J. & Wickens, M. J. (1989). Understanding Vapour Cloud Explosions – An experimental   study. *Inst Gas Engineers 55th Autumn Meeting, Comm 1408.*

Harrison, A. J. & Eyre, A. J. (1987). External Explosion as a result of Explosion venting. *Combustion Sceince and Technology,* 52**:** 91-106.

Hazardex. (2013). *South Korean chemical plant blast kills seven* [Online]. Available: http://www.hazardexonthenet.net/article/56911/South-Korean-chemical-plant-blast-kills-seven.aspx [Accessed 15 October 2014].

Hermanns, R. T. E., Konnov, A. A., Bastiaans, R. J. M., de Goey, L. P. H., Lucka, K. & Köhne, H. (2010). Effects of temperature and composition on the laminar burning velocity of CH4 + H2 + O2 + N2 flames. *Fuel,* 89**:** 114-121.

Hjertager, B. H. (1984). Influence of turbulence on gas explosions. *Journal of Hazardous Materials,* 9**:** 315-346.

Howard, W. B. & Russell, W. W. (1974). A procedure for designing gas combustion venting systems. IChemE Symposium Series

Howard, W. N. (1972). Interpretation of a Building Explosion Accident. *Loss Prevention, ,* 6**:** 68-73.

James, H. (2001). Detonation. HSE TDS/039.

Jiang, X., Fan, B., Ye, J. & Dong, G. (2005). Experimental investigations on the external pressure during venting. *Journal of Loss Prevention in the Process Industries,* 18**:** 21-26.

Johnson, D. M. (2010). The potential for vapour cloud explosions – Lessons from the Buncefield accident. *Journal of Loss Prevention in the Process Industries,* 23**:** 921-927.

Kasmani, R. M. 2008a. *Vented Gas Explosion.* PhD, University of Leeds.

Kasmani, R. M. 2008b. *Vented gas explosions.* PhD, ·   University of eeds.

Kasmani, R. M., Andrews, G. E. & Phylaktou, H. N. (2013). Experimental study on vented gas explosion in a cylindrical vessel with a vent duct. *Process Safety and Environmental Protection,* 91**:** 245-252.

Kasmani, R. M., Andrews, G. E., Phylaktou, H. N. & Willacy, S. K. (2010a). The Influence of Vessel Volume and Equivalence Ratio of Hydrocarbon/air Mixtures in Vented Explosions 4th International Conference on Safety & Environment in Process Industry, Florence. Chemical Engineering Transactions, p.463-468.

Kasmani, R. M., Fakandu, B. M., Kumar, P., Andrews, G. E. & Phylaktou, H. N. (2010b). Vented Gas Explosions in Small Vessels with an L/D of 2. *6th Int. Sem. on Fire and explosion Hazards.* University of Leeds. Leeds, United Kingdom.

Kasmani, R. M., Willacy, S., Phylaktou, H. & Andrews, G. (2006). Self accelerating gas flames in large vented explosion volumes that are not accounted for in current vent design correlations. 2nd International Conference on Safety & Environment in Process Industry, Naples. Chemical Engineering Transactions: 245-250.

Koshigoe, S., Gutmark, E. a. & Schadow, K. C. (1989). Initial Development of Noncircular Jets Leads to Axis Switching. *AIAA J,* Vol.27.

Kumar, R. K., Bowles, E. M. & Mintz, K. J. (1992). Large-scale dust explosion experiments to determine the effects of scaling on explosion parameters. *Combustion and Flame,* 89**:** 320-332.

Kumar, R. K., Dewit, W. A. & Greig, D. R. (1989). Vented Explosion of Hydrogen-Air Mixtures in a Large Volume. *Combustion Science and Technology,* 66**:** 251-266.

Lewis, B. & Elbe, G. v. (1987). *Combustion, flames and explosions of gases.* Acad. Pr., Orlando, Fla. [u.a.].

Lewis, B. & von Elbe (1951). *Combustion, flames and explosions of gases.* Acad. Pr., Orlando, Fla. [u.a.].

Lowesmith, B. J., Mumby, C., Hankinson, G. & Puttock, J. S. (2011). Vented confined explosions involving methane/hydrogen mixtures. *International Journal of Hydrogen Energy,* 36**:** 2337-2343.

Lunn, G. (1984). Gas and Dust Venting. *IChemE*.

Maidstone, R. J. (1973). Hazard of Internal Blast in buildings. *Building Research Station Paper CP*.

Maisey, H. R. (1965). Gaseous and dust explosion venting- Part 1. *Chemical and Process Engineering***:** 527-535.

Marshall, M. R. (1977). Calcualtion of gas explosion relief requirements: The use of emperical equations. ICheme symposium series no 49.

McCann, D. P. J., Thomas, G. O. & Edwards, D. H. (1985). Gasdynamics of vented explosions part I: Experimental studies. *Combustion and Flame,* 59**:** 233-250.

Moen, I. O., Lee, J. H. S., Hjertager, B. H., Fuhre, K. & Eckhoff, R. K. (1982). Pressure development due to turbulent flame propagation in large-scale methane---air explosions. *Combustion and Flame,* 47**:** 31-52.

Molkov, V. (1999a). Explosion Safety Engineering: NFPA 68 and the improved vent sizing technology. *Proceedings of 8th International conference on INTERFLAME'99.* Edinburg.

Molkov, V., Dobashi, R., Suzuki, M. & Hirano, T. (1999). Modeling of vented hydrogen-air deflagrations and correlations for vent sizing. *Journal of Loss Prevention in the Process Industries,* 12**:** 147-156.

Molkov, V., Dobashi, R., Suzuki, M. & Hirano, T. (2000). Venting of deflagrations: hydrocarbon-air and hydrogen-air systems. *Journal of Loss Prevention in the Process Industries,* 13**:** 397-409.

Molkov, V., Makarov, D. & Puttock, J. The nature and large eddy simulation of coherent deflagrations in a vented enclosure-atmosphere system. *Journal of Loss Prevention in the Process Industries,* 19**:** 121-129.

Molkov, V. a. & Bragin, M. V. (2013). A Novel Correlation for Vented Hydrogen-Air Deflagrations. 7th Proceedings of the Seventh International Seminar on Fire and Explosion Hazards, Providence, RI, USA.

Molkov, V. V. (1999b). Explosions in buildings: modeling and interpretation of real accidents. *Fire Safety Journal,* 33**:** 45-56.

Molkov, V. V. (2001a). Turbulence Generated During Vented Gaseous Deflagrations and Scaling Issue In Explosion Protection. IChem E Symposium Series. 279-292.

Molkov, V. V. (2001b). Unified correlations for vent sizing of enclosures at atmospheric and elevated pressures. *Journal of Loss Prevention in the Process Industries,* 14**:** 567-574.

Molkov, V. V. & Alexandrov, S. V. (1995). Venting of deflagrations: the influence of "External explosions". *Fire Safety Journal,* 25**:** 372-372.

Munday, G. (1963). The calculation of venting areas for pressure relief of explosions in vessels. Second symposium on process chemcal hazard. IChemE.

Na'inna, A. M., Phylaktou, H. N. & Andrews, G. E. (2013). The acceleration of flames in tube explosions with two obstacles as a function of the obstacle separation distance. *Journal of Loss Prevention in the Process Industries,* 26**:** 1597-1603.

Na'inna, A. M. 2013. *Effects of Obstacle Separation Distance on Gas Explosions.* University of Leeds.

Na'inna, A. M., Phylaktou, H. N. a. & Andrews, G. E. (2012). The Acceleration of Flames in Tube Explosions with Two Obstacles as a Function of the Obstacle Separation Distance,. Proceedings of 9th International symposium on hazards, prevention and mitigation of industrial explosion, , Crakow,Poland.

Nagy, J. & Verakis, H. C. (1983). *Development and Control of Dust Explosions.* MARCEL DEKKER, INC, New York.

Nettleton, M. A. (1975). Pressure as a function of time and distance in a vented vessel. *Combustion and Flame,* 24**:** 65-77.

NFPA68, N. F. P. A. (2007a). Guide for Venting of Deflagrations. National Fire Protection Association Batterymarch Park, Quincy, MA.

NFPA68, N. F. P. A. (2007b). Guide for Venting of Deflagrations, NFPA 68. National Fire Protection Association. 2007.

NFPA68, N. F. P. A. (2013). Standard on Explosion Protection by Deflagration Venting. National Fire Protection Association Batterymarch Park, Quincy, MA.

NFPA 68 (2007). Guide for Venting of Deflagrations. National Fire Protection Association Batterymarch Park, Quincy, MA.

NFPA 68 (2013). Standard on Explosion Protection by Deflagration Venting. National Fire Protection Association Batterymarch Park, Quincy, MA.

Palmer, K. N. & Rogowski, Z. W. (1968). USE OF FLAME ARRESTERS FOR PROTECTION OF ENCLOSED EQUIPMENT IN PROPANE-AIR ATMOSPHERES. IChemE Symposium Series No 25. 76-85.

Pappas, J. A. & Foyn, T. (1983). Gas Explosion Research Programme. *Final Report 83-1334, Det Norsk Veritas.*

Pareja, J., Burbano, H. J. & Ogami, Y. (2010). Measurements of the laminar burning velocity of hydrogen-air premixed flames. *International Journal of Hydrogen Energy,* 35**:** 1812-1818.

Pasman, H. L., Groothuizen, T. M. & de Gooijer, H. (1974). Design of pressure relief vents. *Loss Prevention and Safety Promotion in the Process Industries***:** 185-189.

Phylaktou, H. & Andrews, a. G. E. (1990). Gas Explosions in Long Closed Vessels. *Combustion Sceince and Technology,* 1-3**:** 27-39.

Phylaktou, H. & Andrews, G. E. (1991a). The acceleration of flame propagation in a tube by an obstacle. *Combustion and Flame,* 85**:** 363-379.

Phylaktou, H. & Andrews, G. E. (1991b). Gas Explosions in Long Closed Vessels. *Combustion Science and Technology,* 77**:** 27-39.

Phylaktou, H. & Andrews, G. E. (1993). Gas explosions in linked vessels. *Journal of Loss Prevention in the Process Industries,* 6**:** 15-19.

Phylaktou, H. & Andrews, G. E. (1994). Prediction of the maximum turbulence intensities generated by grid-plate obstacles in explosion-induced flows. *Symposium (International) on Combustion,* 25**:** 103-110.

Phylaktou, H. N. 1993. *Gas explosion in Long closed vessels with obstacles.* PhD, University of Leeds.

Phylaktou, H. N., Andrews, G. E. & Herath, P. (1990). Fast flame speeds and rates of pressure rise in the initial period of gas explosions in large L/D cylindrical enclosures. *Journal of Loss Prevention in the Process Industries,* 3**:** 355-364.

Phylaktou, H. N., Liu, Y., and & Andrews, G. E. (1994). A Study of the Influence of the Obstacle Scale. I. ChemE Symposium No. 134, 19-21 April

Phylaktou, H. N. a. & Andrews, a. G. E. (1995). Application of turbulent combustion models to explosion scaling. *Process Safety and Environmental Protection,* 73**:** 3-10.

Ponizy, B., Henneton, N., Claverie, A. & Veyssiere, B. (2014). Detailed investigation of flame transmission from a vessel to a discharge duct. *Combustion and Flame,* 161**:** 1348-1364.

Ponizy, B. & Leyer, J. C. (1999a). Flame dynamics in a vented vessel connected to a duct: 1. Mechanism of vessel-duct interaction. *Combustion and Flame,* 116**:** 259-271.

Ponizy, B. & Leyer, J. C. (1999b). Flame dynamics in a vented vessel connected to a duct: 2. Influence of ignition site, membrane rupture, and turbulence. *Combustion and Flame,* 116**:** 272-281.

Raezer, S. D. & Olsen, H. L. (1962). Measurement of laminar flame speeds of ethylene-air and propane-air mixtures by the double kernel method. *Combustion and Flame,* 6**:** 227-232.

Rasbash, D., Drysdale, D. D. & Kemp N. (1976). Design of an Explosion Relief System for a Building Handling Liquefied Fuel Gases. IChem.E.Symp. Series, . 145-156.

Rasbash, D. J. (1969). The relief of Gas and Vapour Explosions in Domestic Structures. Fire Research Notes

Rasbash, D. J. & Rogowski, Z. W. (1960). Relief of explosions in duct systems. Proceedings of the Institution of Chemical Engineers Symposium on Chemical Process Hazards with Special Reference to Plant Design, Mar 29-31 1960. 58-68.

Razus, D., Brinzea, V., Mitu, M. & Oancea, D. (2009). Explosion characteristics of LPG-air mixtures in closed vessels. *Journal of Hazardous Materials,* 165**:** 1248-1252.

Razus, D., Movileanu, C., Brinzea, V. & Oancea, D. (2006). Explosion pressures of hydrocarbon-air mixtures in closed vessels. *Journal of Hazardous Materials,* 135**:** 58-65.

Razus, D., Oancea, D., Brinzea, V., Mitu, M. & Movileanu, C. (2010). Experimental and computed burning velocities of propane-air mixtures. *Energy Conversion and Management,* 51**:** 2979-2984.

Razus, D., Oancea, D., Chirila, F. & Ionescu, N. I. (2003). Transmission of an explosion between linked vessels. *Fire Safety Journal,* 38**:** 147-163.

Razus, D. M. & Krause, U. (2001). Comparison of empirical and semi-empirical calculation methods for venting of gas explosions. *Fire Safety Journal,* 36**:** 1-23.

Runes, E. (1972). Explosion venting in Loss Prevention. *Proceedings of the 6th Symposium on Loss Prevention in the Chemical Industry* New York.

Sato, K., Tano, S. a. & Maeda, Y. (2010). Observations of Venting Explosions in a Small Cubic Vessel with Rich Propane-Air Mixtures. *In:* D. BRADLEY, G. M., V. MOLKOV ed. Proceedings of the Sixth International Seminar onFire and Explosion Hazards, Leeds, UK, 11 – 16 April

Sato, Y., Iwabuchi, H., Groethe, M., Merilo, E. & Chiba, S. (2006). Experiments on hydrogen deflagration. *Journal of Power Sources,* 159**:** 144-148.

Sattar, H., Andrews, G. E., Phylaktou, H. N. & Gibbs, B. M. (2014). Turbulent Flames Speeds and Laminar Burning Velocities of Dusts using the ISO 1 m3 Dust Explosion Method. *Chemical Engineering Transactions,* 36.

Scholte, T. G. & Vaags, P. B. (1958). The Burning Velocity of Hydrogen-air mixtures and mixtures of some Hydrocarbons. 495-501.

Shallcross, D. C. (2013). Using concept maps to assess learning of safety case studies – The Piper Alpha disaster. *Education for Chemical Engineers,* 8**:** e1-e11.

SifyNews. (2014). *Gas cylinder blasts injures 30 in Surat* [Online]. Available: http://www.sify.com/news/gas-cylinder-blasts-injures-30-in-surat-news-national-ofmwJhcdaae.html [Accessed 29 May 2014].

Singer, J. M. (1952). *Proc. Combust. Inst,* 4**:** 352.

Siwek, R. (1996). Explosion venting technology. *Journal of Loss Prevention in the Process Industries,* 9**:** 81-90.

Solberg, D. M., Pappas, J. A. & Skramstad, E. (1981). Observations of flame instabilities in large scale vented gas explosions. *Symposium (International) on Combustion,* 18**:** 1607-1614.

Swift, I. (1988). Design of deflagration protection systems. *Journal of Loss Prevention in the Process Industries,* 1**:** 5-15.

Swift, I. (1989). NFPA 68 guide for venting of deflagrations: what's new and how it affects you. *Journal of Loss Prevention in the Process Industries,* 2**:** 5-15.

Tamanini, F. (2001). Scaling parameters for vented gas and dust explosions. *Journal of Loss Prevention in the Process Industries,* 14**:** 455-461.

Tamanini, F. & Chaffee, J. L. (1991). Turbulent unvented gas explosions under dynamic mixture injection conditions. *Symposium (International) on Combustion,* 23**:** 851-858.

Tang, C., Huang, Z., Jin, C., He, J., Wang, J., Wang, X. & Miao, H. (2009). Explosion characteristics of hydrogen–nitrogen–air mixtures at elevated pressures and temperatures. *International Journal of Hydrogen Energy,* 34**:** 554-561.

Taylor, G. I. (1946). The Air Wave Surrounding an Expanding Sphere. *Proceedings of the Royal Society of London. Series A, Mathematical and Physical Sciences,* 186**:** 273-292.

Taylor, P. H. a. & Hirst, W. J. S. (1989). The scaling of vapour cloud explosions: A fractal model for size and fuel type. *Twenty Second International Symposium on Combustion* Seattle, USA.

The Daily Times. (2014). *6 injured in Gerdau Ameristeel Mill explosion in Knoxville* [Online]. Available: http://www.thedailytimes.com/news/injured-in-gerdau-ameristeel-mill-explosion-in-knoxville/article_89c2f5c6-d140-5526-8542-bbd170221d2e.html [Accessed 29 May 2014].

The Times of India. (2014). *Six explosions in chemical factory in Tarapur-MIDC* [Online]. [Accessed 29 May 2014].

The World Post. (2014). *Death Toll In Turkish Mining Accident Climbs As Hundreds Found Dead* [Online]. Available: http://www.huffingtonpost.com/2014/05/13/turkey-mining-accident-death-toll_n_5319275.html#TID=19nmokq1mt1govTData [Accessed 29 May 2014].

Tite, J. P., Binding, T. M. & Marshall, M. R. (1991). Explosion Reliefs for Long Vessels, Fire and Explosion Hazards. *The Institute of Energy*.

Tomlina, G. & Johnson, D. M. (2013). A Large Scale Study of the Venting of Confined Explosions into Unobstructed and Congested Flammable Vapour Clouds. *In:* D. BRADLEY, G. M., V. MOLKOV, P. SUNDERLAND, F. TAMANINI ed. Proceedings of the Seventh International Seminar on Fire and Explosion Hazards, Providence, RI, USA.

Ural, E. A. (1993). A simplified method for predicting the effect of ducts connected to explosion vents. *Journal of Loss Prevention in the Process Industries,* 6**:** 3-10.

Watanabe, N., Yonomoto, T., Tamaki, H., Nakamura, T. & Maruyama, Y. (2013). Review of five investigation committees' reports on the Fukushima Dai-Ichi Nuclear Power Plant severe accident: Focusing on accident progression and causes. *Transactions of the Atomic Energy Society of Japan,* 12**:** 113-127.

Willacy, S. K. 2008. *Homogeneous and Stratified vented Gas Explosions.* PhD, University of Leeds.

Willacy, S. K., Phylaktou, H. N., Andrews, G. E. & Ferrara, G. (2007). Stratified Propane-Air Explosions in a Duct Vented Geometry: Effect of Concentration, Ignition and Injection Position. *Process Safety and Environmental Protection,* 85**:** 153-161.

Wireupdate. (2014). *China discloses 31 deaths in tunnel fire after nearly 2 weeks* [Online]. Available: http://wireupdate.com/china-discloses-31-deaths-in-tunnel-fire-after-nearly-2-weeks.html [Accessed 29 May 2014].

Wu, C. K. & Law., a. C. K. (1984). *Proc. Combust. Inst,* 20**:** 1941.

Wu Y & Swithenbank, J. (1992). Experimental studies on gas-dynamics of venting explosions. *Trans IChemE,* 70(PartA)**:** 200–203.

Wu, Y. & Swithenbank , J. (1992). Experimental studies on gas-dynamics of venting explosions. *Trans IChemE,* 70(PartA)**:** 200–203.

Yao, C. (1974). Explosion venting of low-strenght and structures. *Loss prevention,* 8**:** 1-9.

Zalosh, R. G. (1995). Review of gas deflagration venting models. *1st International Fire and Explosion Hazards of Substances and Venting of Deflagrations.*

FACULTY OF ENGINEERING – RISK ASSESSMENT		UNIVERSITY OF LEEDS
Gas explosion study of gas/air mixtures (eg Propane, Methane, Ethylene and Hydrogen) mixtures with air as the oxidant under ambient atmospheric initial pressure conditions in 0.007m^3 cylindrical vessel – (Rig 1)	**Assessment N^o**	
B11	1	

Preliminary notes
● Risk assessment must be conducted by Academic supervisor/Principal Investigator/Manager.
● Other team members and/or people involved or affected by the activities must be consulted in the construction of the risk assessment.
● Academic supervisor/PIs/Managers and other team members must ensure that the control arrangements and safe systems of work are followed.
● Academic supervisor/PIs/Managers must review this risk assessment at least annually, or in the event of incident, accident or changes to operating/maintenance procedures/personnel.
● Review of risk assessment must be conducted by the Academic supervisor/PI/Manager and initialed and dated in the space provided.

Reference information
● Health and Safety at Work etc Act 1974
● Management of Health and Safety at Work Regulations 1999

Copies
● Original signed risk assessment must be retained by the Academic supervisor/PI/Manager in their office.
● A copy (and any appendices or cross-referenced documents) must be retained in the health and safety file in the workplace.
● The Academic Supervisor/PI/Manager must send a copy by email to the Faculty Safety Team before work begins.

Academic supervisor/PI/Manager's approval				
ACADEMIC SUP/PI/MANAGER	**PRINT NAME**	**SIGNATURE**	**EMAIL/TELEPHONE**	**DATE**

RA review [to be dated initialed by Academic supervisor/PI/MANAGER]							
Date of next review due:							
Date review completed:							
Initials:							

Countersignatures (other members of risk assessment team) [Only if applicable – see Faculty RA Procedures]				
ROLE	**PRINT NAME**	**SIGNATURE**	**EMAIL/TELEPHONE**	**DATE**

IDENTIFICATION OF RISKS, CONTROLS & ACTIONS

Consequence/Severity of Harm (C) x Likelihood of harm being realised (L) = Risk Rating [see table following]

HAZARD TYPE	WHO MAY BE HARMED?	RISK RATING WIITHOUT CONTROLS C x L = E,H,M,L,T	CURRENT CONTROL MEASURES (IF ANY)	NEW RISK RATING C x L = E,H,M,L,T	ADDITIONAL CONTROL MEASURES IDENTIFIED	FINAL RISK RATING C x L = E,H,M,L,T	ACTION BY (& DEADLINE)
Pressure rise	Operators	H	The adiabatic pressure generated for Stoichiometric methane/propane/hydrogen-air explosions, initially at 1 bar are of the order of 8 bar max. Vessel is deign to 35 bar.	T			
Transmission of explosion to connected equipments	Operators	H	The test vessel is opened at one end, connected to a dump vessel with the opened end closed by a gate valve.	T	An operating procedure is carried out using a tick box method as attached to ensure that all valves are closed prior to ignition. The vacuum pump is isolated by two valves before mixture ignition	T	
Prevention of Mixture	Operators	E	The intended pre-ignition pressure is 1013.2 mbara. Pre-	T			

pressurization above 1 atm at start of explosion			pressurization is avoided by not allowing air filling form a compressed air source. Air is sucked into the rig form ambient. The integrity of the gas supply line all the valves an joints in the system is maintained by ensuring that the required pressures remain constant at the required values.				
Personal safety during testing	Operators	M	Lab B11 is divided into two areas; the Control room and the Test room separated by concrete walls. Two bolted-doors are used for access between the rooms. As part of procedure, all personnel are required to leave the test room before ignition. All authorized operators must wear approved safety boots while undertaking experimental work and laboratory coats and appropriate protective equipment	T			

			when required.				
Rupture of pressurized gas lines	Operators	H	Pipes hoses and couplings are suitable for the purpose pressure tested and within their lifespan.	T			
Fall of heavy objects	Operators	M	Main covers are securely closed; possible all off bolts-consequences mitigated by safety foot wear. Overhead crane for heavy objects i.e lifting up weigh in order for vent orifice to be fitted safely.	T			
Fall and trip injuries	Operators	M	Maintenance of surrounding area, clean and free of obstacles and the platform for loading and access to the hatch is sturdy and leveled and are inspected.	T			
Exposure to Gas during mixing and purging of the vessel	Operators	H	The gas lines are connected to test vessel through a Fix and connect horse and regulating valves. The tick-box operating procedure assists in preventing leaks. Though when left open.	T			

| Fire in the control room while personnel are in the test room | Operators | L | A signed escape route through a hinged door in a roller shutter is available with access steps. All new personnel are made aware of this before being allowed to participate in testing. | T | For gas/air explosion tests, all fuel gas bottle are present in the test room with standard valves and regulators. | T | |

COMMUNICATION OF RISK ASSESSMENT FINDINGS TO THOSE INVOLVED				
	METHOD	**YES**	**DATE**	**COMMENTS**
METHODS OF COMMUNICATION USED	Local induction			
	Details of risk assessment discussed and agreed			
	Copy of risk assessment available			
	Controls covered by local protocols & procedures			
	Safety Handbook location notified			
	Toolbox talk			
	Team meeting			
	Email circulation			
	Other -			

Consequence/Severity of Harm (C)	Likelihood of harm being realised (L)				
	Remote Possibility	**Possible**	**Likely**	**Highly probable**	**Virtual Certainty**
Minor injury or illness	Trivial	Trivial	Low	Low	Low
Injury/illness requiring medical attention	Trivial	Low	Medium	Medium	High
Injury/illness involving more than 3 days off work	Low	Medium	Medium	High	High
Major injury or long term illness	Low	Medium	High	Extreme	Extreme
Fatal injury/illness	Low	High	High	Extreme	Extreme

RISK RATING = (C x L/S)		ACTION & TIMESCALES
Extreme	E	Work must not be started or continued until the risk level has been reduced. While the control measures should be cost-effective, the legal duty to reduce the risk is absolute. This means that if it is not possible to reduce the risk, even with unlimited resources, then the work must not be started or must remain prohibited.
High	H	Work must not be started until the risk has been reduced. Considerable resources may have to be allocated to reduce the risk. Where the risk involves work in progress, the problem should be remedied as quickly as possible. (Action within 1 Week)
Medium	M	Efforts should be made to reduce the risk, but the costs of prevention should be carefully measured and limited. Depending on the number of people exposed to the hazard risk reduction measures should normally be implemented (Action within 1 Month)
Low	L	Consideration should be given to cost-effective solutions, or improvements that impose minimal operating standards which will maintain Low level of risk. Monitoring is required to ensure that the controls are maintained. (Review Assessment Annually)
Trivial	T	No action is required to deal with trivial risks, and no documentary records need be kept (insignificant risk)(Review Assessment Annually)

APPENDIX 2 TO

EXPERIMENTAL METHODS

DATED: NOVEMBER 2014

OPERATING PROCEDURE
FOR 162MM DIAMETER SMALL TEST VESSEL(10L)

Date:				Fuel Mixture:
Test No:		Previous Test No:		Concentration:
BR:	Kv:		Remark:	Ignition:
Authorised by:				Injection:

Note: Ensure area around Rig in use is cleared to avoid trip hazards   ☐

DESCRIPTION

	A. Initial Conditions				
1.	Power the Barocel		12.	Test the spark plug from control room	
2.	Ambient Pressure:		13.	Close the gate valve	
3.	Ambient Temperature:		14.	open the door	
4.	Humidity:		15.	Open FR1	
B.	**System Purging**		16.	Check the bottle pressure	
1.	Close the gate valve (check the switch light in control room)		17.	Open Two stage regulator to set F2 to 2bar and F3 to 5bar.	
2.	Push to connect P2 to RP2 (ensure a click sound)		**E.**	**Fuel Mixture Preparation**	
3.	Push to connect P1 to RP1 (ensure a click sound)		1.	Ensure 2WV to test	
			2.	Ensure AV1 is closed	
4.	Open RV1		3.	Push to connect P2 to RP2	
5.	Turn 2WV to test		4.	Push to connect P1 to RP1	
6.	Open VAV1		5	Open VAV1	
7.	Switch on Vac A and monitor Test-Rig pressure		6.	Switch on Vac A (until test-rig pressure less than 50mbar)	
8.	Allow vacuum pressure to go down below 200mbar		7.	Close VAV1	
			8.	Switch-off Vac A	
9.	Close VAV1		9.	Is test-rig pressure Change less than 0.5mbar/minute? Yes☐ No ☐	
10.	Switch-off Vac A				
11.	Open AV2 and allow pressure to reach ambient		10.	If No to step E9, then ABANDON procedure and go to [CONTRUCTION] or consult technician/authorised personnel.	
12.	Close AV2		11.	If Yes to E9 then continue as normal	
13.	Repeat A6 to A12 for at least three times		12.	Note: Vacuum Pressure(P_1):............................ mbar Fuel Pressure Required(P_2):................. mbar Total fill required($P_1 + P_2$):...................... mbar	
14.	Close RV1				
15.	Disconnect P2 from RP2				
16.	Disconnect P1 form RP1		13.	Open FV1	
C.	**Pretest Condition**		14.	Open FV2	
1.	Power on the data logger		15.	Turn 4WV to fuel	
2.	Switch on the computer		16.	Open RV1	
3.	Open the wavecap software Record Time base in use: µs		17.	Carefully open and control FR2 and monitor Barocel readout to obtain the Total fill pressure required in E12	
D.	**Pretest Checks**		18.	If at the point "excess pressure" is obtained than required pressure in Step E17. If Yes go to [EXCESS FUEL] in the [Special Procedure]. If NO go to E19 and continue as normal	Ye ☐ No ☐
1.	Ensure AV1 is close				
2.	Ensure AV2 is close				
3.	Ensure CV1 is close				
4.	Ensure CV2 is close				
5.	Ensure RV1 is close				
6.	Power IB		19.	Close FR2	
7.	Leave the Lab		20.	Close FV2	
8.	Close the doors		21.	Close RV1	
9.	Turn-on both switches on LG6/1		22.	Close FV1	
10.	Open the gate valve				

F.	Air Filling	
1.	Carefully open and control AV2	
2.	Monitor Barocel readout until the pressure reaches to ambient. Also, monitor pressure gauge reading (to ensure pressure is same as recorded in step A2).	
3.	Close AV2	
4.	Record test-rig pressure:................... mbar	
5.	Disconnect P1 from RP1 and fit to interlock.	
6.	Disconnect P2 to RP2	

G.	System Checks	
1.	Check RV1 is close	
2.	Check AV1 is close	
3.	Check AV2 is close	
4.	Check FV1 is close	
5.	Check FV2 is close	
6.	Check CV1 is close	
7.	Check CV2 is close	
8.	Check CR3 is close	
9.	Check VAV1 is close	
10.	Check P1 disconnected and fitted in lock	
11.	Check P2 disconnected	
12.	Check IB switched on	
13.	Connect spark plug to test vessel (if not)	
14.	Check 4WV is turned to close	

H.	Ignition Procedure	
1.	All personnel go into control room	
2.	Close all doors to test room	
3.	Lock all locks.	
4.	On the ignition panel check the following indicator lights.	
4a	Door locked	
4b	Door latched.	
5.	ARM the data logger system	
6.	Open gate valve	
7.	Check on ignition panel "the gate valve open/Fuel line disconnected" indicator light is on. If no go to step G1-14. If yes proceed as normal.	Yes ☐ No ☐
8.	Press "Fire" button	
9.	Close the gate valve	
10.	Save Data	
11.	Check whether the data logger tripped. If "No" then go to [NO IGNITION] in the [SPECIAL PROCEDURE], if "Yes" proceed as normal.	Yes ☐ No ☐
12.	Open doors	
13.	Turn-off both switches LG6/1	

I.	System Purging	
1.	Ensure the gate valve is closed (check the switch light in control room)	
2.	Ensure the Barocel is powered	
3.	Push to connect P2 to RP2 (ensure a click sound)	
4.	Push to connect P1 to RP1 (ensure a click sound)	
5.	Open RV1	
6.	Open VAV1	
7.	Turn 2WV to test	
8.	Switch on Vac A and monitor Test-Rig pressure	
9.	Allow vacuum pressure to go down below 200mbar	
10.	Switch-off Vac A	
11.	Open AV2 and allow pressure to reach ambient	
12.	Close AV2	
13.	Repeat A8 to A12 for at least three times	
14.	Close VAV1	
15.	Close RV1	
16.	Disconnect P2 from RP2	
17.	Disconnect P1 form RP1	

J.	Data Checking	
1.	Load all test result on FAMOS	
2.	Record Pressures: PT0: P_{fv}...................P_{ext}...............(bar) PT1: P_{fv}...................P_{ext}...............(bar) PT2: ....(bar) PT3:...............................(bar)	
3.	Record Flame arrival times: T4:........................ms T1:.................ms T5:........................ms T2:.................ms T6:........................ms T3:.................ms T7:........................ms	

If this is the last test of the day go to step K1-6

K.	End of Day Procedure	
1.	Ensure disconnect P1 ☐ P2 ☐	
2.	Ensure all valves closed AV1 ☐ RV1 ☐ VAV1 ☐ AV2 ☐ CV1 ☐ CV2 ☐ CV3 ☐ FV1 ☐ FV2 ☐	
3.	Dump vessel purging: Open VBV1 ☐ Switch on Vac B (allow at least 10 miniutes pump operation) ☐	
4.	Switch-off Vac B	
5.	Close VBV1	
6.	Turn-off : Barocel ☐ Data logger ☐ IB ☐	